CELL JOURNAL

(Yakhteh)

Vol 22, Suppl 1, Autumn 2020, Pages: 1-168

ISSN: 2228-5806
eISSN: 2228-5814

www.celljournal.org

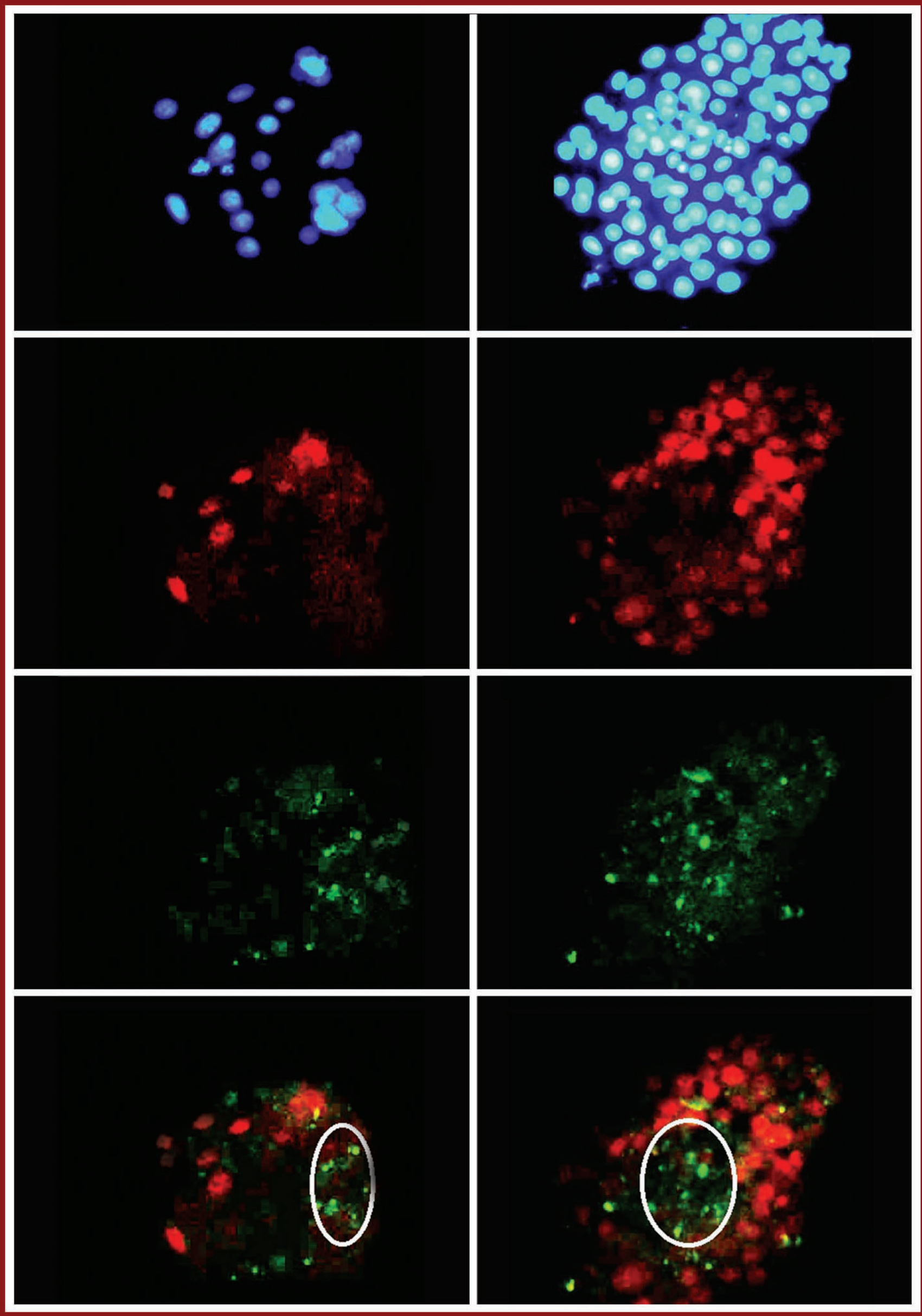

A Quarterly Publication of the Royan Institute

پژوهشگاه رویان

Cell Journal (Yakhteh)

Guide for Authors

Aims and Scope: The "Cell Journal (Yakhteh)" is a peer review and quarterly English publication of Royan Institute of Iran. The aim of the journal is to disseminate information through publishing the most recent scientific research studies on exclusively Cellular, Molecular and other related topics. **Cell J**, has been certified by the Ministry of Culture and Islamic Guidance since 1999 and also accredited as a scientific and research journal by HBI (Health and Biomedical Information) Journal Accreditation Commission since 2000 which is an open access journal. **This journal holds the membership of the Committee on Publication Ethics (COPE).**

1. Types of articles

The articles in the field of Cellular and Molecular can be considered for publications in **Cell J.** These articles are as below:

A. Original articles Original articles are scientific reports of the original research studies. The article consists of English Abstract (structured), Introduction, Materials and Methods, Results, Discussion, Conclusion, Acknowledgements, Author's Contributions, and References **(Up to 40).**

B. Review articles Review articles are the articles written by well experienced authors and those who have excellence in the related fields. The corresponding author of the review article must be one of the authors of at least three published articles appearing in the references. The review article consists of English Abstract (unstructured), Introduction, Conclusion, Author's Contributions, and References **(Up to 70).**

C. Systematic Reviews

Systematic reviews are a type of literature review that collect and critically analyzes multiple research studies or papers. The Systematic reviews consist of English Abstract (unstructured), Introduction, Materials and Methods, Results, Discussion, Conclusion, Acknowledgements, Author's Contributions, and References **(Up to 70).**

D. Short communications: Short communications are articles containing new findings. Submissions should be brief reports of ongoing researches. The short communication consists of English Abstract (unstructured), the body of the manuscript (should not hold heading or subheading), Acknowledgements, Author's Contributions, and References **(Up to 30).**

E. Case reports: Case reports are short discussions of a case or case series with unique features not previously described which make an important teaching point or scientific observation. They may describe novel techniques or use equipment, or new information on diseases of importance. It consists of English Abstracts (Unstructured), Introduction, Case Report, Discussion, Acknowledgements, Author's Contributions, and References **(Up to 30).**

F. Editorial: Editorial should be written by either the editor in chief or the editorial board.

G. Imaging in biology: Images in biology should focus on a single case with an interesting illustration such as a photograph, histological specimen or investigation. Color images are welcomed. The text should be brief and informative.

H. Letter to the editors: Letter to editors are welcome in response to previously published **Cell J** articles, and may also include interesting cases that do not meet the requirement of being truly exceptional, as well as other brief technical or clinical notes of general interest.

I. Debate.

2. Submission process

It is recommended to see the guidelines for reporting different kinds of manuscripts here. This guide explains how to prepare the manuscript for submission. Before submitting, we suggest authors to familiarize themselves with **Cell J** format and content by reading the journal via the website (www.celljournal.com). The corresponding author ensures that all authors are included in the author list and agree with its order, and they must be aware of the manuscript submission.

A. Author contributions statements

It is essential for authors to include a statement of responsibility in the manuscript that specifies the contribution of every one of them. This participation must include conception and design of the manuscript, data acquisition or data analysis and interpretation, drafting of the manuscript and/or revising it for critically important intellectual content, revision and final approval of the manuscript and statistical analysis, obtaining funding, administrative, technical, or material support, or supervision. Authors who do not meet the above criteria should be acknowledged in the **Acknowledgments section.**

B. Cover letter

Each manuscript should be accompanied by a cover letter, signed by all authors specifying the following statement: "The

manuscript has been seen and approved by all authors and is not under active consideration for publication. It has neither been accepted for publication nor published in another journal fully or partially (except in abstract form). I hereby assign the copyright of the enclosed manuscript to **Cell J.** Corresponding author must confirm the proof of the manuscript before online publishing. Also, is it needed to suggest three peer reviewers in the field of their manuscript.

C. Manuscript preparation

Authors whose first language is not English encouraged to consult a native English speaker in order to confirm his manuscripts to American or British (not a mixture) English usage and grammar. It is necessary to mention that we will check the plagiarism of your manuscript by iThenticate Software. The manuscript should be prepared in accordance with the "International Committee of Medical Journal Editors (ICMJE)". Please send your manuscript in two formats Word and Pdf (including: title, name of all the authors with their degree, abstract, full text, references, tables and figures) and Also send tables and figures separately in the site. The abstract and text pages should have consecutive line numbers in the left margin beginning with the title page and continuing through the last page of the written text. Each abbreviation must be defined in the abstract and text when they are mentioned for the first time. Avoid using abbreviation in the title. Please use the international and standard abbreviations and symbols

It should be added that an essential step toward the integration and linking of scientific information reported in published literature is using standardized nomenclature in all fields of science and medicine. Species names must be italicized (*e.g., Homo sapiens*) and also the full genus and species written out in full, both in the title of the manuscript and at the first mention of an organism in a paper.

It is necessary to mention that genes, mutations, genotypes, and alleles must be indicated in italics. Please use the recommended name by consulting the appropriate genetic nomenclature database, e.g., HUGO for human genes. In another words; if it is a human gene, you must write all the letters in capital and italic (*e.g., OCT4, c-MYC*). If not, only write the first letter in capital and italic (*e.g., Oct4, c-Myc*). **In addition, protein designations are the same as the gene symbol but are not italicized.**

Of note, Cell J will only consider publishing genetic association study papers that are novel and statistically robust. Authors are advised to adhere to the recommendations outlined in the STREGA statement (http://www.strega-statement.org). The following criteria must be met for all submissions:

1. Hardy-Weinberg Equilibrium (HWE) calculations must be carried out and reported along with the P-values if applicable [see Namipashaki et al. 2015 (Cell J, Vol 17, N 2, Pages: 187-192) for a discussion].

2. Linkage disequilibrium (LD) structure between SNPs (if multiple SNPs are reported) must be presented.

3. Appropriate multiple testing correction (if multiple independent SNPs are reported) must be included.

Submissions that fail to meet the above criteria will be rejected before being sent out for review.

Each of the following manuscript components should begin in the following sequence:

Authors' names and order of them must be carefully considered (full name(s), highest awarded academic degree(s), email(s), and institutional affiliation(s) of all the authors in English. Also, you must send mobile number and full postal address of the corresponding author).

Changes to Authorship such as addition, deletion or rearrangement of author names must be made only before the manuscript has been accepted in the case of approving by the journal editor. In this case, the corresponding author must explain the reason of changing and confirm them (which has been signed by all authors of the manuscript). If the manuscript has already been published in an online issue, an erratum is needed.

Title is providing the full title of the research (do not use abbreviations in title).

Running title is providing a maximum of 7 words (no more than 50 characters).

Abstract must include Objective, Materials and Methods, Results, and Conclusion (no more than 300 words).

Keywords, three to five, must be supplied by the authors at the foot of the abstract chosen from the Medical Subject Heading (MeSH). Therefore; they must be specific and relevant to the paper.

The following components should be identified after the abstract:

Introduction: The Introduction should provide a brief background to the subject of the paper, explain the importance of the study, and state a precise study question or purpose.

Materials and Methods: It includes the exact methods or observations of experiments. If an apparatus is used, its manufacturer's name and address should be stipulated in parenthesis. If the method is established, give reference but if the method is new, give enough information so that another author can perform it. If a drug is used, its generic name, dose, and

route of administration must be given. Standard units of measurements and chemical symbols of elements do not need to be defined.

Statistical analysis: Type of study and statistical methods should be mentioned and specified by any general computer program used.

Ethical considerations*:* Please state that informed consent was obtained from all human adult participants and from the parents or legal guardians of minors and include the name of the appropriate institutional review board that approved the project. It is necessary to indicate in the text that the maintenance and care of experimental animals complies with National Institutes of Health guidelines for the humane use of laboratory animals, or those of your Institute or agency.

Clinical trial registration: All of the Clinical Trials performing in Iran must be registered in Iranian Registry of Clinical Trials (www.irct.ir). The clinical trials performed abroad, could be considered for publication if they register in a registration site approved by WHO or www.clinicaltrials.gov. If you are reporting phase II or phase III randomized controlled trials, you must refer to the CONSORT Statement for recommendations to facilitate the complete and transparent reporting of trial findings. Reports that do not conform to the CONSORT guidelines may need to be revised before peer-reviewing.

Results: They must be presented in the form of text, tables, and figures. Take care that the text does not repeat data that are presented in tables and/or figures. Only emphasize and summarize the essential features of the main results. Tables and figures must be numbered consecutively as appeared in the text and should be organized in separate pages at the end of the manuscript while their location should be mentioned in the main text.

Tables and figures: If the result of your manuscript is too short, it is better to use the text instead of tables & figures. Tables should have a short descriptive heading above them and also any footnotes. Figure's legend should contain a brief title for the whole figure and continue with a short explanation of each part and also the symbols used (no more than 100 words). All figures must be prepared based on cell journal's guideline in color (no more than 6 Figures and Tables) and also in GIF or JPEG format.

Of Note: Please put the tables & figures of the result in the results section not any other section of the manuscript.

Supplementary materials would be published on the online version of the journal. This material is important to the understanding and interpretation of the report and should not repeat material within the print article. The amount of supplementary material should be limited. Supplementary material should be original and not previously published and will undergo editorial and peer review with the main manuscript. Also, they must be cited in the manuscript text in parentheses, in a similar way as when citing a figure or a table. Provide a legend for each supplementary material submitted.

Discussion: It should emphasize the present findings and the variations or similarities with other researches done by other researchers. The detailed results should not be repeated in the discussion again. It must emphasize the new and important aspects of the study.

Conclusion: It emphasizes the new and important aspects of the study. All conclusions are justified by the results of the study.

Acknowledgements: This part includes a statement thanking those who contributed substantially with work relevant to the study but does not have authorship criteria. It includes those who provided technical help, writing assistance and name of departments that provided only general support. You must mention financial support in the study. Otherwise; write this sentence "There is no financial support in this study".

Conflict of interest: Any conflict of interest (financial or otherwise) and sources of financial support must be listed in the Acknowledgements. It includes providers of supplies and services from a commercial organization. Any commercial affiliation must be disclosed, regardless of providing the funding or not.

References: The references must be written based on the Vancouver style. Thus the references are cited numerically in the text and listed in the bibliography by the order of their appearance. The titles of journals must be abbreviated according to the style used in the list of Journals Indexed in PubMed. Write surname and initials of all authors when there are six or less. In the case of seven or more authors, the names of the first six authors followed by "et al." must be listed. You can download Endnote file for Journal references style: endnote file

The reference of information must be based on the following order:

Article:

Surname(s) and first letter of name &middle name(s) of author(s) .Manuscript title. Journal title (abbr).publication date (year); Volume & Issue: Page number.

Example: Manicardi GC, Bianchi PG, Pantano S, Azzoni P, Bizzaro D, Bianchi U, et al. Presence of endogenous nicks in DNA of ejaculated human spermatozoa and its relationship to chromomycin A3 accessibility. Biol Reprod. 1995; 52(4): 864-867.

Book:

Surname(s) and first letter of name & middle name(s) of author(s).Book title. Edition. Publication place: publisher name; publication date (year); Page number.

Example: Edelman CL, Mandle CL. Health promotion throughout the lifespan. 2nd ed. ST Louis: Mosby; 1998; 145-163.

Chapter of book:

Surname(s) and first letter of name & middle name(s) of author(s).Chapter title. In: Surname(s) and first letter of name & middle name(s) of editor(s), editors. Book title. Edition. Publication place: publisher name; publication date (year); Page number.

Example: Phillips SJ, Whisnant JP. Hypertension and stroke. In: Laragh JH, Brenner BM, editors. Hypertension: pathophysiology, diagnosis, and management. 2nd ed. New York: Raven Press; 1995; 465-478.

Abstract book:

Example: Amini rad O.The antioxidant effect of pomegranate juice on sperm parameters and fertility potential in mice. Cell J. 2008;10 Suppl 1:38.

Thesis:

Name of author. Thesis title. Degree. City name. University. Publication date (year).

Example: Eftekhari Yazdi P. Comparison of fragment removal and co-culture with Vero cell monolayers on development of human fragmented embryos. Presented for the Ph.D., Tehran. Tarbiyat Modarres University. 2004.

Internet references

Article:

Example: Jahanshahi A, Mirnajafi-Zadeh J, Javan M, Mohammad-Zadeh M, Rohani M. Effect of low-frequency stimulation on adenosineA1 and A2A receptors gene expression in dentate gyrus of perforant path kindled rats. Cell J. 2008; 10 (2): 87-92. Available from: http://www.celljournal.org. (20 Oct 2008).

Book:

Example: Anderson SC, Poulsen KB. Anderson's electronic atlas of hematology.[CD-ROM]. Philadelphia: Lippincott Williams & Wilkins; 2002.

D. Proofs are sent by email as PDF files and should be checked and returned within 72 hours of receipt. It is the authors' responsibility to check that all the text and data as contained in the page proofs are correct and suitable for publication. **We are requested to pay particular attention to author's names and affiliations as it is essential that these details be accurate when the article is published.**

E. Pay for publication: Publishing an article in Cell J requires Article Processing Charges (APC) that will be billed to the submitting author following the acceptance of an article for publication. For more information please see www.celljournal.org.

F. Ethics of scientific publication: Manuscripts that have been published elsewhere with the same intellectual material will refer to duplicate publication. If authors have used their own previously published work or work that is currently under review, as the basis for a submitted manuscript, they are required to cite the previous work and indicate how their submitted manuscript offers novel contributions beyond those of the previous work. Research and publication misconduct is considered a serious breach of ethics.

The Journal systematically employs iThenticate, plagiarism detection and prevention software designed to ensure the originality of written work before publication. Plagiarism of text from a previously published manuscript by the same or another author is a serious publication offence. Some parts of text may be used, only where the source of the quoted material is clearly acknowledged.

3. General information

A. You can send your manuscript via online submission system which is available on our website. If the manuscript is not prepared according to the format of **Cell J**, it will be returned to authors.

B. The order of article appearance in the Journal is not demonstrating the scientific characters of the authors.

C. Cell J has authority to accept or reject the manuscript.

D. The received manuscript will be evaluated by associate editor. **Cell J** uses a single-blind peer review system and if the manuscript suits the journal criteria, we select the reviewers. If three reviewers pass their judgments on the manuscript,

it will be presented to the editorial board of **Cell J.** If the editorial board has a positive judgment about the manuscript, reviewers' comments will be presented to the corresponding author (the identification of the reviewers will not be revealed). The executive member of journal will contact the corresponding author directly within 3-4 weeks by email. If authors do not receive any reply from journal office after the specified time, they can contact journal office. Finally, executive manager will respond promptly to authors' request.

The Final Checklist

The authors must ensure that before submitting the manuscript for publication, they have to consider the following parts:

1. Title page should contain title, name of the author/coauthors, their academic qualifications, designation & institutions they are affiliated with, mailing address for future correspondence, email address, phone, and fax number.

2. Text of manuscript and References prepared as stated in the "guide for authors" section.

3. Tables and figures should be uploaded separately except in the main manuscript. Figures must be sent in color and also in GIF or JPEG format with 300 dpi resolutions.

4. Cover Letter should be uploaded with signature of all authors.

The Editor-in-Chief: Ahmad Hosseini, Ph.D.

Cell Journal (Yakhteh),

P.O. Box: 16635-148, Iran

Tel/Fax: + 98-21-22510895

Emails: Celljournal@royaninstitute.org

info@celljournal.org

Dr. Saeed Kazemi Ashtiani

IN THE NAME OF GOD

Gone But not Forgotten

In the memory of the late Director of Royan Institute, Founder of Stem Cells Research in Iran and Chairman of ***Cell Journal*** *(Yakhteh)*. May he rest in peace.

PUBLISHED & SPONSORED BY:
Publication of Royan Institute (ACECR)

Indexed in:
1. Thomson Reuters (ISI)
2. PubMed
3. PubMed Central (PMC)
4. National Library Medicine (NLM)
5. Biosis Preview
6. Index Medicus for the Eastern Mediterranean Region (IMEMR)
7. Regional Information Center for Sciences and Technology (RICeST)
8. Index Copernicus International
9. Cambridge Scientific Abstract (CSA)
10. EMBASE
11. Scopus
12. Cinahl Database
13. Google Scholar
14. Chemical Abstract Service (CAS)
15. Proquest
16. Directory of Open Access Journals (DOAJ)
17. Open Academic Journals Index (OAJI)
18. Directory of Research Journals Indexing (DRJI)
19. Scientific Information Database (SID)
20. Iranmedex
21. Islamic World Science Citation Center (ISC)
22. Magiran
23. Science Library Index
24. Biological Abstracts
25. Essential Science Indicators
26. EuroPub

ACECR

Editorial Office Address (Dr. Ahmad Hosseini):
Royan Institute, P.O.Box: 16635-148,
Tehran, Iran
Tel & Fax: (+9821)22510895
Website: www.celljournal.org
Emails: info@celljournal.org
celljournal@royaninstitute.org

Printing Company:
Naghshe e Johar Co.
No. 103, Fajr alley, Tehranpars Street,
Tehran, Iran.

Cell Journal (Yakhteh), Vol 22, Suppl 1, Autumn 2020, Pages: 1-168

CONTENTS

Review Article

Original Articles

Short Communication Articles

Letter to The Editor Article

• **Front page of Cell Journal$_{(Yakhteh)}$: Figure 3D, Page: 78**

Review Article

Induced Pluripotent Stem Cell Meets Severe Combined Immunodeficiency

Reza Kouchaki, B.Sc.[1], Bahareh Abd-Nikfarjam, Ph.D.[2], Amirhosein Maali, M.Sc.[3], Saeid Abroun, Ph.D.[4], Farshad Foroughi, Ph.D.[2], Sasan Ghaffari, M.Sc.[5], Mehdi Azad, Ph.D.[1]*

1. Faculty of Allied Medicine, Qazvin University of Medical Sciences, Qazvin, Iran
2. Department of Immunology, School of Medicine, Qazvin University of Medical Sciences, Qazvin, Iran
3. Student Research Committee, Pasteur Institute of Iran, Tehran, Iran
4. Department of Hematology and Blood Banking, Faculty of Medical Sciences, Tarbiat Modares University, Tehran, Iran
5. Hematology Department, School of Allied Medicine, Tehran University of Medical Sciences, Tehran, Iran

Corresponding Address: P.O.Box: 34197-59811, Faculty of Allied Medicine, Qazvin University of Medical Sciences, Qazvin, Iran
Email: haematologicca@gmail.com

Received: 16/April/2019, Accepted: 27/August/2019

Abstract

Severe combined immunodeficiency (SCID) is classified as a primary immunodeficiency, which is characterized by impaired T-lymphocytes differentiation. *IL2RG, IL7Ralpha, JAK3, ADA, RAG1/RAG2,* and *DCLE1C* (Artemis) are the most defective genes in SCID. The most recent SCID therapies are based on gene therapy (GT) of hematopoietic stem cells (HSC), which are faced with many challenges. The new studies in the field of stem cells have made great progress in overcoming the challenges ahead. In 2006, Yamanaka et al. achieved "reprogramming" technology by introducing four transcription factors known as Yamanaka factors, which generate induced pluripotent stem cells (iPSC) from somatic cells. It is possible to apply iPSC-derived HSC for transplantation in patients with abnormality or loss of function in specific cells or damaged tissue, such as T-cells and NK-cells in the context of SCID. The iPSC-based HSC transplantation in SCID and other hereditary disorders needs gene correction before transplantation. Furthermore, iPSC technology has been introduced as a promising tool in cellular-molecular disease modeling and drug discovery. In this article, we review iPSC-based GT and modeling for SCID disease and novel approaches of iPSC application in SCID.

Keywords: Hematopoietic Stem Cell Transplantation, Induced Pluripotent Stem Cell, Primary Immunodeficiency, Severe Combined Immunodeficiency

Cell Journal(Yakhteh), Vol 22, Suppl 1, Autumn 2020, Pages: 1-10

Citation: **Kouchaki R, Abd-Nikfarjam B, Maali AH, Abroun S, Foroughi F, Ghaffari S, Azad M. Induced pluripotent stem cell meets severe combined immunodeficiency T. Cell J. 2020; 22 Suppl 1: 1-10. doi: 10.22074/cellj.2020.6849.**

Introduction

Severe combined immunodeficiency (SCID) is classified as a primary immunodeficiency (PID), which is characterized by impaired T-lymphocyte differentiation. SCID is a monogenic, heterogeneous, and life-threatening syndrome (1). Considering that both humoral and cellular adaptive immunity are involved, this immunodeficiency is called "combined" because in T^-B^- phenotypes of SCID, T-cell development, as well as B-cell development is affected. In T^-B^+ phenotypes, the absence of normal T-helpers leads to defective antibody production by normal B-cells. In some subtypes of SCID, the disease can also be accompanied by defective natural killer (NK) cells. These different phenotypes are due to mutations in several genes, which lead to appear in different stages of T-cell development (Fig.1). The worldwide prevalence of SCID is estimated to be in 50,000 to 100,000 of the young population and constitutes 7% of PID patients. Approximately 90% of genetic defects in different forms of SCID have been identified (2, 3). The latest therapies regarding SCID are based on gene therapies (Table 1), which so far are faced with many difficulties (4-18). The new studies in the field of stem cells have made considerable progress in overcoming the challenges ahead.

A review on induced pluripotent stem cell

In 2006, Takahashi et al. (19) achieved "Reprogramming" technology by introducing OCT4, KLF4, SOX2, and C-MYC reprogramming factors (RFs), which are responsible for embryonic-like state, into human fibroblasts. These RFs, known as OKSM factors, generate induced pluripotent stem cells (iPSC) from a somatic cell and reverse its state back into embryonic status, which can later differentiate to various human cells. IPSC-derived pre-differentiated or differentiated cells can be used for transplantation in patients with abnormal or poorly functional specific cell lineage. Considering that harvested cells are autologous, there is no risk of immunological rejection (fully matched HLA-profile) and no concern regarding the low number of transplantable cells. Furthermore, preparing these pluripotent stem cells is a non-invasive method (20).

In addition to other aspects of iPSC-based therapies, there are various studies in the field of cancer and immunodeficiency that led to the creation of iPSC-derived cytotoxic T-lymphocytes (iCTL) and iNKT-Cells, which have major roles in the immune system. The medical applications of iPSC are not limited to cell therapy. Recently, iPSC technology has been introduced as a promising tool for *in vitro* cellular-molecular disease modeling, drug discovery, and *ex-vivo* regenerative medicine, including organogenesis and GT (21, 22).

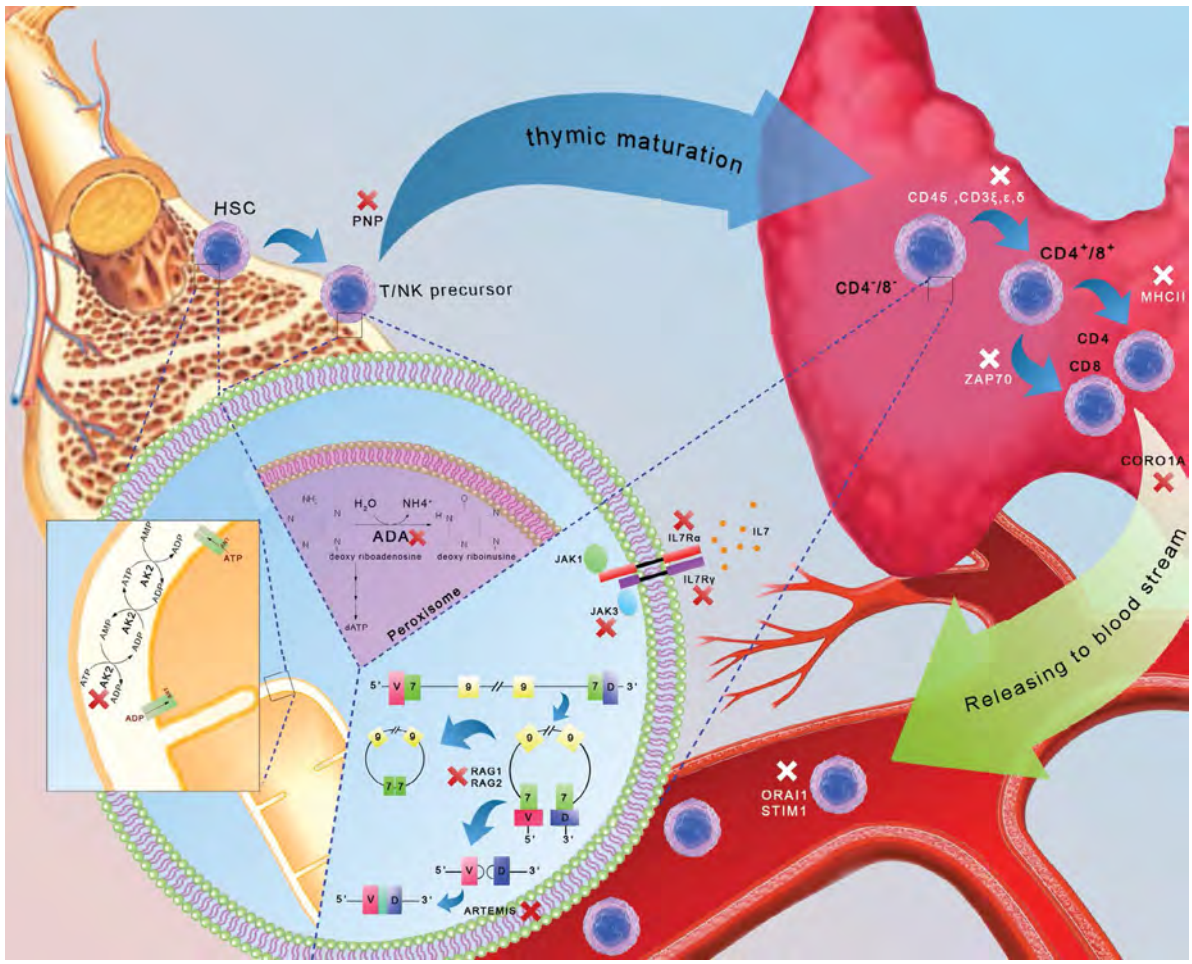

Fig.1: A depiction of the most common types of SCID. The deficiencies appear in different stages of T-cell development. AK2-deficiency, ADA-SCID, and PNP-SCID are caused by a deficiency in the developmental stages of the bone marrow. The defective signals from the pre-TCR and TCR (CD45, CD3ξ, CD3ε, CD3δ), ILR γ and α, RAG1/2, JAK3, ZAP70, MHCII, and ARTEMIS deficiencies occur in thymus developmental stages. SCID; Severe combined immunodeficiency, ADA; Adenosine-deaminase, PNP; Purine nucleo-side phosphorylase, and TCR; T-cell receptor.

The standard severe combined immunodeficiency treatments and challenges

Supportive care, such as intravenous immunoglobulin (IVIG) and antimicrobial agents, may be required for SCID. For example, cotrimoxazole is prescribed as prophylactic agent against *P. jirovecii*, acyclovir is used for patients with a history of herpes simplex virus infection, and antifungal prophylaxis should also be used. ADA-SCID can also be treated by enzyme replacement therapy (ERT), which consists of ADA coupled to polyethylene glycol (PEG-ADA), but the intramuscular injection is needed at least once a week to eliminate toxic waste. This is a life-saving therapy when other treatments are unavailable or less effective. This treatment is effective in approximately 90% of the patients. However, in some cases, after a period, the dose of PEG-ADA must be increased, mainly when anti-ADA antibodies have been produced. Systemic ERT may also ameliorate hepatic and neurologic dysfunctions in some ADA-SCID patients. A concern regarding ERT is lymphoid and possibly hepatic malignancies and progression of chronic pulmonary insufficiency. ERT before bone marrow transplantation may prevent donor cell engraftment by enhancing endogenous T-cell recovery (23).

Hematopoietic stem cell transplantation (HSCT) is the only definitive treatment for SCID and has more than a 90% chance of success (from geno-identical donors). There are some serious adverse effects, such as graft versus host disease (GvHD) or graft rejection, following the allogenic immune conflict between donor and recipient (24, 25). On the other hand, granulocyte colony-stimulating factors (G-CSF), such as filgrastim and lenograstim, which are used to release HSCs into the peripheral blood before leukapheresis, can also be mutagenic. However, chronic infection and thymus problems, which are related to the age of the recipient, can reduce the chance of success or cause damage to specific organs, like liver, kidney, or lung. In NK^- phenotypes of SCID, myeloablation or immunosuppression is not required for HSCT. NK cells can reduce the survival rate after transplantation of haplo-incompatible HLA. Due to the perpetual B-cell dysfunction, lifelong immunoglobulin substitution may be required to prevent infections caused by inadequate antibody responses (26).

Table 1: Review on common types of severe combined immunodeficiencies

Deficiency	Impaired gene	Locus	Inheritance pattern	Mechanisms	Lymphocyte profile	Frequency	Treatment	References
Signaling of IL7R	IL2RG	Xq13.1	XLR	Deficiency in common γ chain in IL7R and IL15R (associated with thymocytes and NK-cells differentiation signaling pathways, respectively)	$T^-B^+ K^-$	48%	GT HSCT	(4-6)
	IL7R alpha	5p13	AR	A decrease in expression of IL7Rα on the surface of lymphocyte progenitor cells	$T^-B^+NK^+$	10%	HSCT	(8 ,7)
	JAK3	19p13.1	AR	Deficiency in the JAK3 tyrosine kinase	$T^-B^+NK^-$	6%	HSCT	(10 ,9)
Purine Metabolism	ADA	20q13.11	AR	The absence of ADA leads to accumulation of dAdo and dATP, which have functional and developmental deleterious roles in lymphocytes	$T^-B^-NK^-$	16%	ERT GT HSCT	(11-13)
V(D)J Recombination	RAG1/RAG2	11p13	AR	Ceases the initiation stages of VDJ recombination process	$T^-B^-NK^+$	6%	HSCT+Myeloablation	(14 ,10)
	DCLE1C (Artemis)	10p	AR	Impairment in NHEJ (used for opening the hairpins during VDJ recombination) and disability of T-cell in rearranging TRG and TRB	$T^-B^-NK^+$	5%	HSCT+Meloablation	(15-17)

AR; Autosomal recessive, XLR; x linked recessive, GT; Gene therapy, HSCT; Hematopoietic stem cell transplantation, ERT; Enzyme replacement therapy, SCID; Severe combined immunodeficiency, PNP; Purine nucleo-side phosphorylase, and TCR; T-cell receptor.

Transplantation from mismatched donors is still associated with high mortality. GT, as an alternative for haplotype HSCT procedure, is on clinical trials for both ADA-SCID and X-SCID, which will eventually determine the role of GT as a therapeutic option. The first vector that was used in GT was the γ-retroviral vector, which increases the expression of *MDS-EVI1* and *LMO2* (two insertional hotspots in HSC for γ-retroviral vector) and causes T-cell acute lymphoblastic leukemia (ALL) in some X-linked SCID patients (27-29). Nevertheless, it has been used in ADA-SCID patients with a mild conditioning regimen, while no genotoxicity was seen. Self-inactivation (SIN) retroviral vector design has deletions in the U3 region of 5´LTR beside an internal heterologous promoter, which leads to the reduced incidence or even absence of proto-oncogene activation. Preclinical investigations on retroviral-mediated *JAK3* gene transfer shows expression of the exogenous JAK3 protein in animal models. SIN lentiviral vectors (LVs), which are based on the human immunodeficiency virus, have a better safety profile and reduce the risk of insertional mutagenesis. In addition, LVs are superior to γ-retroviral vectors in manipulating human HSCs and maintaining sustained transgene expression. SIN-lentiviral vector GT succeeded in preclinical murine models for ADA-SCID, RAG1-SCID, RAG2-SCID, and Artemis-SCID (30, 31). Considering all the challenges and therapeutic potentials of iPSC, the road to treating SCID seems clear, which ultimately leads to shorter and more efficacious treatment courses with fewer side effects.

Induced pluripotent stem cells-based gene therapy meets severe combined immunodeficiency

The invention of iPSC technology has allowed scientists to cure single-gene disorders by creating a healthy cell line from the patient in *ex vivo* conditions. After a biopsy of healthy cells, they are monitored in the laboratory. Lentiviruses and retroviruses were the first vectors that were used for transferring OKSM factors into somatic cells. The major problem with the use of these vectors is their mutagenicity, but lentiviral vectors are deemed to be less mutagenic than retroviral vectors (32). It has been shown that polycistronic lentiviral viruses, which have been combined with 2A self-cleaving peptides and internal Ribosomal Entry Site (IRES), are sufficient for the integration of RFs. Hence, the recombination of a polycistronic vector system with a lentiviral vector facilitates the clinical applications of iPSC.

There are other methods to generate iPSC. These include non-integrating viruses, such as adenovirus, and non-viral approaches, such as plasmids, DNA-demethylating agents, histone deacethylating agents, and dimethyl transferases (33).

After the gene introduction, a particular time is required to allow the expression of factors and induction of pluripotency. Ultimately, iPSC gains immortality and self-renewal capacity (34). Direct iPSC-based cell therapy is used in non-hereditary diseases. In hereditary disorders, the iPSC-based cell therapy should be combined with GT to correct the defective gene(s). Due to the congenital deficiency in SCID, which is present in HSC, the primary step in iPSC-based treatment is generating "corrected" HSC. Each subtype of SCID results in different molecular mutagenic disorders. The most common ones are listed in Table 2. GT is used to modify these mutations and manipulate normal products by using iPSC-based GT.

There are many targeting vectors when genetically manipulating iPSC. These include classic targeting vectors, DSB-mediated targeting vector, BAC targeting vector, piggyBac targeting vector. Also, helper-dependent adenovirus targeting vector, single-strand oligonucleotides (ssODN), and Adeno-associated virus (AAV) targeting vector are among advanced vectors. The nucleases bind to specific sites of DNA and catalyze it to a double-strand break (DSB). In the presence of donor DNA (targeting gene), homologous recombination occurs at a specific genomic site. The CRISPR-Cas9, meganucleases, zinc-finger nucleases (ZFN), transcription activator-like effector nucleases (TALEN) more recently have been engineered for this purpose. They decrease the dysregulation of gene expression and the off-targeting genotoxicity (40-43). After the correction of mutation, the iPSCs differentiate to HSCs, which is also influenced by specific hematopoietic cytokines and HOXB4 (44). In the next step, SCID patients are treated with induced HSCs transplantation with adequate dosage.

As discussed, many clinical trials have been performed in the field of iPSC-based GT. In 2007, Zou et al. (45) conducted the first iPSC-based GT for the treatment of sickle cell anemia. They reported the successful iPSC-based GT in sickle cell anemia in mice. There are other clinical trials, in iPSC-based SCID GT. In 2015, Chang et al. (46) attempted to correct JAK3 deficiency in SCID human iPSCs (hiPSC) using CRISPR/Cas9-enhanced gene targeting. It resulted in restoring normal T-cell development after gene correction. In 2015, Menon et al. (47) treated X1-SCID by generating the corrected iPSC line, which was modified by TALEN. Prior to this, in 2009, Lei et al. (48) differentiated T-Lineage from iPSCs and used it to treat RAG-deficient mice. In 2015, Howden et al. (49) modified reprogramming and gene correction by somatic cells of SCID patients using the CRISPR-Cas9 system. In 2016, Li et al. (50) edited IL-2RG locus in iPSC with a recombinant Adeno-associated virus (rAAV)-targeting vector. Despite the common problems in routine GT methods, there is no risk of immunological rejection and GvHD in iPSC-based GT (Table 3).

Table 2: Genetic alterations in common types of severe combined immunodeficiency

			Types /number of mutations						
Defective gene	**Gene size**	**Number of exons**	**Missense**	**Nonsense**	**Splice-site**	**Insertion**	**Deletion**	**Hotspot**	**References**
IL7R	20738	8	3	1	1	-	-	In exon 4	(7)
IL2RG	5447	8	55	33	33	10	32	CG dinucleotides at cDNA 690-691 and cDNA 879	(4)
JAK3	24029	25	13	7	3	1	2	-	(35)
RAG1	12544	2	36	10	-	1 (frameshift)	12 (frameshift)	-	(36)
RAG2	7092	2	15	2	-	1 (frameshift)	1 (frameshift) 1 (in-frame) 1 (gross)	-	(37)
ARTEMIS	56665	18		1	3	-	3 (frameshift)	-	(38)
ADA	33003	10	37	3	9	-	4 (frameshift) 1 (in-frame and gross)	-	(39)

Table 3: Current studies on iPSC-based trials on severe combined immunodeficiency

Year	Scientists	Disease	Type of investigation	Origin of iPSC	Reprogramming vector	Reprogramming factor	Gene editing vector	Results	References
2009	Lei F *et al.*	RAG-SCID	Modeling	Mouse embryonic fibroblast (MEF)	Retroviral	OCT3/4, SOX2, KLF4, c-MYC	-	The first report of T-cell generation from iPSCs (iPSCs were converted into T-cells, which contained TCRβ and CD3. T-cells were stimulated by anti-CD3 and anti-CD28 antibodies to secrete IL2 and INFγ. Then, by transferring them into RAG-SCID mice, it led to the reconstituting of T-cell pools).	(48)
2015	Chang CW *et al.*	JAK3-SCID	Modeling (+Gene editing)	Keratinocyte	lentiviral	OCT4, SOX2, KLF4, c-MYC	CRISPR/ Cas9	The iPSC was derived from a JAK3-SCID patient and showed that the differentiation of T-cells that contained this defect stops at early developmental stages. The correction of JAK3-mutation via CRISPR/Cas9 led to regular development and production of mature NK and T-cells with a broad TCR repertoire.	(46)
2015	Howden SE *et al.*	ADA-SCID	Gene editing	Fibroblast	episomal	OCT4, SOX2, KLF4, c-MYC, NANOG, LIN28, SV40 large T-antigen	CRISPR/ Cas9	Reprogramming and gene targeting in a one-step process significantly reduce the time and resources, as well as the risks of cell cultures, drug selection, and multiple clonal events.	(49)
2016	Menon T *et al.*	X-SCID	Modeling (+gene editing)	BM-MSC (bone marrow mesenchymal stem cell)	lentiviral	-	TALEN	The mutant X1-SCID iPSC can produce hematopoietic and myeloid precursors, but the wild type and the gene-corrected iPSC can also provide mature NK and T-cell precursors with healthy IL2Rγ production.	(47)
2016	Li LB *et al.*	X-SCID	Modeling (+gene editing)	MSCs (mesenchymal stem/stromal cells)	Lentiviral	OCT4, SOX2, NANOG, LIN28	rAAV	Illustrated the role of IL2RG in the developmental evolution of NK-cells and T-cells, and the application of correcting IL2RG mutation in iPSC in regenerative medicine to prevent GvHD.	(50)
2015	Brauer PM *et al.*	RAG1-SCID (and RAG1-OS)	Modeling	Modeling	Lentiviral	OCT4, SOX2, KLF4, c-MYC	-	Evaluation and comparison of T-cell development, along with TCR V(D) J recombination in OS and SCID patients, and showing the correlation of genotype-phenotype in different patients with different mutations in the same gene.	(51)

SCID; Severe combined immunodeficiency and iPSCs; Induced pluripotent stem cells.

Severe combined immunodeficiency modeling based on induced pluripotent stem cells

In addition to all its clinical benefits, iPSC technology is also used in the human disease modeling to identify the exact genomic and molecular pathological pathways of a disorder. It is also used in drug discovery to design efficient, safe, and novel drugs and screen their efficacy and toxicity. The use of animals for human disease modeling have ethical issues, limitation in completely resembling human disease phenotypes due to fundamental differences between human and animal genomes. Furthermore, the inaccessibility to animals and difficult preparation (impossible in some cases) of specific cell-line *in vitro* makes this method more problematic.

In contrast, patient-derived iPSC has enabled scientists to provide high numbers of disease-specific cell-lines in laboratory conditions and help them overcome the mentioned problems. Moreover, healthy iPS cells, which are derived from the patient, can be used as a control in the modeling process. As mentioned, the accurate recognition of monogenic mutations is a key step in understanding the pathogenesis of the disease (52). Consequently, the action to reverse this mutation is a major step in the treatment of genetic disorders. The *in vitro* modeling of gene editing is an introduction to the application of *in vivo* GT. There are conventional tools for gene modification that are used in GT in clinics and modeling. Among the programmable site-specific nucleases, CRISPR-Cas9 system has been highly regarded for its ability to create a wide range of isogenic controls for iPSC-based modeling and its simplicity in design and use (53).

Since the inception of this technology, many studies have been conducted based on iPSC-disease modeling, such as Ciliopathy, Parkinson's disease, hematopoietic abnormalities, cardiac disorders, insulin resistance, and metabolic syndrome, skeletal muscle disorders, schizophrenia pathogenesis, amyotrophic lateral sclerosis, mitochondrial disorders, etc. (54-56). The use of iPS cells in the modeling of primary immunodeficiencies, such as chronic granulomatous disease (CGD) and SCID, has also been successful (19).

In 2008, one of the first PID models based on iPSC was done by Park et al. (57). In 2015, Chang et al. (46) recognized that the Jak3-deficient T-cell progenitor development is blocked in early stages by using iPSCs derived from SCID patients. In this study, gene editing by the CRISPR-Cas9 system restored the development of early T-cell progenitors. These modified progenitors could differentiate into healthy NK cells and T-cells. In 2016, Brauer et al. (51) modeled T-cell development by iPSCs from RAG1-SCID patients. They recognized that *RAG1* mutation has low recombination capability and results in cleavage defects. These studies are powerful tools for identifying the PID mechanisms, pharmacological tests, and GT trials (Fig.2). There are other applications of iPSCs in the field of immunodeficiency (Table 4).

Induced pluripotent stem cell application in secondary diseases of severe combined immunodeficiency and another sight

IPSC can also generate B-cells in T^-B^- phenotypes of SCID. In advanced SCID, secondary diseases are often seen. In addition to the primary treatment of SCID that restores the immune system, the application of regenerative iPSC technology can also be used for secondary diseases of SCID. Sensorineural hearing loss (SNHL), which is the result of reticular dysgenesis progression, is caused by damage or deficiency in cochlear, which is followed by SCID.

Moreover, deterioration of bone (leading to costochondral dysplasia), thymic epithelium, lung, liver, and brain tissues results in progressive ADA-SCID. PNP-SCID causes neurological abnormalities. RHOH deficiency induces Burkitt lymphoma. ORAI1 and STMI1 deficiencies lead to non-progressive myopathy and ectodermal. MATG1 deficiency can also cause neoplasia (70). Most of the aforementioned disorders are characterized by specific cell-line deficiency. IPSC-derived cells, prepared *in vitro*, can replace faulty cell-lines. In organopathies, there are clinical approaches to organogenesis and histogenesis based on iPS cells, which were inaccessible before. Malignancies and other disorders are also in the context of iPSC technology. DiGeorge syndrome, characterized by the impaired thymus, leads to SCID. The standard treatment for DiGeorge syndrome is allograft thymus transplantation. The risk of immunological graft rejection can be eliminated by iPSC regenerative technology. Therefore, iPSC appears to be a suitable and comprehensive therapeutic option for SCID patients.

SCID is a fatal PID characterized by impairment in T-cells development. Standard therapeutic plans for SCID are not safe. In grafted cases, there is a risk of GvHD and immune rejection due to the impairment in the immune system. The Side effects of ERT and myeloablation cause a systemic defect in patients. Altogether, we do not have access to optimal therapy for SCID yet.

We discussed different aspects of a critical key in SCID treatment in the future: iPSC therapy, which potentially is optima for SCID therapy. However, many challenges are facing to iPSC technology. As discussed, it could be achieved to the high-pure cell products based on iPSC, including iCTL, iNK cells, HSC, etc., making a safe procedure to transplantation (no immune rejection, no GvHD) as an autologous graft in SCID patients. However, due to the pluripotency state of iPSCs, there is a teratogenesis risk that limited clinical administrations of iPSCs for now. However, there are some reports to overcoming on teratogenesis of iPSCs and entrance in clinical trials. So, iPSC is a promising window for "Bubble boys" in the future, not so far.

Table 4: Current studies on iPSC-based trials on other immunodeficiency disorders

Disease	Year	Conducted by	Type	Results	References
AIDS	2010	Kamata et al.	Modeling (+gene editing)	Application of chimeric MLV (murine leukemia virus)/ lentiviral vectors for iPSCs reprogramming (to take advantage of both vectors) and CCR5 shRNA (short-hairpin RNA) as an anti-HIV factor in GT based on iPSCs.	(58)
	2011	Kambal et al.	Modeling (+gene editing)	Generation of the immune cells derived from iPSCs that are resistant to HIV-1 via CCR5 shRNA and human/ rhesus chimeric TRIMα gene as a pre-integration inhibitor.	(59)
	2012	Yao et al.	Modeling (+gene editing)	Destruction of CCR5 locus in hiPSCs via ZFN to generate healthy hematopoietic colonies in AIDS treatment.	(60)
	2015	Kang et al.	Modeling (+gene editing)	Destruction of CCR5 locus in hiPSCs via CRISPR/Cas9 to generate healthy hematopoietic colonies. The iPSCs-derived macrophages are resistant to CCR5-tropic viruses.	(61)
CGD	2011	Mukherjee et al.	Modeling (+GT)	Generation of iPSCs from X-CGD mice and comparison of the differentiation potential of these iPSCs to myeloid precursors and neutrophil compared to wild type iPSCs. GT by transferring gp^{91phox} and using a lentiviral vector regenerates the activity of NADPH oxidase in X-CGD iPSC-derived neutrophils.	(62)
	2011	Zou et al.	Modeling (+Gene editing)	Reproducing the pathognomonic CGD oxidase negative phenotype to show ROS deficiency in neutrophils derived from X-CGD iPSCs, and gp^{91phox} correction via ZFN and restoration of ROS production in neutrophils.	(63)
	2012	Jiang et al.	Modeling	The iPSCs generation from X-CGD and AR47-CGD patients, differentiation to monocytes, and macrophages by a similar cytokine profile to blood-derived macrophages. These macrophages have typical phagocytic properties but lack ROS production.	(64)
	2014	Brault et al.	Modeling	Presentation of the optimized protocols to generate macrophages and neutrophils derived from iPSCs in three types of CGD patients (i.e., x^0-linked, $AR47^0$, and $AR22^0$for the first time).	(65)
	2015	Laugsch et al.	Modeling (+gene editing)	Restoration of NADPH oxidase activity in X-CGD iPSCs after differentiation to neutrophils in two ways: transposon-mediated integration of a BAC vector carrying the *CYBB* gene, and the correction of mutation via homologous recombination.	(66)
	2017	Brault J et al.	Modeling	The research on enzyme therapy by recombinant NOX2/ p^{22phox} liposomes in macrophages derived from X-CGD iPSCs that led to the successful delivery of NOX2 and p^{22phox} to the plasma membrane and regeneration of NADPH oxidase complex and production of superoxide anions.	(67)
WAS	2015	Suphapeetiporn et al.	Modeling (+GT)	Correction of pro-platelet structures by overexpression of WASp in WAS iPSCs via lentiviral vectors.	(68)
	2016	Laskowski et al.	Modeling (+gene editing)	Correction of WASp in WAS-iPSCs via ZFN that led to the expression of WASp in all of hematopoietic lineages and repair of T-cells and NK-cells defect.	(69)

AIDS; Acquired immunodeficiency syndrome, CGD; Chronic granulomatous disease, WAS; Wiskott-Aldrich syndrome, iPSC; induced Pluripotent stem cell, and GT; Gene therapy.

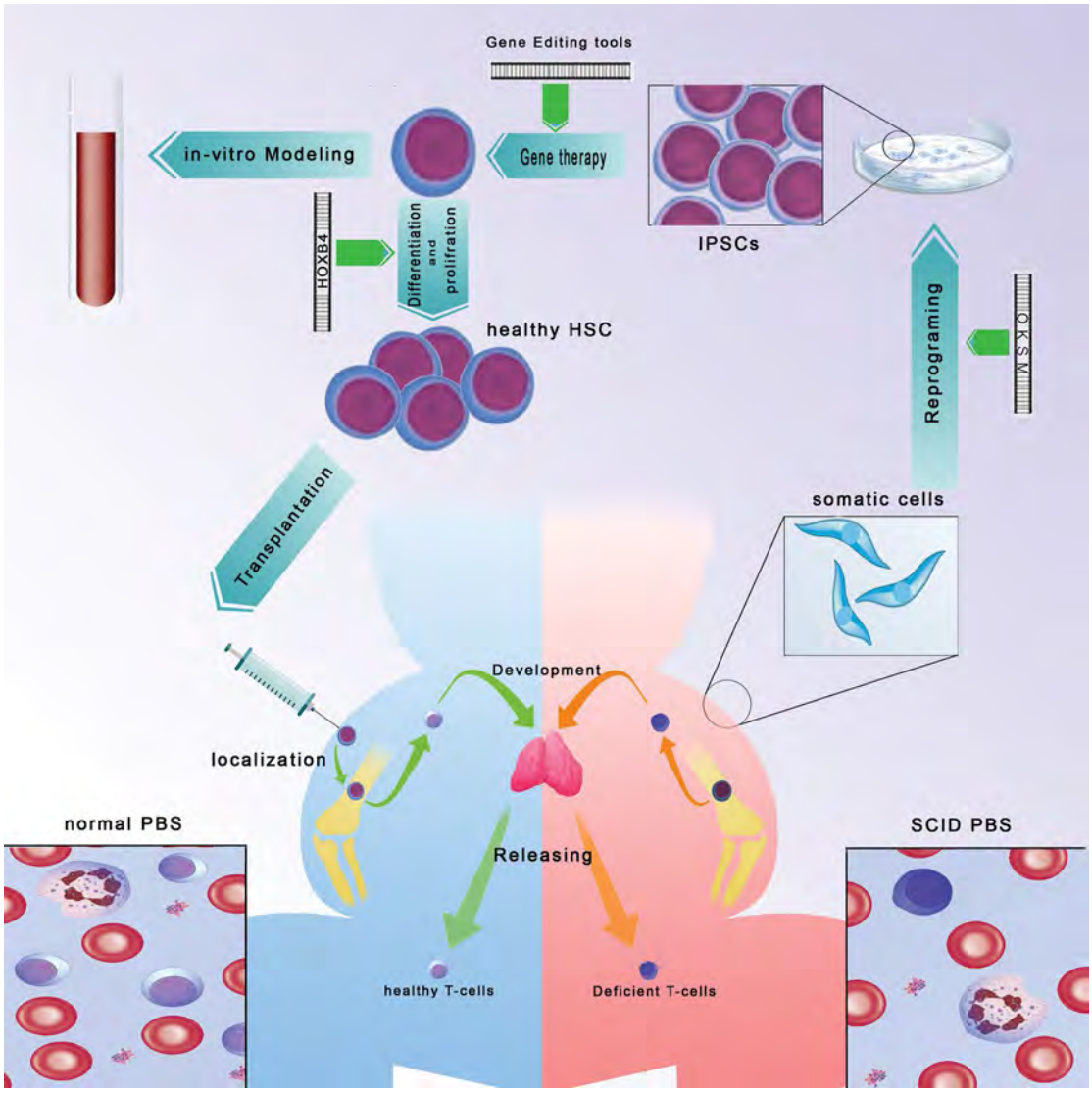

Fig.2: A review of iPSC technology applications in SCID. OKSM RFs reprogram somatic cells to iPSCs. Hematopoietic RFs are used to induce hematopoiesis in iPSCs. The prepared cells are used for *in vitro* modeling and HSCT (after GT).
SCID; severe combined immunodeficiency, OKSM; OCT4, KLF4, SOX2 and c-MYC, RFs; Reprogramming factors, iPSCs; Induced pluripotent stem cell, HSCT; Hematopoietic stem cell transplantation, and GT; Gene therapy.

Conclusion

The technology of iPSC demonstrates a promising future in clinical applications. Since its invention, there is extensive research regarding various reprogramming methods to achieve iPSC. Many researchers have studied its differentiation, application in identifying disease pathogenesis, drug design, histogenesis, organogenesis, and cell therapy. The combination of iPSCs and GT has expanded its therapeutic potential and other aspects of this technology. Most of the clinical applications of iPSC, such as application in SCID, are still in the study phase. Although its introduction to the clinic is not far. As technology is increasingly used by scientists, the treatment of various diseases by iPSC technology is close.

Acknowledgment

There is no financial support and conflict of interest in this study.

Authors' Contributions

R.K., A.H.M.; Contributed in this study as main authors, data collecting and drafting. B.A.-N., F.F.; Performed a precise advising on the immunologic aspect of this manuscript. S.A.; Revised study from hematological aspects. S.Gh.; Contributed as language editor. M.A.; Supervised all aspect of this paper. All authors performed editing and approving the final version of this paper for submission, also participated in the finalization of the manuscript and approved the final draft.

References

1. Rosen FS. Severe combined immunodeficiency: a pediatric emergency. J Pediatr. 1997; 130(3): 345-346.
2. Gaspar HB, Qasim W, Davies EG, Rao K, Amrolia PJ, Veys P. How I treat severe combined immunodeficiency. Blood. 2013; 122(23): 3749-3758.
3. Sahmani M, Vatanmakanian M, Goudarzi M, Mobarra N, Azad M. Microchips and their significance in isolation of circulating tumor cells and monitoring of cancers. Asian Pac J Cancer Prev. 2016;

17(3): 879-894.
4. Mou W, He J, Chen X, Zhang H, Ren X, Wu X, et al. A novel deletion mutation in IL2RG gene results in X-linked severe combined immunodeficiency with an atypical phenotype. Immunogenetics. 2017; 69(1): 29-38.
5. Hiramoto T, Li LB, Funk SE, Hirata RK, Russell DW. Nuclease-free adeno-associated virus-mediated Il2rg gene editing in X-SCID mice. Mol Ther. 2018; 26(5): 1255-1265.
6. Maali AH, Ferdosi-Shahandashti E, Azad M. Drug switching, a creative approach to leukemia therapy. IJBC. 2019; 11(3): 111-112.
7. Puel A, Ziegler SF, Buckley RH, Leonard WJ. Defective IL7R expression in T-B+ NK+ severe combined immunodeficiency. Nat Genet. 1998; 20(4): 394-397.
8. Puck JM. Newborn screening for severe combined immunodeficiency and T-cell lymphopenia. Immunol Rev. 2019; 287(1): 241-252.
9. Robinette ML, Cella M, Telliez JB, Ulland TK, Barrow AD, Capuder K, et al. Jak3 deficiency blocks innate lymphoid cell development. Mucosal Immunol. 2018; 11(1): 50-60.
10. Schuetz C, Neven B, Dvorak CC, Leroy S, Ege MJ, Pannicke U, et al. SCID patients with ARTEMIS vs RAG deficiencies following HCT: increased risk of late toxicity in ARTEMIS-deficient SCID. Blood. 2014; 123(2): 281-289.
11. Aiuti A, Slavin S, Aker M, Ficara F, Deola S, Mortellaro A, et al. Correction of ADA-SCID by stem cell gene therapy combined with nonmyeloablative conditioning. Science. 2002; 296(5577): 2410-2413.
12. Lanfranchi A, Lougaris V, Notarangelo LD, Soncini E, Comini M, Beghin A, et al. Maternal T-cell engraftment impedes with diagnosis of a SCID-ADA patient. Clin Immunol. 2018; 193: 118-120.
13. Aiuti A, Roncarolo MG, Naldini L. Gene therapy for ADA-SCID, the first marketing approval of an ex vivo gene therapy in Europe: paving the road for the next generation of advanced therapy medicinal products. EMBO Mol Med. 2017; 9(6): 737-740.
14. Munoz IG, Prieto J, Subramanian S, Coloma J, Redondo P, Villate M, et al. Molecular basis of engineered meganuclease targeting of the endogenous human RAG1 locus. Nucleic Acids Res. 2011; 39(2): 729-743.
15. Volk T, Pannicke U, Reisli I, Bulashevska A, Ritter J, Bjorkman A, et al. DCLRE1C (ARTEMIS) mutations causing phenotypes ranging from atypical severe combined immunodeficiency to mere antibody deficiency. Hum Mol Genet. 2015; 24(25): 7361-7372.
16. Punwani D, Kawahara M, Yu J, Sanford U, Roy S, Patel K, et al. Lentivirus mediated correction of artemis-deficient severe combined immunodeficiency. Hum Gene Ther. 2017; 28(1): 112-1124.
17. Rahmani T, Azad M, Chahardouli B, Nasiri H, Vatanmakanian M, Kaviani S. Patterns of DNMT1 promoter methylation in patients with acute lymphoblastic leukemia. Int J Hematol Oncol Stem Cell Res. 2017; 11(3): 172-177.
18. Cossu F. Genetics of SCID. Ital J Pediatr. 2010; 36: 76.
19. Takahashi K, Tanabe K, Ohnuki M, Narita M, Ichisaka T, Tomoda K, et al. Induction of pluripotent stem cells from adult human fibroblasts by defined factors. Cell. 2007; 131(5): 861-872.
20. Zomer HD, Vidane AS, Goncalves NN, Ambrosio CE. Mesenchymal and induced pluripotent stem cells: general insights and clinical perspectives. Stem Cells Cloning. 2015; 8: 125-134.
21. Maali A, Atashi A, Ghaffari S, Kouchaki R, Abdolmaleki F, Azad M. A review on leukemia and iPSC technology: application in novel treatment and future. Curr Stem Cell Res Ther. 2018; 13(8): 665-675.
22. Azad M, Biniaz RB, Goudarzi M, Mobarra N, Alizadeh S, Nasiri H, et al. Short view of leukemia diagnosis and treatment in Iran. Int J Hematol Stem Cell Ress. 2015; 9(2): 88-94.
23. Gaspar HB, Aiuti A, Porta F, Candotti F, Hershfield MS, Notarangelo LD. How I treat ADA deficiency. Blood. 2009; 114(17): 3524-3532.
24. Azad M, Kaviani S, Noruzinia M, Mortazavi Y, Mobarra N, Alizadeh S, et al. Gene expression status and methylation pattern in promoter of P15INK4b and P16INK4a in cord blood CD34+ stem cells. Iran J Basic Med Sci. 2013; 16(7): 822-828.
25. Miggelbrink AM, Logan BR, Buckley RH, Parrott RE, Dvorak CC, Kapoor N, et al. B-cell differentiation and IL-21 response in IL2RG/JAK3 SCID patients after hematopoietic stem cell transplantation. Blood. 2018; 131(26): 2967-2977.
26. Dehghanifard A, Kaviani S, Abroun S, Mehdizadeh M, Saiedi S, Maali A, et al. Various signaling pathways in multiple myeloma cells and effects of treatment on these pathways. Clin Lymphome Leuk. 2018; 18(5): 311-320.
27. Kaufmann KB, Buning H, Galy A, Schambach A, Grez M. Gene therapy on the move. EMBO Mol Med. 2013; 5(11): 1642-1661.
28. Hacein-Bey-Abina S, Von Kalle C, Schmidt M, McCormack MP, Wulffraat N, Leboulch P, et al. LMO2-associated clonal T cell proliferation in two patients after gene therapy for SCID-X1. Science. 2003; 302(5644): 415-419.
29. Fischer A, Notarangelo LD, Neven B, Cavazzana M, Puck JM. Severe combined immunodeficiencies and related disorders. Nat Rev Dis Primers. 2015; 1: 15061.
30. Mortellaro A, Hernandez RJ, Guerrini MM, Carlucci F, Tabucchi A, Ponzoni M, et al. Ex vivo gene therapy with lentiviral vectors rescues adenosine deaminase (ADA)-deficient mice and corrects their immune and metabolic defects. Blood. 2006; 108(9): 2979-2988.
31. Pike-Overzet K, Rodijk M, Ng YY, Baert MR, Lagresle-Peyrou C, Schambach A, et al. Correction of murine Rag1 deficiency by self-inactivating lentiviral vector-mediated gene transfer. Leukemia. 2011; 25(9): 1471-1483.
32. Duinsbergen D, Salvatori D, Eriksson M, Mikkers H. Tumors originating from induced pluripotent stem cells and methods for their prevention. Ann N Y Acad Sci. 2009; 1176: 197-204.
33. Shi Y, Do JT, Desponts C, Hahm HS, Schöler HR, Ding S. A combined chemical and genetic approach for the generation of induced pluripotent stem cells. Cell Stem Cell. 2008; 2(6): 525-528.
34. Takebe T, Zhang RR, Koike H, Kimura M, Yoshizawa E, Enomura M, et al. Generation of a vascularized and functional human liver from an iPSC-derived organ bud transplant. Nat Protoc. 2014; 9(2): 396-409.
35. Puck JM, Pepper AE, Henthorn PS, Candotti F, Isakov J, Whitwam T, et al. Mutation analysis of IL2RG in human X-linked severe combined immunodeficiency. Blood. 1997; 89(6): 1968-1977.
36. Koo GC, Tan SY, Tang T, Poon SL, Allen GE, Tan L, et al. Janus kinase 3-activating mutations identified in natural killer/T-cell Lymphoma. Cancer Discov. 2012; 2(7): 591-597.
37. Ghorban K, Shanaki M, Mobarra N, Azad M, Asadi J, Pakzad R, et al. Apolipoproteins A1, B, and other prognostic biochemical cardiovascular risk factors in patients with beta-thalassemia major. Hematology. 2016; 21(2):113-120.
38. Li L, Moshous D, Zhou Y, Wang J, Xie G, Salido E, et al. A founder mutation in Artemis, an SNM1-like protein, causes SCID in Athabascan-speaking Native Americans. J Immunol. 2002; 168(12): 6323-6329.
39. Arredondo-Vega FX, Santisteban I, Daniels S, Toutain S, Hershfield MS. Adenosine deaminase deficiency: genotype-phenotype correlations based on expressed activity of 29 mutant alleles. Am J Hum Genet. 1998; 63(4): 1049-1059.
40. Hotta A, Yamanaka S. From genomics to gene therapy: induced pluripotent stem cells meet genome editing. Annu Rev Genet. 2015; 49: 47-70.
41. Mussolino C, Cathomen T. RNA guides genome engineering. Nat Biotechnol. 2013; 31(3): 208-209.
42. Segal DJ, Meckler JF. Genome engineering at the dawn of the golden age. Annu Rev Genomics Hum Genet. 2013; 14: 135-158.
43. Samavarchi Tehrani S, Mahmoodzadeh Hosseini H, Yousefi T, Abolghasemi M, Qujeq D, Maniati M, et al. The crosstalk between trace elements with DNA damage response, repair, and oxidative stress in cancer. J Cell Biochem. 2019; 120(2): 1080.
44. Daniel MG, Pereira CF, Lemischka IR, Moore KA. Making a hematopoietic stem cell. Trends Cell Biol. 2016; 26(3): 202-214.
45. Zou J, Mali P, Huang X, Dowey SN, Cheng L. Site-specific gene correction of a point mutation in human iPS cells derived from an adult patient with sickle cell disease. Blood. 2011; 118(17): 4599-4608.
46. Chang CW, Lai YS, Westin E, Khodadadi-Jamayran A, Pawlik KM, Lamb LS Jr, et al. Modeling human severe combined immunodeficiency and correction by CRISPR/Cas9-enhanced gene targeting. Cell Rep. 2015; 12(10): 1668-1677.
47. Menon T, Firth AL, Scripture-Adams DD, Galic Z, Qualls SJ, Gilmore WB, et al. Lymphoid regeneration from gene-corrected SCID-X1 subject-derived iPSCs. Cell Stem Cell. 2015; 16(4): 367-372.
48. Lei F , Haque R, Weiler L, Vrana KE, Song J. T lineage differentiation from induced pluripotent stem cells. Cell Immunol. 2009; 260(1): 1-5.
49. Howden SE, Maufort JP, Duffin BM, Elefanty AG, Stanley EG, Thomson JA. Simultaneous reprogramming and gene correction of patient fibroblasts. Stem Cell Reports. 2015; 5(6): 1109-1118.
50. Li LB, Ma C, Awong G, Kennedy M, Gornalusse G, Keller G, et al. Silent IL2RG gene editing in human pluripotent stem cells. Mol Ther. 2016; 24(3): 582-591.
51. Brauer PM , Pessach IM, Clarke E, Rowe JH, Ott de Bruin L, Lee YN, et al. Modeling altered T-cell development with induced pluripotent stem cells from patients with RAG1-dependent immune deficiencies. Blood. 2016; 128(6): 783-793.

52. Onos KD, Sukoff Rizzo SJ, Howell GR, Sasner M. Toward more predictive genetic mouse models of Alzheimer's disease. Brain Res Bull. 2016; 122: 1-11.
53. Shi Y , Inoue H, Wu JC, Yamanaka S. Induced pluripotent stem cell technology: a decade of progress. Nat Rev Drug Discov. 2017; 16(2): 115-130.
54. Shimada H, Lu Q, Insinna-Kettenhofen C, Nagashima K, English MA, Semler EM, et al. In vitro modeling using ciliopathy-patient-derived cells reveals distinct cilia dysfunctions caused by CEP290 mutations. Cell Rep. 2017; 20(2): 384-396.
55. Holmqvist S , Lehtonen S, Chumarina M, Puttonen KA, Azevedo C, Lebedeva O, et al. Creation of a library of induced pluripotent stem cells from parkinsonian patients. NPJ Parkinsons Dis. 2016; 2: 16009.
56. Gandre-Babbe S, Paluru P, Aribeana C, Chou ST, Bresolin S, Lu L, et al. Patient-derived induced pluripotent stem cells recapitulate hematopoietic abnormalities of juvenile myelomonocytic leukemia. Blood. 2013; 121(24): 4925-4929.
57. Park IH, Arora N, Huo H, Maherali N, Ahfeldt T, Shimamura A, et al. Disease-specific induced pluripotent stem cells. Cell. 2008; 134(5): 877-886.
58. Kamata M, Liu S, Liang M, Nagaoka Y, Chen IS. Generation of human induced pluripotent stem cells bearing an anti-HIV transgene by a lentiviral vector carrying an internal murine leukemia virus promoter. Hum Gene Ther. 2010; 21(11): 1555-1567.
59. Kambal A, Mitchell G, Cary W, Gruenloh W, Jung Y, Kalomoiris S, et al. Generation of HIV-1 resistant and functional macrophages from hematopoietic stem cell-derived induced pluripotent stem cells. Mol Ther. 2011; 19(3): 584-593.
60. Yao Y, Nashun B, Zhou T, Qin L, Qin L, Zhao S, et al. Generation of CD34+ cells from CCR5-disrupted human embryonic and induced pluripotent stem cells. Hum Gene Ther. 2012; 23(2): 238-2342.
61. Kang H, Minder P, Park MA, Mesquitta WT, Torbett BE, Slukvin II. CCR5 disruption in induced pluripotent stem cells using CRISPR/Cas9 provides selective resistance of immune cells to CCR5-tropic HIV-1 virus. Mol Ther Nucleic Acids. 2015; 4: e268.
62. Mukherjee S, Santilili G, Blundell MP, Navarro S, Bueren JA, Thrasher AJ. Generation of functional neutrophils from a mouse model of X-linked chronic granulomatous disorder using induced pluripotent stem cells. PLoS One. 2011; 6(3): e17565.
63. Zou J, Sweeney CL, Chou BK, Choi U, Pan J, Wang H, et al. Oxidase-deficient neutrophils from X-linked chronic granulomatous disease iPS cells: functional correction by zinc finger nuclease-mediated safe harbor targeting. Blood. 2011; 117(21): 5561-5572.
64. Jiang Y, Cowley S, Siler U, Melguizo D, Tilgner K, Browne C, et al. Derivation and functional analysis of patient-specific induced pluripotent stem cells as an in vitro model of chronic granulomatous disease. Stem Cells. 2012; 30(4): 599-611.
65. Brault J, Goutagny E, Telugu N, Shao K, Baquié M, Satre V, et al. Optimized generation of functional neutrophils and macrophages from patient-specific induced pluripotent stem cells: ex vivo models of X(0)-Linked, AR22(0)- and AR47(0)- chronic granulomatous diseases. Biores Open Access. 2014; 3(6): 311-326.
66. Laugsch M, Rosovskaya M, Velychko S, Richter C, Zimmer A, Klink B, et al. Functional restoration of gp91phox-oxidase activity by BAC transgenesis and gene targeting in X-linked chronic granulomatous disease iPSCs. Mol Ther. 2016; 24(4): 812-822.
67. Brault J, Vaganay G, Le Roy A, Lenormand JL, Cortes S, Stasia MJ. Therapeutic effects of proteoliposomes on X-linked chronic granulomatous disease: proof of concept using macrophages differentiated from patient-specific induced pluripotent stem cells. Int J Nanomedicine. 2017; 12 : 2161-2177.
68. Ingrungruanglert P, Amarinthnukrowh P, Rungsiwiwut R, Maneesri-le Grand S, Sosothikul D, Suphapeetiporn K1, et al. Wiskott-Aldrich syndrome iPS cells produce megakaryocytes with defects in cytoskeletal rearrangement and proplatelet formation. Thromb Haemost. 2015; 113(4): 792-805.
69. Laskowski TJ, Van CY, Pourebrahim R, Ma C, Ni Z, Garate Z, et al. Gene correction of iPSCs from a Wiskott-Aldrich syndrome patient normalizes the lymphoid developmental and functionanal defects. Stem Cell Reports. 2016; 7(2): 139-148.
70. Li FY, Chaigne-Delalande B, Kanellopoulou C, Davis JC, Matthews HF, Douek DC, et al. Second messenger role for Mg2+ revealed by human T-cell immunodeficiency. Nature. 2011; 475(7357): 471-476.

Original Article

Intralesional Injection of Mouse Mesenchymal Stem Cells Reduces IL-10 Production and Parasite Burden in *L. major* Infected BALB/c Mice

Elham Zanganeh, M.Sc., Sara Soudi, Ph.D.*, Ahmad Zavaran Hosseini, Ph.D.

Department of Immunology, Faculty of Medical Sciences, Tarbiat Modares University, Tehran, Iran

Corresponding Address: P.O.Box: 14115-331, Department of Immunology, Faculty of Medical Sciences, Tarbiat Modares University, Tehran, Iran
Email: soudi@modares.ac.ir

Received: 26/March/2019, Accepted: 04/September/2019

Abstract

Objective: Leishmaniasis is of public health problems, especially in endemic areas. The activation of macrophages, as the main host of leishmania and promotion of the TH1 immune responses, are the main goal of im-munotherapy methods. Recently, the immunomodulatory role of mesenchymal stem cells (MSCs) in infectious disease has been considered. Different *in vitro* studies demonstrated the immunostimulatory effect of MSCs on macrophages in response to *L.major*. In this study, the effect of MSCs on cutaneous leishmaniasis in BALB/c mice was assessed.

Materials and Methods: To do this experimental research, BALB/c mice infected with *L. major* that was followed by multiple subcutaneous injections of MSCs at infection site at different intervals. Footpad thickness, spleen parasite burden, lymph node, and spleen cytokine production were measured to determine the efficacy of cell therapy.

Results: Significant ($P<0.05$) reduction in footpad thickness and delayed wound formation was observed in MSCs treated group. The spleen of the MSCs-treated group indicated a two-fold reduction in parasite burden compared with non-treated infected mice. In addition, nitric oxide (NO), interleukin-10 (IL-10), and tumor necrosis factor-alpha (TNF-α) production of lymph node isolated cells and splenocytes changed to the benefit of macrophage activation in response to *L. major* in MSCs treated group. A two-fold increase in interferon-gamma (IFN-γ) production in the lymph node was determined in the MSCs-treated group.

Conclusion: Although MSCs therapy could not clear the parasite, the results confirm the ability of MSCs to enhance immune responses against leishmania by induction of inflammatory responses and slowing down the spread of parasites. However, further studies needed to improve the efficacy of this method and provide a therapeutic protocol.

Keywords: *Leishmania major*, Macrophage, Mesenchymal Stem Cell

Cell Journal(Yakhteh), Vol 22, Suppl 1, Autumn 2020, Pages: 11-18

Citation: Zanganeh E, Soudi S, Zavaran Hosseini A. Intralesional injection of mouse mesen-chymal stem cells reduces IL-10 production and parasite burden in L. major infected BALB/c mice. Cell J. 22 Suppl 1: 11-18. doi: 10.22074/cellj.2020.6838.

Introduction

Leishmaniasis is among uncontrolled parasitic diseases, which manifests a wide variety of clinical symptoms that may lead to death. These clinical manifestations depend on Leishmania species and the host immune system (1). Cutaneous leishmaniasis is caused by Leishmania major (*L. major*) and afflicts 0.7-1.2 million cases in the world annually. Cutaneous leismaniasis has clinical manifestation from self-limiting to chronic signs in hosts, such as humans and mice (2). Due to the extracellular matrix interfaces, immediately after entering the parasite, pathogen identification, nitric oxide (NO), and hydrogen peroxide production by phagocytes is suppressed (3). In resistant mice, (C57BL/6) immune response is oriented to Th1, associated with the production of interferon-gamma (IFN-γ) and interleukin-12 (IL-12) at the site of infection, which inhibite parasite development. Susceptible mice (BALB/c) extend Th2 immune response associated with IL-4 production that terminated to systemic dissemination of the parasite (4).

Different approaches have been made for leishmaniasis treatment. The use of antibiotics, such as pentavalent antimonials, Amphotericin B, and other drugs, are among these therapeutic approaches. Because of their side effects, toxicity, cost, long term of treatment, and incomplete elimination of parasite, none of them is an ideal medicine (5). Different vaccine generations have been developed based on the killed parasite, live-attenuated parasites, and DNA vaccine; however, they failed to be used in human vaccination because of their limitations, such as lesion development or long-lasting recovery (6, 7). Immunotherapy by cytokines like IFN-γ for humans and the use of monoclonal antibodies for mice are other approaches (8, 9). Nowadays, cell therapy is a modern method to treat a broad range of infectious diseases. Some studies have shown that dendritic cells and macrophages can be used to treat leishmaniasis (7, 10).

Mesenchymal stem cells (MSCs) with self-renewal property and differentiation potential to multiple cell lineage are used for repairing tissues and rebuilding damaged organs (11, 12). They have some receptors that enable them to sense inflammatory conditions and switch inflammatory responses by secretion of soluble factors and interaction with immune cells

(13, 14). In 2010, pro-inflammatory MSCs1 and anti-inflammatory MSCs2 were identified, that can emerge as immune stimulator cells or immune suppressor cells, respectively, depending on cytokine milieu (15). MSCs migrate to the inflammation site and induce angiogenesis and extracellular matrix remodeling by the direction of MQ-M2 responses that terminated to repair damaged tissues (16). MSCs secrete antimicrobial peptides that enable them to fight against sepsis, acute respiratory distress syndrome, and cystic fibrosis-related infections (17). So, MSCs are good candidates for infectious disease therapy, including Tuberculosis, Malaria, sepsis, human immunodeficiency virus (HIV), and *Trypanosoma cruzi* (18). Although the previous report rejects the effectiveness of MSCs in the treatment of leishmaniasis, our previous findings indicate that MSCs can interact with macrophages and enhance their immune response by increasing the tumor necrosis factor-alpha (TNF-α)/IL-10 ratio against *L. major* (19-21).

In the present study, the effect of the repeated local injection of MSCs was investigated on the induction of TH1/TH2 immune responses against *L. major* and parasite dissemination. For this purpose, *L. major* in their footpad injected BALB/c mice and then received adipose-derived mesenchymal stem cells (AD-MSCs) subcutaneously. Footpad swelling was monitored weekly, and *L. major* dissemination was determined by parasite burden analysis. In addition, splenocytes and lymph node cells were assessed for cytokine and NO production.

Materials and Methods

Animals

Six-to-eight weeks old female BALB/c mice were obtained from the Pasture Institute, Tehran, Iran. The mice were used for three purposes: *L. major* proliferation, AD-MSCs isolation and as experimental groups. The Ethics Committee of Tarbiat Modares University approved the projects with an ethical code IR.TMU.REC.1394.180.

L. major culture and Leishmania antigen preparation

L. major promastigotes (MRHO/IR/75/ER strain) were isolated from the lymph node of the parasite reservoir BALB/c mice. Infected organs were transferred to the liquid phase of the Novy-MaccNeal-Nicolle medium. The released promastigotes were proliferated at 26˚C in RPMI (Biowest, France) medium containing 5% fetal bovine serum (FBS, Gibco, USA). The stationary phase promastigotes were used to infect the mice.

In order to prepare soluble leishmania antigen (SLA), 10^9 parasites/ml were undergone eight cycles of freezing and thawing. SLA containing supernatant was collected after centrifugation of this suspension at 8000 g for 15 minutes at 4˚C and stored at -70˚C. Soluble antigen protein was measured by Bradford assay.

Isolation of adipose-derived mesenchymal stem cells

Abdominal adipose tissues of BALB/c mice were removed aseptically. Adipose tissues were minced and digested with 0.075% type I collagenase in Dulbecco's modified Eagle's medium (DMEM, Gibco, USA) for 15-20 minutes at 37˚C. After centrifugation at 500 g for 5 minutes, the pellets were resuspended and cultured in DMEM supplemented with 10% FBS, 2 mM L-glutamine supplementary, and 1% Pen/Strep (Gibco, USA). The cells incubated in humified air containing 5% CO_2 at 37˚C. Expanded adipose-derived MSCs (AD-MSCs) used for injection into mice and characterization.

Characterization of adipose-derived mesenchymal stem cells

The cell surface markers of AD-MSCs at passage 3 were analyzed by Flowcytometry using monoclonal antibodies against mice CD45, CD34, CD90, CD105, CD73, and CD29 (all of them were purchased from eBioscience, USA). The cell surface markers were analyzed by the FACScalibur flowcytometer (BD Biosciences, USA) and Cyflogics software (CyFlo Ltd., Finland). The ability of AD-MSCs to differentiate into adipocyte and osteocyte was examined by Oil Red O (ORO) and Alizarin Red (AR), respectively. Adipogenic differentiation was induced by culturing AD-MSCs in a cell differentiation medium containing 10% FBS, 250 nM dexamethasone (Sigma-Aldrich, USA), 5 mM insulin (Sigma-Aldrich, USA), 0.5 nM 3-isobutyl-1 methylxanthine (Sigma-Aldrich, USA) and 100 mM indomethacin (Sigma-Aldrich, USA) for 21 days. For the purpose of osteogenic differentiation, the cells were cultured in a cell differentiation medium containing 50 mg/ml ascorbic acid-2- phosphate (Sigma-Aldrich, USA), 100 nM dexamethasone (Sigma-Aldrich, USA) and 10 mM beta-glycerophosphate (Merck, UK) for 21 days.

Experimental groups and treatment protocol

The present research was based on an experimental study. Three study groups, each with 10 mice, were considered in this study. Groups I and II were infected by the footpad injection of 50 µL phosphate buffered saline (PBS, BioIdea, Iran) containing 1×10^5 stationary phase *L. major* promastigotes. Group III received only 50 µL of PBS by footpad injection and was kept as control. Group I was treated by the subcutaneous injection of 1×10^5 of AD-MSCs at the infection site. The injection was repeated four times at 7, 14, 21, and 28 days post-infection. Group II was treated with cell-free PBS at the same periods at the infection site. The infected mice were checked daily. After observing the first symptom of swelling, footpad thickness was measured weekly by a digital caliper and noted. The experimental groups and their treatment protocol are shown in Figure 1.

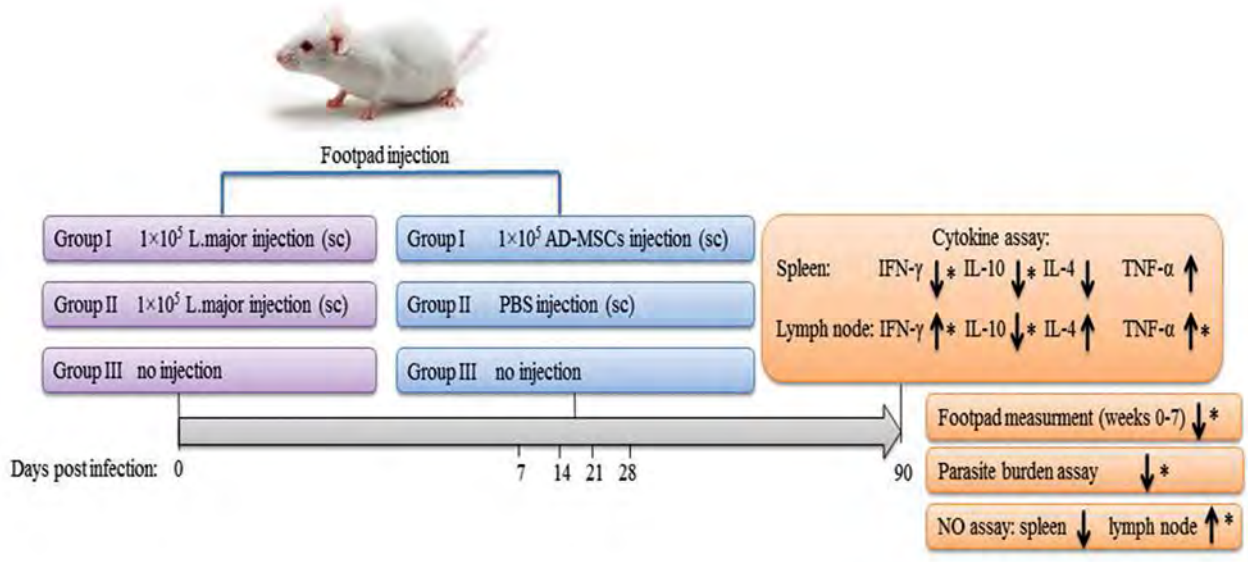

Fig.1: Depiction of experimental groups and treatment schedule.

Parasite burden

The spleens of the infected mice were excised, and the number of parasites was counted by the limiting dilution assay. Briefly, 90 days post-infection, a small fragment of the infected tissues (spleen) was weighted, homogenized in 2 mL of the Schnider's Drosophila medium (Biological Industries, USA) supplemented with 10% FBS and 0.1% Gentamicin. Serial dilution (10^{-1} to 10^{-40}) was provided and transferred into 96 well culture plates in triplicate and incubated at 26˚C for 2 weeks. The existence of parasite was observed by an inverted microscope. The last well containing at least a motile promastigote was noted as parasite dilution. Parasite burden was calculated with this formula:

Parasite burden=$-\log_{10}$ (parasite dilution/tissue weight)

Nitric oxide measurement

Splenocyte and inguinal lymph node cells of five mice from each group were harvested. After red blood cell (RBC) lysis, the cells were cultured at 2×10^{6} cell/well of 6-well plates in the RPMI medium containing 10% FBS. Each experimental group was re-stimulated in vitro with SLA (10 µg/ml) and lipopolysaccharide (LPS, 1 µg/ml) or media. After 72 hours of the stimulation, the presence of NO was measured by the Griess method. The absorbance of the developed color was read at 540 nm and converted to NO amount (µM) according to the standard curve obtained by sodium nitrite (Merck, UK) standard concentrations. All the *in vitro* treatments were performed in triplicate.

Cytokine detection by ELISA

Inguinal lymph node cells and splenocytes of mice from each group were isolated at 90 days post-infection. About 10^6 cells/well were cultured in 4-well plates in triplicate and *in vitro* stimulated with either media or 10 µg/mL of SLA or 1 µg/mL of phytohemagglutinin (PHA). 72 hours after incubation, the supernatants were collected and analyzed for the presence of IL-10, IL-4, IFN-γ, and TNF-α by the ELISA method using kits from R&D Systems (Minneapolis, MN, USA) according to the manufacturer's instructions.

Statistical analysis

All parts of this study were repeated three times as three independent experiments. Three experimental groups, each with 10 mice, were considered in this study. So, the data are shown as mean ± standard deviation (SD) of 30 mice. Data analysis was carried out according to the SPSS 13.0 (IBM, USA) software, and statistically significant differences were set at $P<0.05$.

Results

Adipose-derived mesenchymal stem cells characterization

The AD-MSCs revealed the fibroblast-like morphology and were able to differentiate into osteocytes and adipocytes are indicated in Figure 2A, B, C, respectively. As indicated in Figure 2D, AD-MSCs expressed CD45, CD34, CD90, CD105, CD73 and CD29 cell surface markers at percentages of 1.54, 1.12, 44.68, 61.55, 46.82 and 95.7%, respectively.

Footpad swelling measurement

The *L. major* infected mice were checked daily, and footpad thickness was measured until 7 weeks after the challenge. The first symptom of swelling without lesion was observed in the first-week post-infection in both infected groups. In the second-week post-infection, lesion development was observed in group II, while in the AD-MSCs recipient group, footpad swelling increased

without lesion formation. The footpad thickness of Group II significantly (P<0.05) increased from the third week to the seventh week, as in the seventh week, lesion led to footpad necrosis. A significant decrease (P<0.05) was observed in footpad thickness between the AD-MSCs treated group and non-treated group at weeks 4 to 7 post-infection. In addition, lesion formation in the AD-MSCs-treated group occurred with high latency and less severity. Group III was considered as the control without any challenge or cell treatment (Fig.3A).

Parasite burden of the spleen

The parasite burden of the spleen was measured 90 days post-infection. The result demonstrated that the injection of AD-MSCs at the infection site affected the *L. major* proliferation. As shown in Figure 3B, parasite load in group I treated with AD-MSCs, was significantly (P<0.05) less than that of the non-treated group (group II).

Nitric oxide production

NO production was measured 90 days post-infection by the Griess method. The *in vitro* LPS treatment could induce the NO production of all the study groups compared with SLA stimulation (Fig.4A). In addition, the AD-MSCs treatment (group I) did not affect the NO production of splenocytes compared with the non-treated *L. major* infected group (group II). Unlike the spleen, the NO production of the groin lymph node isolated cells was affected by the AD-MSCs injection. NO production of both the SLA and LPS stimulated groups was significantly (P<0.05) higher in the AD-MSCs treated group (P<0.05) compared with the non-treated *L. major* infected group (Fig.4B).

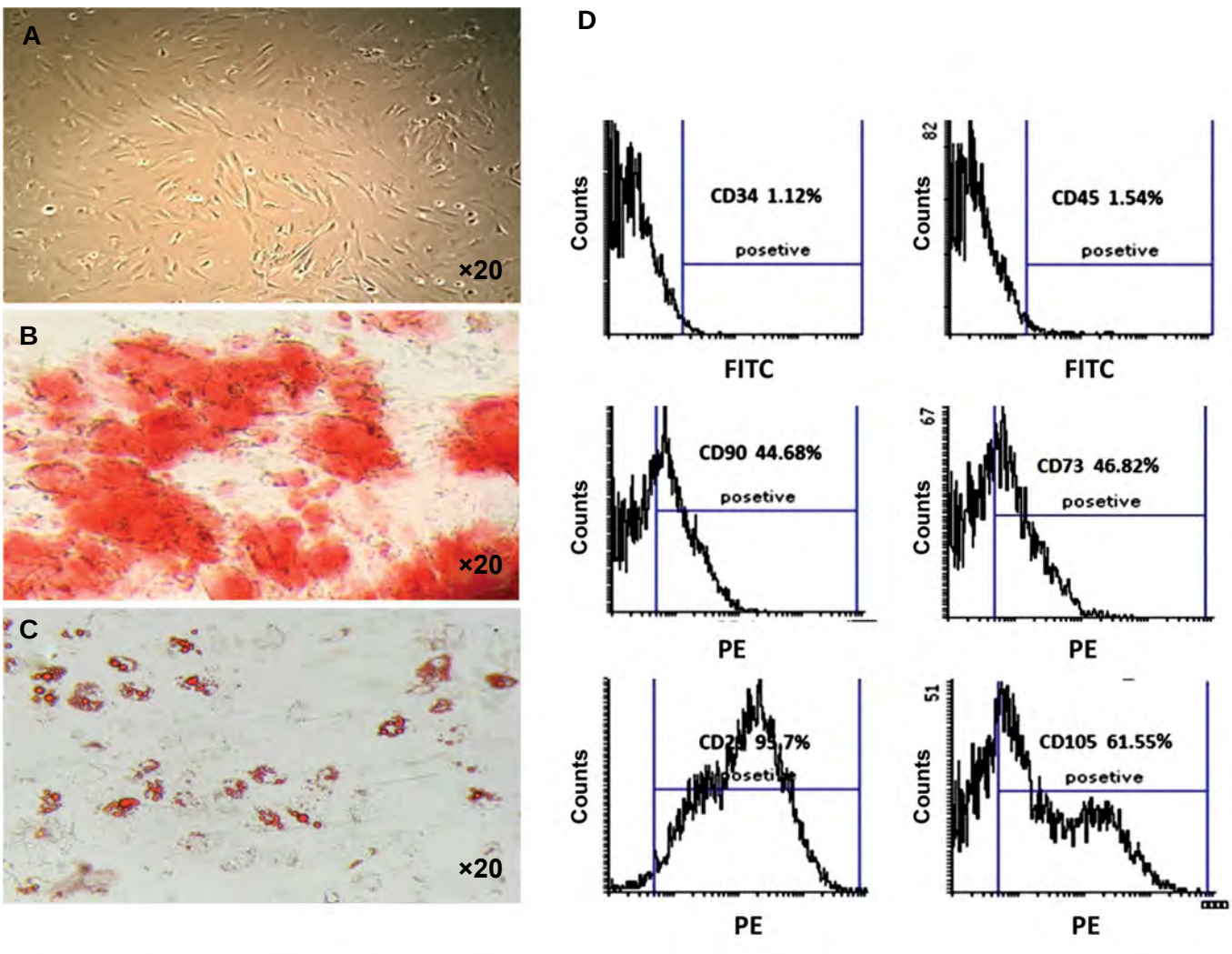

Fig.2: Characterization of adipose-derived mesenchymal stem cells (AD-MSCs). **A.** Fibroblast-like AD-MSCs were isolated from the BALB/c mice (×20). **B.** Alizarin red staining displayed calcium mineralization of AD-MSCs in osteocyte differentiation (×20) and **C.** Oil Red O staining display lipid droplets of AD-MSCs in adipocyte differentiation (×20). **D.** The mean percent of the cell surface markers of AD-MSCs analyzed by flow cytometry.

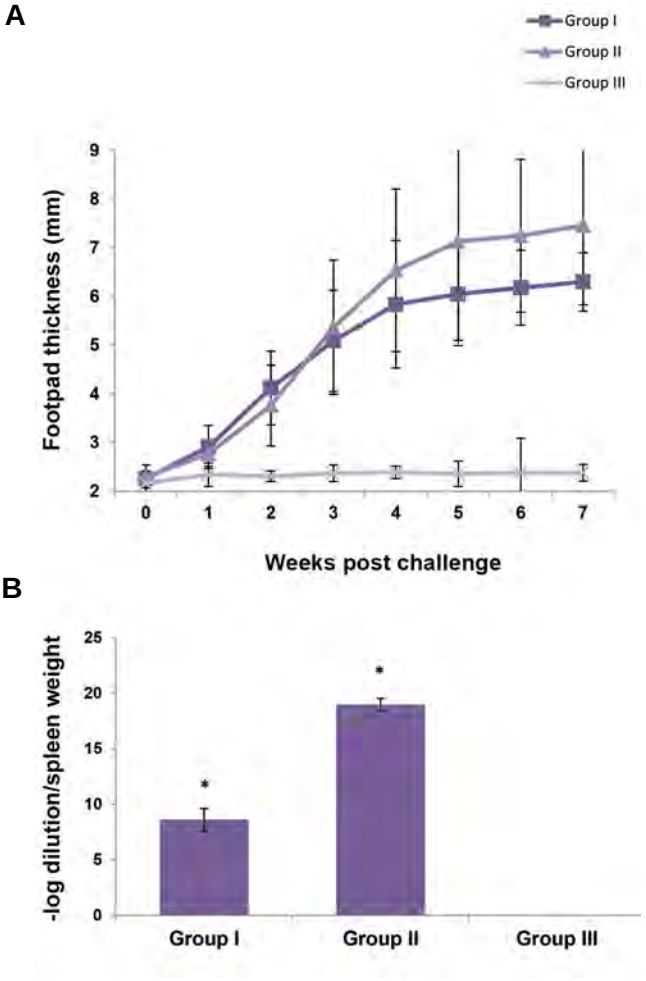

Fig.3: Evaluation of parasite proliferation and dissemination. **A.** Footpad thickness of the AD-MSCs treated group (group I), non-treated group (group II), and control group (group III). **B.** The number of parasites in the spleen counted by limiting dilution assay at 90 days post-infection. BALB/c mice were infected with 1×10^6 of *L. major* parasite by footpad injection at day 0. At days 7, 14, 21, and 28 post-infection, the first infected group (group I) was treated with 5×10^5 of AD-MSCs. The same volume of PBS (60 µL) was injected subcutaneously to the second infected group (group II). Data were reported as means ± SD of 30 mice. The P value was considered significantly at <0.05. A significant difference between the groups was determined by repeated measure analysis of varience (ANOVA) by the SPSS software.
AD-MSCs; Adipose derived mesenchymal stem cells and PBS; Phosphate buffered saline.

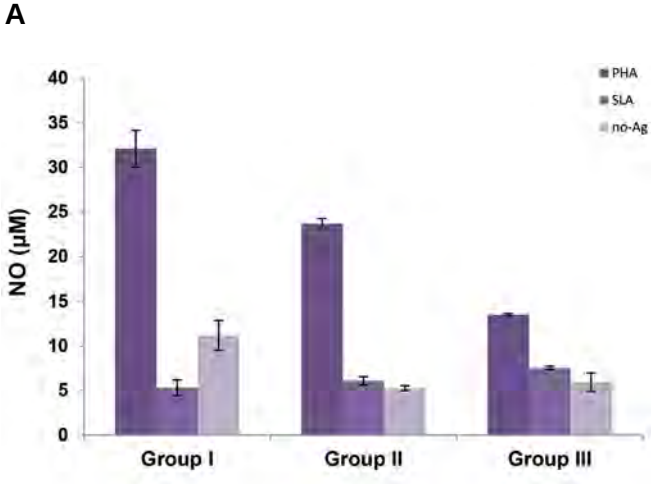

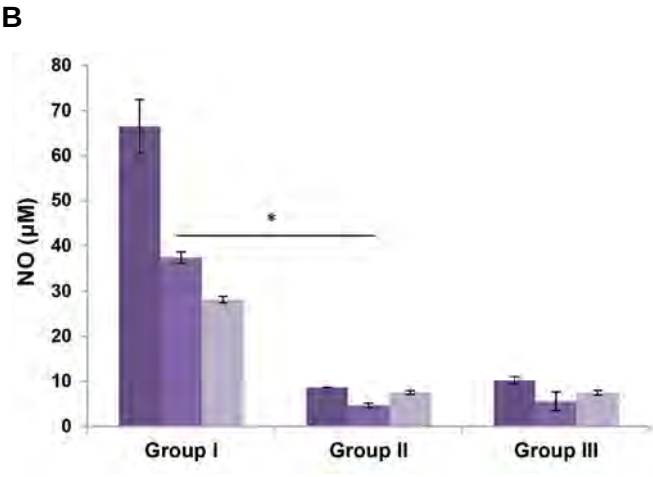

Fig.4: Nitric oxide (NO) production in the supernatant of experimental groups. **A.** Spleen and **B.** Lymph nodes isolated cells at 90 days post infection. Data were reported as means ± SD of 30 mice. The groups having significant differences are indicated by an asterisk (*) sign (P<0.05).

Splenocyte cytokine production

Splenocyte of each group was isolated and treated with media, SLA, and PHA. After 72 hours of incubation, the supernatants were collected and evaluated for IFN-γ, IL-10, IL-4, and TNF-α cytokine analysis by the ELISA method. As indicated in Figure 5A and 5C, IFN-γ, and IL-4 production increased in the *L. major* infected groups compared with the non-infected control group. However, no significant difference was observed in terms of IL-4 production between the AD-MSCs treated (group I) and non-treated (group II) groups. IL-10 and TNF-α production increased in splenocytes of the *L. major* infected groups at 90 days post-infection. According to Figure 5B, D, the AD-MSCs treatment could induce higher IL-10 and TNF-α production in response to LPS and SLA stimulation, compared with the non-treated group (group II).

Cytokine production in the lymph node

The lymph node cells of each group were isolated and then treated with media, SLA, or PHA. After 72 hours of incubation, IFN-γ, IL-10, IL-4, and TNF-α cytokine production was measured by the ELISA method. As indicated in Figure 6A and 6B, the production of IFN-γ and TNF-α was induced significantly (P<0.05) in the lymph node of the AD-MSCs-treated group compared with the non-treated infected mice. Although interleukin-10 production was more in the *L. major* infected group than in control, the increase in the AD-MSCs treated group (group I) was significantly lower than that in the non-treated group (group II) (Fig.6C). Moreover, there was no significant difference in IL-4 production of both the AD-MSCs treated and non-treated *L. major* infected groups (Fig.6D).

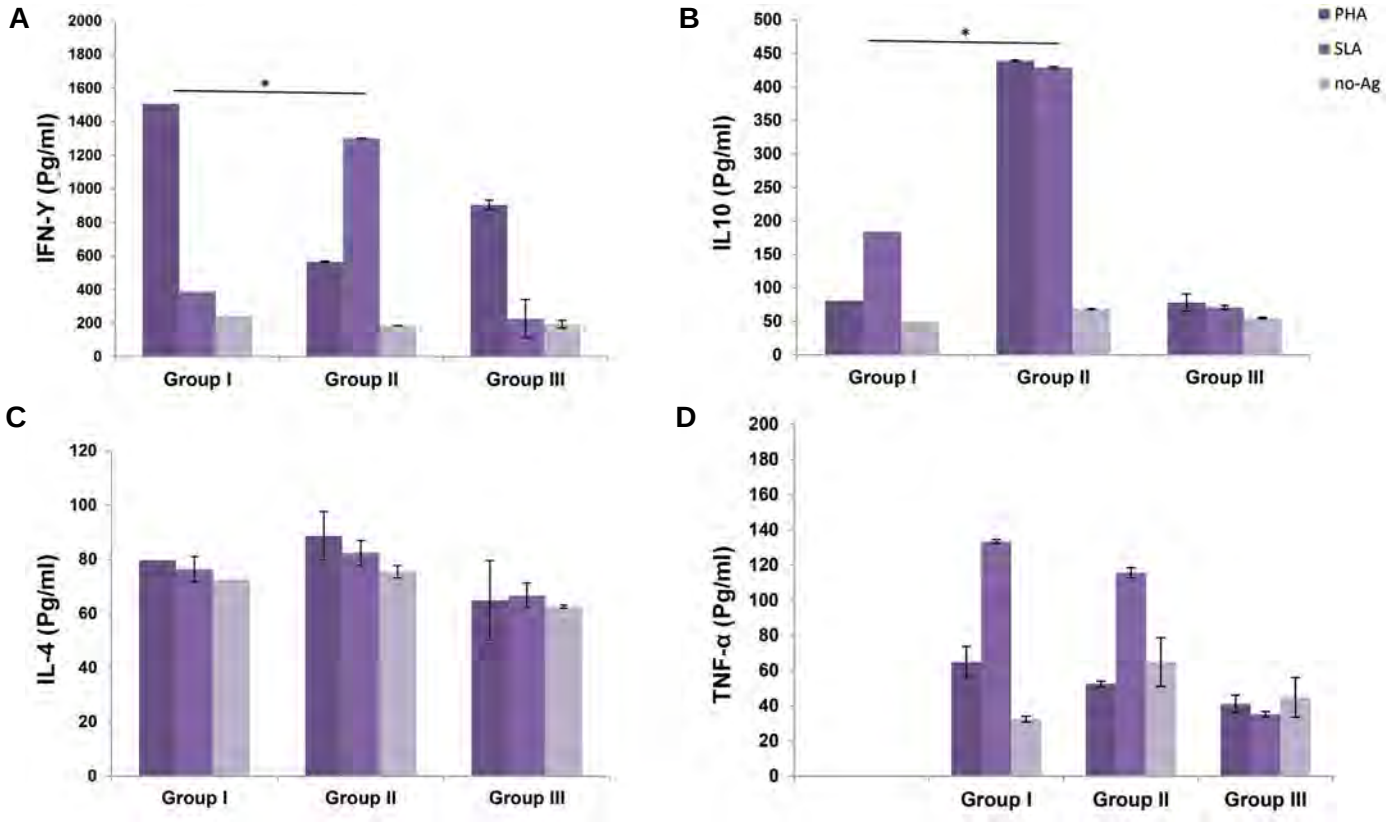

Fig.5: Cytokine assays in the supernatants of the splenocytes of different experimental groups. **A.** Interferon gamma (IFN-γ), **B.** Interleukin-10 (IL-10), **C.** IL-4, and **D.** Tumor necrosis factor-alpha (TNF-α). Data were reported as means ± SD of 30 mice. The groups having significant differences (P≤0.05) are indicated by an asterisk (*) sign.

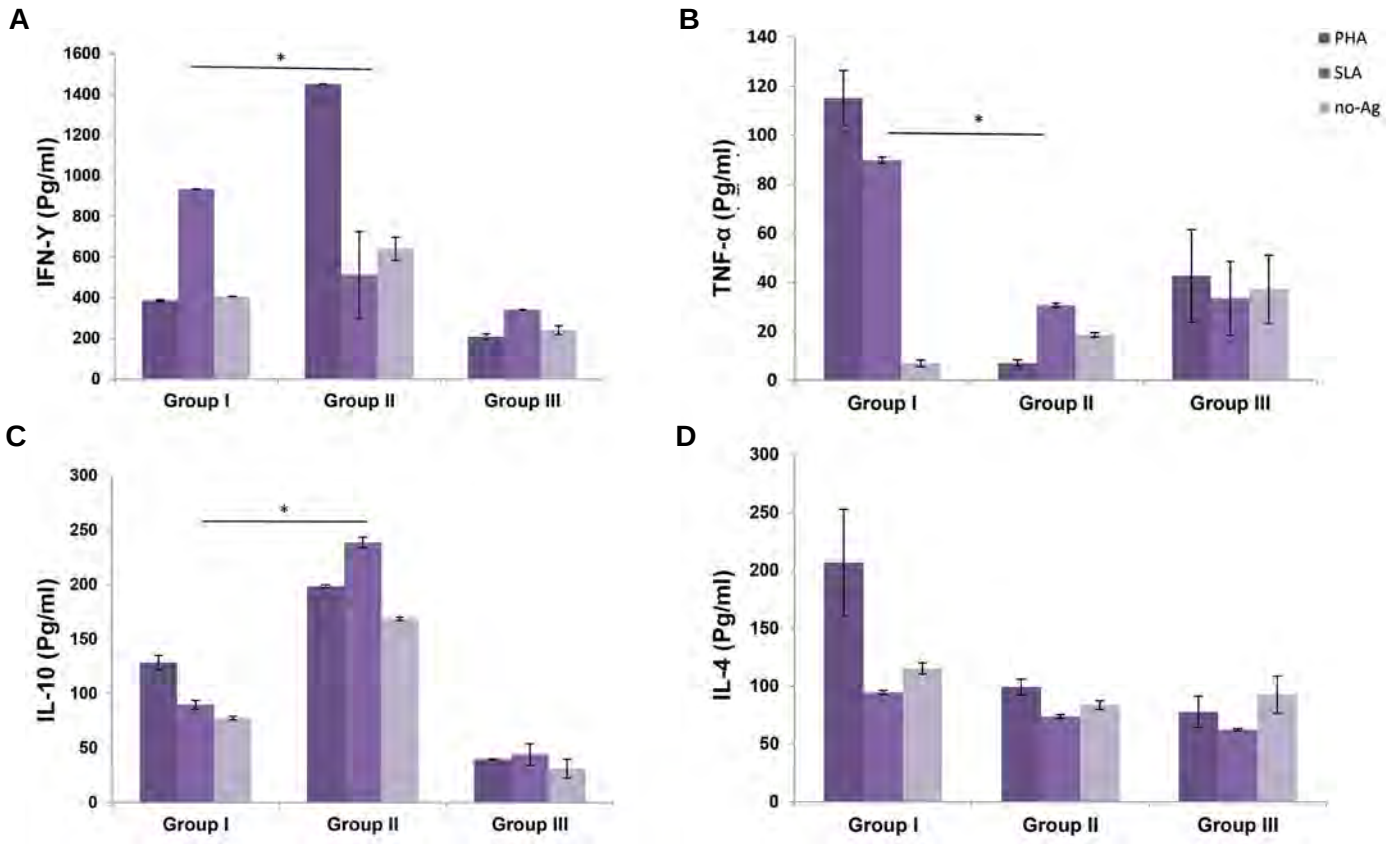

Fig.6: Cytokine assays in tha supernatants of the lymph node isolated cells at 90 days post-infection. **A.** Interferon gamma (IFN-γ), **B.** Interleukin-10 (IL-10), **C.** IL-4, and **D.** Tumor necrosis factor alpha (TNF-α). Data were reported as means ± SD of 30 mice. The groups having significant differences (P≤0.05) are indicated by an asterisk (*) sign.

Discussion

Leishmaniasis is one of the neglected parasitic diseases that is transmitted by sandflies in tropical areas (22). These intracellular pathogens spread by targeting immune cells and induction of inappropriate immune responses that terminated to loss of proper functioning of the infected organs (23). Drug toxicity and the emergence of resistance, along with the lack of approved protective vaccines, indicated the need for new therapeutic approaches (7, 24). The ability of MSCs to modulate immune responses made them as therapeutic tools of inflammatory disorders, including infectious disease (25). Different studies demonstrated the direct or indirect effect of MSCs therapy on T-cell count and differentiation in infectious disease. Allam et al. (26) showed that MSCs therapy of HIV patients induces a significant increase in naïve and memory CD4+T cells and restores their ability to produce IL-2 and IFN-γ in response to HIV antigens. In another study, Thakur et al. (27) introduced the protective role of MSCs in malaria infection by the suppression of IL10 and regulatory T-cell differentiation and induction of IL-12 production. In the current study, the potential effects of the adipose-derived MSC therapy evaluated on parasite dissemination and induction of TH1/TH2 responses in a murine model of cutaneous leishmaniasis. AD-MSCs considered in this research because the preparation of human adipose tissue is easy, non-invasive, and ethically accepted (28). In addition, adipose-derived MSCs have a more homogeneous population than those derived from bone marrow (29).

Following the footpad injection of leishmania, the immune cells migrated into the infection site, and inflammatory responses appeared, resulting in an increase in the thickness of the footpad. If the protective innate immune responses developed, the proliferation of the parasite would be limited, and the inflammatory responses would decrease. In other words, if the unprotected inflammatory responses were created, the accelerated proliferation of the parasite, ulcers, and necrosis would appear at the infection site (30). The current results demonstrated the efficacy of AD-MSCs administration for the control of lesion formation and footpad necrosis. In addition, the footpad thickness in the AD-MSCs treated group was significantly less than that the non-treated group on weeks 4 to 7 post-infection, indicating a decrease in the severity of inflammation. The lower parasite load in the spleen of mice that received AD-MSCs demonstrated the control of *L. major* proliferation at the infected site and its dessemination to other organs.

Activation of NO synthase and respiratory burst terminated to produce NO and reactive oxygen species (ROS) is among the important mechanisms that macrophages use to kill Leishmania parasites (31). Different studies indicated that the amount of NO production by macrophages and neutrophils was associated with resistance to leishmaniasis and control of parasite proliferation (32). The obtained results represented the enhanced production of NO by the lymph node isolated cells in the AD-MSCs treated group. This increase can be one of the reasons for the lower parasite burden, and slow wound formation in the footpad of the AD-MSCs treated group compared with the non-treated one. IL-10 cytokine production is one of the important indicators of failure or victory against leishmaniasis. Different studies demonstrated that an increase in IL-10 production affected the anti-leishmania activity of innate immune cells and inhibited Th1 cell development and IFN-γ production (33, 34). In addition, the persistence of IL-10 at the infected skin causes the persistence of *L. major* after clinical cure and reactivation of the disease (35). In the current study, the significant reduction in IL-10 production in both the spleen and lymph node of the AD-MSCs treated group demonstrated the efficacy of MSCs in the treatment of leishmaniasis. TNF-α is another protective cytokine, the importance of which differs depending on parasite strains (36). However, the ability of TNF-α in the induction of NO and the increased risk of animal death in the absence of TNF-α reflected its protective role (37). The ELISA study showed that the level of TNF-α production in the spleen of the infected mice was higher than that of the lymph node. The local administration of AD-MSCs can significantly increase the amount of this cytokine in the lymph node. All the experiences in the study of leishmaniasis in resistant and susceptible mice indicated a key role in inducing Th1 immune responses in controlling and treating leishmaniasis (38). In this research, the AD-MSCs treatment could induce IFN-γ production of the lymph node at the infected site through attenuation of IL-10 production. Considering that in the previous study, MSCs therapy could not have a positive role in the control of leishmaniasis, different results of the current study indicate the importance of the injection route and the frequency of injection in the success of cell therapy. Since the present study does not investigate the mechanism of MSCs' action in reducing IL-10, it is not possible to discuss it clearly. However, it seems that multiple injections of MSCs help to generate sequential waves of pro-inflammatory type I MSCs (15) that terminated to induction of TNF-α, reduction in IL-10, and control of parasite dissemination. Different studies have shown the efficacy of multiple MSCs injection in the improvement of the disease.

Conclusion

Multiple intralesional injections of MSCs can induce the formation of protective responses at the early phase of *L. major* infection. However, this positive effect was not long-lasting and ultimately led to parasite dissemination and death of susceptible infected mice. We need to find a solution that can help to maintain the effectiveness of stem cells and remove barriers in this way.

Acknowledgement

This study (Research code: 1091) had grant support from Tarbiat Modares University. The authors declare no

conflict of interest.

Author's Contributions

E.Z.; Isolated and cultured *L.major*, infected BALB/c mice, performed parasite burden, cytokine assay, measured footpad swelling, monitored animal weight, participated in data analysis, and manuscript writing. S.S.; Designed the study, isolated, cultured and characterized MSCs, treated mice by intralesional injection of MSCs, participated in data analysis and manuscript writing. A.ZH.; Participated in study design and scientific edition of the manuscript. All authors read and approved the final manuscript.

References

1. Torres-Guerrero E, Quintanilla-Cedillo MR, Ruiz-Esmenjaud J, Arenas R. Leishmaniasis: a review. F1000Res. 2017; 6: 750.
2. Okwor I, Uzonna J. Social and economic burden of human leishmaniasis. Am J Trop Med Hyg. 2016; 94(3): 489-493.
3. De Menezes JP, Saraiva EM, da Rocha-Azevedo B. The site of the bite: Leishmania interaction with macrophages, neutrophils and the extracellular matrix in the dermis. Parasit Vectors. 2016; 9: 264.
4. Loeuillet C, Bañuls AL, Hide M. Study of Leishmania pathogenesis in mice: Experimental considerations. Parasit Vectors. 2016; 9: 144.
5. de Menezes JP, Guedes CE, Petersen AL, Fraga DB, Veras PS. Advances in development of new treatment for leishmaniasis. Biomed Res Int. 2015; 2015: 815023.
6. Srivastava S, Shankar P, Mishra J, Singh S. Possibilities and challenges for developing a successful vaccine for leishmaniasis. Parasit Vectors. 2016; 9(1): 277.
7. Whyte DC, Zufferey R. Cutaneous leishmaniasis: update on vaccine development. Hum Parasit Dis (Auckl). 2017; 9.
8. Roatt BM, Aguiar-Soares RD, Coura-Vital W, Ker HG, Moreira Nd, Vitoriano-Souza J, et al. Immunotherapy and immunochemotherapy in visceral leishmaniasis: promising treatments for this neglected disease. Front Immunol. 2014; 5: 272.
9. Singh OP, Sundar S. Immunotherapy and targeted therapies in treatment of visceral leishmaniasis: Current status and future prospects. Front Immunol. 2014; 5: 296.
10. Manna PP, Hira SK, Basu A, Bandyopadhyay S. Cellular therapy by allogeneic macrophages against visceral leishmaniasis: role of TNF-α. Cell Immunol. 2014; 290(1): 152-163.
11. Dostert G, Mesure B, Menu P, Velot É. How Do Mesenchymal Stem Cells Influence or Are Influenced by Microenvironment through Extracellular Vesicles Communication? Front Cell Dev Biol. 2017; 5: 6.
12. Gao F, Chiu SM, Motan DA, Zhang Z, Chen L, Ji HL, et al. Mesenchymal stem cells and immunomodulation: current status and future prospects. Cell Death Dis. 2016; 7: e2062.
13. Castro-Manrreza ME, Montesinos JJ. Immunoregulation by mesenchymal stem cells: biological aspects and clinical applications. J Immunol Res. 2015; 2015: 394917.
14. Bernardo ME, Fibbe WE. Mesenchymal stromal cells: sensors and switchers of inflammation. Cell Stem Cell. 2013; 13(4): 392-402.
15. Wang Y, Chen X, Cao W, Shi Y. Plasticity of mesenchymal stem cells in immunomodulation: pathological and therapeutic implications. Nat Immunol. 2014; 15(11): 1009-1016.
16. Lee DE, Ayoub N, Agrawal DK. Mesenchymal stem cells and cutaneous wound healing: Novel methods to increase cell delivery and therapeutic efficacy. Stem Cell Res Ther. 2016; 7: 37.
17. Sung DK, Chang YS, Sung SI, Yoo HS, Ahn SY, Park WS. Antibacterial effect of mesenchymal stem cells against Escherichia coli is mediated by secretion of beta- defensin- 2 via toll- like receptor 4 signalling. Cell Microbiol. 2016; 18(3): 424-436.
18. Bhattacharya D, Dwivedi VP, Mona, Yadav V, Das G. Understanding the role of mesenchymal stem cells in infectious diseases : focus on tuberculosis , malaria , sepsis and HIV. Electron J Biol. 2016; 12(3): 247-253.
19. Pereira JC, Ramos TD, Silva JD, de Mello MF, Pratti JES, da Fonseca-Martins AM, et al. Effects of bone marrow mesenchymal stromal cell therapy in experimental cutaneous leishmaniasis in BALB/c mice induced by leishmania amazonensis. Front Immunol. 2017; 8: 893.
20. Khosrowpour Z, Hashemi SM, Mohammadi-Yeganeh S, Soudi S. Pretreatment of mesenchymal stem cells with leishmania major soluble antigens induce anti-inflammatory properties in mouse peritoneal macrophages. J Cell Biochem. 2017; 118(9): 2764-2779.
21. Dameshghi S, Zavaran-Hosseini A, Soudi S, Shirazi FJ, Nojehdehi S, Hashemi SM. Mesenchymal stem cells alter macrophage immune responses to Leishmania major infection in both susceptible and resistance mice. Immunol Lett. 2016; 170: 15-26.
22. Scorza BM, Carvalho EM, Wilson ME. Cutaneous manifestations of human and murine leishmaniasis. Int J Mol Sci. 2017; 18(6). pii: E1296.
23. Alemayehu B, Alemayehu M. Leishmaniasis: a review on parasite, vector and reservoir host. Heal Sci J. 2017; 11(4): 1-6.
24. Kumar R, Engwerda C. Vaccines to prevent leishmaniasis. Clin Transl Immunology. 2014; 3(3): e13.
25. Parekkadan B, Milwid JM. Mesenchymal stem cells as therapeutics. Annu Rev Biomed Eng. 2010; 12: 87-117.
26. Allam O, Samarani S, Ahmad A. Mesenchymal stem cell therapy in HIV-infected HAART-treated nonimmune responders restores immune competence. AIDS. 2013; 27(8): 1349-1352.
27. Thakur RS, Tousif S, Awasthi V, Sanyal A, Atul PK, Punia P, et al. Mesenchymal stem cells play an important role in host protective immune responses against malaria by modulating regulatory T cells. Eur J Immunol. 2013; 43(8): 2070-2077.
28. Kim JH, Jo CH, Kim HR, Hwang YI.Comparison of Immunological characteristics of mesenchymal stem cells from the periodontal ligament, umbilical cord, and adipose tissue. Stem Cells Int. 2018; 2018: 8429042.
29. Ahmadbeigi N, Soleimani M, Gheisari Y, Vasei M, Amanpour S, Bagherizadeh I, et al. Dormant phase and multinuclear cells: two key phenomena in early culture of murine bone marrow mesenchymal stem cells. Stem Cells Dev. 2011; 20(8): 1337-1347.
30. 30. Maspi N, Abdoli A, Ghaffarifar F. Pro- and anti-inflammatory cytokines in cutaneous leishmaniasis: a review. Pathog Glob Health. 2016; 110(6): 247-260.
31. Horta MF, Mendes BP, Roma EH, Noronha FS, Macêdo JP, Oliveira LS, et al. Reactive oxygen species and nitric oxide in cutaneous leishmaniasis. J Parasitol Res. 2012; 2012: 203818.
32. Charmoy M, Megnekou R, Allenbach C, Zweifel C, Perez C, Monnat K, et al. Leishmania major induces distinct neutrophil phenotypes in mice that are resistant or susceptible to infection. J Leukoc Biol. 2007; 82(2): 288-299.
33. Girard-Madoux MJH, Kautz-Neu K, Lorenz B, Ober-Blobaum JL, von Stebut E, Clausen BE. IL-10 signaling in dendritic cells attenuates anti-Leishmania major immunity without affecting protective memory responses. J Invest Dermatol. 2015; 135(11): 2890-2894.
34. Chatelain R, Mauze S, Coffman RL. Experimental Leishmania major infection in mice: role of IL-10. Parasite Immunol. 1999; 21(4): 211-218.
35. Belkaid Y, Hoffmann KF, Mendez S, Kamhawi S, Udey MC, Wynn TA, et al. The role of interleukin (IL)-10 in the persistence of Leishmania major in the skin after healing and the therapeutic potential of anti-IL-10 receptor antibody for sterile cure. J Exp Med. 2001; 194(10): 1497-1506.
36. Ritter U, Mattner J, Rocha JS, Bogdan C, Korner H. The control of Leishmania (Leishmania) major by TNF in vivo is dependent on the parasite strain. Microbes Infect. 2004; 6(6): 559-565.
37. Fromm PD, Kling JC, Remke A, Bogdan C, Korner H. Fatal Leishmaniasis in the absence of TNF despite a strong Th1 response. Front Microbiol. 2015; 6: 1520.
38. Walton SF. The immunology of susceptibility and resistance to scabies. Parasite Immunol. 2010; 32(8): 532-540.

Original Article

Role of Vascular Endothelial Growth Factor and Human Umbilical Vein Endothelial Cells in Designing An *In Vitro* Vascular-Muscle Cellular Model Using Adipose-Derived Stem Cells

Abbas Heidari-Moghadam, M.Sc.[1, 2], Vahid Bayati, Ph.D.[1, 2*], Mahmoud Orazizadeh, Ph.D.[1, 2], Mohammad Rashno, Ph.D.[3]

1. Cellular and Molecular Research Center, Ahvaz Jundishapur University of Medical Sciences, Ahvaz, Iran
2. Department of Anatomical Sciences, Faculty of Medicine, Ahvaz Jundishapur University of Medical Sciences, Ahvaz, Iran
3. Department of Immunology, Faculty of Medicine, Ahvaz Jundishapur University of Medical Sciences, Ahvaz, Iran

Corresponding Address: P.O.Box: 45, Cellular and Molecular Research Center, Ahvaz Jundishapur University of Medical Sciences, Ahvaz, Iran
Email: bayati-v@ajums.ac.ir

Received: 30/June/2019, Accepted: 26/August/2019

Abstract

Objective: Researchers have been interested in the creation of a favorable cellular model for use in vascular-muscle tissue engineering. The main objective of this study is to determine the myogenic effects of vascular endothelial growth factor (VEGF) and human umbilical vein endothelial cells (HUVECs) on adipose-derived stem cells (ADSCs) to achieve an *in vitro* vascular-muscle cellular model.

Materials and Methods: The present experimental research was conducted on two primary groups, namely ADSCs monoculture and ADSCs/HUVECs co-culture that were divided into control, horse serum (HS), and HS/VEGF differentiation subgroups. HUVECs were co-cultured by ADSC in a ratio of 1:1. The myogenic differentiation was evaluated using the reverse transcription-polymerase chain reaction (RT-PCR) and immunofluorescence in different experimental groups. The interaction between ADSCs and HUVECs, as well as the role of ADSCs conditional medium, was investigated for endothelial tube formation assay.

Results: Immunofluorescence staining indicated that Tropomyosin was positive in ADSCs and ADSCs and HUVECs co-culture groups on HS and HS/VEGF culture medium. Furthermore, the *MyHC2* gene expression significantly increased in HS and HS/VEGF groups in comparison with the control group ($P<0.001$). More importantly, there was a significant difference in the mRNA expression of this gene between ADSCs and ADSCs and HUVECs co-culture groups on HS/VEGF culture medium ($P<0.05$). Current data revealed that the co-culture of ADSCs and HUVECs could develop endothelial network formation in the VEGF-loaded group. Also, the ADSCs-conditioned medium improved the viability and formation of the endothelial tube in the HS and VEGF groups, respectively.

Conclusion: It was concluded that ADSCs/HUVECs co-culture and dual effects of VEGF can lead to the formation of differentiated myoblasts in proximity to endothelial network formations. These *in vitro* cellular models could be potentially used in vascular-muscle tissue engineering implanted into organ defects where muscle tissue and vascular regeneration were required.

Keywords: Human Umbilical Vein Endothelial Cells, Mesenchymal Stem Cells, Myogenic Differentiation, Vascular Endothelial Growth Factor

Cell Journal(Yakhteh), Vol 22, Suppl 1, Autumn 2020, Pages: 19-28

Citation: **Heidari-Moghadam A, Bayati V, Orazizadeh M, Rashno M. Role of vascular endothelial growth factor and human umbilical vein endothelial cells in designing an in vitro vascular-muscle cellular model using adipose-derived stem cells. Cell J. 22 Suppl 1: 19-28. doi: 10.22074/cellj.2020.7034.**

Introduction

Skeletal muscle tissue plays a major role in body movement, keeping posture, and supporting the skeletal system that accounts for about half of human body weight (1). Due to its specific resident progenitor cells, called satellite cells, this tissue has an innate capacity to self-repair after injury (2). It should be noted that these cells have limited capacity; hence, in the case of intensive damage to muscle tissue (which destroys the basal membrane of cells), it is stem cells cannot repair the damaged area and remains as a permanent disability (3). The specific tissue damage called "Volumetric Muscle Loss" (VML) was considered to define the research pathway. VML is irreversible damage (both volumetric and contractile) of muscle tissue and can occur because of tumors, surgery, accidents, etc. (4, 5). It is found that there are insufficient treatment options of VML, and there is no proper, effective, and promising treatment for it (5). In recent years, new methods, such as regenerative medicine with its high potential for replacing and repairing tissues and organs have been promising for researchers to solve these problems (6). Designing in-vitro favorable cellular models for use in tissue engineering can improve the therapeutic choices for numerous serious health challenges, such as VML (7). Since two decades ago, the use of stem cells in research has attracted much attention. A specific stem cell called adipose-derived stem cell (ADSC) has been gradually introduced with increasing research (8, 9). These cells are ideal options in regenerative medicine because of features such as the

ease of isolation and cultivation and their control, high ability of growth and differentiation, nonaggression, and finally, the absence of ethical issues about them (9). Creating an ideal cellular composition for differentiation and forming of myofibrils along with the development of vascular and neural structures have always been complicated and challenging. The co-culture of endothelial cells with other types of cells is a new approach to construct a vascular cellular composition for use in tissue engineering (10). For instance, the co-culture of endothelial cells with fibroblasts (11), primary osteoblasts, or smooth muscle cells have been able to significantly increase vascular sprouts and structures *in vitro* (11, 12). The vascular endothelial growth factor (VEGF) is a key factor and regulator of embryonic angiogenesis. This factor has inductive effects on endothelial cells (in the creation of vascular networks) (13), neurons, hepatocytes, and myoblast in stimulating cell migration, protecting them against apoptosis, and inducing myoblasts to form muscle fibers (14, 15). Therefore, the present study was designed to determine the myogenic effects of VEGF and human umbilical vein endothelial cells (HUVECs) on ADSCs to achieve an ideal cellular model and create an *in vitro* differentiated vascular-muscle structure.

Material and Methods

Adipose-derived stem cells isolation and culture

In this experimental study, isolation of ADSCs was performed based on previous protocols (16). So, after excision, the gonadal fat tissues of Wistar rats were washed three times with phosphate-buffered saline (PBS, Invitrogen, USA), containing 1% penicillin/ streptomycin (Gibco, USA) to remove blood vessels and debris, and then cut into small pieces to facilitate enzymatic digestion. Samples were incubated with 0.1% collagenase type I at 37˚C for 30-50 minutes and then neutralized enzymatic activity by adding cell culture media Dulbecco's Modified Eagle Medium (DMEM, Invitrogen, USA), 10% fetal bovine serum (FBS, Sigma, USA) to the solution. For the separation of mature adipocytes from the remaining stromal-vascular fraction (SVF), the cellular mixture was centrifuged at 2000 rpm for 5 minutes. The supernatant was removed, and the cell plate was resuspended in 3 ml growth media containing (DMEM) supplemented with 10% FBS, 1% L-glutamine, and 1% penicillin/streptomycin. SVF cells were plated at 2.5×10^4 cells/cm^2 per 25 cm^2 cell culture flasks and incubated at 37˚C in 5% CO_2. The non-adherent cells were removed after the substitution of the cell culture medium following 48 hours. At passage 4, the surface antigens of cells, including CD44, CD73, and CD90 as positive markers and CD45 as a negative marker, were evaluated for ADSCs characterization by flow cytometry assay. To promote myogenic differentiation, determined ADSCs were cultured in DMEM containing 10% FBS and 3_M 5-Azacytidine (Sigma, NY, USA) for 24 hours and then in DMEM supplemented with 5% horse serum (HS, Gibco, NY, USA) for 7 days. Supplemented media was replaced every 48 hours.

Ethical consideration

This study was approved by the Ethics Committee of Ahvaz Jundishapur University of Medical Sciences (IR. AJUMS.REC.1396.282). All protocols, such as animal care, anesthesia, and euthanasia procedures, were performed in accordance with the guidelines of the Ethics Committee of Ahvaz Jundishapur University of Medical Sciences.

Co-culture models

HUVECs were purchased from the National Center for Genetic and Biological Resources (Tehran, Iran) and cultured in DMEM containing Ham's F12 (1:1), 20% FBS, 10 mM L-Glutamine, 2 mM Sodium Pyruvate, 2 mM nonessential amino acids, 0.5 µg/ml hydrocortisone and 50 µg/ml ascorbic acid with 5% CO_2 and 37˚C after being labeled with Cell Tracker TM CM-DiI (C7000, Sigma, NY, USA) according to its instructions.

In the present study, we designed two primary experimental groups in order to investigate the roles of endothelial cells and VEGF165 (Sigma, NY, USA) on the differentiation of ADSCs as follows:

I. ADSCs
II. ADSCs and HUVECs co-culture

Each group was then divided into 3 subgroups including:

1. Control group (C) in which cells were cultured in DMEM containing Ham's F12 (1:1), supplemented with 10% FBS, 1% L-glutamine and 1% penicillin/ streptomycin

ADSCs/DMEM
ADSCs/HUVECs/DMEM

2. Differentiation group with HS, cultured in the differentiation media (HS and *5-azacytidine*)

ADSCs/HS
ADSCs/HUVECs/HS

3. Differentiation group with HS and VEGF cultured in differentiation media (HS and *5-azacytidine*+50 ng/µl VEGF)

ADSCs/HS/VEGF
ADSCs/HUVECs/HS/VEGF

HUVECs were co-cultured with ADSC in a ratio of 1:1. Cells were treated with 50 ng/µl VEGF for VEGF *in vitro* experiments. Supplemented media was replaced every 48 hours. Figure 1 summarizes the main points of the experiment.

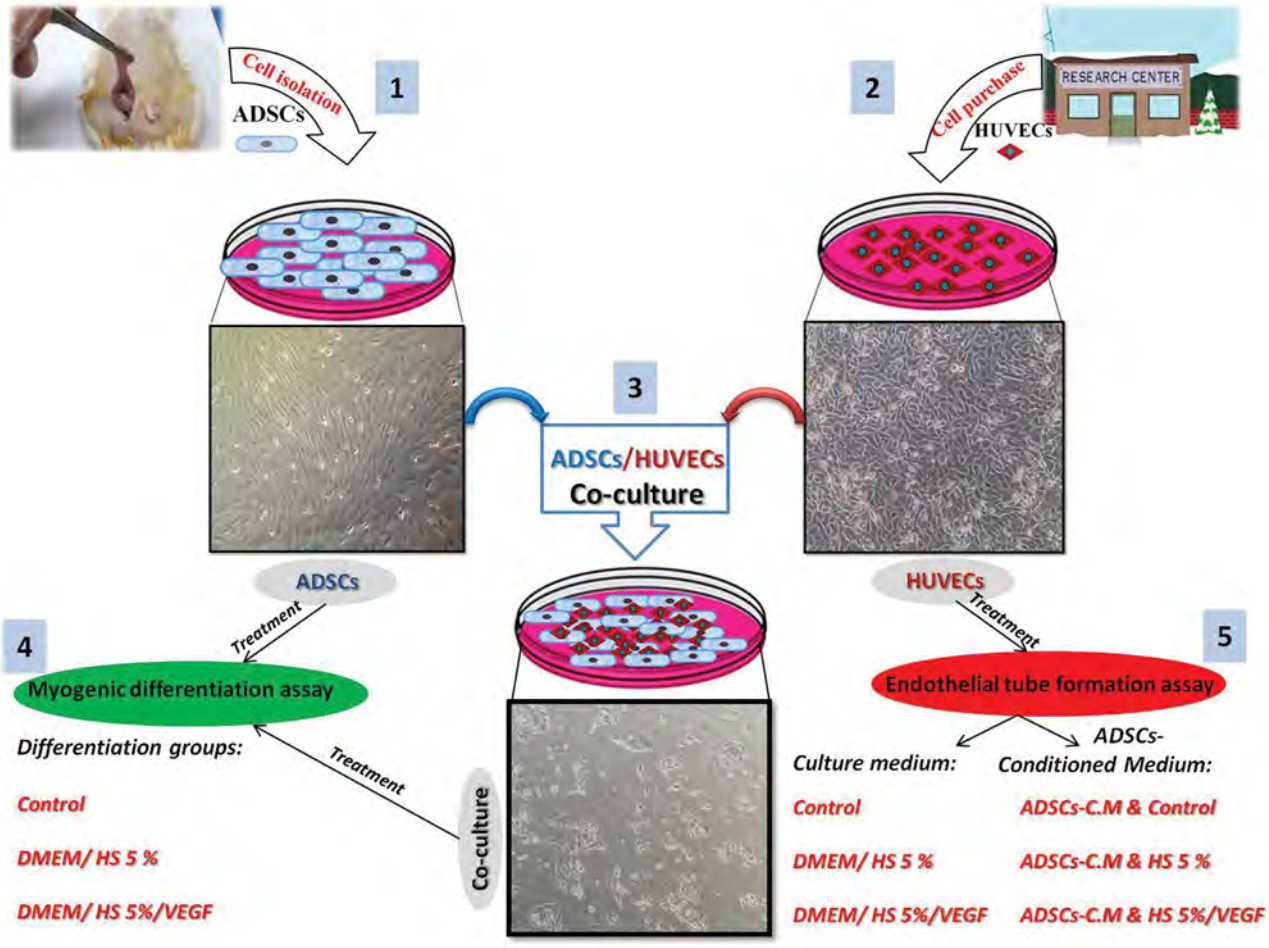

Fig.1: The schematic diagram shows the experimental procedures. Adipose-derived stem cells (ADSCs) and human umbilical vein endothelial cells (HUVECs) cultivation (step 1 and 2) and ADSCs/HUCEVs co-culture (step 3) was described. Step 4 and 5 represents the experimental groups. In this research 3 types of culture medium including myogenic differentiation and ADSCs-conditioned medium (ADSCs-C.M) were designed (step 4 and 5). Myogenic differentiation assay in ADSCs and co-culture groups were evaluated, separately (step 4). And finally, in step 5, HUVECs were treated by different types of culture mediums to examine the endothelial tube formation.

In addition to direct the interaction of ADSCs and HUVECs in the present research, it was also evaluated the role of the conditioned medium of ADSCs (CM-ADSCs) on the growth, proliferation and endothelial network formation of HUVECs. In this regard, HUVECs were divided into two primary groups: HUVECs and induced HUVECs (iHUVECs) groups. Each group was then divided into 3 subgroups as follows:

1. HUVECs/DMEM
2. HUVECs/HS
3. HUVECs/HS/VEGF
4. HUVECs/ADSCs-C.M/ DMEM
5. HUVECs/ADSCs-C.M/ HS
6. HUVECs/ADSCs-C.M/ HS/VEGF

In the iHUVECs group, cells were induced by the ADSC-conditioned medium (ADSC-CM) and HUVEC special culture medium at a ratio of 1:1.

Cell labeling

Endothelial cells were marked with CM-DiI (C7000) according to the manufacturer's instructions. Labeled-HUVECs fluorescence was confirmed by microscopy after 24 hours.

Real-time reverse transcriptase-polymerase chain reaction analysis

We used real-time reverse transcriptase-polymerase chain reaction (RT-PCR) to confirm the expression of *MyHC2* with ABI (STEP1, USA) according to the manufacturer's instructions. So at first, for RNA extraction, the cells were lysed using the RNeasy Plus Mini Kit (Qiagen, Gaithersburg, MD, USA) in Eppendorf tubes. Then the cells were quantified by using a NanoDrop 2000c spectrophotometer (Thermo Scientific, USA). cDNA synthesis was performed using a QuantiTect Reverse Transcription Kit (Qiagen, Gaithersburg, MD, USA). The following primer sequences for amplification were used:

MyHC2-
F: 5′-GGCTGGCTGGACAAGAACA-3′
R: 5′-CCACCACTACTTGCCTCTGC-3′

GAPDH-
F: 5′-TGCTGGTGCTGAGTATGTCGTG-3′
R: 5′-CGGAGATGATGACCCTTTTGG-3′

Immunofluorescence analysis

The cells were washed 3 times with PBS and then with 4% paraformaldehyde were fixed (Sigma, USA) for 20 minutes, washed with PBS and permeable with Triton X-100 (Merck, USA) for 10 minutes, washed again with PBS, subsequently; the cells were incubated with 3% bovine serum albumin (BSA, Sigma, USA) for 2 hours to block any non-specific binding.

ADSCs and ADSCs/HUVECs experimental groups were stained with a primary antibody against the anti-tropomyosin antibody (1:100, Sigma, USA) overnight at 4˚C. Then, the specimens were rinsed three times with PBS and incubated with goat anti-mouse fluorescein isothiocyanate (FITC)-conjugated secondary antibody (1:150, Sigma, USA) for 1 hour. Nuclear staining was done with 4′, 6-diamidino-2-phenylindole (DAPI, 1:400, Sigma, USA) for 15 minutes at room temperature. Ultimately, the plates were washed three times with PBS and then examined by an invert fluorescent microscope (IX 71, Olympus, Japan).

Adipose-derived stem cell-conditioned medium preparation:

ADSCs were cultured in a complete culture medium when reached confluence, and then the medium was replaced with a serum-free or low serum-containing medium. After changing the medium, ADSCs cells were cultured under hypoxia (2% O_2, 5% CO_2) for 48 hours. The conditioned media of ADSCs were collected, centrifuged at 2,000 rpm and 4˚C for 10 minutes, and finally filtered using a 0.22 mm syringe filter.

Endothelial tube formation assay

HUVEC tube formation was analyzed using the Angiogenesis Analyzer of Image J software (version 1.47 from [http://imagej.nih.gov/ij/]). Therefore, the tube formation was calculated by counting numbers of connected cells (meshed network) in random fields with an inverted microscope and by dividing by the total number of cells in the same field.

Statistical analysis

The whole data was presented as the mean ± standard deviation of three triplicated independent experiments. To meet study objectives, data were analyzed using different techniques, including one-way analysis of variance (ANOVA) followed by Tukey's post hoc test for each paired experiment. All analyses were done using GraphPad Prism Software (version 5.1, Graphpad Software Inc., La Jolla, CA, USA). Moreover, $P<0.05$ was *considered* statistically significant.

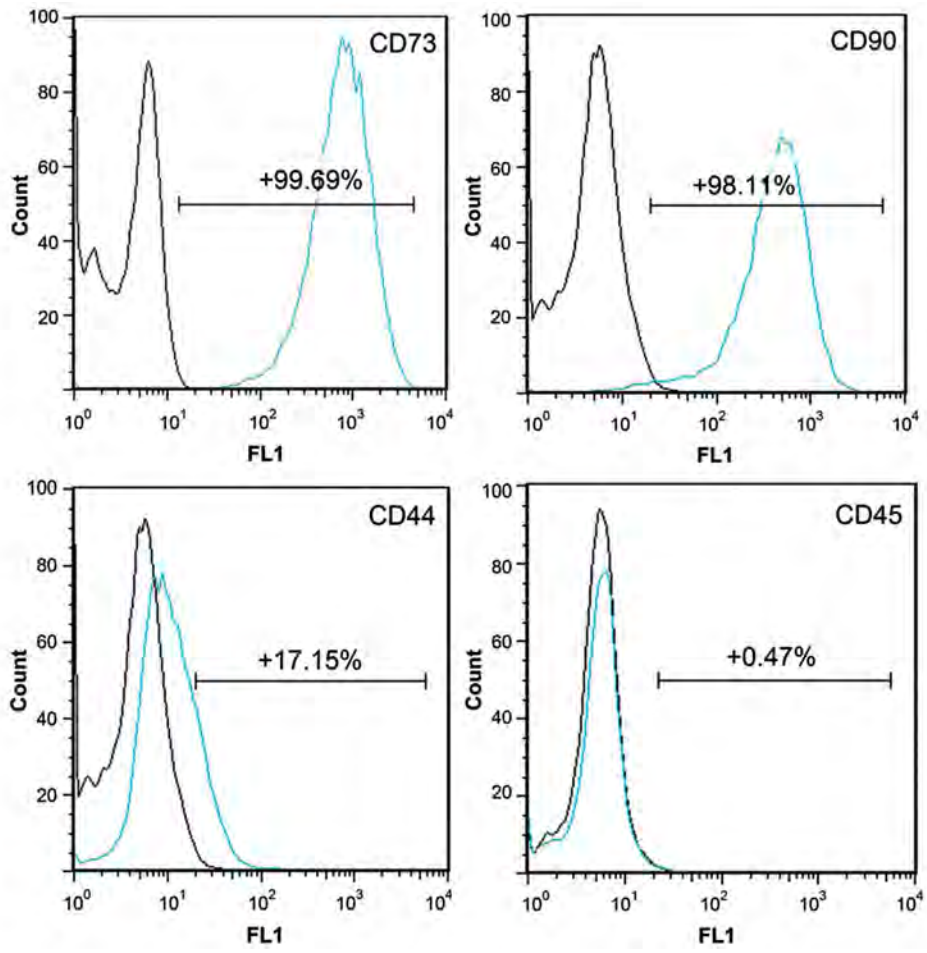

Fig.2: Flow cytometric analysis of cell surface marker expression in adipose-derived stem cells (ADSCs) at 4th passages. Histograms represent the positive mean value of each marker.

Results

Characterization of adipose-derived stem cells

Flow cytometric analysis of passage 4 ADSCs revealed that CD73 (99.69%), CD90 (98.11%), and CD44 (17.15%) were expressed on the cell surface as a positive marker of mesenchymal stem cells. however, only in a few cells, CD45 (0.47%) was expressed as a negative marker (Fig.2).

Changes in gene mRNA expression

Quantitative real-time RT-PCR demonstrated that mRNA expression of *MyHC2* increased significantly in the HS and HS/VEGF groups compared to the control group (P<0.001). There was a significant difference in the mRNA expression of this gene between HS/VEGF and HS group (P<0.05). Most importantly, *MyHC2* expression was *significantly upregulated* on HS/VEGF in the co-culture group compared to the monoculture group (P<0.05). However, the observed gene expression difference was not significant between ADSCs and co-culture groups on HS (Fig.3).

These results showed that VEGF with HUVECs upregulates the expression of *MyHC2* in differentiated ADSCs compared to other groups.

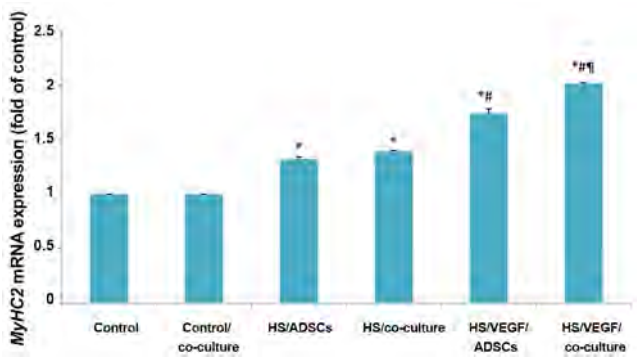

Fig.3: Expression of *MyHC2* mRNA in experimental groups. *MyHC2* mRNA expression increased 1.32 ± 0.02, 1.39 ± 0.01, 1.74 ± 0.04, 2.01 ± 0.01 fold in HS/ADSCs, HS/co-culture, HS/VEGF/ADSCs and HS/VEGF/co-culture groups, respectively. Data are mean ± SD of 3 separate experiments. *, #, and ¶ symbols indicate comparison to control, HS and HS/VEGF groups, respectively.
ADSCs; Adipose-derived stem cells, VEGF; Vascular endothelial growth factor, HS; Horse serum, *; P<0.001, #, and ¶; P<0.05.

Immunofluorescence assay

Immunofluorescence staining showed that the expression of tropomyosin in HS and HS/VEGF differentiation groups was positive compared to the control group (Fig.4A, B). According to the previous protocol, fluorescence intensity measurements were evaluated with image J software (17). As shown in Figure 4C, Corrected Total Cell Fluorescence (CTCF) in HS and HS/VEGF groups was significantly higher than the control group (P<0.001). However, there was no significant difference between HS and HS/VEGF groups (Fig.4C).

In the ADSC groups, the orientation of differentiated cells due to HS was arranged in dense parallel form, while the myoblast-like cells did not have any uniform arrangement on HS/VEGF, which probably due to the role of VEGF in the promotion of ADSCs towards the vascular, skeletal, muscle tissues (Fig.4A).

In the co-culture groups, it seems that the shape and orientation of ADSCs were impressed by two factors: VEGF and HUVEC cells. So that, in the control co-culture group, ADSCs were distributed between the endothelial cells, While, differentiated ADSCs were situated between the endothelial cell colonies (cellular islets) in the HS co-culture group. More interestingly, these cells were arranged in proximity to endothelial cells and looked like the vascular network in the HS/VEGF co-culture group (Fig.4B).

These results suggested that HS/VEGF-loaded medium has dual effects (Myogenesis, Angiogenesis) on both ADSCs monoculture and ADSCs/HUVECs co-culture.

Endothelial tube formation assay

It is interesting to note that besides myogenic differentiation, endothelial tube formation of HUVECs was observed by inverted microscopy in the present study. The endothelial tube formation was quantified by measuring total capillary tube length using image j software. Our findings indicated that the endothelial tube formation was significantly higher than the HS group in HS/VEGF and control co-culture groups (P<0.001). Moreover, there was a significant difference between HS/VEGF and the control group (P<0.001, Fig.5A, B).

The results indicated the endothelial tube formation of HUVECs in control, and more importantly, VEGF-loaded culture media.

Conditional medium assay

It was found that HUVECs had an optimal growth in the HS culture medium in co-culture when compared to the culture of HUVECs alone on the HS medium. Therefore, it seems that the ADSCs culture medium (conditioned medium) has an effect on endothelial cell growth.

According to the conditioned medium of ADSCs in the control group, it was found that the cells retained their natural growth in the culture medium, but no endothelial tube formation was observed. In the HS group, the conditioned medium prevented HUVECs from cell death and apoptosis. Figures showed a remarkable improvement in the cell viability compared to the primary culture medium, while the conditioned medium considerably promoted the endothelial tube formation in the HS/VEGF group after 3 days (Fig.6). Our data indicated that HS/VEGF ADSCs-CM could induce the endothelial tube (network) formation in HUVECs monoculture.

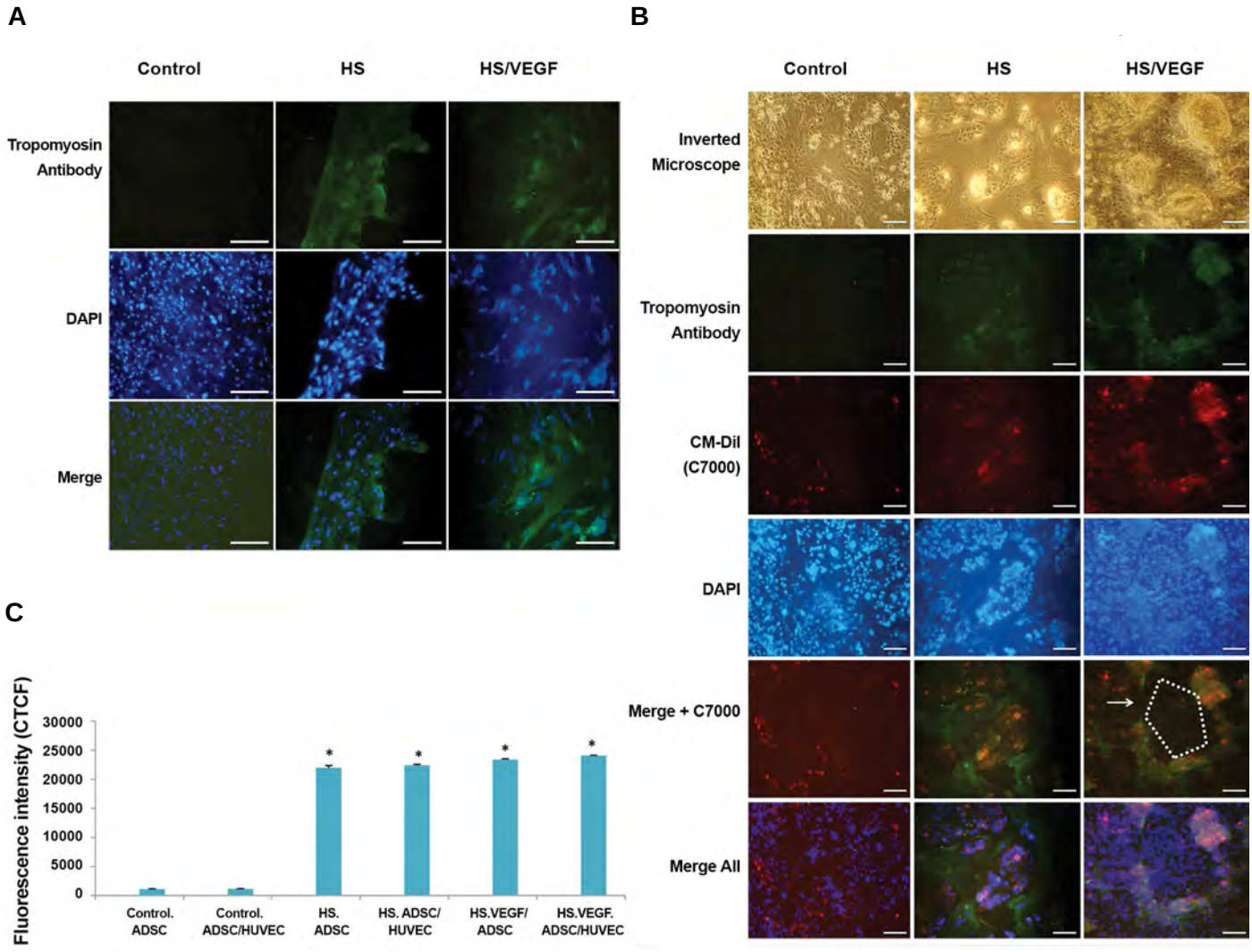

Fig.4: Immunofluorescence and Morphological characterization in experimental groups. (**A.** ADSCs and **B.** ADSCs/HUVECs). Immunofluorescence confirmed the expression of tropomyosin in HS and HS/VEGF groups. Negative control groups were cultured in proliferation (not differentiation) medium and set using both primary and secondary antibodies. The results showed no expression of tropomyosin in these groups. ADSCs were arranged in proximity to endothelial cells and looked like the vascular network in the HS/VEGF co-culture group. Arrows and schematic shapes represent endothelial tube formation. **C.** CTCF assessment of tropomyosin antibody in experimental groups. CTCF in the HS and HS/VEGF groups was significantly increased in comparison to the control group. However, the index of HS/VEGF group showed that there was no significant difference compared to the HS group. * symbol indicates comparison to control groups (scale bare: **A:** 500 µm and **B:** 200 µm).
ADSCs; Adipose-derived stem cells, HUVECs; Human umbilical vein endothelial cells, HS; Horse serum, VEGF; Vascular endothelial growth factor, CTCF; Corrected total cell fluorescence, and *; P<0.001.

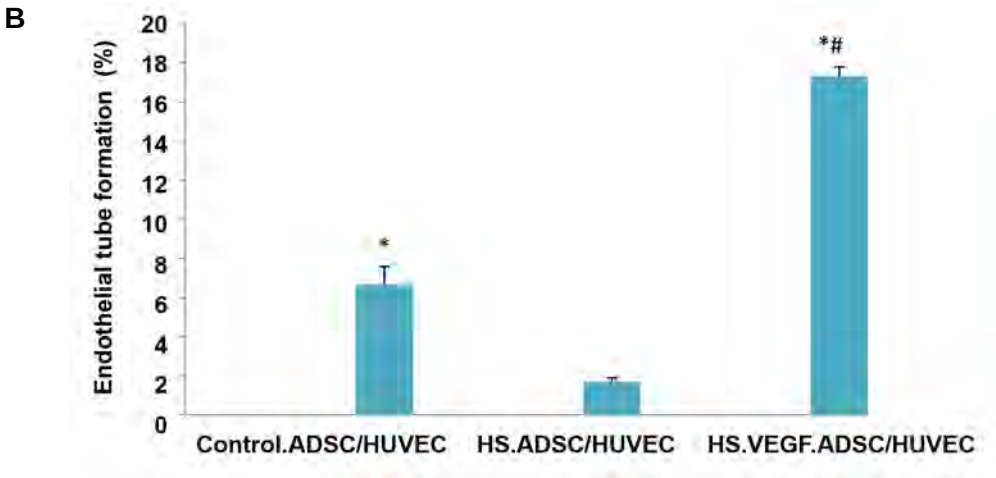

Fig.5: Endothelial tube formation assay (ETFA) in experimental co-culture groups. **A, B.** ETF in the control group indicated a significant increase compared to the HS group. Also, ETF was significantly increased in HS+VEGF group compared to other groups (arrows and schematic shapes represent ETF). *, # symbols indicate comparison to HS and control groups, respectively (scale bare: 1 mm).
ADSCs; Adipose-derived stem cells, HUVECs; Human umbilical vein endothelial cells, HS; Horse serum, VEGF; Vascular endothelial growth factor, *, and #; P<0.001.

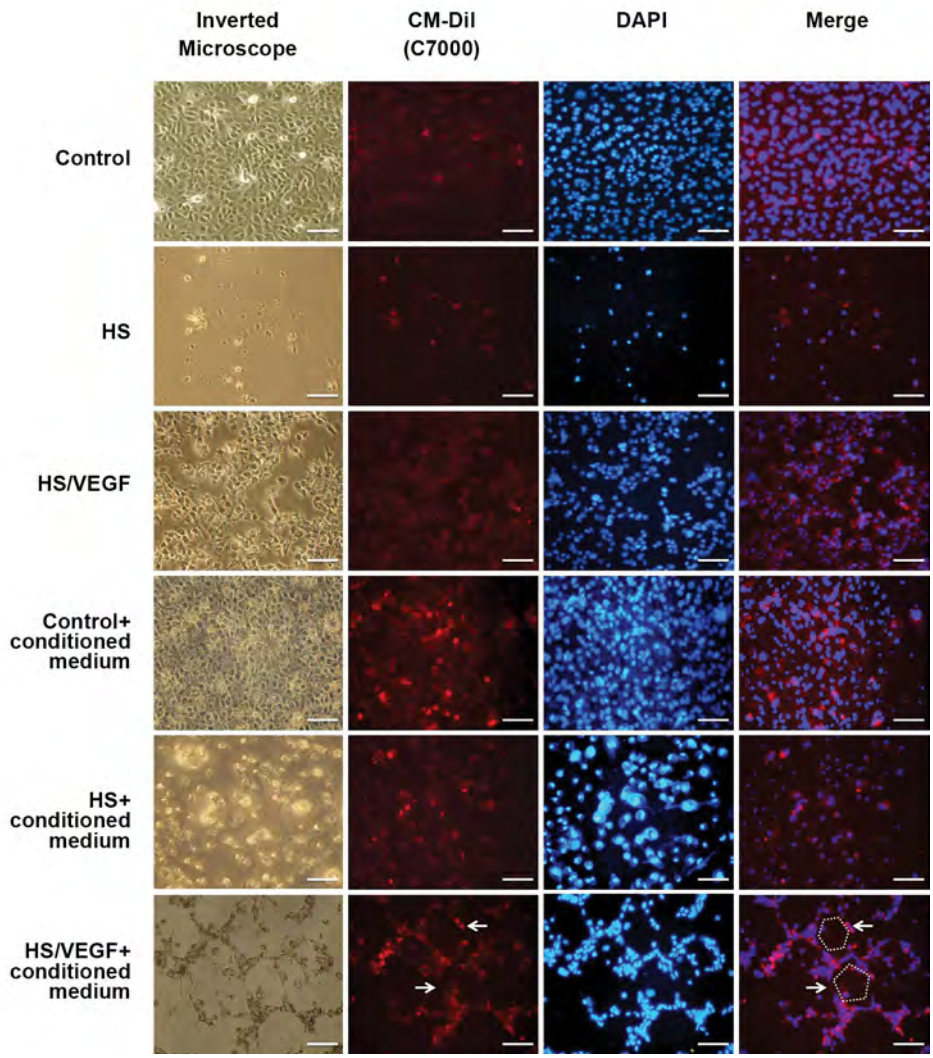

Fig.6: ADSCs conditioned medium effects on HUVECs orientation in experimental groups. In control groups, the cells kept their natural growth in both culture medium and ADSCs-CM. In the HS groups, ADSCs-CM prevented HUVECs from cell death and apoptosis. It can be observed from the figure that endothelial tube formation was promoted in HS/VEGF ADSCs-CM in comparison to other groups (arrows and schematic shapes represent ETF, scale bare: 300 µm).
ADSCs-CM; Adipose-derived stem cells-conditioned medium, HUVECs; Human umbilical vein endothelial cells, HS; Horse serum, and VEGF; Vascular endothelial growth factor.

Discussion

It is now known that skeletal muscle tissue engineering is a complex process that requires the formation of myofibers, construction of functional vasculature, innervation, and an improvement in the extracellular matrix (ECM) that allows for the production of a proper mechanical force (18). In the present experimental research, we investigated the effects of HUVECs and VEGF on myoblast differentiation of ADSCs to achieve acceptable and functional cellular models for use in muscle tissue engineering. In this regard, ADSCs were cultured in a 2D system alone or with HUVECs with or without VEGF in the culture medium. ADSCs/HUVECs were co-cultured in a ratio of 1:1. This ratio was based on previous studies that have been used between ADSCs/HUVECs (19) and myoblast/HUVECs (20).

Results of current research indicated that VEGF could improve the myogenic differentiation of ADSCs in monoculture or co-culture groups. VEGF is a key regulator of angiogenesis, but it is not clear whether it would restore muscle force and aid in muscle regeneration after acute musculoskeletal injuries. Recent studies suggest that VEGF may affect a variety of other cell types such as neurons, hepatocytes, osteoblasts, hematopoietic cells, and myoblasts (13). Moreover, it was demonstrated that VEGF administration in vitro stimulates myoblast migration and survival, protects myogenic cells from apoptosis, and promotes myogenic cell growth (14, 15). Chen et al. (21) and Song et al. (22) in separate studies reported that VEGF was responsible for the cardiomyocyte differentiation of ESCs and ADSCs, respectively.

Furthermore, Kim et al. (23) reported that the VEGF, when combined with ADSCs, could be used as a vascularizing tool for tissue engineering of complex muscle tissue. Based on our investigation, VEGF induced the endothelial tube formation in HS/VEGF co-culture groups besides myoblast differentiation of ADSCs. These data support the idea that appropriate myogenesis will occur along with angiogenesis, and VEGF could promote both of them. It has been suggested that the increased angiogenesis induced by VEGF might improve the muscle function in ischemic tissues (14).

The present findings were consistent with other studies that identified a relationship between angiogenesis and more effective muscle regeneration (10, 24, 25). According to previous studies, in addition to VEGF, it seems necessary to utilize endothelial cells to create ideal vasculature and skeletal muscle (26, 27).

In the present research, ADSCs were co-cultured with HUVECs to investigate myoblast differentiation in stem cells. In this regard, we assessed direct cell-cell interaction and paracrine effects on differentiation, morphology, and directions of cells. It was based on our hypothesis that direct cell-cell interactions between cells probably enhanced the myoblast differentiation.

In this study, it has been demonstrated that HUVECs myogenic effects are impressive when utilized along with VEGF and can promote the development of a favorable vascular-muscle structure. Koffler et al. (28) sought to cultivate muscle progenitor cells (MPCs), endothelial cells (ECs), and fibroblasts on an acellular biological scaffold that was used for abdominal wall defect in nude mice. It was determined that the co-culture of myoblast cells and HUVECs in a sandwich structure could improve vascular formation (29).

The co-culture of ECs with MPCs, in addition to increased angiogenesis, could improve the formation of muscle tissue (18). Previous research found that the VEGF secretion by ECs resulted in the migration of MPCs and protection against apoptosis (15). It is believed that endothelial cells can induce smooth muscle cell differentiation in bone marrow stem cells (BMSCs). It is reported that ECs can promote a contractile phenotype, reduce proliferation, and increase the synthesis of collagen (30). There is insufficient data about ADSCs/HUVECs co-culture in the myogenic differentiation. An advantage of the current study is that it investigated the role of HUVECs in myogenic differentiation as well as the orientation of ADSCs in a co-culture model. As mentioned in previous publications, the myogenesis occurred along with the angiogenesis. Therefore, the endothelial tube formation was evaluated *in vitro* in the present study. We hypothesized that the interaction between ADSCs and HUVECs might lead to the proliferation, improvement of the cellular arrangement, and angiogenesis of endothelial cells, and this process could mutually improve the myoblast differentiation. It is believed that ECs were induced to form capillary-like structures during the reorganization stage of angiogenesis *in vitro.*

It has been reported that ADSCs/ECs co-culture can induce endothelial tube formation and significantly increase numbers of junctions and tubules. Using the ELISA, Holnthoner et al. (31) reported that an increasing amount of ADSCs in the co-culture resulted in the elevation of VEGF-A concentrations. It was mentioned that ADSCs were secreted a considerable amount of VEGF in the conditioned medium (22). Several studies indicated that the simultaneous co-stimulation of MPCs and endothelial tube formation were due to paracrine effects of VEGF as well as IGF-1, HGF, bFGF, and PDGF-BB (32, 33). On the contrary to our findings, Kook et al. (34) suggested that HUVECs co-cultured with ADSCs in the well plate did not observe any capillary formation. They reported that the proliferation, junctional proteins expression, and sprouts of HUVECs in the VEGF-loaded co-culture group were only slightly increased.

Unlike to results of research by Kook et al. (34), our finding study confirmed that ADSCs could induce endothelial tube formation in the VEGF-loaded co-culture group. It may be due to direct cellular interactions and, more importantly, the effects of paracrine secretion of ADSCs such as VEGF, angiopoietin-1, angiopoietin-2, and interleukin-6 that induce the proliferation and endothelial

tube formation of HUVECs (35). The current research revealed that ADSCs conditioned medium (ADSCs-CM) had the potential to promote the vascular tube formation of HUVECs. *In vitro* and *in vivo* investigation revealed that the mesenchymal stem cell-conditioned media (MSC-CM) or ADSC-CM had a therapeutic effect with considerable results (36, 37).

ADSC-CM contained various growth factors such as VEGF, EGF, cytokines, proteins, and exosomes. Results of the present study were consistent with other research indicating that the ADSC-CM could improve the cell arrangement of endothelial cells. It is expected to enhance the proliferation and angiogenesis via paracrine effects of ADSC- CM (38, 39). Similar to finding of studies by Walter et al. (38) and Lee et al. (39), our study showed that the ADSC-CM could induce endothelial tube formation in VEGF-loaded group compared to HS and control groups. Due to the lack of these structures in other groups, it seems that an additional concentration of VEGF could induce endothelial tube formation in the VEGF-loaded group.

Conclusion

It can be generally concluded that ADSCs/HUVECs interaction and dual effects of VEGF can lead to the formation of differentiated myoblasts in proximity to endothelial network formations. Co-culture HUVECs and ADSCs can be a promising approach to achieve a favorable cellular design for tissue engineering of vascularized skeletal muscle. Furthermore, these *in vitro*-cellular models could be potentially used in vascular-muscle tissue engineering implanted into organ defects where muscle tissue and vascular regeneration were required.

Acknowledgements

This manuscript is a part of a Ph.D. thesis, funded by grant no. 9625, from the Cellular and Molecular Research Center (CMRC-9625), of the Ahvaz Jundishapur University of Medical Sciences (AJUMS), Ahvaz, Iran. The authors sincerely thank all individuals who cooperated with this study. There is no conflict of interest in this study.

Authors' Contributions

A.H.-M., V.B., M.O.; Contributed to conception and design. A.H.-M., V.B., M.R.; Contributed to all experimental work, data and statistical analysis, as well as the interpretation of data. V.B., M.O.; Were responsible for overall supervision. A.H.-M., M.R.; Drafted the manuscript, which was revised by V.B., M.O. All authors read and approved the final manuscript.

References

1. Juhas M, Bursac N. Engineering skeletal muscle repair. Curr Opin Biotechnol. 2013; 24(5): 880-886.
2. Su Y, Yu Y, Liu C, Zhang Y, Liu C, Ge M, et al. Fate decision of satellite cell differentiation and self-renewal by miR-31-IL34 axis. Cell Death Differ. 2020; 27(3): 942-965.
3. Corona BT, Rivera JC, Owens JG, Wenke JC, Rathbone CR. Volumetric muscle loss leads to permanent disability following extremity trauma. J Rehabil Res Dev. 2015; 52(7): 785-792.
4. Grogan BF, Hsu JR; Skeletal Trauma Research Consortium. Volumetric muscle loss. J Am Acad Orthop Surg. 2011; 19 Suppl 1: S35-S37.
5. Dienes JA, Hu X, Janson KD, Slater C, Dooley EA, Christ GJ, et al. Analysis and Modeling of rat gait biomechanical deficits in response to volumetric muscle loss injury. Front Bioeng Biotechnol. 2019; 7: 146.
6. Kesireddy V. Evaluation of adipose-derived stem cells for tissue engineered muscle repair construct-mediated repair of a murine model of volumetric muscle loss injury. Int J Nanomedicine. 2016; 11: 1461-1473.
7. Sicari BM, Rubin JP, Dearth CL, Wolf MT, Ambrosio F, Boninger M, et al. An acellular biologic scaffold promotes skeletal muscle formation in mice and humans with volumetric muscle loss. Sci Transl Med. 2014; 6(234): 234ra58.
8. Gorecka A, Salemi S, Haralampieva D, Moalli F, Stroka D, Candinas D, et al. Autologous transplantation of adipose-derived stem cells improves functional recovery of skeletal muscle without direct participation in new myofiber formation. Stem Cell Res Ther. 2018; 9(1): 195.
9. Ogawa R. The importance of adipose-derived stem cells and vascularised tissue regeneration in the field of tissue transplantation. Curr Stem Cell Res Ther. 2006; 1(1): 13-20.
10. Levenberg S, Rouwkema J, Macdonald M, Garfein ES, Kohane DS, Darland DC, et al. Engineering vascularized skeletal muscle tissue. Nat Biotechnol. 2005; 23(7): 879-884.
11. Elbjeirami WM, West JL. Angiogenesis-like activity of endothelial cells co-cultured with VEGF-producing smooth muscle cells. Tissue Eng. 2006; 12(2): 381-390.
12. Ucuzian AA, Bufalino DV, Pang Y, Greisler HP. Angiogenic endothelial cell invasion into fibrin is stimulated by proliferating smooth muscle cells. Microvasc Res. 2013; 90: 40-47.
13. Yoshida K, Ito H, Furuya K, Ukichi T, Noda K, Kurosaka D. Angiogenesis and VEGF-expressing cells are identified predominantly in the fascia rather than in the muscle during the early phase of dermatomyositis. Arthritis Res Ther. 2017; 19(1): 272.
14. Arsic N, Zacchigna S, Zentilin L, Ramirez-Correa G, Pattarini L, Salvi A, et al. Vascular endothelial growth factor stimulates skeletal muscle regeneration in vivo. Mol Ther. 2004; 10(5): 844-854.
15. Germani A, Di Carlo A, Mangoni A, Straino S, Giacinti C, Turrini P, et al. Vascular endothelial growth factor modulates skeletal myoblast function. Am J Pathol. 2003; 163(4): 1417-1428.
16. Bayati V, Hashemitabar M, Gazor R, Nejatbakhsh R, Bijannejad D. Expression of surface markers and myogenic potential of rat bone marrow-and adipose-derived stem cells: a comparative study. Anat Cell Biol. 2013; 46(2): 113-121.
17. Bankhead P. Analyzing fluorescence microscopy images with ImageJ. Image J. 2014; 1: 195.
18. Criswell TL, Corona BT, Wang Z, Zhou Y, Niu G, Xu Y, et al. The role of endothelial cells in myofiber differentiation and the vascularization and innervation of bioengineered muscle tissue in vivo. Biomaterials. 2013; 34(1): 140-149.
19. Carter RN, Casillo SM, Mazzocchi AR, DesOrmeaux JP, Roussie JA, Gaborski TR. Ultrathin transparent membranes for cellular barrier and co-culture models. Biofabrication. 2017; 9(1): 015019.
20. Chen S, Kawazoe N, Chen G. Biomimetic assembly of vascular endothelial cells and muscle cells in microgrooved collagen porous scaffolds. Tissue Eng Part C Methods. 2017; 23(6): 367-376.
21. Chen Y, Amende I, Hampton TG, Yang Y, Ke Q, Min JY, et al. Vascular endothelial growth factor promotes cardiomyocyte differentiation of embryonic stem cells. Am J Physiol Heart Circ Physiol. 2006; 291(4): H1653-H1658.
22. Song YH, Gehmert S, Sadat S, Pinkernell K, Bai X, Matthias N, et al. VEGF is critical for spontaneous differentiation of stem cells into cardiomyocytes. Biochem Biophys Res Commun. 2007; 354(4): 999-1003.
23. Kim MH, Hong HN, Hong JP, Park CJ, Kwon SW, Kim SH, et al. The effect of VEGF on the myogenic differentiation of adipose tissue derived stem cells within thermosensitive hydrogel matrices. Biomaterials. 2010; 31(6): 1213-1218.
24. Law PK, Haider Kh, Fang G, Jiang S, Chua F, Lim YT, et al. Human VEGF165- myoblasts produce concomitant angiogenesis/myogenesis in the regenerative heart. Mol Cell Biochem 2004; 263(1-2): 173-178.
25. Ochoa O, Sun D, Reyes-Reyna SM, Waite LL, Michalek JE, Mc-

Manus LM, et al. Delayed angiogenesis and VEGF production in CCR2-/- mice during impaired skeletal muscle regeneration. Am J Physiol Regul Integr Comp Physiol. 2007; 293(2): R651-R661.
26. Rahman N, Purpura KA, Wylie RG, Zandstra PW, Shoichet MS. The use of vascular endothelial growth factor functionalized agarose to guide pluripotent stem cell aggregates toward blood progenitor cells. Biomaterials. 2010; 31(32): 8262-8270.
27. Wang Z, He Y, Yu X, Fu W, Wang W, Huang H. Rapid vascularization of tissue-engineered vascular grafts in vivo by endothelial cells in co-culture with smooth muscle cells. J Mater Sci Mater Med. 2012; 23(4): 1109-1117.
28. Koffler J, Kaufman-Francis K, Shandalov Y, Egozi D, Pavlov DA, Landesberg A, et al. Improved vascular organization enhances functional integration of engineered skeletal muscle grafts. Proc Natl Acad Sci USA. 2011; 108(36): 14789-14794.
29. Sasagawa T, Shimizu T, Sekiya S, Haraguchi Y, Yamato M, Sawa Y, et al. Design of prevascularized three-dimensional cell-dense tissues using a cell sheet stacking manipulation technology. Biomaterials. 2010; 31(7): 1646-1654.
30. Lin CH, Lilly B. Endothelial Cells direct mesenchymal stem cells toward a smooth muscle cell fate. Stem Cells Dev. 2014; 23(21): 2581-2590.
31. Holnthoner W, Hohenegger K, Husa AM, Muehleder S, Meinl A, Peterbauer-Scherb A, et al. Adipose-derived stem cells induce vascular tube formation of outgrowth endothelial cells in a fibrin matrix. J Tissue Eng Regen Med. 2015; 9(2): 127-136.
32. Doukas J, Blease K, Craig D, Ma C, Chandler LA, Sosnowski BA, et al. Delivery of FGF genes to wound repair cells enhances arteriogenesis and myogenesis in skeletal muscle. Mol Ther. 2002; 5(5 Pt 1): 517-527.
33. Walgenbach KJ, Gratas C, Shestak KC, Becker D. Ischaemia-induced expression of bFGF in normal skeletal muscle: a potential paracrine mechanism for mediating angiogenesis in ischaemic skeletal muscle. Nat Med. 1995; 1(5): 453-459.
34. Kook YM, Kim H, Kim S, Heo CY, Park MH, Lee K, et al. Promotion of vascular morphogenesis of endothelial cells co-cultured with human adipose-derived mesenchymal stem cells using polycaprolactone/gelatin nanofibrous scaffolds. Nanomaterials (Basel). 2018; 8(2): pii: E117.
35. Park KM, Gerecht S. Harnessing developmental processes for vascular engineering and regeneration. Development. 2014; 141(14): 2760-2769.
36. Pawitan JA. Prospect of stem cell conditioned medium in regenerative medicine. Biomed Res Int. 2014; 2014: 965849.
37. Tarcisia T, Damayanti L, Antarianto RD, Moenadjat Y, Pawitan JA. Adipose derived stem cell conditioned medium effect on proliferation phase of wound healing in Sprague Dawley rat. Medical Journal of Indonesia. 2018; 26(4): 239-245.
38. Walter MN, Wright KT, Fuller HR, MacNeil S, Johnson WE. Mesenchymal stem cell-conditioned medium accelerates skin wound healing: an in vitro study of fibroblast and keratinocyte scratch assays. Exp Cell Res. 2010; 316(7): 1271-1281.
39. Lee SH, Jin SY, Song JS, Seo KK, Cho KH. Paracrine effects of adipose-derived stem cells on keratinocytes and dermal fibroblasts. Ann Dermatol. 2012; 24(2): 136-143.

Original Article

Metformin Attenuates Brain Injury by Inhibiting Inflammation and Regulating Tight Junction Proteins in Septic Rats

Fatima Ismail Hassan, Ph.D.[1#], Tina Didari, Ph.D.[1#], Maryam Baeeri, Ph.D.[1], Mahdi Gholami, M.Sc.[2], Hamed Haghi-Aminjan, Ph.D.[3], Madiha Khalid, M.SC.[1], Mona Navaei-Nigjeh, Ph.D.[1], Mahban Rahimifard, M.Sc.[1], Sara Solgi, M.Sc.[1], Mohammad Abdollahi, Ph.D.[1, 2*], Mojtaba Mojtahedzadeh, Pharm.D.[1, 2*]

1. Pharmaceutical Sciences Research Center (PSRC), The Institute of Pharmaceutical Sciences (TIPS), Tehran University of Medical Sciences, Tehran, Iran
2. School of Pharmacy, Tehran University of Medical Sciences, Tehran, Iran
3. Pharmaceutical Sciences Research Center, Ardabil University of Medical Sciences, Ardabil, Iran

#These authors contributed equally to this work.

Corresponding Address: Pharmaceutical Sciences Research Center (PSRC), The Institute of Pharmaceutical Sciences (TIPS), Tehran University of Medical Sciences, Tehran, Iran
Emails: mohammad@tums.ac.ir, mojtahed@tums.ac.ir

Received: 09/July/2019, Accepted: 1/October/2019

Abstract

Objective: Metformin has a potent inhibitory activity against inflammation and oxidative stress, which inevitably occur in sepsis-associated encephalopathy (SAE). The precise mechanisms underlying neuroprotective effects of metformin in SAE, are still unclear. In the present work, the protective effect of metformin on SAE using cecal ligation and puncture (CLP) model of sepsis, was assessed.

Materials and Methods: In this experimental study, CLP procedure was performed in Wistar rats and 50 mg/kg metformin was administered immediately. Specific markers of sepsis severity, inflammation, blood brain barrier (BBB) dysfunction, and brain injury, were investigated. Specific assay kits and real-time polymerase chain reaction (RT-PCR) were used. Histopathological assessment was also carried out.

Results: Treatment with metformin decreased murine sepsis score (MSS), lactate, platelet lymphocyte ratio (PLR), and high mobility group box (HMGB1) levels. The expression levels of claudin 3 (*Cldn3*) and claudin 5 (*Cldn5*) were increased following treatment with metformin. Metformin decreased the expression of *S100b*, neuron specific enolase (*Nse*), and glial fibrillary acidic protein (*Gfap*).

Conclusion: Our study suggests that metformin may inhibit inflammation and increase tight junction protein expressions which may improve BBB function and attenuate CLP-induced brain injury. Hence, the potential beneficial effects of metformin in sepsis, should be considered in future.

Keywords: Brain Injury, Metformin, Molecular Mechanisms, Sepsis

Cell Journal(Yakhteh), Vol 22, Suppl 1, Autumn 2020, Pages: 29-37

Citation: **Ismail Hassan F, Didari T, Baeeri M, Gholami M, Haghi-Aminjan H, Khalid M, Navaei-Nigjeh M, Rahimifard M, Solgi S, Abdollahi M, Mojtahedzadeh M. Metformin attenuates brain injury by inhibiting inflammation and regulating tight junction proteins in septic rats. Cell J. 2020; 22 Suppl 1: 29-37. doi: 10.22074/cellj.2020.7046 .**

Introduction

Sepsis remains the most common disease among the critically ill with no specific diagnosis and treatment. Sepsis-associated encephalopathy (SAE) is the common form of delirium observed in septic patients (1). It affects the blood-brain barrier (BBB) function and other brain cells as a result of dysregulation of cytokines and neurotransmitters production (2). SAE involves the release of inflammatory mediators, oxidative stress induction and increase in other biomarkers that damage brain cells and affect BBB integrity and intracellular metabolism (2, 3). Neuroinflammation, ischemic processes, and neurotransmitter dysfunction are processes involved in the pathophysiology of SAE (4). Previous studies reported that microglial and astrocytes activation affect BBB integrity and stimulate the production of several mediators in the brain as observed in SAE (4, 5). Inflammation and oxidative stress are crucial in SAE and can lead to other detrimental effects.

Metformin was shown to exert its protective role in sepsis partly through its anti-inflammatory and antioxidant properties (6). Neuroprotective effects of metformin were reported to be mediated via these mechanisms. Metformin prevented brain mitochondrial dysfunction by reducing oxidative stress levels in high fat diet-induced insulin resistant rats, promoted neurogenesis and improved spatial memory, protected against cerebral ischemia, and enhanced angiogenesis in post-stroke recovery (7-10). Several studies reported the protective effects of metformin in sepsis (11). Metformin was shown to inhibit pro-inflammatory cytokines production, down-regulate myeloperoxidase expression, and decrease creatine kinase myocardial band, and brain natriuretic peptide in endotoxin-induced myocarditis (12). It protected the lung

of septic rats against neutrophil infiltration, inflammation, and oxidative damage (13). Metformin attenuated sepsis-induced brain injury by inhibiting oxidative stress and decreasing BBB permeability via activating phosphatidylinositol-3 Akt signaling pathway (14). However, the exact mechanism by which metformin exerts its neuroprotective effects is not clear yet. Elucidation of other SAE markers and pathways is necessary.

In this study, the neuroprotective effects of metformin on SAE were investigated, using cecal ligation and puncture (CLP) model. We hypothesized that using CLP model, metformin will improve sepsis severity, restore BBB function, and attenuate brain injury by reducing the levels of inflammatory markers, increasing gene expression of tight junction proteins, and decreasing the gene expression of brain injury markers which will further reduce brain structural damage.

Materials and Methods

In this experimental study, Metformin (>97% purity) was purchased from (Soha Pharmaceutical Company, Iran). Ketamine and xylazine used for anesthesia induction, were purchased from Alfasan, Netherlands, and normal saline was bought from B-braun, Germany. Formalin, rat high-mobility group protein B1 (HMGB1) ELISA and lactate assay kits were obtained from ZellBio GmbH (Germany). RNase solution, iScript cDNA synthesis kit and propidium iodide were obtained from Sigma-Aldrich (Germany).

Experimental design

All protocols and procedures regarding animal handling were approved by Tehran University of Medical Sciences Ethics Committee under the reference number IR.TUMS.VCR.1396.2075. In this experimental study, 36 healthy adult male Wistar rats (200-250 g) aged 8-10 weeks, were obtained from the animal facility of Pharmacy, Tehran University of Medical Sciences (TUMS). All rats were kept at 25 ± 1˚C, with 50% humidity and 12-hour day/night cycle, and had access to standard feed and water ad libitum. Six (6) rats were randomly assigned to each group. Group I: Sham (12 hours), group II: CLP (12 hours), group III: CLP+metformin 50 mg/kg (12 hours), group IV: Sham (24 hours), group V: CLP (24 hours), and group VI: CLP rats administered metformin 50 mg/kg (24 hours). Rats were sacrificed after 12 and 24 hours, depending on the grouping.

Cecal ligation and puncture model

CLP was performed to induce sepsis in rats as previously described (14). Rats were anesthetized with intraperitoneal ketamine/xylazine (110/10 mg/kg body weight). The lower quadrant of the abdomen was shaved and disinfected and then, a longitudinal skin midline incision was made. The mesentery of the cecum was carefully dissected and the cecum was ligated at the designated position for sepsis induction. The cecum was perforated using 18-gauge needle and two punctures. After removing the needle, a small amount (droplet) of feces, was extruded. The cecum was carefully returned into the abdominal cavity. Prewarmed normal saline (37˚C, 5 ml per 100 g body weight) was administered subcutaneously to resuscitate the animals and then, the animals were placed back in cages in a temperature-controlled room (22˚C) with 12-hour light and dark cycles and free access to water and food. All above procedures were performed on sham animals except cecum ligation and puncture.

Murine sepsis score

This scoring was used to determine disease severity and mortality as previously described (15). The method has been successfully carried out in rats (16). This scoring system involves specific variables and numbers that indicate sepsis severity. The score ranged 0 to 4 and involved appearance, level of consciousness, activity, response to stimuli, eyes, respiration rate and quality. Two investigators scored the animals 12 and 24 hours after sepsis induction where one of the investigators was blinded to treatment.

Blood and organ sampling

Blood samples and brains were taken for determination of platelet lymphocyte ratio (PLR), and levels of lactate, high-mobility group box one (HMGB1), genes expression, and histopathological evaluations. Arterial blood (3 ml) was collected from the left arteria carotis into plain and heparinized tubes. The samples in the heparinized bottles were kept for complete blood count analysis while those in plain bottles were centrifuged at 3000 g for 15 minutes. The plasma was separated, kept in different tubes, and stored at -80ºC for further analysis. Brain samples were washed with normal saline and divided into two hemispheres. The first was stored at -8ºC for real-time polymerase chain reaction (RT-PCR) analysis, while the second part was stored in 10% formalin for histopathological studies.

Platelet lymphocyte ratio determination and lactate measurement

PLR determination is used to evaluate inflammatory responses (17) while lactate is an important marker of sepsis severity. PLR was determined from the complete blood count measured using an automated analyzer (Sysmex, America Inc.). Platelet counts obtained were divided by lymphocyte counts for each sample to obtain the platelet/lymphocyte ratio. We measured plasma lactate concentration using a lactate assay kit (ZellBio GmbH, Germany) according to the manufacturer's instruction and calculations were done using the standard formula.

HMGB1 measurement

HMGB1 is an important marker of late sepsis lethality. It was used to evaluate the effect of metformin in late sepsis. HMGB1 measurement was performed in the rat's

brain that was stored at -80°C. The brain sample was homogenized with phosphate buffer and centrifuged. Specific rat ELISA kit (ZellBio GmbH, Germany) was used according to manufacturer's protocol and HMGB1 level was calculated using standard curve.

Gene expression evaluation using real-time polymerase chain reaction

The expression level of gene of the specific markers for BBB integrity and brain injury were evaluated (4, 5, 13). These included claudins 3 (*Cldn3*), claudin 5 (*Cldn5*), *S100b*, neuron specific enolase (*Nse*), and glial fibrillary acidic protein (*Gfap*). Total RNA was extracted from brain samples stored at -80°C using TRIzol® reagent according to the manufacturer's protocol. The genomic DNA was extracted using DNase I, RNase-free kit (Fermentas, Glen Burnie, MD, USA). The concentrations of RNA and DNA were determined by Thermo Scientific NanoDrop 2000c UV-Vis spectrophotometer (Thermo Scientific, USA). Complementary DNA (cDNA) was then reverse transcribed using the Thermo Scientific RevertAid First Strand cDNA synthesis kit as per manufacturer's manual. For analysis of genes expression levels, primer pairs were used with glyceraldehyde-3-phosphate dehydrogenase (*Gapdh*) as the housekeeping gene. Real time RT-PCR, to determine the expression level of *Cldn3*, *Cldn5*, *S100b*, *Nse*, and *Gfap*, was performed on LightCycler® 96 System (Roche) using the SYBR Green master mix. Expression analysis for each sample was done in triplicates. Cycle number of each reaction was calculated from the amplification curve to determine the relative gene expression using the comparative cycle threshold method. The double delta Ct ($2^{-\Delta\Delta ct}$) analysis was done to determine the differences in gene expressions among the groups (18). The primer sequences used for RT-PCR in terms of genes as follows:

Cldn5-
F: 5′-CTTGTGAGGACTTGACCGA-3′
R: 5′-GTAGGAACTGTTAGCGGCA-3′

S100b-
F: 5′-GTATAGCACTGGTTGTAGAC-3′
R: 5′-CAGCATACATTACACCTAAGA-3′

Gfap-
F: 5′-CCAACTAACAGGATACTCAC-3′
R: 5′-ATAACAACAAGGATGAAGGAA-3′

Nse-
F: 5′-GTCGTCTGCCATTACTCTAC-3′
R: 5′-ACCATTGCTAACCTTTCTGT-3′

Cldn3-
F: 5′-ACCAAGATCCTCTATTCCG-3′
R: 5′-TACATCGACGGTTGGTAG-3′

Gapdh-
F: 5′-ACTGAGCAAGAGAGGCCCTA-3′
R: 5′-TATGGGGGTCTGGGATGGAA-3′

Histopathological studies

The harvested tissue (brain) was fixed in 10% neutral buffered formalin (NBF, pH=7.26) for 48 hours, then processed and embedded in paraffin. The 5-µm thick sections were prepared and stained with haemtoxylin and eosin (H&E). Two sections per animal in each group were examined. An independent (blinded) pathologist performed histopathological analysis using light microscopy (Olympus BX51, Olympus, Japan). Histopathological changes, including acute and chronic inflammatory response, liquefactive necrosis, hemorrhage and/or hyperemia in different samples, were evaluated.

Statistical analysis

In the present work, we present our results as mean ± standard deviation (± SD) or as median and interquartile range (25 and 75% quartile). One-way analysis of variance (ANOVA) or Kruskal Wallis's ANOVA followed by Tukey or Dunn's *post hoc* tests for multiple comparisons, was performed. Pearson correlation measurement was also performed. Significance was considered at $P \leq 0.05$ among the groups. (Stats Version 3.2.10).

Results

Murine sepsis score was lower in metformin-treated cecal ligation and puncture rats

Figure 1 shows the effect of metformin administration on sepsis severity. MSS was used to determine disease progression in CLP rats. MSS was considered the sum of scores of all clinical variables for each rat. The inter-rater reliability was excellent (0.97) when calculated using the intra class coefficient (ICC). The average total score was taken to reconcile differences between scorers. The coat of animals in the sham groups (12 and 24 hours) remained smooth, and activity, response to touch, auditory stimuli, posture, respiration rate and quality were also normal. In CLP 12-hour group, patches of hair were piloerected, activity was slow, strong response to touch was observed, and respiration rate and quality were moderately reduced and labored, respectively. In the metformin-treated group (12 hours), patches of hair were mildly piloerected, rats were active but avoided standing upright, activity was slightly suppressed but response to touch was immediate, the eyes were not fully open but respiration rate and quality were normal. In the CLP 24 hour group, rats appeared puffy, activity was impaired and they remained stationary, there was no response to auditory stimuli, eyes were half open with secretions, respiratory rate and quality were severely reduced and labored, respectively. However, in the metformin-treated groups (both 12 and 24 hours), the appearance was normal, rats were active but avoided standing upright, response to auditory stimulus was immediate,

eyes were half open, respiratory rate and quality were normal but slightly labored.

Statistically significant differences (P<0.001) was observed when sham groups were compared with CLP groups at both 12 and 24 hours. Significant difference (P<0.001) was also observed when CLP groups were compared with metformin-treated groups at both 12 and 24 hours (Fig.1).

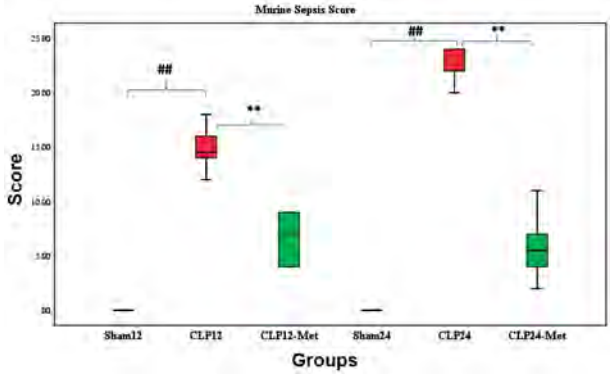

Fig.1: Effect of metformin administration on sepsis severity. Following treatment with metformin 50 mg/kg, sepsis severity was reduced 12 and 24 hours post CLP, as determined by a murine sepsis scoring method. Statistical evaluation of results using Kruskal Wallis's ANOVA followed by Dunn's post hoc revealed a significant difference among the groups for MSS (P<0.001). Values are median and interquartile range. A significant difference was observed between Sham and CLP groups, and between CLP and metformin-treated groups.
CLP; Cecal ligation and puncture, ##; P<0.01 for Sham12 versus CLP12, **; P<0.01 for CLP12 versus CLP12-Met, ##; P<0.01 for Sham24 versus CLP24, and **; P<0.01 for CLP24 versus CLP24-Met, n=6.

Metformin decreased lactate and HMGB1 levels and platelet lymphocyte ratio following cecal ligation and puncture-induced sepsis

Figure 2 presents the changes associated with blood lactate, PLR, and HMGB1 after metformin administration, measured 12- and 24-hour post CLP. No statistically significant difference was observed among the groups after 12 hours in blood lactate (Fig.2A). However, 24 hours post CLP, blood lactate significantly increased when compared with sham (P<0.01). Metformin 50 mg/kg significantly (P<0.01) decreased blood lactate. The PLR was calculated from platelets and lymphocytes count taken 12 and 24 hours after CLP. The PLR values obtained were similar between sham12, CLP12, and CLP-Met12 groups, but 24-hour post CLP, a significant (P<0.001) increase in CLP24 group compared with sham24 was observed. A significant (P<0.001) decrease in metformin-treated group (CLP-Met24) compared with CLP24 group, was also observed (Fig.2B). No significant difference in HMGB1 concentration was observed among the groups. After 24 hours, a significant (P<0.001) increase was observed in CLP group compared with sham (Fig.2C). Metformin treatment did not significantly decrease HMGB1 concentration in CLP rats.

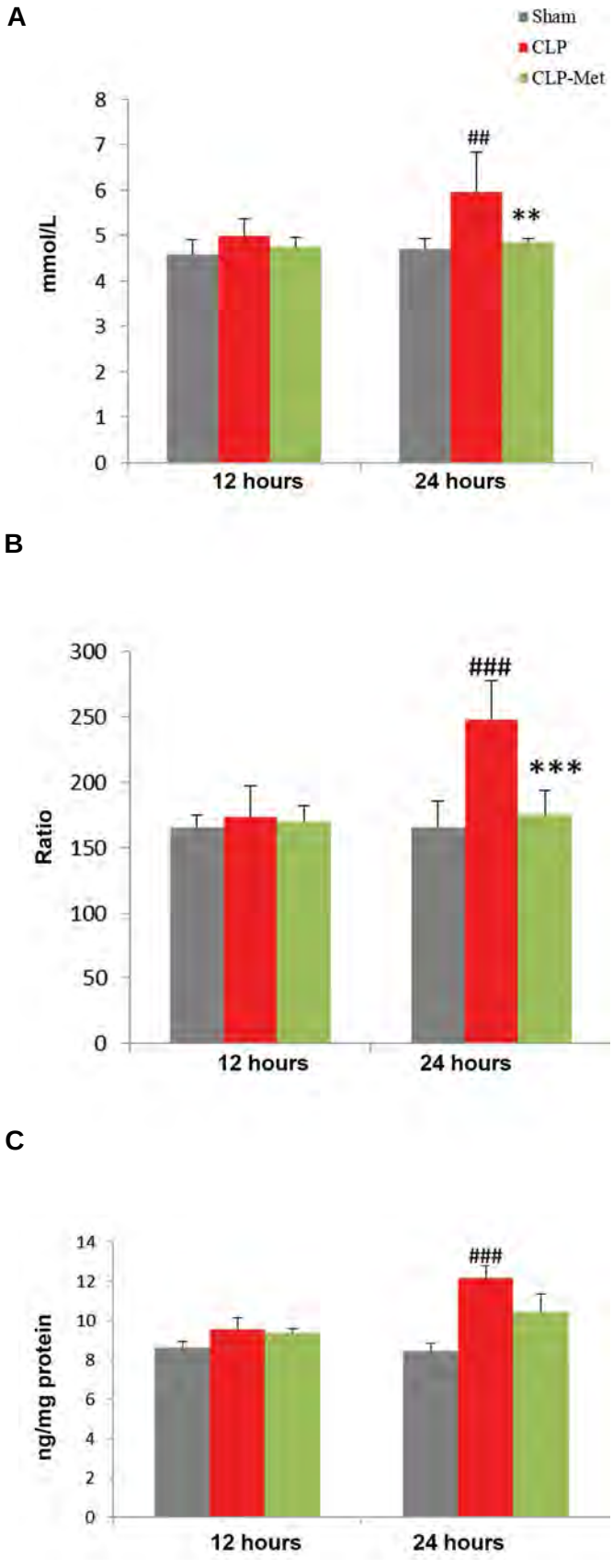

Fig.2: Effect of metformin administration on blood lactate and HMGB1 levels and PLR. **A.** CLP increased blood lactate, **B.** PLR, and **C.** HMGB1 in rats. Values are expressed as mean ± SD, n= 6. Statistical evaluation of results using one-way ANOVA revealed a significant difference among the groups for blood lactate levels (P<0.001), PLR (P<0.001), HMGB1 (P<0.001).
PLR; Platelet lymphocyte ratio, CLP; Cecal ligation and puncture, ##; P<0.01, ###; P<0.001 as CLP compared with sham, **; P<0.01, and ***; P<0.001 between metformin-treated group and the CLP.

Metformin improved blood brain barrier function following cecal ligation and puncture-induced sepsis

Figure 3 presents the expression of tight junction proteins after metformin treatment using real time RT-PCR. Metformin increased the expression of claudin 3 and 5 following a reduction induced by sepsis. No statistically significant difference was observed in the expressions of both *Cldn3* (Fig.3A) and *Cldn5* (Fig.3B) 12 hours post CLP. However, 24 hours post CLP, a significant decrease (P<0.01) was observed in *Cldn3* expression when sham was compared to CLP, but a significant increase was observed when CLP was compared with metformin treated group. For *Cldn5* expression, a significant difference (P<0.001) was observed when sham was compared with CLP group, and a significant (P<0.001) increase in metformin-treated group when compared with CLP group 24 hours post CLP.

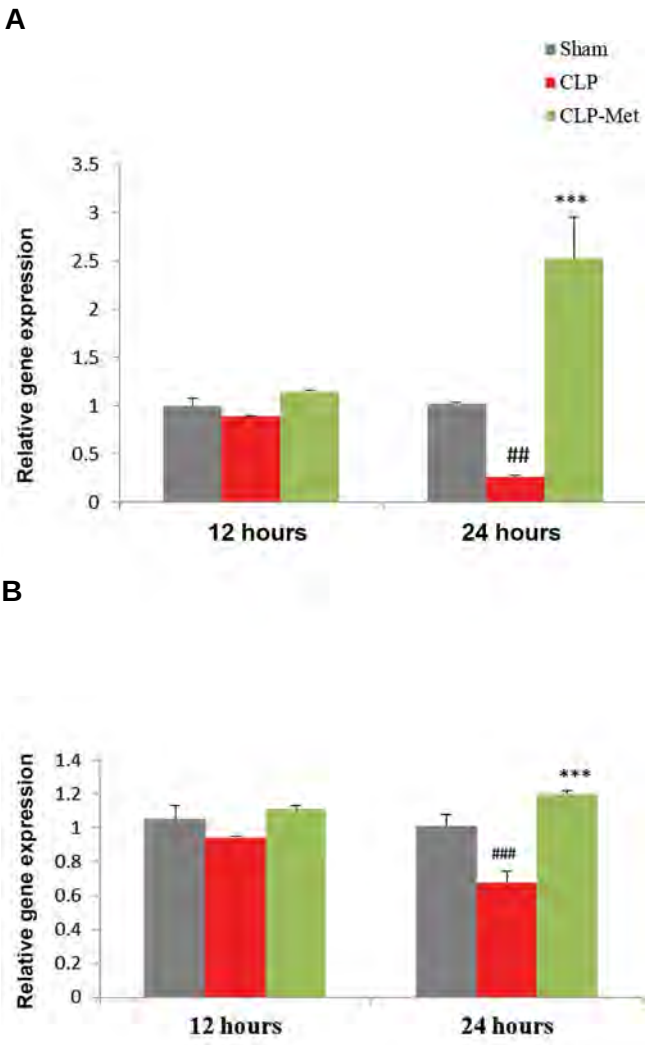

Fig.3: Effect of metformin administration on *Cldn3* and *Cldn5* gene expressions. CLP decreased **A.** *Cldn3* and **B.** *Cldn5* expression in rats. Values are expressed as mean ± SD. Statistical evaluation of results using one-way ANOVA, revealed a significant difference between groups for *Cldn3* (P<0.001), and *Cldn5* (P<0.001).
CLP; Cecal ligation and puncture, ##; P<0.01, ###; P<0.001 as CLP compared with sham, and ***; P<0.001 between metformin-treated group and CLP.

Metformin attenuated brain injury following cecal ligation and puncture-induced sepsis

Figure 4 presents changes in specific brain injury markers after metformin treatment. The expression levels of *S100b*, *Nse*, and *Gfap* were determined using real time RT-PCR. The expression of *S100b* (Fig.4A) was significantly increased (P<0.01 and P<0.001) in CLP (12 and 24 hours) compared to sham (12 and 24 hours) groups respectively. A significant (P<0.05 and P<0.001) decrease was observed in CLP groups compared to metformin-treated groups 12- and 24-hour post CLP, respectively. The expression of *Nse* was significantly increased (P<0.01 and P<0.001) in CLP groups compared to sham and significantly decreased (P<0.01 and P<0.001) in metformin-treated groups compared to CLP groups 12 and 24 hours after CLP (Fig.4B). The expression of *Gfap* was significantly increased (P<0.001) in CLP groups compared to sham 12 and 24 hours (Fig.4C). Metformin significantly decreased (P<0.001) the expression of *Gfap* compared to CLP groups 12 and 24 hours post CLP.

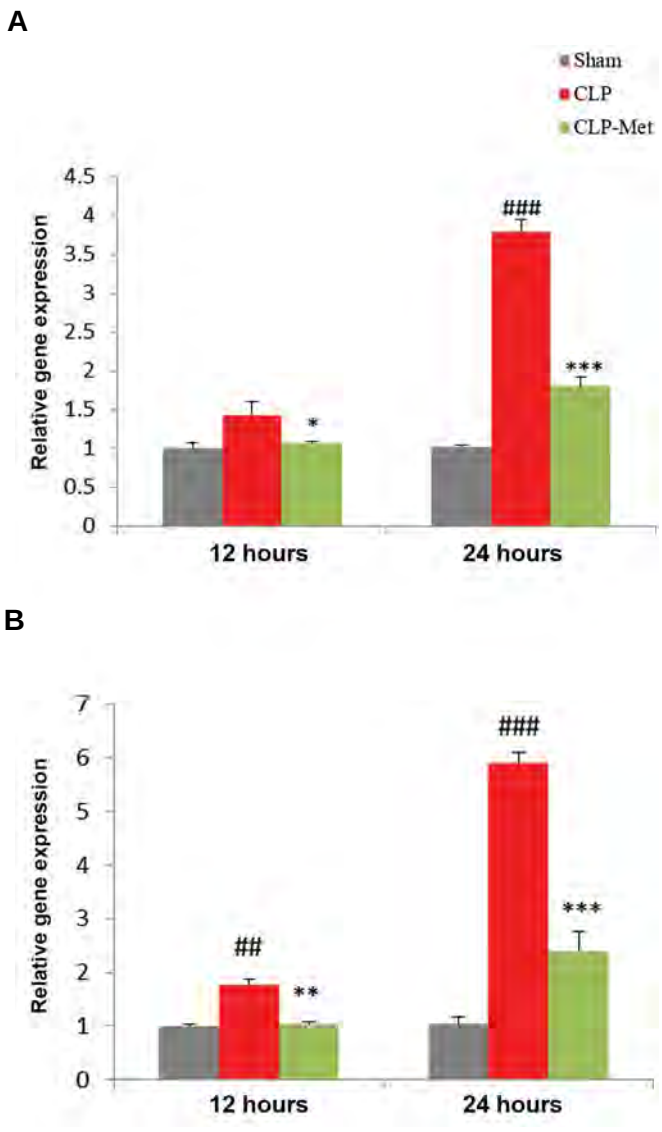

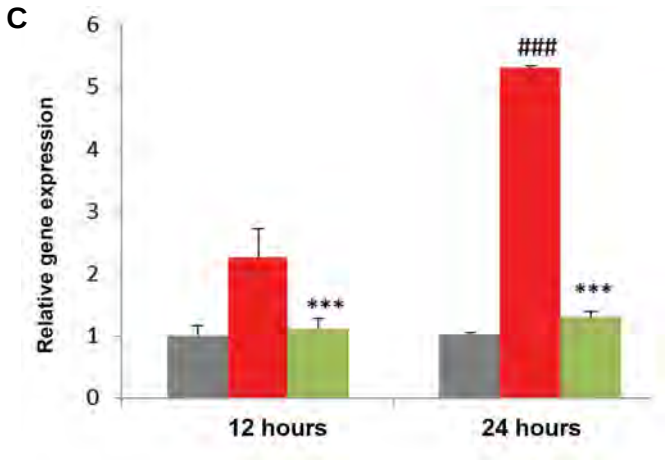

Fig.4: Effect of metformin administration on *S100b*, *Nse*, and *Gfap* gene expressions. **A.** S1006, **B.** Nse and **C.** Gfap. Values are expressed as mean ± SD, (n=6). Statistical evaluation of results using one-way ANOVA revealed a significant difference between groups for *S100b* (P<0.001), *Nse* (P<0.001), and *Gfap* (P<0.001).
CLP; Cecal ligation and puncture, ##; P<0.01, ###; P<0.001 between CLP and sham, *; P<0.05, **; P<0.01, and ***; P<0.001 between metformin-treated group and the CLP.

Metformin improved brain damage caused by the cecal ligation and puncture-induced sepsis

All H&E-stained brain sections from different experimental groups were evaluated histologically. The histopathological micrographs of brain sections in sham group were normal without any histopathological changes. Cerebral hemorrhage and meningitis were observed in the cerebrum 12 hours after CLP. In the 24 hour post-CLP group, meningitis, cerebral necrosis, and infiltration of inflammatory cells were observed. Micrographs of the brain sample in the metformin-treated groups both 12 and 24-hour post CLP, showed normal hippocampus, cerebral cortex, and cerebellum (Fig.5).

Correlations

Correlation analysis between MSS and lactate as markers of sepsis severity, and PLR, and HMGB1 as inflammatory markers; and *Cldn3*, *Cldn5*, *S100b*, *Nse*, and *Gfap* as brain injury markers, are shown in Table 1. By using the Pearson correlation, it was observed that a statistically significant correlation exists between lactate and inflammatory markers (r=0.983, 0.914, P<0.01, P<0.001) and lactate and brain injury markers (r=0.975, 0.974, 0.992, P<0.001, P<0.001). A negative correlation with *Cldn5* (r=-0.868, P<0.05) was observed, while none was observed with *Cldn3* (r=-0.518). A statistically significant correlation was observed between MSS and lactate, inflammatory, and brain injury markers except for claudin 3 and 5 (r=0.928, 0.812, P<0.05, P<0.01).

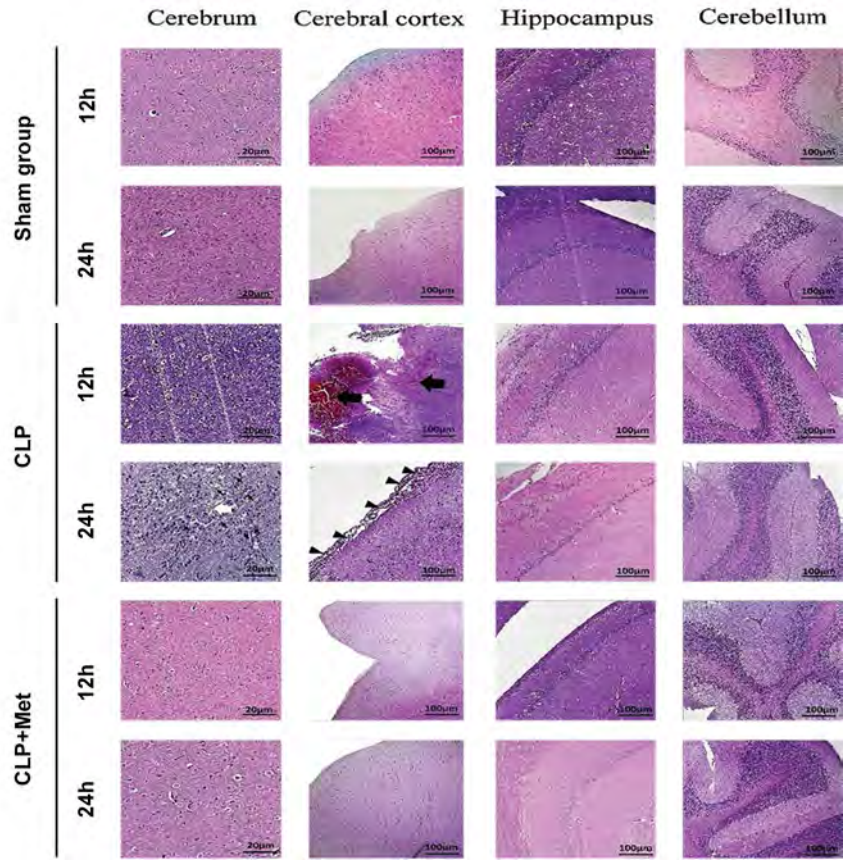

Fig.5: Effect of metformin administration on the morphology of the brain in cecal ligation and puncture (CLP)-induced sepsis. Cerebellum, cerebrum, cerebral cortex, and the hippocampus stained with H&E demonstrating cerebral hemorrhage, necrosis, and infiltration of inflammatory cells. Black thick arrows, white arrows, and thin arrows indicate cerebral hemorrhage, accumulation of inflammatory cells, and infiltration of inflammatory cells (meningitis), respectively. Magnification for cerebrum is ×400 while that of cerebral cortex, hippocampus, and cerebellum is ×200 [scale bars: 20 µm (cerebrum), and 100 µm (cerebral cortex, hippocampus, and cerebellum].

Table 1: Correlation analysis for murine sepsis score (MSS), lactate, inflammatory and brain injury markers

Parameters	Pearson correlation (r)	Lactate (mmol/L)	MSS
Lactate (mmol/L)	R	1	0.928##
	P value		0.01
MSS	R	0.908#	1
	P value	0.05	
PLR	R	0.983###	0.812#
	P value	0.001	0.050
HMGB1	R	0.914#	0.812#
	P value	0.05	0.050
Cldn3	R	-0.465	-0.518
	P value	0.353	0.292
Cldn5	R	-0.868#	-0.522
	P value	0.05	0.288
S100b	R	0.975##	0.812#
	P value	0.001	0.050
Nse	R	0.974##	0.812#
	P value	0.001	0.050
Gfap	R	0.992###	0.928##
	P value	0.001	0.01

#, ##, and ###; Pearson correlation is significant at the level of P<0.05, P<0.01, and P<0.001 (2 tailed), respectively.

Discussion

The present work investigated the effects of metformin on SAE using the CLP sepsis model. The results showed that CLP significantly increased murine sepsis score, and induced inflammation enough for disrupting the BBB and ultimately causing brain injury because of the release of various inflammatory and brain injury biomarkers. However, treatment with metformin 50 mg/kg reduced the inflammation, and improved brain damage, and BBB function thereby attenuating brain injury.

Microcirculatory failure, endothelial activation, BBB disruption, neuroinflammation, and altered brain signaling are complex mechanisms involved in SAE (19). Brain signaling is important in detecting the presence of chemicals released by microorganisms. Circumventricular organs and the vagus nerve are the pathways involved in neuroimmune communications where systemic inflammation is detected via toll-like receptors, CD14, and cytokine receptors, and visceral inflammation via axonal cytokine receptors (20). Neurotoxic substances such as nitric oxide, reactive oxygen species (ROS), cytokines, and glutamate result in cell death within the brain, which is a consequence of cytokine-induced microglial activation (21). Inflammatory cytokines such as tumor necrosis factor-alpha (TNF-α), interleukins, and HMGB1 are crucial in endothelial damage, BBB dysfunction, neuronal damage, and brain cell death (22, 23). In sepsis, microglial and astrocyte activation was linked with the release of inflammatory cytokines, including TNF-α and HMGB1 (23, 24). The BBB prevents neurotoxic substances such as cytokines and ROS from reaching the brain and its breakdown is associated with brain injury and edema which are common features of SAE (25).

The BBB consists of important tight junction proteins present in endothelial cells that regulate the movement of substances. In neurological diseases, the concentration of these proteins is dramatically reduced and this leads to BBB disruption (26). The consequences of BBB disruption involve the passage of neurotoxic substances which interact with brain cells and cause brain injury. Specific proteins in the brain cells such as S100B and GFAP, are released into plasma or cerebrospinal fluid (CSF) during brain injury (27).

CLP model is a gold standard in sepsis research, and it is resulted from polymicrobial infectious origin and closely related to human sepsis (14). Therefore, the beneficial effects of metformin in sepsis may give the researchers insight on how it may work in humans by inhibiting or preventing the deleterious responses associated with the disease.

Metformin was shown to be protective in sepsis. It was reported that metformin is effective in different models of sepsis mainly by inhibiting inflammation, oxidative stress, and apoptosis (12, 13). HMGB1 is implicated in infectious diseases during inflammatory response and tissue damage (28). In sepsis, increased circulating HMGB1 was shown to be associated with apoptosis and decreased survival rate. It is released in response to infection as an inflammatory cytokine and further stimulates an inflammatory response with subsequent tissue damage (29). HMGB1 was shown to cause microglial activation and cognitive dysfunction in lipopolysaccharide (LPS)-treated mice (22). Platelets accumulation was shown to result in organ failure through causing excessive inflammation, disseminated intravascular coagulation (DIC), and microthrombosis in sepsis (30). Platelets initiate inflammation by recruiting neutrophils and other cells to the site of infection or injury (31). This has made platelets important in detecting inflammation in sepsis. PLR is a new and cheap marker of inflammatory response (17). It has been used to detect the early onset of sepsis (32). The inhibitory effects of metformin on inflammation in lipopolysaccharide-treated cells and endotoxemia in mice were shown to be induced by inhibiting the release of HMGB1 a prominent pro-inflammatory cytokine and damage associated molecular pattern (DAMP) (33). In the present study, we found that metformin treatment inhibited inflammatory response by decreasing PLR and HMGB1 levels.

Hyperlactatemia is an important marker of sepsis severity and mortality. Decreased lactate clearance during sepsis was reported as a major cause of hyperlactatemia

(28). Sepsis is believed to cause lactate accumulation by affecting pyruvate dehydrogenase (PDH), an enzyme responsible for the conversion of lactate to pyruvate. A human study reported significant declines in PDH during sepsis that was believed to be responsible for lactate accumulation (34). A distinctive feature of sepsis is impaired microcirculation with concomitant increase in lactate level (35). In the present study, we found that in CLP rats, blood lactate levels significantly increased but reduced by metformin administration. Since hyperlactatemia in sepsis depicts sepsis severity and mortality, the decreased MSS scores observed in metformin-treated groups compared to CLP, may be an indication of metformin's ability to improve sepsis outcome. MSS was shown to exhibit high specificity in predicting sepsis severity and mortality (15).

Furthermore, BBB breakdown and brain injury are important features of SAE which occur as a result of the release of inflammatory mediators and ROS (25). Sepsis was shown to significantly alter the levels of tight junction proteins which are important components of the BBB (14, 36). Agents with anti-inflammatory and anti-oxidant properties have been shown to preserve BBB integrity during sepsis by increasing the concentrations of these proteins (36). Activation of the microglial and astrocytes associated with cytokine production, affects the BBB since they help in maintaining its integrity in conjunction with TJ and transport proteins (22, 24). Metformin attenuated brain injury in CLP mice by inhibiting the inflammatory response, oxidative stress, and apoptosis (13). In our study, the concentration of PLR and HMGB1 (inflammatory markers) was decreased by metformin administration. The expression of *Cldn3* and *Cldn5* decreased significantly after CLP. Metformin treatment improved BBB function as evidenced by the significant increases in *Cldn3* and *Cldn5* expression.

In sepsis, BBB impairment results in the passage of neurotoxic substances which can cause brain injury associated with the release of several markers that damage the astrocytes and neurons (27, 37, 38). The presence of S100B, NSE, and GFAP in the serum indicates a loss in the BBB integrity as they are almost completely produced in the brain (28). An elevated level of these proteins is associated with cytokine activation in sepsis (19, 37, 38). S100B, NSE, and GFAP have been used to diagnose sepsis-induced brain injury (39). Metformin through its anti-inflammatory effects, may prevent BBB breakdown and subsequent brain injury. In the present study, the expressions of *S100b*, *Nse*, and *Gfap* were significantly increased in CLP groups which indicated sepsis-induced brain injury. Metformin treatment decreased these expressions significantly. In this study, obtained results indicated that metformin may improve BBB function and attenuate brain injury, as evidenced by decreased inflammatory markers, increased levels of tight junction proteins, and decreased levels of brain injury markers, and brain damage.

The histopathological studies revealed the presence of cerebral hemorrhage, meningitis, and cerebral necrosis and infiltration of inflammatory cells in the CLP groups, which were abolished in metformin-treated groups. The results of histopathological studies confirmed the inhibitory effects of metformin on inflammatory and brain injury markers release.

The correlation data revealed a strong positive correlation between markers of sepsis severity (MSS and lactate) and inflammatory and brain injury markers but a negative correlation with *Cldn5*. The effectiveness of metformin administration was evidenced by its ability to decrease these markers (sepsis severity, inflammatory, and brain injury) and increase *Cldn3* and *Cldn5* expressions.

Conclusion

Metformin improved sepsis severity, and BBB function, and attenuated brain injury by decreasing sepsis score, lactate levels, inflammatory markers, and expression of brain injury markers, and increasing the expression of tight junction proteins. This study provides evidence on the potential therapeutic effects of metformin in SAE. As far as the authors are concerned, this study is the first document to report PLR and the neuroprotective effects of metformin that were mediated via the inhibition of *S100b*, *Nse*, and *Gfap* expression in a rat model of CLP-induced sepsis.

Acknowledgements

The study was funded in part by Tehran University of Medical Sciences with the code number 94-04-103-34890 received by Mojtaba Mojtahedzadeh. There is no conflict of interest in this study.

Authors' Contributions

M.M., M.A.; Were involved in study design, manuscript drafting and editing. F.I.H., T.D.; Were involved in experimental studies and drafting of the manuscript. M.B., M.G., M.N.-N, S.S., M.R., H.H.-A, M.K.; Were involved in primer design, animal work, real time RT-PCR, ELISA, and data analysis. Authors have read and approved the final manuscript.

References

1. Ely EW, Shintani A, Truman B, Speroff T, Gordon SM, Harrell FE Jr, et al. Delirium as a predictor of mortality in mechanically ventilated patients in the intensive care unit. JAMA. 2004; 291(14): 1753-1762.
2. Lacobone E, Bailly-Salin J, Polito A, Friedman D, Stevens RD, Sharshar T. Sepsis-associated encephalopathy and its differential diagnosis. Crit Care Med. 2009; 37(10 Suppl): S331-S336.
3. Tauber SC, Eiffert H, Brück W, Nau R. Septic encephalopathy and septic encephalitis. Expert Rev Anti Infect Ther. 2017; 15(2): 121-132.
4. Heming N, Mazeraud A, Verdonk F, Bozza FA, Chrétien F, Sharshar T. Neuroanatomy of sepsis-associated encephalopathy. Crit Care. 2017; 21(1): 65.
5. Sharshar T, Annane D, de la Grandmaison GL, Brouland JP, Hopkinson NS, Françoise G. The neuropathology of septic shock. Brain Pathol. 2004; 14(1): 21-33.
6. Ansari G, Mojtahedzadeh M, Kajbaf F, Najafi A, Khajavi MR, Khalili

H, et al. How does blood glucose control with metformin influence intensive insulin protocols? Evidence for involvement of oxidative stress and inflammatory cytokines. Adv Ther. 2008; 25(7): 681-702.
7. Pintana H, Apaijai N, Pratchayasakul W, Chattipakorn N, Chattipakorn SC. Effects of metformin on learning and memory behaviors and brain mitochondrial functions in high fat diet induced insulin resistant rats. Life Sci. 2012; 91(11-12): 409-414.
8. Wang J, Gallagher D, DeVito LM, Cancino GI, Tsui D, He L, et al. Metformin activates an atypical PKC-CBP pathway to promote neurogenesis and enhance spatial memory formation. Cell Stem Cell. 2012; 11(1): 23-35.
9. Jiang T, Yu JT, Zhu XC, Wang HF, Tan MS, Cao L, et al. Acute metformin preconditioning confers neuroprotection against focal cerebral ischaemia by pre-activation of AMPK-dependent autophagy. Br J Pharmacol. 2014; 171(13): 3146-3157.
10. Venna VR, Li J, Hammond MD, Mancini NS, McCullough LD. Chronic metformin treatment improves post-stroke angiogenesis and recovery after experimental stroke. Eur J Neurosci. 2014; 39(12): 2129-2138.
11. Mojtahedzadeh M, Abdollahi M, Didari T. Future of metformin administration in sepsis management. ACC. 2017; 3(1): 267-269.
12. Ghavimi H, Sheidaei S, Vaez H, Zolali E, Asgharian P, Hamishehkar H. Metformin-attenuated sepsis-induced oxidative damages: a novel role for metformin. Iran J Basic Med Sci. 2018; 21(5): 469-475.
13. Tang G, Yang H, Chen J, Shi M, Ge L, Ge X, Zhu G. Metformin ameliorates sepsis-induced brain injury by inhibiting apoptosis, oxidative stress and neuroinflammation via the PI3K/Akt signaling pathway. Oncotarget. 2017; 8(58): 97977-97989.
14. Rittirsch D, Huber-Lang MS, Flierl MA, Ward PA. Immunodesign of experimental sepsis by cecal ligation and puncture. Nat Protoc. 2009; 4(1): 31-36.
15. Shrum B, Anantha RV, Xu SX, Donnelly M, Haeryfar SM, McCormick JK, et al. A robust scoring system to evaluate sepsis severity in an animal model. BMC Res Notes. 2014; 7: 233.
16. Zhai X, Yang Z, Zheng G, Yu T, Wang P, Liu X, et al. Lactate as a potential biomarker of sepsis in a rat cecal ligation and puncture model. Mediators Inflamm. 2018; 2018: 8352727.
17. Qin B, Ma N, Tang Q, Wei T, Yang M, Fu H, Hu Z, Liang Y, Yang Z, Zhong R. Neutrophil to lymphocyte ratio (NLR) and platelet to lymphocyte ratio (PLR) were useful markers in assessment of inflammatory response and disease activity in SLE patients. Mod Rheumatol. 2016; 26(3): 372-376.
18. Livak KJ, Schmittgen TD. Analysis of relative gene expression data using real-time quantitative PCR and the 2(-Delta Delta C(T)) method. Methods. 2001; 25(4): 402-408.
19. Rothermundt M, Peters M, Prehn JH, Arolt V. S100B in brain damage and neurodegeneration. Microscopy Res Tech. 2003; 60(6): 614-632.
20. Akrout N, Sharshar T, Annane D. Mechanisms of brain signaling during sepsis. Curr Neuropharmacol. 2009; 7(4): 296-301.
21. Van Gool WA, van de Beek D, Eikelenboom P. Systemic infection and delirium: when cytokines and acetylcholine collide. Lancet. 2010; 375(9716): 773-775.
22. Terrando N, Rei Fidalgo A, Vizcaychipi M, Cibelli M, Ma D, Monaco C, et al. The impact of IL-1 modulation on the development of lipopolysaccharide-induced cognitive dysfunction. Crit Care. 2010; 14(3): R88.
23. Chaudhry N, Duggal AK. Sepsis associated encephalopathy. Adv Med. 2014; 2014: 1-16.
24. Alexander JJ, Jacob A, Cunningham P, Hensley L, Quigg RJ. TNF is a key mediator of septic encephalopathy acting through its receptor, TNF receptor-1. Neurochemistr Int. 2008; 52(3): 447-456.
25. Sharshar T, Carlier R, Bernard F, Guidoux C, Brouland JP, Nardi O, et al. Brain lesions in septic shock: a magnetic resonance imaging study. Intensive Care Med. 2007; 33(5): 798-806.
26. Nitta T, Hata M, Gotoh S, Seo Y, Sasaki H, Hashimoto N, et al. Size-selective loosening of the blood-brain barrier in claudin-5-deficient mice. J Cell Biol. 2003; 161(3): 653-660.
27. Zenaide PV, Gusmao-Flores D. Biomarkers in septic encephalopathy: a systematic review of clinical studies. Rev Bras Ter Intensiva. 2013; 25(1): 56-62.
28. Severin PN, Uhing MR, Beno DW, Kimura RE. Endotoxin-induced hyperlactatemia results from decreased lactate clearance in hemodynamically stable rats. Crit Care Med. 2002; 30(11): 2509-2514.
29. Huston JM, Wang H, Ochani M, Ochani K, Rosas-Ballina M, Gallowitsch-Puerta M, et al. Splenectomy protects against sepsis lethality and reduces serum HMGB1 levels. J Immunol. 2008; 181(5): 3535-3539.
30. de Stoppelaar SF, van't Veer C, van der Poll T. The role of platelets in sepsis. Thromb Haemost. 2014; 112(04): 666-677.
31. Sreeramkumar V, Adrover JM, Ballesteros I, Cuartero MI, Rossaint J, Bilbao I, et al. Neutrophils scan for activated platelets to initiate inflammation. Science. 2014; 346(6214): 1234-1238.
32. Can E, Hamilcikan S, Can C. The value of neutrophil to lymphocyte ratio and platelet to lymphocyte ratio for detecting early-onset neonatal sepsis. J Pediatr Hematol Oncol. 2018; 40(4): e229-e232.
33. Tsoyi K, Jang HJ, Nizamutdinova IT, Kim YM, Lee YS, Kim HJ, et al. Metformin inhibits HMGB1 release in LPS-treated RAW 264.7 cells and increases survival rate of endotoxaemic mice. Br J Pharmacol. 2011; 162(7): 1498-1508.
34. Nuzzo E, Liu X, Berg K, Andersen L, Doninno M. Pyruvate dehydrogenase levels are low in sepsis. Crit Care. 2015; 19 Suppl 1: P33.
35. Bakker J. Lactate levels and hemodynamic coherence in acute circulatory failure. Best Pract Res Clin Anaesthesiol. 2016; 30(4): 523-530.
36. Yeh CT, Kao MC, Chen CH, Huang CJ. Platonin preserves blood-brain barrier integrity in septic rats. Acta Anaesthesiol Taiwan. 2015; 53(1): 12-15.
37. Semmler A, Okulla T, Sastre M, Dumitrescu-Ozimek L, Heneka MT. Systemic inflammation induces apoptosis with variable vulnerability of different brain regions. J Chem Neuroanat. 2005; 30(2-3): 144-157.
38. Chen Q, Yu W, Shi J, Shen J, Gao T, Zhang J, Xi F, Li J, Li N. Insulin alleviates the inflammatory response and oxidative stress injury in cerebral tissues in septic rats. J Inflamm (Lond). 2014; 11: 18.
39. Nguyen DN, Spapen H, Su F, Schiettecatte J, Shi L, Hachimi-Idrissi S, et al. Elevated serum levels of S-100beta protein and neuron-specific enolase are associated with brain injury in patients with severe sepsis and septic shock. Crit Care Med. 2006; 34(7): 1967-1974.

Original Article

Investigating The Alterations of Oxidative Stress Status, Antioxidant Defense Mechanisms, MAP Kinase and Mitochondrial Apoptotic Pathway in Adipose-Derived Mesenchymal Stem Cells from STZ Diabetic Rats

Azadeh Aminzadeh, Ph.D.[1#], Neda Tekiyeh Maroof, M.Sc.[2#], Mehrnaz Mehrabani, Ph.D.[3], Kobra Bahrampour Juybari, Ph.D.[4], Ali Mohammad Sharifi, Ph.D. [2, 5*]

1. Department of Pharmacology and Toxicology, School of Pharmacy, Kerman University of Medical Sciences, Kerman, Iran
2. Razi Drug Research Center, Department of Pharmacology, School of Medicine, Iran University of Medical Sciences, Tehran, Iran
3. Physiology Research Center, Institute of Basic and Clinical Physiology Sciences, Kerman University of Medical Sciences, Kerman, Iran
4. Department of Pharmacology, Semnan University of Medical Science, Semnan, Iran
5. Department of Tissue Engineering and Regenerative Medicine, School of Advanced Technologies in Medicine, Iran University of Medical Sciences, Tehran, Iran

#These authors contributed equally to this work.

Corresponding Address: P.O.Box: 1449614535, Department of Tissue Engineering and Regenerative Medicine, School of Advanced Technologies in Medicine, Iran University of Medical Sciences, Tehran, Iran
Email: Sharifalim@gmail.com

Received: 23/May/2019, Accepted: 13/October/2019

Abstract

Objective: This study aimed to investigate the reliability of diabetic adipose-derived stem cells (ADSCs) for autologous cell-based therapies by exploring the functionality of signalling pathways involved in regulating oxidative stress and apoptosis.

Materials and Methods: In this experimental study, ADSCs were isolated from streptozotocin (STZ)-induced diabetic rats (dADSCs) and normal rats (nADSCs). The colonies derived from dADSCs and nADSCs were compared by colony-forming unit (CFU) assay. Reactive oxygen species (ROS) formation and total antioxidant power (TAP) were also measured. Furthermore, the expression of antioxidant enzymes, including catalase (*Cat*), superoxide dismutase (*Sod*)-1 and -3, glutathione peroxidase (*Gpx*)-1, -3 and -4 was measured at mRNA level by semi-quantitative reverse transcriptase polymerase chain reaction assay. The expression of Bax, Bcl2, caspase-3, total and phosphorylated c-Jun N-terminal kinase (JNK) and P38 Mitogen-Activated Protein Kinase (MAPK) at protein level was analyzed by western blotting.

Results: The results of this study indicated that viability and plating efficiency of dADSCs were significantly lower than those of nADSCs. ROS generation and TAP level were respectively higher and lower in dADSCs. The gene expression of antioxidant enzymes, including *Cat, Sod-1*, *Gpx-3* and *Gpx-4* in dADSCs was significantly greater than that in nADSCs. However, *Sod-3* and *Gpx-1* mRNA levels were decreased in dADSCs. Moreover, Bax/Bcl-2 protein ratio, caspase-3 protein expression and phosphorylation of JNK and P38 proteins were increased in dADSCs compared to nADSCs.

Conclusion: Taken together, diabetes might impair the cellular functions of dADSCs as candidates for autologous cell-based therapies. This impairment seems to be mediated by JNK, P38 MAPKs, and mitochondria pathway of apoptosis and partly by disruption of antioxidant capacity.

Keywords: Adipose-Derived Stem Cells, Antioxidant, Apoptosis, Cell Therapy, Diabetes

Cell Journal(Yakhteh), Vol 22, Suppl 1, Autumn 2020, Pages: 38-48

Citation: **Aminzadeh A, Tekiyeh Maroof N, Mehrabani M, Bahrampour Juybari K, Sharifi AM. Investigating the alterations of oxidative stress status, antioxidant defense mechanisms, MAP kinase and mitochondrial apoptotic pathway in adipose-derived mesenchymal stem cells from STZ diabetic rats. Cell J. 2020; 22 Suppl 1: 38-48. doi: 10.22074/cellj.2020.6958.**

Introduction

In type 1 diabetes, destruction of beta cells located in the pancreas, leads to elevated blood glucose levels and pathological changes in different organs (1). Currently, insulin therapy is the most common therapeutic strategy used for type 1 diabetes. Since, in some cases, insulin therapy could not properly control the progression of diabetes and its complications (2), other alternative therapies might be desirable (3, 4). Modern therapeutic approaches not only mitigate the symptoms of the disease but also improve organs' function. Stem cell therapy has been proposed as a promising therapeutic strategy for a number of degenerative disorders including type 1 diabetes (5).

Adipose derived stem cells (ADSCs) exhibit the ability to self-renew and differentiate into various functional cell types. Moreover, ADSCs have higher availability, require minimal invasive harvesting procedure and exert a larger yield as compared with other mesenchymal stem cells. Therefore, ADSCs are known as suitable candidates for cell therapy (6).

Oxidative stress is considered to play an important role in the development of various diseases including diabetes mellitus. Free radicals like superoxide radical (O_2^-) that are abundantly produced under diabetic conditions, may hamper the normal function of mesenchymal stem cells (7, 8). For example, it was shown that diabetes impeded the growth and differentiation ability of bone marrow mesenchymal stem cells (BMSCs) (9) and mitigated the angiogenic potential of ADSCs (10). In normal situations, natural enzymatic and non-enzymatic antioxidant defense system protects the body's organs against free radical damage. Free radicals could be eliminated by antioxidant enzymes, such as catalase (CAT), superoxide dismutase (SOD) and glutathione peroxidase (GPx) (11) which were shown to be affected by diabetes (12). There is controversial data in the literature regarding the effects of diabetes on antioxidant enzymes (13) that may be due to differences between organs or experimental conditions like the duration of diabetes induction (14, 15). Moreover, the involvement of mitogen-activated protein kinases (MAPKs) and Bcl-2 family in diabetes progression, was shown (16). MAPKs include c-Jun NH2-terminal kinases (JNK), P38 and extracellular signal-regulated kinase1/2 (ERK1/2) and play key roles in cell viability and death (17). The Bcl-2 family is engaged with apoptosis and survival control, and Bax and Bcl-2 are known as pro- and anti-apoptotic proteins, respectively (18). However, the effect of diabetes on MAPKs, Bcl-2 family and antioxidant enzymes in ADSCs, is still unknown. Therefore, the aim of the current study was to investigate diabetes-induced impaired mechanisms, in particular those related to regulation of oxidative stress and apoptosis, in ADSCs.

Materials and Methods

Fluorescein isothiocyanate (FITC)-conjugated CD90 and CD45 antibodies and purified anti-rat antibody to CD73 were purchased from BD Biosciences Pharmingen (San Diego, CA, USA). FITC-conjugated CD11b antibody was bought from GeneTex, Inc. (USA). FITC-conjugated CD31 and 44 antibodies were purchased from Serotec (Oxford, UK). Bax and Bcl-2 antibodies were bought from Abcam (Cambridge, UK). Horseradish peroxidase (HRP)-conjugated secondary antibody, caspase-3, β-actin, c-Jun N-terminal kinase (JNK), P38, Phospho-JNK and P38 antibodies were obtained from Cell Signaling (Danvers, MA, USA). 2, 4, 6-tri (2-pyridyl)-s-triazine (TPTZ) was bought from Merck (Germany) and 3-(4, 5-dimethylthiazol-2-yl)-2, 5-diphenyl tetrazolium bromide (MTT), streptozotocin (STZ), collagenase type I and 2, 7-dichlorofluorescein diacetate (DCF-DA) were bought from Sigma (Sigma Aldrich, St. Louis, MO, USA). All cell culture materials were obtained from Gibco (Carlsbad, CA, USA).

Animals, study design and induction of diabetes

In this experimental study, young male Wistar rats (200-250 g) were obtained from Pasteur Institute, Tehran, Iran and kept at room temperature (22 ± 2 ˚C) with humidity of 45-55% and 12:12 hours light-dark cycle. The experiment was conducted in accordance with the guidelines of the Ethics Committee of Iran University of Medical Sciences, based on National Institutes of Health Principles of Laboratory Animal Care (NIH Publications No. 8023, revised 1978). Two equal groups were randomly selected from 20 male Wistar rats. Control group was injected with a single intra-peritoneal injection of normal saline as solvent of STZ. Diabetic group was injected with a single intra-peritoneal injection of STZ (55 mg/kg) dissolved in normal saline. Blood glucose level was monitored 7 days later. Only rats with blood glucose levels of >300 mg/dl were considered diabetic and kept for four months. During this period, blood glucose levels were measured monthly. Levels of haemoglobin A1C (HbA1c) were tested in rats before being euthanized and only rats with an HbA1c≥ 6.5 were included.

Isolation and culture of adipose-derived stem cells

Rats were euthanized using ketamine/xylazine overdose and then, adipose tissues were obtained from epididymal fat pads of rats. Adipose tissues were minced, washed extensively in PBS (Sigma Aldrich, St. Louis, MO, USA) containing 5% antibiotic (100 U/ml penicillin and 100 µg /ml streptomycin) and digested using 0.075% collagenase I (prepared in PBS) at 37˚C for 30 minutes. After adding α-modified Eagle's medium (α-MEM), containing 10% fetal bovine serum (FBS, Gibco, Carlsbad, CA, USA) to neutralize collagenase, cell suspension was centrifuged at 2000 rpm for 10 minutes and the supernatant was discarded. Pellet was washed with PBS and filtered using 100 µm nylon mesh. Then, filtered fraction was centrifuged at 2000 rpm for 10 minutes and the pellet was incubated at 37˚C in 5% CO_2 with 95% humidity in the growth medium (α-MEM with 20% FBS and 100 U/ml penicillin and 100 µg /ml streptomycin). After 72 hours, non-adherent cells were removed and the growth medium was changed every 72 hours. All ADSCs used in this study, were from passage 3-4 (10).

Characterizations of adipose-derived stem cells

To characterize the phenotypes of the isolated ADSCs, the cultured ADSCs were harvested and stained with antibodies against CD44, CD73, CD90, CD45, CD11b and CD31. Cell phenotyping was performed using flow cytometry analysis by a FACS caliber cytometer (Becton Dickinson, San Diego, CA, USA).

Colony-forming unit assay

To compare the number of nADSCs- and dADSCs-derived colonies, CFU test was performed. Briefly, cells at early passages were cultured in 6-well plates. Two weeks later, all wells were washed with PBS and 5 ml of crystal violet solution (0.5% prepared in methanol) was added. After 30 min, wells were washed with PBS, and the numbers of colonies with a minimum of 50 cells were assessed using NIH Image J software (http://rsbweb.nih.

gov/ij). Then, plating efficiency was calculated according to the following formula:

Plating efficiency=The number of colony /number of cells plated×100.

MTT and propidium iodide assay

Propidium iodide (PI) staining and MTT assays were used to assess apoptosis and cell prolifration rate, respectively. dADSCs and nADSCs cells were seeded in 96-well plates. After 24, 48 and 72 hours, cells were exposed to MTT dye for 4 hours. Subsequently, the media were discarded, and dimethyl sulfoxide (DMSO) was added. The absorbance was measured at 570 nm using a micro-plate reader. Cell proliferation rate was measured as percentage of control. In PI method, the cells were harvested and fixed in ethanol (70%) on ice for 4 hours. The cells were treated with RNase and incubated with PI staining solution. The stained cells were analyzed by flow cytometry (Becton and Dickinson Co., USA) (7).

Measurement of intracellular reactive oxygen species

DCFH-DA is a lipophilic compound that can pass through the plasma membrane. Intracellular ROS oxidizes non-fluorescent DCF-DA to the highly fluorescent 2′-7′-dichlorofluorescein (DCF). Briefly, nADSCs and dADSCs were harvested in 24-well plates for 72 hours. After discarding media and rinsing cells with PBS, ADSCs were incubated with DCF-DA for 30 minutes. For the last time, cells were washed with PBS and medium was added. Then, the absorbance of DCF was assessed at 485/20 (nm) excitation and 528/20 (nm) emission wavelength using a multi-detection microplate reader.

Measurement of total antioxidant power

In this assay, reduction of ferric tripyridyltriazine to a blue ferrous complex by samples, is considered an indicator of TAP. At first, 290 µl of fresh working solution (25 ml acetate buffer (300 mM), 2.5 ml TPTZ (2, 4, 6 tripyridyl-s-triazine) solution (10 mM in 40 mM HCl), and 2.5 ml $FeCl_3.6H_2O$) was added to 10 µl of cells supernatants. The mixture was incubated at 37˚C for 10 minutes and the absorbance of the blue complex between Fe^{2+} and TPTZ, was read at 593 nm (Bio-Tek ELX800, USA) (19).

Western blot analysis

Firstly, dADSCs and nADSCs were exposed to 1X RIPA lysis buffer that contained 10 µl protease and phosphatase inhibitor cocktail. The resultant mixture was centrifuged for 20 min at 15,000 g at 4˚C. Total protein concentration was determined by Bradford method (20). The supernatant was stored at -80˚C. Equal amount of samples (70 µg) was separated on 10-12% sodium dodecyl sulfate polyacrylamide gel electrophoresis (SDS-PAGE) gel. The proteins were transferred to a polyvinylidene fluoride (PVDF) membrane. It was followed by incubation with primary antibodies overnight at 4˚C and then, HRP-labeled secondary antibody for 1 hour. An enhanced chemiluminescence kit (Amersham Pharmacia Biotech, NJ, USA) was used to visualize the protein bands. β-actin was used as the internal control. Then, band density was quantified by total Lab software (UK) (21).

Semi-quantitative reverse transcriptase polymerase chain reaction

Total RNA was extracted from the nADSCs and dADSCs using *RNX*-PLUS kit (*Cinnagen*, Iran) according to the manufacturer's instructions. Afterwards, cDNA was synthesized using RNA (1 µg), oligo-dT primer (2 µg, Fermentase, USA) and MMLV (200 U, Fermentase, USA) in a total volume of 20 µl. Reaction was done at 42°C for 1 hour, and continued at 72°C for 10 minutes. Finally, polymerase chain reaction (PCR) reaction was done using cDNA (5 µl) and specific primers (Table 1). *β-actin* was used as the internal control. Final products were run on agarose gels (2%) and stained with Nancy-2*5*0. Then, band was quantified by total lab software (UK).

Table 1: Primers used for semi-quantitative reverse transcriptase polymerase chain reaction

Gene	Primer sequence (5′-3′)	Product size (bp)
Cat	F: GGTAACTGGGACCTTGTGGG	222
	R: GCCATTCATGTGCCGATGTC	
Sod1	F: AAGCGGTGAACCAGTTGTGG	187
	R: ATTGCCCAGGTCTCCAACAT	
Sod3	F: GCTTGTCAGGTGTGGAACC	172
	R: CAGGTCTTTGGAGTGCGTG	
Gpx1	F: ACCGTGTATGCCTTCTCC	221
	R: TTGCCATTCTCCTGATGTCC	
Gpx3	F: ACCATCTGTGCTCACGGTTT	187
	R: GAAGGAGGTGGTGGCATAG	
Gpx4	F: GGAGCCCCAGGTGATAGAG	137
	R: CTGGTTTTCAGGCAGACCGT	
β-actin	F: TGTCCACCTTCCAGCAGATGT	101
	R: AGCTCAGTAACAGTCCGCCTAGA	

Statistical analysis

Data are presented as the mean ± S.E.M. Data were analyzed by unpaired student's t test for comparisons between two groups. A $P<0.05$ was considered statistically significant. All data were analyzed by Graphpad Prism 5.0.

Results

Flow cytometry analysis of CD markers

Phenotype of nADSCs or dADSCs was confirmed by flow cytometry analysis. The cell surface markers including CD44, CD73 and CD90, were positive while CD45, CD11b and CD31 were negative. These results indicated that the cultured cells could be considered mesenchymal stem cells (Fig.1A).

Effect of diabetes on plating efficiency of dADSCs and nADSCs

CFU assays demonstrated that plating efficiency of dADSCs (9 ± 0.57) was remarkably lower than that of nADSCs (12.33 ± 0.66, P<0.05, Fig.1B, C).

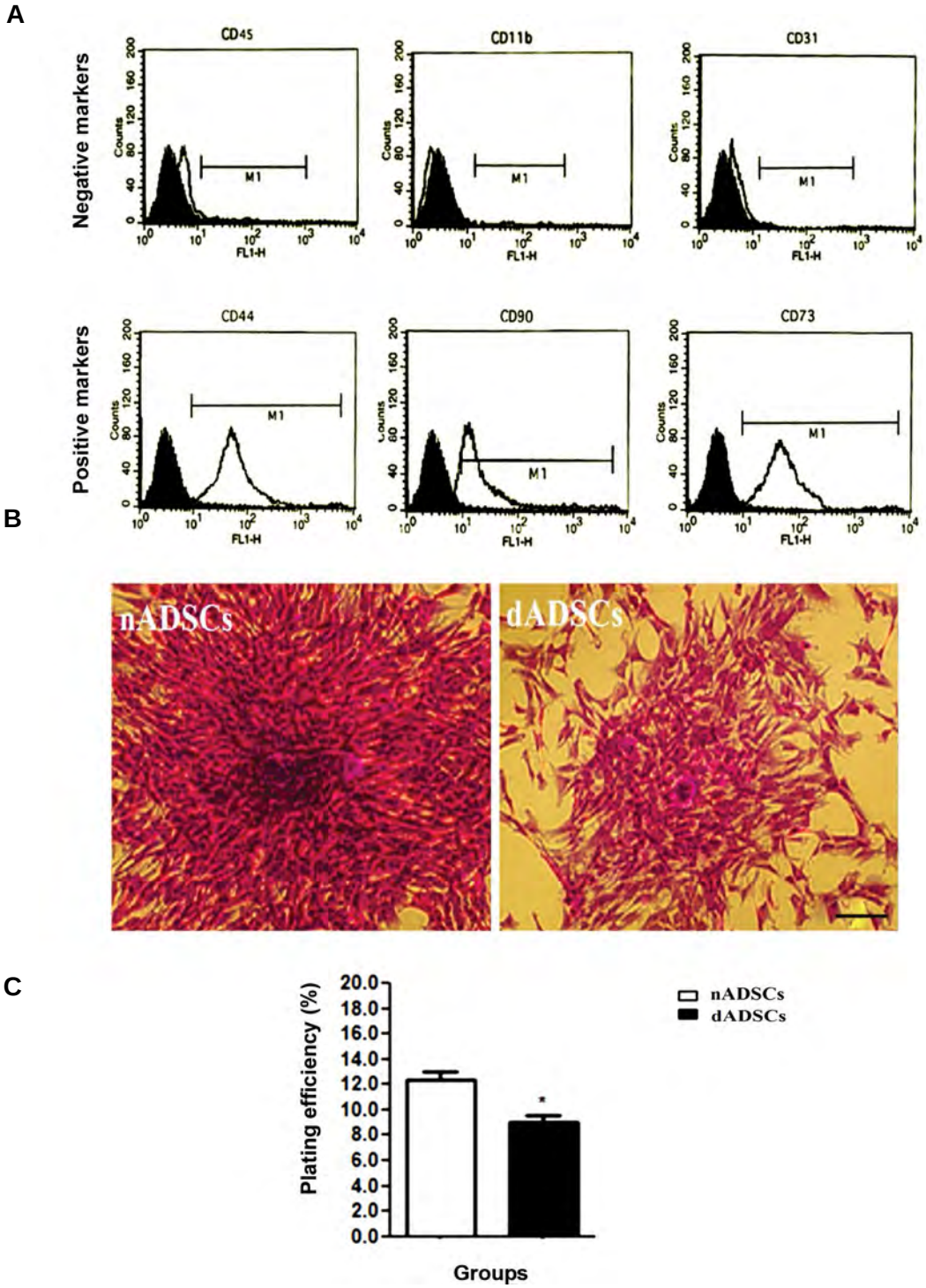

Fig.1: Identification of ADSCs and assessment of their plating efficiency. **A.** Flow cytometry analysis showed that surface markers including CD44, CD73 and CD90 were positive. While CD45, CD11b and CD31 were negative. **B.** Representative images of colonies derived from nADSCs and dADSCs, obtained by light microscopy. **C.** Assessment of plating efficiency of nADSCs and dADSCs. Results are shown as the mean S.E.M (n=3). *; P<0.05 shows significant differences versus control, nADSCs; Normal adipose-derived mesenchymal stem cells, and dADSCs; Diabetic adipose-derived mesenchymal stem cells.

Effect of diabetes on cell proliferation rate and apoptosis

nADSCs and dADSCs were cultured for 24, 48 and 72 hours and proliferation rate was measured. As shown in Figure 2A, the proliferation rate of dADSCs was significantly lower when compared with nADSCs after 72 hours incubation (P<0.001). To determine the effects of diabetes on cell apoptosis, PI staining was conducted. As shown in Figure 2B, diabetes pushed cells to commit apoptosis.

Effect of diabetes on intracellular reactive oxygen species and total antioxidant power level

As shown in Figure 2C, diabetes significantly increased DCF fluorescence as compared with the control group (P<0.05). Figure 2D shows that TAP value decreased in the diabetic group as compared with the control group (P<0.01).

Effects of diabetes on Bax and Bcl-2 protein levels and caspase-3 activation

The protein expression of Bax and Bcl-2 and cleaved caspase-3 was measured by western blotting. As shown in Figure 3A, the results revealed that Bax/Bcl-2 ratio in dADSCs was significantly greater than that in nADSCs (P<0.001). Furthermore, as previously shown, active form of caspases is produced by proteolytic cleavage (22). Hence, we examined cleaved caspase-3 protein expression. Results indicated that cleaved caspase-3 levels markedly increased in dADSCs as compared with nADSCs controls (P<0.001, Fig.3B).

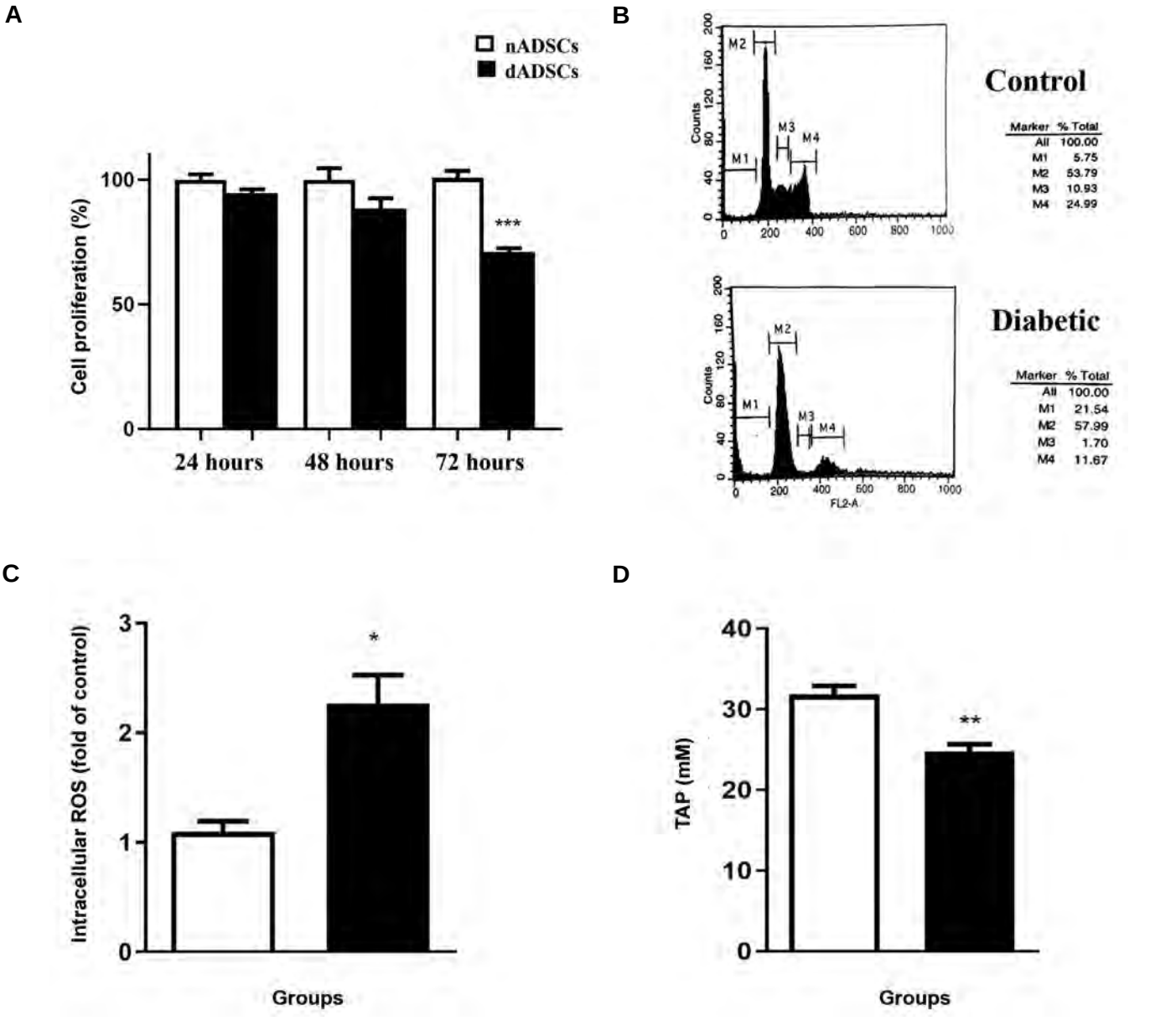

Fig.2: Effect of diabetes on proliferation rate, apoptosis and antioxidant status of ADSCs. **A.** Effect of diabetes on proliferation rate of ADSCs. **B.** Effect of diabetes on apoptosis rate of ADSCs; Sub-G_1, G_1, S and G_2/M phases were separated by gates M1, M2, M3 and M4, respectively. **C.** ROS formation and **D.** Total antioxidant power. Results are shown as the mean S.E.M (n=3).
*; P<0.05, **; P<0.01, and ***; P<0.001 Show significant differences versus controls, ADSCs; Adipose-derived stem cells, and ROS; Reactive oxygen species.

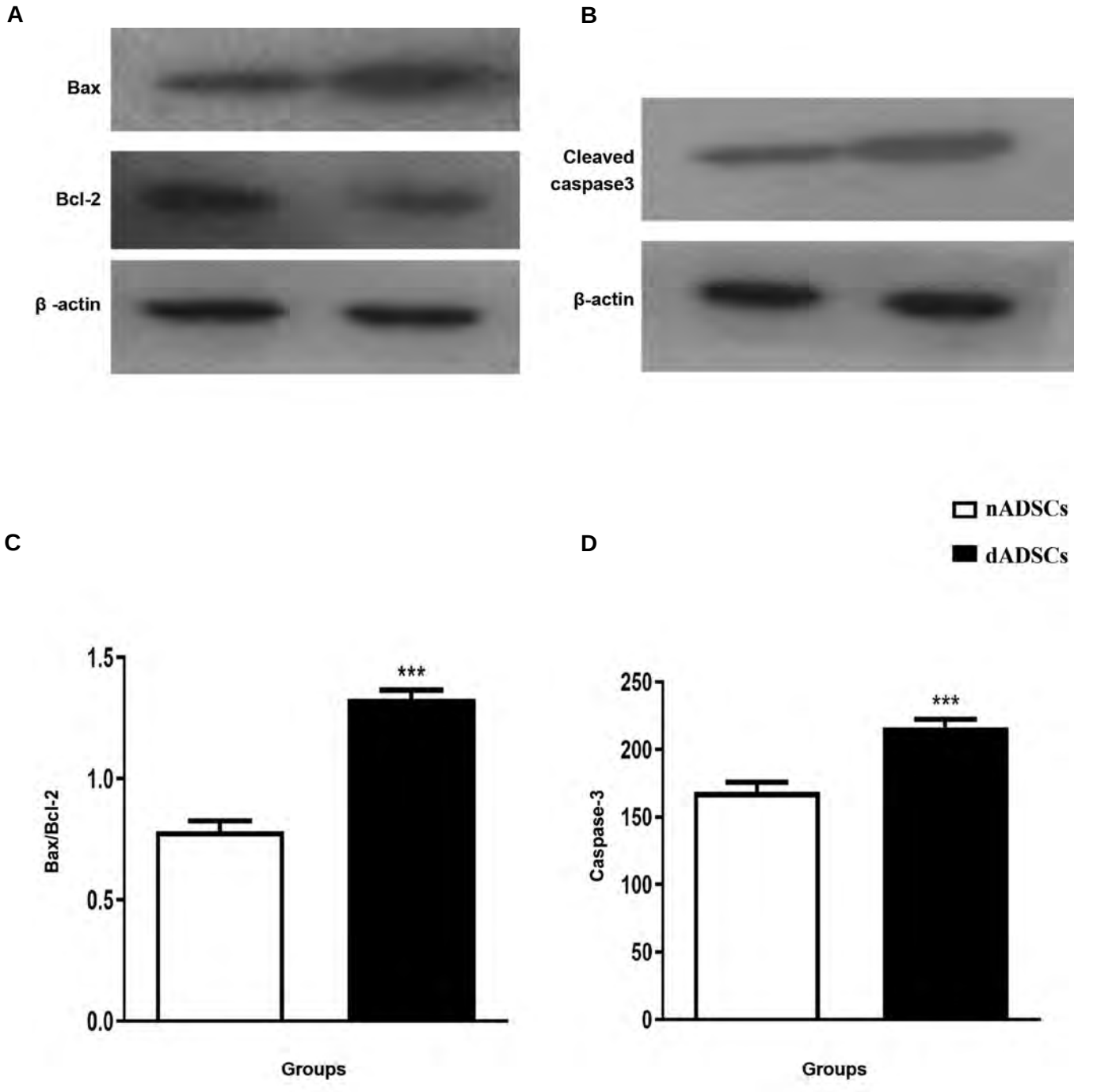

Fig.3: Effects of diabetes on the Bax/Bcl-2 proteins ratio and cleaved caspase-3 protein. Effects of diabetes on the **A.** Bax/Bcl-2 proteins ratio, and **B.** Cleaved caspase-3 protein in nADSCs and dADSCs. Results are shown as the mean ± SEM (n=3).
***; P<0.001 Shows significant differences versus controls, nADSCs; Normal adipose-derived mesenchymal stem cells, and dADSCs; Diabetic adipose-derived mesenchymal stem cells.

Effects of diabetes on JNK and P38 MAPKs protein phosphorylation

Western blotting was performed to determine whether dADSCs had different expression of JNK and P38 compared to nADSCs controls. Current results revealed that phosphorylated JNK and P38 were significantly increased in dADSCs as compared with the controls (P<0.001). Total JNK and P38 protein levels did not differ between the two groups (Fig.4).

Effect of diabetes on mRNA levels of antioxidant enzymes

Antioxidant enzymes mRNA levels were measured by sqRT-PCR using gene-specific primers (Table 1). A significant decrease in *Sod-3* (P<0.001) and *Gpx-1* (P<0.05) mRNA levels was observed in dADSCs as compared with the control group. Furthermore, a significant increase in *Cat* (P< 0.001), *Sod-1* (P<0. 001), *Gpx-3* (P<0.05) and *Gpx-4* (P<0.001) mRNA levels was detected in dADSCs in comparison with the control group (Fig.5).

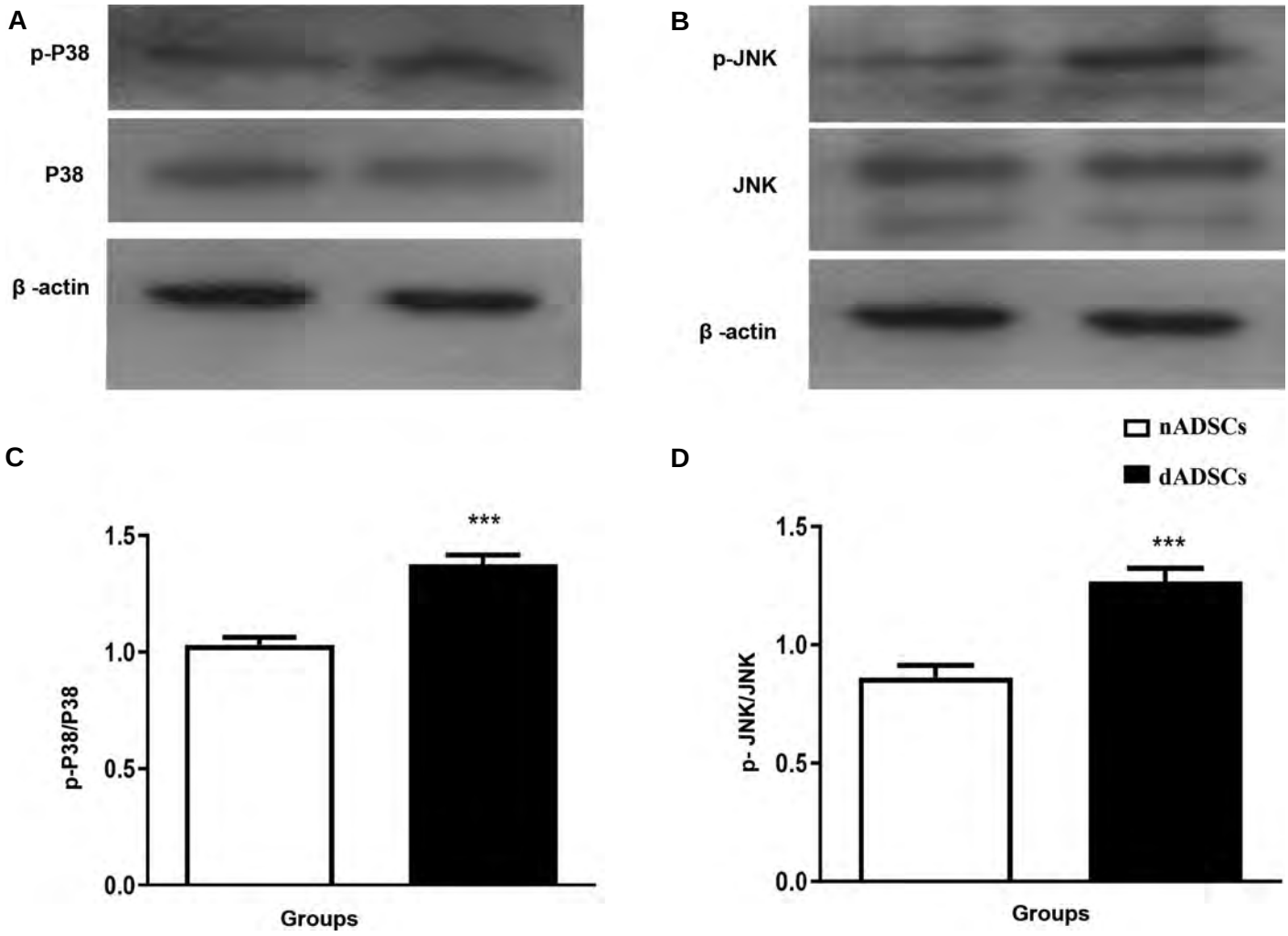

Fig.4: Effects of diabetes on phosphorylation of P38 and JNK MAPKs in nADSCs and dADSCs. **A.** The density of phosphorylated and total P38 were determined and the ratio was calculated. **B.** The density of phosphorylated and total JNK were determined and the ratio was calculated. Results are shown as the mean ± SEM (n=3). ***; P<0.001 shows significant differences versus controls, nADSCs; Normal adipose-derived mesenchymal stem cells, and dADSCs; Diabetic adipose-derived mesenchymal stem cells.

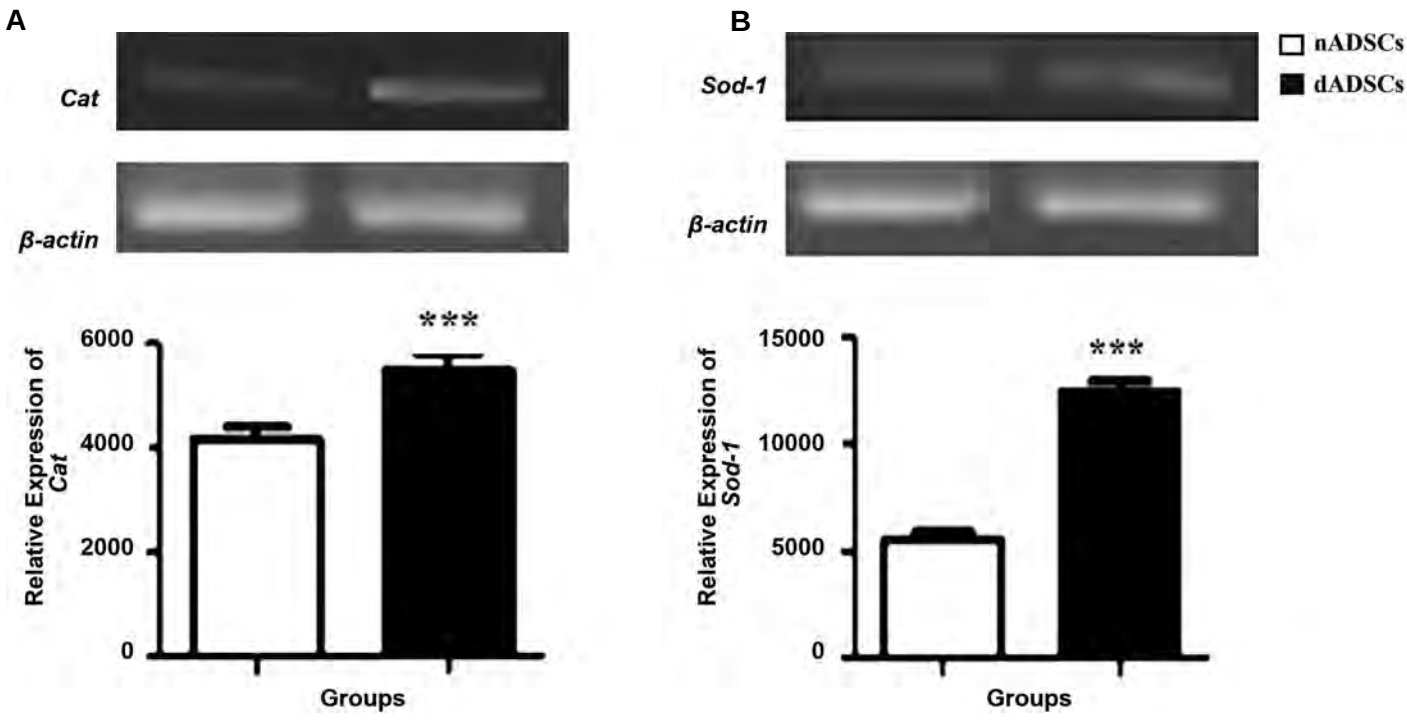

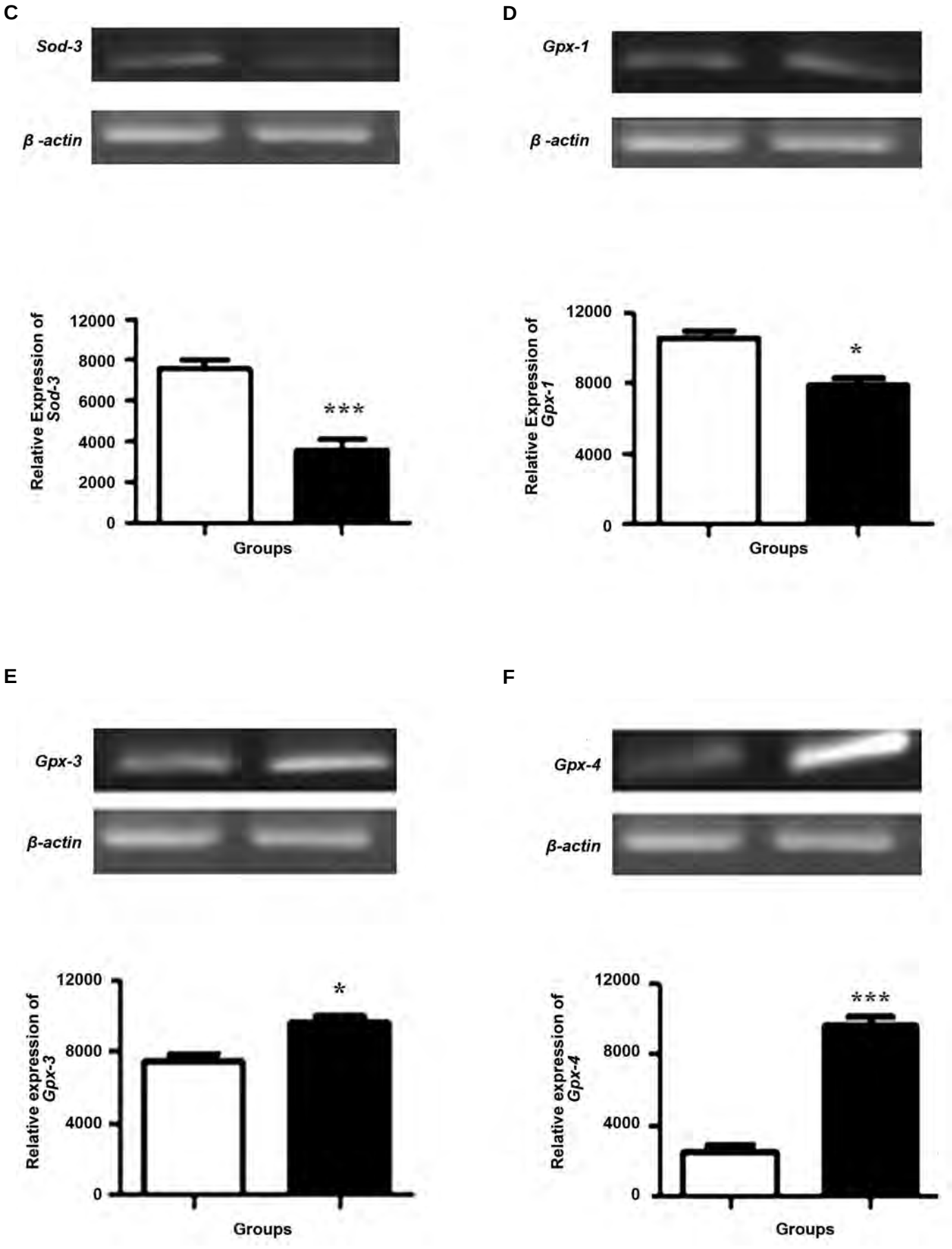

Fig.5: Effects of diabetes on relative mRNA expression level of antioxidant enzymes. Effects of diabetes on relative mRNA expression level of **A.** *Cat*, **B.** *Sod-1*, **C.** *Sod-3*, **D.** *Gpx-1*, **E.** *Gpx-3*, and **F.** *Gpx-4* in the dADSCs in comparison with the control group. Results are shown as the mean ± SEM (n=3).
*; P<0.05, ***; P<0.001 show significant differences versus controls, and dADSCs; Diabetic adipose-derived mesenchymal stem cells.

Discussion

The current study showed that proliferation rate and plating efficiency of dADSCs was considerably lower in comparison with nADSCs. Furthermore, ROS generation and TAP level in dADSCs were respectively higher and lower compared to those of nADSCs. The gene expression of antioxidant enzymes including *Cat, Sod-1, Gpx-3* and *Gpx-4* was significantly increased in dADSCs as compared with nADSCs. In contrast, *Sod-3* and *Gpx-1* mRNA levels were decreased in dADSCs. Bax/Bcl-2 protein ratio, cleaved caspase-3 protein and phosphorylation rate of JNK and P38 proteins were increased in dADSCs as compared with nADSCs.

Recently, stem cell therapy has been proposed as an appropriate alternative approach for treatment of various disorders including diabetes. However, diabetes could induce many changes at molecular levels in cells including stem cells causing serious functional impairment (10). Therefore, there is a need to identify intrinsic mechanisms disrupted by diabetes. Current study investigated the effect of diabetes-induced alterations in ADSCs isolated from diabetic rats to elucidate some signalling pathways involved in oxidative stress and consequently mitochondrial apoptosis.

Our results indicated that proliferation rate of dADSCs was lower than that of non-diabetic controls and apoptotic cell death in dADSCs was higher compared to nADSCs. This is in agreement with our previous report which demonstrated that diabetic stem cells showed significantly lower proliferation (10) rate. Furthermore, a higher apoptosis rate was shown for diabetic stem cells as compared with controls (23). In contrast, there is a report indicating similar proliferation rate in dADSCs and nADSCs of mice (24). However, differences between experimental conditions like duration of diabetes induction may cause this discrepancy.

It was also shown that higher ROS levels in diabetes may be linked to cell senescence and death (23). Excess production of ROS, an important apoptotic mediator, can cause organ injuries (25). Our results showed that ROS concentration was elevated in dADSCs. In agreement with our findings, a previous study showed that oxidative stress leads to impaired self-renewal of adult stem cells *in vitro* (26).

Under oxidative stress conditions, anti-oxidative enzymes such as CAT, SOD, and GPx act as a defense barrier against oxidative damages (27). Hydrogen peroxide is quickly reduced to superoxide by SOD which can be detoxified by activities of GPx and CAT (28). In this study, we found that total antioxidant capacity reduced in diabetic ADSCs, whereas there were various alterations in antioxidants enzyme mRNA expression. This result may emphasize the fact that the expressions of some of these enzyme have been elevated in response to oxidative stress in a compensatory manner to protect against the insult to the cells. In agreement with this result, a previous study demonstrated that mRNA levels of renal *Sod-1, Cat* and *Gpx* of diabetic rats enhanced as compared with controls (29). In opposite, a previous study performed on diabetic heart, showed that total SOD and total GPx expression/activity were declined whereas CAT expression/activity were enhanced (30). Moreover, another study conducted on the brain tissue demonstrated a significant decrease in mRNA transcription levels of *Sod, Cat,* and *Gpx* in the diabetic group compared to the controls (31).

Our results indicated that diabetes affects apoptotic pathways in dADSCs. In intrinsic pathway, Bax dimmers form mitochondrial membrane pores increase membrane permeability allowing the release of pro-apoptotic factors. Bcl-2 could form heterodimers with Bax, preventing oligomerization and pore assembly in mitochondrial membrane (32). Our results revealed that Bax/ Bcl-2 ratio significantly augmented in dADSCs. In line with these results, we previously demonstrated similar results indicating that high glucose levels can cause apoptosis through elevating Bax/Bcl-2 ratio in PC12 cells (18). Another study showed that in BMSCs from patients with systemic lupus erythematous, the levels of Bcl-2 expression were significantly decreased while the Bax expression was remarkably increased as compared with normal controls (18, 33). As final stage of apoptosis, caspase-3 is activated to induce DNA fragmentation and cell death (34). Our results demonstrated that diabetes could elevate the expression of caspase-3 as an ultimate determinant of apoptosis. A former study on PC12 cells demonstrated that high glucose levels increased the expression of caspase-3, caspase-8 and caspase-9 (35).

In addition to Bcl2 family and caspase, MAPKs containing JNK and P38 are important regulators of apoptosis. It was indicated that activation of JNK and P38 is involved in apoptosis induced by various cellular stresses (36). Moreover, it was shown that hyperglycemia could activate JNK and p38 in PC12 neuronal cell (37). Oxidative stress and apoptosis might be inhibited by preventing JNK and p38 phosphorylation. We demonstrated that p-JNK/JNK and p-P38/P38 were increased in dADSCs. This finding is in agreement with a previous study demonstrating a higher level of expression and activation of JNK and p38 in sural nerve of type I and II diabetic patients (38). Taking together, our results suggested that dADSCs showed an overall enhancement in various apoptotic pathways as compared with the controls. It was also suggested that oxidative stress and advanced glycation end products (AGES) are major factors contributing to alterations in MSCs (39).

To explain how this impairment could affect cellular function and lead to complications in diabetes, it is important to realize that, normal MSCs are present in various tissues and have the potential to differentiate into multiple cell types, playing a central role in maintaining tissue homeostasis under both physiological and pathological conditions (40). Moreover, it was previously shown that autologous ADSCs have the

ability to secret many potent angiogenic factors including vascular endothelial growth factor (VEGF), fibroblast growth factor (FGF), and insulin growth factor-1 (IGF-1) and may also play an important role in enhancement of angiogenesis and anti-apoptotic ability in diabetes (9, 10). Consequently, loss of action or functional impairment of dADSCs may be responsible for some of the diabetes complications.

Conclusion

It could be concluded that hyperglycemia might stimulate oxidative stress, resulting into ADSCs damage. Although the current study revealed a significant increase in most of mRNA levels of antioxidant enzymes in ADSCs from STZ-induced diabetic rats, the total antioxidant capacity reduced in these cells. It may be suggested that this compensatory response may no longer survive and hyperglycemia could induce apoptosis leading to impaired cellular functions causing ADSCs death. It may also be concluded that dADSCs may be unsuitable stem cell sources for cell therapy and it may also be speculated that other diabetes complications may possibly be associated with some of these impaired mechanisms.

Acknowledgements

This study was financially supported by a grant from Research section of Iran University of Medical Sciences (grant number: 24838). There is no conflict of interest in this study.

Authors' Contributions

A.A., M.M., N.T.M.; Contributed to data collection and analysis. A.A., K.B.J; Wrote the manuscript and contributed to data analysis. A.M.Sh.; Substantially contributed to the conception and design of the study. All authors read and approved the final manuscript.

References

1. Robertson RP. Chronic oxidative stress as a central mechanism for glucose toxicity in pancreatic islet beta cells in diabetes. J Biol Chem. 2004; 279(41): 42351-42354.
2. Nanji SA, Shapiro A. Advances in pancreatic islet transplantation in humans. Diabetes Obes Metab. 2006; 8(1): 15-25.
3. Vija L, Farge D, Gautier JF, Vexiau P, Dumitrache C, Bourgarit A, et al. Mesenchymal stem cells: Stem cell therapy perspectives for type 1 diabetes. Diabetes Metab. 2009; 35(2): 85-93.
4. Mehrabani M, Heidary M, Mehrabani M. Study of acute and chronic antihyperglycemic activity of methanolic extract of Salvia mirzayanii Rech. & Esfand. in rats. J Med Plants. 2010; 4(36): 106-116.
5. Weir GC, Cavelti-Weder C, Bonner-Weir S. Stem cell approaches for diabetes: towards beta cell replacement. Genome Med. 2011; 3(9): 61.
6. Baer PC, Geiger H. Adipose-derived mesenchymal stromal/stem cells: tissue localization, characterization, and heterogeneity. Stem Cells Int. 2012; 2012: 812693.
7. Mirzamohammadi S, Mehrabani M, Tekiyehmaroof N, Sharifi AM. Protective effect of 17β-estradiol on serum deprivation-induced apoptosis and oxidative stress in bone marrow-derived mesenchymal stem cells. Hum Exp Toxicol. 2016; 35(3): 312-322.
8. Mirzamohammadi S, Nematollahi MH, Mehrbani M, Mehrabani M. Ferulic acid pretreatment could improve prognosis of autologous mesenchymal stromal cell transplantation for diabetic neuropathy. Cytotherapy. 2016; 18(7): 925-927.
9. Jin P, Zhang X, Wu Y, Li L, Yin Q, Zheng L, et al. Streptozotocin-induced diabetic rat–derived bone marrow mesenchymal stem cells have impaired abilities in proliferation, paracrine, antiapoptosis, and myogenic differentiation. Transplant Proc. 2010; 42(7): 2745-2752.
10. Mehrabani M, Najafi M, Kamarul T, Mansouri K, Iranpour M, Nematollahi MH, et al. Deferoxamine preconditioning to restore impaired HIF-1α- mediated angiogenic mechanisms in adipose-derived stem cells from STZ- induced type 1 diabetic rats. Cell Prolif. 2015; 48(5): 532-549.
11. Mehrzadi S, Bahrami N, Mehrabani M, Motevalian M, Mansouri E, Goudarzi M. Ellagic acid: a promising protective remedy against testicular toxicity induced by arsenic. Biomed Pharmacother. 2018; 103: 1464-1472.
12. Maritim AC, Sanders RA, Watkins JB 3rd. Diabetes, oxidative stress, and antioxidants: a review. J Biochem Mol Toxicol . 2003; 17(1): 24-38.
13. Szaleczky E, Prechl J, Fehér J, Somogyi A. Alterations in enzymatic antioxidant defence in diabetes mellitus--a rational approach. Postgrad Med J. 1999; 75(879): 13-17.
14. Wohaieb SA, Godin DV. Alterations in free radical tissue-defense mechanisms in streptozocin-induced diabetes in rat. Effects of insulin treatment. Diabetes. 1987; 36(9): 1014-1018.
15. Kakkar R, Kalra J, Mantha SV, Prasad K. Lipid peroxidation and activity of antioxidant enzymes in diabetic rats. Mol Cell Biochem. 1995; 151(2): 113-119.
16. Allen DA, Yaqoob MM, Harwood SM. Mechanisms of high glucose-induced apoptosis and its relationship to diabetic complications. J Nutr Biochem. 2005; 16(12): 705-713.
17. Plotnikov A, Zehorai E, Procaccia S, Seger R. The MAPK cascades: signaling components, nuclear roles and mechanisms of nuclear translocation. Biochim Biophys Acta. 2011; 1813(9): 1619-1633.
18. Sharifi AM, Mousavi SH, Farhadi M, Larijani B. Study of high glucose-induced apoptosis in PC12 cells: role of bax protein. J Pharmacol Sci . 2007; 104(3): 258-262.
19. Juybari KB, Ebrahimi G, Momeni Moghaddam MA, Asadikaram G, Torkzadeh-Mahani M, Akbari M, et al. Evaluation of serum arsenic and its effects on antioxidant alterations in relapsing-remitting multiple sclerosis patients. Mult Scler Relat Disord. 2018; 19: 79-84.
20. Bradford MM. A rapid and sensitive method for the quantitation of microgram quantities of protein utilizing the principle of protein-dye binding. Anal Biochem. 1976; 72: 248-254.
21. Raeiszadeh M, Esmaeili-Tarzi M, Bahrampour-Juybari K, Nematollahi-mahani S, Pardakhty A, Nematollahi M, et al. Evaluation the effect of Myrtus communis L. extract on several underlying mechanisms involved in wound healing: An in vitro study. S Afr J Bot. 2018; 118: 144-150.
22. Wang ZB, Liu YQ, Cui YF. Pathways to caspase activation. Cell Biol Int. 2005; 29(7): 489-496.
23. Rota M, LeCapitaine N, Hosoda T, Boni A, De Angelis A, Padin-Iruegas ME, et al. Diabetes promotes cardiac stem cell aging and heart failure, which are prevented by deletion of the p66shc gene. Circ Res. 2006; 99(1): 42-52.
24. Nambu M, Ishihara M, Kishimoto S, Yanagibayashi S, Yamamoto N, Azuma R, et al. Stimulatory effect of autologous adipose tissue-derived stromal cells in an atelocollagen matrix on wound healing in diabetic db/db mice. J Tissue Eng. 2011; 2011: 158105.
25. Marchi S, Giorgi C, Suski JM, Agnoletto C, Bononi A, Bonora M, et al. Mitochondria-ros crosstalk in the control of cell death and aging. J Signal Transduct. 2012; 2012: 329635.
26. Song JS, Cho HH, Lee BJ, Bae YC, Jung JS. Role of thioredoxin 1 and thioredoxin 2 on proliferation of human adipose tissue-derived mesenchymal stem cells. Stem Cells Dev. 2010; 20(9): 1529-1537.
27. Benzi G, Marzatico F, Pastoris O, Villa RF. Relationship between aging, drug treatment and the cerebral enzymatic antioxidant system. Exp Gerontol . 1989; 24(2): 137-148.
28. Ghaznavi H, Fatemi I, Kalantari H, Hosseini Tabatabaei SMT, Mehrabani M, Gholamine B, et al. Ameliorative effects of gallic acid on gentamicin-induced nephrotoxicity in rats. J Asian Nat Prod Res. 2018; 20(12): 1182-1193.
29. Limaye PV, Raghuram N, Sivakami S. Oxidative stress and gene expression of antioxidant enzymes in the renal cortex of streptozotocin-induced diabetic rats. Mol Cell Biochem. 2003; 243(1-2): 147-152.
30. Kaul N, Siveski-Iliskovic N, Hill M, Khaper N, Seneviratne C, Singal PK. Probucol treatment reverses antioxidant and functional deficit in diabetic cardiomyopathy. Mol Cell Biochem. 1996; 160-161:

283-288.
31. Aydin M, Celik S. Effects of lycopene on plasma glucose, insulin levels, oxidative stress, and body weights of streptozotocin-induced diabetic rats. Turk J Med Sci. 2012; 42 Suppl 2: 1406-1413.
32. Sharifi AM, Mousavi SH. Studying the effects of lead on DNA fragmentation and proapoptotic Bax and antiapoptotic Bcl-2 protein expression in PC12 cells. Toxicol Mech Methods. 2008; 18(1): 75-79.
33. Li X, Liu L, Meng D, Wang D, Zhang J, Shi D, et al. Enhanced apoptosis and senescence of bone-marrow-derived mesenchymal stem cells in patients with systemic lupus erythematosus. Stem Cells Dev. 2012; 21(13): 2387-2394.
34. Fan T-J, Han L-H, Cong R-S, Liang J. Caspase family proteases and apoptosis. Acta Biochim Biophys Sin (Shanghai). 2005; 37(11): 719-727.
35. Sharifi AM, Eslami H, Larijani B, Davoodi J. Involvement of caspase-8,-9, and-3 in high glucose-induced apoptosis in PC12 cells. Neurosci Lett. 2009; 459(2): 47-51.
36. Cai B, Chang SH, Becker EB, Bonni A, Xia Z. p38 MAP kinase mediates apoptosis through phosphorylation of BimEL at Ser-65. J Biol Chem. 2006; 281(35): 25215-25222.
37. Aminzadeh A, Dehpour AR, Safa M, Mirzamohammadi S, Sharifi AM. Investigating the protective effect of lithium against high glucose-induced neurotoxicity in PC12 cells: involvements of ROS, JNK and P38 MAPKs, and apoptotic mitochondria pathway. Cell Mol Neurobiol. 2014; 34(8): 1143-1150.
38. Purves T, Middlemas A, Agthong S, Jude EB, Boulton AJ, Fernyhough P, et al. A role for mitogen-activated protein kinases in the etiology of diabetic neuropathy. FASEB J. 2001; 15(13): 2508-2514.
39. Stolzing A, Sellers D, Llewelyn O, Scutt A. Diabetes induced changes in rat mesenchymal stem cells. Cells Tissues Organs. 2010; 191(6): 453-465.
40. Prockop DJ. Marrow stromal cells as stem cells for nonhematopoietic tissues. Science. 1997; 276(5309): 71-74.

Original Article

Applicability of Hyaluronic Acid-Alginate Hydrogel and Ovarian Cells for *In Vitro* Development of Mouse Preantral Follicles

Parisa Jamalzaei, Ph.D.[1], Mojtaba Rezazadeh Valojerdi, Ph.D.[1*, 2], Leila Montazeri, Ph.D.[3], Hossein Baharvand, Ph.D.[4, 5*]

1. Department of Anatomy, Faculty of Medical Sciences, Tarbiat Modares University, Tehran, Iran
2. Department of Embryology, Reproductive Biomedicine Research Center, Royan Institute for Reproductive Biomedicine, ACECR, Tehran, Iran
3. Department of Cell Engineering, Cell Science Research Center, Royan Institute for Stem Cell Biology and Technology, ACECR, Tehran, Iran
4. Department of Developmental Biology, University of Science and Culture, Tehran, Iran
5. Department of Stem Cells and Developmental Biology, Cell Science Research Center, Royan Institute for Stem Cell Biology and Technology, ACECR, Tehran, Iran

Corresponding Addresses: P.O.Box: 14115-111, Department of Anatomy, Faculty of Medical Sciences, Tarbiat Modares University, Tehran, Iran
P.O. Box: 13145-871, Department of Developmental Biology, University of Science and Culture, Tehran, Iran
P.O.Box: 16635-148, Department of Stem Cells and Developmental Biology, Cell Science Research Center, Royan Institute for Stem Cell Biology and Technology, ACECR, Tehran, Iran
Emails: mr_valojerdi@modares.ac.ir, baharvand@royaninstitute.org

Received: 26/April/2019, Accepted: 11/December/2019

Abstract

Objective: In the present study, the applicability of hyaluronic acid-alginate (HAA) hydrogel and ovarian cells (OCs) for the culture of mouse ovarian follicles were investigated and compared with those of alginate (ALG) and fibrin-alginate (FA) hydrogels.

Materials and Methods: In the first step of this experimental study, mechanically isolated preantral follicles from the ovaries of two-week-old mice were encapsulated in the absence or presence of OCs in ALG, HAA, and FA hydrogels and cultured for 14 days. The morphology, diameter, survival and antrum formation rates of the follicles and the maturation and quality of the oocytes were evaluated during culture. In the second step, preantral follicles were cultured similar to the first step, but for 13 days, and their gene expressions and hormonal secretion were assessed on the last day of culture.

Results: In the absence of OCs, higher numbers of ALG- and HAA-encapsulated follicles reached the antral stage compared to FA-encapsulated follicles (P<0.05). However, a higher percentage of HAA-developed oocytes resumed meiosis up to the germinal vesicle breakdown (GVBD)/metaphase II (MII) stages in comparison with ALG-developed oocytes (P<0.05). HAA-encapsulated follicles had significant overexpression of most of the growth and differentiation genes, and secreted higher levels of estradiol (E2) compared to ALG- and FA-encapsulated follicles (P<0.05). The co-culture condition increased the diameter of ALG-encapsulated follicles on day 13 of culture (P<0.05). It also increased the survival and maturation rates of ALG- and FA-encapsulated follicles, respectively (P<0.05). The co-culture condition improved cortical granule distribution in all groups, increased E2 and progesterone (P4) secretions in the ALG and FA groups, and androstenedione (A4) secretion in the FA group (P<0.05).

Conclusion: The present study results show that HAA hydrogel is a promising hydrogel for follicle culture. OCs utilization could ameliorate the culture conditions regardless of the type of hydrogel.

Keywords: Alginate, Fibrin, Hyaluronic Acid, Ovarian Cells, Preantral Follicle

Cell Journal(Yakhteh), Vol 22, Suppl 1, Autumn 2020, Pages: 49-60

Citation: **Jamalzaei P, Rezazadeh Valojerdi M, Montazeri L, Baharvand H. Applicability of hyaluronic acid-alginate hydrogel and ovarian cells for in vitro development of mouse preantral follicles. Cell J. 22 Suppl 1: 49-60. doi: 10.22074/cellj.2020.6925.**

Introduction

Today, *in vitro* culture of isolated immature ovarian follicles would be a potential alternative for fertility preservation in adult or prepubertal patients with cancers that can metastasize to the ovaries (1, 2). In this regard, two systems namely, two-dimensional (2D, attachment) and three-dimensional (3D, non-attachment) have been developed. These systems support the growth of immature follicles *in vitro* to produce oocytes that can mature, become fertilized and result in live births in mice (3, 4). Unlike the 3D system, in the 2D system, follicle integrity is not preserved because of the poor correlation between the cultured follicle microenvironment and *in vivo* conditions (5). Therefore, in recent years, the 3D system has attracted more attention for follicle culture compared to the 2D technique and it has been proven that this system is more successful when translating to larger species (6).

One of the challenges that face the follicle culture in a 3D system is how to mimic the properties of the follicles in a physiological environment. Thus, it is important to

apply appropriate biomaterials for follicle encapsulation (7). There are many potential natural and synthetic hydrogels, including agarose, hyaluronic acid (HA), collagen, fibrin, Matrigel, alginate (ALG), poly ethylene glycol (PEG) and their derivatives, which have been used for follicle culture (6, 8-11). ALG, a naturally-derived polysaccharide hydrogel produced from brown algae, has many of the characteristics that an optimal hydrogel requires for follicle culture (6). Follicles cultured in ALG hydrogel can grow and secrete hormones properly (6, 12). Despite documented positive outcomes, there are disadvantages associated with utilization of ALG hydrogel. The ALG degradation rate is not consistent with follicle growth rate, and this may affect oocyte maturation and increase abnormalities in cortical granule distribution, spindle formation, and chromosomal alignment (8, 13). Thus, oocytes that are cultured in ALG hydrogel have quite limited chances of becoming fertilized and reaching the blastocyst stage (12). In addition, ALG does not interact with the cells' integrins, and this property affects the survival and proliferation of the follicular cells (14). To overcome these limitations, ALG can be combined with degradable compounds to make more appropriate hydrogels for the culture of the follicles without affecting its ideal properties. For example, Shikanov et al. added fibrin, as a degradable part to ALG (resulting in fibrin-alginate hydrogel [FA]), and produced oocytes with higher quality and maturation rate (8). Fibrin is a protein derived from fibrinogen that is involved in blood clotting. It facilitates cell adhesion and is degraded by substances secreted by growing follicles. Therefore, fibrin provides dynamic cell-responsive biological and mechanical properties (15).

HA is an anionic glycosaminoglycan that can be combined with ALG to make a composite hydrogel suitable for follicle culture. HA is a primary component of the extracellular matrix (ECM) and is present in many organs, including the ovaries (16). The favourable properties of HA, such as its important role in cell migration, proliferation, and morphogenesis, enable it to make a physiologic milieu for follicle growth and development (9, 17, 18). Although it was shown that preantral follicles encapsulated in a HA hydrogel were able to resume meiosis, they lose out to increase the survival and antrum formation rates in comparison with ALG (18). These results might be attributed to the poor mechanical properties or lack of pores in the HA microstructure, which are necessary for follicle nutrition and growth (19). One way to optimize the poor mechanical properties of HA and form a porous microstructure is the creation of a composite hydrogel that consists of HA and ALG [hyaluronic acid-alginate hydrogel (HAA)]. Interestingly, the combination of ALG and HA in an HAA hydrogel can enhance both bioactivity and biodegradability of the ALG (20).

Although in many studies, ALG and FA have been used for encapsulation and culture of preantral follicles, the HAA hydrogel has not been used for this purpose. Importantly, no study has compared the effectiveness of these three types of hydrogels to introduce the most appropriate one for mouse ovarian follicle culture. Experimental evidence has emphasized the importance of molecular support for the ovarian environment, as well as its physical properties for follicular development (21). In this regard, recent studies have reported a stimulatory effect for ovarian cells (OCs) on the growth and differentiation of the follicles *in vitro* (22, 23). Hence, in the present study, the growth, survival, maturation, oocyte quality, gene expressions and hormonal secretions of the preantral follicles encapsulated in an HAA hydrogel in the absence or presence of OCs (-OCs and +OCs, respectively) were evaluated in two steps. The results were compared with ALG- and FA-encapsulated follicles, which served as the control groups.

Materials and Methods

Study design

In the first step of the present experimental study, preantral follicles were isolated from mice ovaries in five independent replicates; randomly assigned to encapsulate in ALG, HAA and FA hydrogels in the absence or presence of OCs; and cultured for 14 days. The diameter and morphological appearance of the growing follicles were measured on days 1, 6, and 13 of culture. Moreover, on day 13 of culture, the survival rate of the follicles was evaluated, and the surviving follicles were assessed for antrum formation rate. After inducing the antral follicles with 2.25 IU/ml human chorionic gonadotropin (hCG, Choriomon, Switzerland) on day 13 of culture, the developmental stages of the oocytes obtained from induced antral follicles were determined on day 14 of culture. Finally, the qualities of MII oocytes in terms of cortical granule distribution, spindle formation, and chromosomal alignment were assessed. In the second step, follicles were isolated and cultured similar to the first step, but without hCG induction and in three independent replicates. On day 13 of culture, follicles were collected to evaluate their gene expressions, and the conditioned media were also gathered to measure follicle hormonal secretions. The study design has been summarized in Figure S1 (See Supplementary Online Information at www.celljournal.org).

Animals

Female NMRI mice (Pasteur Institute of Iran) were kept in the animal house at Royan Institute with an adjusted temperature (20-25˚C) and lighting (12 hours light: 12 hours dark). They were handled according to the ethical guidelines set by Royan Institute (number: IR.ACECR.ROYAN.REC.1395.93).

Ovarian cell isolation and culture

To obtain OCs (including theca/stromal cells, immune cells, endothelial cells, and smooth muscle cells), 20 mice that were three to four-weeks-old were sacrificed by

cervical dislocation, and their ovaries were removed by an aseptic technique. Isolated ovaries were placed in ice-cold base medium that contained Dulbecco's Modified Eagle's medium (DMEM, Gibco, UK), streptomycin sulphate (Gibco, UK), penicillin (Gibco, UK), sodium bicarbonate ($NaHCO_3$, Sigma, USA), and 10% foetal bovine serum (FBS, Gibco, UK). Next, the bursa and adipose tissues were removed under a stereomicroscope (SZ61, Olympus, Japan). Oocytes and granulosa cells were isolated from the ovaries by puncturing follicles using two 29G insulin syringes and then discarded. The remaining husks were minced and incubated for 45 minutes at 37˚C in 200 µl per ovary of collagenase solution that contained 4 mg/ml collagenase IV (Gibco, UK) in a serum-free base medium. During this time, the ovarian tissues were pipetted at least 20 times every 10-15 minutes. The enzyme was inactivated by adding the same volume of the base medium. The digested cell solution was then filtered through a sterilized 40 µm filter mesh (Falcon, Mexico) and centrifuged at 1800 rpm for 5 minutes. The obtained cells were washed three times and the final pellet was resuspended in a certain volume of base medium. The cells were transferred to T25 culture flasks that contained 4 ml of base medium supplemented with 1% insulin-transferrin-selenium (ITS, Gibco, UK), 1% non-essential amino acids (Gibco, UK), 1% L-glutamine (Sigma, USA), and 0.1% β-mercaptoethanol (Sigma, USA), and then cultured at 37˚C in a water-saturated atmosphere of 95% air and 5% CO_2 until confluent. Then, the OCs were trypsinized, washed, and after centrifugation at 1800 rpm for 5 minutes, they were counted using a Neubauer chamber, and the cell survival was defined by Trypan blue staining (24). Finally, the cells were pelleted again in a 14 ml conical tube and 5×10^5 cells were concentrated in 900 µl FBS. Then, 100 µl of dimethyl sulfoxide (DMSO, Sigma, USA) was added to the cell suspension. Afterward, 1 ml aliquots of the 10% DMSO solution were added to 1 ml cryovials and frozen at -80˚C until use.

Follicle isolation

A total number of 60 mice (two-weeks-old) were sacrificed by cervical dislocation. Mouse ovaries were dissected under a stereomicroscope at 37˚C using two 29G insulin syringes in alpha minimum essential medium (α-MEM, Gibco, UK) supplemented with penicillin, streptomycin, $NaHCO_3$, and 10% FBS. Only healthy preantral follicles that were 100-130 µm in diameter and two-three layers of granulosa cells were selected and divided randomly into the experimental groups.

Hydrogel preparation

Alginic acid sodium salt (10 mg/ml, Sigma, USA), 4-(2-hydroxyethyl)-1-piperazineethanesulfonic acid (HEPES, 25 mM Sigma, USA), and sodium chloride (NaCl, 150 mM, Sigma, USA) were dissolved in deionized water to make a 1.0% (w/v) ALG solution (20). Immediately before use, the sterilized ALG solution was reconstituted with sterile 1X phosphate-buffered saline (PBS, Takara, Japan) without calcium and magnesium to yield a 0.5% (w/v) concentration. FA solution was prepared by mixing fibrinogen solution [50 mg/ml fibrinogen (Sigma, USA) in 3000 KIU/mL aprotinin (Roche, Germany)] with 1% ALG solution at 1:1 ratio. HAA solution was made by the addition of HA [5 mg/ml, Nano Zist Arrayeh (NZA), Iran] to a 0.5% ALG solution (8, 20).

In order to prepare the hydrogels, cross-linking solutions [50 mM calcium chloride ($CaCl_2$, Sigma, USA)/140 mM NaCl for making ALG and HAA, and 50 mM $CaCl_2$/140 mM NaCl with the equal volume of 50 IU/ml thrombin solution for FA] were mixed with the hydrogel solutions.

Encapsulation and culture

In the first step of the study, groups of 94.66 ± 1.54 preantral follicles were individually encapsulated in ALG, HAA, and FA solutions and in the absence or presence of OCs, in five independent replicates. A schematic representation of the co-encapsulation of follicles and OCs is depicted in Figure S2 (See Supplementary Online Information at www.celljournal.org). In detail, for cell encapsulation, thawed and cultured OCs were washed twice in PBS, detached using trypsin-EDTA, and counted. After pelleting, a certain number of cells (5×10^3 cells per follicle based on the best results obtained in the pilot stage of the study) was mixed with hydrogel solutions and pipetted in 5 µl droplets on sterile ultra-low attachment culture dishes (Dow Corning, USA). Follicles were individually cultured in microdrops (5 µl) and cross-linking solutions were gently pipetted on top of each droplet, and then incubated at 37˚C for 2 and 5 minutes. After incubation, ALG, HAA, and FA beads were rinsed with medium and then placed into 96-well plates (TPP, Switzerland). Each well contained one bead in 100 µl culture medium [α-MEM supplemented with 5% FBS, 1% ITS, 10 mIU/ml follicle stimulating hormone (FSH, Merck, Germany)]. Finally, the plates were incubated in 5% CO_2 at 37˚C for 13 days and 50 µl of the medium was replaced every 3 days.

Evaluation of follicle diameters, survival, and antrum formation rates

On days 1, 6, and 13 of culture, morphological features of the follicles were assessed, and the diameters of the growing follicles were defined as the average of two perpendicular diameters of every follicle using ImageJ software (U.S. National Institutes of Health). On day 13 of culture, the survival rate of the cultured follicles and antrum formation rate of the surviving follicles were observationally evaluated. For assessment of follicle survival rate, extrusion of the oocytes and a dark appearance of the oocytes and surrounding granulosa cells were considered to be signs of degeneration. In addition, antrum formation was defined as a noticeable lucid cavity within masses of granulosa cells.

Determination of oocyte maturation

On day 13 of culture, *in vitro* maturation (IVM) and ovulation of antral follicles were induced by 2.25 IU/ml hCG. To determine oocyte maturation, 20–22 hours after stimulation, cumulus-oocyte complexes (COCs) were isolated from induced follicles by their suction into Pasteur pipettes, their cumulus cells were eliminated by gentle pipetting, and the number of germinal vesicle (GV), germinal vesicle breakdown/MII (GVBD/MII), and degenerated oocytes were calculated.

Assessment of cortical granule distribution, spindle formation, and chromosomal alignment

A total number of 15 *in vivo*- and 90 *in vitro*-developed MII oocytes (15 oocytes per group) were randomly collected in three independent replicates for this assessment. To obtain *in vivo*-developed oocytes as the control group, three female 6–8 week-old mice were injected intraperitoneally with 7.5 IU of pregnant mare serum gonadotropin (PMSG, Sigma, USA) followed by administration of 7.5 IU hCG 48 hours later. After 18 hours, the mice were sacrificed, their COCs were removed from the oviduct ampulla and denuded by gentle pipetting in 0.3% hyaluronidase solution (Sigma, USA). Then, the zona pellucida of *in vivo*-developed MII oocytes along with *in vitro*-developed ones were removed by 0.5 mg/ml pronase (Sigma, USA) in PBS at 37˚C and then the oocytes were fixed in 4% paraformaldehyde for at least 1 hour. After washing in PBS with 0.01% Tween 20 (Sigma, USA), the oocytes were permeabilized in PBS with 0.3% bovine serum albumin (BSA, Gibco, UK) and 0.1% Triton X-100 (Sigma, USA) for 15 minutes, and then blocked in PBS that contained 0.3% BSA. In order to visualize the meiosis spindle and cortical granules, the oocytes were incubated with a mixture of anti-alpha-tubulin antibody-microtubule marker (FITC, 1:100; Abcam, UK) and rhodamine-labeled Lens Culinaris Agglutinin (LCA, 1:500, Vector Laboratories, USA) in blocking solution for 1 hour at 37˚C. Finally, the stained oocytes were washed thoroughly in PBS-T, counterstained with Hoechst 33342 (1 mg/ml in 1X PBS, Sigma, USA) for 5 minutes at 37˚C and mounted on adhesion slides (13). Fluorescence was detected using an inverted fluorescence microscope (Eclipse 50i, Nikon, Japan) and images were processed using Adobe Photoshop software (CS5.1, Adobe Systems, Inc., San Jose, CA, USA). The absence of a cortical granule-free domain (CGFD) around the spindle and lack of a cortical distribution, and disorganized spindle configuration or misaligned chromosomes were respectively considered as the signs of cortical granule and spindle abnormalities.

Evaluation of gene expression

In the second step, to evaluate gene expressions, a total number of 75 antral follicles (25 follicles per replicate) that survived were pooled in each group, in three replicates, on day 13 of culture. The follicles were retrieved from the hydrogel beads by gentle suction into Pasteur pipettes. Total RNA was extracted using the RNeasy Micro Kit (Qiagen, Germany) according to the manufacturer's protocol. Synthesis of cDNA was performed using a RevertAid first-strand cDNA synthesis kit (Fermentas, Germany) and random hexamer based on the manufacturer's instructions. The expressions of seven growth and differentiation genes, five apoptotic genes, and five genes involved in steroidogenesis were assessed using RT-qPCR. Primers for the mentioned and housekeeping genes (GAPDH) were designed using Allele ID (v.6, Premier Biosoft, USA) and PerlPrimer (v.1.1.21, http://perlprimer.sourceforge.net/) primer design softwares (Table S1, See Supplementary Online Information at www.celljournal.org). The polymerase chain reaction (PCR) mix for each well contained 5 ml Power SYBR Green PCR Master Mix (Takara, Japan), 1 ml dH_2O, 1 ml of each of the forward and reverse primers (5 pmol/ml), and 2 ml of single-strand cDNA in a final reaction volume of 10 ml. PCR was performed on the ABI StepOnePlus real-time PCR system (Applied Biosystems) using the following program: stage 1: 95˚C for 10 minutes; stage 2: 40 cycles of 95˚C for 15 seconds and 60˚C for 1 minute; and stage 3: 95˚C for 15 seconds, 60˚C for 15 seconds, and 95˚C for 15 seconds. Product specificity was confirmed by melting curve analysis. All samples were assessed in duplicate, and for each reaction, a no-template control reaction (NTC) was run. The expression of genes was compared between groups using the ΔCT method. Gene expression levels were normalized against *GAPDH*.

Measurement of hormonal secretions

Following evaluation of gene expression, the levels of estradiol (E2), progesterone (P4), and androstenedione (A4) were also measured in conditioned media collected from 30 cultured antral follicles per group (10 follicles per replicate) on day 13 of culture. Hormonal secretions were assessed by mouse ELISA kits (Bioassay Technology Laboratory, China) according to the kits' instructions. Data were calculated for each follicle by dividing each of the measured hormone secretions by the number of the follicles. According to the kits' datasheets, the sensitivity assays for E2, P4 and A4 were 1.51, 0.28 and 0.022 ng/ml, respectively.

Statistical analysis

Binary data, including the proportion of the follicle survival and antrum formation rates, oocyte maturation and abnormality rates were analysed using the GENMOD procedure including the logit link function model. The GENMOD procedure produced the odds ratio (OR) as the strength of the difference between groups. Data associated with follicle diameter over the course of the culture were analysed by the MIXED procedure including RANDOM and REPEATED statements in the model to specify between and within covariances, respectively. Data pertaining to gene expression and hormonal secretion were analysed using the GLM procedure. In

addition, the LSMEANS statement was included in the model to perform multiple comparisons. All analyses were conducted in SAS version 9.4 (SAS Institute Inc., NC, USA). Differences were considered significant at $P<0.05$.

Results

Follicle morphological characteristic and diameter

Assessment of morphological changes and follicle diameter after 1, 6, and 13 days of culture showed that there was no significant difference in the morphology and diameter of the follicles encapsulated in different hydrogels, either in the absence or presence of OCs. Nevertheless, the follicles co-cultured with OCs had a more spherical shape and a larger diameter. On day 13 of culture, the difference in diameter of -OCs and +OCs follicles was significant in ALG encapsulated ones (327.59 ± 8.74 vs. 402.73 ± 22.63 µm, respectively; $P<0.05$, Fig.1A, B).

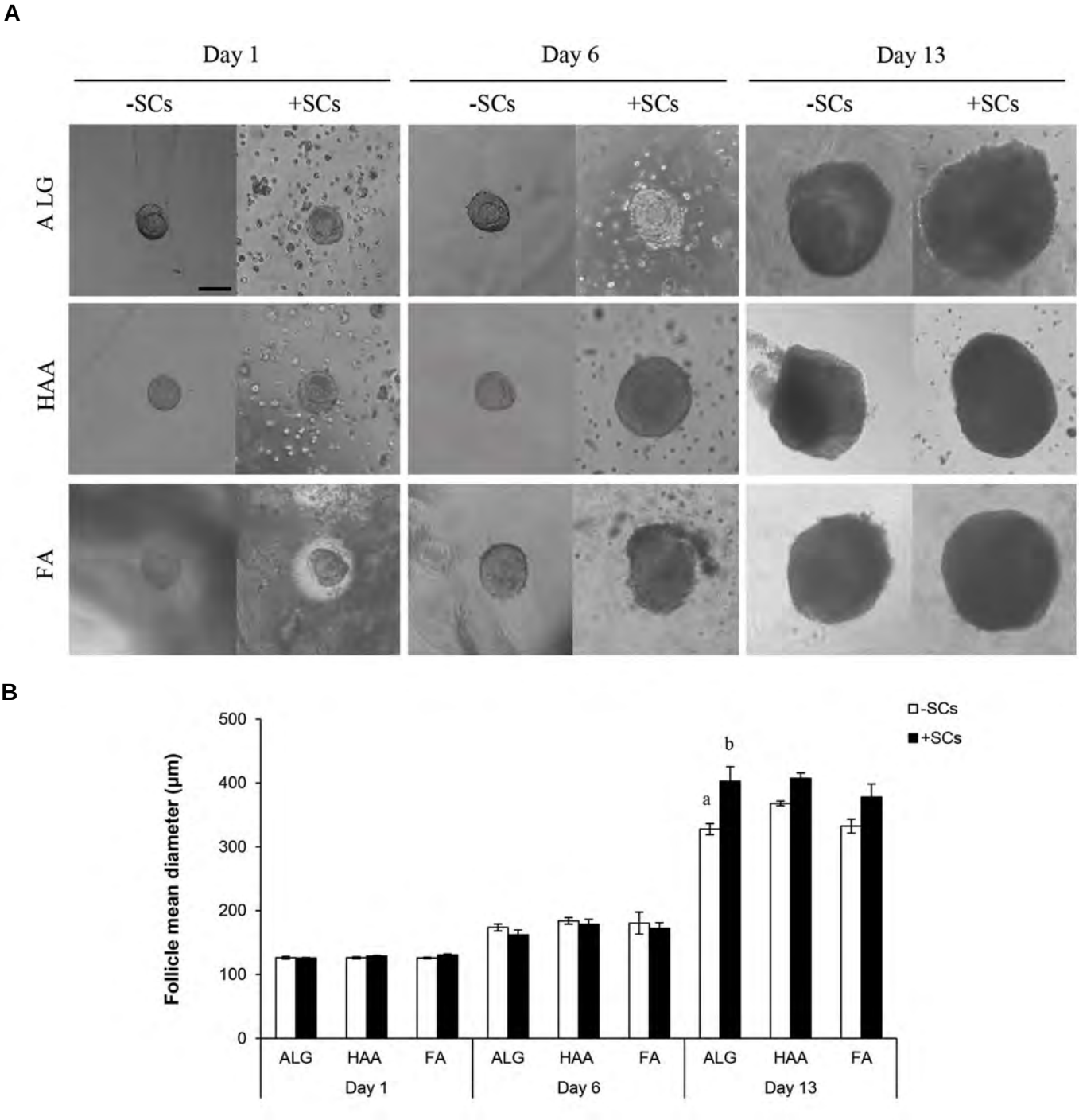

Fig.1: Growth of preantral follicles encapsulated and cultured in alginate (ALG), hyaluronic acid-alginate (HAA) and fibrin-alginate (FA) hydrogels in the absence or presence of ovarian cells (-OCs and +OCs, respectively). **A.** Morphological changes and **B.** Diameters of the surviving follicles on days 1, 6, and 13 of culture. Data are presented as mean diameter ± standard error (SE). Data points a and b differ significantly ($P<0.05$, scale bar: 100 µm). OCs; ovarian Cells.

Survival rate and antrum formation

Evaluation of survival rate after 13 days of culture showed that in the absence of OCs, the survival rate of ALG-encapsulated follicles (69.47%) was significantly higher than FA-encapsulated (53.06%, P<0.05, Table 1). However, in the presence of OCs, the survival rate of ALG-, HAA- and FA-encapsulated follicles did not differ. On the other hand, the addition of OCs to FA hydrogel beads significantly increased the number of surviving follicles (53.06 vs. 75% for FA-OCs and FA+OCs, P<0.05, Table 1).

Antrum formation results revealed that in the absence of OCs, higher numbers of ALG- (81.81%) and HAA- (82.25%) encapsulated follicles reached the antral stage compared to FA-encapsulated follicles (69.23%, P<0.05, Table 1). Nonetheless, in the presence of OCs, the antrum formation did not vary significantly between the ALG, HAA, and FA groups. Also, a comparison of the -OCs and +OCs groups showed that the co-culture of follicles with OCs did not influence follicle antrum formation.

Oocyte maturation

Table 1 shows various developmental stages of oocytes obtained from follicles cultured in ALG, HAA, and FA hydrogels, in the absence or presence of OCs. Data revealed that in the absence of OCs, a higher percentage of HAA-developed oocytes resumed meiosis up to the GVBD/MII stages in comparison with ALG-developed oocytes (74.50 vs. 55.55%, P<0.05), while in the presence of OCs there was no significant difference between groups. Assessment of -OCs and +OCs groups also confirmed that the oocytes which were co-cultured with OCs were more likely to break down their GVs and reach the GVBD/MII stages, whereas in the ALG group this difference was remarkable (GV% oocytes: 29.62 vs. 10.14%, GVBD /MII% oocytes: 55.55 vs. 72.46% for -OCs and +OCs, respectively, P<0.05).

Cortical granule distribution, spindle formation, and chromosomal alignment

Figure 2 shows the features of the normal and abnormal MII oocytes in terms of cortical granule distribution, meiotic spindle organization, and chromosomal alignment.

Data indicated that none of the *in vivo* developed oocytes showed any abnormalities in cortical granule distribution, whereas it appeared to be impaired in the oocytes from all of the *in vitro* groups (P<0.05). Evaluation of *in vitro* developed oocytes revealed that there was no significant difference between the ALG, HAA, and FA groups neither in the absence nor in the presence of OCs. However, a comparison of the -OCs and +OCs groups showed that co-culturing with OCs improved the abnormalities in the distribution of the cortical granules (P<0.05, Table 2).

In terms of meiotic spindle and chromosomal alignment, abnormalities were observed in both *in vivo* and *in vitro* developed oocytes. Importantly, neither the type of hydrogel nor the presence of OCs had significant effects on the rate of abnormalities (Table 2).

Gene expression

In the second step of the study, the expressions of some of the genes involved in growth and differentiation of follicles (*Gdf9*, *Bmp15*, *Zp3*, *Gja4*, *Gja1*, *Bmp4*, and *Bmp7*), apoptosis (*Trp53*, *Casp3*, *Bax*, and *Bcl2*) and steroidogenesis (*Fshr*, *Lhcgr*, *Cyp11a1*, *Cyp17a1*, and *Cyp19a1*) were studied (Fig. 3).

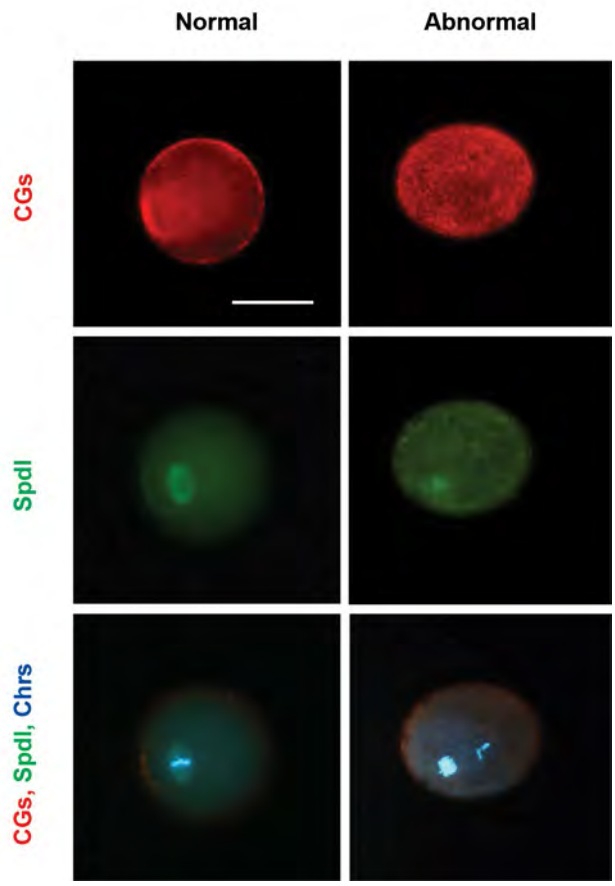

Fig.2: Immunofluorescence staining of cortical granules (CGs, red), meiotic spindle (SpdI, green) and chromosomes (Chrs, blue) in normal and abnormal metaphase II (MII) oocytes. The absence of a cortical granule-free domain (CGFD) around the spindle and lack of a cortical distribution, and disorganized spindle configuration or misaligned chromosomes were respectively considered the signs of cortical granules and spindle abnormalities (scale bar: 50 µm).

Table 1: Development of preantral follicles cultured in ALG, HAA and FA hydrogels in the absence or presence of OCs for 14 days

Groups	Survival rate		Antrum formation rate		Oocyte maturation					
					GV		GVBD/MII		Degenerated	
	-OCs	+OCs	-OCs	+OCs	-OCs	+OCs	-OCs	+OCs	-OCs	+OCs
ALG	66/95 (69.47)^{A}	78/98 (79.59)	54/66 (81.81)^{A}	69/78 (88.46)	16/54 (29.62)^{a}	7/69 (10.14)^{b}	30/54 (55.55)^{Aa}	50/69 (72.46)^{b}	8/54 (14.81)	12/69 (17.39)
HAA	62/93 (66.66)	71/96 (73.95)	51/62 (82.25)^{A}	63/71 (88.73)	7/51 (13.72)	6/63 (9.52)	38/51 (74.50)^{B}	53/63 (84.12)	6/51 (11.76)	4/63 (6.34)
FA	52/98 (53.06)^{Ba}	66/88 (75)^{b}	36/52 (69.23)^{B}	50/66 (75.75)	10/36 (27.77)	7/50 (14)	23/36 (63.88)	38/50 (76)	3/36 (8.33)	5/50 (10)

Data are presented as n (%). Data points A and B in each column, a and b in each row differ significantly (P<0.05). ALG; Alginate, HAA; Hyaluronic acid-alginate, FA; Fibrin-alginate, -OCs; Culture in the absence of stromal cells, +OCs; Culture in the presence of stromal cells, GV; Germinal vesicle, GVBD; Germinal vesicle breakdown, and MII; Metaphase II.

Table 2: Abnormality rate of *in vivo* and *in vitro* developed MII oocytes on day 14 of culture

Groups	*In vivo*	ALG		HAA		FA	
		-OCs	+OCs	-OCs	+OCs	-OCs	+OCs
Abnormal CGs	0/15 (0)^{a}	10/15 (66.66)^{bc}	6/15 (40)^{bd}	15/15 (100)^{be}	9/15 (60)^{bf}	15/15 (100)^{bg}	8/15 (53.33)^{bh}
Abnormal Spdl and Chrs	3/15 (20)	7/15 (46.66)	7/15 (46.66)	4/15 (26.66)	7/15 (46.66)	3/15 (20)	4/15 (26.66)

Data are presented as n (%). Data points a and b, c and d, e and f, g and h differ significantly (P<0.05).
MII; Metaphase II, ALG; Alginate, HAA; Hyaluronic acid-alginate, FA; Fibrin-alginate, -OCs; Culture in the absence of stromal cells, +OCs; Culture in the presence of stromal cells, CGs; Cortical granules, Spdl; Spindle, and Chrs; Chromosomes.

In general, in the absence of OCs, all growth and differentiation genes, except for *Gja1* and *Bmp4*, were significantly overexpressed in the HAA group (P<0.05), while the expressions of pro-apoptotic genes, *Trp53* and *Bax* in the ALG group were significantly higher than those of the FA group (P<0.05). *Bax* expression was also significantly higher in the HAA group (P<0.05). Moreover, the investigation of pro-apoptotic and anti-apoptotic genes and *Bax/Bcl2* ratio revealed a higher tendency for apoptosis in the follicular cells of the ALG group in comparison to the HAA and FA groups. On the other hand, FA-encapsulated follicles expressed *Lhcgr*, *Cyp17a1*, and *Cyp19a*, as steroidogenic genes, at much higher levels compared to HAA-encapsulated and ALG-encapsulated follicles (P<0.05); however, the expressions of *Fshr* and *Cyp11a1* genes did not differ significantly between groups.

In the presence of OCs, only the expression level of *Bmp7* was higher in HAA-encapsulated follicles compared to ALG- encapsulated and FA-encapsulated follicles (P<0.05). No significant difference in the expressions of the apoptotic genes was observed between groups; nonetheless, like -OCs, FA-encapsulated follicles expressed *Cyp19a1* at much higher levels compared to the ALG-encapsulated and HAA-encapsulated follicles (P<0.05).

Finally, comparable results between the -OCs and +OCs groups indicated that adding OCs to the hydrogel beads did not have any significant effect on expressions of the growth and differentiation genes, but it did decrease the expressions of *Trp53* in the ALG group and *Bax* in the ALG and HAA groups (P<0.05), and decreased the expression of *Lhcgr* in the FA group (P<0.05).

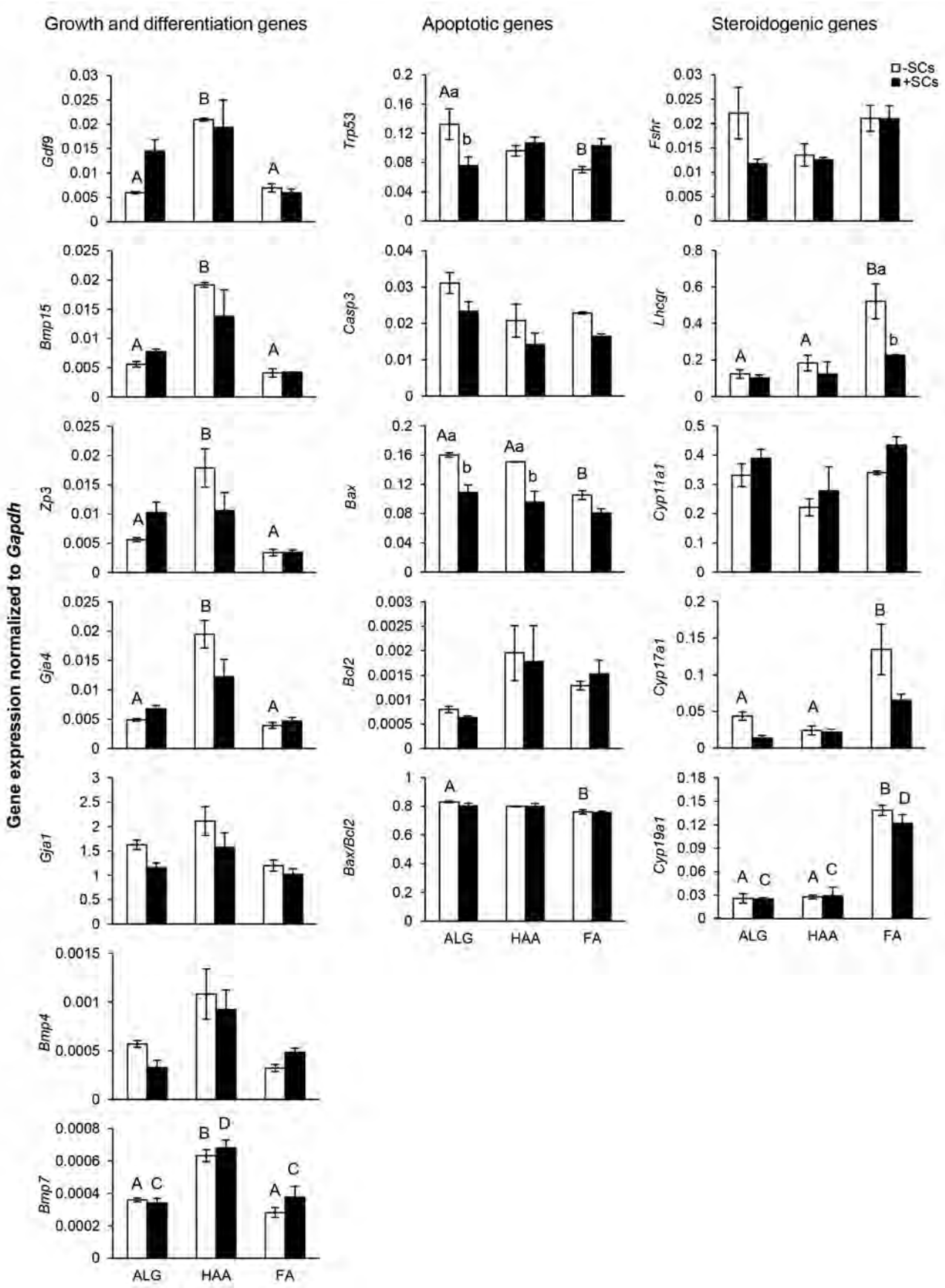

Fig.3: Expression of growth and differentiation (*Gdf9, Bmp15, Zp3, Gja4, Gja1, Bmp4,* and *Bmp7*), apoptotic (*Trp53, Casp3, Bax,* and *Bcl2*) and steroidogenic (*Fshr, Lhcgr, Cyp11a1, Cyp17a1,* and *Cyp19a1*) genes in follicles encapsulated and cultured in alginate (ALG), hyaluronic acid-alginate (HAA) and fibrin-alginate (FA) hydrogels in the absence or presence of ovarian cells (-OCs and +OCs, respectively). Antral follicles were collected on day 13 of culture. Expression levels were normalized to *GAPDH* as the endogenous control. Data are presented as mean ± standard error (SE). Data points A and B, C and D, a and b differ significantly (P<0.05).

Hormonal secretion

We assessed the E2, P4, and A4 secretions by the cultured follicles, and the P4/E2 and E2/A4 ratios (Fig.4). Data indicated that in the absence of OCs, HAA-encapsulated follicles (28.27 ± 1.67 ng/ml) secreted higher levels of E2 compared to ALG-encapsulated (10.08 ± 0.79 ng/ml) and FA-encapsulated (13.26 ± 0.06 ng/ml, P<0.05) follicles; however, no significant difference was found between groups in the levels of P4 and A4. Furthermore, the P4/E2 ratio did not significantly vary between groups, but the E2/A4 ratio in the HAA group was higher than the other groups due to higher E2 levels in the HAA group (P<0.05). Nonetheless, in the presence of OCs, there was no significant difference in E2 and P4 secretions between groups, but the A4 level in FA-encapsulated follicles was significantly higher than the ALG-encapsulated and HAA-encapsulated (0.86 ± 0.02 vs. 0.33 ± 0.01 and 0.45 ± 0.02 ng/ml, P<0.05) follicles. In the presence of OCs, the P4/E2 ratio did not vary significantly between groups, but the E2/A4 ratio in the ALG group was higher than the FA group (P<0.05). Finally, a comparison of the -OCs and +OCs groups showed that co-culture of the follicles with OCs increased E2 secretion in the ALG (10.08 ± 0.79 ng/ml) and FA groups (31.74 ± 0.30 ng/ml) for -OCs and in the ALG (13.26 ± 0.06 ng/ml) versus FA (34.57 ± 1.12 ng/ml) groups for +OCs (P<0.05). There was also increased P4 secretion in the ALG and FA groups (1.59 ± 0.03 vs. 2.86 ± 0.35 and 2.32 ± 0.09 vs. 3.87 ± 0.63 ng/ml for -OCs and +OCs, respectively, P<0.05). There was increased A4 secretion in the FA group (0.39 ± 0.02 vs. 0.86 ± 0.02 ng/ml for -OCs and +OCs, respectively, P<0.05). Additionally, the P4/E2 and E2/A4 ratios in ALG-OCs group were significantly higher and lower than that of the ALG+OCs group, respectively (P<0.05).

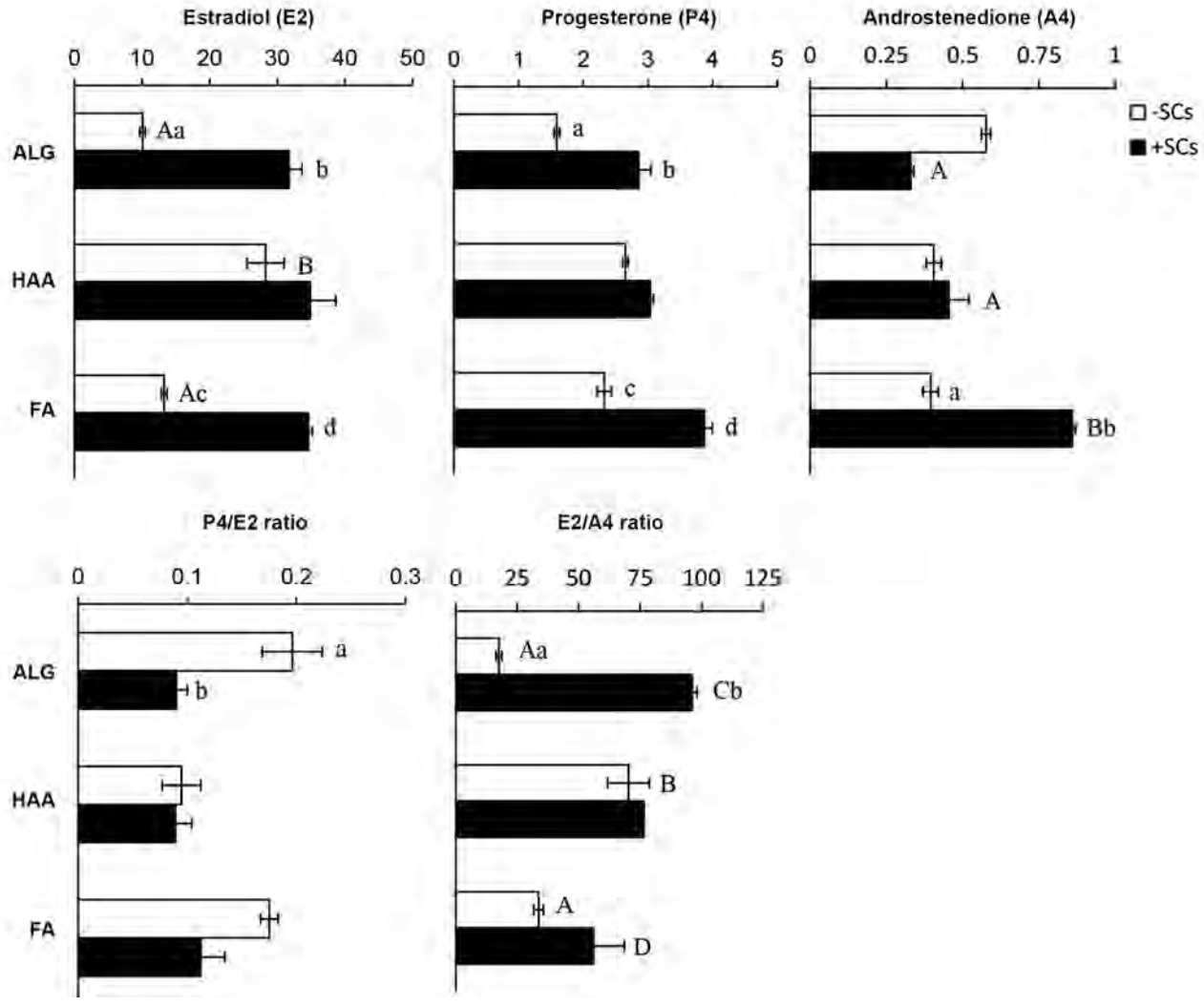

Fig.4: Secretion of estradiol (E2), progesterone (P4), and androstenedione (A4) by follicles encapsulated and cultured in alginate (ALG), hyaluronic acid-alginate (HAA) and fibrin-alginate (FA) hydrogels in the absence or presence of ovarian cells (-OCs and +OCs, respectively). Conditioned media were collected on day 13 of culture. Data are presented as mean ± standard error (SE). Data points A and B, C and D, a and b differ significantly (P<0.05).

Discussion

The aim of the present study was to investigate the applicability of HAA hydrogel and OCs for the culture of ovarian follicles. In this regard, the diameter, survival and antrum formation rates, gene expression profile, and steroidogenic activity of cultured follicles, and developmental competence and quality of obtained oocytes were evaluated.

In the absence of OCs, a comparison of the ALG, HAA, and FA groups showed that the antrum formation and GV to GVBD/MII transition rates in the HAA group were relatively higher than the ALG and FA groups. Based on the mentioned results, it could be proposed that HAA hydrogel supported the growth and development of follicles better than the other evaluated hydrogels.

Nevertheless, the majority of the cultured oocytes in -OCs groups (HAA, ALG, and FA) did not show a normal distribution of cortical granules (important granules within oocyte cytoplasm that are involved in polyspermy-preventing mechanisms) (25). These observations were in line with Mainigi et al., who reported that oocytes obtained from follicles cultured in ALG hydrogel exhibited abnormalities in cortical granule distribution (13). The stated findings could be due to the clumping of cortical granules across the cytoplasm either as a result of increased Ca^{2+} concentration or altered expression of some proteins, which are involved in cortical granule fusion and exocytosis (13, 26). Therefore, it can be suggested that *in vitro* culture of follicles increases the oocyte susceptibility to errors in cortical granule distribution during maturation, regardless of the type of the matrix.

Based on our findings, in the absence of OCs, the HAA-encapsulated follicles highly expressed all growth and differentiation genes with the exception of *Gja1* and *Bmp4*. *Gdf9, BMP15,* and *BMP7* play important roles in follicular growth and development and cumulus expansion (27-29). Moreover, *Gja4* contributes to the gap junctions between the oocyte and the surrounding granulosa cells (30). On the other hand, *Zp3* encodes the most abundant protein in the oocyte's zona pellucida (31). Therefore, overexpression of the mentioned genes in the HAA-OCs group could represent effective oocyte-granulosa cell communication and more marked development of follicles, subsequently, high-quality fertilization and embryo development in this group.

Apoptosis or programmed cell death is modulated by several hormones and growth factors as well as intrinsic factors like TRP53, BAX, BCL2, and CASP3 (32, 33). In our study, in the absence of OCs, the *Bax/Bcl2* ratio, as well as Trp53 and Casp3 expressions in the HAA group, did not significantly differ from those of the ALG and FA groups. Hence, it could be deduced that apoptosis occurred in the HAA group at similar rates to the ALG and FA groups.

Nonetheless, it was shown that in the absence of OCs, ALG-encapsulated and HAA-encapsulated follicles expressed *Lhcgr, Cyp17a1* and *Cyp19a1* genes at a similar level but much lower than those of FA-encapsulated follicles. Gonadotropic hormones, FSH and LH, induce granulosa and theca/stromal cells via their receptors, FSHR and LHCGR, respectively. Afterwards, *CYP17A1* produces P4 and A4 from cholesterol, and *CYP19A1* produces E2 from A4 (34, 35). Accordingly, it is suggested that both the granulosa and theca cells in FA-encapsulated follicles are highly active in steroidogenesis. However, without evaluation of E2, P4, and A4 secretions, it is not possible to approve their health and correct functionality.

In the absence of OCs, FA follicles secreted both E2 and A4 at low levels as reflected by a low E2/A4 ratio. This observation was unexpected as they overexpressed *Cyp17a1* and *Cyp19a1* genes. Since the overexpression of *LHCGR, CYP17A1,* and *CYP19A1,* and the recorded pattern of steroidogenesis are regarded as negative indicators of follicle health, it could be suggested that the FA hydrogel did not have any favourable effects on follicle culture. Presumably, follicle functionality was affected through alteration of regulatory elements such as transcription factors or some intracellular signalling pathways that mediate the expression and translation of steroidogenic genes (36). Unlike ALG and FA, HAA-encapsulated follicles secreted higher amounts of E2, which resulted in a higher E2/A4 ratio. This pattern of the hormonal secretions is acceptable for large antral follicles and may prove the health of the HAA group's follicles and their proper functionality.

In the presence of OCs, there was no significant difference between encapsulated follicles in the ALG, HAA, and FA groups in terms of follicle diameter, survival, antrum formation and maturation rates, oocyte abnormality rate, gene expression (except for *Bmp7* and *Cyp19a1*), E2 and P4 secretions, and the P4/E2 ratio. Therefore, it can be suggested that OCs may relatively change hydrogel bead properties due to the secretion of some enzymes such as protease, and make the culture condition identical to the follicles of all groups (8).

Finally, a comparison of the -OCs and +OCs groups indicated that the follicles in +OCs groups had a more regular shape, better growth and developmental conditions compared to -OCs groups (including a larger diameter, as well as higher survival and GV to GVBD/MII transition rates, but a lower oocyte abnormality rate). Previous studies have shown that OCs have a high secretion activity and can reproduce the theca cell layer when co-cultured with follicles, consequently enhancing the growth and development of follicles *in vitro* (22, 23). In our study, the expression of growth and differentiation genes, especially *Bmp4* and *Bmp7* that are highly expressed in theca/stromal cells, was similar in -OCs and +OCs groups. So, it could be concluded that co-culturing OCs probably did not contribute to the formation of the theca cell layer, and exerted their effect on follicles by secreting growth and development factors that changed the expression of some other genes that we did not check. Furthermore, the co-culture of the follicles with OCs decreased the expressions

of *Trp53* and *Bax* in the ALG and HAA groups. However, it did not significantly affect *Casp3* expression and the *Bax/Bcl2* ratio. Thus, it can be suggested that in contrast to the findings of the previous studies, OCs could not suppress the apoptosis process within the follicular cells (37). The co-culture condition also did not change the expressions of steroidogenic genes, except for *Lhcgr,* in the FA group; nonetheless, it enhanced secretion of E2 in the ALG and FA groups, and A4 in the FA group. This inconsistency between gene expression and hormonal secretion might be explained as follows. The evaluation of gene expression was only performed on large antral follicles without surrounding co-cultured OCs, but hormone secretion was evaluated on conditioned media from both follicles and OCs. In this regard, although no significant difference in gene expression was observed between the -OCs and +OCs groups, hormonal secretion varied significantly between these groups.

Conclusion

The present study showed that, in the absence of OCs, the applied HAA hydrogel caused promising effects on follicle culture. Indeed its suitable stiffness and desirable innate attributes improved growth and development of the follicles by affecting some biochemical pathways that remain to be discovered in future studies. Furthermore, co-culturing the follicles with OCs improved the culture condition regardless of the type of hydrogel they were encapsulated in. These cells could be used properly in follicle culture systems in order to ameliorate the culture condition.

Acknowledgments

This research was financially supported by Royan Institute. We thank all members of the Embryology, Cell Engineering and Germ Cell Groups at Royan Institute for their helpful assistance and comments during this study. The authors have no conflict of interest to disclose.

Author's Contributions

P.J., M.R.V., L.M., H.B.; Contributed to the conception and design of the study. P.J.: Carried out all experimental work, contributed to data and statistical analysis, and interpretation of data. M.R.V., H.B.: Were responsible for overall supervision. P.J.: Drafted the manuscript, which was revised by M.R.V., L.M, and H.B. All authors read and approved the final draft of the manuscript.

References

1. Dolmans MM, Luyckx V, Donnez J, Andersen CY, Greve T. Risk of transferring malignant cells with transplanted frozen-thawed ovarian tissue. Fertil Steril. 2013; 99(6): 1514-1522.
2. Dolmans MM, Marinescu C, Saussoy P, Van Langendonckt A, Amorim C, Donnez J. Reimplantation of cryopreserved ovarian tissue from patients with acute lymphoblastic leukemia is potentially unsafe. Blood. 2010; 116(16): 2908-2914.
3. Eppig JJ, Schroeder AC. Capacity of mouse oocytes from preantral follicles to undergo embryogenesis and development to live young after growth, maturation, and fertilization in vitro. Biol Reprod. 1989; 41(2): 268-276.
4. Xu M, Kreeger PK, Shea LD, Woodruff TK. Tissue-engineered follicles produce live, fertile offspring. Tissue Eng. 2006; 12(10): 2739-2746.
5. Filatov MA, Khramova YV, Semenova ML. In vitro mouse ovarian follicle growth and maturation in alginate hydrogel: current state of the art. Acta Naturae. 2015; 7(2): 48-56.
6. West ER, Shea LD, Woodruff TK. Engineering the follicle microenvironment. Semin Reprod Med. 2007; 25(4): 287-299.
7. Choi JK, Agarwal P, Huang H, Zhao S, He X. The crucial role of mechanical heterogeneity in regulating follicle development and ovulation with engineered ovarian microtissue. Biomaterials. 2014; 35(19): 5122-5128.
8. Shikanov A, Xu M, Woodruff TK, Shea LD. Interpenetrating fibrin-alginate matrices for in vitro ovarian follicle development. Biomaterials. 2009; 30(29): 5476-5485.
9. Desai N, Abdelhafez F, Calabro A, Falcone T. Three dimensional culture of fresh and vitrified mouse pre-antral follicles in a hyaluronan-based hydrogel: a preliminary investigation of a novel biomaterial for in vitro follicle maturation. Reprod Biol Endocrinol. 2012; 10(1): 29.
10. Brito IR, Silva CM, Duarte AB, Lima IM, Rodrigues GQ, Rossetto R, et al. Alginate hydrogel matrix stiffness influences the in vitro development of caprine preantral follicles. Mol Reprod Dev. 2014; 81(7): 636-645.
11. Mendez U, Zhou H, Shikanov A. Synthetic PEG Hydrogel for Engineering the Environment of Ovarian Follicles. Methods Mol Biol. 2018; 1758: 115-128.
12. Xu M, West E, Shea LD, Woodruff TK. Identification of a stage-specific permissive in vitro culture environment for follicle growth and oocyte development. Biol Reprod. 2006; 75(6): 916-923.
13. Mainigi MA, Ord T, Schultz RM. Meiotic and developmental competence in mice are compromised following follicle development in vitro using an alginate-based culture system. Biol Reprod. 2011; 85(2): 269-276.
14. Rowley JA, Madlambayan G, Mooney DJ. Alginate hydrogels as synthetic extracellular matrix materials. Biomaterials. 1999; 20(1): 45-53.
15. Mosesson MW. Fibrinogen and fibrin structure and functions. J Thromb Haemost. 2005; 3(8): 1894-1904.
16. Takahashi N, Tarumi W, Ishizuka B. Involvement of hyaluronan synthesis in ovarian follicle growth in rats. Reproduction. 2014; 147(2): 189-197.
17. Genasetti A, Vigetti D, Viola M, Karousou E, Moretto P, Rizzi M, et al. Hyaluronan and human endothelial cell behavior. Connect Tissue Res. 2008; 49(3): 120-123.
18. Brito IR, Silva GM, Sales AD, Lobo CH, Rodrigues GQ, Sousa RF, et al. Fibrin-alginate hydrogel supports steroidogenesis, in vitro maturation of oocytes and parthenotes production from caprine preantral follicles cultured in group. Reprod Domest Anim. 2016; 51(6): 997-1009.
19. Liu X, Ma PX. Polymeric scaffolds for bone tissue engineering. Ann Biomed Eng. 2004; 32(3): 477-486.
20. Bozza A, Coates EE, Incitti T, Ferlin KM, Messina A, Menna E, et al. Neural differentiation of pluripotent cells in 3D alginate-based cultures. Biomaterials. 2014; 35(16): 4636-4645.
21. Ramesh HS, Gupta PS, Nandi S, Manjunatha BM, Kumar VG, Ravindra JP. Co-culture of buffalo preantral follicles with different somatic cells. Reprod Domest Anim. 2008; 43(5): 520-524.
22. Itami S, Yasuda K, Yoshida Y, Matsui C, Hashiura S, Sakai A, et al. Co-culturing of follicles with interstitial cells in collagen gel reproduce follicular development accompanied with theca cell layer formation. Reprod Biol Endocrinol. 2011; 9: 159.
23. Tingen CM, Kiesewetter SE, Jozefik J, Thomas C, Tagler D, Shea L, et al. A macrophage and theca cell-enriched stromal cell population influences growth and survival of immature murine follicles in vitro. Reproduction. 2011; 141(6): 809-820.
24. 24. Tian Y, Shen W, Lai Z, Shi L, Yang S, Ding T, et al. Isolation and identification of ovarian theca-interstitial cells and granulose cells of immature female mice. Cell Biol Int. 2015; 39(5): 584-590.
25. Ducibella T, Kurasawa S, Duffy P, Kopf GS, Schultz RM. Regulation of the polyspermy block in the mouse egg: maturation-dependent differences in cortical granule exocytosis and zona pellucida modifications induced by inositol 1,4,5-trisphosphate and an activator of protein kinase C. Biol Reprod. 1993; 48(6): 1251-1257.
26. Vogel SS, Zimmerberg J. Proteins on exocytic vesicles mediate calcium-triggered fusion. Proc Natl Acad Sci USA. 1992; 89(10): 4749-4753.
27. Gui LM, Joyce IM. RNA interference evidence that growth differentiation factor-9 mediates oocyte regulation of cumulus expansion in

mice. Biol Reprod. 2005; 72(1): 195-199.
28. Otsuka F, Yao Z, Lee T, Yamamoto S, Erickson GF, Shimasaki S. Bone morphogenetic protein-15. Identification of target cells and biological functions. J Biol Chem. 2000; 275(50): 39523-39528.
29. Glister C, Richards SL, Knight PG. Bone morphogenetic proteins (BMP) -4, -6, and -7 potently suppress basal and luteinizing hormone-induced androgen production by bovine theca interna cells in primary culture: could ovarian hyperandrogenic dysfunction be caused by a defect in thecal BMP signaling? Endocrinology. 2005; 146(4): 1883-1892.
30. Simon AM, Goodenough DA, Li E, Paul DL. Female infertility in mice lacking connexin 37. Nature. 1997; 385(6616): 525-529.
31. Greve JM, Wassarman PM. Mouse egg extracellular coat is a matrix of interconnected filaments possessing a structural repeat. J Mol Biol. 1985; 181(2): 253-264.
32. Tilly JL, Tilly KI, Perez GI. The genes of cell death and cellular susceptibility to apoptosis in the ovary: a hypothesis. Cell Death Differ. 1997; 4(3): 180-187.
33. Rudel T. Caspase inhibitors in prevention of apoptosis. Herz. 1999; 24(3): 236-241.
34. Hanukoglu I. Steroidogenic enzymes: structure, function, and role in regulation of steroid hormone biosynthesis. J Steroid Biochem Mol Biol. 1992; 43(8): 779-804.
35. Simpson ER, Davis SR. Minireview: aromatase and the regulation of estrogen biosynthesis--some new perspectives. Endocrinology. 2001; 142(11): 4589-4594.
36. Ali A, Lange A, Gilles M, Glatzel PS. Morphological and functional characteristics of the dominant follicle and corpus luteum in cattle and their influence on ovarian function. Theriogenology. 2001; 56(4): 569-576.
37. Otala M, Makinen S, Tuuri T, Sjoberg J, Pentikainen V, Matikainen T, et al. Effects of testosterone, dihydrotestosterone, and 17beta-estradiol on human ovarian tissue survival in culture. Fertil Steril. 2004; 82 Suppl 3: 1077-1085.

Original Article

Age Associated Changes in Transcription of *Adiponectin*, *AdipoR1* and *AdipoR2* Genes in Pancreas of Rats

Marziyeh Feyzi, Ph.D.[1, 2], Mohammad Reza Tabandeh, Ph.D.[3, 4*], Mehrdad Shariati, Ph.D.[5], Mohammad Amin Edalatmanesh, Ph.D.[6]

1. Department of Biology, Fars Science and Research Branch, Islamic Azad University, Fars, Iran
2. Department of Biology, Shiraz Branch, Islamic Azad University, Shiraz, Iran
3. Department of Basic Sciences, Division of Biochemistry and Molecular Biology, Faculty of Veterinary Medicine, Shahid Chamran University of Ahvaz, Ahvaz, Iran
4. Stem Cells and Transgenic Technology Research Center, Shahid Chamran University of Ahvaz, Ahvaz, Iran
5. Department of Biology, Kazerun Branch, Islamic Azad University, Kazerun, Iran
6. Department of Biology, College of Sciences, Shiraz Branch, Islamic Azad University, Shiraz, Iran

Corresponding Address: P.O.Box: 61355-145, Department of Basic Sciences, Division of Biochemistry and Molecular Biology, Faculty of Veterinary Medicine, Shahid Chamran University of Ahvaz, Ahvaz, Iran
Email: m.tabandeh@scu.ac.ir

Received: 29/April/2019, Accepted: 02/September/2019

Abstract

Objective: Adiponectin has a crucial role in the function, proliferation and viability of β-cell via action of two receptors: *AdipoR1* and *AdipoR2*. Nevertheless, age related change of *Adiponectin* system genes in pancreas is unclear or controversial. This study sought to investigate the effects of aging process on serum Adiponectin levels, *Adiponectin* and its receptor expression in the rat pancreas.

Materials and Methods: In this experimental study, insulin resistance markers including serum insulin and glucose concentrations, homeostatic model assessment of insulin resistance (HOMA-IR), oral glucose tolerance test (OGTT), glucose induced insulin secretion (GIIS), serum Adiponectin levels, pancreatic expression of *Adiponectin* and its receptors were studied in male Sprague-Dawley rats at the age of 2, 5, 10, 18, 52 and 72 weeks of age.

Results: We found that aging triggered signs of insulin resistance characteristics in rats at 72 age weeks including marked insulin reduction, hyperglycemia and increased HOMA-IR. Circulating Adiponectin as well as pancreatic expression of *Adiponectin* and *AdipoR1* was gradually decreased with age, while the opposite expression pattern of *AdipoR2* was observed in the old rats.

Conclusion: Because Adiponectin and Adiponectin signaling have crucial role in β-cell function and viability, we concluded that reduction of Adiponectin signaling may be involved in aging induced β-cell dysfunction. As a result, manipulation of Adiponectin signaling may be a beneficial approach for improvement of β-cell function in the old people.

Keywords: *Adiponectin, Adiponectin* Receptors, Aging, Pancreas

Cell Journal(Yakhteh), Vol 22, Suppl 1, Autumn 2020, Pages: 61-67

Citation: **Feyzi M, Tabandeh MR, Shariati M, Edalatmanesh MA. Age associated changes in transcription of adiponectin, AdipoR1 and AdipoR2 genes in pancreas of rats. Cell J. 2020; 22 Suppl 1: 61-67. doi: 10.22074/cellj.2020.6921.**

Introduction

Aging is an important risk factor for metabolic disorders, including obesity, impaired glucose tolerance and type 2 diabetes (T2D). T2D has been estimated to be increased monotonically with age, both in animal and human (1, 2). Age associated glucose intolerance, insulin resistance and T2D may result other age related diseases such as cancer, stroke, cardiovascular diseases, Parkinson's disease and Alzheimer's disease (3). The pathophysiologic mechanisms underlying age-induced glucose intolerance remain incompletely understood. Because insulin is the main regulator of glucose homeostasis, peripheral insulin resistance, impaired insulin secretion from β-cells and unusual insulin clearance are considered as the major age-related complications in old rodents as well as humans (4). Pancreatic β-cell mass is another factor affecting development of insulin resistance in old animals and human. Proliferation, apoptosis of β-cells and islet neogenesis are three major factors that tightly regulate β-cell mass (5). It has been shown that age correlates with decreased proliferative activity and enhanced sensitivity to glucose-induced β-cell apoptosis (6). Recent finding has demonstrated that in old Wistar rats increasing glucose concentration induced a higher level of cell death and lower level of β-cell proliferation in relation with those in young animals (7).

New findings suggest the close relationship between adipose tissue dysfunction and endocrine pancreatic health. Adipose tissue is now recognized to be an important endocrine organ that secretes biologically active compounds, known as adipokines (8, 9). Despite the ever-expanding list of adipokines, which now accounts for over 300 secretory products, few have been studied on their roles in β-cell function (10).

Adiponectin, as a 30 kDa secretory protein, was one of the earlier adipokines identified in rodents and human (11, 12). Adiponectin circulate primarily as a multimeric (trimeric, hexameric and high molecular weight) polypeptide and

is locally proteolytically cleaved to a globular (trimeric) form in which the collagen-like amino-terminal domain is released (12). Adiponectin has antidiabetic properties and its circulating concentrations are reduced in patients with visceral obesity, insulin resistance and T2D (9, 13, 14). Adiponectin performs its physiological effects mainly via AdipoR1 and AdipoR2 receptors. Scatcherd plot analysis revealed that AdipoR1 is a receptor for globular Adiponectin, whereas AdipoR2 is a receptor for full-length Adiponectin. *AdipoR1* is abundantly expressed in muscle, while *AdipoR2* is predominantly expressed in liver (13, 14). Adiponectin -AdipoRs interaction results in activation of different signaling pathways such as AMPK, peroxisome proliferator-activated receptors (PPARs) and p38 MAPK (15).

Recent findings have shown that *Adiponectin* and its two receptors are expressed in β-cells and they have substantial roles in viability and insulin secretion potency of β-cells (15-17). Both *AdipoR1* and *AdipoR2* are expressed in rodent pancreatic beta-cells, while the levels of *AdipoR1* mRNA being expressed at a higher level than *AdipoR2* (16, 17). It has been found that Adiponectin can reverse high glucose induced β-cell impairment and apoptosis in INS-1 clonal rat cells (18). Both globular and truncated Adiponectin (gADN and ADN15-36) stimulate expression of the genes related to function of β-cell including insulin and pancreatic and duodenal homeobox 1 (*PDX1*) gene (mRNA) and they increase viability of β-cells (19). *Adiponectin* gene overexpression or ablation in mice has demonstrated that it can protect β-cell against caspase-8-mediated apoptosis (20).

It is clear that Adiponectin have substantial effects on both function and survival of β-cells. This raises the question of whether *Adiponectin* and its two receptors are changed in aging process of pancreatic beta cells and whether this in turn contributes to the age-related change in insulin sensitivity and glucose stimulated insulin secretion (GSIS), *in vivo*. Therefore, the aim of current study was to define relative expression of *Adiponectin, AdipoR1* and *AdipoR2* in the pancreas and their association with insulin resistance markers in aging process of normal rats.

Materials and Methods

Experimental animals

In this experimental study, male Sprague-Dawley rats at different ages were obtained from animal house of faculty of veterinary medicine, Shahid Chamran university of Ahavz (Iran). All rats were housed four per cage in the standard polycarbonate cages with hardwood chip bedding in the Clean Animal Room and they were allowed free access to food and water. They were housed at 22-24˚C and relative humidity of 60% in 12 hours light/dark cycles, with regular ventilation. All experimental protocols were approved by the Ethics Committee of Shahid Chamran University of Ahvaz for animal and human experiments. All the recruited animals were cared according to the guideline for the care and use of laboratory animals by the national academy of sciences (National Institutes of Health publication No. 86-23).

Sampling

Animals were sacrificed at different ages including; 2 (immature group, n=10), 5 (puberty group, n=10), 10 (puberty group, n=10), 18 (young adult group, n=10), 52 (aged group, n=10) and 72 (aged group, n=10) weeks of age. These numbers were based on natural development of pancreas and life cycle curve of rats, as described previously (21). Half of animals in each age group (n=5) were fasted for 12 hours before sampling and scarified by decapitation under anesthesia using combination of ketamine and xylazine (100 mg/kg of ketamine and 10 mg/kg of xylazine). Blood sample was collected and serum was harvested following centrifugation for 5 minutes at 5000 × g and they were next stored at -20˚C until analysis for hormones and metabolites. Pancreas were removed and kept at -80˚C until use. The weight of animals was recorded before scarification.

Oral glucose tolerance test

Oral glucose tolerance test (OGTT) was performed in half of the animals presented in each age group (n=5). After 12 hours fasting, a 20% glucose solution (2 g/kg body weight) was administered to the rats via a polyethylene gastric tube. Blood glucose was measured by tail prick 15, 30, 90 and 120 minutes using hand-held glucometer (EasyGluco, China) (22). At the end of experiment (120 minutes after glucose administration) blood samples were obtained by heart puncture and serum was separated for determination of insulin concentration. Serum was harvested following the centrifugation for 5 minutes at 5000 × g and it was stored at -20˚C until analysis for hormones and metabolites.

Homeostatic model assessment of insulin resistance estimation

The homeostasis model assessment of basal insulin resistance (HOMA-IR) was calculated based on fasting concentrations of plasma glucose (mmol/l) and plasma insulin (μU/ml) as described previously. Lower HOMA-IR values indicated greater insulin sensitivity, whereas higher HOMA-IR values indicated lower insulin sensitivity (insulin resistance) (23).

Biochemical assay

Adiponectin concentration was measured in serum by using rat ELISA kit (EastBiopharm Co Ltd, China). The intra- and inter-assay coefficients of variation were 3.6 and 7.4%, respectively. Insulin concentration in serum was determined with a commercially available ELISA kit (Mercodia, Sweden). The intra- and inter-assay coefficients of variation were 6.1 and 8.5%, respectively. Serum glucose concentration was determined using a commercial kit through enzymatic colorimetry assay (Pars Azmoon Co, Iran).

RNA extraction and cDNA synthesis

Total RNA was isolated from approximately 50 mg pancreas using RNX^{plus} Kit (Sinaclon Inc, Iran) according to manufacturer's protocol. The yield of extracted RNA was determined spectrophotometrically by measuring the optical density at 260 nm using Eppendorf µCuvette G1.0 microvolume measuring cell (Eppendorf, Germany). The purity and quality of extracted RNA were evaluated using measurement of optical density ratio at 260/280 nm. RNA samples with a ratio more than 1.8 were used for quantitative reverse transcription polymerase chain reaction (qRT-PCR) experiments. For each sample, 0.5 µg of total RNA was reverse transcribed by YTA cDNA synthesis kit using random primers as described by the manufacturer (Yektatajhiz, Iran).

Quantitative reverse trasncription polymerase chain reaction analysis

qRT-PCR was carried out on a Lightcycler Detection System (Roche, USA) using qPCR™ Green Master Kit for SYBR Green I® according to the manufacturer's recommendation (Yektatajhiz, Iran). Reactions were carried out in a 12.5 µl total volume containing 6.25 µl qPCR™ Green Master Kit for SYBR Green I® (Yektatajhiz, Iran), 0.25 µl of each primer (200 nM), 3 µl cDNA (100 ng) and 2.25 µl nuclease-free water. The following specific primers were used for:

Adiponectin-
F: 5´-AATCCTGCCCAGTCATGAAG-3´
R: 5´-CATCTCCTGGGTCACCCTTA-3´, (GeneBank Accession No: NM_144744),

Adiponectin Receptor 1 (*AdipoR1*)-
F: 5´-CTTCTACTGCTCCCCACGGC-3´
R: 5´-TCCCAGGAACACTCCTGCTC-3´, (GeneBank Accession No: XM_006249852.3),

Adiponectin Receptor 2 (*AdipoR2*)-
F: 5´-CCACACAACACAAGAATCCG-3´
R:5´-CCCTTCTTCTTGGGAGAATGG-3´, (GeneBank Accession No: 006237183.2)

GAPDH-
F: 5´-AGTTCAACGGCACAGTCAAG-3´
R: 5´-TACTCAGCACCAGCATCACC-3´. (Takapouzist, Iran).

PCR protocol was consisted of 5 minutes denaturation at 94˚C followed by 45 cycles of 94ºC for 15 seconds and 60ºC for 30 seconds. Two separate reactions without cDNA or with RNA were performed in parallel as controls. Gene expression level of each sample was standardized to the house-keeping gene, *GAPDH* (GenBank: NM-017008) using the ΔΔCt method. The relative gene expression levels were determined using the comparative threshold cycle ($2^{-\Delta\Delta CT}$) method and Lightcycler 96® software. Primer amplification efficiency of the individual genes was performed as previously described (24). All qRT-PCR analysis was performed according to The Minimum Information for Publication of Quantitative Real-Time PCR Experiments (MIQE) guideline (25).

Statistical analysis

All data were expressed as means ± standard error of mean (SEM) and analyzed with SPSS software, version 18.0 (IBM SPSS Inc, USA). One way analysis of variance (ANOVA) and Tukey post hoc test were applied for multiple comparisons between groups. A value of $P<0.05$ was considered statistically significant.

Results

Age related changes of weight, insulin and glucose concentrations

As shown in Figure 1, body weight was increased steadily between 5 and 72 weeks of age. Thus, it reached the maximal level at 72 weeks of age ($P=0.024$). As demonstrated in Figure 2A, glucose concentration had the minimum value in the rats with 2 weeks of age ($P<0.05$), while it increased in an age dependent manner. Glucose concentration showed constant level in the 5, 10 and 18 weeks old rats and it reached the maximum level in advanced age groups (52-72 weeks of age, $P<0.05$, Fig.2A). Additionally, changes in serum insulin levels of the rats through aging process have been shown in Figure 2B. Serum insulin concentration showed constant level in the rats with 5, 10 and 18 weeks of age, while it reached the maximum level in 52 weeks age group ($P<0.05$, Fig.2B). The median insulin level was decreased with advancing age in 72 weeks old group ($P<0.05$, Fig.2B) .Our results showed no change in *HOMA-IR* of different age groups (2-18 weeks of age, Fig.2C), while it was increased in an age dependent manner in the 52 and 72 weeks old rats ($P<0.05$, Fig.2C). The highest level of HOMA-IR was determined in the 52 weeks old rats ($P<0.05$, Fig.2C).

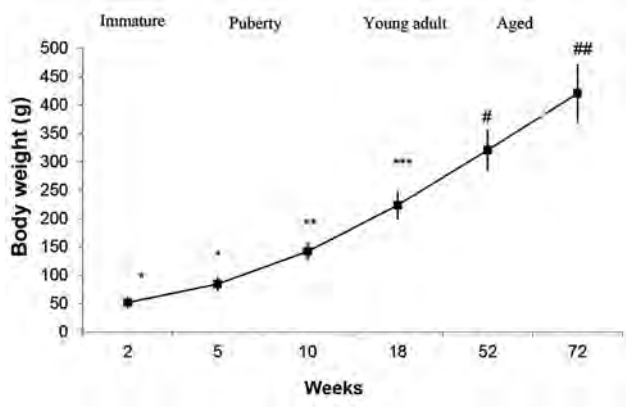

Fig.1: Age-related changes in the body weight of immature (2 weeks old), puberty (5 and 10 weeks old), young adult (18 weeks old) and aged (52 and 72 years old) healthy rats. Data represent means ± SEM for 5 animals in each age group. Comparisons between the groups labeled with different marks were statistically significant ($P<0.05$).

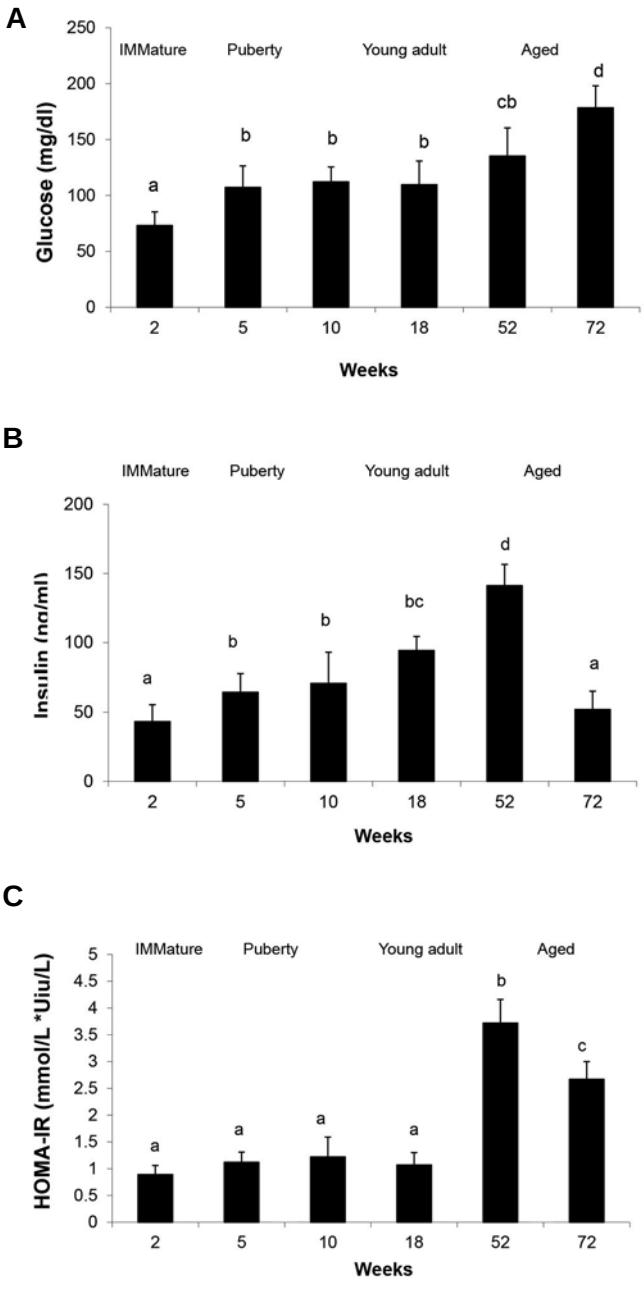

Fig.2: The mean ± SEM for biochemical parameters related to insulin sensivity. **A.** Fasting serum glucose, **B.** Insulin, and **C.** Homeostatic model assessment of insulin resistance (HOMA-IR) values that were examined in immature (2 weeks old), puberty (5 and 10 weeks old), young adult (18 weeks old), and aged (52 and 72 years old) healthy rats. Data was collected from five animals in each age group. Comparisons between the groups labeled with different letters were statistically significant (P<0.05).

Effect of aging on oral glucose tolerance test and glucose stimulated insulin secretion

Figure 3A shows levels of the blood glucose before and after (15, 30, 90, 120 minutes) glucose load during oral glucose tolerance test. As expected, oral glucose administration resulted in an immediate increase in the blood glucose level, which peaked at 15 minutes and then gradually returned to baseline over the following 30 minutes, in young animals. It was found that glucose concentration returned to normal value 30 minutes after OGTT in rats younger than 18 weeks of age, while the 52 and 72 weeks old age groups were increased glucose concentration at the end of OGTT (Fig.3A).

Results verified that 120 minutes after glucose ingestion, blood insulin concentration of the aged groups (52 and 72 weeks old) tended to be higher than those of the younger rats. In the animals with 2, 5, 10 and 18 weeks of age, insulin level returned to fasting level, 2 hours after glucose load. While in the 52 and 72 weeks old rats, insulin concentration was remained high until the end of experiment (P<0.05, Fig.3B).

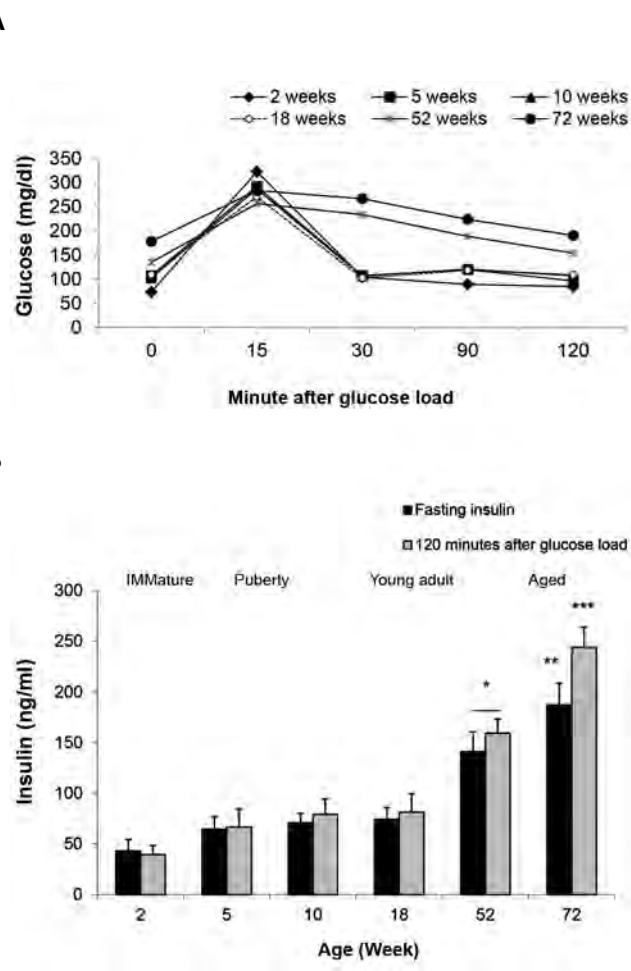

Fig.3: Results of oral glucose tolerance test (OGTT) and glucose stimulated insulin secretion test (GSIS) during aging of rats. **A.** Blood glucose values during the OGTT. Data was collected before and 15, 30, 60, 120 minutes after oral administration of 20% glucose solution in healthy rats with different ages, between 2-72 weeks old. **B.** Blood insulin concentration during the glucose stimulated insulin secretion test (GSIS). Insulin concentration was examined before and 120 minutes after oral administration of 20% glucose solution in healthy rats with different ages, between 2-72 weeks old. Data was collected from five animals in each age group. Comparisons between the groups labeled with different marks were statistically significant (P<0.05).

Alteration of serum Adiponectin level during aging

Our results showed no significant difference in serum Adiponectin concentration detected in the rats with age of 2, 5, 10 and 18 weeks (P>0.05), while it was gradually decreased in old rats with 52-72 weeks of age (P<0.05, Fig.4).

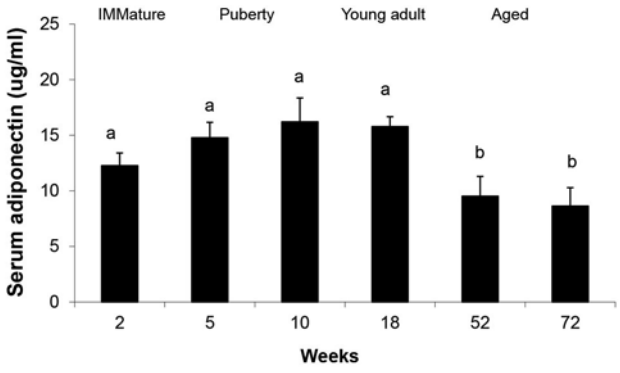

Fig.4: Age-related changes in serum Adiponectin concentration of immature (2 weeks old), puberty (5 and 10 weeks old), young adult (18 weeks old), and aged (52 and 72 years old) healthy rats. Data represent means ± SEM for five animals in each age group. Comparisons between the groups labeled with different marks were statistically significant (P<0.05).

Age related changes in expression of *Adiponectin* and its two receptors in pancrease

An age dependent increase was observed in pancreatic expression of *Adiponectin* in the rats with ages of 2, 5, 10 and 18 weeks (P<0.05, Fig.5A). *Adiponectin* mRNA levels were decreased in the aged rat groups (72 weeks old group) exhibiting the lowest transcription level (P<0.05, Fig.5A). As illustrated in Figure 5B, expression of *AdipoR1* gene in rat aged between 5 and 10 weeks was constant, while it showed significant upregulation at 18 and 52 weeks of age (P<0.05). *AdipoR1* transcription was reduced to the minimum level in the 72 weeks old group (P<0.05). Figure 5C shows the expression levels of *AdipoR2* in pancreas of rats with different ages. It was found that the rats between 2 and 10 weeks of age had similar *AdipoR2* transcription level. *AdipoR2* mRNA level was significantly higher in the 18 and 52 weeks old rats compared to younger animals (P<0.05). *AdipoR2* expression was significantly reduced to the minimum level in the 72 weeks old rats (P<0.05, Fig.5C).

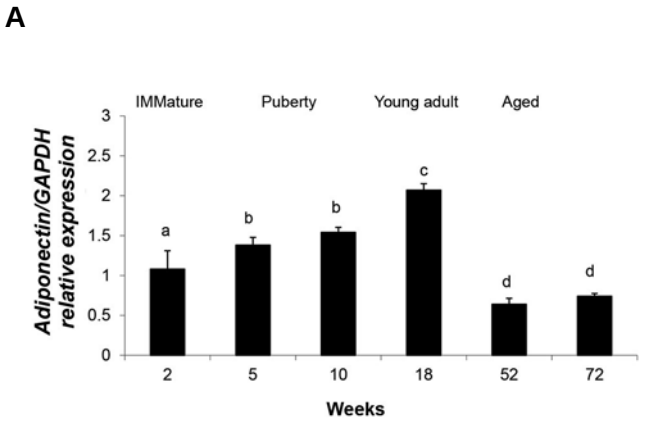

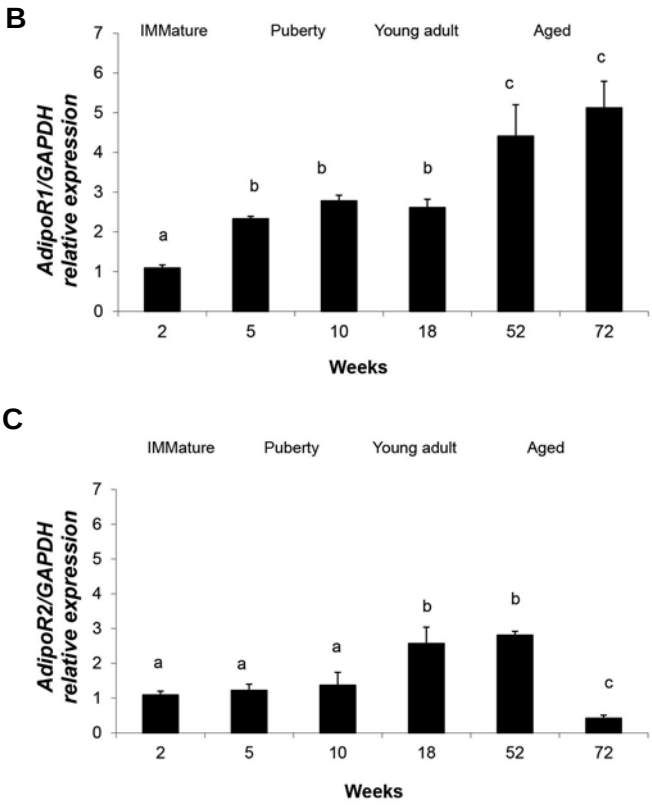

Fig.5: Relative expedition of *Adiponectin* and it's to receptors in pancreas of rats at different ages. mRNA levels of **A.** *Adiponectin*, **B.** *AdipoRI* and **C.** *AdipoRII* in pancrease of immature (2 weeks old), puberty (5 and 10 weeks old), young adult (18 weeks old) and aged (52 and 72 years old) healthy rats. Data represent means ± SEM for five animals in each age group. Comparisons between the groups labeled with different marks were statistically significant (P<0.05).

Discussion

Normal aging is usually associated with progressive β-ell dysfunction that may be responsible for serious disturbances of physiological homeostasis, particularly, glucose tolerance (2, 4, 5). Recently, there has been increasing evidences that Adiponectin, one of the most abundant circulating adipokines, is involved in the regulation of pancreatic β-cell function (10, 14-16). Although expression and function of Adiponectin have been studied in β-cells, little data are available regarding the effect of aging on the expression of *Adiponectin* system genes in pancreas among the aging process. The current study analyzed pancreatic expression of *Adiponectin*, its two receptors and several metabolic markers related to glucose tolerance in normal aging process of rat.

In agreement with the previous studies in both rodents and humans, our results showed that ageing can change anthropometric characteristics and insulin resistance features, such as increasing body weight, serum glucose concentration and HOMA-IR (22, 23). The results of the OGTT and GSIS at 2, 5, 10, 18, 52 and 72 weeks of age of rats demonstrated that glucose tolerance and insulin sensitivity were affected in old animals. Our results showed that, beginning of aging in 52 weeks old animals was associated with marked elevation of serum insulin and glucose levels, while in the advanced age group (72 weeks

old animals) insulin level was decreased to the minimum level. Increase in serum insulin levels at the beginning of aging was not in accordance with our assumptions. These changes may be described by the recently coined term "glucose allostasis" theory indicating that the slightly higher glucose levels in insulin-resistant states drive the β-cells to produce higher levels of insulin (26). Glucose allostasis may be a compensatory mechanism can regulate normal glucose metabolism during insulin resistance. Moreover, recent researches have shown that hyperinsulinemia along with moderate hyperglycemia are the first events in developing insulin resistance in human and experimental animals. In accordance with our observation, *Marban* and coworkers showed that mice, stably transfected with extra copies of the human insulin gene, elevated basal plasma insulin level despite the normal weight and fasting glucose, but they display elevated postprandial glucose and diminished insulin tolerance test (27). Taken together we concluded that the onset of aging is associated with hyperinsulinemia, moderate hyperglycemia and diminished GGT, while advanced aging is accomplished with reduction of insulin production along with elevated glucose concentration.

Our results showed reduction of serum Adiponectin in the aged rats. In accordance with our findings, Li et al. (28) showed that plasma Adiponectin levels and visceral fat ratio in the 24months old mice were lower compared to the 2 and 6months old mice. Mori et al. (29) has also shown that circulating Adiponectin level were remarkably lower in dogs aged 8-12 years than dogs aged 0-7 years. Reduction of plasma Adiponectin concentration in early phases of obesity and in parallel to the progressive development of insulin resistance has been reported in obese and diabetic rhesus monkey (30). Prospective studies in Pima Indians demonstrated that high concentrations of Adiponectin were protective against the development of T2D (31). Furthermore, circulating plasma Adiponectin levels and expressions of both *AdipoRs* are reduced in the subjects with a family history of T2D (32). Based on the incidence of insulin resistance in aged rats and previous data, it was concluded that circulating Adiponectin level was reduced with age, indicating that Adiponectin probably played an important role in aging-related diseases, such as insulin resistance. To support this hypothesis, Yamauchi et al. (33) showed that administration of Adiponectin can lead to improvement of insulin sensitivity, glucose tolerance and correction obesity-related hyperglycemia.

Our results showed that *Adiponectin* and *AdipoR2* expression were down-regulated in pancreas of old animals with 72 weeks of age, while *AdipoR1* expression was increased in the advanced age. Recent findings have clarified that Adiponectin and Adiponectin signaling is important regulators of β-cell function and defects in the expression/secretion of *Adiponectin* or its receptors in pancreas of the old rats may be a contributory factor to β-cell dysfunction. This could diminish insulin secretion during the aging process. Recently Okamoto et al. (34) has shown that Adiponectin stimulates insulin secretion from pancreatic islets, confirming that down-regulation of *Adiponectin* in pancreas of the old rats may affect insulin expression or secretion among the aging process. Molecular *reason* for observing opposite pattern of expression of *AdipoR1* and *AdipoR2* in pancreas of the aged animals is unknown. *AdipoR1* act as a major receptor of Adiponectin in pancreas, regarding the level of *AdipoR1* mRNA expressed at a higher level than *AdipoR2* in pancreas (16, 17). Increased *AdipoR1* expression in pancreas of the aged rats may act as a compensatory mechanism to restore the Adiponectin signaling and sensitize the pancreatic cells to the Adiponectin, when its expression or secretion is reduced. Further investigations are needed to give a better insight into the molecular mechanisms of *Adiponectin* receptors transcription in the aged animals.

Several researchers shifted the focus of their interest on the effect of aging on biology of islet, with particular attention to the proliferative capacity and apoptosis of β-cells. Adiponectin is a candidate molecule because it is a positive regulator of pancreatic β mass. In line with these observations, findings have shown that Adiponectin activates Erk and Akt in clonal β-cells, increases their proliferative activity and regulates their cell cycle (15). It has been found that in INS-1 clonal β-cells, Adiponectin can protect against palmitate or ceramide induced apoptosis (35). Furthermore *Adiponectin* gene overexpression in mice can attenuate caspase-8 mediated apoptosis in β-cells (36). Recently, transcriptome analysis revealed that Adiponectin can boost β-cells regeneration by improving pancreatic islet lipid metabolism and this antilipotoxic effect are attributed to up-regulation of two key transcription factors, including hepatocyte nuclear factor 4 (HNF4) and peroxisome proliferator activated receptor α (PPARα) (35). These data suggest that Adiponectin can maintain a normoglycaemic environment in pancreatic islet in the face of decreases in insulin sensitivity. This could be performed preservation of the β-cell mass and diminishing *Adiponectin* expression or its signaling pathway. These alterations may have important physiological role in progressing β-cell dysfunction and decreasing insulin secretion in the old animals.

One of the major finding of our study was the increased expression of pancreatic *AdipoR1* in the aged rats, despite up-regulation of *Adiponectin* and *AdipoR1*. It remains unclear whether an increase in *AdipoR1* expression of the pancreas with age is a positive feedback regulation induced by decreased *Adiponectin* expression, or the compensatory mechanism for improvement of Adiponectin action in pancrease, which deserves further investigation.

Conclusion

Circulating Adiponectin as well as the pancreatic expression of *Adiponectin* and *AdipoR1* reduced with age, which is accompanied by the increased insulin resistance markers in old rats. Because Adiponectin and Adiponectin signaling have crucial role in β-cell function and viability, we concluded that reduction of Adiponectin signaling

may be involved in aging induced β-cell dysfunction and related metabolic complications, in old animals or humans. Given the findings of our study direct activation of the *Adiponectin* receptors, via small molecule agonists, may be used in future for modulation of Adiponectin system and improvement of β-cell function in the aged people.

Acknowledgements

This work was funded by a Grant obtained from Shahid Chamran University of Ahvaz Research Council (Grant No: 96/3/02/16670). There is no conflict of interest in this study.

Authors' Contributions

M.R.T., M.S., M.A.E.; Designed the study and analyzed the results. M.F.; Performed the study and collected the data. M.R.T., M.F.; Drafted the manuscript. M.R.T., M.S.; Revised the manuscript critically for important intellectual content. M.R.T.; Is the guarantor of this work who has full access to all the data in the study, takes responsibility for the integrity of the data, and the accuracy of the data analysis. All authors performed final approval of the manuscript.

References

1. Lee PG, Halter JB. The pathophysiology of hyperglycemia in older adults: clinical considerations. Diabetes Care. 2017; 40(4): 444-452.
2. De Tata V. Age-related impairment of pancreatic Beta-cell function: pathophysiological and cellular mechanisms. Front Endocrinol (Lausanne). 2014; 5: 138.
3. Yeap BB. Hormones and health outcomes in aging men. Exp Gerontol. 2013; 48(7): 677-681.
4. Gunasekaran U, Gannon M. Type 2 diabetes and the aging pancreatic beta cell. Aging (Albany NY). 2011; 3(6): 565-575.
5. Aguayo-Mazzucato C, van Haaren M, Mruk M, Lee TB Jr, Crawford C, Hollister-Lock J, et al. β Cell aging markers have heterogeneous distribution and are induced by insulin resistance. Cell Metab. 2017; 25(4): 898-910.
6. Tschen SI, Dhawan S, Gurlo T, Bhushan A. Age-dependent decline in cell proliferation restricts the capacity of cell regeneration in mice. Diabetes. 2009; 58(6): 1312-1320.
7. Gu Z, Du Y, Liu Y, Ma L, Li L, Gong Y, et al. Effect of aging on islet beta-cell function and its mechanisms in Wistar rats. Age (Dordr). 2012; 34(6): 1393-1403.
8. Tabandeh MR, Jafari H, Hosseini SA, Hashemitabar M. Ginsenoside Rb1 stimulates adiponectin signaling in C2C12 muscle cellsthrough up-regulation of AdipoR1 and AdipoR2 proteins. Pharm Biol. 2015; 53(1): 125-132.
9. Nazari M, Moghimipour E, Tabandeh MR. Betaine down regulates apelin gene expression in cardiac and adipose tissues of insulin resistant diabetic rats fed by high-calorie diet. Int J Peptide Res Therap. 2017; 23(2): 181-190
10. Dunmore SJ, Brown JE. The role of adipokines in β-cell failure of type 2 diabetes. J Endocrinol. 2013; 216(1): T37-T45.
11. Wang ZV, Scherer PE. Adiponectin, the past two decades. J Mol Cell Biol. 2016; 8(2): 93-100.
12. Scherer PE, Williams S, Fogliano M, Baldini G, Lodish HF. A novel serum protein similar to C1q, produced exclusively in adipocytes. J Biol Chem. 1995; 270(45): 26746-26749.
13. Yamauchi T, Kamon J, Ito Y, Tsuchida A, Yokomizo T, Kita S, et al. Cloning of adiponectin receptors that mediate antidiabetic metabolic effects. Nature. 2003; 423(6941): 762-769.
14. Ruan H, Dong LQ. Adiponectin signaling and function in insulin target tissues. J Mol Cell Biol. 2016; 8(2): 101-109.
15. Wijesekara N, Krishnamurthy M, Bhattacharjee A, Suhail A, Sweeney G, Wheeler MB. Adiponectin-induced ERK and Akt phosphorylation protects against pancreatic beta cell apoptosis and increases insulin gene expression and secretion. J Biol Chem. 2010; 285(44): 33623-33631.
16. Wade TE, Mathur A, Lu D, Swartz-Basile DA, Pitt HA, Zyromski NJ. Adiponectin receptor-1 expression is decreased in the pancreas of obese mice. J Surg Res. 2009; 154(1): 78-84.
17. Kharroubi I, Rasschaert J, Dizirik DL, Cnop M. Expression of adiponectin receptors in pancreatic b cells. Biochem Biophy Res Communic. 2003; 312(4): 1118-1122.
18. Lin P, Chen L, Li D, Liu J, Yang N, Sun Y, et al. Adiponectin reduces glucotoxicity-induced apoptosis of INS-1 rat insulin-secreting cells on a microfluidic chip. Tohoku J Exp Med. 2009; 217(1): 59-65.
19. Brown JE, Conner AC, Digby JE, Ward KL, Ramanjaneya M, Randeva HS, et al. Regulation of beta-cell viability and gene expression by distinct agonist fragments of adiponectin. Peptides. 2010; 31(5): 944-949.
20. Liadis N, Salmena L, Kwan E, Tajmir P, Schroer SA, Radziszewska A, et al. Distinct in vivo roles of caspase-8 in beta-cells in physiological and diabetes models. Diabetes. 2007; 56(9): 2302-2311.
21. Bonner-Weir S, Aguayo-Mazzucato C, Weir GC. Dynamic development of the pancreas from birth to adulthood. Ups J Med Sci. 2016; 121(2): 155-158.
22. Ghezzi AC, Cambri LT, Botezelli JD, Ribeiro C, Dalia RA, de Mello MA. Metabolic syndrome markers in wistar rats of different ages. Diabetol Metab Syndr. 2012; 4(1): 16.
23. Bowe JE, Franklin ZJ, Hauge-Evans AC, King AJ, Persaud SJ, Jones PM. Assessing glucose homeostasis in rodent models. J Endocrin. 2014; 222: G13-G25.
24. Tabandeh MR, Hosseini A, Saeb M, Kafi M, Saeb S. Changes in the gene expression of adiponectin and adiponectin receptors (AdipoR1 and AdipoR2) in ovarian follicular cells of dairy cow at different stages of development. Theriogenology. 2010; 73 (5): 659-669.
25. Bustin SA, Benes V, Garson JA, Hellemans J, Huggett J, Kubista M, et al. The MIQE guidelines: Minimum information for publication of quantitative real-time PCR experiments. Clin Chem. 2009; 55(4): 611-622.
26. Cerf ME. Beta cell dynamics: beta cell replenishment, beta cell compensation and diabetes. Endocrine. 2013; 44(2): 303-311.
27. Marban SL, Roth J. Transgenic hyperinsulinemia: a mouse model of insulin resistance and glucose intolerance without obesity. Shafrir E, editor. In: Lessons from animal diabetes VI. 6th ed. Boston: Birkhauser; 1996; 201-224.
28. Li B, Nishida M, Kaimoto K, Asakawa A, Chaolu H, Cheng KC, et al. Effects of aging on the plasma levels of nesfatin-1 and adiponectin. Biomed Rep. 2014; 2(1): 152-156.
29. Mori N, Kawasumi K, Arai T. Comparison of the plasma insulin and adiponectin concentrations as metabolic markers in clinically healthy dogs with ageing. J Anim Vet Adv. 2012; 11(7): 971-974.
30. Hotta K, Funahashi T, Bodkin NL, Ortmeyer HK, Arita Y, Hansen BC, et al. Circulating concentrations of the adipocyte protein adiponectin are decreased in parallel with reduced insulin sensitivity during the progression to type 2 diabetes in rhesus monkeys. Diabetes. 2001; 50(5): 1126-1133.
31. Lindsay RS, Funahashi T, Hanson RL, Matsuzawa Y, Tanaka S, Tataranni PA, et al. Adiponectin and development of type 2 diabetes in the Pima Indian population. Lancet. 2002; 360(9326): 57-58.
32. Civitarese AE, Jenkinson CP, Richardson D, Bajaj M, Cusi K, Kashyap S, et al. Adiponectin receptors gene expression and insulin sensitivity in non-diabetic Mexican Americans with or without a family history of Type 2 diabetes. Diabetologia. 2004; 47(5): 816-820.
33. Yamauchi T, Kamon J, Waki H, Terauchi Y, Kubota N, Hara K, et al. The fat-derived hormone adiponectin reverses insulin resistance associated with both lipoatrophy and obesity. Nat Med. 2001; 7(8): 941-946.
34. Okamoto M, Ohara-Imaizumi M, Kubota N, Hashimoto S, Eto K, Kanno T, et al. Adiponectin induces insulin secretion in vitro and in vivo at a low glucose concentration. Diabetologia. 2008; 51(5): 827-835.
35. Ye R, Wang M, Wang QA, Scherer PE. Adiponectin-mediated antilipotoxic effects in regenerating pancreatic islets. Endocrinology. 2015; 156(6): 2019-2028.
36. Lin P, Chen L, Li D, Liu J, Yang N, Sun Y, et al. Adiponectin reduces glucotoxicity-induced apoptosis of INS-1 rat insulin-secreting cells on a microfluidic chip. Tohoku J Exp Med. 2009; 217(1): 59-65.

Original Article

MYC Participates in Lipopolysaccharide-Induced Sepsis via Promoting Cell Proliferation and Inhibiting Apoptosis

Yin Li, M.M.[1#], Chengqi Kong, M.M.[2#], Lei Feng, M.M.[1], Wenliang Tang, M.M.[1], Mengwei Chen, M.M.[2*], Zhiyuan Zheng, M.M.[2*]

1. Emergency Department of Huadong Hospital, Fudan University, Yan'an Xi Road, Shanghai, China
2. Cardiovascular Department of Huadong Hospital, Fudan University, Shanghai, China

#These authors contributed equally to this work.

Corresponding Address: Cardiovascular Department of Huadong Hospital, Fudan University, Shanghai, China
Emails: andychenmw@hotmail.com, dora_zzy@hotmail.com

Received: 20/May/2019, Accepted: 14/September/2019

Abstract

Objective: This study aimed to explore the potential mechanism of *MYC* proto-oncogene, BHLH Transcription Factor (*MYC*) gene, on sepsis.

Materials and Methods: In this experimental study, rat-derived H9C2 cardiomyocyte cells were cultured *in vitro*, followed by lipopolysaccharide (LPS) treatment with different concentration gradients. The cholecystokinin octapeptide (CCK-8) assay, enzyme-linked immunoassay (ELISA) assay, quantitative reverse transcription polymerase chain reaction (qRT-PCR), cell transfection, Western blot and flow cytometry were used to observe the cellular apoptosis and proliferation of cells in both treated LPS groups and normal control group.

Results: The result of CCK-8 assay showed that silencing *MYC* inhibited cellular proliferation of sepsis in absence or presence of LPS treatment. ELISA assay showed that the expressions of tumor necrosis factor-α (TNF-α) and interleukin-6 (IL-6) were decreased in *MYC* silenced group, but they were increased after LPS treatment. Moreover, Flow cytometry assay showed that *MYC* silencing contributed to the apoptosis of sepsis cells. Furthermore, the expression of inflammatory factors showed that *MYC* silencing elevated the expression of inflammation factors.

Conclusion: *MYC* might take part in the process of LPS induced sepsis through suppressing apoptosis and inducing cell proliferation. Moreover, *MYC* might reduce inflammation during the progression of LPS induced sepsis.

Keywords: Cell Apoptosis, Cell Proliferation, Inflammation, Lipopolysaccharide, *MYC*, Sepsis

Cell Journal(Yakhteh), Vol 22, Suppl 1, Autumn 2020, Pages: 68-73

Citation: Li Y, Kong Ch, Feng L, Tang W, Chen M, Zheng Z. MYC participates in lipopolysaccharide-induced sepsis via promoting cell proliferation and inhibiting apoptosis. Cell J. 2020; 22 Suppl 1: 68-73. doi: 10.22074/cellj.2020.6961.

Introduction

Sepsis is a kind of systemic inflammatory response syndrome (SIRS), caused by the infection (1). As the most common reason for the hospitalized death, the incidence of sepsis is 18 million cases per year worldwide (2). Poor organ function or insufficient blood flow is the outcome of severe sepsis in clinic (3). Although the influence factors and interventions for sepsis have been widely studied in both animal models and clinic (4, 5), details of the pathogenesis mechanisms are still unclear.

MYC proto-oncogene, BHLH Transcription Factor (*MYC*) are a group of early oncogenes including C-myc, N-myc and L-myc. The corresponding RNAs regulated by MYC participate in various biological functions including cell death, proliferation and mechanisms of drug resistance (6). *MYC* silencing by small interfering RNAs (siRNAs) revealed the importance of biological function of *MYC* in disease (7). Previous study showed that *MYC* signaling in inflammatory response can be used as a therapeutic target during the disease progression (8). Although sepsis is caused by the inflammatory immune response (9), detail of the function of *MYC* in this system is unknown. In our previous gene expression analysis, *MYC* were proved to participate in the pathogenesis of sepsis (10). Although these results provided a genomics information for sepsis progression, detail of the gene functions like *MYC* in pathogenesis of sepsis is yet unclear. Therefore, in the current study, we aimed to explore the potential function of *MYC* on sepsis progression through observing the differences of proliferation and apoptosis of cells in the treated lipopolysaccharide (LPS) groups and normal control group. This will provide new sight for gene-based target therapy of sepsis.

Materials and Methods

Cell culture and grouping

In this experimental study, rat-derived H9C2 cardiomyocyte cell line (Chinese Academy of Sciences, Shanghai, China) were cultured in Dulbecco's Modified Eagle Medium (DMEM) culture medium (Gibco BRL, USA) containing 10% fetal bovine serum (FBS, Gibco BRL, USA) and 1% penicillin/streptomycin, followed by incubation at 37˚C with 5% CO_2. Then, the H9C2 cells in logarithmic growth phase were digested with trypsin (0.25%, Gibco BRL, USA) and cultured in the 96-well plates (2×10^5 cells/well, 37˚C, 5% CO_2) for 24 hours.

When the cell density in plates was above 90%, they were divided into five groups including normal control (NC), LPS1 (treated with 1 μg/ml LPS), LPS10 (treated with 10 μg/ml LPS), LPS20 (treated with 20 μg/ml LPS) and LPS40 (treated with 40 μg/ml LPS) groups. Treatment time for all of these groups was 4, 8 and 24 hours, respectively.

CCK-8 assay

A total of 5 mg/ml CCK solution (BIYUNTIAN Biotechnological Co., China) was used for the CCK-8 assay on H9C2 cells at 24, 48 and 72 hours. Subsequently, the plates were incubated at 37˚C with 5% CO_2 for 24 hours and the absorbance at 450 nm was recorded by a microplate reader (Gene Co., Germany).

ELISA assay

ELISA assay was performed to reveal the expression of MYC in each group. Briefly, interleukin-6 (IL-6) and tumor necrosis factor-α (TNF-α) levels were tested in the samples by ELISA kit (BioSource International, USA). Absorbance (OD) of each hole was measured at 450 nm wavelength in sequence by a microplate reader (Gene Co.).

Quantitative reverse transcription-polymerase chain reaction assay

Total RNA extraction was performed using TRizol reagent (TaKaRa, Japan), and reverse transcribed using RevertAidTM First Strand cDNA Synthesis Kit (Thermo Fisher Scientific, USA). Quantitative reverse transcription-polymerase chain reaction (qRT-PCR) assay was performed on ABI7900FAST (Thermo Fisher Scientific, USA) and the primers were as follows:

MYC-
F: 5´-CCTCGCGTTATTTGAAGCCTG-3´
R: 5´-CACCGAGTCGTAGTCGAGGT-3´

GAPDH-
F: 5´-AGACAGCCGCATCTTCTTGT-3´
R: 5´-CTTGCCGTGGGTAGAGTCAT-3´.

PCR program was performed with thermocycling conditions: 50˚C for 3 minutes, 95˚C for 3 minutes, 40 cycles of 95˚C for 10 seconds, 60˚C for 30 second and melt curve of 60˚C to 95˚C (Increment 0.5˚C for 10 seconds). The method of $2^{-\Delta\Delta Ct}$ (11) was used for the investigation of gene expression.

Cell transfection

Specific shRNA sequence was designed and synthesized in the current study. Simply, shRNAs were inserted into the vector of pLKO.1-Puro at the restriction sites of AgeI and EcoRI. Then, the recombinant pLKO.1-Puro was transformed into DH5α competent cell, followed by the sequence identification of positive clones. The confirmed plasmid by DNA sequencing was extracted by CP6 adsorption column (Tiangen, China). The cells were transfected with plasmid carrying shRNA sequence by the lipofectamine 2000 (Thermo Fisher Scientific, USA). After 48 hours of transfection, the transfected cells were collected for further assay.

Western blot

Total proteins of H9C2 were extracted by RIPA lysis buffer (BIYUNTIAN Biotechnological Co.). After centrifugation, the proteins were separated by SDS-polyacrylamide gel electrophoresis (10%), and transferred to the polyvinylidenefluoride membrane (Millipore, USA). 5% skimmed milk (0.75 g milk powder+15 ml PBS) was used for blocking the membrane for 1-2 hour(s) and incubated with primary antibodies (C-myc, rabbit monoclonal antibody, 57 kDa, 1:1000; Pax-2, rabbit monoclonal antibody, 45 kDa, 1:5000; GAPDH, rat monoclonal antibody, 36 kDa, 1:1000; Santa Cruz Biotechnology Inc., USA) overnight at 4˚C. Then, the samples were treated with the secondary antibody (anti-rabbit, 1:10000; anti-rat, 1:5000; Cwbio, China) for 2 hours at 37˚C. Protein brands were visualized with Millipore ECL Gel imaging system (Millipore, USA). Finally, the results were analyzed by TanonImage 4600 (Tanon, China).

Flow cytometer

Apoptosis of the transfected cells was detected by flow cytometry. Briefly, the cells were digested by 0.25% trypsin (Gibco BRL, USA) and seeded at a 9-well plates (1×10^6 cells/well), followed by incubation at 37˚C with 5% CO_2 for 24 hours. Eugenol was added the next day and apoptosis was detected after 24 hours, 48 hours and 72 hours respectively. For detection, the samples were digested with 0.25% trypsin and resuspended with 400 ul of 1× Binding Buffer for CK groups and 100 ul 1× Binding Buffer for treated LPS groups. Then, the samples were mixed with 5 μl FITC-Annexin V, as well as 5 μl PI. CK group were divided into non-dyeing group, FITC-Annexin V group, PI group, FITC-Annexin V and PI group. The progression of cell cycle was subsequently monitored based on flow cytometry, and the result was analyzed based on Multi-Cycle AV software (Phoenix Flow Systems, USA).

Statistical analyses

All data were expressed as mean ± standard deviation (SD). Statistical analysis was conducted with Graphpad prism 5 (Graphpad Software, USA). Furhtermore, the $P<0.05$ was considered to be significantly different.

Results

MYC silencing on different loci in H9C2 cells

The effect of *MYC* gene silencing on sepsis cells had been investigated by qRT-PCR and Western blot. Compared to NC, silencing efficiency of the three loci (H9C2-652, H9C2-595 and H9C2-1840) was decreased significantly ($P<0.01$, Fig.1A). Rather than NC, expression of the

proteins was inhibited in all *MYC* silencing samples. Meanwhile, silencing efficiency of shMYC-595 was significant, compared to the other two loci (Fig.1B).

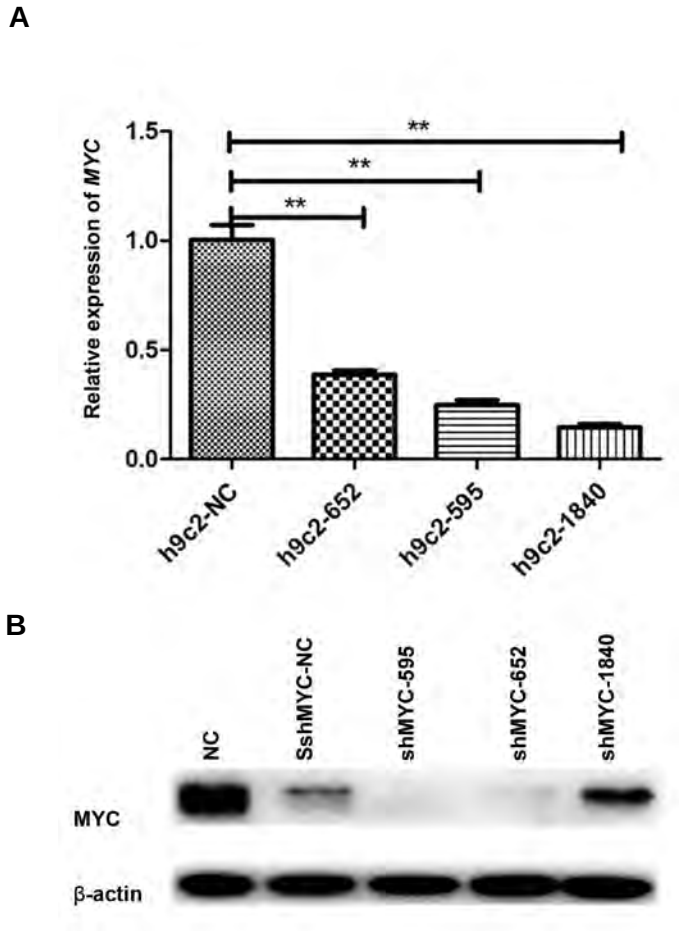

Fig.1: Result of *MYC* gene silencing in the current cell lines. **A.** Analysis of quantitative reverse transcription-polymerase chain reaction (qRT-PCR) to detect the effect of *MYC* silencing. **B.** Result of Western blot for protein expression in MYC silencing cells. **; P<0.01 and NC; Black control.

MYC silencing inhibited H9C2 cell proliferation

Cell proliferation in different groups was analyzed by CCK-8 assay (Fig.2A). The result showed that compared to NC group, *MYC* silencing significantly inhibited proliferation of H9C2 cells. After LPS treatment, *MYC* silencing continued to inhibit proliferation of H9C2 cells. Moreover, in comparison with untreated cells, LPS treatment inhibited proliferation of H9C2 cells (P<0.01).

MYC silencing regulated expressions of TNF-*α* and IL-6

The contents of TNF-α and IL-6 in H9C2 cells were analyzed by ELISA assay. The results showed that expressions of TNF-α and IL-6 were significantly decreased in *MYC* silencing group, compared to the NC group (P<0.01 for the both molecules; Fig.2B). After LPS treatment, expressions of TNF-α and IL-6 were significantly increased in *MYC* silencing group (P<0.01, Fig.2C).

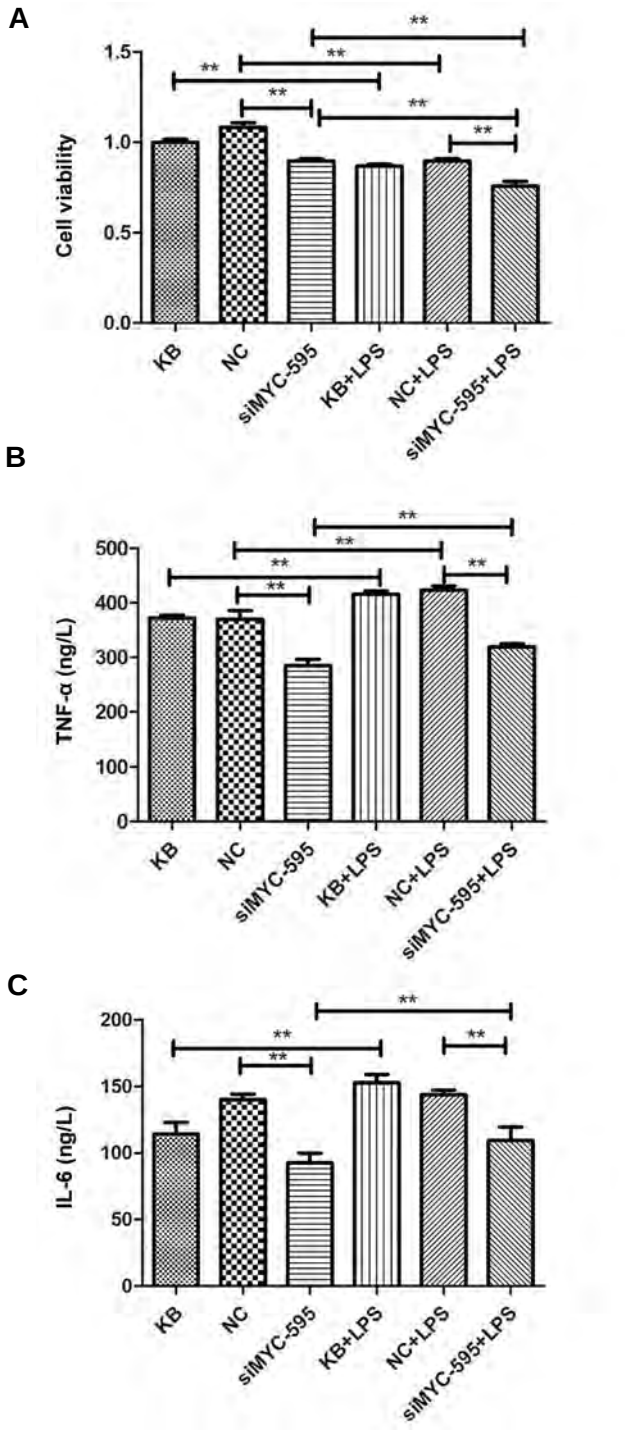

Fig.2: Result of CCK-8 assay and ELISA analysis. **A.** Detection of cell proliferation by CCK-8 assay. **B.** Content of TNF-α in the samples detected by ELISA. **C.** Content of IL-6 in the samples detected by ELISA. **; P<0.01 and NC; Black control.

MYC silencing contributed to the apoptosis of H9C2 cells

The result showed that compared to the non-LPS treatment groups (KB, NC and siMYC-595), the ratio of apoptosis of H9C2 cells in LPS treatment groups (KB+LPS, NC+LPS and siMYC-595+LPS) were increased (P<0.05, Fig.3A). Moreover, compared to the NC+LPS group, apoptosis in the siMYC-595+LPS group was increased (P<0.05, Fig.3B).

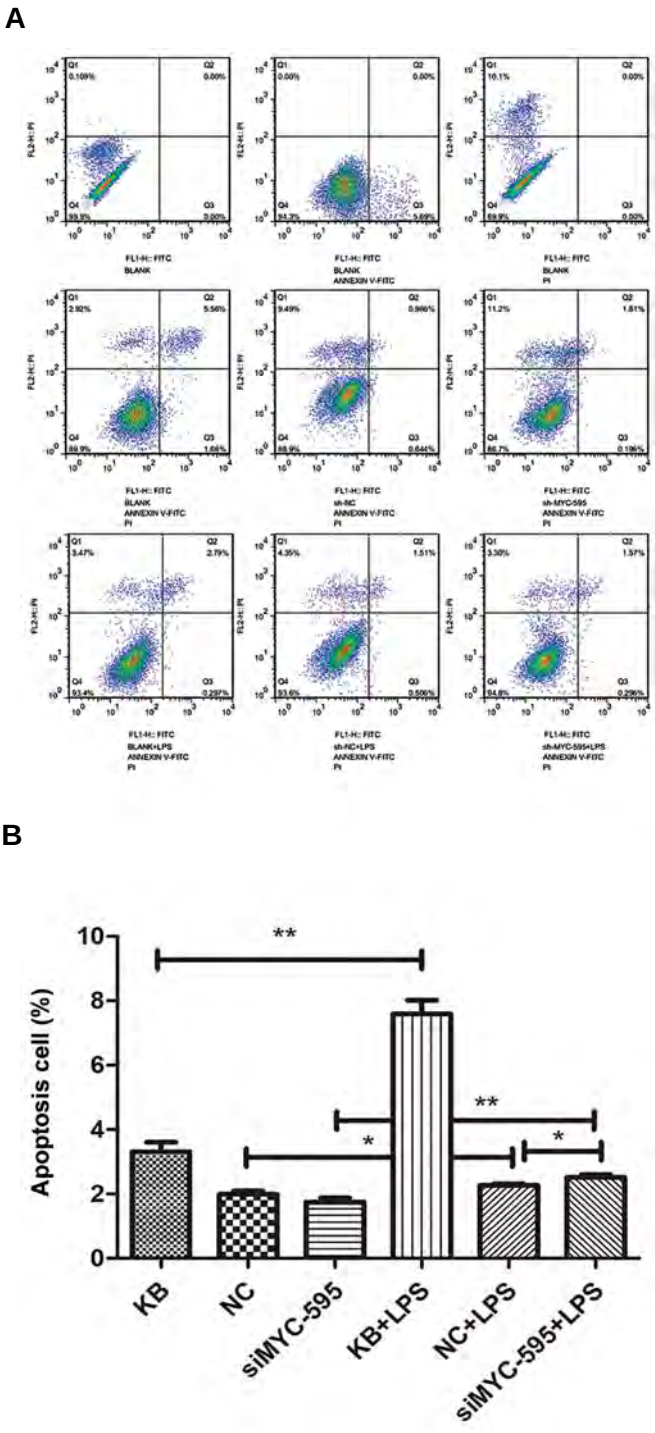

Fig.3: Result of flow cytometry assay for apoptosis. **A.** Result of two-dimensional scatter plot for cell apoptosis in each group. PI and annexin V were represented in X-axis and Y-axis, respectively. PI-stained cells represented dead cells, annexin V-stained cells represented early apoptotic cells, and double-stained cells represented middle apoptotic cells. **B.** Apoptosis rate in different groups. PI; Propidium iodine, *; P<0.05, **; P<0.01, and NC; Black control.

Inflammation factors analysis

The inflammation factors in cells from different groups were investigated by Western blot (Fig.4A). The level of p-IKB-a in the cells treated with LPS was obviously higher than that in the untreated cells (P<0.01, Fig.4B). Meanwhile, the expression level of p-IKB-a was significantly higher in *MYC* group, in comparison with the NC group (P<0.01). Moreover, in the treated LPS group, the level of p-NFKB P65 in NC and siMYC group was observably higher than that in the non-LPS treatment group (P<0.01, Fig.4C). Compared to the NC group, expression level of p-NFKB P65 was significantly higher in silent *MYC* group (P<0.01). Meanwhile, the expression level of p-P38 was significantly higher in both siMYC and KB group in comparison to non-treated LPS group (P<0.01, Fig.4D). Furthermore, compared to the NC group, expression level of p-P38 was significantly lower in siMYC group (P<0.01).

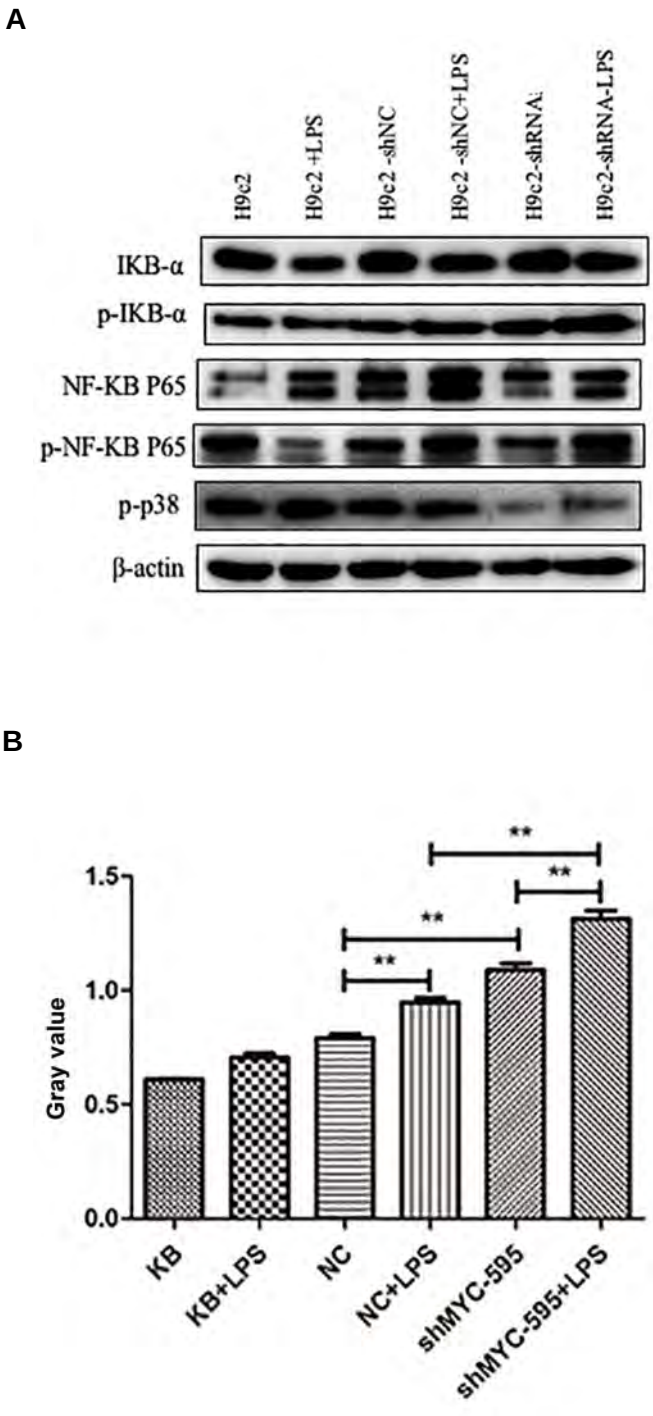

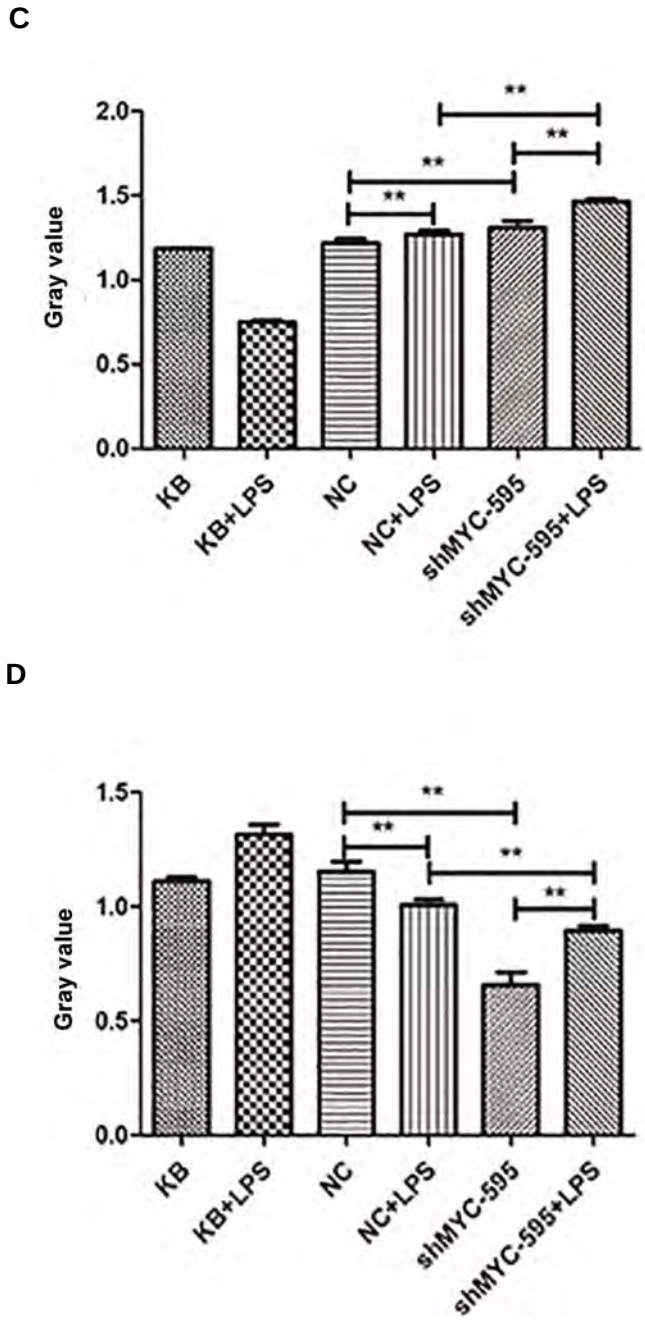

Fig.4: Result of Western blot for detection of inflammation factors. **A.** Electrophoresis results for some inflammation factors including pIKB-α, p-NF-KB P65 and p-P38 in different groups. **B-D.** Expression of some factors including pIKB-α, p-NF-KB P65 and p-P38 in different groups. **; P<0.01 and NC; Black control.

Discussion

The incidence of sepsis still remains high worldwide (12). Although genes such as *MYC* are thought to be associated with sepsis (10), detail of the mechanism of these genes on sepsis progression is yet unclear. This study explored the potential mechanism of *MYC* in sepsis. The result of CCK-8 assay showed that silencing *MYC* significantly inhibited cellular proliferation cells with or without LPS treatment. ELISA assay showed that expressions of TNF-α and IL-6 were decreased in *MYC* silencing group, but increased after LPS treatment. Moreover, flow cytometry assay showed that *MYC* silencing contributed to the apoptosis of sepsis cells. Furthermore, the expression of inflammatory factors investigated by Western blot showed that *MYC* silencing elevated the expression of p-IKB-a and p-NF-KB P65.

MYC proteins are key regulators of mammalian cell proliferation (13). A previous study showed that overexpression of *MYC* gene contributed to the cell proliferation during development of renal clear cell carcinoma (14). Developmental vascular regression is regulated by *MYC* associated pathway that controls cell proliferation (15). Wang et al. (16) indicated that *MYC* participated in the proliferation of breast cancer by promoting the gene expression including SNHG12. Moreover, the function of *MYC* in cell proliferation can be verified by *MYC* gene silencing. For example, Nayak et al. revealed that the down-regulation of *MYC* led to the tumor cell growth in human gastric cancer (17). The *MYC* silencing suppressed the interleukin-1β-induced rat chondrocyte cell proliferation and cytokine expression (18). In the hepatocellular carcinoma, RNAi silencing of *MYC* is proved to inhibit not only migration but also proliferation (19). In the current study, CCK-8 assay showed that *MYC* silencing inhibited proliferation in LPS induced sepsis cells. Thus, we speculated that *MYC* might contribute to the cell proliferation in LPS-induced sepsis.

Actually, deregulated expression of *MYC* not only promotes proliferation, but also can either induce or sensitize cells to apoptosis (20). A previous study showed that *MYC* regulates epithelial cell proliferation and control apoptosis in a positive autocrine feedback loop (21). *MYC* can induce apoptosis in various diseases such as liver and colorectal cancers (22, 23). However, flow cytometry assay in this study showed that silencing *MYC* promoted apoptosis in sepsis cells. This result indicated that *MYC* might suppress but not induce apoptosis within progression of disease.

Sepsis is caused by an inflammatory immune response triggered by an infection (9). Previous study demonstrated an important role of *MYC* in inflammatory phenotype, further indicating the vital physiological function of *MYC* in the process of inflammation (24). Due to the association with inflammation, *MYC* is a critical prognostic factor in the development of hepatoma carcinoma cell (25). A recent study shows that by programming inflammation and immune suppression, the acute activation of high levels of *MYC* can induce cellular proliferation (26). In chronic liver disease, *MYC* play a vital role in the development of disease via interacting with mediators of inflammation (27). In this study, Western blot analysis showed that deregulation of inflammation factors induced by LPS was enhanced by *MYC* silencing. Thus, we speculated that *MYC* might reduce inflammation during the progression of LPS induced sepsis. However, there were some limitations in the current study such as small simple size and lack of verification analysis. Thus, further verification studies based on the large sample size are needed to confirm all speculations in this study.

Conclusion

MYC might take part in the process of LPS induced sepsis via promoting cell proliferation and inhibiting cell apoptosis. Moreover, *MYC* might reduce inflammation during the progression of LPS induced sepsis.

Acknowledgements

There is no financial support and conflict of interest in this study.

Authors' Contributions

M.C., C.K.; Carried out the conception and design of the research, acquisition of data, analysis and interpretation of data. Z.Z.; Carried out the experiments, analysis, and interpretation of data. Y.L.; Carried out the analysis and interpretation of data, and drafted the manuscript. L.F., W.T.; Carried out the conception and design of the research and acquisition of data. All authors read and approved the final manuscript.

References

1. Shankarhari M, Phillips GS, Levy ML, Seymour CW, Liu VX, Deutschman CS, et al. Developing a new definition and assessing new clinical criteria for septic shock: for the third international consensus definitions for sepsis and septic shock (Sepsis-3). JAMA. 2016; 315(8): 775-787.
2. Lyle NH, Pena OM, Boyd JH, Hancock RE. Barriers to the effective treatment of sepsis: antimicrobial agents, sepsis definitions, and host-directed therapies. Ann N Y Acad Sci. 2014; 1323: 101-114.
3. Sganga G. Surgical sepsis. Urologia. 2015; 82(2): 75-83.
4. Saad DY, Baiomy AA, Mansour AA. Antiseptic effect of sea cucumber (Holothuria atra) against multi-organ failure induced by sepsis: molecular and histopathological study. Exp Ther Med. 2016; 12(1): 222-230.
5. Saugel B, Schmid RM. Argatroban for heparin-induced thrombocytopenia therapy in ICU patients with sepsis or multiple organ dysfunction syndrome. Crit Care. 2009; 13(Suppl 1): P442.
6. Fallah Y, Brundage J, Allegakoen P, Shajahan-Haq AN. MYC-driven pathways in breast cancer subtypes. Biomolecules. 2017; 7(3). pii: E53.
7. Napoli S, Pastori C, Magistri M, Carbone GM, Catapano CV. Promoter-specific transcriptional interference and c-myc gene silencing by siRNAs in human cells. EMBO J. 2009; 28(12): 1708-1719.
8. Sipos F, Firneisz G, Műzes G. Therapeutic aspects of c-MYC signaling in inflammatory and cancerous colonic diseases. World J Gastroenterol. 2016; 22(35): 7938-7950.
9. Castellheim A, Brekke OL, Espevik T, Harboe M, Mollnes TE. Innate immune responses to danger signals in systemic inflammatory response syndrome and sepsis. Scand J Immunol. 2009; 69(6): 479-491.
10. Li Y, Zhang F, Cong Y, Zhao Y. Identification of potential genes and miRNAs associated with sepsis based on microarray analysis. Mol Med Rep. 2018; 17(5): 6227-6234.
11. Livak KJ, Schmittgen TD. Analysis of relative gene expression data using real-time quantitative PCR and the 2(-Delta Delta C(T)) method. Methods. 2001; 25(4): 402-408.
12. Jawad I, Lukšić I, Rafnsson SB. Assessing available information on the burden of sepsis: global estimates of incidence, prevalence and mortality. J Glob Health. 2012; 2(1): 010404.
13. Bouchard C, Staller P, Eilers M. Control of cell proliferation by Myc. Trends Cell Biol. 1998; 8(5): 202-206.
14. Gordan JD, Bertout JA, Hu CJ, Diehl JA, Simon MC. HIF-2alpha promotes hypoxic cell proliferation by enhancing c-myc transcriptional activity. Cancer Cell. 2007; 11(4): 335-347.
15. Nayak G, Odaka Y, Prasad V, Solano AF, Yeo EJ, Vemaraju S, et al. Developmental vascular regression is regulated by a Wnt/β-catenin, MYC and CDKN1A pathway that controls cell proliferation and cell death. Development. 2018; 145(12). pii: dev154898.
16. Wang O, Yang F, Liu Y, Lv L, Ma R, Chen C, et al. C-MYC-induced upregulation of lncRNA SNHG12 regulates cell proliferation, apoptosis and migration in triple-negative breast cancer. Am J Transl Res. 2017; 9(2): 533-545.
17. Wang F, Zhang D, Mao J, Ke XX, Zhang R, Yin C, et al. Morusin inhibits cell proliferation and tumor growth by downregulating c-Myc in human gastric cancer. Oncotarget. 2017; 8(34): 57187-57200.
18. Zou J, Li XL, Shi ZM, Xue JF. Effects of C - myc gene silencing on interleukin-1β-induced rat chondrocyte cell proliferation, apoptosis and cytokine expression. J Bone Miner Metab. 2018; 36(3): 286-296.
19. Zhao Y, Jian W, Gao W, Zheng YX, Wang YK, Zhou ZQ, et al. RNAi silencing of c-Myc inhibits cell migration, invasion, and proliferation in HepG(2) human hepatocellular carcinoma cell line: c-Myc silencing in hepatocellular carcinoma cell. Cancer Cell Int. 2013; 13(1): 23.
20. Hoffman B, Liebermann DA. The proto-oncogene c-myc and apoptosis. Oncogene. 1998; 17(25): 3351-3357.
21. Zhang SL, Chen YW, Tran S, Liu F, Nestoridi E, Hébert MJ, et al. Pax-2 and N-myc regulate epithelial cell proliferation and apoptosis in a positive autocrine feedback loop. Pediatr Nephrol. 2007; 22(6): 813-824.
22. Ladu S, Calvisi DF, Conner EA, Farina M, Factor VM, Thorgeirsson SS. E2F1 Inhibits c-Myc-driven apoptosis via PIK3CA/Akt/mTOR and COX-2 in a Mouse model of human liver cancer. Gastroenterology. 2008; 135(4): 1322-1332.
23. Tai J, Wang G, Liu T, Wang L, Lin C, Li F. Effects of siRNA targeting c-Myc and VEGF on human colorectal cancer Volo cells. J Biochem Mol Toxicol. 2012; 26(12): 499-505.
24. Florea V, Bhagavatula N, Simovic G, Macedo FY, Fock RA, Rodrigues CO. c-Myc is essential to prevent endothelial pro-inflammatory senescent phenotype. PLoS One. 2013; 8(9): e73146.
25. Dai CX, Gao Q, Qiu SJ, Ju MJ, Cai MY, Xu YF, et al. Hypoxia-inducible factor-1 alpha, in association with inflammation, angiogenesis and MYC, is a critical prognostic factor in patients with HCC after surgery. BMC Cancer. 2009; 9: 418.
26. Kortlever RM, Sodir NM, Wilson CH, Burkhart DL, Pellegrinet L, Brown Swigart L, et al. Myc Cooperates with ras by programming inflammation and immune suppression. Cell. 2017; 171(6): 1301-1315. e14.
27. Liu T, Zhou Y, Ko KS, Yang H. Interactions between Myc and mediators of inflammation in chronic liver diseases. Mediators Inflamm. 2015; 2015: 276850.

Original Article

Effect of Maternal Age on Hippo Pathway Related Gene Expressions and Protein Localization Pattern in Human Embryos

Sahar Gharanfoli, M.Sc.[1, 2], Abdolhossein Shahverdi, Ph.D.[2], Azam Dalman, Ph.D.[2], Pooneh Ghaznavi, D.V.M.[2], Hiva Alipour, Ph.D.[3], Poopak Eftekhari-Yazdi, Ph.D.[2]*

1. Department of Developmental Biology, University of Science and Culture, Tehran, Iran
2. Department of Embryology, Reproductive Biomedicine Research Center, Royan Institute for Reproductive Biomedicine, ACECR, Tehran, Iran
3. Biomedicine Group, Department of Health Science and Technology, Faculty of Medicine, Aalborg University, Aalborg, Denmark

**Corresponding Address: P.O.Box: 16635-148, Department of Embryology, Reproductive Biomedicine Research Center, Royan Institute for Reproductive Biomedicine, ACECR, Tehran, Iran*
Email: eftekhari@royaninstitute.org

Received: 27/March/2019, Accepted: 11/August/2019

Abstract

Objective: The Hippo pathway plays an important role in embryo development, and separation of trophectoderm (TE) and inner cell mass (ICM) cell lines. Therefore, this study investigated effect of maternal age on activity of Hippo pathway in human embryos.

Materials and Methods: In this experimental study, the developed up embryos to the blastocyst stage and the embryos whose growth stopped at the morula stage were collected from women aged 20-30 years old (young group, 94 embryos) and >37 years (old group, 89 embryos). Expression of *OCT4, SOX2, CDX2, GATA3, YAP* genes and the relevant proteins, in the both groups were evaluated using respectively quantitative reverse transcription-polymerase chain reaction (qRT-PCR) and immunofluorescence methods.

Results: There was no significant difference in the expression level of *OCT4, SOX2, CDX2, GATA3* and *YAP* genes in blastocyst and morula stages, between the two groups. However, *SOX2* and *CDX2* gene expressions in morula stage embryos of the old group was statistically lower than that of the young group (P=0.007 and P=0.008, respectively). Additionally, in the embryos collected from women with >37 years of age, at the blastocyst stage, phospho-YAP (p-YAP) protein was found to be accumulated in the TE, but it was almost disappeared from the ICM. Additionally, in the old group, contrary to the expectation, YAP protein was expressed in the ICM, rather than TE.

Conclusion: The results of this study showed that YAP and P-YAP among the Hippo signalling pathway may be altered by increasing age.

Keywords: Embryonic Development, Hippo Signalling, Maternal Age

Cell Journal(Yakhteh), Vol 22, Suppl 1, Autumn 2020, Pages: 74-80

Citation: Gharanfoli S, Shahverdi A, Dalman A, Ghaznavi P, Alipour H, Eftekhari-Yazdi P. Effect of maternal age on Hippo pathway related gene expressions and protein localization pattern in human embryos. Cell J. 2020; 22 Suppl 1: 74-80. doi: 10.22074/cellj.2020.6860.

Introduction

Pre-implantation development starts from fertilization and continues with repeated divisions. It leads to the formation of a complex structure called blastocyst (1, 2). The major developmental events are embryo cleavage, compaction and polarization, trophectoderm/inner cell mass (ICM) specification and blastocyst formation with two different cell lines (3, 4). Trophectoderm (TE) plays an important role in implantation as it interacts with the mother's uterus and participates in the formation of placenta (5). After implantation, ICM forms three germ layers, ultimately generating all tissues of the body (6, 7). Several mechanisms including FGF, Erk/Mapk and Hippo signalling pathways are involved in this differentiation process (8, 9). Hippo signalling pathway, along with the inside-outside axis of embryo, regulates cell-fate switch by modulating transcription factor Tead4 activity (10, 11). While Tead4 is active in outside-cells and promotes TE development, it is suppressed in inside-cells by cell contact- and phosphorylation-mediated inhibition of nuclear localization of the Tead4 coactivator Yes-associated protein (YAP) (12-14).

In the outer cells of embryo, Hippo signalling is likely suppressed by another signal which is produced by the cell polarity. YAP is translocated to the nucleus, where it increases *CDX2* and *GATA3* gene expressions together with TEAD4, which in turn induces trophoblast formation and *OCT4* down-regulation (12, 13, 15). In the ICM, where Hippo signalling is active, YAP is phosphorylated by LATS. Therefore, YAP remains in the cytoplasm. In the absence of a nuclear YAP, since TEAD4 remains inactive, *CDX2* and *GATA3* genes are not expressed and the initial expression of *OCT4* is maintained (16, 17). Many factors -such as culture medium, oxygen concentration, developmental stage and age- can affect developmental gene expression and likely Hippo signalling pathway. Mantikou et al. (18) in 2015 investigated the effect of women's age on gene expression in three groups of ≤35, 36-38, and ≥39 years old. The results showed significant differences between the three groups. Since the expression of developmental genes are under the control of various signalling pathways, in this study, effect of women's age on activity of the Hippo signalling pathway was investigated. According to a previous study performed by Bellieni et al. (19) in 2016, the woman's optimal age for reproduction is 20-30 years, regarding that the number of oocytes is decreased in women after ≥35 years of age. In the present study, due to the importance of Hippo signaling pathway in the embryo

development, and separating TE and ICM cell lines, effect of women's age on Hippo signalling pathway activity of human embryos was investigated.

Materials and Methods

This experimental study was in accordance with the Declaration of Helsinki, following the approval of Ethical Committee of Royan Institute (Tehran, Iran; approval number: IR.ACECR.ROYAN.REC.1395.8). The patients were selected based on age, body mass index (BMI), cause of infertility, type of control ovarian stimulation (agonist and antagonist), Number of *in vitro* fertilization/intracytoplasmic sperm injection (IVF/ICSI) procedure as well as the oocyte and embryo quality, ovarian reserve and number of treatment cycles. Inclusion criteria for the study encompass the quality of embryo, women's age and lack of genetic diseases.

Exclusion criteria include embryos of the patients which were not developed to morula and blastocyst stages. Fresh and frozen embryos from consenting couples attending Royan Institute for infertility treatment (after signing written consent) were cultured in $G_1V_5^{TM}$ medium (Vitrolife, Sweden) for three days, before transferring to the $G_2V_5^{TM}$ medium (Vitrolife). The embryos (either those stopped at the morula stage or those reaching the blastocyst stage) were collected on day 5 and divided into two groups: the embryos collected from women aged 20-30 (young group) and the embryos belonging to women >37 years of age (old group).

Gene expression analysis

Total RNA from embryos that either reached to the blastocyst stage or stopped at the morula stage, were extracted using the RNeasy micro Kit (Qiagen, Germany), before, synthesizing complementary DNA (cDNA) by Fermentase kit (Germany) (20). PCR reaction was run as follow in a total volume of 25 µl: master mix (10 µl, Thermo, USA), forward and reverse specific primers (each 1 µl), cDNA (1 µl) and nuclease free water (12 µl). quantitative reverse transcription polymerase chain reaction (qRT-PCR) protocol was carried out using SYBER Green (Takara, Japan) according to the following program: initiation step at 94˚C for 300 seconds; 35 cycles at 94˚C for 40 seconds followed by 60˚C for 40 seconds and 72˚C for 40 seconds, terminated by incubating at 72˚C for 10 seconds. For presentation of data, products specificity was confirmed by melt curve analysis. Then, the qRT-PCR results were estimated using $2^{-\Delta\Delta Ct}$ formula. Gene expression analysis was performed for pluripotency markers (*OCT4, CDX2, GATA3* and *SOX2)* and Hippo signalling marker (*YAP*). *GAPDH* was considered as housekeeping gene. The oligonucleotide primers were designed using NCBI site, Perl Primer and Gene Runner software. The utilized primers in the present work are listed in Table 1.

Immunocytochemical analysis

The embryos were fixed in 4% paraformaldehyde solution (Merck, Germany) for 15 minutes at room temperature and placed in 0.25% Triton X-100 (Sigma, USA) soluble in phosphate-buffered saline (PBS, Gibco, USA) for 30 minutes at room temperature. Then, the embryos were incubated with 5% BSA in donkey serum for 60 minutes at room temperature to block unspecific binding of the antibodies, before being incubated with the following primary antibodies: OCT4 (mouse monoclonal; Santa Cruz, USA, 1:100 dilution), CDX2 (Goat polyclonal IgG, Santa Cruz, USA, 1:100 dilution), YAP (Rabbit polyclonal; Proteintech, USA, 1:100 dilution) or P-YAP (Rabbit polyclonal; Abcam, UK, 1:100 dilution) overnight at 4˚C, as previously described (6). Incubation was continued with conjugated donkey anti-rabbit IgG (Invitrogen, USA, 1:600 dilution) for YAP and P-YAP, donkey anti-mouse IgG (Invitrogen, USA, 1:600 dilution) for OCT4 and donkey anti-goat IgG (Invitrogen; 1:600 dilution) for CDX2 for one hour at room temperature. Nuclei were stained with 1 µg/ml 4',6-diamidino-2-phenylindole (DAPI, Sigma, USA) for 5 minutes. For negative control, the samples were only treated with the secondary antibodies. All images were acquired by a camera (Eclipse 50i, Nikon, Japan) coupled to a fluorescence microscope (21). Then, the Image J software (V1.515) was utilized to evaluate, based on the intensity and the results which turned to be quantitative.

Table 1: Primers used for quantitative reverse transcription-polymerase chain reaction

Gene	Primer sequencing (5´-3´)	Product size
YAP	F: TAGCCCTGCGTAGCCAGTTA	177
	R: TCATGCTTAGTCCACTGTCTGT	
CDX2	F: GCAGAGCAAAGGAGAGAGGAAA	136
	R: AAGGGCTCTGGGACACTTCT	
SOX2	F: GGGAAATGGAAGGGGTGCAAAAGA	151
	R: TTGCGTGAGTGTGGATGGGATTGGT	
OCT4	F: CTGGGTTGATCCTCGGACCT	128
	R: CACAGAACTCATACGGCGGG	
GATA3	F: CCTCATTAAGCCCAAGCGA	185
	R: TGCCTTCCTTCTTCATAGTCAG	
GAPDH	F: CTCATTTCCTGGTATGACAACGA	119
	R: CTTCCTGTGCTCTTGCT	

Statistical analysis

All experiments were performed using four independent biological replicates. Data were analysed using t test (for gene expression evaluation), chi-square (for protein expression and demographic information), or Mann Whitney tests (for comparison of the cycle numbers) using the SPSS statistical software (Ver. 16.0, IBM, USA). Differences were considered significant at $P<0.05$.

Table 2: Patient characteristics in the young and old groups

Patient characteristics	Young n=34	Old n=20	Significance P value
Number of male factor	14 (45)	9 (45)	-
Number of female factor	1 (2)	0	-
Number of male and female fact	5 (14)	2 (5)	-
Number of recurrent abortion	1 (2)	2 (1)	-
Number of thalassemia	2 (8)	0	-
Number of sex determination	4 (11)	0	-
Number of unexplained	7 (17)	7 (35)	-
Number of agonist protocol	31 (91)	15 (75)	-
Number of antagonist protocol	3 (8)	5 (25)	-
Number of ICSI	19 (55)	8 (40)	-
Number of ICSI+IVF	15 (44)	12 (60)	-
Number of morula	38	17	-
Number of early blastocyst	10	8	-
Number of mid blastocyst	9	9	-
Number of expand blastocyst	18	8	-
Number of hatching blastocyst	7	3	-
Number of total oocyte	18.2 ± 7	11.6 ± 7	0.001
Number of GV	1.88 ± 1	2.44 ± 2	-
Number of Ml	1.44 ± 0.8	1.90 ± 1	-
Number of Mll	14.8 ± 7	8.76 ± 4	0.001
Mean BMI (Kg/m^2)	26 ± 3	26.25 ± 4	-
Mean number of cycle	1.27 ± 0.5	2.55 ± 1.7	0.001
Female age (Y)	27 ± 2	38 ± 2	0.000
Male age (Y)	34 ± 1	42 ± 1	0.000

Data are presented as n (%) or mean ± SD. Significantly different at $P<0.05$. ICSI; Intracytoplasmic sperm injection, IVF; *In vitro* fertilization, GV; Germinal vesicle, MI; Metaphase I, MII; Metaphase II, and BMI; Body mass index.

Results

Patient demographic information

Table 2 shows that demographic information of the participants, total number of oocytes as well as MII oocytes in the young group was significantly higher than that of the old group (P<0.05). On the other hand, number of cycles in the young group was significantly lower than that of the old group (P<0.05). Additionally, mean age of the participants in these groups was significantly different (P<0.05). Based on the demographic data, it seems that ovarian resources begin to decline in women with >37 years of age.

Quantitative reverse transcription-polymerase chain reaction analysis

There was no significant difference between these two groups, in the expression of Hippo signaling marker (*YAP*) and pluripotency genes (*OCT4* and *GATA3*) at the Morula stage. However, *SOX2* and *CDX2* genes at the Morula stage had significantly higher expression levels in the young group, compared to the old group (P<0.05, Fig.1).

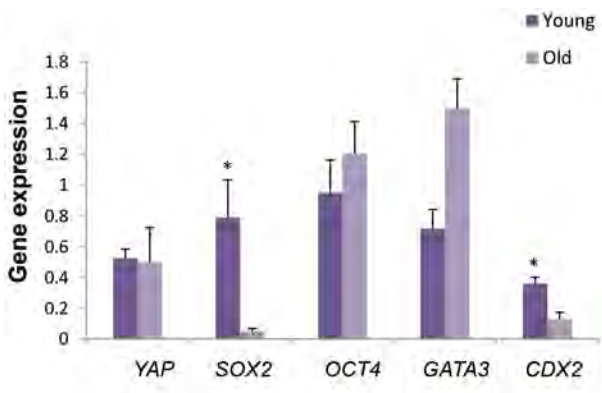

Fig.1: *YAP*, *SOX2*, *OCT4*, *CDX2* and *GATA3* gene expression levels in morula stage of the two groups. Data are presented as mean ± SE. *; Significant difference at P<0.05.

There was no difference between these groups, in the expression of genes (*OCT4*, *CDX2*, *SOX2*, *GATA3* and *YAP*) at the blastocyst stage (Fig.2).

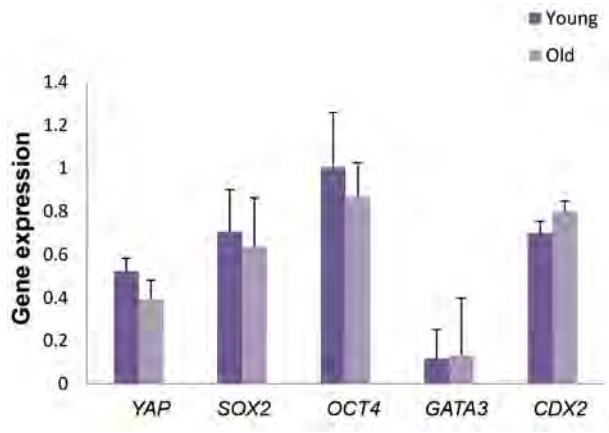

Fig.2: *YAP*, *SOX2*, *OCT4*, *CDX2* and *GATA3* gene expression levels in blastocyst stage of the two groups. Data are presented as mean ± SE.

Immunocytochemical analysis

Protein expression of OCT4, CDX2, YAP and phospho-YAP (p-YAP) at the blastocyst stage did not show significant variation, by comparing the young and old groups (Table 3).

In the old group, at the blastocyst stage, P-YAP protein was found to be accumulated in the TE, but it was almost disappeared from the ICM. Additionally, contrary to the expectations, in the old group, YAP protein was expressed in the ICM rather than TE (Fig.3).

Table 3: Expression intensity of CDX2, OCT4, YAP and P-YAP proteins in the young and old groups

Proteins		Young group		Old group	
OCT4	CDX2	19.4 ± 2	22.1 ± 4	12.2 ± 5	10.4 ± 5
OCT4	YAP	31.8 ± 5	34.5 ± 3	13.8 ± 3	31 ± 2
OCT4	P-YAP	15.4 ± 1	35.4 ± 9	20.7 ± 4	24.9 ± 3
CDX2	YAP	41.6 ± 6	13.3 ± 1	30.18 ± 6	16.3 ± 2
CDX2	P-YAP	16.1 ± 2	24.3 ± 2	17.7 ± 6	27.7 ± 5

The data was evaluated based on the intensity. The signal intensities were quantified using Image J analysis software (V1.515). Data are presented as mean ± SD.

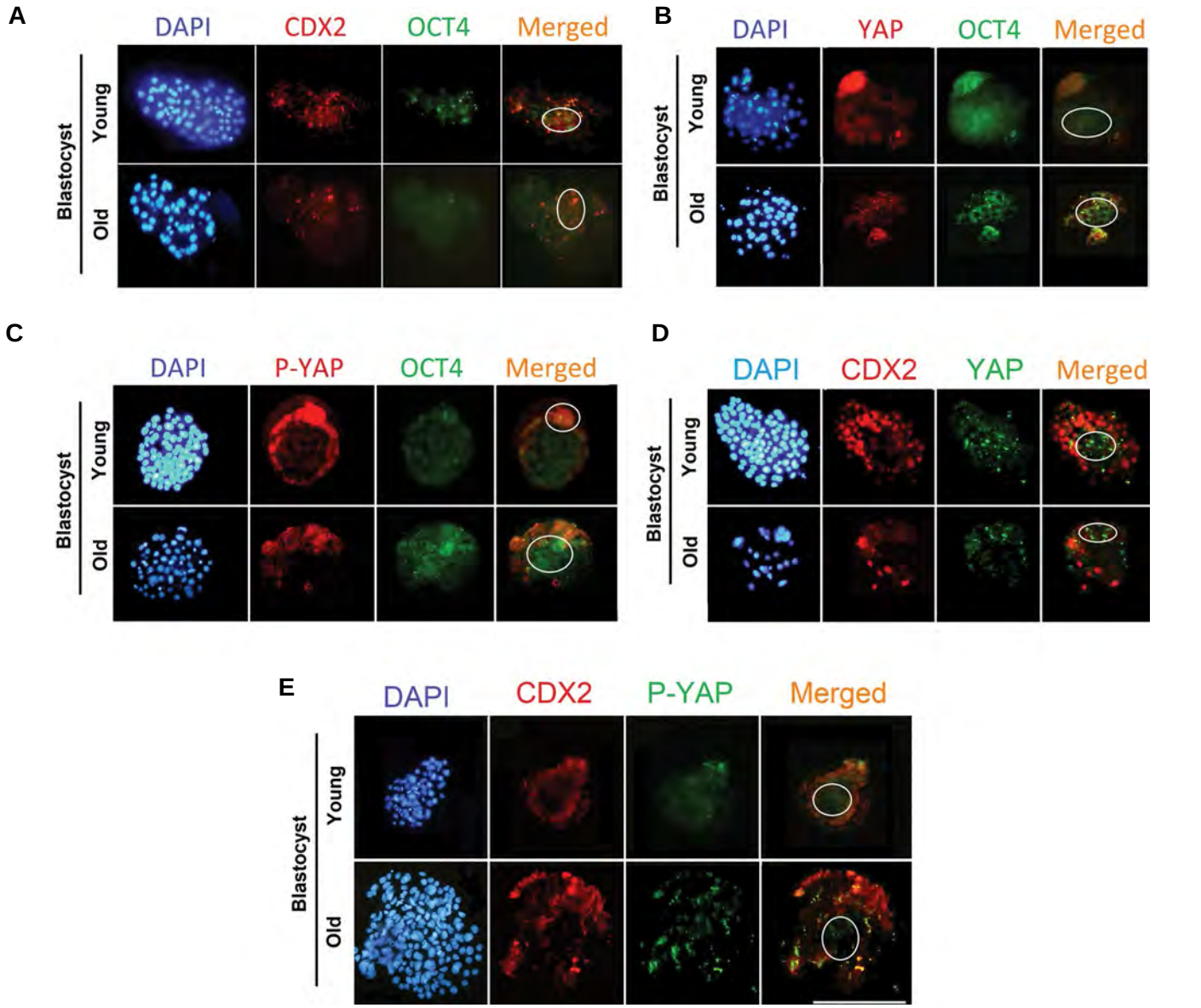

Fig.3: Immunofluorescence staining of developmental proteins (OCT4, CDX2, YAP and P-YAP) at the blastocyst stage. **A.** DAPI staining, immunofluorescence staining of CDX2 and OCT4 in the same cells as well as the merged DAPI and primary antibody-secondary antibody-FITC staining of CDX2 and OCT4 in blastocyst. **B.** DAPI staining, immunofluorescence staining of YAP and OCT4 in the same cells as well as the merged DAPI and primary antibody-secondary antibody-FITC staining of YAP and OCT4 in blastocyst. **C.** DAPI staining, immunofluorescence staining of P-YAP and OCT4 in the same cells as well as the merged DAPI and primary antibody-secondary antibody-FITC staining of P-YAP and OCT4 in blastocyst. **D.** DAPI staining, immunofluorescence staining of CDX2 and YAP in the same cells as well as the merged DAPI and primary antibody-secondary antibody-FITC staining of CDX2 and YAP in blastocyst. **E.** DAPI staining, immunofluorescence staining of CDX2 and P-YAP in the same cells as well as the merged DAPI and primary antibody-secondary antibody-FITC staining of CDX2 and P-YAP in blastocyst. ICM localization was distinguished by a circle (scale bars: 200 µm).

Discussion

During differentiation of the blastomeres, cell polarity and position govern formation of TE and ICM (22). This process is mediated by various signalling pathways, such as Hippo signalling pathway which is the main regulator of cell growth, proliferation, differentiation and death (9, 14). In 2013, Lorthongpanich et al. (23) reported that inhibition of the components of Hippo signaling pathway disrupted the blastomeres differentiation into ICM. After LATS kinase decrease, they observed that *SOX2* and *OCT4* genes (ICM genes) were significantly reduced. On this basis, it can be said that Hippo pathway plays an important role in the early embryo differentiation by affecting these gene. Moreover, in they showed that *SOX2* and *CDX2* genes play an important role in development of embryos. *CDX2* gene is necessary for gastrulation. The mutation in this gene disturbs WNT, FGF and Hippo signalling. *SOX2* is initially expressed in the most of cells during morula stage. But, in the blastocyst stage, it is only expressed in ICM. Various factors can affect the embryo development from a zygote to a blastocyst, including quality of gametes, type of culture medium and oxygen concentration, as well as women's age.

The infertility problems in 10% of women are associated with higher ages. As mentioned in the introduction, the best reproductive age for women is 20-30 years and women with >35 years show decrement of fertility potentiality (19). A study performed by Tehraninezhad

et al. (24) in 2016, suggested age, as the most important underlying cause of infertility in women. Many of the infertility problems observed in older women are due to reduced ovarian reserve, producing fewer oocytes with lower quality. Several factors may reduce ovarian reserve, but one of the most important factors is the women's age. In this study, interesting results in terms of the expression of proteins were obtained by immunofluorescence staining. The location of YAP and the expression levels of P-YAP protein in the blastocyst embryos of the older group were not appropriate. In the older group, YAP protein expression was observed in TE cells, whereas in the blastocyst of women aged 20-30 years old, YAP was expressed in ICM. Furthermore, contrary to the expectation, expression of P-YAP in blastocyst collected from women aged >37 years old was observed in both ICM and TE cells. Therefore, with the age increase, it seems that Hippo pathway proteins are removed from their appropriate locations. According to the study performed by Hartley et al. (25) in 2015, if the protein processing step is not correctly taken after translation, the protein may be degraded by endopeptidase, thus negatively affecting the function or location of protein. To the best of our knowledge, there is no information in literature, regarding the gene expression of Hippo signaling pathway and its relationship with the women's age in human embryo. In 2015, Li et al. (20) explored the Hippo signaling pathway and expression of *MVH*/*OCT4* genes in the mouse ovarian cortex. The level *LATS2*, *MST1*, *MVH* and *OCT4* were significantly decreased with increasing the age. YAP was also observed in the ovarian cortex of two-months old, but not 20-months old mice. In addition, YAP phosphorylation was found in ovarian cortex of seven-days old compared to 20-months old mice. Moreover, the amount of P-YAP/YAP was decreased, as 7-days old mice grew to 20 months. These results show that expressions of Hippo signaling pathway proteins are altered with increasing the age of ovary. A study performed by Pelissier et al. (21) in 2014 was conducted on breast epithelial progenitor cells and showed that biochemical, molecular and functional phenotypes differed before and after menopause. Moreover, Hippo pathway dysregulation affects differentiation and specificity of the cells. In previous studies, the expression of developmental and Hippo signaling pathway genes at the pre-implantation stage was decreased with increasing age in women. In the present study, no significant difference was observed in the expression of genes between these two groups, but immunofluorescent results showed that expression level of Hippo pathway proteins might be changed with increasing age.

This study has a few shortcomings which need to be considered in future studies. Our aim was to compare the gene expression of both young and old groups in two stages of morula and blastocyst, which required the same morphology. For this reason and according to the previous articles which have been done, total mRNA was extracted (23).

Conclusion

The result of this study showed that although the levels of *YAP* and *P-YAP* gene expression were not significantly different between young and old groups, in blastocyst stage, P-YAP protein was found to be accumulated in the TE and it was almost disappeared from ICM. Contrary to expectations, in the old (women with more than 37 years old) group, YAP protein expression was expressed in ICM rather than TE. These data may indicate the inappropriate functionality of Hippo signaling pathway at the advanced ages. More accurate results could be obtained, if immunestaining was performed for all four proteins in the embryo.

Acknowledgments

This study was conducted at Royan Research Institute. This research did not receive any specific grant from funding agencies in the public, commercial or not-for-profit sectors. There is no conflict of interest in this study.

Authors' Contributions

S.G.; Contributed to all experimental work, data and statistical analysis, and interpretation of data. A.D.; Conducted molecular and immunofluorescence experiments as well as the analysis of data. P.E.Y., A.Sh.; Were responsible for overall supervision and provided scientific advice throughout the project and preparation of manuscript P.Gh.; Contributed to molecular experiments and data collection. H.A.; Study design and data analysis. All authors read and approved the final manuscript.

References

1. Bleil JD, Wassarman PM. Mammalian sperm-egg interaction: identification of a glycoprotein in mouse egg zonae pellucidae possessing receptor activity for sperm. Cell. 1980; 20(3): 873-882.
2. Florman HM, Storey BT. Mouse gamete interactions: the zona pellucida is the site of the acrosome reaction leading to fertilization in vitro. Dev Biol. 1982; 91(1): 121-130.
3. Oron E, Ivanova N. Cell fate regulation in early mammalian development. Phys Biol. 2012; 9(4): 045002.
4. Tarkowski AK, Wróblewska J. Development of blastomeres of mouse eggs isolated at the 4-and 8-cell stage. Development. 1967; 18(1): 155-180.
5. Takaoka K, Hamada H. Cell fate decisions and axis determination in the early mouse embryo. Development. 2012; 139(1): 3-14.
6. Dietrich J-E, Hiiragi T. Stochastic patterning in the mouse pre-implantation embryo. Development. 2007; 134(23): 4219-4231.
7. Zernicka-Goetz M, Morris SA, Bruce AW. Making a firm decision: multifaceted regulation of cell fate in the early mouse embryo. Nat Rev Genet. 2009; 10(7): 467-477.
8. Yamanaka Y, Lanner F, Rossant J. FGF signal-dependent segregation of primitive endoderm and epiblast in the mouse blastocyst. Development. 2010; 137(5): 715-724.
9. Yu F-X, Zhao B, Guan K-L. Hippo pathway in organ size control, tissue homeostasis, and cancer. Cell. 2015; 163(4): 811-828.
10. Reddy BVVG, Irvine KD. Regulation of Hippo signaling by EGFR-MAPK signaling through Ajuba family proteins. Dev Cell. 2013; 24(5): 459-471.
11. Sasaki H. Roles and regulations of Hippo signaling during preimplantation mouse development. Dev Growth Differ. 2017; 59(1):12-20.
12. Cockburn K, Biechele S, Garner J, Rossant J. The Hippo pathway member Nf2 is required for inner cell mass specification. Curr Biol. 2013; 23(13): 1195-1201.
13. Yu F-X, Guan K-L. The Hippo pathway: regulators and regulations.

Genes Dev. 2013; 27(4): 355-371.
14. Varelas X. The Hippo pathway effectors TAZ and YAP in development, homeostasis and disease. Development. 2014; 141(8): 1614-1626.
15. Nishioka N, Inoue K, Adachi K, Kiyonari H, Ota M, Ralston A, et al. The Hippo signaling pathway components Lats and Yap pattern Tead4 activity to distinguish mouse trophectoderm from inner cell mass. Dev Cell. 2009; 16(3): 398-410.
16. Lorthongpanich C, Issaragrisil S. Emerging role of the Hippo signaling pathway in position sensing and lineage specification in mammalian preimplantation embryos. Biol Reprod. 2015; 92(6): 143-143.
17. Wicklow E, Blij S, Frum T, Hirate Y, Lang RA, Sasaki H, et al. Hippo pathway members restrict SOX2 to the inner cell mass where it promotes ICM fates in the mouse blastocys. PLoS Genet. 2014; 10(10): e1004618.
18. Mantikou E, Jonker MJ, Wong KM, van Montfoort APA, de Jong M, Breit TM, et al. Factors affecting the gene expression of in vitro cultured human preimplantation embryos. Hum Reprod. 2015; 298-311.
19. Bellieni C. The best age for pregnancy and undue pressures. J Fam Reprod Health. 2016; 10(3): 104-107.
20. Li J, Zhou F, Zheng T, Pan Z, Liang X, Huang J, et al. Ovarian germline stem cells (OGSCs) and the Hippo signaling pathway association with physiological and pathological ovarian aging in mice. Cell Physiol Biochem. 2015; 36(5): 1712-1724.
21. Pelissier FA, Garbe JC, Ananthanarayanan B, Miyano M, Lin C, Jokela T, et al. Age-related dysfunction in mechanotransduction impairs differentiation of human mammary epithelial progenitors. Cell Rep. 2014; 7(6): 1926-1939.
22. Manzanares M, Rodriguez TA. Development: Hippo signalling turns the emberyo inside out. Current Biology. 2013: 23(13): R559-R561.
23. Lorthongpanich C, Messerschmidt DM, Chan SW, Hong W, Knowles BB, Solter D. Temporal reduction of LATS kinases in the early preimplantation embryo prevents ICM lineage differentiation. Genes Dev. 2013; 27(13): 1441-1446.
24. Tehraninezhad ES, Mehrabi F, Taati R, Kalantar V, Aziminekoo E, Tarafdari A. Analysis of ovarian reserve markers (AMH, FSH, AFC) in different age strata in IVF/ICSI patients. Int J Reprod Biomed. 2016; 14(8): 501-506.
25. Hartley AM, Zaki AJ, McGarrity AR, Robert-Ansart C, Moskalenko AV, Jones GF, et al. Functional modulation and directed assembly of an enzyme through designed non-natural post-translation modification. Chem Sci. 2015; 6(7): 3712-3717.

Original Article

Assessment of DNA Repair Gene Expressions in Vitrified Mouse Preantral Follicles

Zahra Khodavandpour, M.Sc.[1], Saeed Zavareh, Ph.D.[2, 3*], Parisa Farrokh, Ph.D.[2, 3], Meysam Nasiri, Ph.D.[2, 3]

1. Department of Biology, Damghan Branch, Islamic Azad University, Damghan, Iran
2. School of Biology, Damghan University, Damghan, Iran
3. Institute of Biological Sciences, Damghan University, Damghan, Iran

Corresponding Address: P.O.Box: 41167-36716, School of Biology, Damghan University, Damghan, Iran
Email: zavareh.s@du.ac.ir

Received: 19/March/2019, Accepted: 19/August/2019

Abstract

Objective: Vitrification of the ovarian tissue is one of the techniques recommended for preserving the fertility of women who are dealing with infertility. Despite its benefits, our information about the molecular aspects of ovarian follicles vitrification is somehow ambiguous. Therefore, the aim of this study was to evaluate the expression pattern of DNA repair genes in vitrified preantral follicles.

Materials and Methods: In this experimental study, the isolated preantral follicles (n=906) from 14-16 days old mice (n=12) were divided into three groups: fresh, toxic and vitrified which were cultured *in vitro* for 12 days. Preantral follicles were vitrified using cryotop followed by exposure to equilibration solution for five minutes and vitrification solution (VS) for 30 seconds. In the toxic group, preantral follicles were only placed in equilibration and vitrification media and they were then placed in the warming solutions without exposure to liquid nitrogen. On the second and sixth days of the culture period, real-time quantitative reverse transcription-polymerase chain reaction (qRT-PCR) was carried out to evaluate expression of the selected genes involved in DNA repair, including *Msh6* (MutS homolog 6), *Mre11* (Meiotic recombination 11), *Brca1* (Breast cancer type 1), *Rad51* (RAD51 recombinase), *Pcna* (Proliferating cell nuclear antigen) and *Atm* (ATM serine/threonine kinase). In addition, developmental parameters including growth, survival rate, antrum cavity formation and ovulation were analyzed.

Results: The relative mRNA expression of *Msh6, Mre11, Brca1, Rad51, Pcna* and *Atm* on the second and sixth days of the culture period in vitrified group was significantly higher than those of the control and toxic groups, but there was no significant difference between the toxic and control groups. In addition, developmental parameters of follicles were similar in both toxic and control groups, while both were significantly higher than that of vitrified group.

Conclusion: Vitrification changes the expression pattern of DNA repair genes of the mouse preantral follicles.

Keywords: DNA Repair, Ovarian Follicles, Vitrification

Cell Journal(Yakhteh), Vol 22, Suppl 1, Autumn 2020, Pages:81-88

Citation: **Khodavandpour Z, Zavareh S, Farrokh P, Nasiri M. Assessment of DNA repair gene expressions in vitrified mouse preantral follicles. Cell J. 2021; 22 Suppl 1: 81-88. doi: 10.22074/cellj.2020.6865.**

Introduction

Not only it is vital to survive the patient who are dealing with cancer, but also increase the quality of life and patient satisfaction following treatment is important (1). The cytotoxic effect of radiation and chemical factors in cancer often results in premature ovarian failure (2). In this regard, assisted reproduction techniques such as vitrification of ovarian tissue, follicle, oocyte and embryo can preserve the fertility. Vitrification methods allow long-term storage of any types of cells. However, vitrification may have negative effects on the molecular level, such as DNA, mRNA and proteins, which their manifestations are not immediately expressed after thawing and sometimes does not cause death (3). It has been proposed that vitrification leads to DNA damage and results in damage to cytoplasmic mRNA (4). However, there are some debated results about the effects of vitrification on gene expression levels of ovarian follicles (5, 6). But, there are not any reports about the effect of vitrification on DNA repair genes of ovarian follicles. However, In this regard Fatehi et al. (7) have showed the vitrification of follicles did not change gene expression pattern related to folliculogenesis such as *Bmp15*, *Gdf9*, *BmprII*, *Alk6*, *Alk5*, *Has2*, and *Ptgs*. Additionally, Sampaio da Silva et al. (8) have recently reported that vitrification decreased proliferation of granulosa cells in developing follicles via changing the expression of *Cx43* gene. Moreover, Asadzadeh et al. (9) showed that expression of gelatinase related genes altered in follicles isolated from vitrified ovarian tissue.

Stressors, either internal or external, which lead to DNA damages may result in activation of DNA repair systems (10, 11). One of the DNA repair pathways is DNA mismatch repair (MMR), activated during 99% of the DNA damages. PCNA and MSH6 proteins play key roles in identifying and repairing DNA mismatches (11). In addition, PCNA plays an important role in many essential cellular processes, such as DNA replication, cell cycle control, cell survival and regulation of ovarian follicles development (10). Another pathway in DNA repair is homologous recombination (*HR*). In this pathway, ATM protein, along with other factors, plays a key role in the binding of broken DNA strands. Previous studies have demonstrated that ATM protein deficiency

may result in oocyte apoptosis at the prophase stage and female infertility (10-12). Any failure in the double-stranded DNA structure activate ATM protein which interacts with RAD51C/BRCA2 and form a complex to repair DNA, using an intact strand as a template (10-12). Formation of the Mre11a3, Rad50 and Nsb1 complexes is essential for HR repair pathway (10-13) and any defection in this complex causes cell apoptosis. Furthermore, the interaction of BRCA, FANC1/FANC2 and RAD 51 is also essential to complete HR repair pathway. Thus, any mutation in *Brca* genes are associated with the increasing of breast and ovarian cancers (10, 12). The *BRCA1* and *BRCA2* tumor suppressor genes prevent tumor development through repair of DNA damage. Any mutation in aforementioned genes result in malignancy (14). It was demonstrated that BRCA1, in collaboration with RAD51 has a key role in HR repair pathway (10-12).

Regarding to the importance of DNA repair process in the control of cell growth and developmental competence in ovarian follicles (3, 12), the aim of this study was to investigate effect of vitrification of mice preantral follicles on the DNA repair gene expressions.

Materials and Methods

All chemicals were purchased from Sigma-Aldrich (UK) Company, otherwise those mentioned in the text, as well as culture media made with the Deionized water (Milli-Q).

Animals

In this experimental study, NMRI mice (14-16 days old, n=12) were obtained from the Razi Vaccine and Serum Research Institute of Iran and they were kept in appropriate conditions including: 12 hours of darkness and 12 hours of light, temperature of 20-24˚C and 40-50% of moisture with free access to the food and water. Experiments of the present study has been reviewed and approved by Ethical Committee of the School of Biology, Damghan University (IR. BSDU.REC.1397.14). All applicable institutional guidelines for the care and use of animals were followed in accordance with declaration of Helsinki as revised in Tokyo 2004.

Isolation of preantral follicles

The mice were euthanized through cervical dislocation and the ovaries were removed and placed in 200 µl drops of α-MEM medium containing 10% fetal bovine serum (FBS, Sigma-Aldrich, Australia), 2.2 g/l sodium bicarbonate, 100 IU/ml penicillin, 75 µg/ml streptomycin and 25 mM HEPES. Preantral follicles were isolated mechanically as described previously (15) using a G29 needle connected to an insulin syringe under a stereomicroscope (Olympus, Japan) ×25 magnification. After that, preantral follicles with an approximate diameter of 140-160 µm containing a central oocyte and 2-3 layers of granulosa cells were considered healthy and selected for culture *in vitro*.

Experimental design

The preantral follicles were randomly divided into three groups (1). Control group: fresh preantral follicles that were cultured for 12 days, immediately after isolation (2). Vitrification group: vitrified preantral follicles thawed and cultured for 12 days (3). Toxic group: preantral follicles without exposure to liquid nitrogen were only placed in equilibration and vitrification media and they were cultured for 12 days. The experiment was conducted in two steps. First, the growth and development of preantral follicles were evaluated and then DNA repair gene expressions were assessed separately.

Vitrification of preantral follicles

The vitrification of preantral follicles were carried out as described previously by Hatami et al. (16) with slightly modifications. The preantral follicles were kept in an equilibrium solution (ES) composed of phosphate-buffered saline (PBS) supplemented with ethylene glycol (EG, 7.5% V/V), dimethyl sulfoxide (DMSO, 7.5% V/V) and FBS (20%) for 5 minutes. After that, the preantral follicles were transferred to vitrification solution (VS) composed of PBS supplemented with EG (15% V/V), DMSO (15% V/V), FBS (20%) and sucrose (0.5 M) and they were kept for 30 seconds. Subsequently, preantral follicles were immediately removed from VS using a Pasteur pipette and loaded to the thin end of the cryotop tape and transferred to the liquid nitrogen. For warming, the preantral follicles were kept in PBS solution supplemented with a descending concentration of sucrose (1, 0.5, 0.25 and 0.125 M sucrose) at an interval of 5 minutes. In the toxic group: preantral follicles were only placed in equilibration and vitrification media and then without exposure to liquid nitrogen placed in the warming solutions (descending concentration of sucrose: 1, 0.5, 0.25 and, 0.125 M sucrose at an interval of 5 minutes) to remove cryoprotectant.

In vitro culture of preantral follicles

Preantral follicles were cultured in 25 µl drops of α-MEM culture medium enriched with 5% FBS, 0.1 IU/ml human follicle stimulating hormone (hFSH), 1% insulin, transferring and selenium (ITS), 10 ng/ml of epidermal growth factor (EGF), 2.2 g/l sodium bicarbonate, 100 IU/ml penicillin and 75 µg/ ml streptomycin under mineral oil in incubator at 37˚C, 90% humidity and 5% CO_2 for 12 days. Every 48 hours, approximately 15 µl of the culture medium from each drop was replaced by a fresh medium.

During the culture period, diameter and morphological changes were evaluated. Follicle diameter was measured by an inverted microscope (Nikon, Japan) under ×400 magnification through calculating the average of two perpendicular diameters with a precalibrated ocular micrometer at the initial time (day 0), in addition to the second and fourth days of the culture period. Darkness of follicles and follicles without an oocyte or naked oocyte were considered as degenerated follicles. The antral cavity was defined as a lucent area among the granulosa cells. Survival rate was calculated by the ratio

of survived follicles to the total follicles.

Induction of ovulation

In order to induce ovulation, on the tenth day of the culture period, 1.5 IU/ml of human chorionic gonadotropin (hCG, Choriomon, Switzerland) was added to the culture medium. After 16-48 hours, ovulation rate was considered under invert microscope (Nikon, Japan) and the released oocytes were categorized into three groups: germinal vesicle (GV), metaphase I (MI) and metaphase II (MII).

RNA extraction

RNA extraction was performed using Trizol® (*Qiagen, Germany)* according to the manufacture's protocol. In brief, 100 preantral follicles were homogenized in 100 µl of Trizol solution, with vigorously vortex for 3 minutes, followed by incubation at room temperature for 5 minutes. After that 50 µl chloroform was added, gently mixed and incubated at room temperature for 3 minutes. It was then centrifuged in 12000 g for 15 minutes at 4˚C. The upper aqueous phase containing total RNA was carefully removed and placed in a new centrifuge tube. 125 µl of Isopropyl alcohol was added and incubates at room temperature for 3 minutes, followed by centrifugation in 12,000 g for 30 minutes at 4˚C. The resultant pellet was washed with 1 ml of 75% ethanol and centrifuged in 7500 g for 5 minutes at 4˚C. The resultant pellet dried at RT and solved in 20 µl sterile water. The integrity and purity of extracted RNA was evaluated by density ratio of 28S to 18S rRNA bands on the agarose gel electrophoresis and measuring the absorbance ratio of 280/260 nm using spectrophotometer, respectively. Samples with 260/280 nm ratio of 1.8-2.0 were acceptable and used for reverse transcription.

cDNA synthesis and quantitative reverse transcription-polymerase chain reaction

Synthesis of cDNA from 500 ng of total RNA was performed using Takara kit (Takara, Japan) according to the manufacturer's instructions.

Quantitative reverse transcription polymerase chain reaction (qRT-PCR) was carried out to assess relative mRNA expressions of *Msh6, Mre11, Brca1, Rad51, Pcna* and *Atm* genes in preantral follicles on the second and sixth days of culture period. The primer sets were designed to include the introns or span exon/exon junction to avoid residual genomic DNA amplification using the Allele ID software version 7.8 (Premier Biosoft Int, USA, Table 1). All primer pairs were tested to be specific for the target genes. Amplification of no genomic DNA was confirmed using PCR on the none-reverse transcribed RNA as template. Additionally, cDNA of each gene was used as a positive control in a separate microtube in PCR reaction. qRT-PCR was carried out on the Rotor-gen 6000 machine (Corbett Life Science, USA) using the SYBR green (Takara, Japan). The reactions mixture included SYBR green (5 µl), forward primer (0.5 µl), reverse primer (0.5 µl) and cDNA (4 µl) in 10 µl final volume. PCR reactions were set as 95˚C for 30 seconds, followed by 40 cycles of denaturation at 95˚C for 10 seconds and annealing/extension at 60˚C for 45 seconds. The *Pfaffl* method was applied to calculate relative mRNA expressions. Relative expression level of the target genes were normalized to *Ef1*. The specificity of qRT-PCR was assessed by analysis of melting curve and a no-template negative control sample for each gene.

Table 1: Oligonucleotide primer sequences for quantitative reverse transcription-polymerase chain reaction

Gene	Primer sequence (5´-3´)	Nucleotides	Product size	Melting temperature	Accession number in NCBI
Msh6	F: AGGAGACAGAGGTGCATGAG	20	135	61.7	NM_010830.2
	R: CAGTTCTTCGCTGCCCAGT	20		62.7	
Mre11	F: ACTTTGAATCAGATGAGGATG	22	119	55.8	NM_001310728.1
	R: CGTACTACGTCCTTCTTTAGT	22		59.4	
Brca1	F: CTGTCTACATTGAACTAGACTC	22	125	51.1	NM_009764.3
	R: GACCTCTACTTCCGTTCGAC	20		53.8	
Rad51	F: CTCTGGCAGCGATGTCCTAG	20	121	55.9	NM_011234.4
	R: AGGTCCATACGTGACGAATAA	22		50.5	
PCNA	F: GTCTCACGTCTCCTTGGTAC	20	113	53.8	NM_011045.2
	R: CTTGGAGTGGTCGTACAGG	20		53.2	
ATM	F: CAGCCTGTAAACCTTCTAGTC	21	152	52.4	NM_007499.2
	R: CTCAGTTATTACTCCACCGAG	21		52.4	
Ef1	F: AGTCGCCTTGGACGTTCTT	19	124	51.1	NM_010106
	R: GTGTAGTTGTAGCATTAGCC	23		55.3	

Statistical analysis

SPSS software (version 24, IBM, USA) was used for analyzing all data. The Shapiro-Wilk test was used to test the normality of data. If the Sig. value of the Shapiro-Wilk Test is greater than 0.05, the data is normal. The statistical significance of differences in the relative gene expression levels was evaluated by one way analysis of variance (ANOVA) test and post hoc Dunnet test, among the groups. One way ANOVA and post hoc tukey's tests were applied for assess significant differences in growth and developmental parameters among the groups. Data are presented as mean ± standard deviation of the mean (SD). A $P<0.05$ was considered statistically significant. Experiments were repeated at least four times.

Results

Growth and development of preantral follicles

At the initial time of culture, follicles with similar diameter (140-160 µm) were selected and analyzed. No significant difference was detected among the all groups. On the second day, the diameter of follicles was increased. The follicles attached to the bottom of plate and immobilized due to proliferation of granulosa cells. On the second day, diameter of the preantral follicles of the vitrified group was significantly lower in comparison with the groups of fresh and toxic follicles, while there was no significant difference between toxic and fresh groups (Table 2). On the fourth day of culture, the growth rate increased. So that the shape of follicles became irregular and measuring diameter was impossible. From the sixth day onwards, some spaces were observed among the granulosa cells, which were considered as antrum cavities. In addition, on the fourth day of culturing period, diameter of preantral follicle in the vitrified group was significantly less than those of the control and toxic groups. However, there was no significant difference between follicle diameters of the control and toxicity groups (Table 2). Furthermore, the percentage of degeneration of vitrified follicles (22.5%) was significantly higher than that of follicles of fresh (14.5%) and toxic (14.5%) groups. However, there was no significant difference between degeneration of follicles in the control and toxic group. The rate of antrum cavity was 65.25% in the vitrified group, which was significantly lower than that of control (82.5%) and toxic groups (81.5%, $P<0.05$). However, there was no significant difference between the rate of antrum cavity formation of the control and the toxic groups. After induction of ovulation, although there was no significant difference between the ovulation rate in the follicles of fresh (78.25%) and the toxic (74.25%) groups, ovulation rate of follicles in both groups were significantly higher than vitrified group (64.75%). As shown in the Table 3, the rate of GV oocytes obtained from preantral follicles in the vitrified group (19.00%) was significantly higher than those of obtained from preantral follicles in the control (13.00%) and the toxic (13.75%) groups ($P<0.05$). Rate of the germinal vesicle breakdown (GVBD) oocytes in the vitrified group was significantly lower compared to those of control and toxic groups ($P<0.05$). However, there was no significant difference in the rate of GVBD oocytes between the control and toxic groups. Percentage of MII oocytes obtained from the preantral follicles of vitrified group (29.75) was significantly lower than that of control (46.00) and toxicity (43.50%) groups. While, there was no significant difference between the rates of MII oocyte in the control and the toxicity groups (Table 3).

Table 2: Diameter of the preantral follicles during the culture period

Groups	Number of follicles	Follicle diameters		
	n	Mean (µm ± SD)		
		Initial time	2nd day	4th day
Control	300	146.36 ± 6.31	196.92 ± 8.69	294.56 ± 12.36
Toxicity	296	146.00 ± 5.92	202.18 ± 9.40	302.13 ± 8.65
Vitrification	310	146.56 ± 6.05	184.99 ± 14.77*	238.02 ± 34.34*

In all cases, at least four experimental replicates were performed. *; Indicate significant difference within the groups ($P<0.05$).

Table 3: Maturation rates of cultured preantral follicles

Groups	Number of follicles	Survived	Antrum formation	Ovulated follicles	Stages of oocyte development		
					GV oocytes	MI oocytes	MII oocytes
Control (fresh follicles)	300	256	248	234	40	56	138
		(85.50 ± 1.73)	(82.50 ± 1.73)	(78.25 ± 2.50)	(13.00 ± 1.83)	(18.75 ± 1.26	(46.00 ± 1.41)
Toxicity follicles	296	252	229	220	37	55	128
		(86.00 ± 2.16)	(81.50 ± 5.92)	(74.25 ± 2.99)	(13.75 ± 1.89)	(18.75 ± 3.10	(43.50 ± 4.43)
Vitrified follicles	310	239*	202*	200*	58*	50*	92*
		(77.25 ± 1.71)	(65.25 ± 2.63)	(64.75 ± 1.71)	(19.00 ± 0.82)	(16.00 ± 0.82)	(29.75 ± 1.50)

In all cases, at least four experimental replicates were performed. Data are presented as n (% ± SD).
*; Indicates significant difference within the groups ($P<0.05$), GV; Germinal vesicle oocyte, MI; Metaphase I oocyte, and MII; Metaphase II oocyte.

Expression of genes

Results of the statistical analysis of data for all three groups of control, vitrification and toxicity are presented in Figure 1 and Figure 2. Dunnett post hoc test showed that relative expression levels of *Atr*, *Pcna*, *Brca1*, *Rad51*, *Msh6* and *Mre11* genes in the vitrification group was significantly higher than control and toxic groups, on the second and sixth days of culture period. While, the relative expression level of the aforementioned genes in the control and toxic groups was not significantly different.

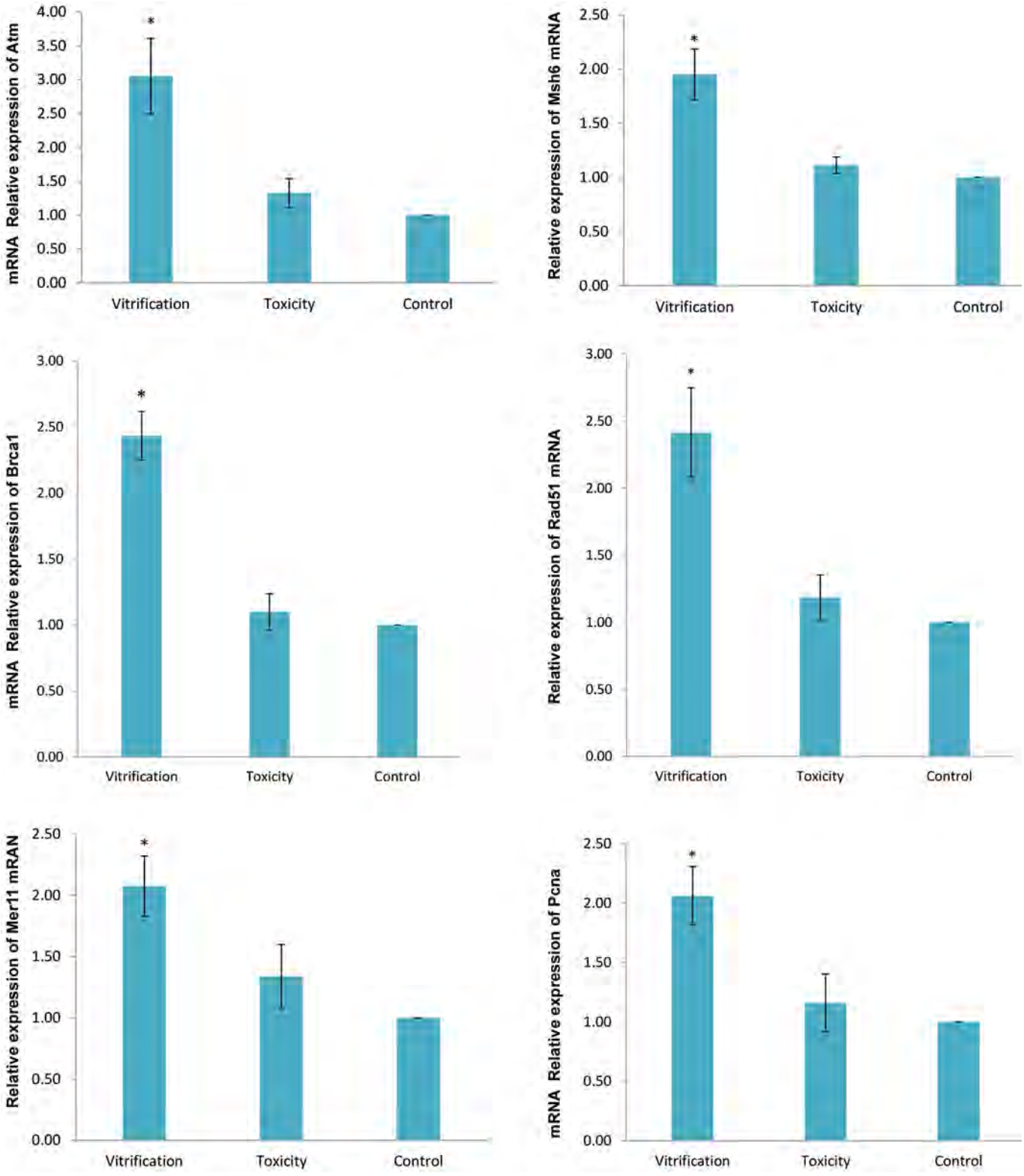

Fig.1: Relative mRNA expression levels of *Atr*, *Pcna*, *Brca1*, *Rad51*, *Msh6* and *Mre11* in preantral follicles on the second day of cultivation period. Data are presented as mean ± SD. *; Indicates significant difference compared to the control (P<0.05).

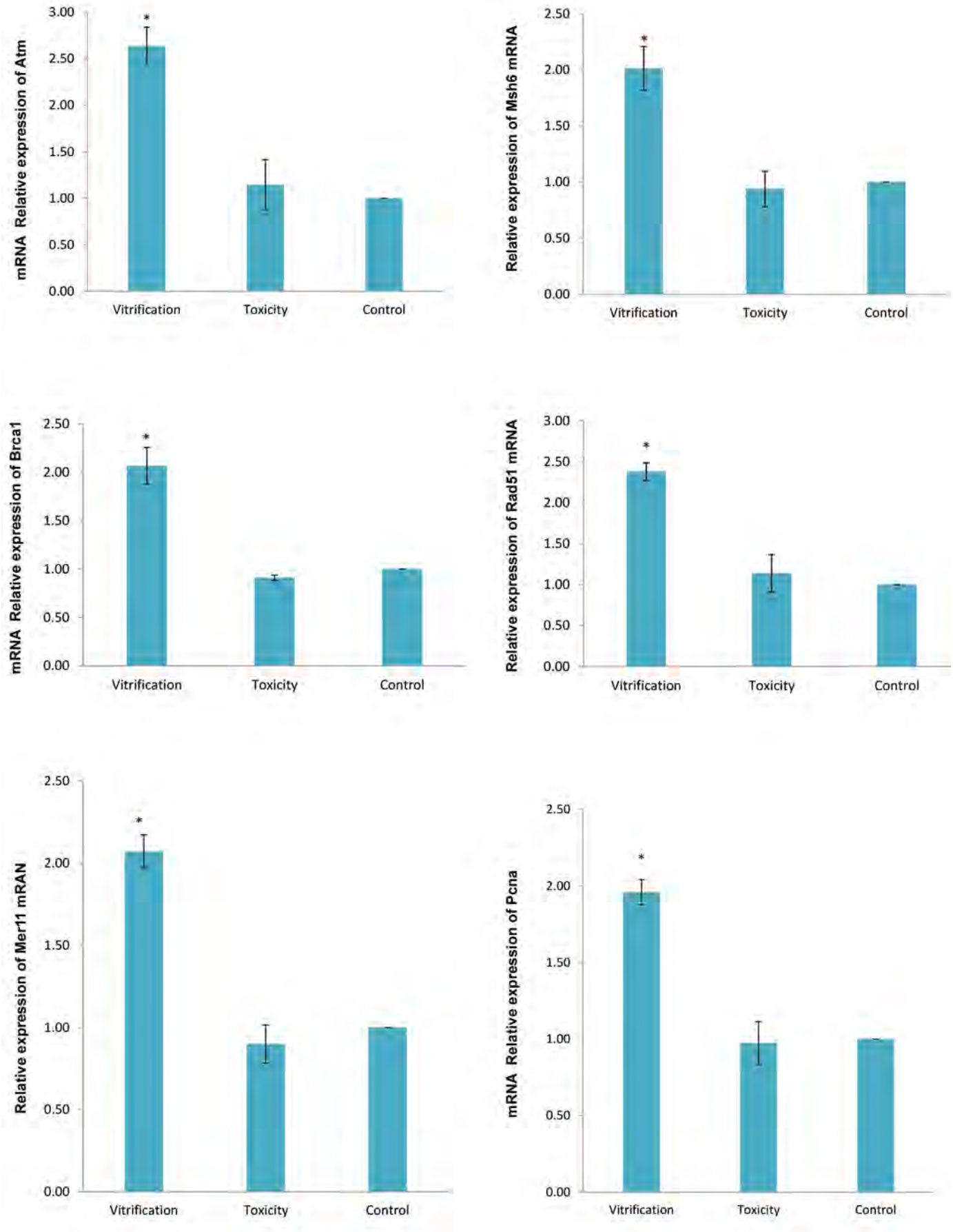

Fig.2: Relative mRNA expression levels of *Atr*, *Pcna*, *Brca1*, *Rad51*, *Msh6* and *Mre11* in preantral follicles on the sixth day of cultivation period. Data are presented as mean ± SD. *; Indicates significant difference compared to control (P<0.05).

Discussion

Cryopreservation methods allow long-term preservation of any types of biological cells and tissues such as ovaries, ovarian follicles, oocytes, embryos and stem cells. While, various degrees of cell damage may occur during cryopreservation, which are depends on several factors such as size, shape, permeability, quality and sensitivity of the cell or tissue (17, 18). These damages in oocyte and embryo can include dispersion of cellular skeleton, releasing cortical granules, zona hardening and disruption of plasma membrane which in turn negatively affect developmental competence of oocyte and embryo (19). However, some effects of vitrification on the molecular structure, including DNA and mRNA expression of the genes, is not immediately expressed after warming and therefore does not necessarily cause cell degeneration, while they can disturb growth and development of the cell (3, 20-22).

The present study was aimed to investigate this issue and examine the effect of vitrification on the developmental competence of mouse ovarian preantral follicles and expression of some DNA repair genes. Results of the first step of the present study showed that the rates of growth, survival, antrum formation and ovulation in the vitrified group were significantly reduced compared to the control and toxicity groups. In agreement with these observations, other studies showed that growth and rate of developmental competence of preantral follicles isolated from the vitrified ovarian tissue is slower than the non-vitrified preantral follicles (9, 21). However, Mazoochi et al. showed that there was no significant difference between the rates of growth and survival of follicles obtained from vitrified ovaries and fresh ovaries (17, 18). The differences in the recent and other studies can be attributed to the different protocols and materials. One of the important factors in regulation of follicular development is growth factors secreted by granulosa cells (23). Choi et al. (24) observed that number of granulosa cells was decreased in the vitrified group compared to the fresh group. Whereas, concentration of growth factors did not change in vitrified follicles.

Since DNA repair pathways are important in genetic preservation of ovarian follicles, in the second step of present study, effect of vitrification on the expression pattern of some genes involved in DNA repair pathways of mouse preantral follicles were investigated. The results showed that relative expression of *Msh6*, *Pcna*, *Rad51*, *Brca1*, *Mre11* and *Atm* genes in the preantral follicles of the vitrified group were significantly increased in comparison with those of the control and toxicity groups on the second and sixth days of culture period. It seems that an increase in the expression of DNA repair genes is a response to the damages resulted from the vitrification on the DNA structure. In addition, similar relative expression of DNA repair gene in the control and toxicity groups might indicate that exposure to the cryoprotectants has no deleterious effect on the DNA structure.

Maintaining genomic integrity of the germ cells is vital role in cell cycles, because it allows the genetic information to be correctly transmitted to the next progeny (25, 26). It was demonstrated that DNA repair genes in the oocyte are more expressed than embryos, in response to DNA damage (12, 27). In this regard, Ménézo et al. (12) showed that DNA repair genes including *MSH6*, *BRCA1*, *MRE11* and *PCNA* were widely expressed in human GV oocytes. Moreover, it was established that the number of ovarian follicles in the mutated Brca1 mice was significantly reduced (13). During repair of DNA double strand breaks, a complex of the Brca1, Rad50, Mre11 and Atm proteins accompanied with forming Brca2 and Rad51 proteins complex to repair these lesions. If this repair does not occur, the cell eventually becomes apoptotic (10-12). Titus et al. showed that reduction in the expression of *Brca1* was associated with a significant decrease in the developmental competence of oocytes (13). *Other researchers investigated* the effect of cryopreservation on the gene expression involved in folliculogenesis (3, 28, 29). It was shown that cryopreservation decreased expression of *Fagl* gene, while increased expression of *Fshr* and *Gdf9* genes. This in turn confirmd that cryopreservation changed the gene expression patterns (30). Furthermore, in a study conducted by Ménézo et al. (12) effect of the slow freezing and vitrification on gene expression pattern of human MII oocytes were investigated and it was shown that pattern of gene expression was changed in the both methods. They showed that slow freezing increased expression of *BRCA1* gene. This finding is constant with the results of present study. While others found conflicting results, regarding the other genes (17, 18).

There may be some possible limitations in this study, including efficiency of the preantral follicle maturation and extruded oocyte maturation. One possible reason could be attributed to their culture condition *in vitro*. In the present study, there may be several differences between the follicle growth *in vivo* and follicle maturation *in vitro*. In the current *in vitro* culture system, intra-ovarian nutritional factors and growth factors improving follicles development through autocrine and paracrine manners were absent. However, supplementation of maturation medium with some of these factors may be efficient for follicle development. Another reason for the weakness of follicle growth rate in the present study may be resulted from culturing in the two-dimensional culture system. Three-dimensional culture system *in vitro* might be supportive to eliminate this problem. More investigations will be needed to verify this hypothesis. Another limitation of this study is the identification of growing follicles during dissecting from ovarian tissue. In the ovarian follicular development, a vital step is recruitment of follicles into growing cohort. Our culture system is potentially compatible with the conventional microscopically methods for assessment the follicles. Further criteria is essential for the identification of recruited follicles.

Conclusion

The results of this study indicate that increasing expression of DNA repair genes can be a response of preantral follicles to repair DNA damages after vitrification.

Acknowledgements

This study was funded by Damghan University, Damghan, Iran. The authors are grateful to Mr. Abutaleb Koosha for providing technical assistance. The authors declare that they have no conflict of interest.

Authors' Contributions

Z.Kh.; Performed experiments and collected data. S.Z.; Developed the concept and designed experiments, analyzed data, and wrote the manuscript. P.F.; Participated in study design, reviewed the literature and gave technical support. M.N.; Conducted the qRT-PCR and revised manuscript, contributed in interpretation of the data and the conclusion. All authors performed editing and approving the final version of this manuscript for submission and they participated in the finalization of manuscript and approved the final draft.

References

1. Donnez J, Dolmans MM. Fertility preservation in women. N Engl J Med. 2017; 377(17): 1657-1665.
2. Revel A, Revel-Vilk S. Pediatric fertility preservation: is it time to offer testicular tissue cryopreservation? Mol Cell Endocrinol. 2008; 282(1-2): 143-149.
3. Lin C, Tsai S. The effect of cryopreservation on DNA damage, gene expression and protein abundance in vertebrate. Ital J Anim Sci. 2012; 11(1): 119-122.
4. Chen JY, Li XX, Xu YK, Wu H, Zheng JJ, Yu XL. Developmental competence and gene expression of immature oocytes following liquid helium vitrification in bovine. Cryobiology. 2014; 69(3): 428-433.
5. Jafarabadi M, Abdollahi M, Salehnia M. Assessment of vitrification outcome by xenotransplantation of ovarian cortex pieces in γ-irradiated mice: morphological and molecular analyses of apoptosis. J Assist Reprod Genet. 2015; 32(2): 195-205.
6. Sales AD, Duarte AB, Santos RR, Alves KA, Lima LF, Rodrigues GQ, et al. Modulation of aquaporins 3 and 9 after exposure of ovine ovarian tissue to cryoprotectants followed by in vitro culture. Cell Tissue Res. 2016; 365(2): 415-424.
7. Fatehi R, Ebrahimi B, Shahhosseini M, Farrokhi A, Fathi R. Effect of ovarian tissue vitrification method on mice preantral follicular development and gene expression. Theriogenology. 2014; 81(2): 302-308.
8. Sampaio da Silva AM, Bruno JB, de Lima LF, Ribeiro de Sá NA, Lunardi FO, Ferreira AC, et al. Connexin 37 and 43 gene and protein expression and developmental competence of isolated ovine secondary follicles cultured in vitro after vitrification of ovarian tissue. Theriogenology. 2016; 85(8): 1457-1467.
9. Asadzadeh R, Khosravi S, Zavareh S, Ghorbanian MT, Paylakhi SH, Mohebbi SR. Vitrification affects the expression of matrix metalloproteinases and their tissue inhibitors of mouse ovarian tissue. Int J Reprod Biomed. 2016; 14(3): 173-180.
10. Friedberg EC, Walker GC, Siede W, Wood RD, Schultz RA, Ellenberger T. DNA repair and mutagenesis. 2nd ed. Washington: American Society for Microbiology Press; 2005.
11. Altieri F, Grillo C, Maceroni M, Chichiarelli S. DNA damage and repair: from molecular mechanisms to health implications. Antioxid Redox Signal. 2008; 10(5): 891-937.
12. Ménézo Y, Dale B, Cohen M. DNA damage and repair in human oocytes and embryos: a review. Zygote. 2010; 18(4): 357-365.
13. Titus S, Li F, Stobezki R, Akula K, Unsal E, Jeong K, et al. Impairment of BRCA1-related DNA double-strand break repair leads to ovarian aging in mice and humans. Sci Transl Med. 2013; 5(172): 172ra21.
14. Mersch J, Jackson MA, Park M, Nebgen D, Peterson SK, Singletary C, et al. Cancers associated with BRCA 1 and BRCA 2 mutations other than breast and ovarian. Cancer. 2015; 121(2): 269-275.
15. Abedelahi A, Salehnia M, Allameh AA, Davoodi D. Sodium selenite improves the in vitro follicular development by reducing the reactive oxygen species level and increasing the total antioxidant capacity and glutathione peroxide activity. Hum Reprod. 2010; 25(4): 977-985.
16. Hatami S, Zavareh S, Salehnia M, Lashkarbolouki T, Ghorbanian MT, Karimi I. The impact of alpha lipoic acid on developmental competence of mouse vitrified pre-antral follicles in comparison to those isolated from vitrified ovaries. Iran J Reprod Med. 2014; 12(1): 57-64.
17. Mazoochi T, Salehnia M, Pourbeiranvand S, Forouzandeh M, Mowla SJ, Hajizadeh E. Analysis of apoptosis and expression of genes related to apoptosis in cultures of follicles derived from vitrified and non-vitrified ovaries. Mol Hum Reprod. 2009; 15(3): 155-164.
18. Mazoochi T, Salehnia M, Valojerdi MR, Mowla SJ. Morphologic, ultrastructural, and biochemical identification of apoptosis in vitrified-warmed mouse ovarian tissue. Fertil Steril. 2008; 90 Suppl 4: 1480-1486.
19. Herrero L, Martínez M, Garcia-Velasco JA. Current status of human oocyte and embryo cryopreservation. Curr Opin Obstet Gynecol. 2011; 23(4): 245-250.
20. Park SE, Son WY, Lee SH, Lee KA, Ko JJ, Cha KY. Chromosome and spindle configurations of human oocytes matured in vitro after cryopreservation at the germinal vesicle stage. Fertil Steril. 1997; 68(5): 920-926.
21. Salehnia M, Töhönen V, Zavareh S, Inzunza J. Does cryopreservation of ovarian tissue affect the distribution and function of germinal vesicle oocytes mitochondria? Biomed Res Int. 2013; 2013: 489032.
22. Barik M, Bajpai M, Patnaik S, Mishra P, Behera P, Dwivedi SN. Development of new method and protocol for cryopreservation related to embryo and oocytes freezing in terms of fertilization rate: A comparative study including review of literature. Adv Biomed Res. 2016; 5: 117.
23. Rimon-Dahari N, Yerushalmi-Heinemann L, Alyagor L, Dekel N. Ovarian folliculogenesis. Results Probl Cell Differ. 2016; 58: 167-190.
24. Choi WJ, Yeo HJ, Shin JK, Lee SA, Lee JH, Paik WY. Effect of vitrification method on survivability, follicular growth and ovulation of preantral follicles in mice. J Obste Gynaecol Res. 2007; 33(2): 128-133.
25. Hotamisligil S, Toner M, Douglas Powers R. Changes in membrane integrity, cytoskeletal structure, and developmental potential of murine oocytes after vitrification in ethylene glycol. Biol Reprod. 1996; 55(1): 161-168.
26. Mathias FJ, D'Souza F, Uppangala S, Salian SR, Kalthur G, Adiga SK. Ovarian tissue vitrification is more efficient than slow freezing in protecting oocyte and granulosa cell DNA integrity. Syst Biol Reprod Med. 2014; 60(6): 317-322.
27. Menezo Y Jr, Russo G, Tosti E, El Mouatassim S, Benkhalifa M. Expression profile of genes coding for DNA repair in human oocytes using pangenomic microarrays, with a special focus on ROS linked decays. J Assist Reprod Genet. 2007; 24(11): 513-520.
28. Liu HC, He Z, Rosenwaks Z. Mouse ovarian tissue cryopreservation has only a minor effect on in vitro follicular maturation and gene expression. J Assist Reprod Genet. 2003; 20(10): 421-431.
29. Tao T, Del Valle A. Human oocyte and ovarian tissue cryopreservation and its application. J Assist Reprod Genet. 2008; 25(7): 287-296.
30. Shams Mofarahe Z, Salehnia M, Ghaffari Novin M, Ghorbanmehr N, Fesharaki MG. Expression of folliculogenesis-related genes in vitrified human Ovarian tissue after two weeks in vitro culture. Cell J. 2017; 19(1): 18-26.

Original Article

Overexpression of *GATA5* Stimulates Paclitaxel to Inhibit Malignant Behaviors of Hepatocellular Carcinoma Cells

Haipeng Feng, M.Sc.[1#], Bo Lin, Ph.D.[1#], Yifei Zheng, M.D.[1], Junnv Xu, M.D.[1, 2], Ying Zhou, M.D.[1], Kun Liu, M.Sc.[1], Mingyue Zhu, Ph.D.[1], Mengsen Li, Ph.D.[1, 3*]

1. Hainan Provincial Key Laboratory of Carcinogenesis and Intervention, Hainan Medical College, Haikou, Hainan Province, China
2. Department of Tumor Internal Medicine, Second affiliated Hospital of Hainan Medical College, Haikou, Hainan Province, China
3. Institution of Tumor, Hainan Medical College, Haikou, Hainan Province, China

#These authors contributed equally to this work.

Corresponding Address: Hainan Provincial Key Laboratory of Carcinogenesis and Intervention, Hainan Medical College, 3 Xueyuan Road, Longhua District, Haikou 571199, Hainan Province, China
Email: mengsenli@163.com

Received: 17/April/2019, Accepted: 15/September/2019

Abstract

Objective: Explore the effect of *GATA5* expression on Paclitaxel inhibiting growth of hepatocellular carcinoma (HCC) cells.

Materials and Methods: In the experimental study, HCC cell lines (HLE, Bel7402 and PLC/PRF/5) were treated with different concentrations of Paclitaxel (5-20 mg/ml) for 24 hours. HLE cells were transfected with *GATA5*-siRNA vector, while Bel7402 and PLC/PRF/5 cells were transfected with overexpressed *GATA5* vector for 24 hours, followed by treatment of the cells with Paclitaxel (10 mg/ml) for 24 hours and subsequently 3-(4,5-dimethyl-2-thiazolyl)-2,5-diphenyl-2-H-tetrazolium bromide (MTT) assay to detect growth of HCC cells. Soft agar cultured was used to analyze formation of colony. Apoptosis of HCC cells were detected by Flow cytometer. Migration of HCC cells was observed by trawell assays. Western blotting and laser confocal microscopy were utilized to detect expression and location of the proteins.

Results: Inhibiting expression of *GATA5* reduced sensitivity of HLE cells to Paclitaxel, while overexpression of *GATA5* increased sensitivity of Bel7402 cells and PLC/PRF/5 cells to Paclitaxel. Overexpression of *GATA5* played a role in stimulating Paclitaxel to inhibit growth, colony formation and migration, as well as enhance apoptosis in HCC cells. Overexpression of *GATA5* also promoted Paclitaxel to inhibit expression of reprogramming genes, such as *Nanog, EpCAM, c-Myc* and *Sox2* in Bel7402 and PLC/PRF/5 cells. Inhibited expression of *GATA5* led to enhancement of the expression of CD44 and CD133, in HLE cells. Overexpression of *GATA5* was not only alone but also synergized with Paclitaxel to inhibit expression of CD44 and CD133 in Bel7402 or PLC/PRF/5 cells.

Conclusion: Overexpression of *GATA5* played a role in enhancing Paclitaxel to inhibit the malignant behaviors of HCC cells. It was involved in suppressing expression of the reprogramming genes and stemness markers. Targeting *GATA5* is an available strategy for applying paclitaxel to therapy of patients with HCC.

Keywords: *GATA5*, Hepatocellular Carcinoma Cells, Paclitaxel, Reprogramming Genes, Stemness Marker

Cell Journal(Yakhteh), Vol 22, Suppl 1, Autumn 2020, Pages: 89-100

Citation: **Feng H, Lin B, Zheng Y, Xu J, Zhou Y, Liu K, Zhu M, Li M. Overexpression of GATA5 stimulates paclitaxel to inhibit malignant behaviors of hepatocellular carcinoma cells. Cell J. 2020; 22 Suppl 1: 89-100. doi: 10.22074/cellj.2020.6894.**

Introduction

Paclitaxel is an effective chemotherapeutic drug that is widely applied in the treatment of a number of cancer types. It promotes cell death through apoptotic pathway (1, 2), while it causes drug resistance in the cancer cells (3). Hepatocellular carcinoma (HCC) is the fifth most frequent type of cancer and the rate of drug-resistance in HCC patients is high (3, 4). Surgery is considered as the best method for the treatment of liver cancer. However, many patients are diagnosed in the middle and late stages of disease and they loss chance of surgery. Thus, the mortality rate of liver cancer patients is higher than many other types of malignant tumor (3, 5). There is an imperative need to explore the mechanism of HCC cell resistance to drug therapy and to develop new strategy for treating drug-resistance of HCC patients.

GATA family regulates cell reprogramming to induce stem cell differentiation and normal function of cells (6). This family includes GATA1-6, while GATA3 plays a key role in the regulating breast cancer suppression (7). GATA5 also inhibits proliferation, invasion and migration of cholangiocarcinoma cells (8). Hypermethylation of gene promoter suppresses *GATA5* expression, leading to promoting growth and colony formation in HCC cells (9). Paclitaxel is a valid chemotherapy drug in HCC patients, although the corresponding drug-resistance has frequently been observed during treatment of these patients. GATA5 is an optional bio-target for treatment of HCC, however, the effect of *GATA5* expression on Paclitaxel during treatment of HCC patients is not clear yet.

Previously, evidences indicated high expression of some reprogramming genes and stemness markers in HCC cells (10-13). In this study, we investigated how GATA5 influenced proliferation, apoptosis, migration and invasion of HCC cells after treatment with Paclitaxel. The results displayed that overexpression of *GATA5*

stimulates Paclitaxel effect to decrease expression of the reprogramming genes *Nanog*, *EpCAM*, *c-Myc*, *Sox2* and two stemness marker (CD44 and CD133) in the HCC cells *in vitro*. Our results revealed that GATA5 played an important role in Paclitaxel inhibiting the malignant behaviors of HCC cells by blocking expression of the reprogramming related genes and stemness markers.

Materials and Methods

Cell culture

In the experimental study, three human liver cancer cell lines (HLE, Bel7402 and PLC/PRF/5) were selected to test, the HCC cells were purchased from the Institution of Cellular Biology, Shanghai Academy of Life Science, China Academy of Science (Shanghai, China). These cells were cultured in RPMI-1640 medium supplemented with 10% heat-inactivated fetal calf serum (FCS) at 37˚C in a humidified atmosphere containing 5% CO_2. The culture medium was replaced or the cells were passaged according to their growth state after 1-2 days. This study protocol was approved by the Ethical Committee of Hainan Medical College (code: 20170106).

Construction and transfection of the *GATA5* expression vector

The construct of stable expression vector CDH-*GATA5* was as follows: the full-length human *GATA5* cDNA (residue 1-397, NCBI: NM_080473) was synthesized and amplified by polymerase chain reaction (PCR) using the following primers:

F: 5´-CCGAAGCTTGCCACCATGTACCAGAGCCT-3´
R:5´-CGGGCGGCCGCCTAGGCCAAGGCCAGCGC-3´.

They were then ligated into the expression vector pCDH-CMV-MCS-EF1-coGFP (Systembio, USA) by the HindIII and NotI restriction enzymes (Takara Bio Inc., China). The expression vector was transfected into HCC cells by Lipofectamine 2000 (Invitrogen, USA). To obtain the stable expression vector CDH-*GATA5*, Puromycin was used to screen the stable cell clones. The transfected Bel7402 and PLC/PFR/5 cells with CDH-*GATA5* were respectively named Bel7402-CDH-*GATA5* and PLC/PFR/5-CDH-*GATA5*.

RNA interference

Transfection of siRNA-*GATA5* or its negative control siRNA-scramble into HLE cells was as follows: the cells were seeded into 6-wells plate until they reached 70-80% confluence. The siRNA-*GATA5* or siRNA-scramble was transfected in each well, in the absence of serum by Lipofectamine 2000. The siRNA-*GATA5* sequence was as follows: 5´-AAAGUCCUCAGGCUCGAAC-3´ (8). The transfected HLE cells with siRNA-*GATA5* were named HLE-siRNA-*GATA5*.

MTT assay

1.5×10^4 cells/ml of HLE, Bel7402, PLC/PRF/5, HLE-siRNA-*GATA5*, Bel7402-CDH-*GATA5* and PLC/PRF/5-CDH-*GATA5* were cultured in 96-wells plate in RPMI-1640 medium supplemented with 10% FCS at 37˚C in a humidified atmosphere of 5% CO_2 for 48 hours. These cells were refreshed with culture medium containing with 10% FCS and they were next treated with different concentrations (5-20 μg/ml) of Paclitaxel (Sigma-Aldrich, USA) for 24 hours. Effect of Paclitaxel on cell growth was measured by the methylthiazolyldiphenyl-tetrazolium bromide (MTT) assay. Absorbance of the experimental group was measured by a microplate reader at a wavelength of 490 nm. Growth ratio was calculated using the following formula: growth ratio=(control group A_{490}-treated group A_{490})/control group $A_{490}\times100\%$ (14).

Analyses of the cell morphology, cell death and cellular nucleus

The HLE, Bel7402, PLC/PRF/5, HLE-siRNA-*GATA5*, Bel7402-CDH-*GATA5*, and PLC/PRF/5-CDH-*GATA5* cells were inoculated into a 6-wells plate with the concentration of 2.5×10^4 cells/ml. Then, the cells were cultured in complete medium, containing 10% FCS for 24 hours and they were refreshed with serum-free medium after 12 hours, followed by treating with 10 μg/ml Paclitaxel for 24 hours (in complete medium, containing 10% FCS). Morphology of the cells was observed under a light microscope. Trypan blue staining was used to observe dead cells by microscopy. The cells were also stained with 4,6-diamidino-2-phenylindole dihydrochloride (DAPI) solution to determine potential changes of the cellular nucleus. The cells were imaged using a microscopy at ×100 magnification. The cellular apoptosis condition was assessed under a microscope, and these criteria were described in the previous reports (14-16).

Soft agar colony formation assay

Approximately 1000 cells were plated in the 6-wells plate and they were cultured in complete medium containing 20% FCS, mixing with 0.7% soft agar (1:1) to lay the upper layer. Then, the cells were incubated for 14 days at 37˚C. The colonies were photographed and counted using a Nikon inverted microscope (Nikon, Japan) (9).

Crystal violet staining observation of the colony formation

The cells were transferred into the fresh 6-wells plate Petri-dishes at a concentration of 800 cells/well, followed by growth selection using 400 mg/ml of G418 (Beijing Baiaolaibo Science and Technology Ltd., China). After 14 days of incubation, the cells were fixed with 75% ethanol for 30 minutes. They were subsequently stained with 0.2% crystal violet (Beijing Zhongshan Biotechnology Co., China) for colony visualization and counting (9).

Flow cytometry

The HLE, Bel7402 and PLC/PRF/5 cells were cultured in RPMI-1640 medium supplemented with 10% FCS at

37˚C in a humidified atmosphere of 5% CO_2. The cells were transfected with siRNA-*GATA5* or CDH-*GATA5* for 48 hours, followed by treatment with Paclitaxel (20 μg/ml) for 48 hours. Apoptosis of the cells were analyzed by flow cytometer (Thermo Fisher Scientific, China) using the method as described previously (14).

Cells migration assays

The transwell method was used for observing the cells migration, and it was performed according to the manufacturer's protocol (Biofavor Biotech, China) and as described previously (17, 18). The HLE, Bel7402 and PLC/PRF/5 cells (1.5×10^4) were transfected with siRNA-*GATA5* or CDH-*GATA5* for 48 hours. The cells were added to the upper chamber, cultured in serum-free RPMI-1640 medium and treated with Paclitaxel (10 μg/ml) for 48 hours, while the lower chamber was filled with 20% FCS. The complete medium was manipulated according to the previously described methods (18). Number of the cells migrated through the wells was quantified by counting five independent fields, using a microscopy with a ×20 objective lens (Olympus Corporation, Japan).

Western blotting

To evaluate the effect of Paclitaxel on migration-related proteins, reprogramming genes and stemness markers, the cells were transfected with siRNA-*GATA5* or CDH-*GATA5* followed by treatment with Paclitaxel (10 μg/ml) for 48 hours. A Western blot analysis of the metastasis-associated proteins MMP2 and MMP9 as well as the reprogramming related genes *Nanog, c-Myc, Sox2,* and *EpCAM* were performed. The experimental method was described previously (14, 19).

Detection of proteins expression by laser confocal microscopy

Expression of the stemness markers (CD44 and CD133) was observed by laser confocal microscopy after drug screening. HLE, Bel7402 and PLC/PRF/5 cells were transfected with siRNA-*GATA5* or CDH-*GATA5* for 24 hours. They were then inoculated into the laser confocal culture chamber for 12 hours, followed by treating with Paclitaxel (10 μg/ml) for 48 hours. The remaining cells were incubated with rabbit anti-human primary CD44 and CD133 antibodies (Abcam Corp., USA) for 12 hours. Next, they were incubated with fluorescent Alex488 and Alex647 (Beyotime Corporation, China) secondary antibodies for 2 hours. Then, they were washed with PBS and DAPI was added. Expression and localization of CD44 and CD133 were subsequently observed by laser confocal microscopy (Fuji, Japan). The experimental method was described previously (20, 21).

Statistical analysis

The data are presented as the mean ± SD. Statistical analysis was performed using Student's t test (for two experimental groups) and F-test (SPSS 11.5 software for Windows, SPSS Inc., USA). The statistical significance was set at $P<0.05$.

Results

GATA5 stimulated Paclitaxel to inhibit the growth of hepatocellular carcinoma cells

To investigate the influence of GATA5 on Paclitaxel regulating growth of HCC cells, we first conducted a MTT assay to analyze the influence of different concentrations of Paclitaxel (5-20 μg/ml) on proliferation of HCC cells. When the optimal concentration of paclitaxel was determined as >10 μg/ml, growth of these HCC cells was significantly inhibited (Fig.1A). Then, we used Western blot to test GATA5 expression in the HCC cells. Result showed that the HLE cells had high expression of endogenous GATA5, but the endogenous expression of GATA5 in the Bel7402 and PLC/PRF/5 cells was low (Fig.1B). Thus, we silenced GATA5 expression in the HLE cells by transfecting the cells with siRNA-*GATA5,* and enhanced *GATA5* expression in the Bel7402 and PLC/PRF/5 cells by transfecting with the CDH-*GATA5* expression vector. The MTT result indicated that silencing *GATA5* expression in the HLE cells stimulated growth, which was inhibited by Paclitaxel. Enhancing *GATA5* expression in the Bel7402 and PLC/PRF/5 cells inhibited the growth to a higher degree, synergizing with Paclitaxel (Fig.1C). The results indicated that overexpression of *GATA5* was able to enhance sensitivity of HCC cells to Paclitaxel *in vitro*.

GATA5 enhanced Paclitaxel to promote apoptosis of hepatocellular carcinoma cells

In this study, we also investigated whether GATA5 was able to enhance Paclitaxel to induce apoptosis of HCC cells by microscopy observations, trypan blue exclude staining, DAPI staining and a flow cytometry analysis. The HCC cells were treated with Paclitaxel for 48 hours followed by transfection with siRNA-*GATA5* or CDH-*GATA5* for 48 hours. The results obtained from light microscopy observation (Fig.2A), trypan blue exclude staining observation (Fig.2B) and DAPI staining observation (Fig.2C) showed that Paclitaxel promoted apoptosis of HCC cells. Silencing *GATA5* expression by transfecting with siRNA-*GATA5* in the HLE cell antagonized the influence of HCC cell apoptosis, which was induced by Paclitaxel. Increasing expression of GATA5 by transfecting with CDH-*GATA5* in the Bel7402 and PLC/PRF/5 cells could enhance Paclitaxel to induce apoptosis of these HCC cells. The flow cytometry analysis also confirmed that GATA5 was able to promote Paclitaxel-induced apoptosis of the HCC cells. The results showed that number of apoptotic cells was significantly higher in the Paclitaxel+siRNA-scramble group compared to the untreated group. HLE cells were treated with Paclitaxel followed by transfecting with siRNA-*GATA5* to silence expression of this gene (Paclitaxel +siRNA-

GATA5 group). The obtained cells displayed that the number of apoptotic cells was reduced compared to Paclitaxel+siRNA-scramble group. Bel7402 and PLC/PRF/5 cells were treated with Paclitaxel followed by increasing *GATA5* expression by transfecting with CDH-*GATA5* (Paclitaxel+CDH-*GATA5* group). The obtained cells showed that the number of apoptotic cells was increased compared to the transfected cells with the CDH empty vector (Paclitaxel+CDH group, Fig.2D). These results indicated that GATA5 has a trait to enhance the effect of Paclitaxel on inducing apoptosis of HCC cells.

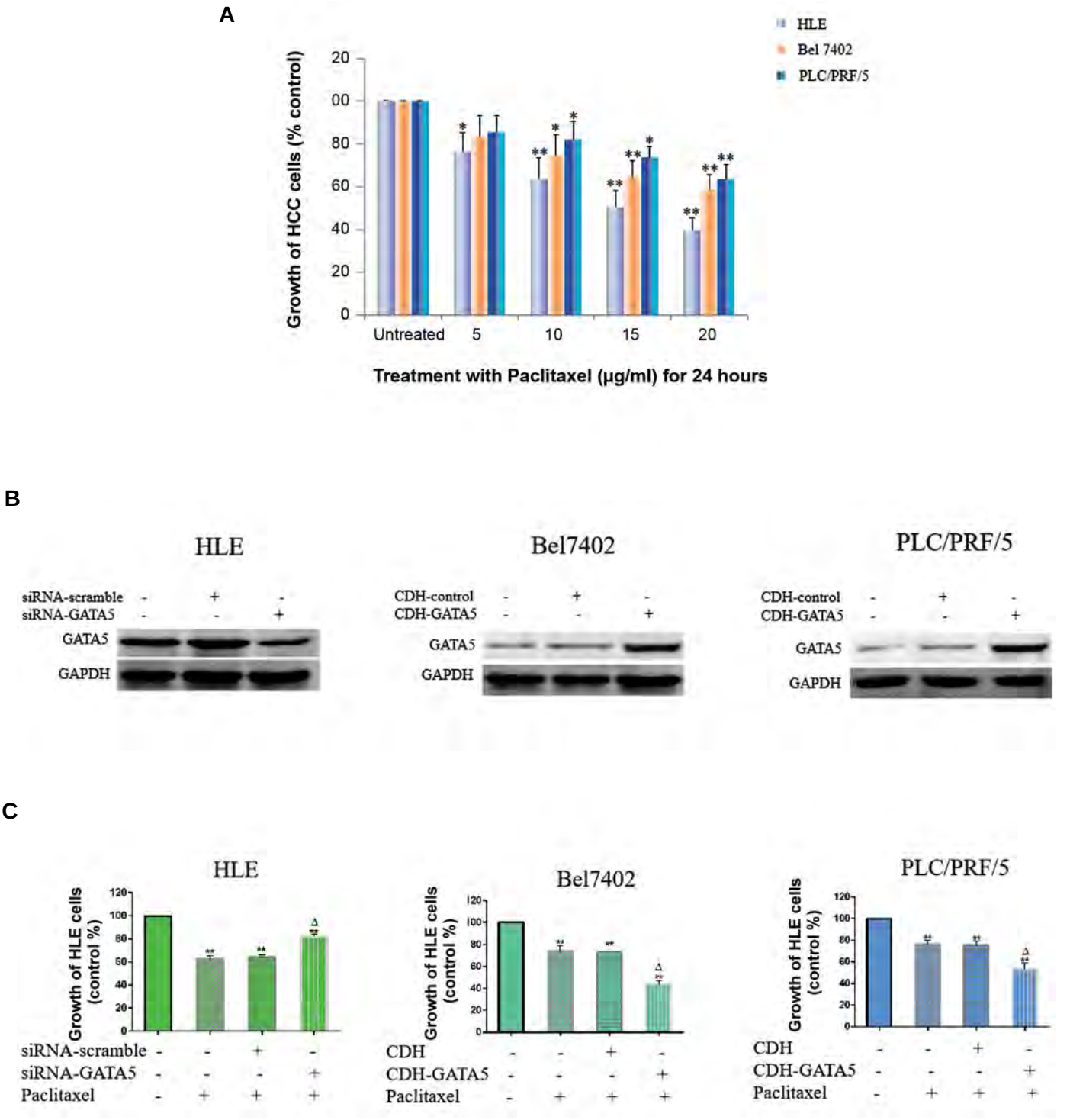

Fig.1: Effect of GATA5 and Paclitaxel on the growth of hepatocellular carcinoma cells (HCC). **A.** HLE, Bel7402 and PLC/PRF/5 cells were treated with different concentrations of Paclitaxel (0, 5, 10, 15 and 20 μg/ml) for 24 hours. Growth of the cells was measured by MTT assay. **B.** Western blotting was carried out to test expression of GATA5 in the HLE cells, Bel7402 and PLC/PRF/5 cells. **C.** The HLE cells were transfected with siRNA-scramble or siRNA-*GATA5* vectors for 24 hours followed by treatment with Paclitaxel (10 μg/ml) for 24 hours. The Bel7402 and PLC/PRF/5 cells were transfected with the CDH empty vectors or CDH-*GATA5* vectors for 24 hours followed by treatment with Paclitaxel (10 μg/ml) for 24 hours. Growth of the cells was measured by an MTT assay. N=6, *; P<0.05, **; P<0.01 versus the control groups, and $^{\Delta}$; P<0.01 versus the empty vector groups or the empty vector groups plus the Paclitaxel-treated groups. Three independent experiments were performed for these data.

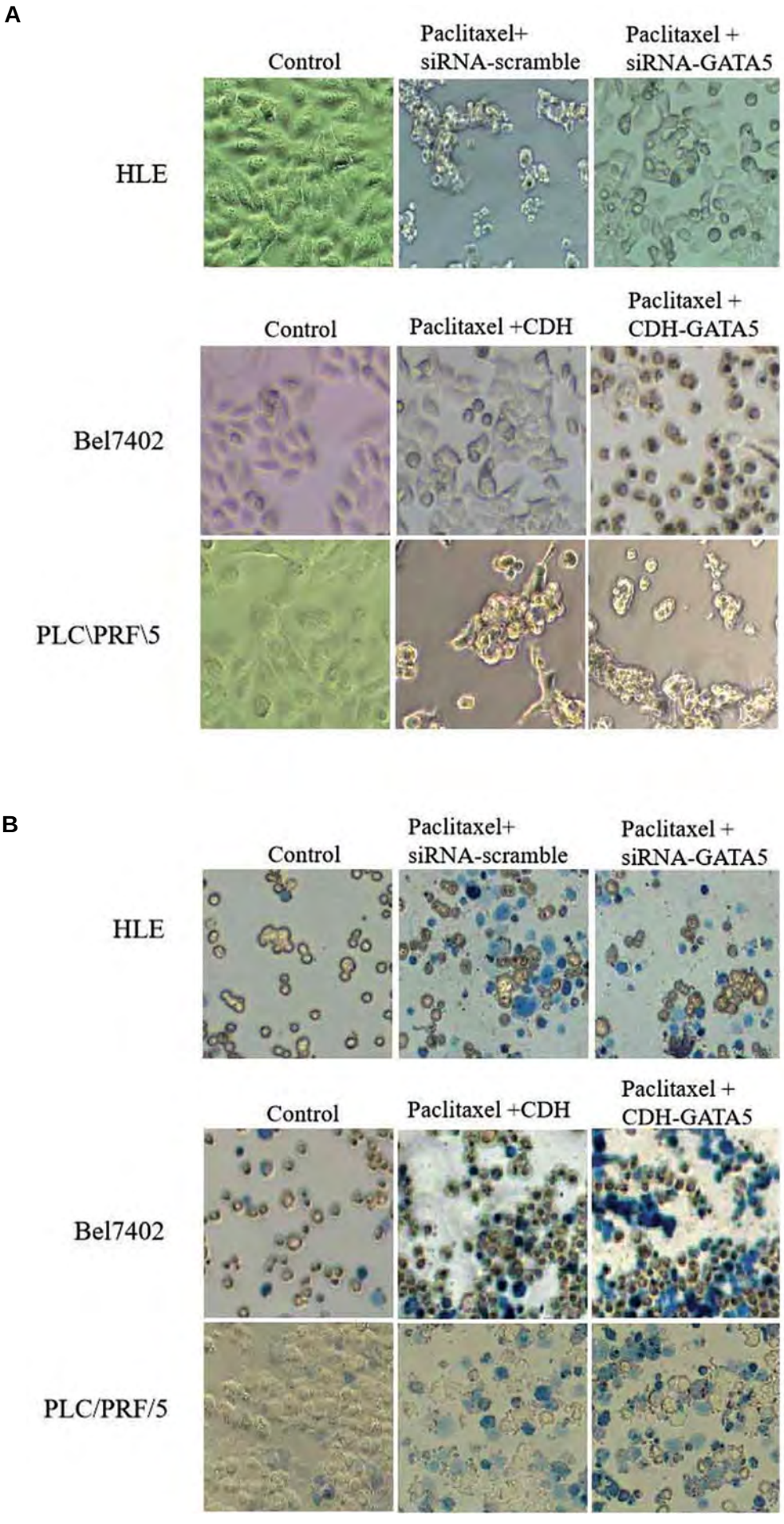
A
Control
Paclitaxel+ siRNA-scramble
Paclitaxel + siRNA-GATA5
HLE
Control
Paclitaxel +CDH
Paclitaxel + CDH-GATA5
Bel7402
PLC\PRF\5
B
Control
Paclitaxel+ siRNA-scramble
Paclitaxel + siRNA-GATA5
HLE
Control
Paclitaxel +CDH
Paclitaxel + CDH-GATA5
Bel7402
PLC/PRF/5

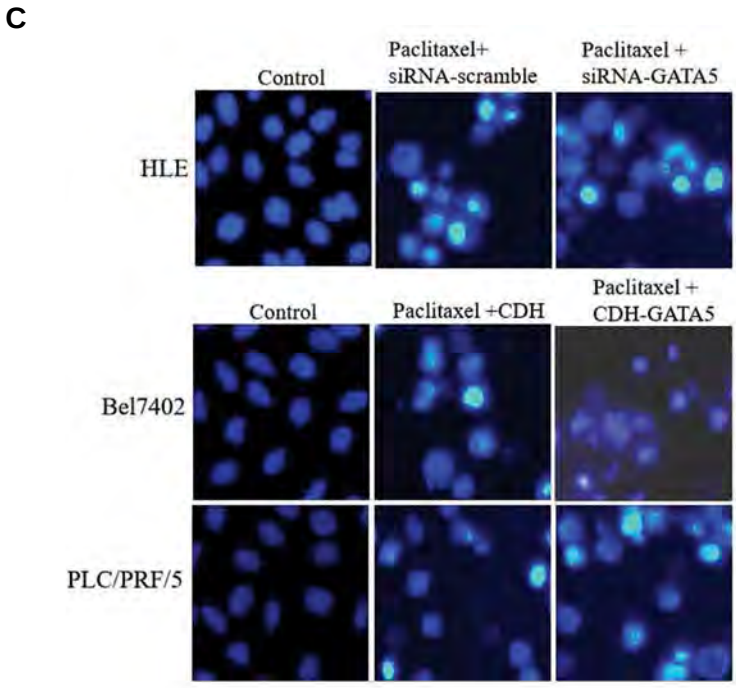

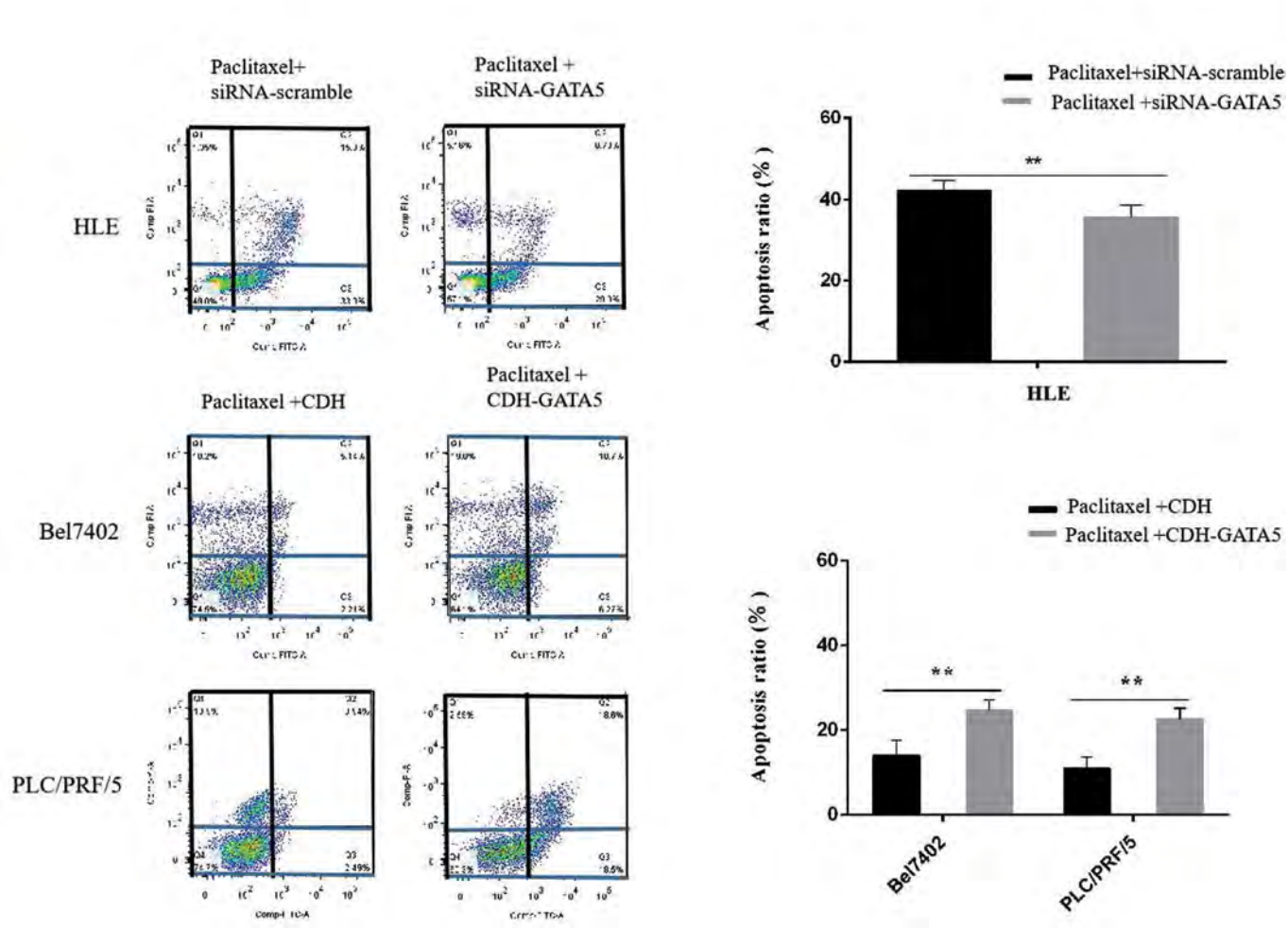

Fig.2: Effect of the GATA5 and Paclitaxel on the apoptosis of hepatocellular carcinoma cells (HCC). The HLE cells were transfected with siRNA-scramble or siRNA-*GATA5* for 24 hours. The Bel7402 and PLC/PRF/5 cell were transfected with the CDH empty vectors or CDH-*GATA5* vectors for 24 hours. Next, these cells were treated with Paclitaxel (20 μg/ml) for 48 hours. Then, apoptosis of the cells was analyzed. **A.** Light microscopy was used to observe morphological changes of the HCC cells (×100). **B.** Trypan blue excluded staining and observations by microscopy (scale bar: ×100). **C.** DAPI staining and morphological observation by microscopy (scale bar: 20 μM). **D.** Flow cytometry was applied to detect apoptosis of HCC cells. The low columnar graph indicates quantity of the cell apoptosis. Three independent experiments were performed for these data.
N=5, **; P<0.05 versus siRNA-scramble vectors groups or CDH empty vectors groups.

GATA5 enhanced the effect of Paclitaxel on inhibiting migration and invasion of HCC cells

In this study, we also investigated whether GATA5 synergizes with Paclitaxel to inhibit HCC migration by a transwell analysis. The microscopic observations showed that after silencing *GATA5* expression by transfecting with siRNA-*GATA5* in the Paclitaxel treated HLE cells (Paclitaxel+siRNA-*GATA5* group), pore transfer capacity of the cells was significantly increased compared to the cells transfected with siRNA-scramble (Paclitaxel+siRNA-scramble group). Enhancing *GATA5* expression by transfecting with CDH-*GATA5* in the Paclitaxel-treated Bel7402 and PLC/PRF/5 cells (Paclitaxel+CDH-*GATA5* group), showed that pore migration capacity of the HCC cells was decreased compared to the cells transfected with the CDH empty vector (Paclitaxel+CDH group, Fig.3A, B). These data indicated that GATA5 synergized with Paclitaxel to inhibit HCC cells migration and invasion.

We also assessed the influence of GATA5 on the expression of the metastasis-related factors, MMP2 and MMP9. In the present study, Western blot results indicated that after silencing expression of *GATA5* by transfecting with siRNA-*GATA5* in the Paclitaxel-treated HLE cells (Paclitaxel+siRNA-*GATA5* group), there was a higher expression of MMP2 and MMP9, compared to the cells transfected with siRNA-scramble (Paclitaxel+siRNA-scramble group). Enhancing GATA5 expression by transfecting with CDH-*GATA5* in Bel7402 and PLC/PRF/5 cells (Paclitaxel+CDH-*GATA5* group) revealed a reduced expression of MMP2 and MMP9, compared to the cells transfected with the CDH empty vector (Paclitaxel+CDH group, Fig.3C). These results demonstrated that GATA5 played a role in synergizing with Paclitaxel to down-regulate expression of the metastasis-related factors, MMP2 and MMP9.

GATA5 increased the effect of Paclitaxel on inhibiting colony formation of hepatocellular carcinoma cells

In addition, we investigated whether GATA5 was able to enhance the effect of Paclitaxel on inhibiting colony formation of the HCC cells. The crystal violet staining and microscopy (×100) observations showed that HLE cells treated with Paclitaxel and transfected with siRNA-scramble (Paclitaxel+siRNA-scramble group) inhibited colony formation. Silencing *GATA5* expression by transfecting with siRNA-*GATA5* in the paclitaxel-treated HLE cells (Paclitaxel+siRNA-*GATA5* group) restored more capacity of colony formation compared to the Paclitaxel+siRNA-scramble group. Bel7402 and PLC/PRF/5 cells treated with Paclitaxel and transfected with the empty vector CDH (Paclitaxel+CDH group) showed that number and volume of cellular colony were significantly decreased compared to the control. Increasing expression of GATA5 by transfecting with CDH-*GATA5* in the Bel7402 and PLC/PRF/5 cells (Paclitaxel+CDH-*GATA5* group) demonstrated that number and volume of cellular colony were inhibited compared to the control group and the Paclitaxel+CDH group (Fig.4). These results indicated that GATA5 played a key role in enhancing the effect of Paclitaxel on inhibiting the colony formation of HCC cells.

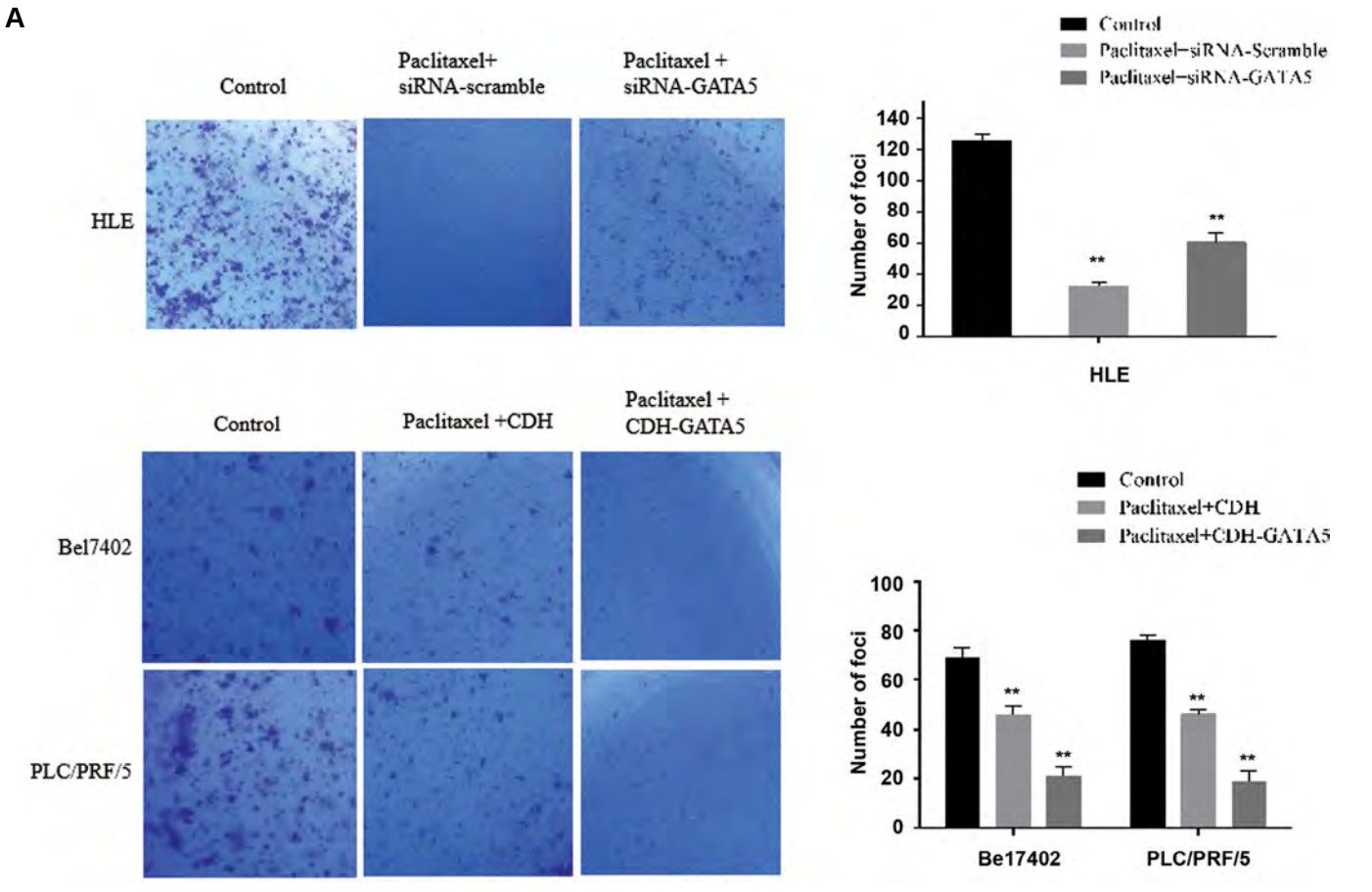

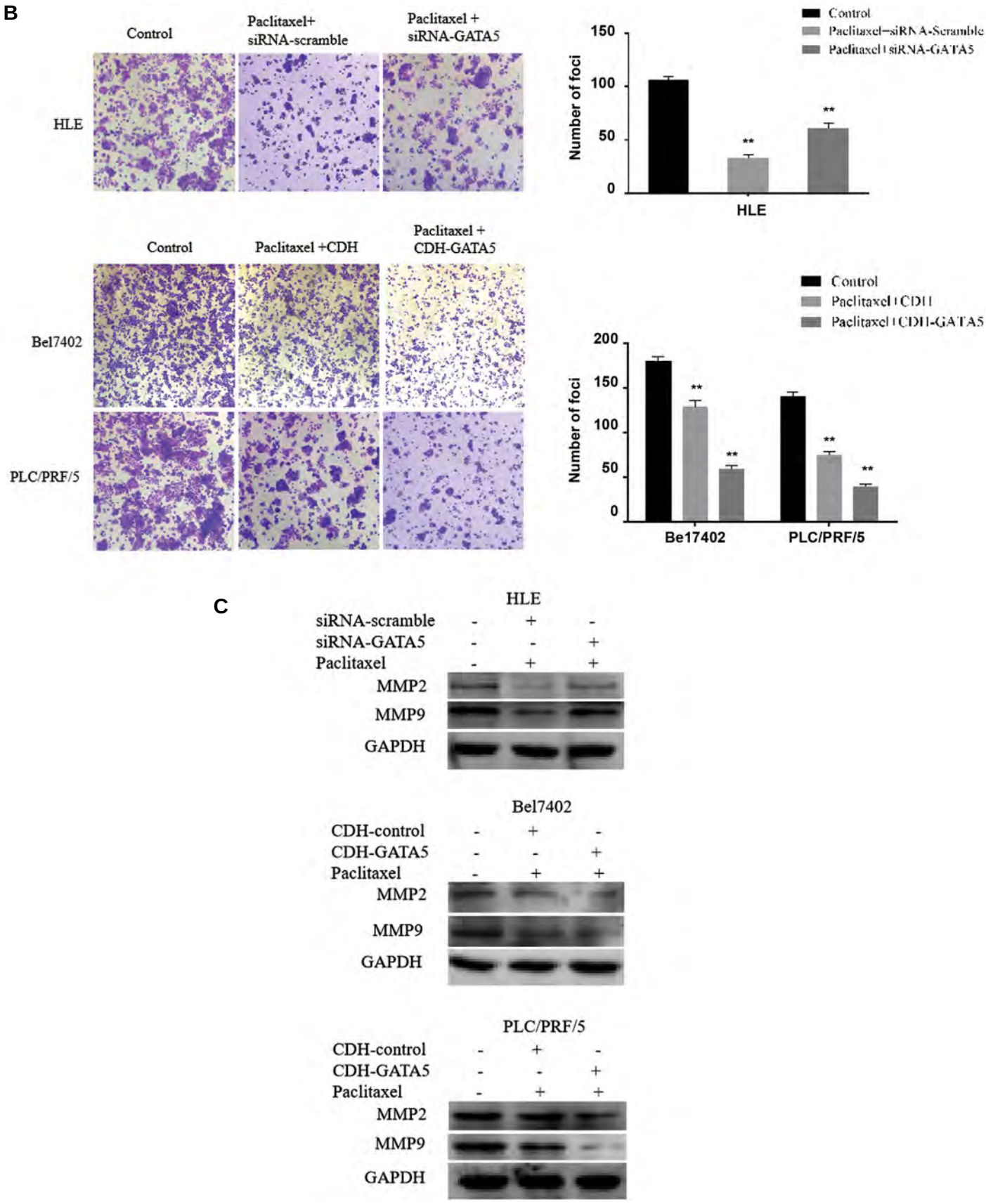

Fig.3: Influence of GATA5 and Paclitaxel on the migration, invasion and expression of the migration-related proteins in hepatocellular carcinoma cells (HCC). The HLE cells were transfected with siRNA-scramble or siRNA-*GATA5*. The Bel7402 and PLC/PRF/5 cell were transfected with the CDH empty vectors or CDH−*GATA5* vectors for 24 hours followed by treatment with Paclitaxel (10 μg/ml) for 48 hours. **A, B.** The migratory and invasive cells were stained with 0.1% crystal violet and they were observed by microscopy. The right columnar graph indicates quantity of the migratory cells (×100). **C.** Western blotting was used to analyze the expression of MMP2 and MMP9 in the HLE, Bel7402 and PLC/PRF/5 cells. Three independent experiments were performed for these data.
N=8, **; P<0.05 versus the control group.

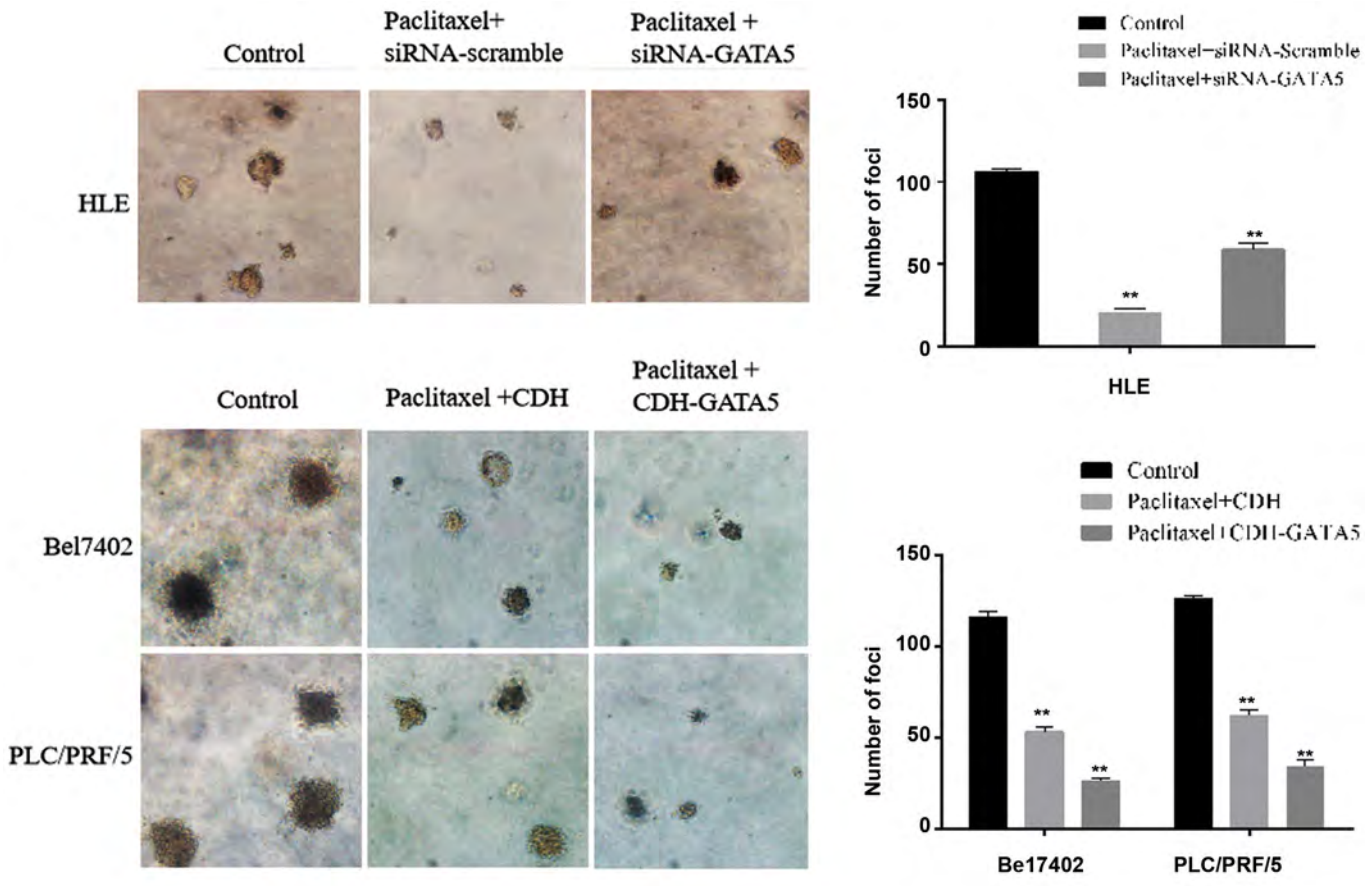

Fig.4: Influence of GATA5 and Paclitaxel on the colony formation of hepatocellular carcinoma cells (HCC). The HLE cells were treated with Paclitaxel and they were transfected with siRNA-scramble vectors or siRNA-*GATA5* vectors. The Bel7402 and PLC/PRF/5 cells were transfected with the CDH empty vectors or CDH−*GATA5* vectors followed by treatment with Paclitaxel (10 μg/ml) for 14 days. The colonies were observed by microscopy (×40). The right columnar graph indicates quantity of colony formation. N=6, **; P<0.05 versus the control group.

GATA5 increased the effect of Paclitaxel on inhibiting expression of the reprogramming genes

To investigate how GATA5 mechanistically stimulated Paclitaxel to suppress malignant behaviors of HCC cells, we analyzed expression of the cancer stem cell reprogramming genes, Nanog, EpCAM, c-Myc and Sox2 in the cells by Western blotting. The results indicated that after silencing expression of GATA5 by transfecting the HLE cells with siRNA-*GATA5* (Paclitaxel+siRNA-*GATA5* group) the reprogramming genes were upregulated in comparison with the cells transfected with siRNA-scramble (Paclitaxel+siRNA-scramble group). After enhancing expression of GATA5 by transfecting with CDH-*GATA5* in Bel7402 and PLC/PRF/5 cells (Paclitaxel+CDH-*GATA5* group), expression of the reprogramming genes was reduced compared to the cells transfected with the CDH empty vector (Paclitaxel+CDH group, Fig.5). These results indicated that GATA5 enhanced Paclitaxel to inhibit expression of Nanog, EpCAM, c-Myc and Sox2 in HCC cells.

GATA5 promoted Paclitaxel to inhibit expression of stemness markers, CD44 and CD133 in hepatocellular carcinoma cells

The stemness markers CD44 and CD133 play a key role in maintaining the malignancy of HCC. Thus, in this study, we investigated whether GATA5 was able to play a role in stimulating Paclitaxel to suppress expression of CD44 and CD133 in HCC cells. Western blot was performed to assay expression of these proteins and laser confocal microscope observation was applied to detect expression and location of these markers in the HCC cells. The results indicated that silencing expression of *GATA5* (transfected cell with siRNA-*GATA5*) resulted in a higher expression of CD44 and CD133 compared to the HLE cells transfected with siRNA-scramble. After enhancing expression of *GATA5* (transfected cells with CDH-*GATA5*) in the Bel7402 and PLC/PRF/5 cells, expressions of CD44 and CD133 were suppressed, compared to the cells transfected with CDH empty vector (Fig.6A, B). These results showed that GATA5 played a role in promoting Paclitaxel to inhibit expression of the stemness markers, CD44 and CD133 in HCC cells.

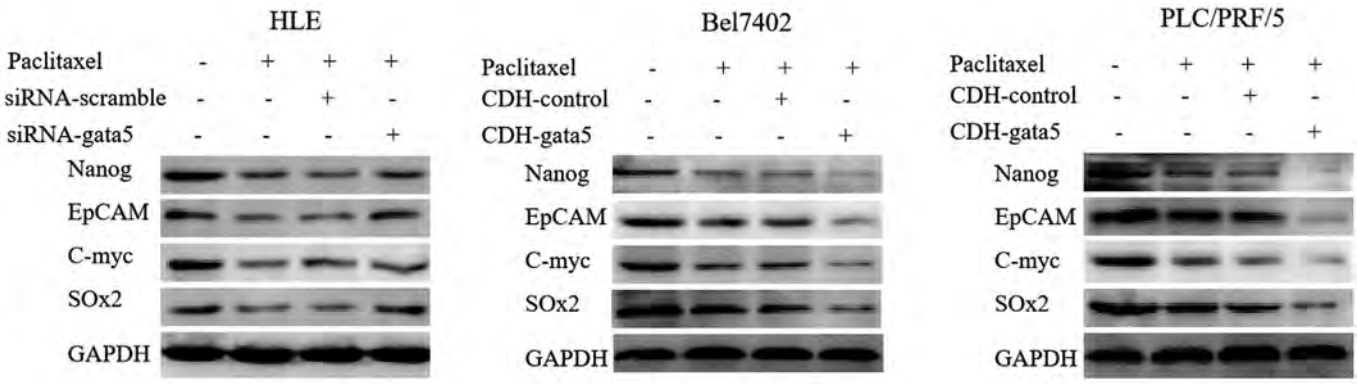

Fig.5: Effect of GATA5 and Paclitaxel on the expression of reprogramming genes in the hepatocellular carcinoma cells (HCC). The HLE cells were transfected with siRNA-scramble vectors or siRNA-*GATA5* vectors. The Bel7402 and PLC/PRF/5 cells were transfected with the CDH empty vectors or CDH-*GATA5* vectors for 24 hours followed by treatment with Paclitaxel (10 μg/ml) for 48 hours. Then, Western blotting was applied to analyze expression of the reprogramming genes: *Nanog, EpCAM, c-Myc* and *Sox2*. The images are representative of three independent experiments.

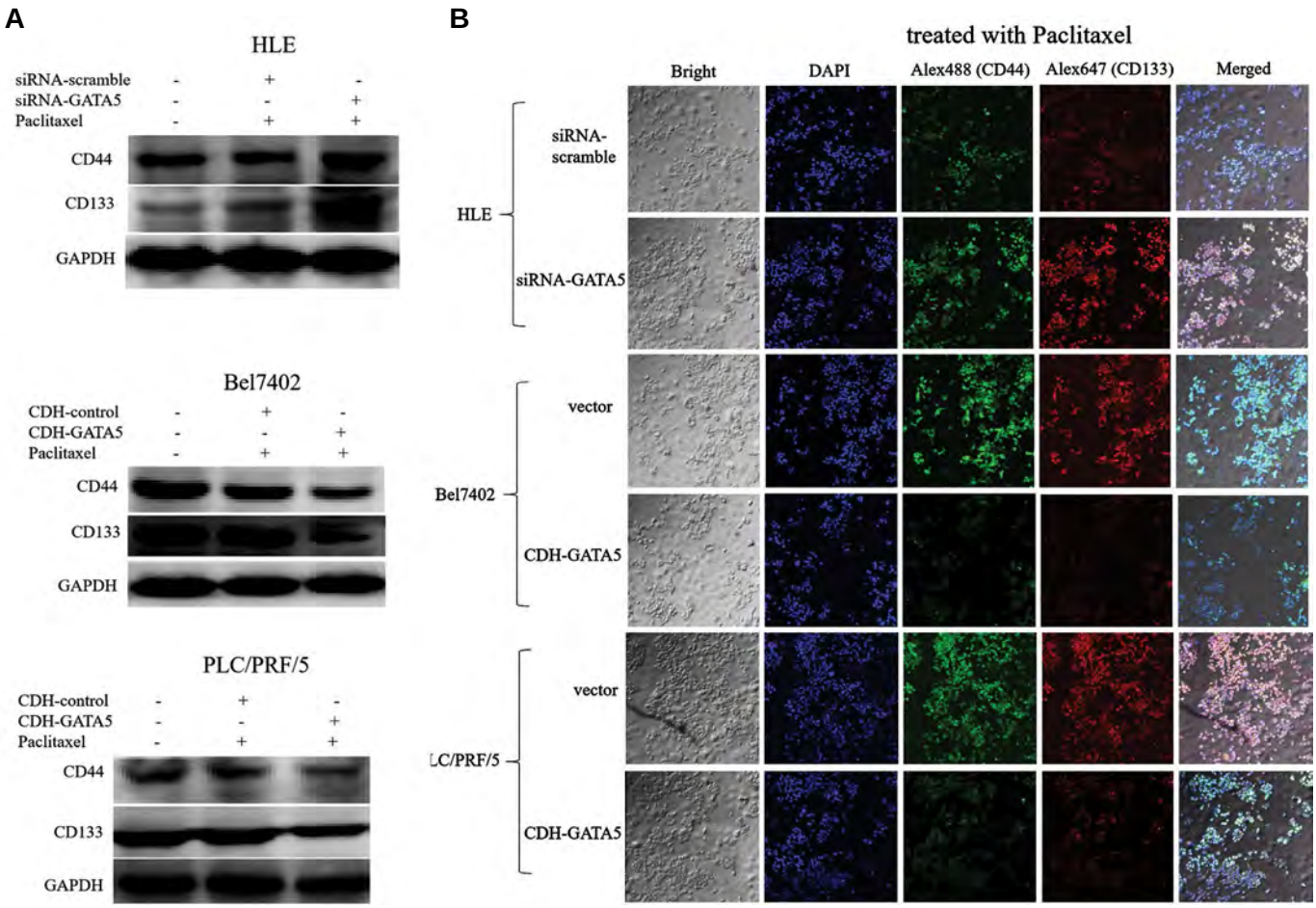

Fig.6: Effect of GATA5 and Paclitaxel on the expression of stemness markers, CD44 and CD133 in the HCC cells. The HLE cells were transfected with siRNA-scramble vectors or siRNA-*GATA5* vectors for 24 hours. The Bel7402 and PLC/PRF/5 cells were transfected with the CDH empty vectors or CDH-*GATA5* vectors for 24 hours, and then the cells were treated with Paclitaxel (10 μg/ml) for 48 hours. **A.** Western blotting was used to analyze expressions of CD44 and CD133 in the HCC cells. **B.** The expression and localization of CD44 and CD133 in the HCC cells were visualized by laser confocal microscopy. The nuclei were stained with DAPI (blue). CD44 (green) and CD133 (red) were labeled with Alex488 and Alex647, respectively (×40). Three independent experiments were performed for these data.

Discussion

Paclitaxel is now widely used as a chemotherapeutic drug for treatment of many types of cancer. It blocks the M/G2 cell cycle and stimulates caspase signal transduction to promote apoptosis in cancer cells (22, 23). Due to the inherent or late acquired drug resistance of liver cancer cells, sensitivity of HCC cells to Paclitaxel is reduced, limiting application of Paclitaxel in the treatment of liver cancer (24, 25). Drug resistance in the liver cancer cells is a crucial problem in clinical treatment. Our study

showed that the endogenous expression of GATA5 was higher in the HLE cells than in Bel7402 and PLC/PRF/5 cells. Thus, we silenced expression of *GATA5* in the HLE cells and enhanced expression of *GATA5* in the Bel7402 and PLC/PRF/5 cells. Silencing *GATA5* expression in the HLE cells could antagonize Paclitaxel to inhibit proliferation and stimulate apoptosis of the HCC cells. Inversely, enhancing *GATA5* expression in the Bel7402 and PLC/PRF/5 cells was capable to promote Paclitaxel to inhibit proliferation and stimulate apoptosis of these HCC cells. The results indicated that GATA5 has a trait to inhibit growth and stimulate apoptosis of HCC cells. Additionally, findings suggested that GATA5 was able to increase sensitivity of HCC cells to Paclitaxel.

To further demonstrate whether GATA5 synergized with Paclitaxel to suppress malignant behaviors of HCC cells, we performed HCC cellular colony formation, migration and invasion assays to assess the influence of GATA5 in the HCC cells accompanied by the treatment with Paclitaxel. Colony formation assay indicated that GATA5 synergizes with Paclitaxel to significantly inhibit cellular colony formation in the HCC cells. The cell migration and invasion assay indicated that GATA5 synergized with Paclitaxel to significantly reduce pore migratory capacity of the HCC cells and overexpression of GATA5 enhanced Paclitaxel to inhibit expression of the migration-related factors, MMP2 and MMP9. These results further demonstrated that GATA5 promoted Paclitaxel to induce apoptosis of HCC cells. Enhancing expression of GATA5 was able to synergize with Paclitaxel to inhibit HCC cells migration and invasion. GATA5 increased the sensitivity of HCC cells to Paclitaxel which maybe involved in suppressing expression of MMP2 and MMP9.

Cancer stem cells play pivotal role in malignant cells transformation (26, 27). Reprogramming genes, such as *Nanog, KLF4, EpCAM, c-Myc, Sox2* and *p-Oct4* induce the origin of CSCs (10, 11, 21). In the present study, we performed a Western blot analysis to assess influence of GATA5 and Paclitaxel on expression of reprogramming genes in HCC cells. Silencing *GATA5* expression in HLE cells (accompanied with treatment by Paclitaxel) stimulated expression of the reprogramming genes, while enhancing expression of GATA5 in the Bel7402 and PLC/PRF/5 cells (accompanied with treatment by Paclitaxel) could inhibit expression of the reprogramming genes, such as *Nanog, c-Myc* and *Sox2*. The results indicated that GATA5 played a role in promoting Paclitaxel to inhibit expression of the reprogramming genes in HCC cells, which enhanced sensitivity of the HCC cells to Paclitaxel, and also inhibiting cancer stem cell formation and cancer cells aggressiveness. Previously, we found that hepatitis virus B x protein (HBx) promoted liver cancer stem cell genesis by stimulating expression of alpha fetoprotein (AFP); so that AFP promoted expressions of CD44 and CD133 (21). AFP is a critical molecule to promote malignant transformation of liver cells and inhibit autophagy of HCC cells (28). These results implicated that expression of CD44 and CD133 in liver cancer cells is related to the malignant behaviors. CD44 is a stemness marker involved in cell adhesion and tumor metastasis (12, 29). CD133 is considered a stemness marker of cancer cells which plays a critical role in cancer recurrence (12). Recently, we found that GATA5 played role in inhibiting expression of reprogramming genes in HCC cells (30). In the present study, we also found that GATA5 synergized with Paclitaxel to inhibit expression of the stemness markers CD44 and CD133 in the cancer stem cells. These results further demonstrated that overexpression of GATA5 was able to enhance the effect of Paclitaxel on inhibiting HCC cells malignant behaviors. These mechanisms maybe involved in suppressing the expression of reprogramming genes.

Conclusion

This is the first report indicating that GATA5 plays a role in promoting Paclitaxel to inhibit the growth, migration, invasion and colony formation of HCC cells, in addition to stimulating apoptosis in these cells. All together, we revealed that in terms of molecular mechanism, GATA5 synergizes with Paclitaxel to inhibit the malignant behaviors of HCC cells which maybe involved in suppressing expression of reprogramming genes and stemness markers. These findings suggest that enhanced expression of GATA5 may be an available strategy for applying Paclitaxel to treat HCC patients.

Acknowledgements

This work was supported by the National Natural Science Foundation of China (Nos. 81660463, 81560450, 31560243). The Natural Science Foundation of Hainan Province (Nos. 2019CXTD406, 20168263 and 814293); Hainan Provincial Association for Science and Technology Program of Youth Science Talent and Academic Innovation (No.QCXM 201922); The Hainan Graduate Students Innovate Program (Hys2017-178, Hys2017-180, Hys2018-277, Hys2018-278, Hys2018-279). The authors declare that they have no competing interest.

Authors' Contributions

H.F., B.L., Y.Z., JX., Y.Z.; Performed the experiments. K.L., M.L.; Analyzed the clinical data and discussed the results. B.L., M.L.; Drafted the manuscript. M.Z., M.L.; Designed the experiments and revised the results. All the authors contributed to the manuscript editing and approval.

Reference

1. Hu P, Huang Q, Li Z, Wu X, Ouyang Q, Chen J, et al. Silencing MAP3K1 expression through RNA interference enhances paclitaxel-induced cell cycle arrest in human breast cancer cells. Mol Biol Rep. 2014; 41(1): 19-24.
2. Liu K, Cang S, Ma Y, ChiaoJW. Synergistic effect of paclitaxel and epigenetic agent phenethyl isothiocyanate on growth inhibition, cell cycle arrest and apoptosis in breast cancer cells. Cancer Cell Int. 2013; 13(1): 10.
3. Zhu M, Li W, Lu Y, Dong X, Chen Y, Lin B, et al. Alpha fetoprotein antagonizes apoptosis induced by paclitaxel in hepatoma cells in vitro. Sci Rep. 2016; 6: 26472.

4. Torre LA, Bray F, Siegel RL, Ferlay J, Lortet-Tieulent J, Jemal A. Global cancer statistics, 2012. CA Cancer J Clin. 2015; 65(2): 87-108.
5. Zhu GQ, Shi KQ, Yu HJ, He SY, Braddock M, Zhou MT, et al. Optimal adjuvant therapy for resected hepatocellular carcinoma: a systematic review with network meta-analysis. Oncotarget. 2015; 6(20): 18151-18161.
6. Shu J, Zhang K, Zhang M, Yao A, Shao S, Du F, et al. GATA family members as inducers for cellular reprogramming to pluripotency. Cell Res. 2015; 25(2): 169-180.
7. Mehra R, Varambally S, Ding L, Shen R, Sabel MS, Ghosh D, et al. Identification of GATA3 as a breast cancer prognostic marker by global gene expression meta-analysis. Cancer Res. 2005; 65(24): 11259-11264.
8. Liu P, Zhou TF, Qiu BA, Yang YX, Zhu YJ, An Y, et al. Methylation-mediated silencing of GATA5 gene suppresses cholangiocarcinoma cell proliferation and metastasis. Transl Oncol. 2018; 11(3): 585-592.
9. Xia L, Gong Y, Zhang A, Cai S, Zeng Q. Loss of GATA5 expression due to gene promoter methylation induces growth and colony formation of hepatocellular carcinoma cells. Oncol Lett. 2016; 11(1): 861-869.
10. Liang G, Taranova O, Xia K, Zhang Y. Butyrate promotes induced pluripotent stem cell generation. J Biol Chem. 2010; 285(33): 25516-25521.
11. Nagy K, Sung HK, Zhang P, Laflamme S, Vincent P, Agha-Mohammadi S, et al. Induced pluripotent stem cell lines derived from equine fibroblasts. Stem Cell Rev Rep. 2011; 7(3): 693-702.
12. Zhu Z, Hao X, Yan M, Yao M, Ge C, Gu J, et al. Cancer stem/progenitor cells are highly enriched in CD133+CD44+ population in hepatocellular carcinoma. Int J Cancer. 2010; 126(9): 2067-2078.
13. Yang XR, Xu Y, Yu B, Zhou J, Qiu SJ, Shi GM, et al. High expression levelsof putative hepatic stem/progenitor cell biomarkersrelated to tumour angiogenesis and poor prognosis of hepatocellular carcinoma. Gut. 2010; 59(7): 953-962.
14. Li M, Li H, Li C, Guo L, Liu H, Zhou S, et al. Cytoplasmic alpha-fetoprotein functions as a co-repressor in RA-RAR signaling to promote the growth of human hepatoma Bel 7402 cells. Cancer Lett. 2009; 285(2): 190-199.
15. Li C, Wang S, Jiang W, Li H, Liu Z, Zhang C, et al. Impact of intracellular alpha fetoprotein on retinoic acid receptors-mediated expression of GADD153 in human hepatoma cell lines. Int J Cancer. 2012; 130(4): 754-764.
16. Li M, Zhou S, Liu X, Li P, McNutt MA, Li G. Alpha-Fetoprotein shields hepatocellular carcinoma cells from apoptosis induced by tumor necrosis factor-related apoptosis-inducing ligand. Cancer Lett. 2007; 249(2): 227-234.
17. Zhu M, Li W, Dong X, Chen Y, Lu Y, Lin B, et al. Benzyl-isothiocyanate induces apoptosis and inhibits migration and invasion of hepatocellular carcinoma cells in vitro. J Cancer. 2017; 8(2): 240-248.
18. Lu Y, Zhu M, Li W, Lin B, Dong X, Chen Y, et al. Alpha fetoprotein plays a critical role in promoting metastasis of hepatocellular carcinoma cells. J Cell Mol Med. 2016; 20(3): 549-558.
19. Li MS, Li PF, He SP, Du GG, Li G. The promoting molecular mechanism of alpha-fetoprotein on the growth of human hepatoma Bel7402 cell line. World J Gastroenterol. 2002; 8(3): 469-475.
20. Li M, Li H, Li C, Zhou S, Guo L, Liu H, et al. Alpha fetoprotein is a novel protein-binding partner for caspase-3 and blocks the apoptotic signaling pathway in human hepatoma cells. Int J Cancer. 2009; 124(12): 2845-2854.
21. Zhu M, Li W, Lu Y, Dong X, Lin B, Chen Y, et al. HBx drives alpha fetoprotein expression to promote initiation of liver cancer stem cells through activating PI3K/AKT signal pathway. Int J Cancer. 2017; 140(6): 1346-1355.
22. Chao Y, Chan WK, Birkhofer MJ, Hu OY, Wang SS, Huang YS, et al. Phase II and pharmacokinetic study of paclitaxel therapy for unresectable hepatocellular carcinoma patients. Br J Cancer. 1998; 78(1): 34-39.
23. Chun E, Lee KY. Bcl-2 and Bcl-xL are important for the induction of paclitaxel resistance in human hepatocellular carcinoma cells. Biochem Biophys Res Commun. 2004; 315(3): 771-779.
24. Sutter AP, Maaser K, Grabowski P, Bradacs G, Vormbrock K, Höpfner M, et al. Peripheral benzodiazepine receptor ligands induce apoptosis and cell cycle arrest in human hepatocellular carcinoma cells and enhance chemosensitivity to paclitaxel, docetaxel, doxorubicin and the Bcl-2 inhibitor HA14-1. J Hepatol. 2004; 41(5): 799-807.
25. Gagandeep S, Novikoff PM, Ott M, Gupta, S. Paclitaxel shows cytotoxic activity in human hepatocellular carcinoma cell lines. Cancer Lett. 1999; 136(1): 109-118.
26. Kawai T, Yasuchika K, Ishii T, Katayama H, Yoshitoshi EY, Ogiso S, et al. Keratin 19, a cancer stem cell marker in human hepatocellular carcinoma. Clin Cancer Res. 2015; 21(13): 3081-3091.
27. Chiba T, Kita K, Zheng YW, Yokosuka O, Saisho H, Iwama A, et al. Side population purified from hepatocellular carcinoma cells harbors cancer stem cell-like properties. Hepatology. 2006; 44(1): 240-251.
28. Wang S, Zhu M, Wang Q, Hou Y, Li L, Weng H, et al. Alpha-fetoprotein inhibits autophagy to promote malignant behaviour in hepatocellular carcinoma cells by activating PI3K/AKT/mTOR signalling. Cell Death Dis. 2018; 9(10): 1027.
29. Chou YE, Hsieh MJ, Chiou HL, Lee HL, Yang SF, Chen TY. CD44 gene polymorphisms on hepatocellular carcinoma susceptibility and clinicopathologic features. Biomed Res Int. 2014; 2014: 231474.
30. Feng H, Zhu M, Zhang R, Wang Q, Li W, Dong X, et al. GATA5 inhibits hepatocellular carcinoma cells malignant behaviors by blocking expression of reprogramming genes. J Cell Mol Med. 2019; 23(4): 2536-2548.

Original Article

Integrative Analysis of lncRNAs in Kidney Cancer to Discover A New lncRNA *(LINC00847)* as A Therapeutic Target for Staphylococcal Enterotoxin *tst* Gene

Maryam Safarpour-Dehkordi, Ph.D.[1], Abbas Doosti, Ph.D.[1*], Mohammad-Saied Jami, Ph.D.[2, 3]

1. Department of Biology, Faculty of Basic Sciences, Shahrekord Branch, Islamic Azad University, Shahrekord, Iran
2. Cellular and Molecular Research Center, Basic Health Sciences Institute, Shahrekord University of Medical Sciences, Shahrekord, Iran
3. Department of Neurology, David Geffen School of Medicine, University of California Los Angeles (UCLA), USA

Corresponding Address: P.O.Box: 166, Department of Biology, Faculty of Basic Sciences, Shahrekord Branch, Islamic Azad University, Shahrekord, Iran
Email: abbasdoosti@yahoo.com

Received: 4/June/2019, Accepted: 28/September/2019

Abstract

Objective: Bacterial toxin can cause cell death through induction of apoptosis in cancer cell lines as well as changes in the expression patterns of long non-coding RNAs (lncRNAs) and genes. In the present study, the effect of *tst* gene on ACHN cell lines was reported along with proposing a novel pathway of apoptosis in kidney cancer.

Materials and Methods: In this experimental study, effective lncRNAs and genes were predicted from different criteria for renal cell carcinoma (RCC) by bioinformatics methods and lncRNA-miRNA-mRNA interaction was constructed; then the effect of Staphylococcus aureus *tst* gene on induction of apoptosis pathways on ACHN and HDF cell lines was investigated.

Results: After creation of lncRNA-miRNA-mRNA interaction, changes in expression levels of lncRNA *LINC00847* (P=0.0024) and *PTEN* gene (P=0.0027) were identified, as potential apoptosis biomarkers for kidney cancer, after treating ACHN cell line by pCDNA3.1 (+)-*tst* compared to the empty vector. In contrast, there was no statistically significant difference in *DICER1* expression levels in ACHN-*tst* cell (P≥0.05). In addition, transfection by pcDNA3.1 (+)-*tst* could increase ACHN cell apoptosis level (P<0.0001) compared to the pcDNA3.1 (+) group; but no significant effect was observed on normal cells.

Conclusion: It is suggested that lncRNA LINC00847, discovered in this study, could provide a new landscape for researches aimed to determine relationship between functional lncRNA and RCC pathways. pcDNA3.1 (+)-*tst* was found to increase apoptosis in the transfected cells.

Keywords: Apoptosis, Long Non-Coding RNA, microRNA, mRNA, TSST-1 Toxin

Cell Journal(Yakhteh), Vol 22, Suppl 1, Autumn 2020, Pages: 101-109

Citation: **Safarpour-Dehkordi M, Doosti A, Jami MS. Integrative analysis of lncRNAs in kidney cancer to discover a new lncRNA (LINC00847) as a therapeutic target for staphylococcal enterotoxin tst gene. Cell J. 2020; 22 Suppl 1: 101-109. doi: 10.22074/cellj.2020.6996.**

Introduction

Nowadays, cancer not only is known as one of the most common health problems, but also is prominent cause of death in societies all over the world (1). World Health Organization (WHO) reports that kidney cancer as an urologic cancer ranks first among the malignant tumors (2). Kidney cancer is the most fatal genitourinary cancer and the most significant cancer due to the new known advances on genetic mutations using the knowledge obtained from targeted systemic cures (3). Unlike the other types of disease, kidney cancer is not a single disease and according to the scientists, kidney cancer includes different types of malignancy each of which has different clinical course, responding differently to treatment, different histology and it is caused by different genes (4). Increasing prevalence of kidney cancer has been observed in different countries during the past decades, but it is difficult to treat it, because of the limited evidences for its evaluation (5, 6).

In adults, kidney cancer occurs as a result of malignant tumors increasing from renal pelvis and renal parenchyma. On the other hand, in children, kidney cancer is caused by Wilms tumor (nephroblastoma). Prevalence of nephroblastoma is about 1.1% compared to all kidney cancers. Almost all renal pelvis cancers are transitional cell carcinoma. In 90% of kidney carcinomas, adenocarcinomas arise essentially in renal parenchyma (7). There are some risk factors for kidney cancer, such as cigarette smoking, obesity, hypertension, other preexisting conditions, reproductive and hormonal factors, physical activity, diet and beverages, occupation and the environment (8). Renal cell carcinoma (RCC) is caused by the cancer originated from renal tubular epithelial cells accounting for majority of kidney cancer-related deaths. RCC is the ninth most common types of cancer in the world accounting for ~90% of all kidney neoplasms and 2-3% of adult malignant tumors. Despite extensive research about this carcinoma, few facts have been introduced about the role of RCC-specific long non-coding RNAs (lncRNAs) (2, 9).

lncRNAs activated in cytosolic or nuclear fractions have more than 200 bp sequence length (10, 11). lncRNAs have been known as a new element, transcribed in nuclear genome using new genome sequencing

techniques. Mounting evidences approved tumorigenesis role and regulation of gene expression at the various levels of lncRNAs in kidney cancer. This gene expression might appear through transcription, post-transcription processing and chromatin modification (12). New recent approaches indicated that lncRNAs illustrate a pleiotropic pattern in different human diseases. For instance, they are involved in promotion, progression and initiation of tumors (13).

Bacterial toxins have a great therapeutic potential to treat the cancer. In several studies (*in vitro* and *in vivo*), these toxins showed an effective cell-killing capacity for cancer cells. *S. aureus* is one of main human pathogens causing apoptosis during infection. Atopic dermatitis and sepsis are examples of diseases in which the *S. aureus* affects intensity and result of a disease by inducing apoptosis. Intensity of sepsis caused by *S. aureus* is related to staphylococcal toxins with properties of a super antigen such as Toxic Shock Syndrome Toxin-1 (TSST-1) of *tst* gene. TSST-1 stimulates host immune system and causes release of interleukin (1 and 2), activating a significant amount of T-cells and tumor necrosis factor-alpha (TNF-a) (14-17).

Kidney cancer is one of the most common cancers diagnosed in the world in recent decades. There are limited techniques for diagnosis and treatment of this disease. Like other types of cancer, kidney cancer is resistant to treatment methods including chemotherapy and radiation therapy, highlighting the need for identification (ID) of new biomarkers and treatment methods.

Thus, the present study was carried out to discover a new potential apoptosis pathway and integrate Staphylococcal *tst* gene in ACHN cancer cell line to measure apoptosis and expression level of the lncRNAs and related genes.

Materials and Methods

Recognition of the expressed lncRNAs and miRNAs

In this experimental study (The study was approved by Islamic Azad University, Shahrekord, Iran), as the first step to show contribution of lncRNA in kidney cancer, an online database was used to predict differentially-expressed genes. ID, transcripts and chromosomal locations of every lncRNA were recovered from Ensembl GRCh37 for more analysis. Total lncRNAs were recruited from HUGO Gene Nomenclature Committee (http://www.genennames.org). Kidney cancer dataset was recognized from TCGA (The Cancer Genome Atlas) at the cBioPortal for Cancer Genomics including 1,105 samples (http://www.cbioportal.org/). FASTA format of each lncRNA was located into LncDisease software and the lncRNAs with higher expression profile in kidney cancer were selected. The Ensembl GRCh37, HUGO and miRWalk servers were used to select microRNAs (miRNAs). Eventually, the disease-associated lncRNAs were identified through miRNA interactions. Additionally, the Human microRNA Disease Database (HMDD) was used to conduct more studies on kidney cancer miRNAs, based on tool for microRNA set enrichment analysis (TAM) (18) method.

Analysis of interaction between lncRNA and miRNA

Regarding analysis of binding of folded lncRNAs to folded miRNAs, bioinformatics tool of RegRNA 2.0 (http://regrna2.mbc.nctu.edu.tw/detection.html) was used to identify lncRNA-miRNA interaction. Protein sequence was provided using the NCBI database (National Center for Biotechnology Information). The least folding free energy was regulated under <-25 and system score was set at >160 to predict miRNA target sites. An increased score represents the ability for stronger binding. lncRNAs falling above the 15% alteration frequency were selected among many lncRNAs expressed in kidney cancer. Homo-sapiens lncRNA sequences were also searched in the NCBI database.

miRNA target checking and making the lncRNA-miRNA-mRNA network

Investigative analysis of PicTar (http://pictar.mdc-berlin.de/cgi-bin/PicTarvertebrate.cgi), TargetScan (http://www.targetscan.org/vert_72/) and microcosm Targets (http://ebi.ac.uk/Enright-srv/microcosm/htdocs/targets/v5) databases were used to identify the genes for targeting through screening miRNAs. All of the genes determined using three databases were used to restrict number of false positive results. It was also confirmed that lncRNAs exhibited alterations by >15%, until maximum clarity in the network diagram. Cytoscape 3.6.0 software was used to visualize lncRNA-miRNA-mRNA interaction of significant genes (http://www.cytoscape.org/download.php).

Gene ontology analysis

GO enrichment of target genes was performed using the Enrichr to further study biological pathways of the genes involved in RCC.

Recombinant plasmid preparation and confirmation

The mammalian expression vector, pcDNA3.1(+) containing *tst* encoding gene was purchased from GenRay Biotechnology (China) and the pcDNA3.1(+) (Invitrogen, USA) plasmid was used in this program as empty plasmid. The recombinant vector (pcDNA3.1(+)-*tst*) was digested using the restriction enzymes *NotI* and *EcoRV* (both from New England BioLabs, USA) to confirm the presence of *tst* gene in the recombinant plasmid.

Cell transfection

Human renal cell adenocarcinoma (ACHN) and human dermal fibroblasts-normal (HDF) cells were provided from the National Cell Bank of Iran (Pasteur Institute, Iran). The cells were cultured in RPMI-1640 medium with 10% heat-inactivated fetal bovine serum (FBS, Gipco, USA), 100 U/ml penicillin and 100 µg/ml streptomycin (Invitrogen, USA) at 37˚C in a humidified atmosphere containing 5% carbon dioxide (CO_2). Transfection of ACHN and HDF cells were carried out in 6-well plate according to the instructions for the Lipofectamine 2000™ reagent (Invitrogen, USA). Two micrograms of

the pcDNA3.1(+)-*tst* and 2 µg of the empty pcDNA3.1(+) were transfected separately into cells. The transfected cells were selected with 600 µg/ml G418 (Invitrogen, USA) (19). In addition, there was one group from each cell, cultured in the same condition in 6-wells plate without any transfection. The cells were treated with G418, as control groups to assess the accurate performance of this aminoglycoside antibiotic.

Annexin V-FITC assay

Cell apoptosis caused by recombinant (pcDNA3.1(+)-*tst*) and empty vector (pcDNA3.1(+)) was measured using FITC Annexin V Apoptosis Detection Kit I (BD Biosciences Pharmingen, USA) by flow-cytometer. Experiments were done in duplicate; briefly, 3×10^5 of each cell (ACHN and HDF) were washed twice with ice-cold phosphate buffer solution (PBS, BIO-IDEA, Iran). Then, the cells were resuspended in 100 µl of 1X binding buffer (provided in the kit) and 100 µl of suspended cells was transferred into flow-cytometer micro-tube. They were next stained with 5 µl of FITC- Annexin-V (10 mg/ml) and 10 µl of propidium iodide (PI, 50 mg/ml, BD Biosciences Pharmingen, USA). After incubating the cells at 25˚C for 15 minutes in the dark, 400 µl binding buffer was added and the solution was analyzed by a flow cytometer apparatus (BD, USA).

RNA isolation and cDNA synthesis

RNX-Plus reagent (SinaClon, Iran) was used to isolate total RNA, according to the manufacturer's protocol. RNA was quantified, and the concentration and purity were measured based on absorption rate of 260/280 nm using a Nanodrop spectrophotometer (Nanodrop 2000, Thermo Scientific, USA). Total RNA samples were treated with RNase-free DNase (Thermo Scientific, USA) before quantitative reverse transcription polymerase chain reaction (qRT-PCR). A RevertAid First Strand cDNA Synthesis Kit (Thermo Scientific, USA) was used to synthesize complementary DNA (cDNA) from total RNA. A PCR test was applied using *tst* specific primers on cDNA to confirm *tst* gene expression after lipofection. Primer sequences were as follows:

tst-
Sense: 5´-GCACAAACGACAACATTAAGGACC-3´
Antisense: 5´-TTGTCCGCTTTGTGTTGAGGTC-3´.

Quantitative reverse transcription polymerase chain reaction analysis

Transcription levels were measured in triplicate by qRT-PCR using SYBR®Premix Ex TaqTM II kit (TaKaRa, Japan). Measurements were performed using *LINC00847*, *PTEN* and *DICER1* specific primer pairs (in ACHN cell line) in Rotor-Gene 6000 Real-Time PCR Machine (Qiagen, Germany). *LINC00847* was evaluated as pro-apoptotic lncRNA in HDF cells. *GAPDH* was monitored as a reference gene and expression level of the specific genes was normalized according to *GAPDH* transcript. Different transcription levels were calculated by using $2^{-\Delta\Delta Ct}$ method (20). Primer sequences were as follows:

LINC00847-
Sense: 5´-AACGCTGCCTCTGTGGAAGTCTC-3´
Antisense: 5´-CGCTCTGCTCTCCCGCCATC-3´,

PTEN-
Sense: 5´-ACACGACGGGAAGACAAGTT-3´
Antisense: 5´-CTGGTCCTGGATTGAAGAAGT-3´,

DICER1-
Sense: 5´-GTGCGAGAATTGCTTGAA-3´
Antisense: 5´-CACAGTGACTCTGACCTT-3´,

GAPDH-
Sense: 5´-GCCAAAAGGGTCATCATCTCTCTGC-3´
Antisense: 5´-GGTCACGAGTCCTTCCACGATAC-3´.

Statistical analysis

All data was presented as mean ± standard error (SE). Paired Student's t test was performed for statistical analysis. Differences with a $P<0.05$ were considered statistically significant. GraphPad Prism (version 8, GraphPad software, USA) was used to perform the aforementioned statistical analyses.

Results

Differentially expressed lncRNAs and microRNAs

As shown in Figure 1, in this study, a total of 3994 known lncRNAs were selected as lineage-specific lncRNAs with an expressed profile above 3 (0.2%). in terms of miRNAs, 37 molecules (1.91%) were selected among 1933 miRNAs having an expressed profile above than 2.5.

lncRNA-miRNA interactions network

miRNAs have been found to regulate some of the protein-coding genes, but it is not completely known whether miRNAs can also regulate lncRNAs or not. RegRNA 2.0 database was used to analyze interaction between lncRNAs and miRNAs to identify accurate mechanism underlying the role of lncRNAs and miRNAs in kidney cancer. RegRNA 2.0 was used as a unified web server to compare mRNA sequence against insertion of homologs of regulatory RNA motifs and elements. The proposed miRNAs from this database must be intersected with kidney cancer dataset from cBioPortal. Five hindered and eighty eight miRNAs can use regulatory functions on 93 lncRNAs between differentially expressed lncRNAs with a threshold alteration frequency > 2.5%. At first, four lncRNAs with the most alteration frequencies were selected including *CARMN*, *LINC00847*, *CHRLOS*, and *LINC00852*. Results showed that only one of them interacted with RCC-related miRNA and genes. A new lncRNA named *LINC00847*, targeted by 71 miRNAs is related to kidney cancer. For example, it was predicted that *hsa-miR-15a-5p*, *hsa-miR-93-5p*, *hsa-miR-671-5p* and 67 other miRNAs may be used to regulate *LINC00847*. Folded RNA structure of miRNAs and lncRNAs was analyzed using RegRNA2.0 software, and Figure 2 shows limited reliability data of pair possibilities.

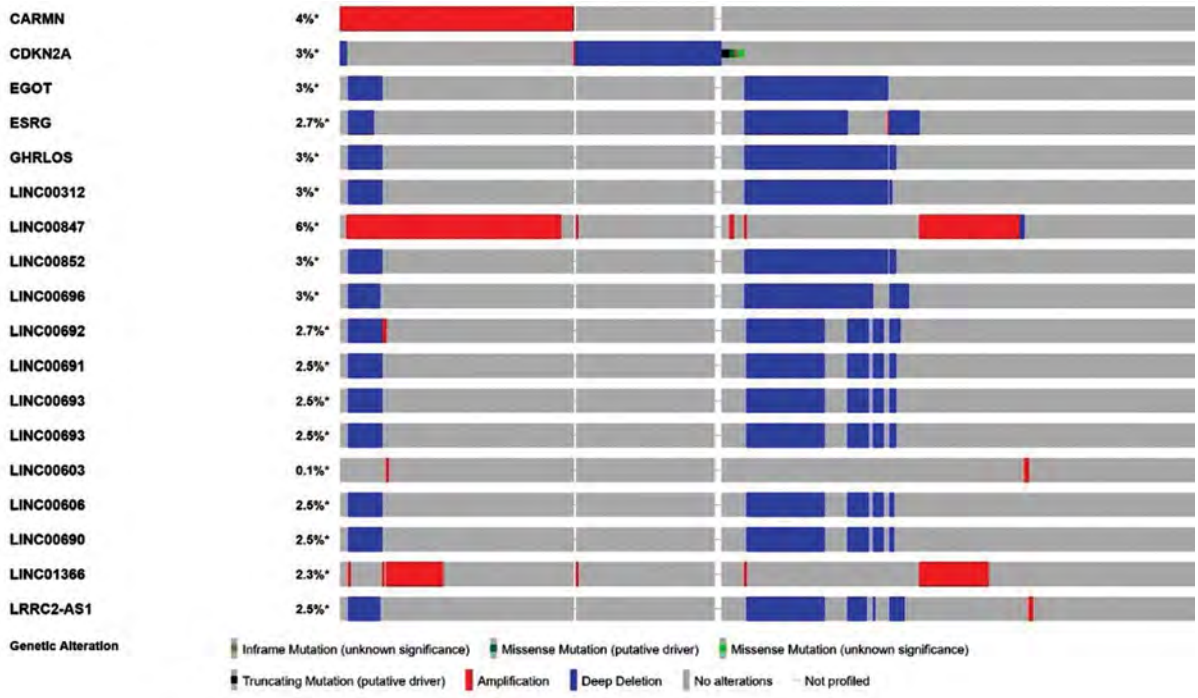

Fig.1: Identification of differentially expressed lncRNAs from The TCGA. Alternation frequency > 3%.

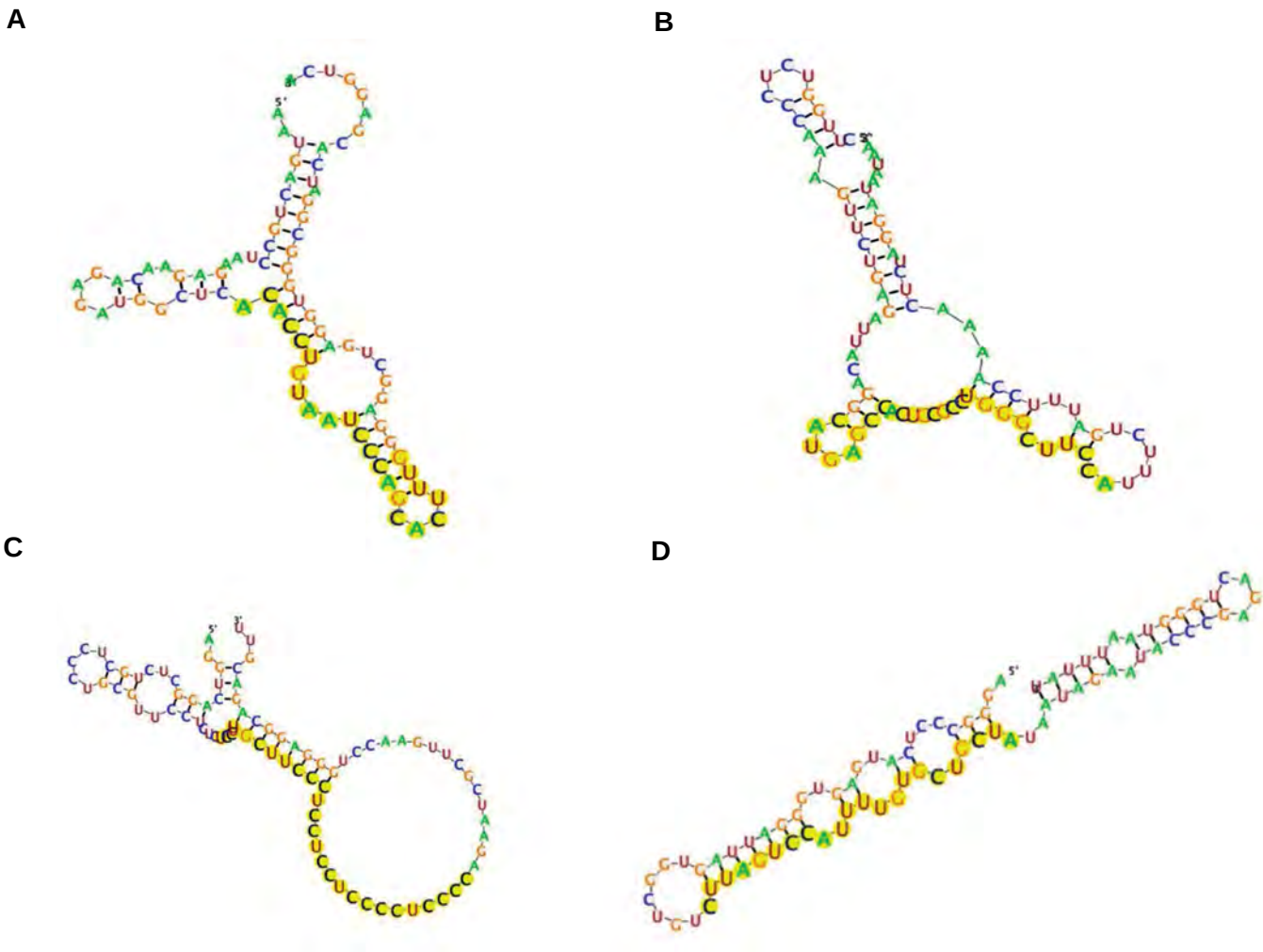

Fig.2: Top four RNA fold reliability data of probable lncRNA-microRNA pairs. **A.** *LINC00847-hsa-miR-93-5p*. **B.** *LINC00847-hsa-miR-671-5p*. **C.** *LINC00847-hsa-miR-4728*. **D.** *LINC00847-hsa-miR-15a-5p*. LINC, long intervening non-coding; miR, microRNA.

Creating lncRNA-miRNA-mRNA network

In this study, 37 miRNAs were recognized to be differentially-expressed in kidney cancer. Only, miRNA-mRNA pairs were simultaneously predicted by ≥ 2 applications in order to remove wrong positive rates of target prognostication. Interaction of all miRNAs with mRNAs was studied. One hundred and seventy six genes were predicted as targets of miRNA. Target genes were involved in different mechanisms of the cancer including apoptosis, cell cycle, cell proliferation and cell size. Cytoscape 3.6.0 software was used to visualize results. miRNA-mRNA network was created in this study as presented in network diagram (Fig.3), multiple miRNAs can target one gene. Regulation of *LINC00847-hsa-mir-15a-5p-DICER1* was observed as a new pathway in kidney cancer according to lncRNA-miRNA-mRNA regulatory network constructed in this study. *LINC00847-hsa-miR-93-5p-PTEN* was also identified as another new pathway in kidney cancer. In the next step, the effects of *tst* gene on expression level of these identified genes were investigated.

Functional enrichment analysis

Functional enrichment analyses, such as biological processes, were performed for *PTEN* and *DICER1* genes. GO class enrichments, according to threshold of enrichment, were rated with scores >1.0 and P<0.05. Enrichment genes may contribute to multiple biological processes including apoptotic signaling pathway, apoptotic DNA fragmentation, cell cycle and cell size, as shown in Figure 4.

Confirmation of recombinant plasmid

Presence of *S. aureus tst* gene in the pcDNA3.1 (+)-*tst* recombinant vector was confirmed by EcoRV/*NotI* restriction enzymes double digestion. Therefore, two fragments of 5 kb and 740 bp were observed after double digestion of pcDNA3.1(+) plasmid and *tst* gene, respectively (data not shown).

Flow cytometry assay

Results of flow cytometry experiments showed that apoptosis and necrosis in ACHN cells transfected with pcDNA3.1 (+)-*tst* recombinant vector were increased significantly (P<0.0001) compared to the control group (cells with empty plasmid). After *tst* treatment, death percentage of ACHN cells was clearly increased. Flow cytometry results showed that 68.02% of *tst* -treated ACHN cells were dead (due to necrosis and apoptosis), while 19.1% of cell death occurred in the control group (P<0.05, Fig.5A). In contrast, no statistically significant difference was observed in apoptosis and necrosis of HDF cells transfected with the pcDNA3.1(+)-*tst* recombinant vector (as normal cells) compared to the pcDNA3.1(+) plasmid (P=0.3246, Fig.5B).

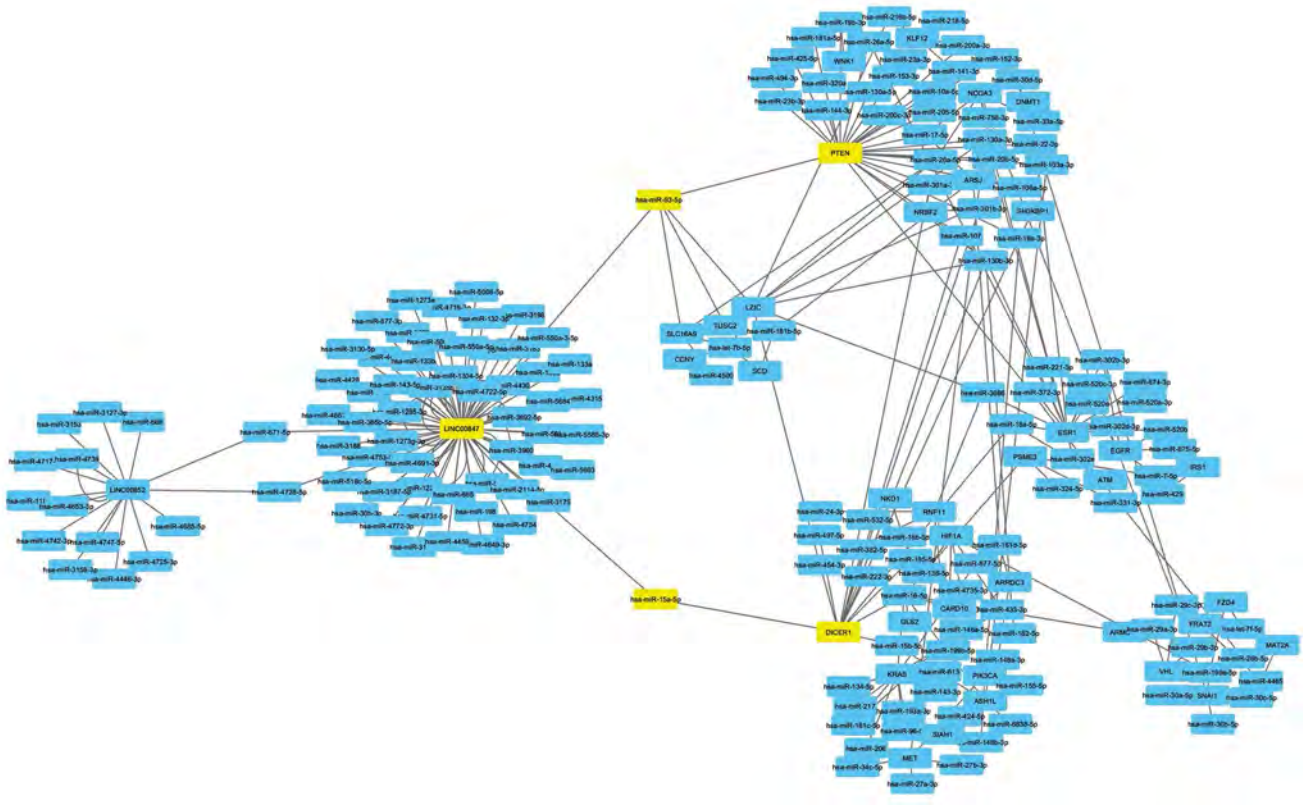

Fig.3: Interaction network of lncRNA-miRNA-mRNA in renal cell carcinoma (RCC). Differentially expressed mRNAs in kidney cancer were retrieved, their proximities to the selected miRNAs and lncRNAs were analyzed and visualized in Cytoscape.

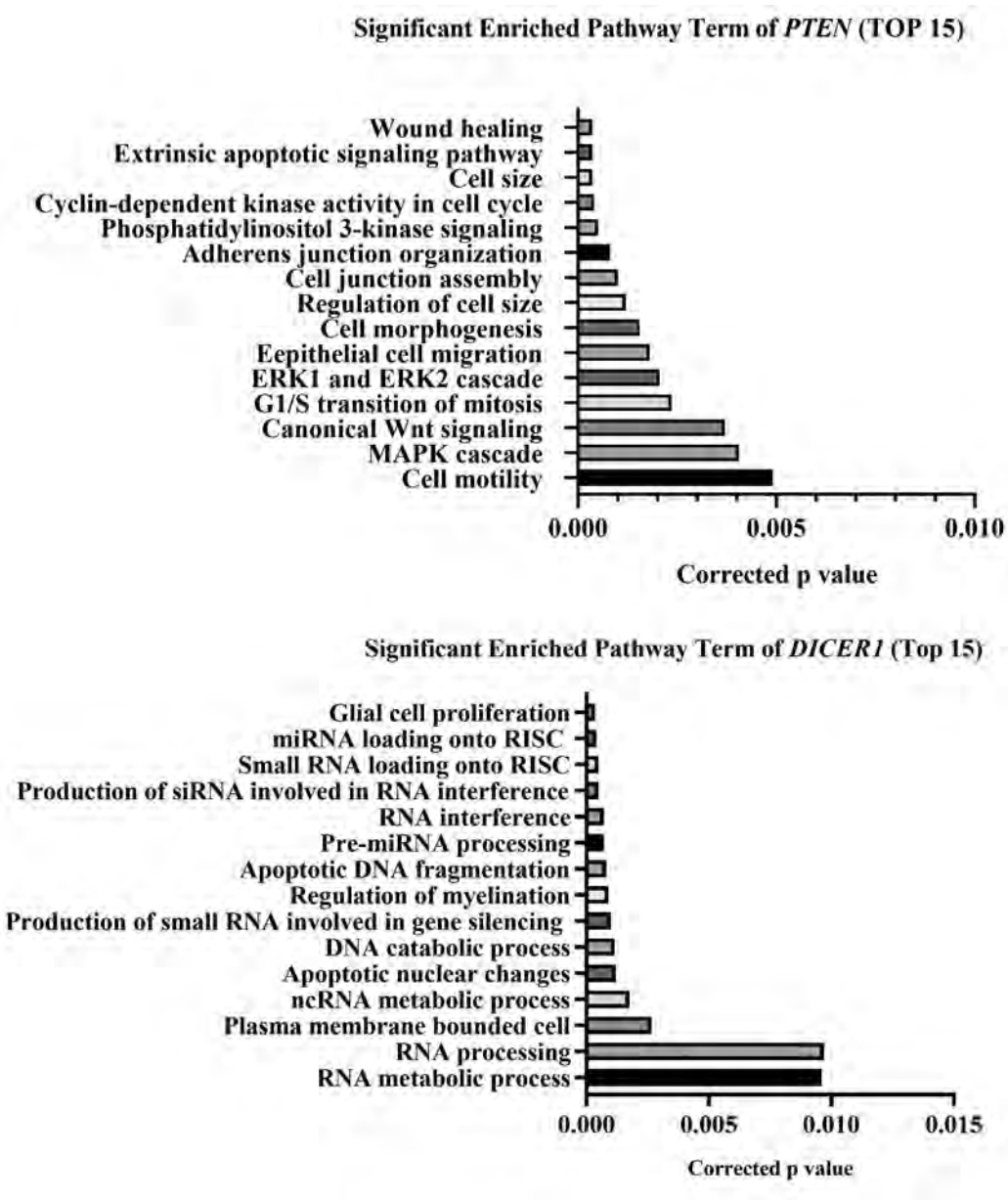

Fig.4: Enrichment pathway analysis. Top 15 pathways for the *PTEN* and *DICER1* genes based on biological process pathways. The lower P value is the most important activities of the genes that are shown on the top of graphs of the *PTEN* and *DICER1* genes.

Mammalian expression of *tst* gene

ACHN and HDF cells transfected with recombinant pcDNA3.1 (+)-*tst* expression vector were harvested 10 days post-transfection. RT-PCR results showed that 207 bp fragment was amplified for *tst* gene, suggesting that recombinant plasmid was successfully transfected into ACHN and HDF cells (data not shown).

Significant changes in the expression level of specific lncRNA and related genes in RCC cell line

Expression levels of the selected lncRNA and related genes in RCC cell line were measured after lipofection, compared to the empty plasmid group. qRT-PCR results showed a significant increase in the *LINC00847* expression in ACHN-*tst* group compared to pcDNA3.1(+) group (P=0.0024). A significant difference was found in the expression intensity (>3-fold change); therefore, *LINC00847* was introduced as a pro-apoptotic gene. Moreover, *PTEN* gene related to apoptosis pathway and their exclusive miRNA was increased in the ACHN-*tst* group compared to the pcDNA3.1 (+) group (P=0.0027 and ≥3-fold change). In contrast, no statistically significant difference was found in the expression levels of *DICER1* in the pcDNA3.1 (+)-*tst* transfected cells compared to the pcDNA3.1(+) group (P=0.4498, Fig.6). Additionally, no statistically significant difference was observed in the expression levels of *LINC00847* in the pcDNA3.1(+)-*tst* -HDF cells compared to the pcDNA3.1(+) group (P=0.3043, Fig.6). This indicates that *tst* gene had no statistically significant effect on the normal cells.

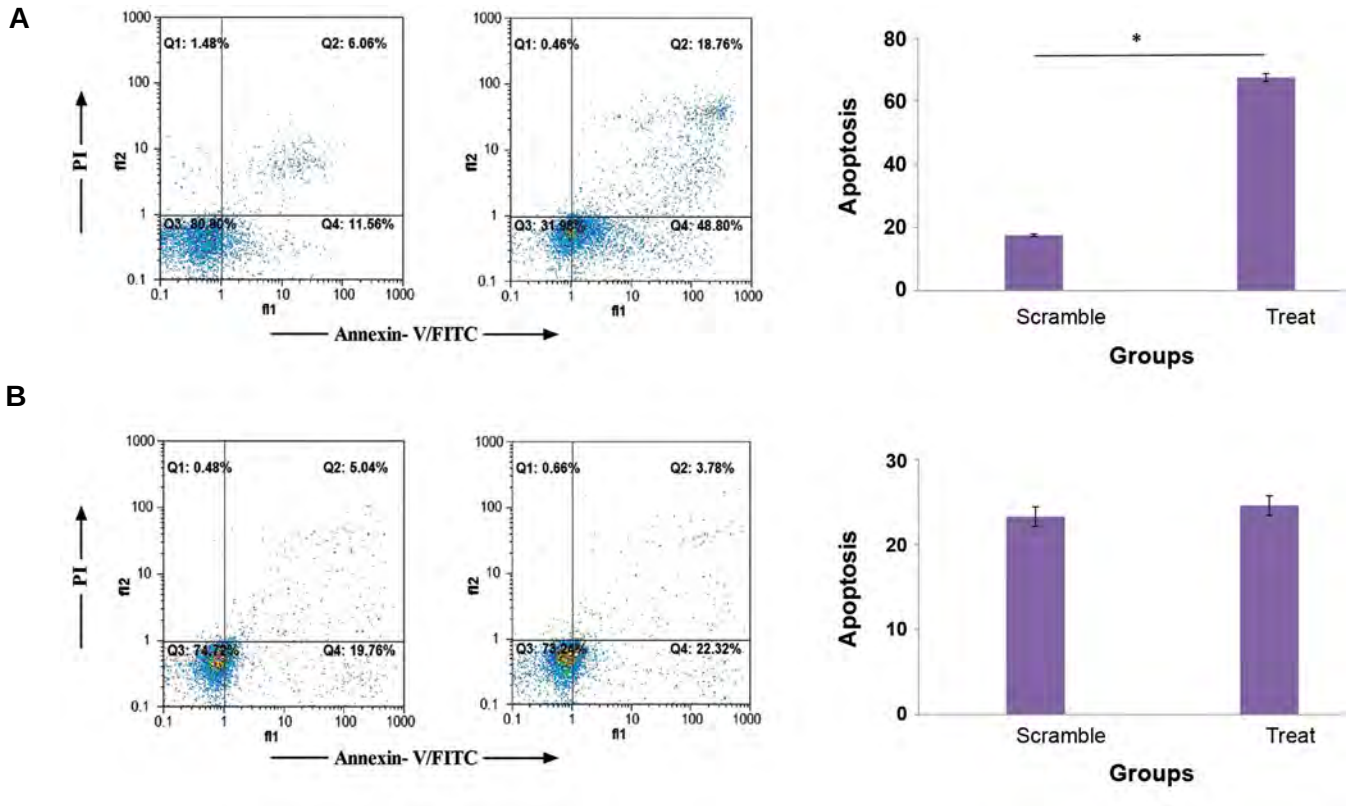

Fig.5: The results of apoptosis assay by FITC Annexin V for ACHN and HDF cells (Scale of axis: percentage (%)). **A.** Percentage of death in the ACHN treated group is 68.02%, after detection by flow cytometry assay, while it is 19.1% in the control group. **B.** The *tst*-treated HDF cells showed no statistically significant apoptotic cell death, compared to the control group. FITC; Fluorescein isothiocyanate, ACHN; Human renal cell adenocarcinoma, and HDF; Human Dermal Fibroblasts.

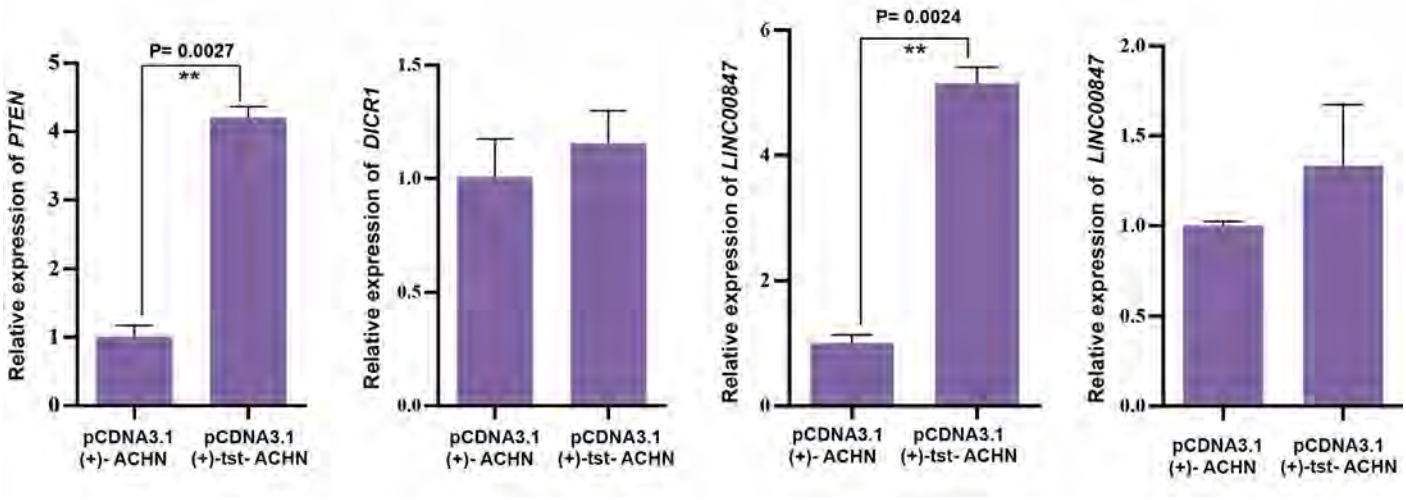

Fig.6: Expression levels of *PTEN*, *DICER1,* and *LINC00847* in the ACHN kidney cancer cell and *LINC00847* in the HDF normal cells treated by *tst* gene. Relative expression of the genes were examined by quantitative reverse transcription polymerase chain reaction (qRT-PCR) and they were compared to the treated and control cells by ΔΔCt method. Asterisks show significant differences to the controls (*; P<0.05, **; P<0.01, ***; P<0.001). ACHN; Human renal cell adenocarcinoma, and HDF; Human Dermal Fibroblasts. ACHN; Human renal cell adenocarcinoma, and HDF; Human Dermal Fibroblasts.

Discussion

In this study, the effects of non-coding RNAs were analyzed to prepare a network for elucidating lncRNA-miRNA-mRNA interaction in kidney cancer followed by measuring efficiency of recombinant plasmid in apoptosis of cancer cell lines. General analysis procedures have been used to find unique expressed genes, lncRNAs and miRNAs in biological processes or diseases. Few studies have been conducted on interactions within lncRNAs, miRNAs and target genes in kidney cancer. In this study, the obtained results regarding the expression level used to recognize abnormally expressed miRNAs and lncRNAs, in addition to the interaction network of lncRNA-miRNA-mRNA, was provided in kidney cancer. Data of miRNA and lncRNA expression levels related to kidney cancer

were achieved by the Cancer Genome Atlas, to find genes which are likely to be related to the cancer. It is suggested to explain more completely the process of lncRNAs in RCC, in future empirical researches. Initially, it was believed that lncRNAs are 'transcription noise'. However, lncRNAs have now been identified as significant players in gene regulation and they are related to a majority types of cancer (22, 23).

RegRNA software was used to predict interactions between lncRNAs and miRNAs. A total of 176 genes were targeted by miRNAs in this study, according to the results of ≥ 2 different algorithms, *hsa-miR-93-5p* and *hsa-mir-15a-5p* are the main elements in the constructed network. Created network showed an interaction within lncRNAs, miRNAs and mRNAs in relation to the development or occurrence of RCC. Our results (a relationship was identified between lncRNAs and mRNAs) showed that lncRNAs were related to miRNAs and vice versa. It was hypothesized that lncRNAs may also be related to clinical and pathological features of kidney cancer, just like miRNAs. Results of this study showed that one lncRNA, termed *LINC00847*, exhibited the possibility of interaction with *PTEN* and *DICER1* genes. Enrichr was used to analyze GO biological process in order to further study biological effects of aberrantly-expressed *PTEN* and *DICER1* in kidney cancer. Prognostication data showed that these genes may be involved in some biological processes including apoptotic signaling pathway, apoptotic DNA fragmentation, cell cycle and cell size. Nowadays, functional roles of most of the lncRNAs are obscure in cancers, but the role of *HOTAIR* is well-known. Liu et al. (24) showed that *HOTAIR* acting as a competing endogenous RNA (CeRNA) was a target of *miR-331-3P*. It can impose an additional level of post-transcriptional regulation and thereby modulating de-repression of *HER2*. Therefore, lncRNAs, miRNAs and mRNAs showed a regulatory network to co-interact with gene expression.

Hence, more disease-associated lncRNAs can be found using these methods in particular cells. The present report provided a new perspective into molecular pathway of RCC. However, these mechanisms have some limitations. For example, all of the miRNAs cannot be concurrently registered in prediction software algorithms. On the other hand, in vivo and in vitro studies will be required later due to lncRNA-miRNA-mRNA regulatory network proposed in this report, using a bioinformatics approach. Herein, *LINC00847*, *PTEN* and *DICER1* were identified based on the different servers. In fact, it was found that *LINC00847*, *PTEN* and *DICER1* are involved in apoptotic pathways in kidney cancer, and interaction network of lncRNA-miRNA-mRNA in RCC was also created. Correlation of these genes is based on the significance level of P value. On the other hand, this study was conducted to investigate the effect of *tst* gene on apoptosis. For this reason, expressions of *LINC00847*, *PTEN* and *DICER1* were investigated after lipofection. Therefore, a new therapeutic method was designed. Bacterial toxin can cause cell death by inducing apoptosis in cancer cell lines (25). As a result, efficiency of recombinant plasmid was studied in cancer cell lines. The pcDNA3.1 (+) mammalian expression vector was used to insert encoding *tst* gene. ACHN and HDF cell lines were transfected with pcDNA3.1 (+)-*tst* and pcDNA3.1 (+) as empty plasmid, and cell death was evaluated in the tested cells using Annexin V/PI staining and flow cytometer to measure the extent of necrosis and apoptosis. Our results significantly showed more cell death in the ACHN cell lipofected with pcDNA3.1 (+)-*tst* compared to the control groups. Cell death percentage caused by apoptosis in treated and control ACHN cells was equal to 68.02% and 19.1%, respectively. While, there was no significant necrosis and apoptosis in the HDF cells (as normal cells) in comparison with the control groups.

qRT-PCR of *LINC00847* showed up-regulation in ACHN treated cells compared to the controls. To find out whether lncRNA related to apoptosis (*LINC00847*) can influence on expression of the related genes or not, *PTEN* and *DICER1* gene expressions in the treated ACHN cells were studied, in comparison with the controls. Results obtained from *PTEN* expression indicated that this gene is indeed responsible for the increased level of apoptosis. So that, *PTEN* expression levels in the ACHN cells transfected with pcDNA3.1(+)-*tst* was significantly increased in comparison with the ACHN cells transfected with empty pcDNA3.1(+) vector. *PTEN* is known as a tumor suppressor gene, which activates apoptosis pathway by reducing intracellular phosphatidylinositol-3,4,5-triphosphate (PIP3). Protein abundance of *PTEN* decreases PIP3 level in cells and causes a decrease in the Akt protein on plasma membrane. This in turn decreases cell proliferation potential and increases apoptosis (26). Results of this study showed that expression level of *PTEN* was increased in ACHN-*tst*, compared to pcDNA3.1 (+) group, indicating that apoptosis induction was achieved in ACHN-*tst* group. Therefore, it can be stated that an increase in the expression of these genes could cause cell death in the *tst*-treated ACHN cell line. In contrast, expression levels of *DICER1* gene showed no statistically significant difference between *tst*-treated ACHN cells and pcDNA3.1 (+) group. Insufficient capabilities of the software to suggest probable lncRNA-miRNA-mRNA networks might be a reason for high false positive/negative outputs and finding no significant difference in the expression levels of *DICER1*. Expression of *LINC00847*, as a pro-apoptotic lncRNA, in the *tst*-treated HDF cell showed no statistically significant difference between the *tst*-treated cells and pcDNA3.1 (+) group. This indicates that *tst* gene had no effect on the normal cells.

As previously mentioned, bacterial toxins have great therapeutic potential to treat the cancers. Bacterial toxins are the most obvious cytotoxic agents, because these genes are native to bacterial physiology. Bacterial toxins are used to induce apoptosis during infection and they are presently considered to be important in disease processes (16, 27). Yu et al. (28) studied the effects of *S. aureus* toxins, SEB and α-toxin, on ECV304 cells. Results of this

study showed apoptosis induction and increase in TNF-α expression, as well as activation of caspase 3 and 8 in ECV304 cells. Findings expressed that SEB and α-toxin induce apoptosis through extrinsic apoptosis pathway. In this study, considering apoptosis induction, similar results were achieved for *S. aureus* toxin TSST-1.

Conclusion

In the current study, a variety of bioinformatic approaches were used, as a result of which a new lncRNA was discovered in the kidney cancer along with apoptosis pathways. lncRNAs and miRNAs were also found to exert regulatory effects on kidney cancer apoptosis, by influencing signaling pathways and biological process. Moreover, the effect of *tst* expression on ACHN cell line was investigated and the results were obtained regarding apoptosis induction. Expression of *LINC00847*, as a cell apoptosis-inducing lncRNA, and *PTEN* gene was up-regulated in the *tst*-treated ACHN cells. These results expressed that *S. aureus* toxin TSST-1 arrested cell cycle and resulted in activation of apoptosis through regulatory lncRNA and associated genes. Generally, *S. aureus* toxin TSST-1 can be used as a therapeutic bacterial toxin to treat the cancer in future.

Acknowledgements

This article is the outcome of Ph.D. thesis and the authors wish to thank the staff of Shahrekord Branch, Islamic Azad University and Cellular and Molecular Research Center of Shahrekord University of Medical Sciences (Shahrekord, Iran) for their helps. There is no financial support and conflict of interest in this study.

Authors' Contributions

A.D.; Contributed to the conception and design. M.S-D.; Contributed to the all experimental works, data and statistical analysis, as well as the interpretation of data. M.S.J.; Are responsible for overall supervision and contributed mainly to critical revision and approval of the final version. All authors read and approved the final manuscript.

References

1. Chen W, Zheng R, Baade PD, Zhang S, Zeng H, Bray F, et al. Cancer statistics in China, 2015. CA Cancer J Clin. 2016; 66(2): 115-132.
2. Qiao HP, Gao WS, Huo JX, Yang ZS. Long non-coding RNA GAS5 functions as a tumor suppressor in renal cell carcinoma. Asian Pac J Cancer Prev. 2013; 14(2): 1077-1082.
3. Leveridge MJ, Jewett MA. Recent developments in kidney cancer. Can Urol Assoc J. 2011; 5(3): 195-203.
4. Linehan WM, Vasselli J, Srinivasan R, Walther MM, Merino M, Choyke P, et al. Genetic basis of cancer of the kidney: disease-specific approaches to therapy. Clin Cancer Res. 2004; 10(18 Pt 2): 6282S-6289S.
5. Levi F, Ferlay J, Galeone C, Lucchini F, Negri E, Boyle P, et al. The changing pattern of kidney cancer incidence and mortality in Europe. BJU Int. 2008; 101(8): 949-958.
6. Scélo G, Brennan P. The epidemiology of bladder and kidney cancer. Nat Clin Pract Urol. 2007; 4(4): 205-217.
7. Chow WH, Dong LM, Devesa SS. Epidemiology and risk factors for kidney cancer. Nat Rev Urol. 2010; 7(5): 245-257.
8. Cheng L, Zhang S, Maclennan GT, Lopez-beltran A, Montironi R. Molecular and cytogenetic insights into the pathogenesis, classification, differential diagnosis, and prognosis of renal epithelial neoplasms. Hum Pathol. 2009; 40(1): 10-29.
9. Hsieh JJ, Purdue MP, Signoretti S, Swanton C, Albiges L, Schmidinger M, et al. Renal cell carcinoma. Nat Rev Dis Primers. 2017; 3: 17009.
10. Gutschner T, Diederichs S. The hallmarks of cancer: a long non-coding RNA point of view. RNA Biol. 2012; 9(6): 703-719.
11. Guttman M, Rinn JL. Modular regulatory principles of large non-coding RNAs. Nature. 2012; 482(7385): 339-346.
12. Cheetham SW, Gruhl F, Mattick JS, Dinger ME. Long noncoding RNAs and the genetics of cancer. Br J Cancer. 2013; 108(12): 2419-2425.
13. Wapinski O, Chang HY. Long noncoding RNAs and human disease. Trends Cell Biol. 2011; 21(6): 354-361.
14. Dinges MM, Orwin PM, Schlievert PM. Exotoxins of Staphylococcus aureus. Clin Microbiol Rev. 2000; 13(1): 16-34.
15. Faulkner L, Cooper A, Fantino C, Altmann DM, Sriskandan S. The mechanism of superantigen-mediated toxic shock: not a simple Th1 cytokine storm. J Immunol. 2005; 175(10): 6870-6877.
16. Pahle J, Menzel L, Niesler N, Kobelt D, Aumann J, Rivera M, et al. Rapid eradication of colon carcinoma by Clostridium perfringens Enterotoxin suicidal gene therapy. BMC Cancer. 2017; 17(1): 129.
17. Zhang X, Hu X, Rao X. Apoptosis induced by Staphylococcus aureus toxins. Microbiol Res. 2017; 205: 19-24.
18. Lu M, Shi B, Wang J, Cao Q, Cui Q. TAM: A method for enrichment and depletion analysis of a microRNA category in a list of microRNAs. BMC Bioinformatics. 2010: 11: 419.
19. Seim I, Jeffery PL, Thomas PB, Walpole CM, Maugham M, Fung JN, et al. Multi-species sequence comparison reveals conservation of ghrelin gene-derived splice variants encoding a truncated ghrelin peptide. Endocrine. 2016; 52(3): 609-617.
20. Livak KJ, Schmittgen TD. Analysis of relative gene expression data using real-time quantitative PCR and the 2(-Delta Delta C(T)) method. Methods. 2001; 25(4): 402-408.
21. Ma X, Fan Y, Gao Y, Zhang Y, Huang Q, Ai Q, et al. Dicer is down-regulated in clear cell renal cell carcinoma and in vitro Dicer knock-down enhances malignant phenotype transformation. Urol Oncol. 2014; 32(1): 46. e9-17.
22. Balas MM, Johnson AM. Exploring the mechanisms behind long noncoding RNAs and cancer. Noncoding RNA Res. 2018; 3(3): 108-117.
23. Zhang Z, Weaver DL, Olsen D, Peng Z, Ashikaga T, Evans MF. Long non-coding RNA chromogenic in situ hybridisation signal pattern correlation with breast tumour pathology. J Clin Pathol. 2016; 69(1): 76-81.
24. Liu XH, Sun M, Nie FQ, Ge YB, Zhang EB, Yin DD, et al. LncRNA HOTAIR functions as a competing endogenous RNA to regulate HER2 expression by sponging miR-331-3p in gastric cancer. Mol Cancer. 2014; 13: 92.
25. Bayles KW. Bacterial programmed cell death: making sense of a paradox. Nat Rev Microbiol. 2014; 12(1): 63-69.
26. Wan X, Yokoyama Y, Shinohara A, Takahashi Y, Tamaya T. PTEN augments staurosporine-induced apoptosis in PTEN-null Ishikawa cells by downregulating PI3K/Akt signaling pathway. Cell Death Differ. 2002; 9: 414–420.
27. Forbes NS. Engineering the perfect (bacterial) cancer therapy. Nat Rev Cancer. 2010; 10(11): 785-794.
28. Yu FL, Liu TT, Zhu X, Yang WX, Zhang T, Lin N, et al. Staphylococcal enterotoxin B and α-toxin induce the apoptosis of ECV304 cells via similar mechanisms. Mol Med Rep. 2013; 8(2): 591-596.

Original Article

hsa-miR-423 rs6505162 Is Associated with The Increased Risk of Breast Cancer in Isfahan Central Province of Iran

Nadia Pourmoshir, M.Sc.[1], Gholamreza Motalleb, Ph.D.[1]*, Sadeq Vallian, Ph.D.[2]*

1. Division of Cell and Molecular Biology, Department of Biology, Faculty of Science, University of Zabol, Zabol, Iran

2. Division of Genetics, Department of Cellular and Molecular Biology and Microbiology, Faculty of Science and Technology, University of Isfahan, Isfahan, Iran

Corresponding Addresses: P.O.Box: 98613-35856, Division of Cell and Molecular Biology, Department of Biology, Faculty of Science, University of Zabol, Zabol, Iran
P.O. Box: 8174573441, Division of Genetics, Department of Cellular and Molecular Biology and Microbiology, Faculty of Science and Technology,, University of Isfahan, Isfahan, Iran
Emails: reza.motaleb@uoz.ac.ir, svallian@sci.ui.ac.ir

Received: 14/June/2019, Accepted: 16/September/2019

Abstract

Objective: Thirteen million cancer deaths and 21.7 million new cancer cases are expected in the world by 2030. Breast cancer is considered as the main cause of cancer mortality in women aged 20-59 years. microRNAs (miRNAs) regulate gene expression at the post-transcriptional level and they are highly expressed in malignancies, including breast cancer. The role of miRNAs in the pathogenesis of breast cancer is not fully understood. In the present study, for the first time, the impact of *hsa-miR-423* rs6505162 on breast cancer risk was investigated in the central province of Iran, Isfahan.

Materials and Methods: This case-control study was conducted on 153 clinicopathological proven breast cancer patients and 153 sex-matched healthy women with no history of any cancer type and relative patients. The patients and controls were genotyped and association of their clinical characteristics with *hsa-miR-423* rs6505162 genotype was analyzed.

Results: The findings indicated that CC genotype of *hsa-miR-423* rs6505162 was associated with the increased risk of breast cancer [odds ratio (OR)=2.37, 95% confidence interval (CI)=1.29-4.35 and P=0.0023, CC vs. AA].

Conclusion: The data suggested that *hsa-miR-423* rs6505162 could be considered as a novel risk factor in breast cancer pathogenesis in Isfahan province of Iran.

Keywords: Breast Cancer, *hsa-miR-423*, microRNA

Cell Journal(Yakhteh), Vol 22, Suppl 1, Autumn 2020, Pages: 110-116

Citation: **Pourmoshir N, Motalleb Gh, Vallian S. hsa-miR-423 rs6505162 is associated with the increased risk of breast cancer in Isfahan central province of Iran. Cell J. 2020; 22 Suppl 1: 110-116. doi: 10.22074/cellj.2020.7011.**

Introduction

The rate of cancers is increasing day by day in the worldwide. Approximately, 30000 Iranians lose their life due to cancer each year (1). Breast cancer is the most frequent carcinoma and the second leading cause of cancer mortality among women in less-developed countries (2). Multiple studies have made progress in many fields of breast cancer investigations to understand the etiology of its carcinogenesis. However, the precise mechanisms of breast cancer carcinogenesis remain largely unknown (3, 4). It is well accepted that environmental and genetic factors are two main groups of risk factors for breast cancer. Several studies have revealed that the sophisticated synergy of genetics, environmental exposures, hormones and diet behaviors may predispose to breast cancer (5). Early detection of breast cancer primary tumors is very important, because it can increment the chance of an effective cure in patients with early stage of the disease. However, majority of the cancers at an early stage are difficult to detect. Therefore, novel biomarkers for identifying high-risk populations as well as new strategies for early detection are urgently required (6, 7).

microRNAs (miRNAs) are an abundant class of ancient, noncoding and small single-stranded molecules (20-22 nucleotides) that participate in transcriptional and translational regulations of their target genes (8). Since miRNAs can regulate several target transcripts, they have been identified to have vital roles in normal biological processes, such as cell differentiation, proliferation, immune system regulation, hematopoiesis and apoptosis through different gene regulation networks (9). Elevated or decreased expression of specific miRNAs has been reported to be implicated in down- or up-regulation of the miRNA putative targets, which could give rise to deregulation of the pathways in which those targets are involved. Aberrant expression of miRNA can occur in the multiple processes of carcinogenesis, including cell growth, apoptosis, differentiation, invasion and angiogenesis of solid cancers, including the breast (10, 11). The wide role of miRNAs opens up a new avenue of investigation for molecular mechanisms of miRNAs in cancer pathogenesis. In this framework, miRNA signatures have obviously been distinguished for certain types of malignancy, in which they can act as either tumor

suppressors or oncogenes (12). miRNA expression can be altered by various mechanisms, such as chromosomal instability, epigenetic changes, genomic mutations, defects in the mechanisms of miRNA biosynthesis and single nucleotide polymorphisms (SNPs) in their coding genes (13).

In modern genetics, phenotypic variations for traits with medical importance are of special interests. Some variations are due to SNP in miRNAs, named as MirSNPs, which represent a new class of potential biomarkers. These markers have attracted increasing interests due to their potential role in the development of various types of cancer (14). In fact, MirSNPs could be used as new biomarkers for molecular diagnosis of genetic diseases and cancer (15). Many reports indicated that MirSNPs could play functional roles in different ways such as altering the transcription of the primary target genes, affecting pre-miRNA/pre-miRNA processing or by exerting effects on miRNA-mRNA interplays (16, 17). Therefore, MirSNPs seem to be ideal biomarkers for constructing genetic maps and categorizing the direct functional and effective variants correlated with common and even genetically complex diseases like cancer.

Various reports from the studies performed on a number of populations with breast cancer patients have demonstrated that SNPs in the precursor of miRNAs (pre-miRNAs), exclusively miR-423 A/C polymorphism, could affect maturation or expression of the respective mature miRNA (18-20).

To date, there is no report on the impact of *hsa-mirR-423* rs6505162 variants on breast cancer risk in the Iranian population. Therefore, the current study was carried out to find the possible association between *hsa-mirR-423* rs6505162 variants polymorphisms and susceptibility to breast cancer in the Isfahan central province of Iran.

Materials and Methods

Patients and controls

This study was qualified by meeting the following criteria: i. Designed as case-control, ii. Assessed the association between Hsa-miR-423 rs6505162 polymorphism and breast cancer risk, iii. Provided adequate numbers of genotype distribution in case and control groups, in order to calculate the odd ratios (OR) and its 95% confidence interval (CI).

In the present case-control study, 153 genetically-unrelated females with breast cancer from the Omid Hospital (Isfahan, Iran) were investigated between 2011 and 2014. As control, the same numbers of healthy independent females were included in the study. The study design and recruitment procedures were described previously (21). The project was approved by the Scientific and Ethical Advisory Group of the University of Zabol (code: 7611) and University of Isfahan (code: 790205), Iran. All control and patient samples were obtained from Isfahan province, which may indicate approximate similarity of healthy and patient population in terms of environmental factors. The informed consent was obtained from all individuals participated in this study. As indicated, the patients were categorized in two groups, including superficial (levels 0, I and II) and invasive (levels III and IV) based on their tumor grade.

Table 1: Sequence of the primers designed and used for *miR-423* genotyping (rs6505162)

Primers	Primer sequence (5´-3´)	Amplicon size (bp)
*hsa-mir-423*rs6505162 A>C		
Forward outer	TTTAAATGCGCTGGAAGTGAAG	410
Reverse outer	CCTATATGCCTACCCTTTTTCTGTG	410
Forward normal	CCCTCAGTCTTGCTTCCCAA	200
Forward mutant	CCCTCAGTCTTGCTTCCCAC	200

Single nucleotide polymorphisms selection and genotyping

The *hsa-miR-423* rs6505162 polymorphism was selected by considering the following criteria: i. the minor allele frequency (MAF) of selected SNP was < 5% (0.4978), ii. It was functional (22). The International HapMap Project (http://www.hapmap.org), dbSNP (http://www.ncbi.nlm.nih.gov/projects/SNP/) and Mirbase (http://microrna.sanger.ac.uk) were used for evaluation of MAF criteria. F-SNP (http://compbio.cs.queensu.ca/F-SNP) database was used to prioritize the SNPs with potential pathological effect on human health. Genotyping was performed on total genomic DNA. Genomic DNA was extracted from the peripheral blood leukocytes by a standard salting out procedure (23). Genotyping of *hsa-miR-423* rs6505162 polymorphism was carried out by ARMS-PCR using newly designed specific primers (24, 25). Primers were designed using Oligo software and NCBI BLAST search engine as shown in Table 2. The 3´-terminus of each primer was modified to match the corresponding polymorphism in *hsa-miR-423*. Moreover, an artificial mismatch at the antepenultimate base was included in the allele-specific primers to improve the primers/template specificity (26). PCR reactions were performed in two separate tubes in 25 µl total volume. The reaction mixture was composed of 1µg DNA, 3 mM $MgCl_2$, 0.4 mM dNTPs, 1x PCR Buffer, 1 U Taq DNA polymerase and 0.5 µM of each forward and reverse primers. Initial denaturation was accomplished at 94˚C for 5 minutes, followed by 30 cycles including denaturation at 94˚C for 1 minute, annealing temperature at 57˚C for 1 minute, extension at 72˚C for 1 minute, followed by a final extension at 72˚C for 10 minutes. The amplification products were separated in 2% agarose gel and visualized under UV light.

Statistical analysis

Association of the genotypes with breast cancer was assessed by computing the OR and 95% CI. The data were statistically evaluated using Simple Interactive Statistical Analysis (SISA) software (two by two tables available from http://www.quantitativeskills.com/sisa/). The genotypic associations were examined using SNPstats, (http://bioinfo.iconcologia.net/SNPstats_web). The results were considered statistically significant at P≤0.05.

The Pearson's chi-square $\chi 2$ test was used to evaluate the Hardy-Weinberg equilibrium by considering statistical significance at a P≥0.05 (27). Population studies were carried out by using GENEPOP website (http://genepop.curtin.edu.au) and the polymorphism information content (PIC) was computed by PIC calculator website (https://www.liverpool.ac.uk/~kempsj/pic.html).

Determination of the best fitting pattern of inheritance

The patterns of inheritance were determined by Akaike information criterion (AIC) and Bayesian information criterion (BIC) (28).

Results

Clinical and pathological characteristics of the breast ancer patients were summarized in Table 2.

Table 2: Clinicopathological characteristics of the patients with breast cancer

Characteristics	Number	Percentage
Age (Y), mean ± SD		
≤50	93	60.8
>50	60	39.2
Tumor stage		
Invasive	100	65.4
Superficial	53	34.6
Estrogen receptor		
Positive	94	61.4
Negative	59	38.6
Progesterone receptor		
Positive	90	58.8
Negative	63	41.2

Genotyping was performed for *hsa-miR-423* rs6505162 in 153 breast cancer patients (age with mean ± SD of 47.14 ± 10.45 years old] and 153 control individuals [age with mean ± SD of 45.4 ± 12.3 years old]. The results of representative polymerase chain reaction (PCR) products from ARMS-PCR reactions were shown in Figure 1. Data showed that the Pearson Chi-Square significance value was 0.00071 (P<0.05). Analysis of the association of genotyping data with the risk of breast cancer using SNPstats, showed a clear association of *hsa-miR-423* rs6505162 in codominance, recessive and Log-additive patterns with breast cancer. These data showed the presence of possible relationship between *hsa-miR-423* rs6505162 and the incidence of breast cancer. The genotyping data also showed that the CC genotype was associated with the increased risk of breast cancer in codominance (OR=2.37, 95% CI=1.29-4.35, P=0.0023, CC vs. AA), recessive (OR=2.58, 95% CI=1.48-4.52, P=0.0006; CC vs. AA+AC) and Log-additive (OR=1.43, 95% CI=1.07-1.91, P=0.016) pattern of inheritance. This indicated that the *hsa-miRw* rs6505162 C allele in comparison with the A allele could increase the risk of breast cancer (OR=1.56, 95% CI=1.13-2.16, P=0.007). Based on the AIC and BIC factors, the best fitting inheritance pattern would be a recessive model (AIC: 416.5, BIC: 424, Table 3).

Analysis of the data indicated that *hsa-miR-423* rs6505162 was associated with the tumor stage in codominance (P=0.0008, OR=4.55, 95 % CI=1.87–11.08 and OR=2.98, 95% CI=1.32-6.74 for A/C and C/C genotypes, respectively), dominance (OR=3.62, 95% CI=1.80-7.29, P=0.0002), over dominance (OR=2.87, 95% CI=1.26-6.55, P=0.0081) and Log-additive mode of inheritance (OR=1.85, 95% CI=1.21-2.84, P=0.0034). In view of the AIC and BIC factors, the best fitting model would be dominant inheritance model (AIC=187.9, BIC=194, Table 4).

Moreover, as shown in Table 5, *hsa-miR-423* rs6505162 was associated with age of the patient in a codominance (P=0.01, OR=3.01, 95% CI=1.32–6.84 and OR=2.61, 95% CI=1.18-5.78 for A/C and C/C genotypes, respectively), dominance (OR=2.79, 95% CI=1.42-5.50, P=0.0026) and Log-additive pattern (OR=1.68, 95% CI=1.12-2.51, P=0.011). The AIC and BIC indicated the presence of dominant inheritance model as the best fitting model (AIC=19909, BIC=205.9, Table 5). However, there was no association between *hsa-miR-423* rs6505162 and the estrogen and progesterone receptors in the tested inheritance models (P>0.05). Analysis of Hardy-Weinberg Equilibrium showed the presence of equilibrium for this marker in the Isfahan population (P=0.1627). Analysis of the allele frequency and heterozygosity for the indicated marker using GENEPOP website illustrated 0.356 MAF and 41.18% heterozygosity rate for *hsa-miR-423* rs6505162 (data not shown). The estimated PIC value was 0.3534 by determining the frequency of alleles per locus through PIC calculator website.

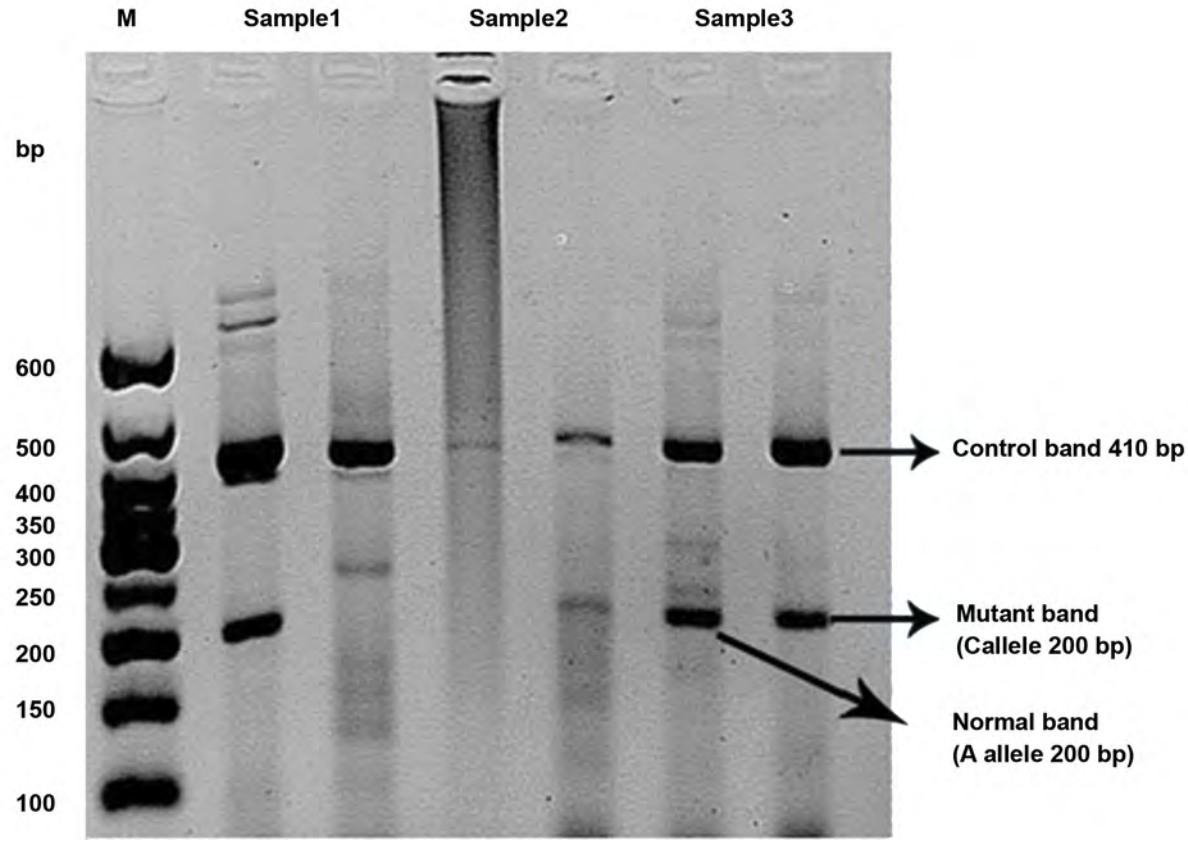

Fig.1: Genotyping of *hsa-miR-423* rs6505162 A>C polymorphism**.** The results of representative amplified products from ARMS-PCR reactions are shown. The PCR products were run on 2% agarose gel and the *hsa-miR-423* rs6505162 A>C genotypes were detected. Each sample consists of two lines: the first line refers to the allele from normal primers (A allele) and second line refers to the allele of mutant primers (C allele). Therefore, as illustrated, sample 1 (line 1-2) represents a normal homozygous individual (AA), sample 2 (lines 3-4) represents a mutant homozygous individual (CC) and sample 3 (lines 5-6) represents a heterozygous individual (AC). M represents DNA size marker.

Table 3: Allele and genotype distribution of *hsa-miR-423* rs6505162 A>C polymorphism in the patient and control group

Model	Genotype	Control	Case	OR (95% CI)	P value	AIC	BIC
Codominant	A/A	67 (43.8)	59 (38.6)	1.00	0.0023	418	429.2
	A/C	63 (41.2)	46 (30.1)	0.83 (0.49-1.39)			
	C/C	23 (15)	48 (31.4)	2.37 (1.29-4.35)			
Dominant	A/A	67 (43.8)	59 (38.6)	1.00	0.35	427.3	434.8
	A/C-C/C	86 (56.2)	94 (61.4)	1.24 (0.79-1.96)			
Recessive	A/A-A/C	130 (85)	105 (68.6)	1.00	6e-04	416.5	424
	C/C	23 (15)	48 (31.4)	2.58 (1.48-4.52)			
Overdominant	A/A-C/C	90 (58.8)	107 (69.9)	1.00	0.042	424.1	431.5
	A/C	63 (41.2)	46 (30.1)	0.61 (0.38-0.98)			
Log-additive	---	---	---	1.43 (1.07-1.91)	0.016	422.4	429.8
Allele	A	164 (53.6)	197 (64.4)	1.00	0.007	-	-
	C	142 (46.4)	109 (35.6)	1.56 (1.13-2.16)			

Data are presented as n (%). CI; C*onfidence interval,* AIC; Akaike information criterion, OR; Odds ratio, and BIC; Bayesian information criterion.

Table 4: Genotype and allele frequency of *hsa-miR-423* rs6505162 A>C polymorphism among the breast cancer patients

Model	Genotype	Superficial	Invasive	(OR (95% CI	P value	AIC	BIC
Codominant	A/A	31 (58.5)	28 (28)	1.00	8e-04	189.2	198.3
	A/C	9 (17)	37 (37)	4.55 (1.87-11.08)			
	C/C	13 (24.5)	35 (35)	2.98 (1.32-6.74)			
Dominant	A/A	31 (58.5)	28 (28)	1.00	2e-04	187.9	194
	A/C-C/C	22 (41.5)	72 (72)	3.62 (1.80-7.29)			
Recessive	A/A-A/C	40 (75.5)	65 (65)	1.00	0.18	199.6	205.7
	C/C	13 (24.5)	35 (35)	1.66 (0.78-3.50)			
Overdominant	A/A-C/C	44 (83)	63 (63)	1.00	0.0081	194.4	200.5
	A/C	9 (17)	37 (37)	2.87 (1.26-6.55)			
Log-additive	---	---	---	1.85 (1.21-2.84)	0.0034	192.9	198.9

Data are presented as n (%). CI; C*onfidence interval,* AIC; Akaike information criterion, OR; Odds ratio, and BIC; Bayesian information criterion.

Table 5: Association of *hsa-miR-423* rs6505162 with tumor stage in the breast cancer patients

Model	Genotype	>50	≤50	OR (95% CI)	P value	AIC	BIC
Codominant	A/A	32 (53.3)	27 (29)	1.00	0.01	201.8	210.9
	A/C	13 (21.7)	33 (35.5)	3.01 (1.32-6.84)			
	C/C	15 (25)	33 (35.5)	2.61 (1.18-5.78)			
Dominant	A/A	32 (53.3)	27 (29)	1.00	0.0026	199.9	205.9
	A/C-C/C	28 (46.7)	66 (71)	2.79 (1.42-5.50)			
Recessive	A/A-A/C	45 (75)	60 (64.5)	1.00	0.17	207	213.1
	C/C	15 (25)	33 (35.5)	1.65 (0.80-3.40)			
Overdominant	A/A-C/C	47 (78.3)	60 (64.5)	1.00	0.065	205.5	211.6
	A/C	13 (21.7)	33 (35.5)	1.99 (0.94-4.20)			
Log-additive	---	---	---	1.68 (1.12-2.51)	0.011	202.5	208.5

Data are presented as n (%). CI; C*onfidence interval,* AIC; Akaike information criterion, OR; Odds ratio, and BIC; Bayesian information criterion.

Discussion

In the present study, the impact of *hsa-miR-423* rs6505162 polymorphism was investigated on 306 breast cancer cases and control individuals in the Isfahan population (central province of Iran). The results indicated that *hsa-mirR-423* rs6505162 polymorphism was associated with susceptibility to increased risk of breast cancer. In this regard, recently genetic susceptibility due to SNP has been one of the major focuses of cancer molecular biology research (29).

It has been reported that MirSNPs could potentially influence miRNA maturation, silencing machinery, the structure or expression level of mature miRNA and the base pairing at the target site, altering miRNA expression. Furthermore, MirSNPs have been shown to play a functional role in miRNA-mediated gene regulation, thereby affecting susceptibility and progression of various cancers (30).

To date, a large number of investigations have been performed to unravel the exact role of MirSNPs in precursor and mature miRNA and their influences on cancer susceptibility (31, 32). *miR-423* is located in the frequently amplified region of chromosome 17q11.2 and lies within the first intron of the nuclear speckle splicing regulatory protein (*NSRP1*) gene, which is involved in alternative splicing of mRNAs. Its pre-miRNA can

produce two mature transcripts, *miR-423-3p* and *miR-423-5p*, that are at the 3′- and 5′-terminus of the pre-*miR-423*, respectively (33). The rs6505162 SNP, located in the pre-*miR-423*, 12 base pairs 5′ of *miR-423-5p* suggests a relationship with development of cancer according to cross phenotype meta-analysis (CPMA).

Up to now, most of the investigations on *miR-423* has focused on expression analyses and showed that abnormal expression of the miRNA could affect different types of cancer during cellular differentiation (34). Previous studies have shown that miRNAs (pre-miRNA SNPs) can influence the binding of nuclear factors associated with miRNA processing. Together with the other recent studies, our bioinformatics investigation suggested that rs6505162 might influence the expression of miR-423 (data not shown). However, some experiments assessing the rs6505162 SNP effect on function of miR-423 are needed.

Moreover, the SNP of rs895819 in pre-*miR-27a* has been reported as a risk factor for breast cancer in younger Chinese populations (35). Experiments on rs6505162 polymorphism and risk of cancer have yielded unpredictable results. Ye et al. (36) reported that C allele of rs6505162 was significantly higher in the cancer patients compared to the controls in 346 Caucasian ESCC patients. Another study showed that the C genotype of rs6505162 SNP decreases breast cancer development risk. Nevertheless, one study showed that the C genotype of rs6505162 suggested an increased risk of developing breast and ovarian cancers in carriers with Breast Cancer Associated 2 (BRCA2) mutation (34).

Genotyping data obtained from this study showed that *hsa-miR-423* rs6505162 could have a positive effect on the incidence of breast cancer with approximately 2.5 folds. This suggested that *hsa-miR-423* rs6505162 could involve in the susceptibility to increase risk of breast cancer in the Isfahan population. Zhao et al. (19) reported that *miR-423* could play potentially an oncogenic role in breast tumorigenesis. Moreover, it has been reported that this MirSNP showed several associations with cancer development in diverse ethnicities (34). One example includes the study performed by Kontorovich et al. (33) and Hu et al. (34), whereby it was illustrated that rs6505162 was associated with a significantly increased risk of ovarian and bladder cancers.

On the other hand, another study showed that *miR-423* could confer a reduced risk of breast and esophageal cancers as well as the recurrence or survival of renal cell carcinoma and prostate cancer (36). Interestingly, we found the association between clinicopathological characteristics and *hsa-miR-423* rs6505162 polymorphism in breast cancer patients. The association analysis indicated that existence of C recessive (minor) allele in patients who were >50 years old had 2-3 folds higher risk of developing breast cancer. Moreover, 2-4.5 folds increase in the risk of developing breast cancer was observed in those with invasive stages of breast cancer progression compared to those at the superficial stages.

Given the association of *hsa-miR-423* rs6505162 polymorphism with increased risk of breast cancer, its allele frequency in control population was investigated. The data showed presence of Hardy-Weinberg equilibrium for *hsa-miR-423* rs6505162 marker in the Isfahan population. The data indicated a high heterozygosity for *hsa-miR-423* rs6505162 variant (with He=41.18%). Moreover, analysis showed PIC=0.3534. This indicated diversity of *hsa-miR-423* rs6505162 in the Isfahan population. In the present study, MAF was compared to the other population based on the 1000 genome project database (data not shown). Data showed that the highest MAF was related to Chinese population (0.8127) indicating a big difference with the Iranian population. The lowest MAF refers to the American population (0.2541).

On the other hand, the British population has the closest distance to the Iranian population for both A and C alleles of *hsa-miR-423* rs6505162 polymorphism. All together, the data from this study showed that there was an association between *hsa-miR-423* rs6505162 A/C polymorphism and susceptibility to breast cancer in the population of Isfahan central province of Iran. We highly suggest using anti-sense RNA of *hsa-miR-423* rs6505162 in animal model to evaluate this point.

Conclusion

Data obtained from this study could suggest *hsa-miR-423* rs6505162 as a new molecular marker in molecular cancer diagnosis and prevention as well as the development of possible individually tailored miRNA-based therapy. Furthermore, these data may indicate that polymorphism in pre-microRNA (*hsa-miR-423* rs6505162) could play a role in the pathogenesis of breast cancer.

Acknowledgements

This research was approved and funded, in part, by University of Zabol, and the University of Isfahan (Isfahan, Iran). The authors are grateful to University of Zabol and University of Isfahan. The authors declare that there is no conflict of interests.

Authors' Contributions

G.M.; Conducted and supervised the study and drafting. N.P.; Contributed to the conception, design, performing data collection, in addition to the all experimental works and drafting. S.V.; Conducted and supervised the study design, data collection and evaluation, drafting, statistical analysis and he was in charge of overall direction and planning. All authors read and approved the final manuscript.

References

1. Motalleb G, Gholipour N, Samaei NM. Association of the human astrocyte elevated gene-1 promoter variants with susceptibility to hepatocellular carcinoma. Med Oncol. 2014; 31(4): 916.
2. Majeed W, Aslam B, Javed I, Khaliq T, Muhammad F, Ali A, et al.

Breast cancer: major risk factors and recent developments in treatment. Asian Pac J Cancer Prev. 2014; 15(8): 3353-3358.
3. Carter D. New global survey shows an increasing cancer burden. Am J Nurs. 2014; 114(3): 17.
4. Hashemi M, Eskandari-Nasab E, Fazaeli A, Taheri M, Rezaei H, Mashhadi M, et al. Association between polymorphisms of glutathione S-transferase genes (GSTM1, GSTP1 and GSTT1) and breast cancer risk in a sample Iranian population. Biomark Med. 2012; 6(6): 797-803.
5. Benz CC. Impact of aging on the biology of breast cancer. Crit Rev Oncol Hematol. 2008; 66(1): 65-74.
6. Zhang N, Huo Q, Wang X, Chen X, Long L, Jiang L, et al. A genetic variant in pre-miR-27a is associated with a reduced breast cancer risk in younger Chinese population. Gene. 2013; 529(1): 125-130.
7. Zhong S, Chen Z, Xu J, Li W, Zhao J. Pre-mir-27a rs895819 polymorphism and cancer risk: a meta-analysis. Mol Biol Rep. 2013; 40(4): 3181-3186.
8. Garzon R, Marcucci G, Croce CM. Targeting microRNAs in cancer: rationale, strategies and challenges. Nat Rev Drug Discov. 2010; 9(10): 775-789.
9. Esquela-Kerscher A, Slack FJ. Oncomirs-microRNAs with a role in cancer. Nat Rev Cancer. 2006; 6(4): 259-269.
10. Wang C, Bian Z, Wei D, Zhang JG. miR-29b regulates migration of human breast cancer cells. Mol Cell Biochem. 2011; 352(1-2): 197-207.
11. Filipowicz W, Bhattacharyya SN, Sonenberg N. Mechanisms of post-transcriptional regulation by microRNAs: are the answers in sight? Nat Rev Genet. 2008; 9(2): 102-114.
12. Gyparaki MT, Basdra EK, Papavassiliou AG. MicroRNAs as regulatory elements in triple negative breast cancer. Cancer Lett. 2014; 354(1): 1-4.
13. Lee YS, Dutta A. MicroRNAs in cancer. Annu Rev Pathol. 2009; 4: 199-227.
14. Ryan BM, Robles AI, Harris CC. Genetic variation in microRNA networks: the implications for cancer research. Nat Rev Cancer. 2010; 10(6): 389-402.
15. Rezaei H, Vallian S. BanI/D13S141/D13S175 represents a novel informative haplotype at the GJB2 gene region in the Iranian population. Cell Mol Neurobiol. 2011; 31(5): 749-754.
16. Chen K, Song F, Calin GA, Wei Q, Hao X, Zhang W. Polymorphisms in microRNA targets: a gold mine for molecular epidemiology. Carcinogenesis. 2008; 29(7): 1306-1311.
17. Sethumadhavan R. Application of computational tools for identification of miRNA and their target sNPs. J Proteomics Bioinform. 2008; 1(7): 359-367.
18. Smith RA, Jedlinski DJ, Gabrovska PN, Weinstein SR, Haupt L, Griffiths LR. A genetic variant located in miR-423 is associated with reduced breast cancer risk. Cancer Genomics Proteomics. 2012; 9(3): 115-118.
19. Zhao H, Gao A, Zhang Z, Tian R, Luo A, Li M, et al. Genetic analysis and preliminary function study of miR-423 in breast cancer. Tumor Biology. 2015; 36(6): 4763-4771.
20. Zheng W, Long J, Gao YT, Li C, Zheng Y, Xiang YB, et al. Genome-wide association study identifies a new breast cancer susceptibility locus at 6q25.1. Nat Genet. 2009; 41(3): 324-328.
21. Hashemi M, Shahkar G, Simforoosh N, Basiri A, Ziaee SA, Narouie B et al. Association of polymorphisms in PRKCI gene and risk of prostate cancer in a sample of Iranian Population. Cell Mol Biol (Noisy-le-grand). 2015; 61(5): 16-21.
22. Qi P, Wang L, Zhou B, Yao W, Xu S, Zhou Y, et al. Associations of miRNA polymorphisms and expression levels with breast cancer risk in the Chinese population. Genet Mol Res. 2015; 14(2): 6289-6296.
23. Miller SA, Dykes DD, Polesky HF. A simple salting out procedure for extracting DNA from human nucleated cells. Nucleic Acids Res. 1988; 16(3): 1215.
24. Kwok PY, Chen X. Detection of single nucleotide polymorphisms. Curr Issues Mol Biol. 2003; 5(2): 43-60.
25. Newton CR, Graham A, Heptinstall LE, Powell SJ, Summers C, Kalsheker N, et al. Analysis of any point mutation in DNA. The amplification refractory mutation system (ARMS). Nucleic Acids Res. 1989; 17(7): 2503-2516.
26. Altschul SF, Gish W, Miller W, Myers EW, Lipman DJ. Basic local alignment search tool. J Mol Biol. 1990; 215(3): 403-410.
27. Solé X, Guinó E, Valls J, Iniesta R, Moreno V. SNPStats: a web tool for the analysis of association studies. Bioinformatics. 2006; 22(15): 1928-1929.
28. Burnham KP, Anderson DR. Multimodel inference understanding AIC and BIC in model selection. Sociol Methods Res. 2004; 33(2): 261-304.
29. Mishra PJ, Mishra PJ, Banerjee D, Bertino JR. MiRSNPs or MiR-polymorphisms, new players in microRNA mediated regulation of the cell: Introducing microRNA pharmacogenomics. Cell Cycle. 2008; 7(7): 853-858.
30. Slaby O, Bienertova-Vasku J, Svoboda M, Vyzula R. Genetic polymorphisms and microRNAs: new direction in molecular epidemiology of solid cancer. J Cell Mol Med. 2012; 16(1): 8-21.
31. Vitale A, Tan H, Jin P. MicroRNAs, SNPs and cancer. Journal of Nucleic Acids Investigation. 2011; 2(1): e6.
32. Kim YD, Lee JY, Oh KM, Araki M, Araki K, Yamamura K, et al. NSrp70 is a novel nuclear speckle-related protein that modulates alternative pre-mRNA splicing in vivo. Nucleic Acids Res. 2011; 39(10): 4300-4314.
33. Kontorovich T, Levy A, Korostishevsky M, Nir U, Friedman E. Single nucleotide polymorphisms in miRNA binding sites and miRNA genes as breast/ovarian cancer risk modifiers in Jewish high-risk women. Int J Cancer. 2010; 127(3): 589-597.
34. Hu Y, Yu CY, Wang JL, Guan J, Chen HY, Fang JY. MicroRNA sequence polymorphisms and the risk of different types of cancer. Sci Rep. 2014; 4: 3648.
35. Zhang N, Huo Q, Wang X, Chen X, Long L, Jiang L, et al. A genetic variant in pre-miR-27a is associated with a reduced breast cancer risk in younger Chinese population. Gene. 2013; 529(1): 125-130.
36. Ye Y, Wang KK, Gu J, Yang H, Lin J, Ajani JA, et al. Genetic variations in microRNA-related genes are novel susceptibility loci for esophageal cancer risk. Cancer Prev Res (Phila). 2008; 1(6): 460-469.

Original Article

α-Lipoic Acid Ameliorates The Changes in Prooxidant-Antioxidant Balance in Liver and Brain Tissues of Propylthiouracil-Induced Hypothyroid Rats

Adile Merve Baki, Ph.D.[1], Abdurrahman Fatih Aydın, M.D.[1], Pervin Vural, M.D.[1]*, Vakur Olgaç, Ph.D.[2], Semra Doğru Abbasoğlu, Ph.D., M.D.[1], Müjdat Uysal, M.D.[1]

1. Department of Biochemistry, Istanbul Faculty of Medicine, Istanbul University, Istanbul, Turkey
2. Institute of Oncology, Department of Pathology, Istanbul University, Istanbul,Turkey

Corresponding Address: Department of Biochemistry, Istanbul Faculty of Medicine, Istanbul University, Istanbul, Turkey
Email: pervinvural@yahoo.com

Received: 12/July/2019, Accepted: 27/August/2019

Abstract

Objective: There are controversial data about the prooxidant-antioxidant balance in hypothyroidism. We aimed to investigate the effect of α-lipoic acid (ALA) on oxidative stress parameters in the liver and brain of propylthiouracil (PTU)-induced hypothyroid rats.

Materials and Methods: In this experimental study, PTU (500 mg/L) was given to rats in drinking water for 10 weeks. ALA (0.2% in diet) alone and together with thyroxine (T4, 20 µg/kg body weight, s.c) were given to hypothyroid rats in the last 5 weeks of the experimental period. The levels of reactive oxygen species, malondialdehyde, protein carbonyl, ferric reducing antioxidant power (FRAP) and glutathione (GSH) levels, superoxide dismutase, and GSH peroxidase activities were determined in the liver and brain of rats. Histopathological examinations were also performed.

Results: Prooxidant parameters were increased in the brain but not liver in hypothyroid rats. ALA treatment alone lowered enhanced brain oxidative stress in hypothyroid rats. Also, ALA was found to ameliorate the changes as a result of oxidative stress arising from T4 replacement therapy.

Conclusion: Our results indicate that ALA alone and together with T4 may be useful in reducing oxidative stress in thyroid dysfunctions.

Keywords: Brain, Hypothyroidism, Lipoic Acid, Liver, Prooxidant-Antioxidant Balance

Cell Journal(Yakhteh), Vol 22, Suppl 1, Autumn 2020, Pages: 117-124

Citation: Baki AM, Aydin AF, Vural P, Olgaç V, Doğru Abbasoğlu S, Uysal M. α-Lipoic acid ameliorates the changes in prooxidant-antioxidant balance in liver and brain tissues of propylthiouracil-induced hypothyroid rats. Cell J. 2020; 22 Suppl 1: 117-124. doi: 10.22074/cellj.2020.7049.

Introduction

Thyroid hormones (THs) (thyroxine and triiodothyronine, T4, and T3) are necessary for various physiological functions such as growth, development, and reproduction, and they regulate lipid and carbohydrate metabolism (1). They control the body's metabolism rate by regulating the rate of tissue oxygen consumption. Therefore, hyperthyroidism is characterized by accentuated oxidative metabolism and reactive oxygen species (ROS) production leading to tissue injury (2). Furthermore, THs control protein, vitamin, and antioxidant enzyme production, and breakdown (3, 4).

Hypothyroidism is a pathological condition related to the hypometabolic state, decreased mitochondrial oxygen utilization, low tissue proliferation, and reduction of ROS formation (5-7). Moreover, many experimental (8-10) and clinical (11, 12) studies showed that hypothyroidism is also related to increased ROS production and oxidative stress in several tissues, as observed in hyperthyroidism. However, the mechanisms are different in two clinical situations. Increased oxidative stress was attributed to the decrease in antioxidant levels and an increase in atherogenic lipids providing a substrate for lipid peroxidation in hypothyroidism (3, 13).

Several studies reported that antioxidant therapy may help prevent the oxidative stress seen in hypothyroidism and may provide support to the conventional L-thyroxine treatment. For this purpose, various antioxidants such as vitamin E, curcumin, and taurine have been used in hypothyroidism, and some favorable results have been obtained (8, 14, 15). α-Lipoic acid (ALA) is a mitochondrial coenzyme with significant antioxidant properties. ALA supports the regeneration of many antioxidants such as vitamin E and C, glutathione (GSH), and coenzyme Q10, repairs oxidized proteins, creates complexes with metal ions such as copper, manganese, and zinc, and prevents the formation of ROS (16). Indeed, it has been reported that ALA possesses beneficial effects on various conditions related to increased oxidative stress (16, 17).

In this study, we wanted to investigate prooxidant-antioxidant balance in liver and brain tissues before and after ALA and/or L-thyroxine (T4) replacement therapy changes in a 6-propyl-2-thiouracil (PTU)- induced hypothyroid rat model. Besides, the determinations of some biochemical indicators in serum and histopathological observations in examined tissues were performed.

Material and Methods

In this experimental study, Sprague-Dawley albino

male rats (weighing 250-350 g), purchased from the Institute of Experimental Medicine of Istanbul University, Turkey, were housed in ordinary metallic cages in a room with the temperature regulated at 21 ± 1˚C and light/dark cycles (12 hours). The experimental procedure met the guidelines of the Institutional Animal Care and Use Committee of Istanbul University (Project No. 2014/111). Used chemicals were obtained from Sigma (Sigma Chemical Co., St. Louis, MO, USA).

Animals were divided into six groups as control, ALA, PTU, PTU+ALA, PTU+T4, and PTU+T4+ALA; each group included 6 rats. Control group: rats were fed with a standard diet and drinking water ad libitum for 10 weeks.

ALA group: rats were fed initially with the standard diet for 5 weeks. For next 5 weeks, rats were fed with ALA (0.2%, w/w) supplemented diet. The utilization of ALA by rats was approximately equivalent to 100 mg/kg body weight/day. Tap water was given as drinking water in this group.

Other groups were fed standard diet and treated with PTU (500 mg/L, w/v) in drinking water for 5 weeks. After 5 weeks, the administration of PTU was continued for another 5-week period in these groups. Rats of PTU and PTU+T4 groups were fed standard diet, while rats of PTU+ALA and PTU+T4+ALA groups were fed with 0.2% (w/w) ALA containing diet for the last 5 weeks. Rats of PTU+T4 and PTU+T4+ALA groups were also treated with L-thyroxine (20 µg/kg/day, s.c.) in this period.

After 10 weeks of the experimental period, the blood samples were drawn by cardiac puncture under pentobarbital anesthesia (50 mg/kg, i.p.) following overnight fasting. Blood samples were centrifuged at 1500 x g for 10 min to obtain serum fraction. Liver and brain tissues were removed immediately after blood collection, rinsed with ice-cold saline and blotted with filter paper. Tissues were homogenized in ice-cold 0.15 M KCl (10%, w/v), and tissue homogenates were centrifuged at 600 x g for 10 minutes to remove crude fractions. In obtained supernatants, ROS, malondialdehyde (MDA), protein carbonyl (PC), ferric reducing antioxidant power (FRAP), and GSH determinations were performed. These samples were centrifuged at 10000 x g for 20 minutes to obtain the postmitochondrial fraction. This fraction was stored at -80˚C for the analysis of superoxide dismutase (SOD) and glutathione peroxidase (GSH-Px) activities.

Determinations in serum

Serum fT3 and fT4 were measured on the Elecsys autoanalyzer (Roche Diagnostics, Germany). Serum glucose, total cholesterol (TC), triglyceride (TG) and albumin levels, alanine aminotransferase (ALT) and aspartate aminotransferase (AST) activities were assayed on Cobas Integra 800 autoanalyzer (Roche Diagnostics, Germany).

Determinations of reactive oxygen species formation, lipid peroxidation, and protein oxidation products

Ultraspec 3000 spectrophotometer (Pharmacia Biotech, Biochrom Ltd. Cambridge, UK) was used for the spectrophotometrical measurements. ROS formation was assayed fluorometrically (18). After 30 minutes of the incubation period with 100 µM 2,7-dichlorodihydrofluorescein diacetate (DCFH-DA), the fluorescence of formed product was read on a fluorometer (Fluoroskan Ascent FL, Thermo Scientific Inc, USA) (excitation - 485 nm, emission - 538 nm). Results were expressed as relative fluorescence units (RFU). Lipid peroxidation was examined spectrophotometrically using the reaction between MDA and thiobarbituric acid at 535 nm (19). The MDA concentrations of samples were calculated using an extinction coefficient of 1.56×10^5 $M^{-1}cm^{-1}$. MDA levels were expressed as pmol MDA/mg protein. The oxidative protein damage (PC levels) was measured by the quantification of carbonyl groups based on their reaction with 2,4-dinitrophenylhydrazine (DNPH). Calculation of results was performed using a molar absorption coefficient of 22,000 $M^{-1}cm^{-1}$ at 360 nm and expressed as nmol carbonyl per mg protein (20).

Determinations of non-enzymatic and enzymatic antioxidants

Total antioxidant status was evaluated using FRAP assay (21). In this assay, a ferric- tripyridyltriazine (Fe^{3+}-TPTZ) complex is reduced to the ferrous form, which can be monitored by measuring the change in absorbance at 593 nm. GSH levels were measured with 5,5-dithiobis-(2-nitrobenzoate) at 412 nm (22). The SOD activity was assayed by its ability to increase the effect of riboflavin-sensitized photooxidation of o-dianisidine (23). GSH-Px activity (24) was assayed using cumene hydroperoxide as a substrate. Protein determination was performed using the bicinchoninic acid method (25).

Histopathologic evaluation

Liver tissues were fixed in 10% buffered formaldehyde, processed, and stained with hematoxylin and eosin (H&E) for histopathologic examination.

Statistical analyses

ANOVA (post hoc Tukey HSD) and Kruskal-Wallis (post hoc Mann-Whitney U) tests were used for statistical evaluation. A $P<0.05$ was considered to be statistically significant. All statistical analyses were performed with IBM SPSS Statistics for Windows (version 21, SPSS Inc., Chicago, IL, USA). The results were expressed as mean ± SD.

Results

Body weight, liver weight, and liver indices

Body and liver weights significantly decreased, while the liver index did not change in PTU and PTU+ALA groups. Giving of T4 to PTU-treated rats resulted in significant increases in body and liver weights and liver index as compared to the PTU group. These parameters remained unaltered in PTU+T4 rats due to ALA treatment (Table 1).

Table 1: Effects of ALA alone or together with T4 treatment on body and liver weights, liver index, serum glucose, TC, TG, albümin levels and ALT and AST activities of PTU administered rats

Parameters	Control	ALA	PTU	PTU+ALA	PTU+T4	PTU+T4+ALA
Body weight (g)	310.8 ± 38	319.5 ± 44.3	217.0 ± 9.32[a]	228.3 ± 6.28[a,b]	259.7 ± 24.5[a,b]	276.5 ± 18.1[b]
Liver weight (g)	7.94 ± 1.21	9.51 ± 1.90	5.32 ± 0.48[a]	5.31 ± 0.44[a]	7.36 ± 0.81[b]	8.43 ± 0.97[b]
Liver index*(%)	2.55 ± 0.16	2.95 ± 0.22[a]	2.45 ± 0.21	2.32 ± 0.14	2.84 ± 0.24[b]	3.04 ± 0.23[a,b]
Free T3 (pmol/L)	3.17 ± 0.40	3.56 ± 0.56	1.35 ± 0.30[a]	1.16 ± 0.13[a]	1.70 ± 0.16[a]	1.78 ± 0.15[a]
Free T4 (pmol/L)	26.3 ± 5.90	28.3 ± 5.76	1.75 ± 0.95[a]	0.98 ± 0.18[a]	48.1 ± 8.87[a,b]	43.6 ± 10.9[a,b]
Glucose (mg/dL)	139.0 ± 8.10	142.6 ± 11.8	103.6 ± 13.5[a]	102.0 ± 5.95[a]	129.6 ± 17.7[b]	133.6 ± 12.4[b]
TC (mg/dL)	56.1 ± 11.1	46.1 ± 6.68	80.7 ± 8.29[a]	79.3 ± 7.95[a]	58.0 ± 10.0[b]	49.1 ± 3.91[b]
TG (mg/dL)	48.6 ± 9.77	40.6 ± 14.3	28.1 ± 4.36[a]	29.3 ± 7.69[a]	28.1 ± 7.41[a]	18.5 ± 4.38[a]
Albumin (g/dL)	3.77 ± 0.28	3.69 ± 0.23	3.57 ± 0.21	3.60 ± 0.17	3.51 ± 0.21	3.68 ± 0.15
ALT (U/L)	44.6 ± 6.50	55.8 ± 16.7	62.8 ± 8.63	105.2 ± 21.2[a,b]	85.6 ± 36.3[a]	74.5 ± 17.1
AST (U/L)	117.0 ± 16.8	111.8 ± 16.9	118.5 ± 18.2	127.2 ± 21.3	180.0 ± 33.8[a,b]	145.1 ± 13.2[c]

Data are presentes as mean ± SD, n=6 each. ALA; α-lipoic acid, TC; Total cholesterol, TG; Triglyceride, ALT; Alanine aminotransferase, AST; Aspartate aminotransferase, PTU; Propylthiouracil, *; Liver weight×100/body weight, [a]; P<0.05 as compared with control, [b]; P<0.05 as compared with PTU group, and [c]; P<0.05 as compared with PTU+T4.

Serum thyroid function tests

PTU administration significantly decreased serum fT3 and fT4 levels. ALA treatment did not change the levels of fT3 and fT4 in hypothyroid rats. When PTU-treated rats were administered with T4, serum fT4 levels increased significantly, while fT3 unchanged as compared to the PTU group. ALA treatment did not change fT3 and fT4 levels in rats of the PTU+T4 group (Table 1).

Serum glucose, lipid profile parameters, and liver function analyses

Serum glucose and TG levels significantly decreased, TC levels significantly increased, while albumin levels, ALT, AST activities did not change in the PTU-treated group. ALA administration caused an increase in ALT activity in the PTU-treated group. However, other serum parameters did not alter. T4 administration to PTU-treated rats resulted in increased glucose levels and AST activity together with lowered TC levels, but TG and albumin levels and ALT activity remained unchanged. In the PTU+T4+ALA group, elevated serum AST activity was found to diminish as compared to the PTU+T4 group (Table 1).

Prooxidant and antioxidant status in the liver tissue

There were no changes in hepatic ROS formation, MDA, and PC levels in PTU-induced hypothyroid rats. ALA administration to PTU-treated rats (PTU+ALA) resulted in significant decreases in hepatic ROS formation, but MDA and PC levels did not alter when compared with the PTU group. Administration of T4 to the PTU-treated group resulted in significant increases in hepatic ROS formation (18.5%) and PC levels (63.7%) as compared to the PTU group. MDA levels were also increased (28.3%), but this increase was not significant. When ALA was administered to rats in the PTU+T4 group, hepatic ROS levels were found to decrease significantly. Hepatic MDA (21.9%) and PC (24.5%) levels were also decreased, but these decreases were not significant (Fig.1).

In PTU-treated rats, no changes were detected in hepatic FRAP and GSH levels, and SOD and GSH-Px activities when compared with control rats. These parameters did not change due to ALA treatment. T4 administration to the PTU-treated group resulted in significant decreases in hepatic GSH levels and SOD activity, but FRAP levels and GSH-Px activity did not

alter as compared to the PTU group. No changes were detected in FRAP levels, SOD and GSH-PX activities, but GSH levels increased in the liver of rats of the PTU+T4+ALA group as compared to the PTU+T4 group (Fig.2).

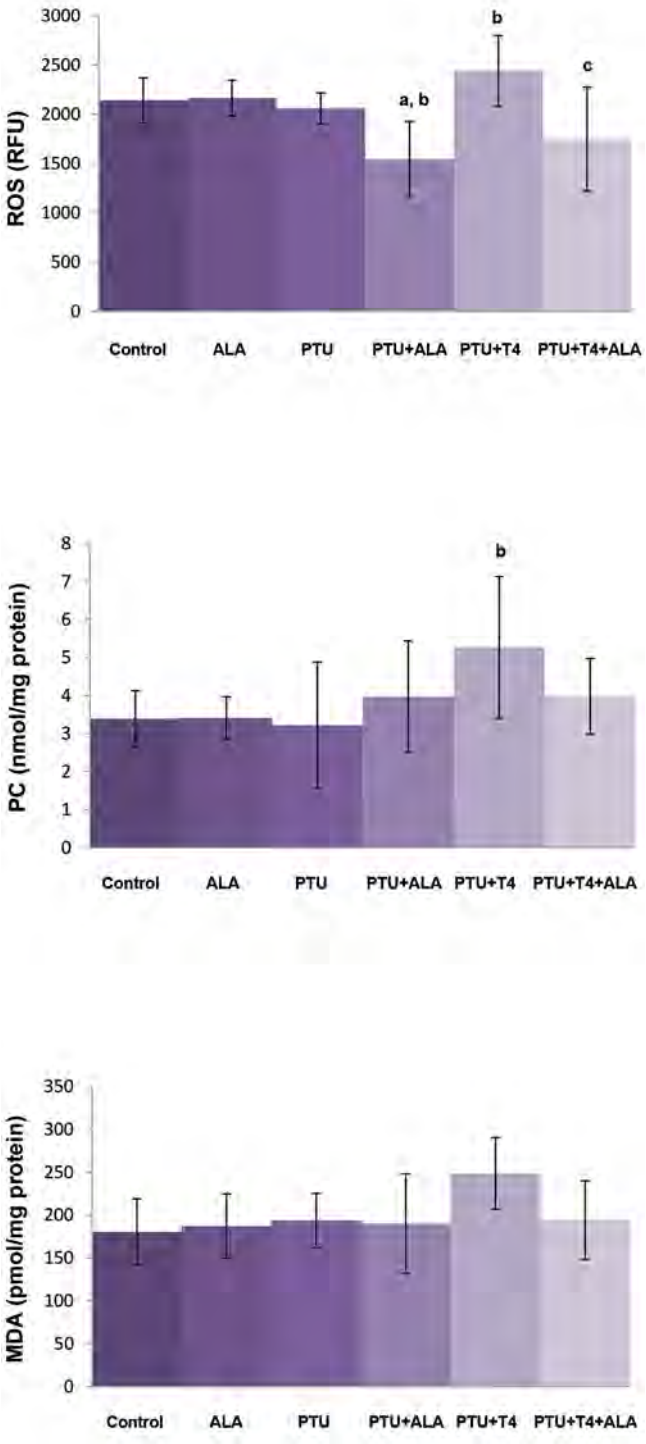

Fig.1: Effects of ALA alone or together with T4 treatment on liver ROS formation, MDA and PC levels in liver tissue of PTU administered rats (mean ± SD).
ALA; α-lipoic acid, ROS; Reactive oxygen species, MDA; Malondialdehyde, PC; Protein carbonyl, PTU; Propylthiouracil, [a]; P<0.05 compared with control, [b]; P<0.05 compared with PTU, and [c]; P<0.05 compared with PTU+T4.

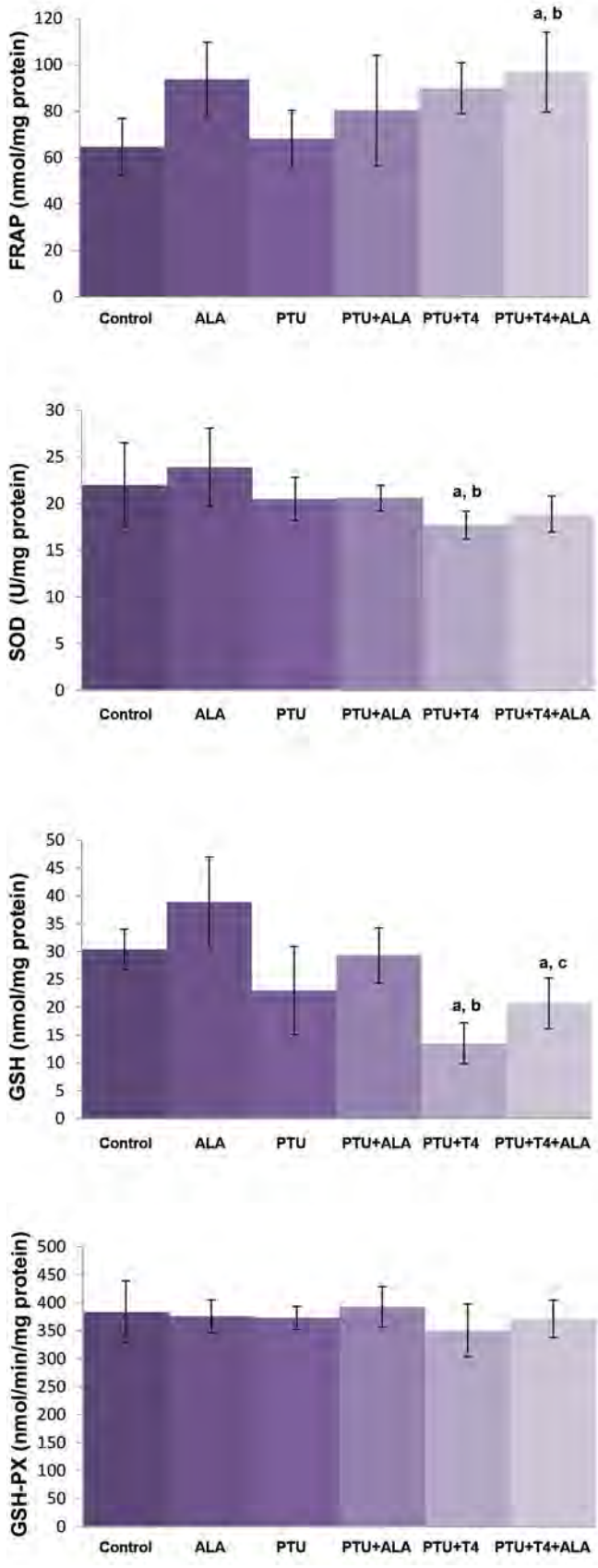

Fig.2: Effects of ALA alone or together with T4 treatment on liver FRAP and GSH levels, SOD and GSH-Px activities in liver tissue of PTU administered rats (mean ± SD).
ALA; α-lipoic acid, FRAP; Ferric reducing antioxidant, GSH; Glutathione, SOD; Superoxide dismutase, GSH-Px; Glutathione peroxidase, PTU; Propylthiouracil, [a]; P<0.05 compared with control, [b]; P<0.05 compared with PTU, and [c]; P<0.05 compared with PTU+T4.

Prooxidant and antioxidant status in the brain tissue

Brain ROS formation, MDA, and PC levels were found to increase in PTU-induced hypothyroid rats. ALA administration to the PTU-treated group (PTU+ALA) decreased MDA and PC levels, but not ROS formation as compared to the PTU group. Although T4 administration to PTU-treated rats caused further increases in brain MDA levels, ROS formation and PC levels did not alter as compared to PTU group. ALA administration to rats of PTU+T4 was found not to alter these parameters in the brain tissue (Fig.3).

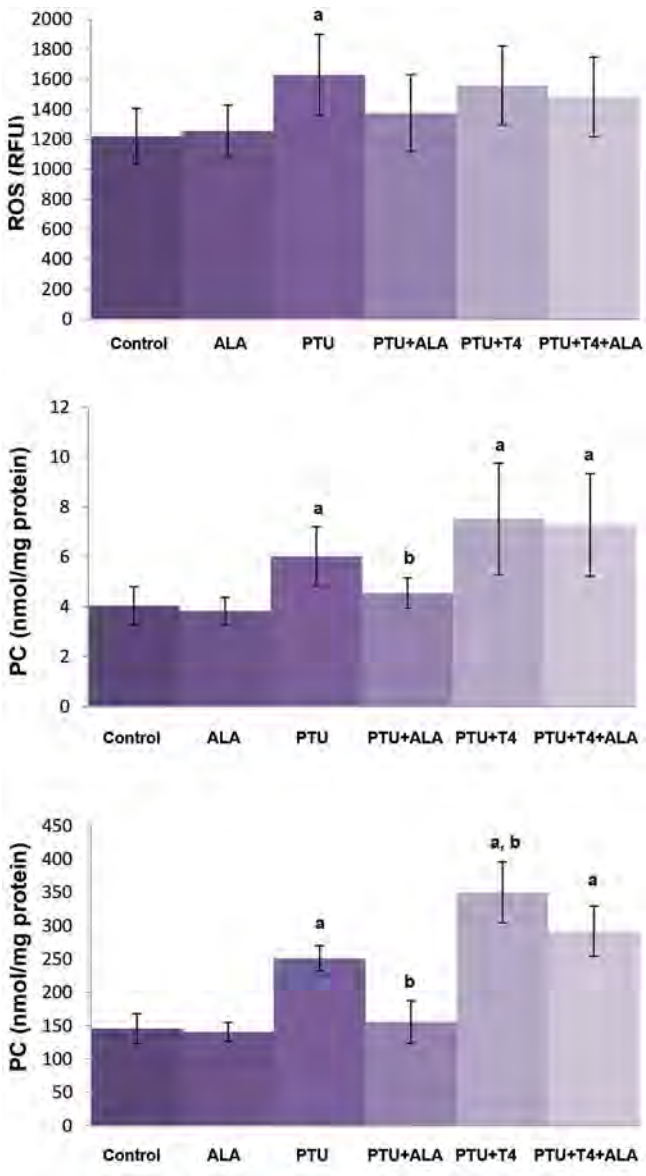

Fig.3: Effects of ALA alone or together with T4 treatment on brain ROS formation, MDA and PC levels in brain tissue of PTU administered rats (mean ± SD).
ALA; α-lipoic acid, ROS; Reactive oxygen species, MDA; Malondialdehyde, PC; Protein carbonyl, PTU; Propylthiouracil, [a]; P<0.05 compared with control, and [b]; P<0.05 compared with PTU.

GSH levels and SOD activity decreased, but FRAP levels and GSH-Px activity did not alter in the brain tissue of PTU-treated rats as compared to the cotrol group. Increases in GSH levels were detected, but FRAP levels, SOD, and GSH-Px activities remained unchanged in the PTU-treated group due to ALA treatment. In PTU+T4 group, brain GSH levels and SOD activity increased, but FRAP levels and GSH-Px activity did not alter as compared to the PTU group. There was no difference in antioxidant parameters between PTU+T4 and PTU+T4+ALA groups (Fig.4).

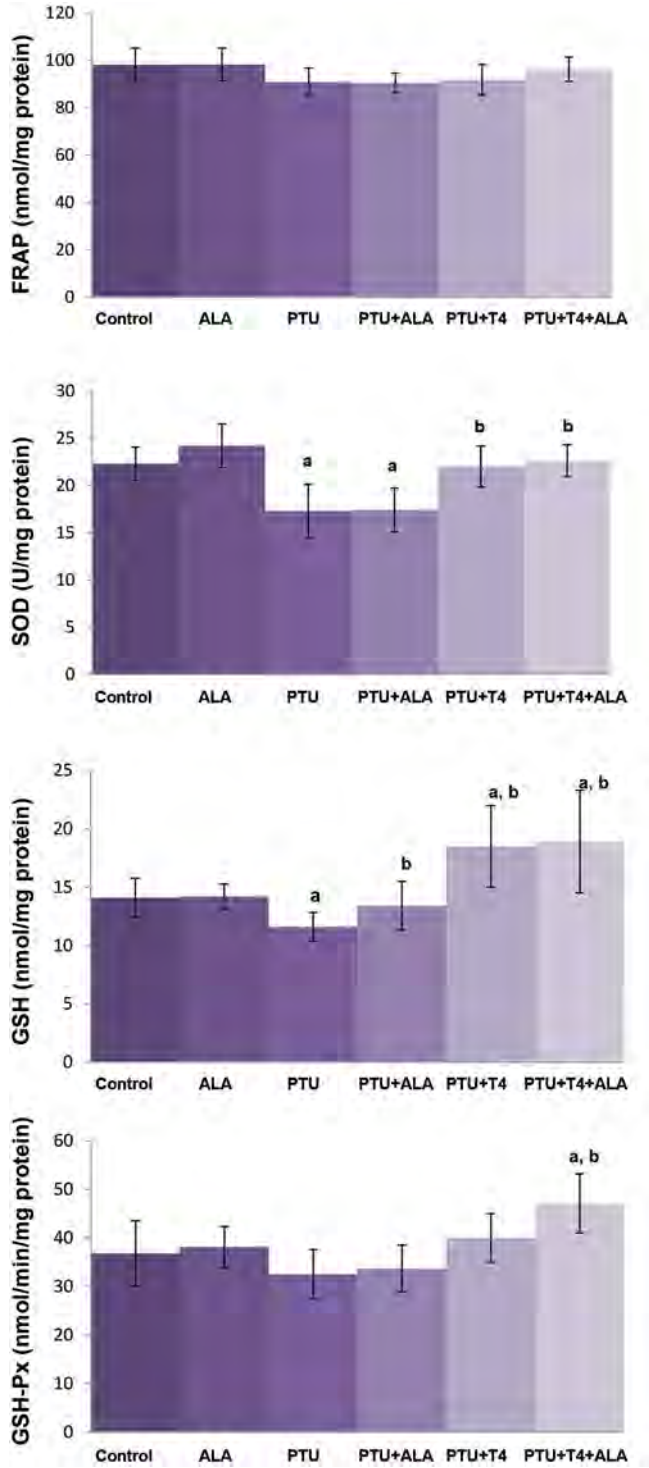

Fig.4: Effects of ALA alone or together with T4 treatment on brain FRAP and GSH levels, SOD and GSH-Px activities in liver tissue of PTU administered rats (mean ± SD).
ALA; α-lipoic acid, FRAP; Ferric reducing antioxidant, GSH; Glutathione, SOD; Superoxide dismutase, GSH-Px; Glutathione peroxidase, PTU; Propylthiouracil, [a]; P<0.05 compared with control, and [b]; P<0.05 compared with PTU.

Histopathological evaluation

The normal histological structure of the liver was observed in control and ALA groups. Hydropic degeneration around the central vein hepatocytes and congestion in sinusoids were observed in the PTU group. There were no changes in histopathological findings between PTU and PTU+ALA groups. However, necrotic and necrobiotic changes in hepatocytes and a decrease in sinusoid spaces were observed in the PTU+T4 group. Similar findings were also observed in the PTU+T4+ALA group, as observed in the PTU+T4 group (Fig.5). There was no difference in histopathological findings between the groups in brain tissue (data not shown).

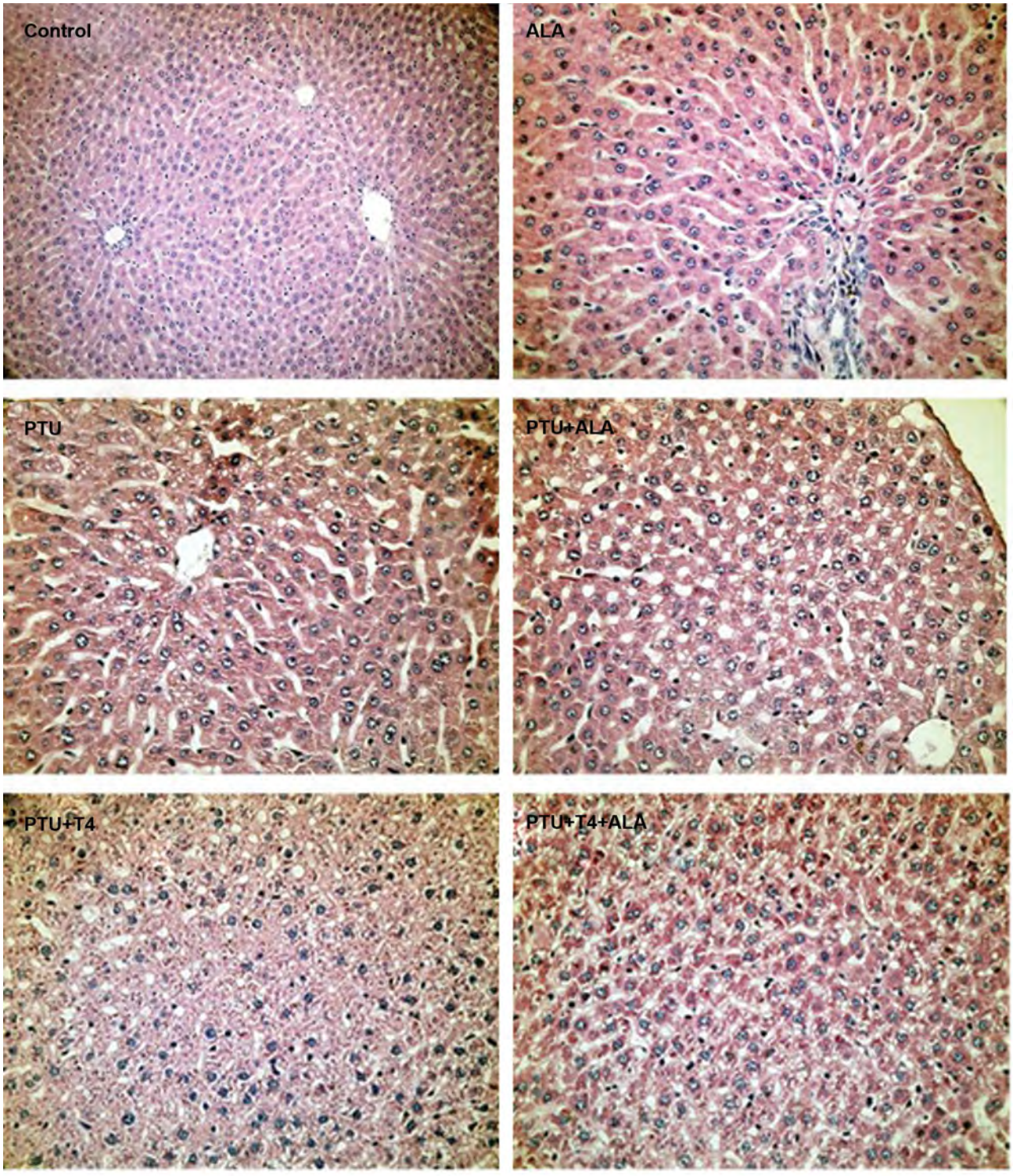

Fig.5: Histopathological findings in liver tissue of propylthiouracil (PTU)- administered rats treated by α-Lipoic acid (ALA) alone or together with T4 treatment (H&E, ×100).

Discussion

Various methods are being used to create an experimental hypothyroid state, including thyroidectomy or drug administration, which suppresses TH synthesis such as PTU/methimazole (4, 9, 15, 26). It has become a matter of debate that methimazole is toxic to various tissues, and whether the effects are due to hypothyroidism or the toxic effect of methimazole (9). Similar to other antithyroid drugs, PTU decreases the synthesis of THs by suppressing thyroid peroxidase and prevents the conversion of T4 into T3 in peripheral tissues (4, 8).

In our study, hypothyroidism was reached by giving of PTU (500 mg/L) to rats in drinking water (4, 8). Indeed, a significant reduction in the levels of fT3 and fT4 was found in the serum of PTU-treated rats. There was a decrease in serum glucose and TG levels and an increase in cholesterol levels in hypothyroid rats. Although there were no differences in ALT and AST activities reflecting liver function, histopathological examination revealed hydropic degeneration around the central vein and constriction of the sinusoids in the liver. These findings are in accordance with previous studies (10, 26).

Many studies examined oxidative stress parameters in various tissues such as the liver, heart, brain, and kidney obtained from hypothyroid animals, such as rodents. Data obtained in these studies are controversial. Various factors such as type of antithyroid drugs used to induce hypothyroidism, duration of administration, the severity of the developed hypothyroid condition, different sensitivity of tissues to oxidative stress, and differences in the methods used to investigate prooxidant-antioxidant balance may explain these contradictory results.

In rat models of hypothyroidism, hepatic lipid and protein oxidation were found to be increased (7, 9, 26), not altered (27), and even decreased (6). Conflicting results have also been reported for antioxidant parameters (9, 27). Similar findings are also obtained in hypothyroid patients (11, 12). In this study, we found that ROS, MDA, and PC levels, together with antioxidant parameters, did not alter in the liver of PTU-induced hypothyroid rats. These findings indicate that hepatic prooxidant-antioxidant balance remained unchanged in hypothyroid rats.

On the other hand, THs possess important effects on brain development, maturation, and function. For this reason, the examination of brain tissue in hypothyroidism has gained particular importance (4, 14, 15). In many studies, increased lipid and protein oxidation products and weakness of the antioxidant system were observed in the total brain or specific brain regions in adult rats (4, 14), although some conflicting results are available (15). In the current study, brain MDA and PC levels were also observed to increase, but GSH levels and SOD activity decreased in PTU-treated rats.

It has been suggested that antioxidant treatment may be useful in the prevention of oxidative stress seen in hypothyroid state and may provide support to conventional treatments. ALA is a disulfide compound naturally found in mitochondria. Exogenous supplemented ALA can act as a powerful antioxidant which alleviates oxidative stress (17, 28, 29). Because ALA is a small lipophilic molecule, it easily crosses biological membranes, thus reaching all cellular compartments. Several studies have also shown that ALA is useful in the amelioration of various oxidative stress-induced pathologies, including atherosclerosis, metabolic syndrome, diabetes mellitus (13, 28). It was reported that ALA administration decreases obesity, thereby restoring blood TH levels and alleviating oxidative stress in the rats with long-term obesity (28). However, there are only two studies about the effects of ALA in hypothyroidism (29, 30). In one clinical study, 300 mg/day ALA was administered for 3 weeks to patients with subclinical hypothyroidism, and an ameliorative effect on endothelial dysfunction together with decreased ROS was observed (29). Also, Tanaka et al. reported that in PTU-exposed offspring, postweaning exposure to ALA may be efficient for improving developmental hypothyroidism-induced disruptive neurogenesis (30).

In our study, ALA was given during the last 5 weeks of PTU treatment. The application of ALA did not affect the observed changes in serum THs levels and examined biochemical parameters except ALT activity in the PTU group. Interestingly, there was an increase in serum ALT levels. Some investigators have suggested that ALA may have a toxic effect on the liver, depending on the ALA dose and duration of administration. However, no difference in the hepatic histopathological findings was found in the PTU and PTU+ALA groups. In addition, although ROS levels were detected to decrease, there were no changes in other hepatic oxidative stress parameters between PTU and PTU+ALA groups. On the contrary, in brain tissue, ROS, MDA, and PC levels decreased, but GSH levels increased in PTU-treated rats due to ALA treatment. These results indicate that ALA treatment was effective to decrease PTU-induced oxidative stress in brain tissue.

In this study, T4 replacement therapy was also applied in hypothyroid rats. However, after this treatment, serum T4 levels were found to be significantly increased when compared with both PTU and control values. This hyperthyroid condition created a change in the direction of prooxidation in the prooxidant-antioxidant balance in the liver tissue, together with increased serum AST activity and hepatic histopathological changes such as necrosis and decrease in sinusoidal spaces were observed. However, when ALA was administered to rats in the PTU+T4 group, serum AST activity decreased, but there were no differences in hepatic histopathological findings. Also, ALA administration was observed to cause a tendency to ameliorate changes in hepatic prooxidant-antioxidant balance observed in PTU+T4 rats.

However, brain MDA levels increased, but ROS and PC levels did not alter in the brain tissue of rats of the PTU group due to T4 treatment. Additionally, significant increases in brain GSH levels and SOD activity were found in PTU+T4-treated rats. These increases may be an

adaptive increase against the oxidative stress observed in brain tissue, and this situation may be a preventive factor against the development of a more intense pro-oxidant environment in brain tissue in PTU-treated rats due to T4 administration. Indeed, no differences in histopathological findings were also observed in brain tissue. When ALA was administered to rats in the PTU+T4 group, oxidative stress parameters and histopathological findings were found to not change in brain tissue.

Conclusion

The susceptibility of liver and brain tissues to oxidative stress appears to be different, and the prooxidant state developed mainly in the brain of PTU-induced hypothyroid rats. ALA treatment has an improving effect on brain oxidative stress. In addition, ALA was also observed to be effective against hepatic oxidative stress arising from T4 replacement therapy. Our results indicate that ALA alone and together with T4 may be useful in reducing oxidative stress in thyroid dysfunctions.

Acknowledgements

The present work was financially supported by the Research Fund of Istanbul University (Project No: 52916). There is no conflict of interest.

Authors' Contributions

A.M.B., P.V., S.D.A., M.U.; Contributed to conception and design. A.M.B., A.F.A., P.V., V.O., M.U..; Contributed to all experimental work, data and statistical analysis, and interpretation of data. P.V., M.U.; Were responsible for overall supervision. P.V.; Drafted the manuscript, which was revised by A.F.A, S.D.A., M.U. All authors read and approved the final manuscript.

References

1. Mancini A, Di Segni C, Raimondo S, Olivieri G, Silvestrini A, Meucci E, et al. Thyroid hormones, oxidative stress, and inflammation. Mediators Inflamm. 2016; 2016: 6757154.
2. Khakisahneh S, Zhang XY, Nouri Z, Hao SY, Chi QS, Wang DH. Thyroid hormones mediate metabolic rate and oxidative, anti-oxidative balance at different temperatures in Mongolian gerbils (Meriones unguiculatus). Comp Biochem Physiol C Toxicol Pharmacol. 2019; 216: 101-109.
3. Mancini A, Raimondo S, Di Segni C, Persano M, Gadotti G, Silvestrini A, et al. Thyroid hormones and antioxidant systems: focus on oxidative stress in cardiovascular and pulmonary diseases. Int J Mol Sci. 2013; 14(12): 23893-23909.
4. Das K, Chainy GB. Thyroid hormone influences antioxidant defense system in adult rat brain. Neurochem Res. 2004; 29(9): 1755-1766.
5. Das K, Chainy GB. Modulation of rat liver mitochondrial antioxidant defence system by thyroid hormone. Biochim Biophys Acta. 2001; 1537(1): 1-13.
6. Brzezińska-Slebodzińska E. Influence of hypothyroidism on lipid peroxidation, erythrocyte resistance and antioxidant plasma properties in rabbits. Acta Vet Hung. 2003; 51(3): 343-351.
7. Petrović N, Cvijić G, Davidović V. The activity of antioxidant enzymes and the content of uncoupling protein-1 in the brown adipose tissue of hypothyroid rats: comparison with effects of iopanoic acid. Physiol Res. 2001; 50(3): 289-297.
8. Taş S, Dirican M, Sarandöl E, Serdar Z. The effect of taurine supplementation on oxidative stress in experimental hypothyroidism. Cell Biochem Funct. 2006; 24(2): 153-158.
9. Oktay S, Uslu L, Emekli N. Effects of altered thyroid states on oxidative stress parameters in rats. J Basic Clin Physiol Pharmacol. 2017; 28(2): 159-165.
10. Messarah M, Boumendjel A, Chouabia A, Klibet F, Abdennour C, Boulakoud MS, et al. Influence of thyroid dysfunction on liver lipid peroxidation and antioxidant status in experimental rats. Exp Toxicol Pathol. 2010; 62(3): 301-310.
11. Shevchenko S, Tsyganenko O, Petrenko S, Stetsyshyn R, Strakhovetskyi V. Dynamıcs of ındıces of oxıdatıve stress ın patıents wıth thyroıd gland surgery dependıng on ıts functıonal actıvıty. Georgian Med News. 2019; (287): 87-90.
12. Öztürk Ü, Vural P, Özderya A, Karadağ B, Doğru-Abbasoğlu S, Uysal M. Oxidative stress parameters in serum and low density lipoproteins of Hashimoto's thyroiditis patients with subclinical and overt hypothyroidism. Int Immunopharmacol. 2012; 14(4): 349-352.
13. Ichiki T. Thyroid hormone and atherosclerosis. Vascul Pharmacol. 2010; 52(3-4): 151-156.
14. Jena S, Anand C, Chainy GB, Dandapat J. Induction of oxidative stress and inhibition of superoxide dismutase expression in rat cerebral cortex and cerebellum by PTU-induced hypothyroidism and its reversal by curcumin. Neurol Sci. 2012; 33(4): 869-873.
15. Pan T, Zhong M, Zhong X, Zhang Y, Zhu D. Levothyroxine replacement therapy with vitamin E supplementation prevents oxidative stress and cognitive deficit in experimental hypothyroidism. Endocrine. 2013; 43(2): 434-439.
16. Rochette L, Ghibu S, Muresan A, Vergely C. Alpha-lipoic acid: molecular mechanisms and therapeutic potential in diabetes. Can J Physiol Pharmacol. 2015; 93(12): 1021-1027.
17. Cimolai MC, Vanasco V, Marchini T, Magnani ND, Evelson P, Alvarez S. α-Lipoic acid protects kidney from oxidative stress and mitochondrial dysfunction associated to inflammatory conditions. Food Funct. 2014; 5(12): 3143-3150.
18. Wang H, Joseph JA. Quantifying cellular oxidative stress by dichlorofluorescein assay using microplate reader. Free Radic Biol Med. 1999; 27(5-6): 612-616.
19. Buege JA, Aust SD. Microsomal lipid peroxidation. Methods Enzymol. 1978; 52: 302-310.
20. Reznick AZ, Packer L. Oxidative damage to proteins: spectrophotometric method for carbonyl assay. Methods Enzymol. 1994; 233: 357-363.
21. Benzie IFF, Strain JJ. The ferric reducing ability of plasma (FRAP) as a measure of "antioxidant power": the FRAP assay. Anal Biochem. 1996; 239(1): 70-76.
22. Beutler E, Duron O, Kelly BM. Improved method for determination of blood glutathione. J Lab Clin Med. 1963; 61: 882-888.
23. Mylroie AA, Collins H, Umbles C, Kyle J. Erythrocyte superoxide dismutase activity and other parameters of copper status in rats ingesting lead acetate. Toxicol Appl Pharmacol. 1986; 82(3): 512-520.
24. Paglia DE, Valentine WN. Studies on the quantitative and qualitative characterization of erythrocyte glutathione peroxidase. J Lab Clin Med. 1967; 70(1): 158-169.
25. Smith PK, Krohn RI, Hermanson GT, Mallia AK, Gartner FH, Provenzano MD, et al. Measurement of protein using bicinchoninic acid. Anal Biochem. 1985; 150(1): 76-85.
26. Santi A, Baldissareli J, Murussi CR, Dias GR, de Menezes CC, Zanini D, et al. Effects of quercetin on oxidative stress biomarkers in methimazole - induced hypothyroid rats. Exp Clin Endocrinol Diabetes. 2014; 122(9): 533-539.
27. Venditti P, Balestrieri M, Di Meo S, De Leo T. Effect of thyroid state on lipid peroxidation, antioxidant defences, and susceptibility to oxidative stress in rat tissues. J Endocrinol. 1997; 155(1): 151-157.
28. Cheserek MJ, Wu G, Li L, Li L, Karangwa E, Shi Y, et al. Cardioprotective effects of lipoic acid, quercetin and resveratrol on oxidative stress related to thyroid hormone alterations in long-term obesity. J Nutr Biochem. 2016; 33: 36-44.
29. G DX, J HP, H LS, L SZ. Alpha-lipoic acid improves endothelial dysfunction in patients with subclinical hypothyroidism. Exp Clin Endocrinol Diabetes. 2010; 118: 625-629.
30. Tanaka T, Masubuchi Y, Okada R, Nakajima K, Nakamura K, Masuda S, et al. Ameliorating effect of postweaning exposure to antioxidant on disruption of hippocampal neurogenesis induced by developmental hypothyroidism in rats. J Toxicol Sci. 2019; 44(5): 357-372.

Original Article

Nicotinamide Phosphoribosyltransferase Knockdown Leads to Lipid Accumulation in HepG2 Cells through The SIRT1-AMPK Pathway

Davod Ilbeigi, Ph.D.[1], Mitra Nourbakhsh, Ph.D.[2, 3*], Parvin Pasalar, Ph.D.[1, 3*], Reza Meshkani, Ph.D.[1], Hajar Shokri Afra, Ph.D.[1], Ghodratollah Panahi, Ph.D.[1], Mohammad Borji, Ph.D.[4], Roya Sharifi, Ph.D.[5]

1. Department of Biochemistry, School of Medicine, Tehran University of Medical Sciences, Tehran, Iran
2. Department of Biochemistry, School of Medicine, Iran University of Medical Sciences, Tehran, Iran
3. Metabolic Disorders Research Center, Endocrinology and Metabolism Molecular, Cellular Sciences Institute, Tehran University of Medical Sciences, Tehran, Iran
4. Department of Biochemistry, School of Medicine, Shiraz University of Medical Sciences, Shiraz, Iran
5. Department of Medical Laboratory Sciences, School of Allied Medical sciences, Iran University of Medical Sciences, Tehran, Iran

**Corresponding Addresses: P.O.Box: 1449614535, Department of Biochemistry , School of Medicine, Iran University of Medical Sciences, Tehran, Iran*
P.O.Box: 1417614418, Department of Biochemistry, School of Medicine, Tehran University of Medical Sciences, Tehran, Iran
Emails: nourbakhsh.m@iums.ac.ir, pasalar@sina.tums.ac.ir

Received: 16/June/2019, Accepted: 24/August/2019

Abstract

Objective: Nicotinamide phosphoribosyltransferase (NAMPT), which is responsible for biosynthesis of nicotinamide adenine dinucleotide (NAD), has a regulatory role in cellular metabolism and thus, might be implicated in non-alcoholic fatty liver disease (NAFLD). This study aimed to show how NAMPT down-regulation in liver cells influences lipid metabolism and sirtiun 1 (SIRT1), as the main NAD-dependent deacetylase enzyme.

Materials and Methods: In this experimental study, HepG2 cells were transfected with NAMPT siRNA and hepatic triglyceride (TG) content and SIRT1 deacetylase activity were measured by colorimetric and fluorometric methods, respectively. Gene expression of fatty acid synthase (FAS) and sterol regulatory element-binding protein-1c (SREBP-1c) was evaluated by real-time polymerase chain reaction (PCR). Total protein level and the phosphorylated form of acetyl-CoA carboxylase (ACC) and AMP-activated protein kinase (AMPK) were also investigated by western blotting.

Results: Knockdown of NAMPT significantly promoted the accumulation of TG in HepG2 cells, accompanied by a remarkable decline in SIRT1 deacetylase activity. A significant rise in the gene expression of two key lipogenic factors, FAS and SREBP-1c was also observed. These effects were also accompanied by decreased phosphorylation of ACC and AMPK. On the other hand, treatment of transfected cells with either NAD, as the SIRT1 substrate or resveratrol, as the SIRT1 activator reversed the outcomes.

Conclusion: These results demonstrated a protective role for NAMPT against NAFLD and its involvement in the regulation of de novo lipogenesis through the SIRT1/AMPK pathway.

Keywords: Acetyl-CoA Carboxylase, Nicotinamide Phosphoribosyltransferase, Non-Alcoholic Fatty Liver Disease, Sirtiun 1, Sterol Regulatory Element-Binding Protein-1c

Cell Journal(Yakhteh), Vol 22, Suppl 1, Autumn 2020, Pages: 125-132

Citation: Ilbeigi D, Nourbakhsh M, Pasalar P, Meshkani R, Shokri Afra H, Panahi Gh, Borji M, Sharifi R. Nicotinamide phosphoribosyltransferase knockdown leads to lipid accumulation in HepG2 cells through the SIRT1-AMPK pathway. Cell J. 2020; 22 Suppl 1: 125-132. doi: 10.22074/cellj.2020.7013.

Introduction

It is believed that non-alcoholic fatty liver disease (NAFLD) ranks among the most common liver disorders worldwide and shows increasing incidence within the past two decades (1). NAFLD ranges from simple fat deposition (steatosis) to non-alcoholic steatohepatitis (NASH), characterized by steatosis and inflammation. NASH can lead to fibrosis, cirrhosis, and eventually hepatocellular carcinoma (HCC) (2).

Liver has a central role in lipid metabolism, and synthesis, and import of free fatty acids, as well as storing and exporting lipids and lipoproteins. In NAFLD, lipid deposition is increased because of elevated hepatic lipogenesis and increased lipid uptake. At the same time, reduced lipid removal caused by decreased β-oxidation and diminished TG export, causes a positive lipid balance in the liver leading to the progression of NAFLD (3). Obesity and its metabolic consequences such as insulin resistance and type 2 diabetes mellitus, are the most prevalent risk factors for dyslipidemia and steatosis development (4).

Approximately 26% of liver lipids are produced by de novo lipogenesis and this pathway is induced in individuals with NAFLD (5). In this pathway, acetyl-CoA carboxylase (ACC) and fatty acid synthase (FAS) are major enzymes that are controlled by important transcription factors like carbohydrate response element-binding protein (ChREBP), sterol regulatory element-binding protein-1c (SREBP-1c) and liver X receptor (LXR) (6).

Nicotinamide phosphoribosyltransferase (NAMPT), an enzyme with two intra- and extracellular forms, is a 52 kDa protein expressed in approximately all tissues/cells (7). Extracellular NAMPT (eNAMPT), generally called visfatin, is secreted by visceral adipose tissue and functions as an adipokine and activates various cellular signaling pathways (8, 9). Intracellular form of the protein (iNAMPT) has an enzymatic activity and functions as the key

enzyme in NAD biosynthesis. NAD is an essential coenzyme in many metabolic reactions and has multiple roles in cellular metabolism (10). NAMPT catalyzes the synthesis of nicotinamide mononucleotide (NMN) from nicotinamide and 5-phosphoribosyl-pyrophosphate (PRPP) (11). Nicotinamide mononucleotide adenylyltransferase (NMNAT) turns NMN into NAD (12). Some enzymes use NAD as substrate for their catalytic reactions such as the sirtuin family of protein deacetylases (13); one of them is silent information regulator 1 (SIRT1) and its inhibition has been shown to be implicated in hepatic steatosis (14). SIRT1 controls the function of AMP-activated protein kinase (AMPK), which is a central enzyme in energy homeostasis and fatty acid metabolism (15, 16). ACC phosphorylation and activity are respectively increased and repressed by AMPK phosphorylation. The subsequent decline in the synthesis of malonyl-CoA causes up-regulation of fatty acid oxidation and suppression of fatty acid synthesis, which lead to decreased levels of hepatocyte lipids (17). Moreover, glucose-induced expression of FAS is impeded by AMPK activation that hampers fatty acid biosynthesis and leads to decreased TG levels (18).

SREBP-1c is one of the main transcription factors that induces the expressions of lipogenic genes such as *FAS, ACC* and glycerol-3-phosphate acyltransferase (*GPAT*), and can affect the production of fatty acids and TG. Thus, SREBP-1c plays a critical role in NAFLD (19). It was found that AMPK can phosphorylate SREBP-1c at Ser 372, suppress its translocation into the nucleus, and therefore repress the expression of its target genes (20). Increased expression of SIRT1 was shown to be a causative factor in SREBP-1c gene expression decline in obese mice (21).

Recent studies suggested that NAMPT is involved in lipid metabolism in the liver; however, its mechanism is still not clearly defined (19, 22). A recent study showed that inhibition of NAMPT by its chemical inhibitor, FK866, aggravated hepatic lipid accumulation and steatosis *in vivo* and *in vitro* (19). Additionally, it was reported that NAMPT is necessary for *de novo* lipid biosynthesis in prostate cancer (PCa) cells (22). NAMPT expression was also shown to be reduced in the serum and liver tissue of patients with NAFLD (23).

Given the regulatory role of SIRT1 and AMPK in fatty acid and lipid metabolism, NAMPT might be related to NAFLD by provision of NAD as the main SIRT1 substrate.

Some studies showed that circulating levels of eNAMPT/visfatin are elevated in NAFLD (24, 25). Conversely, downregulation of iNAMPT was recently reported in hepatic tissue of patients with NAFLD (23). Taken together, these studies point to the involvement of NAMPT in the pathogenesis of NAFLD; however, the associated molecular and metabolic mechanisms are not fully elucidated. In the current study, we inspected the effect of NAMPT knockdown on lipid accumulation, lipogenic factors, and SIRT1 activity in HepG2 cells.

Materials and Methods

This experimental study was approved by the Ethics Committee of Tehran University of Medical Sciences (IR.TUMS.REC1394.2182).

Cell culture and transfection

Human hepatoma cells (HepG2) were obtained and authenticated from Iranian Biological Resource Center (Tehran, Iran). All cell culture reagents were bought from Gibco (UK). HepG2 cells were kept at 37˚C in Dulbecco Modified Eagle medium (DMEM) containing fetal bovine serum (10%) and 100 µg/ml penicillin and streptomycin, in 5% CO_2. Cells were transfected using polyethyleneimine (PEI, Thermo, USA) as transfection reagent. Approximately, 5×10^5 cells were seeded in 2 ml of medium in 6-well plates for 24 hours, prior to transfection. Afterwards, the cells were incubated with serum-free medium for 6 hours and subsequently transfected with PEI alone (mock) or with either siRNA against NAMPT or its negative control (scrambled siRNA) from GenePharma (Shanghai, China). FAM-labeled control siRNA (GenePharma, Shanghai, China) was also used to monitor transfection efficiency. The siRNA was mixed with PEI at the nitrogen/phosphate (N/P) ratio of six (26). Cells were incubated with the transfection complex for 24 hours. Afterwards, the transfection medium was substituted with fresh growth medium and the incubation was continued for another 24 hours. Cells with no treatment were considered control. Knockdown of NAMPT was confirmed by real-time polymerase chain reaction (PCR) and western blotting. Resveratrol was also used to investigate the involvement of SIRT1. For this purpose, two different concentrations of resveratrol (20 and 50 µM) were examined according to the cytotoxicity test done by MTT (27, 28); eventually, because of better cell viability, 20 µM concentration was chosen for the experiments. The transfected cells were treated with resveratrol (20 µM) or NAD (1 mM) separately in fresh medium for 24 hours.

Detection of SIRT1 deacetylase activity

To investigate the relationship between NAMPT knockdown and changes in SIRT1 activity, the effect of NAMPT knockdown by siRNA on SIRT1 deacetylase activity was assessed after transfection for 48 hours using an SIRT1 Activity Assay Kit (Fluorometric, Abcam, Cambridge, UK) following the manufacturer's protocol. Briefly, a mixture including fluoro-substrate peptides and NAD as SIRT1 substrates was mixed with cell extracts or recombinant SIRT1 as the positive control.

Then, a microplate reader was used to measure fluorescence for 60 minutes with 1-2 minute intervals at excitation and emission wavelength of 350 and 460 nm, respectively. Fluorescence intensity relative to untreated control cells was used to express the enzyme activity.

Oil red O staining

About 5×10^5 HepG2 cells were seeded in 2 ml of medium in 6-well plates for 24 hours and transfected as described above. After transfection, cells were washed 3 times with phosphate buffered saline (PBS, Sigma Aldrich, Germany) and fixed

with 4% formaldehyde for 1 hour. Oil Red-O staining solution (0.5% in isopropanol) was added and incubated for 15 minutes at room temperature. Finally, the cells were washed 3 times with PBS. The cells were photographed under light microscopy. Isopropanol was added to the stained lipid droplets and the absorbance was measured at 492 nm.

Intracellular triglyceride measurement

Cells were harvested 48 hours after transfection and the intracellular TG content was measured. Pellets of cells were homogenized in 1 ml of 5% NP-40 solution. Then, slow heating was applied to the mixture to 80-100˚C in a water bath for 5 minutes; afterward, the mixture was let to cool down to room temperature. Then, it was centrifuged for 2 minutes at top speed for eliminating the insoluble materials. Next, a commercial kit (Abcam, UK) was applied to determine TG content of the resulting solution. The concentration of total protein was quantified by bicinchoninic acid (BCA) method by applying Pierce protein assay kit (Thermo, USA), and TG levels were presented as µg of lipid/mg of protein.

Real-time polymerase chain reaction

RNA extraction kit (GeneAll, South Korea) was used for total RNA isolation. Reverse transcription reaction was performed using kit for cDNA synthesis (Thermo Fisher Scientific, Waltham, USA). StepOnePlus real-time PCR System (Applied Biosystems, USA) was applied using SYBR Green PCR Master Mix (Ampliqon, Denmark) to amplify the resulting cDNA. Relative gene expression was analyzed by ΔΔCt method and *β-actin* was used as the normalizer (29). The primer sequences are presented in Table 1.

Table 1: The sequences of the used primers

Primers target	Primer sequence (5´-3´)
NAMPT	F: GGTTCTTGGTGGAGGTTTGCTAC
	R: GAAGACGTTAATCCCAAGGCC
SREBP-1c	F: CACCGAGAGCAGAGATGGC
	R: AAGGAGACGAGCACCAACAG
FAS	F: GAGGAAGGAGGGTGTGTTT
	R: CGGGGATAGAGGTGCTGA
β-actin	F: TCCTTCCTGGGCATGGAGT
	R: ACTGTGTTGGCGTACAGGTC

Western blot analysis

After transfection for 48 hours, cells were lysed by radio-immunoprecipitation assay (RIPA) buffer containing phenylmethylsulfonyl fluoride (PMSF) as the protease inhibitor. The concentration of the extracted protein was assessed using the BCA method. Electrophoresis was performed on 10% sodium dodecyl sulfate (SDS) polyacrylamide gel to separate equal amounts of total proteins; then, they were transferred into polyvinylidene difluoride (PVDF) membranes. Subsequently, blocking was carried out by incubation of membranes for 3 hours at room temperature in tris-buffered saline containing 5% skim milk and 0.1% tween-20 (TBST). Afterward, the membranes were incubated overnight at 4˚C, with rabbit primary antibodies (Cell Signaling Technology, USA) against NAMPT, phospho-AMPK (Thr172), total-AMPK, phosho-ACC (Ser 79), total -ACC, and GAPDH as the loading control at the dilution of 1:1000. Horseradish peroxidase-conjugated anti-rabbit antibody (Cell Signaling Technology, Danvers, USA) at 1:5000 dilution, was used as the secondary antibody. The protein bands were visualized by exposing them to X-ray film after reaction with enhanced chemiluminescence (ECL) detection reagent. Densitometric analysis of the resulting bands was performed by ImageJ software (v1.52, NIH). In order to perform the blotting with different antibodies, the membranes were stripped, re-probed and visualized after blocking and incubating with the primary and secondary antibodies.

Statistical analyses

Data are shown as mean ± SD of at least three separate experiments. One-way analysis of variance (ANOVA) together with Dunnett's multiple comparison post-hoc test was used to evaluate significant differences among groups. GraphPad Prism software (version 5.04., USA) was applied for statistical analysis. A $P<0.05$ was considered statistically significant.

Results

Confirmation of transfection

Transfection efficiency was evaluated by FAM-siRNA under a fluorescence microscope and the results were indicative of efficient transfection (Fig.1A). In addition, knockdown of NAMPT was confirmed by real-time PCR as well as western blotting. Transfection with siRNA significantly downregulated both the mRNA and protein levels of NAMPT (by about 58 and 55 %, respectively), compared to the control ($P<0.001$, Fig.1B, C).

Knockdown of NAMPT reduces SIRT1 activity

Since NAMPT provides the substrate for SIRT1 activity, we first tested the hypothesis that knockdown of NAMPT modulates SIRT1 deacetylase activity. As shown in Figure 2, when cells were transfected with siRNA, SIRT1 deacetylation activity was significantly reduced compared to the untreated control cells. This inhibition was removed when excessive amounts of NAD were provided, confirming that the reduction of SIRT1 activity was due to the loss of NAD production by NAMPT.

Resveratrol, which is a well-characterized activator of SIRT1, also significantly reversed the effect of NAMPT knockdown, further confirming that the reduced SIRT1 activity was due to the down-regulation of NAMPT.

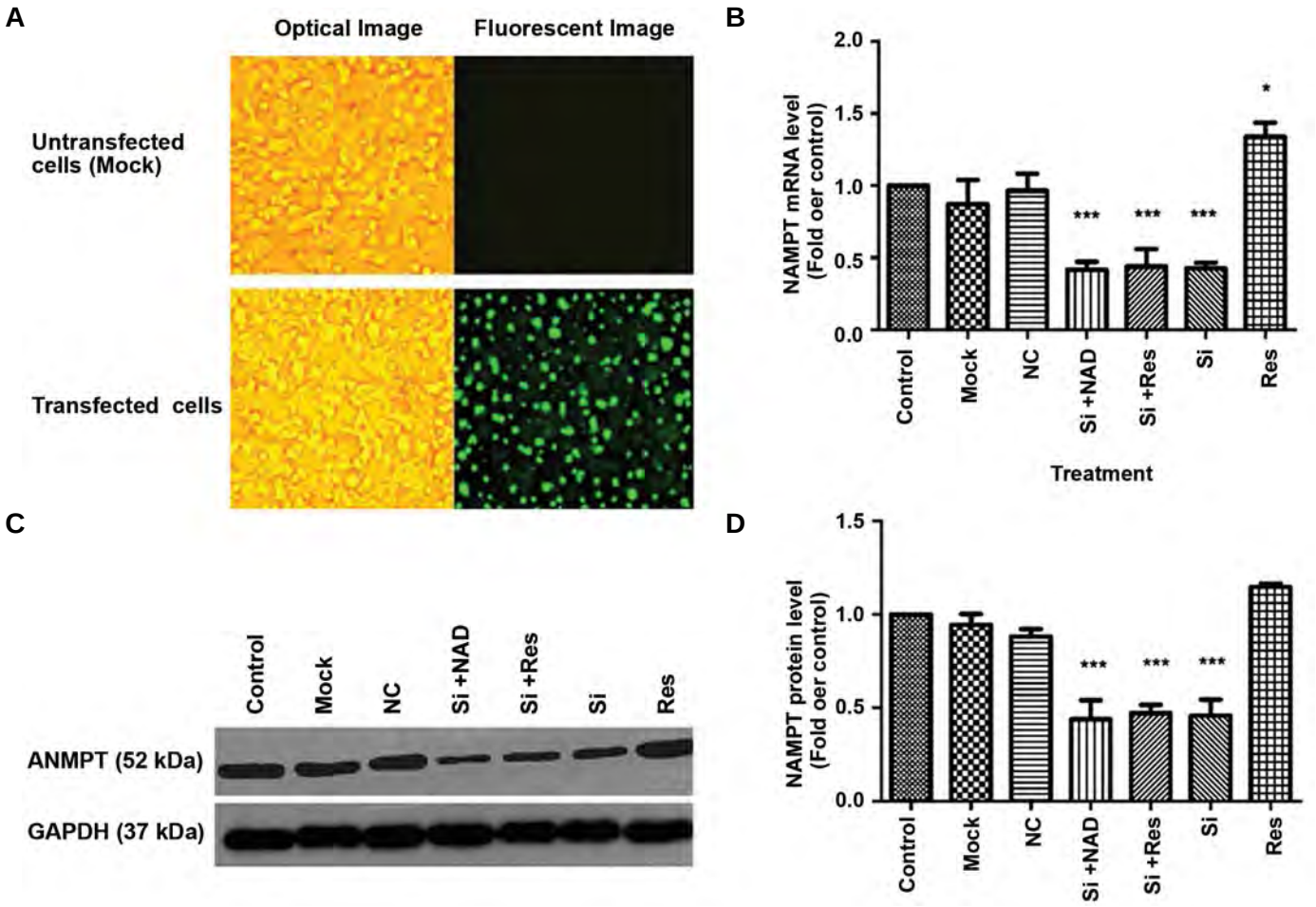

Fig.1: Transfection of HepG2 cells with NAMPT siRNA. **A.** Transfection efficiency was tested by FAM-siRNA under a fluorescence microscope (right panel) compared to the image under the optical microscope (left panel) (scale bar: 50 µm). **B.** Decreased expression of NAMPT mRNA measured by real-time PCR. **C.** Protein levels evaluated by western blotting compared to untreated control cells, after transfection with siRNA (Si), and **D.** A representative blotting image. Transfected cells were also treated with NAD (1 mM) and resveratrol (Res) (20 µM). A representative
blotting image is shown and the data represent the mean ± SD. NAMPT; Nicotinamide phosphoribosyltransferase, PCR; Polymerase chain reaction, NAD; Nicotinamide adenine dinucleotide, *; P<0.05, ***; P<0.001 versus the control, and NC; Negative control (scrambled siRNA).

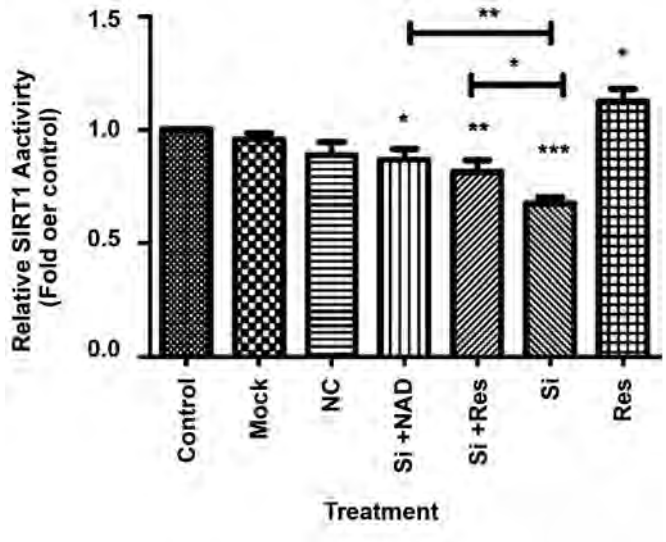

Fig.2: Reduced SIRT1 activity in HepG2 cells after transfection with NAMPT siRNA (Si). Resveratrol (Res) or NAD ameliorated this effect and increased SIRT1 activity. The results are mean ± SD of at least 3 independent experiments. NAMPT; Nicotinamide phosphoribosyltransferase, NAD; Nicotinamide adenine dinucleotide, *; P<0.05, **; P<0.01, ***; P<0.001 versus the control, and NC; Negative control (scrambled siRNA).

NAMPT affects hepatic lipid accumulation via SIRT1

In order to determine whether NAMPT is involved in hepatic steatosis, Oil Red O staining was performed. The results indicated that lipid content of HepG2 cells was significantly increased after NAMPT knockdown (Fig.3A, B). In addition, intracellular TG levels were measured following knockdown of NAMPT in HepG2 cells. As it is shown in Figure 3C, NAMPT knockdown caused a remarkable rise in the TG content of cells compared to the control cells. Elevation of TG levels by NAMPT knockdown was notably reversed by addition of NAD, confirming the effect of NAMPT inhibition on hepatic steatosis. Interestingly, treatment with resveratrol significantly reduced the TG accumulation that indicated the involvement of SIRT1 in the effect of NAMPT on lipid metabolism in HepG2 cells.

NAMPT and SIRT1 cooperate in the regulation of lipid metabolism in liver cells through modulation of FAS and SREBP-1c

To determine the participation of NAMPT in the gene expression of lipogenic factors in hepatocytes, HepG2 cells

were transfected with NAMPT siRNA and the effect of NAMPT silencing was evaluated on *FAS* and *SREBP-1* mRNA expression. We showed that suppression of NAMPT was followed by a significant enhancement of *FAS* and *SREBP-1* expression at mRNA levels. In comparison to the untreated control cells, we achieved 28 and 30% elevation in *SREBP-1* and *FAS* mRNA levels, respectively (Fig.4A, B). The negative control siRNA had no influence on the expression of these genes. On the other hand, treatment with resveratrol or NAD reversed these effects and significantly decreased the *SREBP-1c* and *FAS* mRNA levels compared to the cells transfected with NAMPT siRNA.

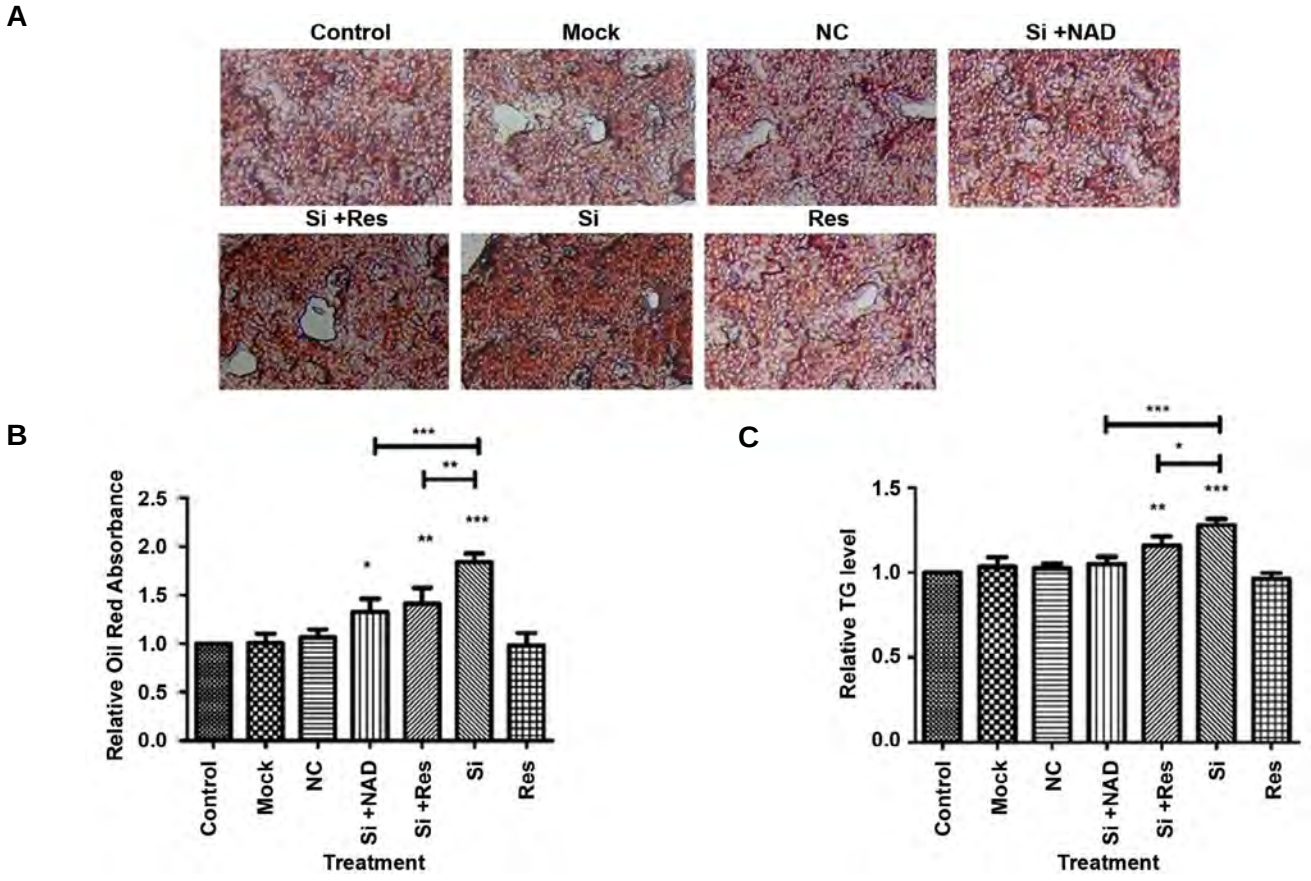

Fig.3: Knockdown of NAMPT with siRNA (Si) promoted TG accumulation in HepG2 cells. **A.** Microscopic images of the intracellular lipid content after Oil Red O staining (scale bar: 50 µm). **B.** Relative intracellular lipid content which was measured spectrophotometrically at 492 nm after solubilization of Oil Red O stain. **C.** Intracellular TG level determined by enzymatic method. The data represent the mean ± SD of at least three independent experiments. NAMPT; Nicotinamide phosphoribosyltransferase, TG; triglyceride, NAD; Nicotinamide adenine dinucleotide, *; P<0.05, **; P<0.01, ***; P<0.001 versus the untreated control, and NC; Negative control (scrambled siRNA).

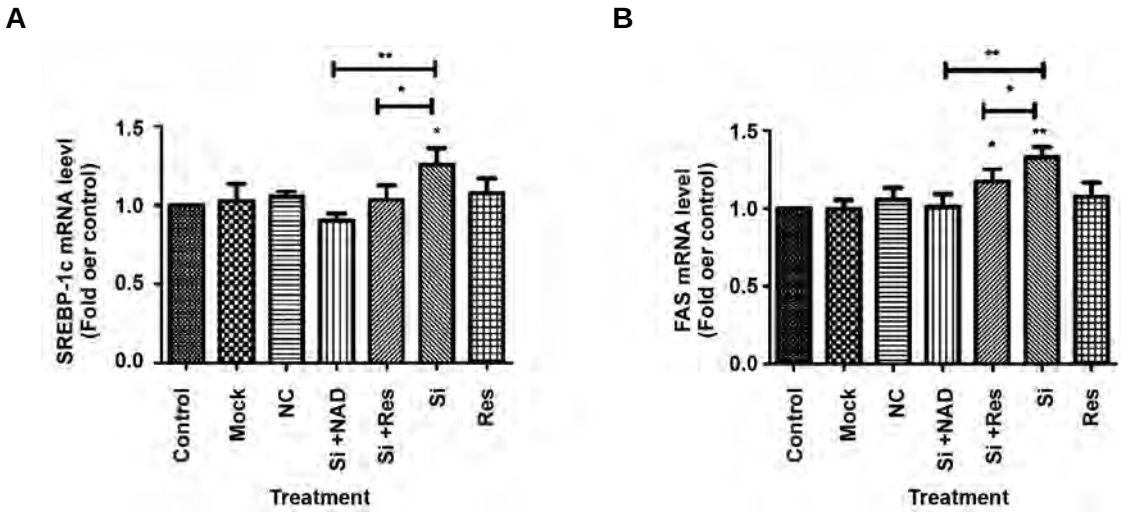

Fig.4: Knockdown of NAMPT with siRNA (Si) in HepG2 cells enhanced the expression of genes involved in lipogenesis. **A.** mRNA levels of *SREBP-1*, **B.** mRNA levels of *FAS*, after knockdown of NAMPT. The results are mean ± SD of at least three independent experiments. NAMPT; Nicotinamide phosphoribosyltransferase, NAD; Nicotinamide adenine dinucleotide, *; P<0.05, **; P<0.01 compared to untreated control, and NC; Negative control (scrambled siRNA).

Down-regulation of NAMPT affects phosphorylation of ACC and AMPK via SIRT1

To characterize whether NAMPT takes part in regulating lipid metabolism in the liver, we assessed the influence of NAMPT knockdown on AMPK and ACC as the regulatory enzymes in lipogenesis. As shown in Figure 5, down-regulation of NAMPT by siRNA caused a significant decline in the phosphorylation levels of AMPK at Thr172 and ACC at Ser 79, by 42 and 32%, respectively, compared to the control cells, while the total levels of both ACC and AMPK protein were not changed. Conversely, treatment of the transfected cells with resveratrol or NAD significantly reversed the effect of NAMPT knockdown, suggesting the requirement of NAD for AMPK phosphorylation and the involvement of SIRT1 in the activation of AMPK and inhibition of ACC.

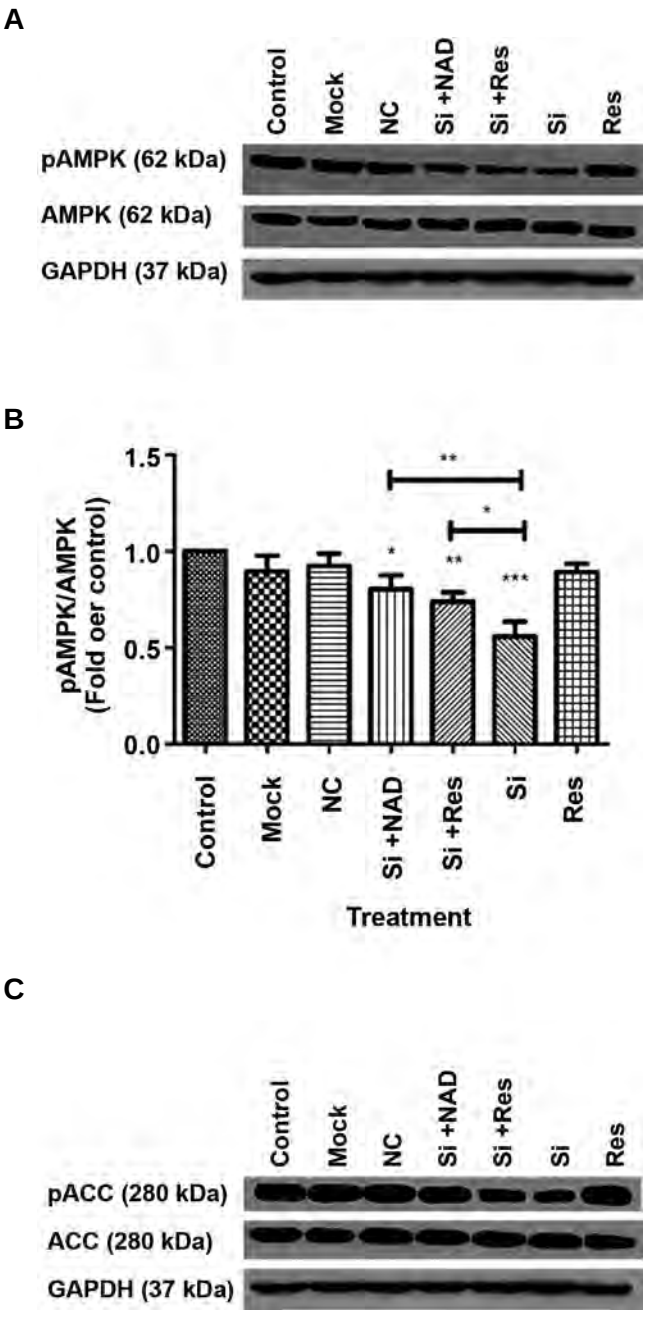

Fig.5: Evaluation of the effect of NAMPT knockdown with siRNA (Si) on AMPK and ACC phosphorylation in HepG2 cells by Western blotting followed by densitometric analysis of the resulting bands. **A.** A representative blotting image for pAMPK and total-AMPK. **B.** quantitative analysis of the ratio of pAMPKα to total-AMPKα. **C.** A representative blotting image for pACC and total-ACC. **D.** Quantitative analysis of the ratio of pACC to total-ACC. The levels of protein were normalized to GAPDH. The data are presented as mean ± SD of at least 3 separate experiments. *; P<0.05, **; P<0.01, ***; P<0.001 versus the untreated control, and NC; Negative control (scrambled siRNA).

Discussion

NAFLD which is considered to be among the most prevalent liver disorders, is defined by the extent of lipid accumulation in liver (30). It is believed that dysregulation of lipid synthesis ranks among the major reasons causing abnormal lipid accumulation in the liver (31).

Recent studies established the involvement of NAMPT in the regulation of lipid metabolism (22, 32). In this research, we examined the effect of NAMPT knockdown by siRNA on TG accumulation, SIRT1 activity, and lipogenic factors in HepG2 liver cells. The current study presents the first direct evidence that NAMPT influences lipid metabolism in HepG2 cells and modulates TG accumulation through SIRT1/AMPK pathway.

One of the main findings of this study was that NAMPT knockdown resulted in lipid accumulation in HepG2 cells. Consistently, Wang et al. (19) and Zhou et al. (33) showed that inhibition of NAMPT aggravated hepatic lipid accumulation and steatosis. Additionally, it was reported that NAMPT is necessary for de novo lipid biosynthesis in cancer (22). These results together with our findings indicate that down-regulation of NAMPT might be an essential element contributing to the pathogenesis of NAFLD. The decreased expression of NAMPT in the hepatic tissue of animals kept on high fat diet as well as its decline in HepG2 cells treated with oleic acid is also suggestive of the role of NAMPT in controlling hepatic lipid metabolism (19, 33). NAMPT was also shown to be reduced in the liver tissue of patients with NAFLD, further confirming the relationship between NAMPT

and hepatic steatosis (23). NAMPT positively regulates SIRT1 activity through the enzymatic synthesis of NAD (19). Furthermore, SIRT1 was shown to be protective against hepatic steatosis (15). The levels of SIRT1 are generally reduced in patients with NAFLD (34). On the other hand, overexpression of SIRT1 prevents high glucose-induced lipid pile-up in HepG2 cells (15). Here we showed that NAMPT knockdown decreased NAD-dependent deacetylase activity of SIRT1, leading to increased TG accumulation in HepG2. Supplementation of cells with NAD compensated the deleterious effect of NAMPT inhibition, pointing out the importance of NAD provision by NAMPT for the function of SIRT1.

Consistent with our results, it was reported that by reestablishing SIRT1 activity and promoting the mitochondrial effectiveness through NAD supplementation, the fatty liver is ameliorated in mice (35, 36). Furthermore, Zhou et al. (33) confirmed that the age-related NAD deficit intensified vulnerability to NAFLD and contributed to diet-induced steatohepatitis.

We also showed that treatment of transfected cells with resveratrol, a well-known and potent SIRT1 activator (37), reversed TG accumulation, confirming the involvement of SIRT1 in the effect of NAMPT on liver cells. Consistently, it was reported that treatment of 3T3-L1 adipocytes with resveratrol decreases TG accumulation and increases SIRT1 gene and protein expression (38).

Another finding of the current study was that NAMPT influenced the phosphorylation of ACC and AMPK. The phosphorylation and subsequent stimulation of AMPK lead to inhibition of ACC through phosphorylation and shift the metabolic pathways from lipogenesis to lipid oxidation. Thus, increased TG accumulation following NAMPT down-regulation, can be attributed to reduced AMPK and increased ACC activities caused by the decline in SIRT1 function.

The mRNA expression of *FAS* and *SREBP-1*, as major transcription factors in lipid metabolism, were also increased in HepG2 cells following NAMPT knockdown, an effect that was attenuated after treatment with NAD. Therefore, increased gene expression of *SREBP-1* as well as *FAS* might serve as another mechanism linking NAMPT to hepatic steatosis. In agreement with our results, Wang et al. (19) showed that NAMPT overexpression caused a dramatic decline in lipid content and decreased the expressions of genes that are responsible for the regulation of lipogenesis such as SREBP-1c, and its downstream targets including FAS and ACC.

We found that the effects of NAMPT on the above lipogenic factors were reversed by resveratrol. It was reported that SIRT1 is able to suppress the expression of FAS via activating AMPK (15). SIRT1 also downregulates hepatic SREBP-1c activity by deacetylation (21). Thus, it is suggested that the modulation of FAS and SREBP-1c by NAMPT may also occur through SIRT1.

Altogether, these results suggest a protective role for NAMPT against NAFLD. Our findings are consistent with the previous observations that serum NAMPT had a significant negative correlation with the hepatic de novo lipogenesis and liver mitochondrial function (39, 40).

Conclusion

These data demonstrate that down-regulation of NAMPT increases hepatic lipid accumulation through modulation of SIRT1/AMPK pathway, leading to increased expression of FAS and SREBP-1c as well as reduced phosphorylation of ACC. Thus, NAMPT might be considered to be central and upstream to pathogenesis of NAFLD and regarded as a therapeutic strategy for this disorder.

Acknowledgements

Tehran University of Medical Sciences and Health Services provided this study with financial support (grant number 95-03-10-30917). The authors declare no conflict of interest.

Authors' Contributions

D.I.; Carried out all experiments and drafted the manuscript. M.N.; Designed and supervised the project and critically revised the manuscript. P.P.; Provided the grant and supervised the conduction of the study. R.M.; Consulted and advised the project and contributed in revising the manuscript. H.S.A., G.P.; Contributed in the analysis of data. M.B., R.S.; Contributed in the conduction of transfection part of the experiments. All authors read and approved the final manuscript.

References

1. Younossi ZM, Stepanova M, Afendy M, Fang Y, Younossi Y, Mir H, et al. Changes in the prevalence of the most common causes of chronic liver diseases in the United States from 1988 to 2008. Clin Gastroenterol Hepatol. 2011; 9(6): 524-530. e521.
2. Perumpail BJ, Khan MA, Yoo ER, Cholankeril G, Kim D, Ahmed A. Clinical epidemiology and disease burden of nonalcoholic fatty liver disease. World J Gastroenterol. 2017; 23(47): 8263-8276.
3. Van Herpen NA, Schrauwen-Hinderling VB. Lipid accumulation in non-adipose tissue and lipotoxicity. Physiol Behav. 2008; 94(2): 231-241.
4. Dixon JB, Bhathal PS, O'brien PE. Nonalcoholic fatty liver disease: predictors of nonalcoholic steatohepatitis and liver fibrosis in the severely obese. Gastroenterology. 2001; 121(1): 91-100.
5. Lee JJ, Lambert JE, Hovhannisyan Y, Ramos-Roman MA, Trombold JR, Wagner DA, et al. Palmitoleic acid is elevated in fatty liver disease and reflects hepatic lipogenesis. Am J Clin Nutr. 2014; 101(1): 34-43.
6. Horton JD, Goldstein JL, Brown MS. SREBPs: activators of the complete program of cholesterol and fatty acid synthesis in the liver. J Clin Invest. 2002; 109(9): 1125-1131.
7. Samal B, Sun Y, Stearns G, Xie C, Suggs S, McNiece I. Cloning and characterization of the cDNA encoding a novel human pre-B-cell colony-enhancing factor. Mol Cell Biol. 1994; 14(2): 1431-1437.
8. Revollo JR, Körner A, Mills KF, Satoh A, Wang T, Garten A, et al. Nampt/PBEF/visfatin regulates insulin secretion in β cells as a systemic NAD biosynthetic enzyme. Cell Metab. 2007; 6(5): 363-375.
9. Gholinejad Z, Kheiripour N, Nourbakhsh M, Ilbeigi D, Behroozfar K, Hesari Z, et al. Extracellular NAMPT/Visfatin induces proliferation through ERK1/2 and AKT and inhibits apoptosis in breast cancer cells. Peptides. 2017; 92: 9-15.
10. Rongvaux A, Shea RJ, Mulks MH, Gigot D, Urbain J, Leo O, et al. Pre-B-cell colony-enhancing factor, whose expression is up-regulated in activated lymphocytes, is a nicotinamide phosphoribosyl-

transferase, a cytosolic enzyme involved in NAD biosynthesis. Eur J Immunol. 2002; 32(11): 3225-3234.
11. Rongvaux A, Andris F, Van Gool F, Leo O. Reconstructing eukaryotic NAD metabolism. Bioessays. 2003; 25(7): 683-690.
12. Yang H, Lavu S, Sinclair DA. Nampt/PBEF/Visfatin: a regulator of mammalian health and longevity? Exp Gerontol. 2006; 41(8): 718-726.
13. Chalkiadaki A, Guarente L. Sirtuins mediate mammalian metabolic responses to nutrient availability. Nat Rev Endocrinol. 2012; 8(5): 287-296.
14. Borji M, Nourbakhsh M, Shafiee SM, Owji AA, Abdolvahabi Z, Hesari Z, et al. Down-regulation of SIRT1 expression by mir-23b contributes to lipid accumulation in HepG2 cells. Biochem Genet. 2019; 57(4): 507-521.
15. Hou X, Xu S, Maitland-Toolan KA, Sato K, Jiang B, Ido Y, et al. SIRT1 regulates hepatocyte lipid metabolism through activating AMP-activated protein kinase. J Biol Chem. 2008; 283(29): 20015-20026.
16. Shokri Afra H, Zangooei M, Meshkani R, Ghahremani MH, Ilbeigi D, Khedri A, et al. Hesperetin is a potent bioactivator that activates SIRT1-AMPK signaling pathway in HepG2 cells. J Physiol Biochem. 2019; 75(2): 125-133.
17. Park SH, Gammon SR, Knippers JD, Paulsen SR, Rubink DS, Winder WW. Phosphorylation-activity relationships of AMPK and acetyl-CoA carboxylase in muscle. J Appl Physiol (1985). 2002; 92(6): 2475-2482.
18. Foretz M, Carling D, Guichard C, Ferré P, Foufelle F. AMP-activated protein kinase inhibits the glucose-activated expression of fatty acid synthase gene in rat hepatocytes. J Biol Chem. 1998; 273(24): 14767-14771.
19. Wang LF, Wang XN, Huang CC, Hu L, Xiao YF, Guan XH, et al. Inhibition of NAMPT aggravates high fat diet-induced hepatic steatosis in mice through regulating Sirt1/AMPKα/SREBP1 signaling pathway. Lipids Health Dis. 2017; 16(1): 82.
20. Li Y, Xu S, Mihaylova MM, Zheng B, Hou X, Jiang B, et al. AMPK phosphorylates and inhibits SREBP activity to attenuate hepatic steatosis and atherosclerosis in diet-induced insulin-resistant mice. Cell Metab. 2011; 13(4): 376-388.
21. Ponugoti B, Kim D-H, Xiao Z, Smith Z, Miao J, Zang M, et al. SIRT1 deacetylates and inhibits SREBP-1C activity in regulation of hepatic lipid metabolism. J Biol Chem. 2010; 285(44): 33959-33970.
22. Bowlby SC, Thomas MJ, D'Agostino RB Jr, Kridel SJ. Nicotinamide phosphoribosyl transferase (Nampt) is required for de novo lipogenesis in tumor cells. PLoS One. 2012; 7(6): e40195.
23. Dahl TB, Haukeland JW, Yndestad A, Ranheim T, Gladhaug IP, Damås JK, et al. Intracellular nicotinamide phosphoribosyltransferase protects against hepatocyte apoptosis and is down-regulated in nonalcoholic fatty liver disease. J Clin Endocrinol Metab. 2010; 95(6): 3039-3047.
24. Akbal E, Koçak E, Taş A, Yüksel E, Köklü S. Visfatin levels in nonalcoholic fatty liver disease. J Clin Lab Anal. 2012; 26(2): 115-119.
25. Auguet T, Terra X, Porras JA, Orellana-Gavaldà JM, Martinez S, Aguilar C, et al. Plasma visfatin levels and gene expression in morbidly obese women with associated fatty liver disease. Clin Biochem. 2013; 46(3): 202-208.
26. Cheraghi R, Alipour M, Nazari M, Hosseinkhani S. Optimization of conditions for gene delivery system based on PEI. Nanomed J. 2017; 4(1): 8-16.
27. Ismail N, Abdel–Mottaleb Y, Ahmed AAE, El-Maraghy NN. Novel combination of thymoquinone and resveratrol enhances anticancer effect on hepatocellular carcinoma cell line. Future Journal of Pharmaceutical Sciences. 2018; 4(1): 41-46.
28. Ou X, Chen Y, Cheng X, Zhang X, He Q. Potentiation of resveratrol-induced apoptosis by matrine in human hepatoma HepG2 cells. Oncol Rep. 2014; 32(6): 2803-2809.
29. Livak KJ, Schmittgen TD. Analysis of relative gene expression data using real-time quantitative PCR and the 2(-Delta Delta C(T)) Method. 2001; 25(4): 402-408.
30. Bambha K, Belt P, Abraham M, Wilson LA, Pabst M, Ferrell L, et al. Ethnicity and nonalcoholic fatty liver disease. Hepatology. 2012; 55(3): 769-780.
31. Musso G, Gambino R, Cassader M. Recent insights into hepatic lipid metabolism in non-alcoholic fatty liver disease (NAFLD). Prog Lipid Res. 2009; 48(1): 1-26.
32. Tao R, Wei D, Gao H, Liu Y, DePinho RA, Dong XC. Hepatic FoxOs regulate lipid metabolism via modulation of expression of the nicotinamide phosphoribosyltransferase gene. J Biol Chem. 2011; 286(16): 14681-14690.
33. Zhou CC, Yang X, Hua X, Liu J, Fan MB, Li GQ, et al. Hepatic NAD+ deficiency as a therapeutic target for non-alcoholic fatty liver disease in ageing. Br J Pharmacol. 2016; 173(15): 2352-2368.
34. Wu T, Liu YH, Fu YC, Liu XM, Zhou XH. Direct evidence of sirtuin downregulation in the liver of non-alcoholic fatty liver disease patients. Ann Clin Lab Sci. 2014; 44(4): 410-418.
35. Gariani K, Menzies KJ, Ryu D, Wegner CJ, Wang X, Ropelle ER, et al. Eliciting the mitochondrial unfolded protein response by nicotinamide adenine dinucleotide repletion reverses fatty liver disease in mice. Hepatology. 2016; 63(4): 1190-1204.
36. Gual P, Postic C. Therapeutic potential of nicotinamide adenine dinucleotide for nonalcoholic fatty liver disease. Hepatology. 2016; 63(4): 1074-1077.
37. Borra MT, Smith BC, Denu JM. Mechanism of human SIRT1 activation by resveratrol. J Biol Chem. 2005; 280(17): 17187-17195.
38. Imamura H, Nagayama D, Ishihara N, Tanaka S, Watanabe R, Watanabe Y, et al. Resveratrol attenuates triglyceride accumulation associated with upregulation of Sirt1 and lipoprotein lipase in 3T3-L1 adipocytes. Mol Genet Metab Rep. 2017; 12: 44-50.
39. Amirkalali B, Sohrabi MR, Esrafily A, Jalali M, Gholami A, Hosseinzadeh P, et al. Association between Nicotinamide Phosphoribosyltransferase and de novo Lipogenesis in Nonalcoholic Fatty Liver Disease. Med Princ Pract. 2017; 26(3): 251-257.
40. Ruiz JR, Lasa A, Simon E, Larrarte E, Labayen I. Lower plasma NAMPT/visfatin levels are associated with impaired hepatic mitochondrial function in non-diabetic obese women: a potential link between obesity and non-alcoholic fatty liver disease. Nutr Metab Cardiovasc Dis. 2012; 22(2): e1-e2.

Original Article

The Changes of Heart miR-1 and miR-133 Expressions following Physiological Hypertrophy Due to Endurance Training

Mohammad Fathi, Ph.D.[1]*, Reza Gharakhanlou, Ph.D.[2], Razieh Rezaei, Ph.D.[3]

1. Department of Physical Education and Sport Sciences, Faculty of Humanities Sciences, Lorestan University, Khorramabad, Iran
2. Department of Physical Education and Sport Sciences, Faculty of Humanities Sciences, Tarbiyat Modares University, Tehran, Iran
3. Faculty of Physical Education and Sport Sciences, Shahid Chamran University of Ahvaz, Ahvaz, Iran

Corresponding Address: P.O.Box: 68151-44316, Department of Physical Education and Sport Sciences, Faculty of Humanity Sciences, Lorestan University, Khorramabad, Iran
Email: Fathi.m@lu.ac.ir

Received: 16/June/2019, Accepted: 12/October/2019

Abstract

Objective: MicroRNAs (miRNAs) play a key role in the development of the heart. Recent studies have shown that miR-1 and miR-133 are key regulators of cardiac hypertrophy. Therefore, we aimed to evaluate the effect of an endurance training (ET) program on the expressions of these miRNAs and their transcriptional network.

Materials and Methods: In this experimental study, cardiac hypertrophy was induced by 14 weeks of ET for 1 hour per day, 6 days per week at 75% VO2 max). The rats (221 ± 23 g) in the experimental (n=7) and control (n=7) groups were anesthetized to evaluate heart morphology changes by echocardiography. Next, we evaluated expressions of miR-1 and miR-133, and heart and neural crest derivatives express 2 *(Hand2), Mef2c*, histone deacetylase 4 (Hdac4) and serum response factor (*Srf*) gene expressions by real-time polymerase chain reaction (*PCR*). Finally, the collected data were evaluated by the independent t test to determine differences between the groups

Results: The echocardiography result confirmed physiological hypertrophy in the experimental group that underwent ET as shown by the increased left ventricular weight/body surface area (LVW/BSA) (P=0.004), LVW/body weight (BW) (P=0.011), left ventricular diameter end-diastolic (LVDd) (P=0.003), and improvements in heart functional indexes such as fractional shortness (FS) (P=0.036) and stroke volume (SV) (P=0.002). There were significant increases in the expressions of miR-1 (P=0.001) and miR-133 (P=0.004). The expressions of *Srf, Hdac4,* and *Hand2* genes significantly increased (P<0.001) in the experimental group Compared with the control group. The expression of *Mef2c* did not significantly change.

Conclusion: The expressions of miR-1 and miR-133 and their target genes appeared to be involved in physiological hypertrophy induced by ET in these rats.

Keywords: Endurance Training, *Hand2, Mef2c*, miR-1, miR-133

Cell Journal(Yakhteh), Vol 22, Suppl 1, Autumn 2020, Pages: 133-140

Citation: **Fathi M, Gharakhanlou R, Rezaei R. The changes of heart miR-1 and miR-133 expressions following physiological hypertrophy due to endurance training. Cell J. 2020; 22 Suppl 1: 133-140. doi: 10.22074/cellj.2020.7014.**

Introduction

In recent years, microRNAs (miRNAs) are considered one of the most important factors involved in myocellular processes, including cell differentiation, proliferation, heart disease, and muscle adaptation (1). Among the known miRNAs, myomiRs (special muscle miRs) are specifically expressed in skeletal and cardiac muscle tissues (2). A wide array of studies have focused on myomiRs functions (3, 4). myomiRs have important roles in myogenesis, embryonic muscle growth, and cardiac function and hypertrophy (5). In a review article, van Rooij et al. (2) introduced a network of transcription factors involved in the regulation of ventricular growth and cardiomyocyte differentiation of the heart, in which myomiRs play a central role. Among the myomiRs, miR-1 and miR-133 are expressed in striated muscle and have different roles. While miR-1 promotes myogenesis by targeting histone deacetylase 4 (*Hdac4*), a transcriptional repressor of muscle gene expression, miR-133 enhances myoblast proliferation by repressing serum response factor (*Srf*) (6).

Srf is a member of the MADS-box family of transcription factors and an important regulator of various genes that are necessary for cardiac function and development. Srf-dependent genes induce some contractile proteins such as skeletal α-actin, β myosin heavy chain (βMHC), cardiac α-actin, myosin light chain-2 (MLC-2v), and dystrophin. The importance of the Srf protein in regulating both contractile protein genes and genes that encode proteins involved in regulating the action of the contractile apparatus suggest that Srf exerts control over multiple aspects of cardiac function (7). Heart and neural crest derivatives express 2 (*Hand2*), a transcription factor that promotes ventricular cardiomyocyte expansion, is a target of miR-1 (8). It has been shown that the *Mef2c* transcription factor, an essential regulator of muscle development, directly activates transcription of a bicistronic primary transcript that encodes miR-1 and miR-133 via an intragenic muscle-specific enhancer located between the miR-1 and miR-133 coding regions (9). As van Roiij et al. (2) showed, the all of mentioned factors is in a transcriptional network that functions in cardiomyocyte proliferation and differentiation, control of cardiac growth, and conductance.

In addition to miRNAs, physical activity, especially endurance activities, causes changes in heart tissue (10) that lead to structural changes and changes in cardiac function such as left ventricle (LV) hypertrophy (physiology hypertrophy) (11), which coincides with an increase in stroke

volume (SV), ejection fraction percent (EF%), and LV mass (12) of the heart.

Thus, the effect of long-term endurance training (ET) on miRNAs and their upstream (*Srf* and *Mef2c*) and downstream (*Hdac4* and *Hand2*) genes (2) in the heart is intriguing. In the field of exercise and cardiac adaptation, few studies have evaluated the effect of ET on expression of miR-1 and miR-133 in a hypertrophied heart (13). No data has assessed both functional and structural heart changes and simultaneously measured miR-1 and miR-133 transcription network changes involved in cardiac hypertrophy, which is very important in cardiomyocyte proliferation and differentiation. Given the probable changes in cardiac remodelling by ET, this study assessed whether 14 weeks of ET would change the expressions of miR-1 and miR-133 and their upstream and downstream genes, and cause hypertrophy of the heart tissue in rats.

Materials and Methods

This experimental investigation was conducted at Tarbiat Modares University, Tehran, Iran. A total of 14 healthy male adult Wistar rats, 10 weeks of age, that weighed between 175 and 200 g (Fig.1) were purchased from Pasteur Institute, Tehran, Iran. The rats were maintained under the following conditions: 12-hour dark (7 p.m. to 7 a.m.)/12-hour light cycle (7 a.m. to7 p.m.), 23 ± 2˚C, and 30- 70% humidity to enable them to acclimate to the laboratory environment. The rats had free access to water and food, which was purchased from Behparvar Animal Chow Company, Iran. The rats were weighed before the start of the protocol. The experimental approved by the Ethics Committee of the Iran National Science Foundation (code: 90003724). Every attempt was made to decrease the number of animals used and their suffering. All of the observations were performed by a single individual. The rats were randomly assigned by simple randomization to a control (CON) group (n=7) and experimental (ET) group (n=7). The ET group was subjected to a prolonged ET program.

Training protocol

After a one-week acclimation period (9 m/minute, 10 minute/day, 4 days a week). The rats were weighed and marked. Rats in the ET group were trained by running on a level motorized rodent treadmill, 6 days per week for 14 weeks. At the start of each session, the rats were allowed to warm up by running for 5 minutes at 12 m/minute. After completion of the warm up period, the main exercise was begun. During the first 6 weeks, the speed of the treadmill and duration of the training sessions were gradually increased, as follows: week 1 (20 m/minute), week 2 (22 m/minute), week 3 (25 m/minute), week 4 (27 m/minute), week 5 (29 m/minute), and week 6 (30 m/minute). On the first day, the exercise duration was 12 minutes, which was increased daily by approximately more than 2 minutes per day until it reached 50 minutes at the end of the third week. We added an incline beginning with the seventh week, which reached 5 degrees by the end of the tenth week. This protocol was maintained until the end of the fourteenth week. According to a study by Wisloff et al. (14) the intensity of this protocol was equal to 75% VO2max in the rats. At the end of the main exercise period, the rats were allowed to cool down at a speed of 9 m/minute for 5 minutes. The endurance protocol was performed between 5-7 pm each day. The measurements were obtained 48 hours after the end of the last training session. With the exception of the training protocol, the other conditions were similar to the CON group.

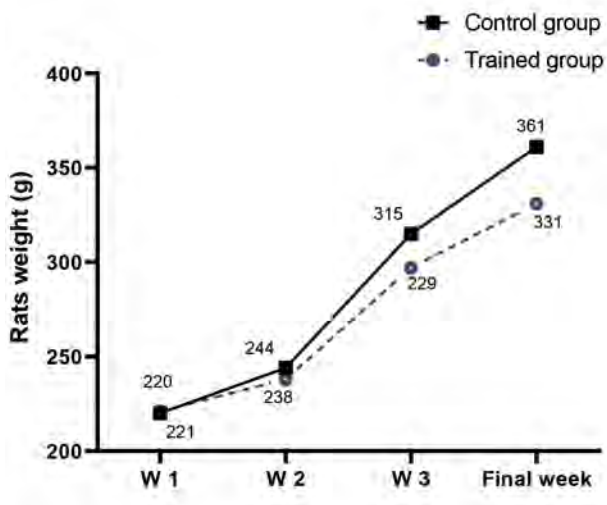

Fig.1: The weight trend (means) in the rats during 14 weeks of endurance training. W; Week.

Echocardiography recording

The rats from both groups were administered a light anaesthesia using ketamine and xylazine, and placed in the supine position. Ultrasound gel was placed on the thorax of each rat to enable optimal visibility. The echocardiography was performed according to the guidelines of the American Society of Echocardiography (15). We used an ultrasound machine (Sonix Touch Ultrasound System, Ultrasonix Medical Corp., Richmond, ON, Canada) and a 14 MHz linear array transducer. Images were obtained with the transducer placed on each animal's shaved chest. The animals were scanned from below at a depth of 2 cm with the focus optimized at 1 cm. Wall thickness and LV dimensions were obtained from a short axis view at the level of the papillary muscles (Fig.2). Echocardiography was completed within 10 to 15 minutes. The fractional shortness percent (FS%) was calculated using the following equation:

(LVDd-LVDs/LVDd)×100

where: LVDd is the left ventricular diameter end-diastolic.

The ejection fraction (EF) was calculated by the following equation:

(LVEDV-LVESV/LVEDV)×100

where: LVDd and LVDs=LV end-diastolic/systolic diameter and LVEDV and LVESV=LV end-diastolic/

systolic volume (16).

The left ventricular end-systolic/diastolic volume was calculated by the Teichholz formula:

$$LVESV=[7.0/(2.4+LVSd)]\times LVSd^3$$

and

$$LVEDV=[7.0/(2.4+LVDd)]\times LVDd^3$$

SV and FS were also calculated as the measured differences between the LVEDV and LVESV and [LVDd-LVDs]/LVDd, respectively (17).

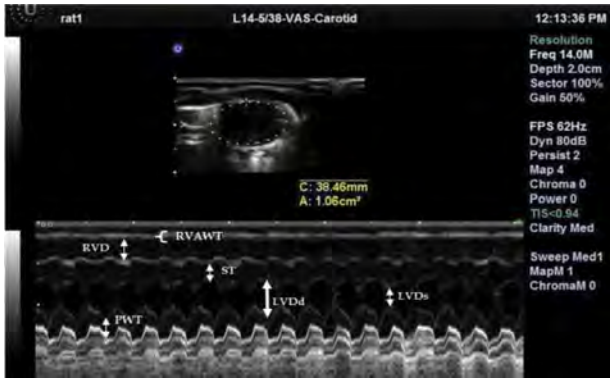

Fig.2: Two-dimensional targeted M-mode echocardiograms from the heart of one rat from the endurance-trained (ET) group.
RVAWT; Right ventricular anterior wall thickness, RVD; Right ventricular dimension, ST; Septum thickness, LVDd; Left ventricular diameter diastole, LVDs; Left ventricular diameter diastole, and PWT; Posterior wall thickness.

Tissue preparation and other measurements

One day following the echocardiographic examination, the animals were weighed first, and subsequently injected with an overdose of ketamine (90 mg/kg) and xylazine (10 mg/kg). The animals were sacrificed by administration of overdoses of ketamine and xylazine 48 hours after the last session. We calculated the body surface area (BSA) of each animal by measuring their lengths (mouth to tail root) while they were unconscious, and then we removed the heart and tibia bone. The heart was rapidly and carefully excised. The dissected heart and left ventricle (including the septum) were weighed to four decimal digits. We measured the tibia length by using a calliper, heart and left ventricular weight (LVW) to normalization, and evaluated the hearts for hypertrophy. After the measurement of LVW and heart weight, the tissue samples of LV and heart were quickly frozen in liquid nitrogen and stored at -80˚C until needed. Tibia length, BSA and body weight (BW) were used to normalize the heart and LVW changes. We used the Excel progam to calculate compounded parameters such as EF, FS, and other indexes.

$$BSA=6.67\times W^{0.7}\times[0.34/(\sqrt[3]{W/L})] \quad (18)$$

RNA isolation and cDNA synthesis

Total RNA was isolated from the frozen left ventricles by using TRIzol (Invitrogen, Inc.) and chloroform (Merck, Germany) according to the manufacturer's instructions. Briefly, the LV extracted tissue was pulverized in liquid nitrogen by a mortar and pestle, and the pulverized sample was transferred to TRIzol 1ml. The final product was centrifuged at 12000 × g for 10 minutes at 4˚C. Then, the samples were mixed with chloroform in 1:5 portions and shaken vigorously for 15 seconds. The supernatant was centrifuged at 12000 × g for 10 minutes at 4˚C and the supernatant were removed. Finally, the portion that contained RNA was removed and mixed with isopropanol in 1:5 portions, allowed to remain for 10 minutes at room temperature, and then centrifuged at 12000 × g at 4˚C for 10 minutes. The RNA was washed and dissolved in 20 µL RNase-free water. RNA purity was determined by UV spectrophotometry (Eppendorf, Germany) at 260 nanometre: RNA purity was determined by calculating the absorbance ratio at 260 and 280 nm. GelRed staining was used to confirm RNA purity. Purification was accepted when the 260/280-nm absorbance ratio was above 1.8. Isolated RNA was stored at -80˚C. Total RNA was converted to cDNA using the Revert Aid First Strand cDNA Synthesis Kit (Thermo Scientific, Waltham, MA, USA) according to the manufacturer's instructions.

Real-time polymerase chain reaction

Real-time polymerase chain reaction (PCR) was performed using the Takara Master Mix (RR820A SYBR® Premix Ex Taq™ II. Tli RNase H Plus) for determining mRNA expression levels of *Hand2, Mef2c, Srf,* and *Hdac4* (Step One Plus™ Real-Time PCR Systems, Applied Biosystem America). The reaction mixture was performed in final volume in 20 µL that included 10 µL of Syber Green, 1 µL of forward primer, 1 µL of reverse primer, 1 µL of cDNA, and 7 µL of DEPC water. Each reaction was run in triplicate. GeneRunner software and NCBI (http://www.ncbi.nlm.nih.gov/tools/primer-blast/), respectively, were used to design and BLAST of the *Hand2, Mef2c, Srf, Hdac4* and glyceraldehyde-3-phosphate dehydrogenase (*Gapdh*) primers according to the NCBI Gene Bank. Table S1 (See Supplementary Online Information at www.celljournal.org) lists the primer sequences used in this experiment. The thermal program used in real-time PCR was 95˚C for 30 seconds, 95˚C for 5 seconds, and 60˚C for 30 seconds (40 cycle repetitions). The standard and melting curves were drawn and analysed for optimization of the experiment and assessment of data accuracy, respectively. *Hand2, Mef2c, Srf* and *Hdac4* mRNA expressions were normalized using *Gapdh* as the housekeeping gene.

MicroRNA detection

We measured the amount of miR-1 expression with the 5′-UGGAAUGUAAAGAAGUAUGUAU-3′ sequence and miR-133 expression with the 5′-UUUGGUCCCCUUCAACCAGCUG-3′ sequence. The reagents for cDNA synthesis (#203300), SYBR Green master mix (#203450), primers miR-1 and miR-133, and U6 (small nuclear RNA as miRNAs housekeeping) were purchased from Exiqon (Vedbaek, Denmark). cDNA synthesis and real-time PCR for miR-1 and miR-133 were done according to the manufacturer's protocols as described in our previous study (19). The equipment used in this experiment were calibrated regularly.

Statistical analysis

All data are presented as mean ± standard deviation (SD). We confirmed that all continuous variables were normally

distributed using the Shapiro-Wilk test and the equality of variances using Levene's test. Next, the independent t-test was used to assess the main effects of the ET prog that included changes in mRNA expressions of miR-1 and miR-133, and echocardiographic indexes after the ET program. All analyses were performed using the SPSS statistical software (version 20,SPSS Inc, Chicago, IL, USA) The significance level was set at $P<0.05$. The graphs were reported based on mean ± SD.

Table 1: Normalized heart and left ventricle based BSA and tibia length of rats (n=14) and BW, HW, tibia length, body surface, and cardiac structural and functional indexes of rats' hearts after 14 weeks of endurance training

Index	Group	Mean ± SD	P value
LVW (g)/tibial length (c)	ET	0.01913 ± 0.00138	0.216
	CON	0.01826 ± 0.00109	
LVW (g)/BSA (cm^2)	ET	0.168 ±0 .0086	0.004**
	CON	0.15 ± 0.0068	
LVW (g)/HW (g)	ET	0.6136 ± 2.73	0.096
	CON	0.6465 ± 3.85	
LVW (g)/BW (kg)	ET	2.3 ± 0.18	0.011*
	CON	2.05 ± 0.12	
LVW (g)	ET	0.75918 ± 0.04904	0.435
	CON	0.73968 ± 0.04472	
BSA (cm^2)	ET	451.19 ± 22.7	0.021*
	CON	481.57 ± 20	
HW (g)	ET	1.23 ± 0.059	0.058
	CON	1.14 ± 0.096	
Final BW (g)	ET	331.2 ± 33.4	0.065
	CON	361.2 ± 16.8	
Tibia length (mm)	ET	39.7 ± 0.95	0.476
	CON	40.57 ± 2.86	
Septum (mm)	ET	1.96 ± 0.499	0.323
	CON	1.7 ± 0.203	
LVDd (mm)	ET	5.001 ± 0.719	0.003**
	CON	3.98 ± 0.13	
RVDd (mm)	ET	1.81 ± 0.47	0.812
	CON	1.77 ± 0.158	
RVAWT (mm)	ET	1.21 ± 0.2	0.379
	CON	1.29 ± 0.11	
RVD (mm)	ET	1.77 ± 0.4	0.841
	CON	1.73 ± 0.32	
PWT (mm)	ET	1.57 ± 0.437	0.939
	CON	1.585 ± 0.166	
FS (%)	ET	63.84 ± 8	0.036*
	CON	55.41 ± 4.9	
EF (%)	ET	91.02 ± 4.8	0.066
	CON	86.1 ± 4.1	
SV (ml)	ET	3.18 ± 0.53	0.002**
	CON	2.2 ± 0.24	

LVW; Left ventricular weight, BSA; Body surface area, EF; Ejection fraction, SV; Stroke volume, HW; Heart weight, BW; Body weight, LVDd; Left ventricular diameter end-systolic, RVDd; Right ventricular diameter end-systolic, RVAWT; Right ventricular anterior wall thickness, RVD; Right ventricular dimension, PWT; Posterior wall thickness, FS; Fractional shortness, ET; Endurance training, and CON; Control.

Results

Table 1 and Figure 1 list the rats' morphology characteristics that included BW, HW, LVW, tibia length, and body length. There was no significant difference between the groups in BW at the start of the protocol (P<0.801). BW of the ET group rats did not change compared with CON group rats at the end of the protocol (P≤ 0.063, Fig.1).

Other studies have used parameters such as tibia length (20) and BSA (18) to normalize heart hypertrophy. Therefore, we calculated these indexes (Table 1) and noted between the two groups in mean HW/BSA and mean BH/BW ratios at significance level of P<0.01.

In the normalized parameter, there was a difference between LVW/BSA (P=0.004) and LV/BW (P=0.011). Table 2 lists the mean echocardiographic parameters after 14 weeks of endurance exercise. There were significant differences between the two groups in LVDd (P=0.003) and FS (P=0.036).

The results of this study showed that the expressions of miR-1 (P=0.001) and miR-133 (P=0.004) in the left ventricle of the trained group significantly increased after 14 weeks of endurance training (Fig.3).

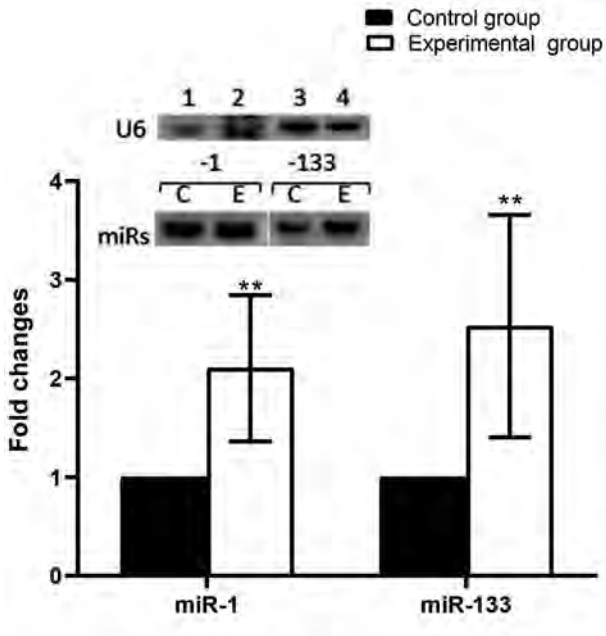

Fig.3: Expressions of miR-1 and miR-133 in the rats. Representative image of real-time polymerase chain reaction (PCR) results for miR-1 and miR-133 in left ventricle tissue from the control (CON) and experimental groups (ET), respectively. The expressions of the microRNAs (miRNAs) were normalized to U6 expression. Histogram of real-time PCR miRNA products showed that both miR-1 and miR-133 had significantly increased expressions of greater than~2.1-fold (P=0.001 and P=0.004, respectively) in response to 14 weeks of endurance training). Values are mean ± SE (n=7). Data were analysed by the independent t test. **; P<0.01.

The expressions of *Hand2* and *Hdac4* genes in the left ventricle of the ET group rats significantly increased (P=0.001) by ~143-fold (Fig.4). *Srf* gene expression significantly increased (P=0.001) by ~5.9-fold in the left ventricle of the ET group rats after 14 weeks of ET There was no change in expression of the *Mef2c* gene (P=0.148, Fig.5).

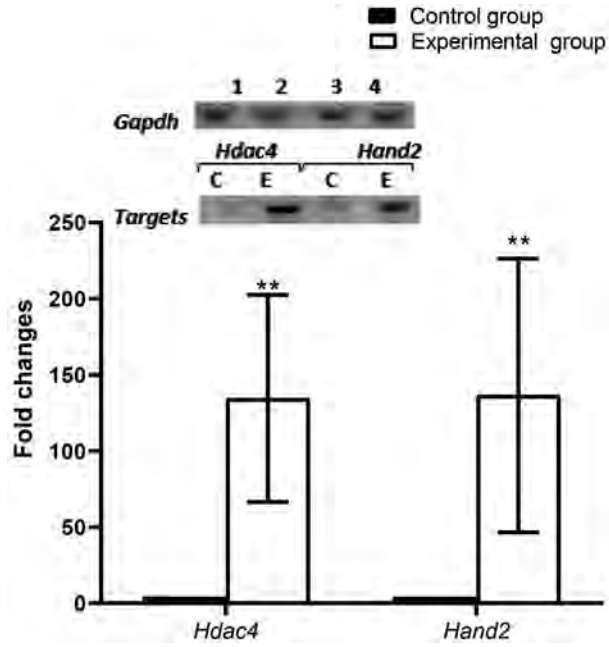

Fig.4: Expressions of histone deacetylase 4 (*Hdac4*) and heart and neural crest derivatives express 2 (*Hand2*) genes in rats. Representative image of real-time polymerase chain reaction (PCR) results for *Hdac4* and *Hand2* in left ventricle tissue from the control (CON) and experimental groups (ET), respectively. Expressions of the genes were normalized to glyceraldehyde-3-phosphate dehydrogenase (*GAPDH*) expression. Histogram of real-time PCR gene products revealed significantly increased expression of both genes by ~143-fold (P=0.001) in response to 14 weeks of endurance training. Values are mean ± SE (n=7). Data were analysed by the independent t test. **; P<0.01.

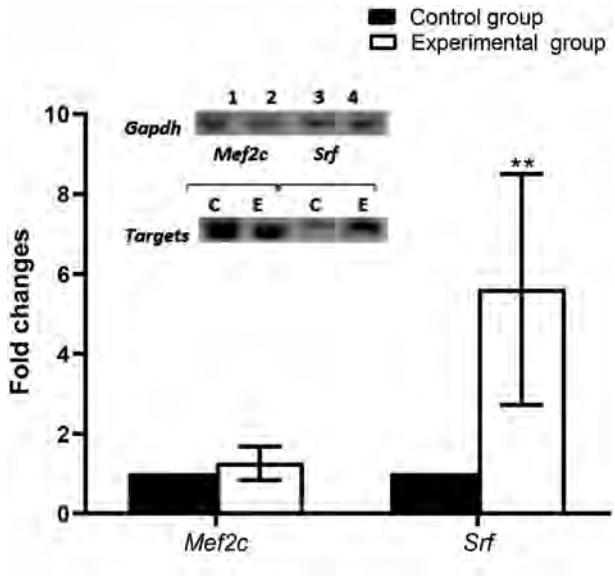

Fig.5: Expressions of *Mef2c* and *Srf* genes in the rats. Representative image of real-time polymerase chain reaction (PCR) results for *Mef2c* and *Srf* genes in left ventricle tissue from the control (CON) and experimental groups (ET), respectively. The gene expressions were normalized to glyceraldehyde-3-phosphate dehydrogenase (*GAPDH*) expression. Histogram of real-time PCR gene products revealed that Srf expression was significantly increased by ~5.9-fold (P=0.001) in response to 14 weeks of endurance training, whereas there was no difference in the expression level of *Mef2c* between the CON and ET groups (P=0.148). Values are mean ± SE (n=7). Data were analysed by the independent t test. **; P<0.01.

Discussion

The present study has demonstrated that 14 weeks of ET was able to change the expressions of the miRNAs and the genes that are part of a transcription network to regulate ventricular growth and cardiomyocyte differentiation of the heart, as has been described by van Rooij et al. (2).

Echocardiography and weighing were used to evaluate heart and left ventricle adaptation to ET. The aim of this study was to determine if the miR-1 and miR-133 network expression changes and the accompanied genes that function to regulate ventricular growth and cardiomyocyte differentiation of the heart mediate ET induced-cardiac hypertrophy.

As in previous studies (21, 22), the results of this study showed that 14 weeks of ET-induced cardiac hypertrophy and improvement in some functional indexes. For example, LVW/BSA and LVW/BW in the experimental group were significantly more than the control group. These findings confirmed cardiac hypertrophy due to ET, as known physiological hypertrophy. The results of this study were in line with those of other studies (22, 23). The obtained data from echocardiography showed an increase in LVDd, which coincided with improved heart functional indexes (SV, FS%, and EF%). Similarly, several studies showed that ET increased SV, FS%, and EF% (24, 25). It is a possibility that the observed changes in heart structural and functional indexes in this study refer to physiological hypertrophy, which occurs without fibrosis and cardiac dysfunction. Aerobic exercise training, such as long-distance running or swimming, is matched with an increased volume overload accompanied by cardiac chamber dilation, and is referred to as eccentric hypertrophy (26). This phenotype is associated with the addition of sarcomeres in series to lengthen the cardiomyocytes and to increase the widths of the cells in parallel.

The interesting findings in this study was when the absolute weight of the heart and LV of the ET group compared with the CON group. There were no significant differences between the groups. In line with these findings, Pluim et al. (27), in a meta-analysis study, reported that the development of an endurance-trained heart (eccentric hypertrophy) and a strength-trained heart (concentric hypertrophy) was not to be considered an absolute and dichotomous concept, but rather a relative concept. However, when the weight of the heart and LV of the experimental group were assessed and compared to the ratio of BSA and BW of the rats, the differences were significant. Both HW/BW and LVW/BSA increased significantly in the experimental group.

As previous studies have pointed out (28, 29), physical activity, especially endurance activity, causes the heart to undergo cardiac remodelling (i.e., changes in left ventricular geometry) to enhance performance. The resulting phenotype is referred to as the "athlete's heart" and is most frequently observed in elite athletes who participate in regular, high-intensity training regimes. A fundamental component of exercise-induced remodelling is physiological cardiac hypertrophy, a process that increases muscle mass by increasing cardiac myocyte size. Physiological cardiac hypertrophy is associated with normal or enhanced cardiac function (26). According to the mentioned studies, the structural and functional changes observed in this study were adaptations to ET and cardiovascular fitness to respond to the challenge of volume overload that occurred during ET.

The most important findings of this study were the increase of the miRNAs in proliferation and differentiation of myocardial cells such as miR-1 and miR-133 with their upstream and downstream genes (except for *Mef2c*).

Muscle-specific miR-1 and miR-133 are part of the myomiRs that play a key role in heart development and function. Both miR-1 and miR-133 are essential for cardiac remodelling in response to different stresses (30), including physical activity which induces physiological hypertrophy. In a clinical study, decreased expression of miR-133 was significantly associated with the severity of patients (31) since physical activity is a stimulator for cardiac remodelling and physiological hypertrophy; therefore, adaptation to this stimulant is necessary. Increases in miR-1 and miR-133 probably provide the base for physiological hypertrophy changes (32). According to a study by van Roij et al. (2), *Srf* and *Mef2c* are located upstream of miR-1 and miR-133 in DNA sequences. According to the result of this study, increased *Srf* expression probably induced increased miR-1 and miR-133 expressions. However, in contrast to our results, Care and colleagues reported decreased expressions of cardiac miR-133 and miR-1 in pathological or physiological cardiac hypertrophy in rats and human pathological cardiac hypertrophy (13). The inconsistent results could be attributed to differences in the type of exercise. Our training protocol was ET and the Care protocol was an interval exercise. It seems the existing paradox could be due to the different types of exercise, because differences exist between interval and ET in the heart's response to physical activity (22).

Srf is a transcription factor required for the regulation of important genes for cardiac structure and function. It has been reported that *Srf* is necessary for spontaneously induced hypertrophic gene expression in mouse cardiomyocytes (7). Probably, the increase in *Srf* gene expression is necessary for cardiac hypertrophy. However, some studies have pointed out that an increase in *Srf* occurs in pathological hypertrophy (33).

The *Mef2c* gene is involved in cardiac morphogenesis and myogenesis, and plays an important role in maintaining the differentiated state of muscle cells (34). Physical activity has been shown to increase *Mef2c* gene expression in rat trained muscles (35). *Mef2c* acts as a nodal point for stress-response and remodelling programs during cardiac hypertrophy and fibre-type switching muscles (36). On the other hand, it has been reported that

physical activity induces fibre type transformation and cardiac hypertrophy, which coincide with mitochondrial biogenesis and other desirable adaptations. We only found one study in the field of exercise and cardiac adaptation. In contrast to our study results, Castro and colleagues reported unchanged and increased expression of cardiac *Mef2c* following medium intensity and high intensity swim training, respectively, in Atlantic salmon (37). It seems the differences are related to the differences in the subject or intensity of physical activity.

The result of this study showed that *Hdac4* gene expression dramatically increased after ET. *Hdac4* is a transcriptional repressor of muscle gene expression with chromatin remodelling. On the other hand, *Mef2c* activates miR-1 expression, which targets *Hdac4* and diminishes its repression (38). We observed increased *Hdac4* expression at the transcription level. However, the most important effects of *Hdac4* occur post-translation after physical activity (39), such as export of the Hdac4 protein from the cell nucleus (40) and phosphorylation of Hdac4 in response to exercise (39). Due to the lack of measurement of the Hdac4 protein, the discussion of increasing *Hdac4* depends on the Hdac4 protein measurement.

However, the important changes in heart (physiological, structural and functional) were measured in this study. We could not measure the protein levels of the miRNA downstream genes; therefore, these findings could not be generalized to protein changes. Additional studies are proposed to measure the level of proteins.

Conclusion

After 14 weeks of ET, our research provided a comprehensive view of the network transcription factors of which miR-1 and miR-133 play a central role and support a relevant role of these myomiRs in the modulation of cardiac physiological hypertrophy. We also provided evidence for the cardiac functional and structural changes during ET that coincided with miR-1 and miR-133 changes, their upstream and downstream genes, and important elements in cardiac structural and functional changes.

Acknowledgments

This work was financial supported by the Iran National Science Foundation. There are no conflicts of interest to declare.

Authors' Contributions

M.F.; Contributed to the study conception and design. R.R.; Contributed to all of the experimental work, data, statistical analysis, and data interpretation. R.Gh.; Drafted the manuscript, which was revised by M.F. All authors read and approved the final manuscript.

References

1. Brennecke J, Stark A, Cohen SM. Not miR-ly muscular: microRNAs and muscle development. Genes Dev. 2005; 19(19): 2261-2264.
2. van Rooij E, Liu N, Olson EN. MicroRNAs flex their muscles. Trends Genet. 2008; 24(4): 159-166.
3. Frias Fde T, de Mendonca M, Martins AR, Gindro AF, Cogliati B, Curi R, et al. MyomiRs as markers of insulin resistance and decreased myogenesis in skeletal muscle of diet-induced obese mice. Front Endocrinol (Lausanne). 2016; 7: 76.
4. Siracusa J, Koulmann N, Banzet S. Circulating myomiRs: a new class of biomarkers to monitor skeletal muscle in physiology and medicine. J Cachexia Sarcopenia Muscle. 2018; 9(1): 20-27.
5. McCarthy JJ. MicroRNA-206: the skeletal muscle-specific myomiR. Biochim Biophys Acta. 2008; 1779(11): 682-691.
6. Chen JF, Mandel EM, Thomson JM, Wu Q, Callis TE, Hammond SM, et al. The role of microRNA-1 and microRNA-133 in skeletal muscle proliferation and differentiation. Nat Genet. 2006; 38(2): 228-233.
7. Nelson TJ, Balza R, Jr., Xiao Q, Misra RP. SRF-dependent gene expression in isolated cardiomyocytes: regulation of genes involved in cardiac hypertrophy. J Mol Cell Cardiol. 2005; 39(3): 479-489.
8. Zhao Y, Samal E, Srivastava D. Serum response factor regulates a muscle-specific microRNA that targets Hand2 during cardiogenesis. Nature. 2005; 436(7048): 214-220.
9. Liu N, Williams AH, Kim Y, McAnally J, Bezprozvannaya S, Sutherland LB, et al. An intragenic MEF2-dependent enhancer directs muscle-specific expression of microRNAs 1 and 133. Proc Natl Acad Sci USA. 2007; 104(52): 20844-20849.
10. Samiei A, Behpour N, Tadibi V, Fathi R. Effect of Eight weeks of aerobic training on some myocardial fibrosis indices in cardiac muscle of diabetic rats. Ann Appl Sport Sci. 2018; 6(4): 1-8.
11. Jakovljevic DG. Physical activity and cardiovascular aging: physiological and molecular insights. Exp Gerontol. 2018; 109: 67-74.
12. Lee BA, Oh DJ. The effects of long-term aerobic exercise on cardiac structure, stroke volume of the left ventricle, and cardiac output. J Exerc Rehabil. 2016; 12(1): 37-41.
13. Care A, Catalucci D, Felicetti F, Bonci D, Addario A, Gallo P, et al. MicroRNA-133 controls cardiac hypertrophy. Nat Med. 2007; 13(5): 613-618.
14. Wisloff U, Helgerud J, Kemi OJ, Ellingsen O. Intensity-controlled treadmill running in rats: VO(2 max) and cardiac hypertrophy. Am J Physiol Heart Circ Physiol. 2001; 280(3): H1301-H1310.
15. Lang RM, Bierig M, Devereux RB, Flachskampf FA, Foster E, Pellikka PA, et al. Recommendations for chamber quantification: a report from the American Society of Echocardiography's Guidelines and Standards Committee and the Chamber Quantification Writing Group, developed in conjunction with the European Association of Echocardiography, a branch of the European Society of Cardiology. J Am Soc Echocardiogr. 2005; 18(12): 1440-1463.
16. Stypmann J, Engelen MA, Troatz C, Rothenburger M, Eckardt L, Tiemann K. Echocardiographic assessment of global left ventricular function in mice. Lab Anim. 2009; 43(2): 127-137.
17. Hayward R, Lien CY. Echocardiographic evaluation of cardiac structure and function during exercise training in the developing Sprague-Dawley rat. J Am Assoc Lab Anim Sci. 2011; 50(4): 454-461.
18. Farriol M, Rossell J, Schwar S. Body surface area in Sprague-Dawley rats. J Anim Physiol Anim Nutr. 1997; 77 (1-5): 61-65.
19. Fathi M, Gharakhanlou R, Soleimani M, Rajabi H. Increased expression of miR-1 in fast-twitch skeletal muscle in response to resistance exercise. Iran Red Crescent Med. 2019; 21(4): e84841.
20. Yin FC, Spurgeon HA, Rakusan K, Weisfeldt ML, Lakatta EG. Use of tibial length to quantify cardiac hypertrophy: application in the aging rat. Am J Physiol. 1982; 243(6): H941-H947.
21. Trachsel LD, Ryffel CP, De Marchi S, Seiler C, Brugger N, Eser P, et al. Exercise-induced cardiac remodeling in non-elite endurance athletes: Comparison of 2-tiered and 4-tiered classification of left ventricular hypertrophy. PLoS One. 2018; 13(2): e0193203.
22. Gharaat MA, Kashef M, Jameie B, Rajabi H. Regulation of PI3K and Hand2 gene on physiological hypertrophy of heart following high-intensity interval, and endurance training. J Res Med Sci. 2019; 24: 32.
23. Zhua SS, Ma JZ, Yong YH, Niu J, Zhang JN. Left ventricular function in physiologic and pathologic hypertrophy in Sprague-Dawley rats. Science & Sports. 2008; 23(6): 299-305.
24. Xu X, Wan W, Powers AS, Li J, Ji LL, Lao S, et al. Effects of exercise training on cardiac function and myocardial remodeling in post myocardial infarction rats. J Mol Cell Cardiol. 2008; 44(1): 114-122.
25. Rodrigues B, Jorge L, Mostarda CT, Rosa KT, Medeiros A, Malfitano C, et al. Aerobic exercise training delays cardiac dysfunction and improves autonomic control of circulation in diabetic rats un-

dergoing myocardial infarction. J Card Fail. 2012; 18(9): 734-744.
26. Mihl C, Dassen WR, Kuipers H. Cardiac remodelling: concentric versus eccentric hypertrophy in strength and endurance athletes. Neth Heart J. 2008; 16(4): 129-133.
27. Pluim BM, Zwinderman AH, van der Laarse A, van der Wall EE. The athlete's heart: a meta-analysis of cardiac structure and function. Circulation. 2000; 101(3): 336-344.
28. Sharma S, Maron BJ, Whyte G, Firoozi S, Elliott PM, McKenna WJ. Physiologic limits of left ventricular hypertrophy in elite junior athletes: relevance to differential diagnosis of athlete's heart and hypertrophic cardiomyopathy. J Am Coll Cardiol. 2002; 40(8): 1431-1436.
29. Nakamura M, Sadoshima J. Mechanisms of physiological and pathological cardiac hypertrophy. Nat Rev Cardiol. 2018; 15(7): 387-407.
30. Matkovich SJ, Wang W, Tu Y, Eschenbacher WH, Dorn LE, Condorelli G, et al. MicroRNA-133a protects against myocardial fibrosis and modulates electrical repolarization without affecting hypertrophy in pressure-overloaded adult hearts. Circ Res. 2010; 106(1): 166-175.
31. Danowski N, Manthey I, Jakob HG, Siffert W, Peters J, Frey UH. Decreased expression of miR-133a but not of miR-1 is associated with signs of heart failure in patients undergoing coronary bypass surgery. Cardiology. 2013; 125(2): 125-130.
32. Karakikes I, Chaanine AH, Kang S, Mukete BN, Jeong D, Zhang S, et al. Therapeutic cardiac-targeted delivery of miR-1 reverses pressure overload-induced cardiac hypertrophy and attenuates pathological remodeling. J Am Heart Assoc. 2013; 2(2): e000078.
33. Parlakian A, Charvet C, Escoubet B, Mericskay M, Molkentin JD, Gary-Bobo G, et al. Temporally controlled onset of dilated cardiomyopathy through disruption of the SRF gene in adult heart. Circulation. 2005; 112(19): 2930-2939.
34. Wang DZ, Valdez MR, McAnally J, Richardson J, Olson EN. The Mef2c gene is a direct transcriptional target of myogenic bHLH and MEF2 proteins during skeletal muscle development. Development. 2001; 128(22): 4623-4633.
35. Wu H, Rothermel B, Kanatous S, Rosenberg P, Naya FJ, Shelton JM, et al. Activation of MEF2 by muscle activity is mediated through a calcineurin-dependent pathway. EMBO J. 2001; 20(22): 6414-6423.
36. Potthoff MJ, Olson EN. MEF2: a central regulator of diverse developmental programs. Development. 2007; 134(23): 4131-4140.
37. Castro V, Grisdale-Helland B, Helland SJ, Torgersen J, Kristensen T, Claireaux G, et al. Cardiac molecular-acclimation mechanisms in response to swimming-induced exercise in Atlantic salmon. PLoS One. 2013; 8(1): e55056.
38. Chen JF, Mandel EM, Thomson JM, Wu QL, Callis TE, Hammond SM, et al. The role of microRNA-1 and microRNA-133 in skeletal muscle proliferation and differentiation. Nat Genet. 2006; 38(2): 228-233.
39. McGee SL. Exercise and MEF2-HDAC interactions. Appl Physiol Nutr Metab. 2007; 32(5): 852-856.
40. Backs J, Backs T, Bezprozvannaya S, McKinsey TA, Olson EN. Histone deacetylase 5 acquires calcium/calmodulin-dependent kinase II responsiveness by oligomerization with histone deacetylase 4. Mol Cell Biol. 2008; 28(10): 3437-3445.

Original Article

Direct Differentiation of Human Primary Fibroblast into Hematopoietic-Like Stem Cells; A New Way without Viral Transduction

Sina Habibi, M.Sc.[1], Gholamreza Khamisipour, Ph.D.[1]*, Narges Obeidi, Ph.D.[1], Saeedeh Zare Jaliseh, M.Sc.[2]

1. Department of Hematology, Faculty of Allied Medicine, Bushehr University of Medical Sciences, Bushehr, Iran
2. Department of Anatomy, Faculty of Medical Sciences, Tarbiat Modares University, Tehran, Iran

Corresponding Address: P.O.Box: 7518759577, Department of Hematology, Faculty of Allied Medicine, Bushehr University of Medical Sciences, Bushehr, Iran
Email: r.khamisipour@bpums.ac.ir

Received: 12/April/2019, Accepted: 24/August/2019

Abstract

Objective: The aim of this study was to investigate the possibility of producing safe hematopoietic stem cells without the use of viral infectious agents that can be used in stem cell transplantation.

Materials and Methods: In this experimental study, after single layer cell formation, human primary fibroblast cells were treated with static electromagnetic fields of 10 and 15 milli Tesla (mT) for 20 minutes each day for seven consecutive days. On the seventh day and immediately after the last radiation, the cells were added to the wells containing specific hematopoietic stem cell expansion media. After 21 days and colony formation, the cells belonging to each group were evaluated in terms of the expression of *CD34, CD38*, and *GATA-1* genes using quantitative real-time polymerase chain reaction (PCR), as well as surface marker expression of CD34 by flow cytometry.

Results: Exposure to 10 mT and 15 mT electromagnetic field increased the expression of *CD34* and *CD38* genes ($P<0.05$). This increase in gene expression levels were 2.85 and 1.84 folds, respectively, in the 10mT group and 6.36 and 3.81 folds, respectively, in the 15 mT group. The expression of the *GATA-1* gene in the 10 mT and 15 mT groups was not significantly different from that of the control group ($P<0.05$). Electromagnetic waves caused a marked increase in the expression of the CD34 marker at the surface of reprogrammed cells. The rate of expression was about 42.3% in the 15 mT group and 23.1% in the 10 mT group.

Conclusion: The presence of human primary fibroblasts exposed to electromagnetic fields can increase the expression of specific hematopoietic genes. This method can be suitable for reprogramming cells differentiated into hematopoietic-like stem cells and does not pose the risks of retroviral use.

Keywords: Direct Differentiation, Electromagnetic Waves, Fibroblast, Hematopoietic Stem Cells, Reprogramming

Cell Journal(Yakhteh), Vol 22, Suppl 1, Autumn 2020, Pages: 141-147

Citation: **Habibi S, Khamisipour Gh, Obeidi N, Zare Jaliseh S. Direct differentiation of human primary fibroblast into hematopoietic-like stem cells; a new way without viral transduction. Cell J. 2020; 22 Suppl 1: 141-147. doi: 10.22074/cellj.2020.6846.**

Introduction

Stem cells are primary cells that can differentiate into various cells, including embryonic stem cells (ES cell) and adult stem cells. These cells can divide and rebuild themselves and become specialized cells, so they can be used to cure different diseases, such as diabetes, arthritis, and spinal cord injury in the future (1).

In recent years, scientists have applied viral vectors containing sex-determining region Y (*SOX2),* octamer-binding transcription factor 4 *(OCT4),* Kruppel-like factor 4 *(KLF4)* and Avian myelocytomatosis virus oncogene cellular homolog (*c-MYC)* genes in somatic cells to produce cells similar to embryonic cells that are able to form cells of all three embryonic layers. These cells called induced pluripotent stem cells (iPSCs) (2-4). Different types of somatic cells obtained from pluripotent stem cells could be used in regenerative medicine (5). Viruses that are used to transfer these genes to cells enter their genetic material (transgenes) into the genome of host cells (6). Transgenes are mainly silenced in iPS cells, but the reactivation of such transgenes (primarily the transgene encoding *c-MYC*) could lead to tumorigenesis (7). These genes can be dangerous, so the clinical use of iPS cells is currently impossible (8, 9).

The iPS cell potentially could overcome two crucial barriers related to human ES cells: immune rejection after transplantation and ethical concerns about the use of human embryos (7, 9).

Michael Faraday first introduced electromagnetic induction. This theory indicates that magnetic field fluctuations can create an electrical current in conductors that are close to it. Whether electromagnetic waves are constant or alternating in time, each one has physical characteristics that interfere with biological organisms [plants, animals, and humans (10)].

From the point of view, organisms are electromagnetic systems, and they use magnetism to emit proteins, interact in molecular systems of cell membrane, and disseminate information through nerve systems. The

interest in interactions between the magnetic field and living organisms triggers a series of epidemiological studies. These studies suggest a weak correlation between exposure to magnetic fields and the incidence of various types of cancer (11).

The effects of a strong magnetic field on the metabolic activity of leukemia cells were investigated. In this experiment, human leukemic cells (HL-60) were subjected to a 1T static magnetic field for 72 hours, resulting in a significant reduction in the metabolic activity of cancer cells (12). The magnetic field affects the non-sexual division of dictyostelium discoideum as a model for human disease. When the protozoa were subjected to the electromagnetic field at a frequency of 50 hertz (Hz) and the intensity of 300 microteslas (μT) for 24 hours, the net rate of non-sexual division of this protozoan was changed (13). *In vitro* studies performed on human cells show increased cell proliferation in immune cells and also promote new angiogenesis in endothelial cells exposed to electromagnetic waves (14).

Huangfu et al. (15) used early fibroblast cells to form iPSCs. In this study, only *OCT4* and *SOX2* genes were used for reprogramming using valproic acid. The results showed that it is possible to reprogramming cells by means of the pure chemicals, and more secure methods can be used for the generation of iPSC. In another study conducted by Baek et al. (16) on the reprogramming of somatic cells, they employed both *OCT4* and *SOX2* genes and the electromagnetic waves, iPSC-like generations were formed in the culture media. It was also observed that electromagnetic waves could be used well instead of using *c-MYC* and *KLF4* genes.

In this study, human fibroblast cells were exposed to static electromagnetic fields, and after transferring to a differentiated media, the production of hematopoietic stem cells in these cells were induced and tested.

Materials and Methods

This study is experimental research approved as a thesis with an Ethical code number of "IR.BPUMS.REC.1395.201" in Bushehr University of Medical Sciences.

Experiments were carried out in two separate groups, which were exposed to static electromagnetic fields under the radiation of 10 and 15 milli Tesla (mT). Each experiment was performed triplicate, and the entire experiment was repeated at three different times.

Electromagnetic field exposure

After single-cell layer formation, cells were exposed to static electromagnetic fields of 10 and 15 mT for 20 minutes each day for seven consecutive days. A device designed and built in the lab produced the electromagnetic field.

Structural design of the electromagnetic field generator device

The generator used to stimulate the cells has been manufactured and calibrated by the Persian Gulf University, Bushehr, Iran. Briefly, three-column coils, 12 cm in diameter and made of 2300 turns of enamel copper wire (0.6 mm in diameter), was mounted in a horizontal arrangement. Two ends of these wires can be connected to a suitable voltage. This device was designed to produce a static electromagnetic field with an energy range between 0 and 320 V and a magnetic field strength range between 0 and 40 mT. A line power supply powered the entire apparatus and connected directly to the variac. The electricity was converted into DC through an AC-DC rectifier. After adjusting the intensity of the field with gaussmeter, a 4-well culture plate was placed at the center of a uniform field area. Temperature near the culture plates was monitored, and no variation was recorded throughout the experiments. The intensity of the electromagnetic field used in this protocol was 10 to 15 mT, and the application time was 20 minutes.

Cell culture

Human primary fibroblasts HU02 (Stem Cell Technology, bonbiotech, Iran) were cultured in 4-well plates containing Dulbecco's Modified Eagle's Medium with Ham's F-12 Nutrient Mixture (DMEM.F12 Medium, Caisson, USA), which included 100 IU/mL penicillin, 100 μg/ml streptomycin in 0.9% saline (Caisson, USA), and 10 % fetal bovine serum (FBS, Gibco, USA), 1% non-essential Amino acid solution (Sigma, USA) and incubated at 37˚C at 5 % CO_2. After 24 hours and single-cell layer formation, non-adherent cells were eliminated by medium exchange, and the plate was exposed to electromagnetic radiation for seven days.

On the seventh day and immediately after the last radiation, the cells were separated from the well with 0.25% trypsin-EDTA (Caisson, USA) enzyme solution. Following the centrifugation of cells, they were transferred to a new 4 well-plate (10,000 cells per well) containing Stem MACS HSC Expansion Media (Miltenyi Biotec, Germany) supplemented with Stem MACS HSC Expansion Cocktail (Miltenyi Biotec, Germany) containing the human recombinant growth factor Flt3-Ligand, stem cell factor (SCF) and thrombopoietin (TPO). After 21 days of proliferation and colony formation, cells were examined for the expression of the specific hematopoietic genes [*CD34*, *CD38*, and GATA-binding factor 1 (*GATA-1)*] by quantitative real-time polymerase chain reaction (qRT-PCR) and hematopoietic surface marker (CD34) by flow cytometry.

The examined genes

The *CD34*, *CD38*, and *GATA-1* genes were studied as target genes. For the determination of the relative gene expression levels, the hypoxanthine-guanine phosphoribosyl transferase (*HPRT*) gene was used as a reference gene.

The sequences of *CD34, CD38, GATA-1,* and *HPRT* genes were extracted from the ncbi.nlm.gov, and related primers were designed using the Gene Runner software version 6.5. After designing, using the NCBI site tool, the primer sequence (Table 1) was blasted with the entire human genome, and the primer properties for complete complementary areas were fully assured.

Quantitative real-time polymerase chain reaction

For the quantitative real-time PCR (qRT-PCR) analysis, RNA was isolated using a YTzol Pure RNA (Yekta Tajhiz Azma, Iran) according to the manufacturer's protocol. Complementary DNA was produced with the cDNA Synthesis kit (Yekta Tajhiz Azma, Iran) according to the manufacturer's protocol. qRT-PCR reactions were set up in triplicate with the Amplicon RealQ Plus 2x Master Mix Green (Amplicon, Denmark) and run on a Step-One plus real-time PCR system (Applied Biosystems, USA) according to the manufacturer's protocol. Gene expression data were reported as relative expression to *HPRT*. qRT-PCR products were checked by gel electrophoresis according to the product sizes.

Flow cytometry analysis

Briefly, after 21 days and colony formation, the colonies of each group were entirely suspended in the medium. Cell suspensions were then transferred into flow cytometry tubes and centrifuged for 5 minutes at 210-230 g. After centrifugation, the supernatants were discarded, and 1 µl of CD34 antibodies (BioLegend, USA) was added to tubes of each group and placed in a dark environment at 4˚C for 30 minutes. Then, the cells were washed three times in phosphate-buffered saline (PBS) Solution (InoClon, Iran) and resuspended in 1 ml PBS solution and examined by flow cytometry instrument (FACSCalibur, BD, USA). In each group, 10,000 cells were analyzed by flow cytometry.

Karyotype analysis

The karyotype analysis of hematopoietic-like stem cells was performed by a protocol developed by Chou et al. (17).

Statistical analysis

Each experiment was performed triplicate, and the entire experiment was repeated at three different times. All data that corresponded to the three separate experiments were expressed as means ± SD. The distribution of parameters was evaluated using the Kolmogorov Smirnov test. The independent t test was used to estimate the difference between groups. Statistical analyses were performed using SPSS-18 software. $P<0.05$ were considered statistically significant.

Results

Quantitative real-time polymerase chain reaction analysis of *CD34, CD38,* and *GATA-1* genes

To determine the differentiation into the hematopoietic lineage using specific *CD34, CD38,* and *GATA-1* genes and quantitative real-time PCR, the change in expression of these genes was analyzed in comparison with the control group. As shown in Figures 1-3, *CD34* and *CD38* expression in exposed groups show a significant increase compared to the control group ($P<0.05$). This increase in gene expression levels were 2.85 and 1.84 folds, respectively, in the 10 mT group and 6.36 and 3.81 folds, respectively, in the 15 mT group. Therefore, electromagnetic waves have played a role in the reprogramming of fibroblast cells. The expression of the *GATA-1* gene in exposed groups was not altered in comparison with the control group ($P<0.05$).

Flow Cytometry analysis of CD34 Marker

Based on flow cytometric results shown in Figure 4, electromagnetic waves have caused the expression of CD34 marker at the surface of reprogrammed cells. This expression is about 42.3% in the 15mT group and 23.1% in the 10 mT group.

Karyotype analysis

Based on the karyotype analysis results shown in Figure 5, the karyotype of Hematopoietic-like stem cells shows normal karyotype.

Table 1: Genes primer sequence

Gene	Primer sequence (5´-3´)	Amplicon size (bp)
CD34	F: CTACAACACCTAGTACCCTTGGA	185
	R: GGTGAACACTGTGCTGATTACA	
CD38	F: AGACTGCCAAAGTGTATGGGA	118
	R: GCAAGGTACGGTCTGAGTTCC	
GATA-1	F: CTGTCCCCAATAGTGCTTATGG	88
	R: GAATAGGCTGCTGAATTGAGGG	
HPRT	F: CCTGGCGTCGTGATTAGTGAT	131
	R: AGACGTTCAGTCCTGTCCATAA	

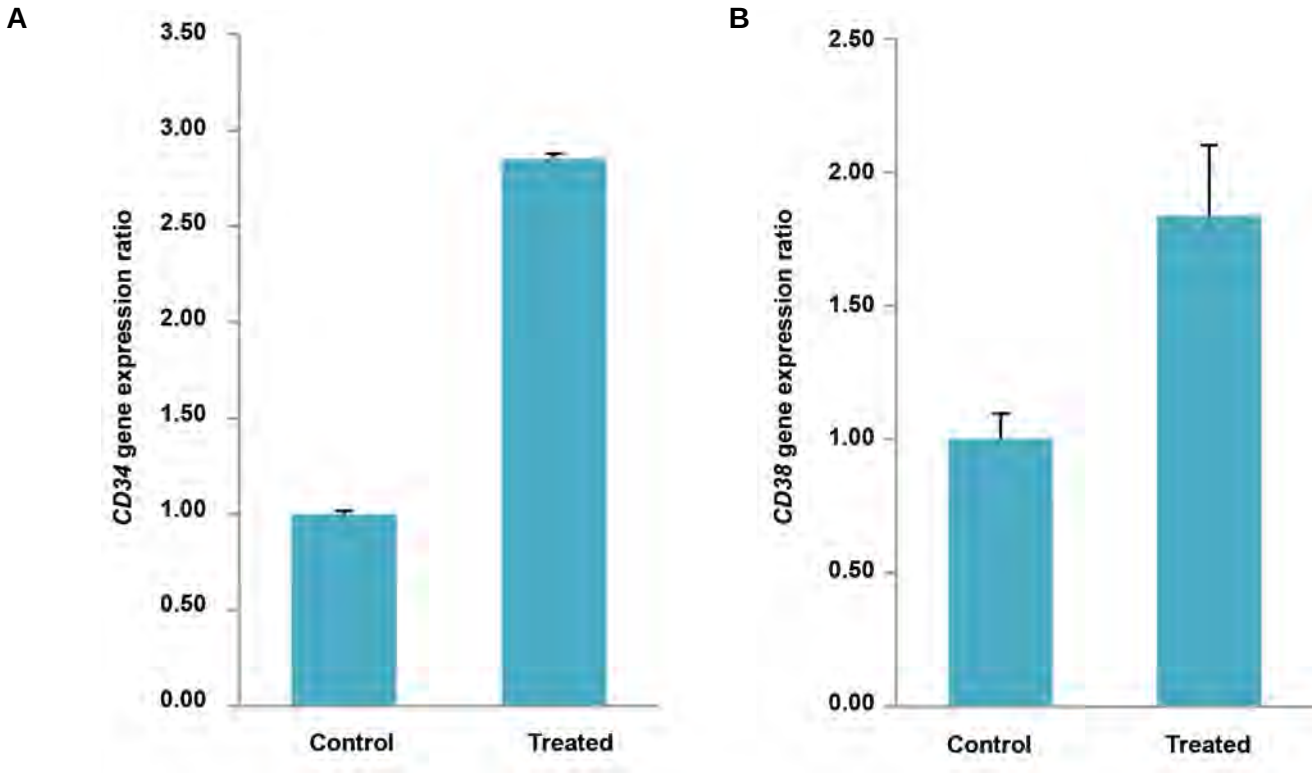

Fig.1: The expression level of hematopoietic-like stem cells genes in the 15 mT group. **A.** The expression level of CD34 gene expression is significantly increased compared to the control group (1.00 ± 0.02 Vs. 6.36 ± 0.08, P<0.001). **B.** The expression level of CD38 gene expression is significantly increased compared to the control group (1.00 ± 0.02 Vs. 3.81 ± 0.30, P<0.005). Data are presented as (mean ± SD).

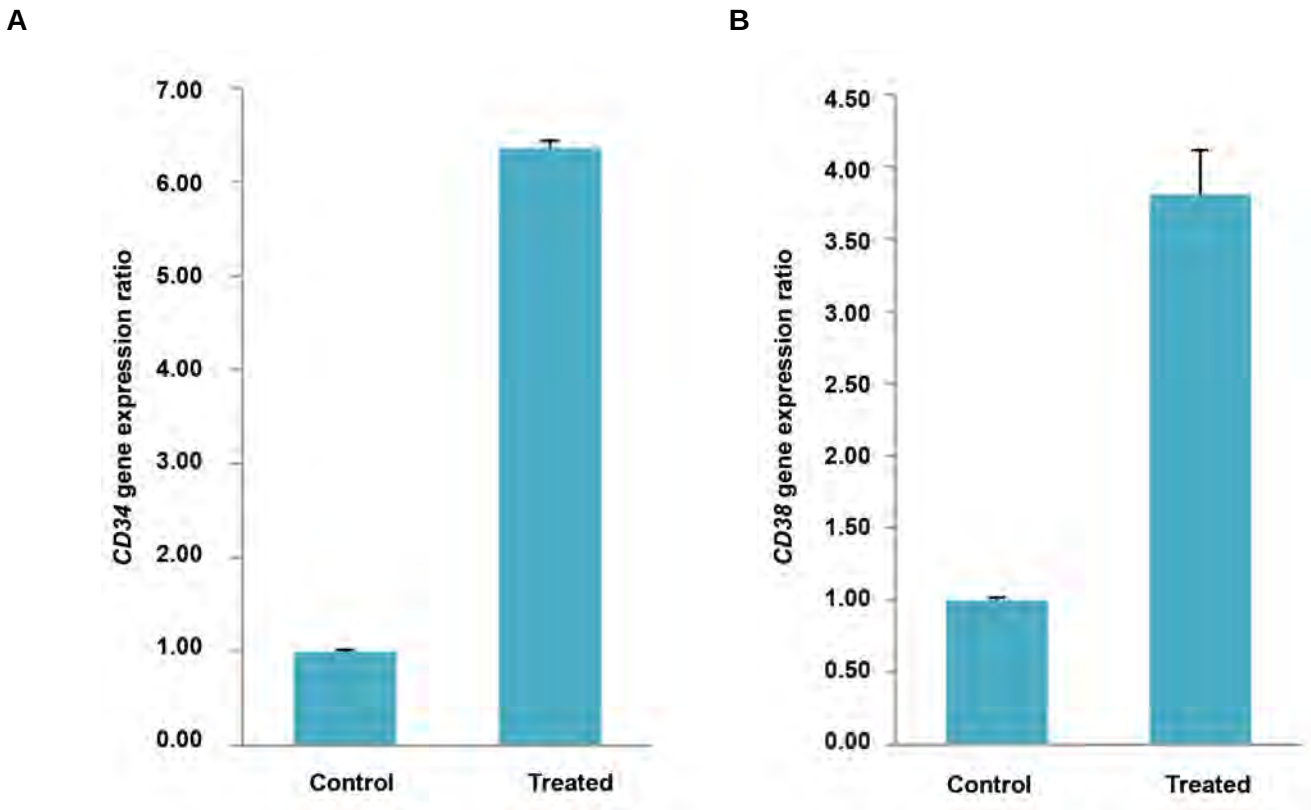

Fig.2: The expression level of hematopoietic-like stem cells genes in the 15 mT group. **A.** The expression level of CD34 gene expression is significantly increased compared to the control group (1.00 ± 0.02 Vs. 6.36 ± 0.08, P<0.001). **B.** The expression level of CD38 gene expression is significantly increased compared to the control group (1.00 ± 0.02 Vs. 3.81 ± 0.30, P<0.005). Data are presented as (mean ± SD).

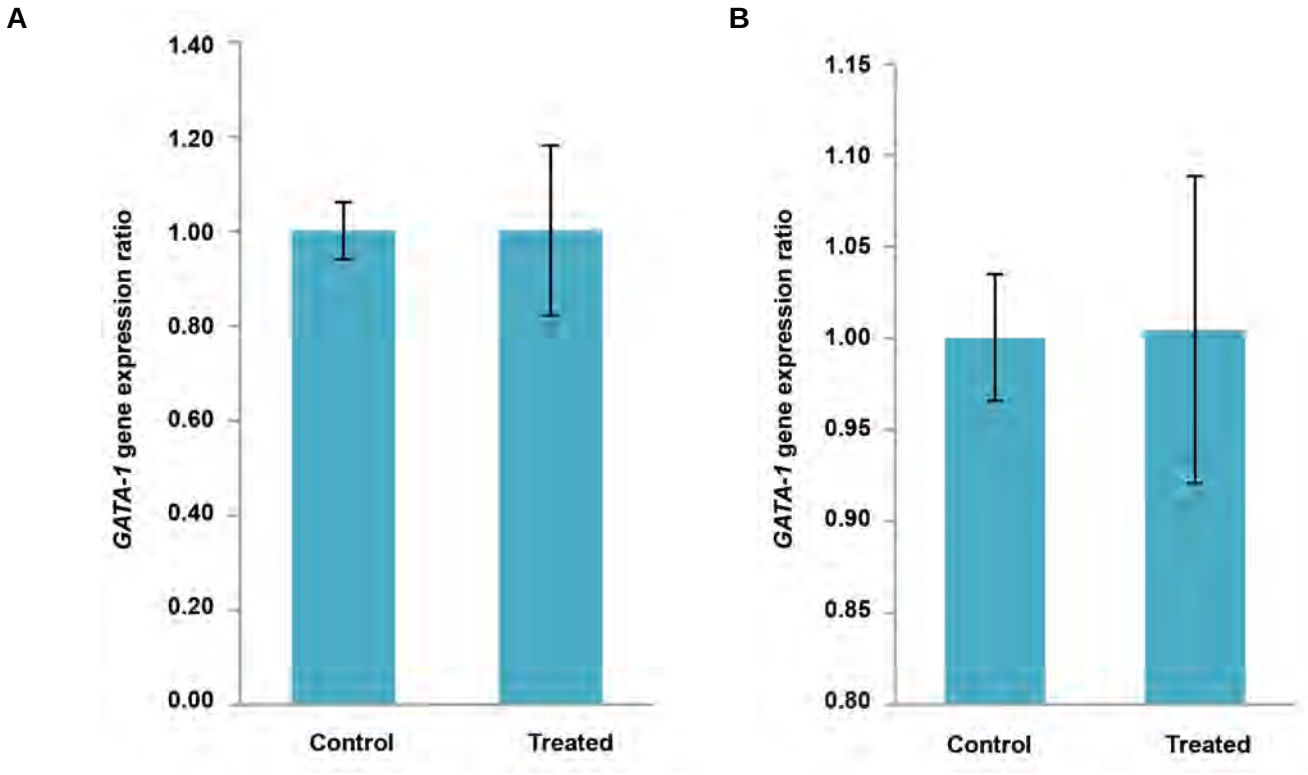

Fig.3: The Expression level of GATA-1 gene in hematopoietic-like stem cells. The expression of the GATA-1 gene did not change compared to the control group. **A.** The expression level of GATA-1 gene in the 10 mT group (1.00 ± 0.06 Vs. 1.00 ± 0.18, P<0.005). **B.** The expression level of GATA-1 gene in the 15 mT group (1.00 ± 0.03 Vs. 1.00 ± 0.08, P<0.005). Data are presented as (mean ± SD).

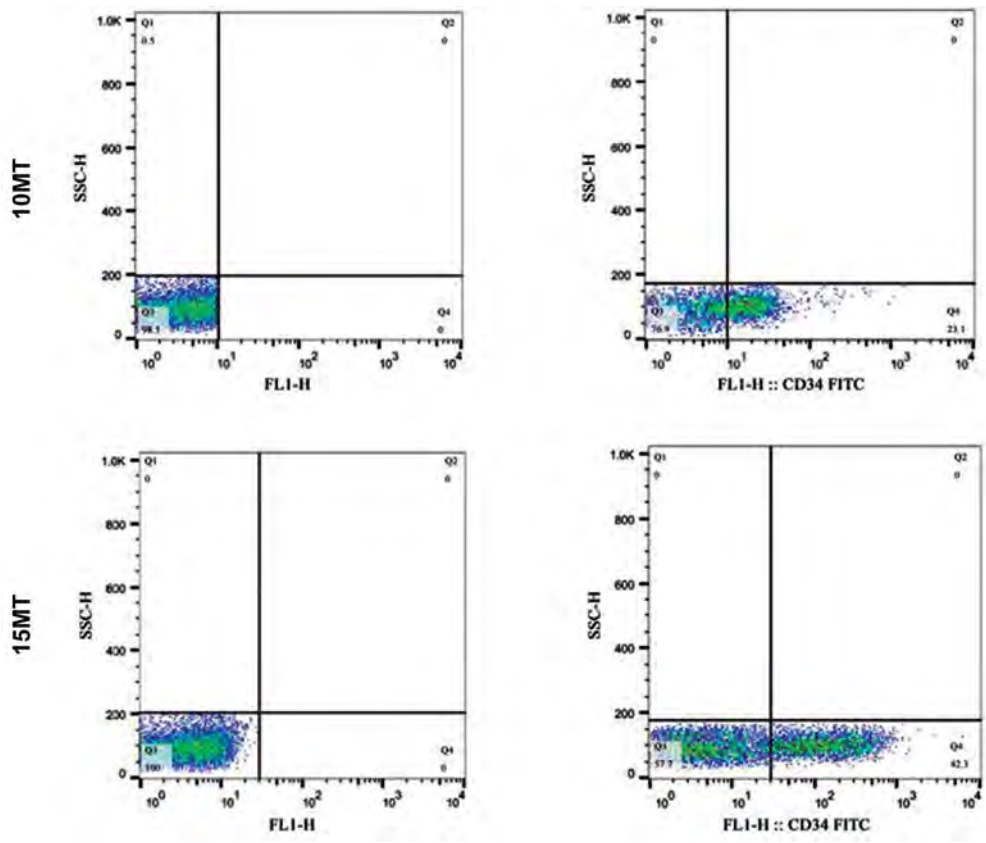

Fig.4: The image shown on the left side is the control sample, and the right model shown the cells treated with the CD34 antibody. The positive regions were adjusted according to the control isotype antibody reaction. (P<0.05).
Upper Image: Flow cytometric results of CD34 antigen in the 10mT group. A total of 2310 (event) cells express the CD34 marker. **Lower Image**: Flow cytometric results of CD34 antigen in the 15mT group. A total of 4230 (event) cells express the CD34 marker.

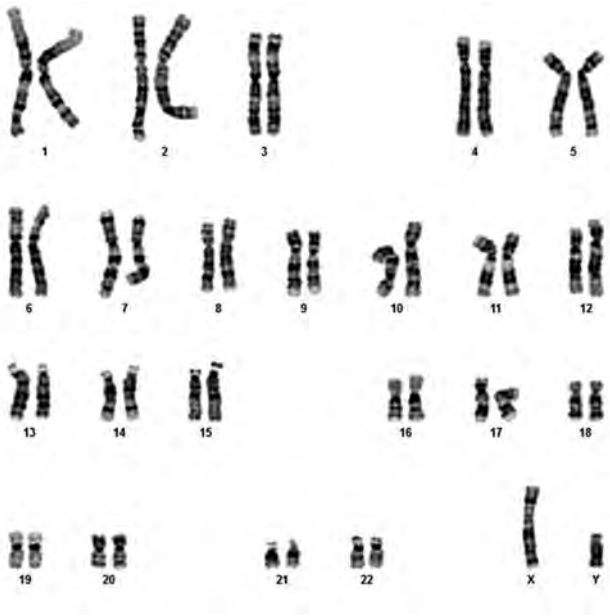

Fig.5: Hematopoietic-like Stem cells shows normal Karyotype.

Discussion

Electromagnetic waves, as one of the critical forces of nature, are physical energy charged by electrical objects and can influence the movement of other contradictory objects in this field. It was shown in this study that this physical energy can reprogram the cell and affect the fate of the cells. Exposure of cells to electromagnetic waves improves programming in somatic cells (18). Interestingly, exposure to electromagnetic waves with only one Yamanaka's agent, Oct4, and electromagnetic waves can fill up other factors, such as Sox2, Klf4, and c-Myc to reprogramming (16). These results provided a new window for the efficient production of iPSCs. Therefore, electromagnetic wave base reprogramming can ultimately offer a solution for the efficient and non-invasive cellular planning in regenerative therapies. The current study is a step forward in defining the main factors for inducing pluripotent cells from human fibroblasts.

Similar to ES cells, iPSCs should not be used directly in cell therapy, since the ability to make tumors is one of the inherent characteristics of these cells (9, 19). The ES cells and iPSCs need to be converted into functional cells before used in cell therapy. Recent advances in the direct reprogramming of cells that reprogram a type of somatic cell into a different kind without passing through the pluripotent state is a new solution for the generation of functional cells (20). The first study, in this case, is the expression of a transcription factor (MyoD) in fibroblast cells and the transformation of these cells into myoblasts (21). To date, many functional cells, including neurons, cardiomyocytes, stem cells, neuronal precursors, hepatocytes, and hematopoietic stem cells, have been obtained *in vitro* from fibroblast cells and other somatic cells (22, 23). The flexibility of fibroblasts and the success of their conversion to different types of cells have led to efforts to produce HSC cells from these cells as an alternative strategy for stem cell-based methods.

In the hematopoietic system, the hematopoietic stem cell is only cells that capable of differentiating into all blood cell types and self-renewal. This ability and the ability of these cells to fill the hematopoietic tissue of the individual after receiving the transplant makes use of these cells in regenerative medicine (24). Allogeneic and autologous stem cell transplantation has a disadvantage despite its widespread use in medicine. In an autologous transplant, patients with hematological diseases have the potential to transmit cancer cells to an individual. Allogeneic transplantation also usually results in Graft versus host disease (GVHD) due to minor differences in HLA type between the donor and the recipient (25). Despite medical advances made in HLA typing of individuals, GVHD is the leading cause of death in 60-80% of recipients of transplantation from non-native relatives (26). For this reason, the achievement of hematopoietic stem cells from another type of individual human cells is one of the primary goals of regenerative medicine.

In this study, it was shown that Human primary fibroblast cells could be directly reprogrammed to hematopoietic-like stem cells by exposure to electromagnetic waves and then cultured in a medium containing hematopoietic growth factors. Human primary fibroblast cells appear to be an accessible and safe cell population for cell reprogramming. Reprogramming cells without the use of viral agents is the most crucial goal of this study.

Conclusion

Because the use of retroviruses has many disadvantages, we are going to reprogram the distinct human fibroblast cells into hematopoietic stem cells by using electromagnetic fields. After exposure of fibroblast cells to electromagnetic fields and then placed in a hematopoietic differentiation medium, the expression of *CD34* and *CD38* genes were measured in 10 and 15 mT groups. The results showed that the expression of these genes after exposure to electromagnetic fields increased. The expression of the CD34 gene in the 10mT and 15mTesla group increased by 2.85 and 6.36 times, respectively, while the expression of the *CD38* gene in the 10 mT group was 1.84 versus 3.81, in the 15 mT group. The expression of the *GATA-1* gene in the 10 mT and 15 mT groups was not significantly different from the control group.

It seems that this method would be suitable for reprogramming the differentiated Human primary fibroblast cells into hematopoietic-like Stem cells and also does not have risks for using retroviruses.

Acknowledgments

This study is part of an M.Sc. thesis of Sina Habibi and financially supported by the Research Council of Bushehr University of Medical Sciences in 2019. There is no conflict of interest.

Author's Contributions

Gh.Kh., S.H.; Participated in study design, contributed to all experimental work, data and statistical analysis, and interpretation of data reviewed the literature for the manuscript. N.O., S.Z.J.; Contributed extensively in interpretation of the data and the conclusion, made substantial contribution to the discussions, wrote, and reviewed. Gh.Kh.; Edited and finalized the manuscript before submission, were responsible for overall supervision. All authors read and approved the final manuscript.

References

1. Dulak J, Szade K, Szade A, Nowak W, Józkowicz A. Adult stem cells: hopes and hypes of regenerative medicine. Acta Biochim Pol. 2015; 62(3): 329-337.
2. Wernig M, Meissner A, Cassady JP, Jaenisch R. c-Myc is dispensable for direct reprogramming of mouse fibroblasts. Cell Stem Cell. 2008; 2(1): 10-12.
3. Okita K, Ichisaka T, Yamanaka S. Generation of germline-competent induced pluripotent stem cells. Nature. 2007; 448(7151): 313-317.
4. Csobonyeiova M, Polak S, Zamborsky R, Danisovic L. iPS cell technologies and their prospect for bone regeneration and disease modeling: A mini review. J Adv Res. 2017; 8(4): 321-327.
5. Eminli S, Foudi A, Stadtfeld M, Maherali N, Ahfeldt T, Mostoslavsky G, et al. Differentiation stage determines potential of hematopoietic cells for reprogramming into induced pluripotent stem cells. Nat Genet. 2009; 41(9): 968-976.
6. Zhou W, Freed CR. Adenoviral gene delivery can reprogram human fibroblasts to induced pluripotent stem cells. Stem Cells. 2009; 27(11): 2667-2674.
7. Inoue H, Nagata N, Kurokawa H, Yamanaka S. iPS cells : a game changer for future medicine. EMBO J. 2014; 33(5): 409-417.
8. Nienhuis AW, Dunbar CE, Sorrentino BP. Genotoxicity of retroviral integration in hematopoietic cells. Mol Ther. 2006; 13(6): 1031-1049.
9. Aoi T. 10th anniversary of iPS cells: the challenges that lie ahead. J Biochem. 2016; 160(3): 121-129.
10. Cho H, Seo YK, Yoon HH, Kim SC, Kim SM, Song KY, et al. Neural stimulation on human bone marrow-derived mesenchymal stem cells by extremely low frequency electromagnetic fields. Biotechnol Prog. 2012; 28(5): 1329-1335.
11. Petri AK, Schmiedchen K, Stunder D, Dechent D, Kraus T, Bailey WH, et al. Biological effects of exposure to static electric fields in humans and vertebrates: a systematic review. Environ Heal. 2017; 16(1): 41.
12. Sabo J, Mirossay L, Horovcak L, Sarissky M, Mirossay A, Mojzis J. Effects of static magnetic field on human leukemic cell line HL-60. Bioelectrochemistry. 2002; 56(1-2): 227-231.
13. Amaroli A, Chessa MG, Bavestrello G, Bianco B. Effects of an extremely low-frequency electromagnetic field on stress factors: A study in Dictyostelium discoideum cells. Eur J Protistol. 2013; 49(3): 400-405.
14. Sun LY, Hsieh DK, Lin PC, Chiu HT, Chiou TW. Pulsed electromagnetic fields accelerate proliferation and osteogenic gene expression in human bone marrow mesenchymal stem cells during osteogenic differentiation. Bioelectromagnetics. 2010; 31(3): 209-219.
15. Huangfu D, Osafune K, Maehr R, Guo W, Eijkelenboom A, Chen S, et al. Induction of pluripotent stem cells from primary human fibroblasts with only Oct4 and Sox2. Nat Biotechnol. 2008; 26(11): 1269-1275.
16. Baek S, Quan X, Kim S, Lengner C, Park JK, Kim J. Electromagnetic fields mediate efficient cell reprogramming into a pluripotent state. ACS Nano. 2014; 8(10): 10125-10138.
17. Chou CH, Yang NK, Liu TY, Tai SK, Hsu DSS, Chen YW, et al. Chromosome instability modulated by BMI1-AURKA signaling drives progression in head and neck cancer. Cancer Res. 2013; 73(2): 953-966.
18. Ardeshirylajimi A, Soleimani M. Enhanced growth and osteogenic differentiation of induced pluripotent stem cells by extremely low-frequency electromagnetic field. Cell Mol Biol (Noisy-le-grand). 2015; 61(1): 36-41.
19. Kurotsu S, Suzuki T, Ieda M. Direct reprogramming, epigenetics, and cardiac regeneration. J Card Fail. 2017; 23(7): 552-557.
20. Xu J, Du Y, Deng H. Direct lineage reprogramming: strategies, mechanisms, and applications. Cell Stem Cell. 2015; 16(2): 119-134.
21. Davis RL, Weintraub H, Lassar AB. Expression of a single transfected cDNA converts fibroblasts to myoblasts. Cell. 1987; 51(6): 987-1000.
22. Lee S, Park C, Han JW, Kim JY, Cho K, Kim EJ, et al. Direct reprogramming of human dermal fibroblasts into endothelial cells using ER71/ETV2. Circ Res. 2017; 120(5): 848-861.
23. Sandler VM, Lis R, Liu Y, Kedem A, James D, Elemento O, et al. Reprogramming human endothelial cells to haematopoietic cells requires vascular induction. Nature. 2014; 511(7509): 312-318.
24. Chivu-Economescu M, Rubach M. Hematopoietic stem cells therapies. Curr Stem Cell Res Ther. 2016; 12(2): 124-133.
25. Amouzegar A, Dey BR, Spitzer TR. Peripheral Blood or bone marrow stem cells? Practical Considerations in hematopoietic stem cell transplantation. Transfus Med Rev. 2019; 33(1): 43-50.
26. Petersdorf EW. The major histocompatibility complex: a model for understanding graft-versus-host disease. Blood. 2013; 122(11): 1863-1872.

Short Communication

Profiling of Initial Available SARS-CoV-2 Sequences from Iranian Related COVID-19 Patients

Najmeh Salehi, Ph.D.[1, 2], Amir Amiri-Yekta, Ph.D.[1], Mehdi Totonchi, Ph.D.[1, 3]*

1. Department of Genetics, Reproductive Biomedicine Research Center, Royan Institute for Reproductive Biomedicine, ACECR, Tehran, Iran
2. Department of Bioinformatics, Institute of Biochemistry and Biophysics, University of Tehran, Tehran, Iran
3. Department of Stem Cells and Developmental Biology, Cell Science Research Center, Royan Institute for Stem Cell Biology and Technology, ACECR, Tehran, Iran

**Corresponding Address: P.O.Box: 16635-148, Department of Genetics, Reproductive Biomedicine Research Center, Royan Institute for Reproductive Biomedicine, ACECR, Tehran, Iran*
Email: m.totonchi@royaninstitute.org

Received: 3/April/2020, Accepted: 4/May/2020

Abstract

The etiologic agent SARS-CoV-2 has caused the outbreak of COVID-19 which is spread widely around the world. It is vital to uncover and investigate the full genome sequence of SARS-CoV-2 throughout the world to track changes in this virus. To this purpose, SARS-CoV-2 full genome sequence profiling of 20 patients in Iran and different countries that already had a travel history to Iran or contacts with Iranian cases were provided from the GISAID database. The bioinformatics analysis showed 44 different nucleotide mutations that caused 26 nonsynonymous mutations in protein sequences with regard to the reference full genome of the SARS-CoV-2 sequence (NC_045512.2). R207C, V378I, M2796I, L3606F, and A6407V in ORF1ab were common mutations in these sequences. Also, some of the detected mutations only were found in Iranian data in comparison with all the available sequences of SARS-CoV-2. The position of S protein mutations showed they were far from the binding site of this protein with angiotensin-converting enzyme-2 (ACE2) as the host cell receptor. These results can be helpful to design specific diagnostic tests, trace the SARS-CoV-2 sequence changes in Iran, and explore therapeutic drugs and vaccines.

Keywords: COVID-19, Nonsynonymous Mutations, SARS-CoV-2, S Protein

Cell Journal(Yakhteh), Vol 22, Suppl 1, Autumn 2020, Pages: 148-150

Citation: Salehi N, Amiri-Yekta A, Totonchi M. Profiling of initial available SARS-CoV-2 sequences from Iranian related COVID-19 patients. Cell J. 2020; 22 Suppl 1: 148-150. doi: 10.22074/cellj.2020.7524.

Coronaviruses (CoVs) are related to the family of Coronaviridae. They contain a single-stranded RNA of 26 to 32 kilobases. Pathogenic human CoVs usually cause mild respiratory diseases (1). In contrast, two highly pathogenic human CoVs were identified that transmitted from animals to humans. Severe acute respiratory syndrome (SARS) coronavirus (SARS-CoV) as the first one was reported in Guangdong, China, in November 2002 that caused more than 8,096 human infections and 774 deaths in 37 countries (2,3). The second one was the Middle East respiratory syndrome (MERS) coronavirus (MERS-CoV), which was first reported in Saudi Arabia in June 2012 that infected 1,728 cases and expired 624 patients in 27 countries (2).

In December 2019, a new human coronavirus, SARS-CoV-2, was identified in patients in Wuhan, Hubei Province, China (4,5). This new infectious respiratory disease is called coronavirus disease 19 (COVID-19), which is quickly spread around the world. The COVID-19 outbreak has a total of 2,072,113 infections and 138,475deaths in 210 countries and territories around the world until 15th April 2020. As it can be seen in Figure 1A, the full genome sequence of SARS-CoV-2 has ten open reading frames (ORFs) that contain four structural proteins; the spike-surface glycoprotein (S), the small envelope protein (E), the membrane glycoprotein (M), and the nucleocapsid protein (N), as well as several nonstructural proteins. In all CoVs, the S protein plays a crucial role in binding to the host cell receptors (6,7). A pairwise sequence alignment between the SARS-CoV-2 with SARS-CoV and MERS-CoV showed about 79% and 50% identity, respectively (8). The complete genome profile of SARS-CoV-2 revealed a high overall genome sequence identity to bat-CoV-RaTG13, Pangolin-CoV, bat-SARSr-CoV-ZC45, and bat-SARSr-CoV-ZXC21 by 96.2%, 91.02%, 87·99%, and 87·23%, respectively (8-10) Therefore, SARS-CoV-2 genome is highly similar to RaTG13 genome (9). However, genes such as ORF1b, the S protein, ORF7a, and ORF10

in pangolin-CoV depict higher identity with SARS-CoV-2 than bat-CoV-RaTG13 (10-12).

The genome sequence of SARS-CoV-2 is being generated by a lot of laboratories around the world, and these are freely available at the global initiative on sharing all influenza data (GISAID) database (13). These data can be helpful to design more specific diagnostic tests, trace the ongoing outbreak, and explore therapeutic processes. By 15th April 2020, twenty-three sequences of SARS-CoV-2 with a length of 87 to 595 bases and one full sequence with a length of 29,828 were available at the GISAID database of Iran's location. Fifteen and eight of these twenty-three sequences were associated with a part of the N gene and the ORF1ab, respectively. Three, four, and one (of eight) sequences of ORF1ab coded a portion of leader protein, RNA polymerase, 3´-to-5´ exonuclease, respectively. All of these twenty-three sequences encoded the related proteins as same as the reference one (NC_045512.2) if we masked the first and last few bases.

On the other hand, nineteen sequences of the full genome sequence of SARS-CoV-2 on the GISAID database from patients in different countries that had a travel history to Iran or contacts with Iranian cases were retrieved from the database. The one full sequence with Iran's location and these Iranian related sequences were translated to the protein sequence in six frames. The multiple nucleotide and protein sequence alignments of these initial available data were performed by MUSCLE and Clustal Omega programs with default parameters, respectively. The mutation results of nucleotide and protein sequences are available in Table S1 and S2 (See Supplementary Online Information at www.celljournal.org), respectively. As it can be seen in the Table S1, these sequences totally revealed 44 different nucleotide mutations that have made 26 nonsynonymous mutations in protein sequences (Table. S2) regarding the full genome of the SARS-CoV-2 sequence isolate Wuhan-Hu-1 (NC_045512.2). These nucleotide mutations should be noticed in designing diagnostic tests to reduce the false-negative results of no binding of primers and probes in qPCR-based tests. Figure 1B presents nucleotide mutations that lead to nonsynonymous mutations in protein sequences. A six-nucleotide and two-amino-acid insertions were detected in the full genome sequence of SARS-CoV-2 with Iran's location. The number of mutation events depicts that some of these mutations occurred more than three times among these 20 sequences such as R207C, V378I, M2796I, L3606F and A6407V in ORF1ab which are highlighted in the light orange columns in Figure 1B. Also, the entropy values of these mutations among the 3927 full genome sequences of the SARS-CoV-2 have retrieved from Nextstrain (14) (https://nextstrain.org/) analyses. The entropy values quantify the uncertainty or variability of amino acid mutations for each position in protein sequences. A position on the protein sequence without any mutation in the whole genome of the SARS-CoV-2 sequence has an entropy of zero (15). The entropy values show that some mutations have occurred just once in Iranian sequences were also rare in the 3927 full genome sequences of SARS-CoV-2 with 0.002 entropy value (Fig.1B). Furthermore, the corresponded protein name for each mutation is identified in Figure 1B. Accordingly, nsp2, nsp4, nsp6, 3´-to-5´ exonuclease, endoRNAse, and S protein contain more mutation positions with higher events in data from these 20 Iranian related patients. Among these proteins, the S protein facilitates viral entry into host cells (6, 7).

Similar to SARS-CoV, angiotensin-converting enzyme-2 (ACE2) is used as a cellular entry receptor for SARS-CoV-2 (16,17). The viral replication rates and disease severity depend on the binding affinity between the S protein and the ACE2 receptor (17). The 3D structure of the SARS-CoV-2 receptor-binding domain (RBD) in complex with human ACE2 protein receptor (PDB ID: 6M17) was superimposed on the S protein of SARS-CoV-2 with a single RBD up (PDB ID: 6VSB) by VMD1.9.3 (18) in Figure 1C. As can be seen, the S protein amino-acids variants in our cases are far from the binding site of the S-ACE complex. So, none of these mutations cause any disruption on the binding of S protein with ACE2. On the other hand, for the SARS-CoV-2 vaccine and drug designing the S protein is a perfect target on the surface of this virus (19, 20) which its mutations should be observed.

In this study, the full genome sequences of SARS-CoV-2 from the 20 Iranian related COVID-19 patients were profiled in detail. The results showed some significant mutations such as R207C, V378I, M2796I, L3606F, and A6407V in ORF1ab which occur more than three times among these 20 Iranian related sequences. Also, some rare mutations were found that only happened in these sequences in comparison with all 3927 full genome sequences of SARS-CoV-2. The structural analysis of S protein showed the S protein mutations in Iranian related sequences were away from the binding site of S protein with ACE2. These data can be of great help for performing researches to trace the SARS-CoV-2 sequence changes, designing more specific diagnostic tests to reduce the false-negative results of no binding of primers and probes in qPCR-based tests, as well as exploring specific therapeutic drugs and vaccines in Iran. It is certainly needed to generate more full genome sequences of SARS-CoV-2 from Iranian patients to find more certain changes of this virus in Iran.

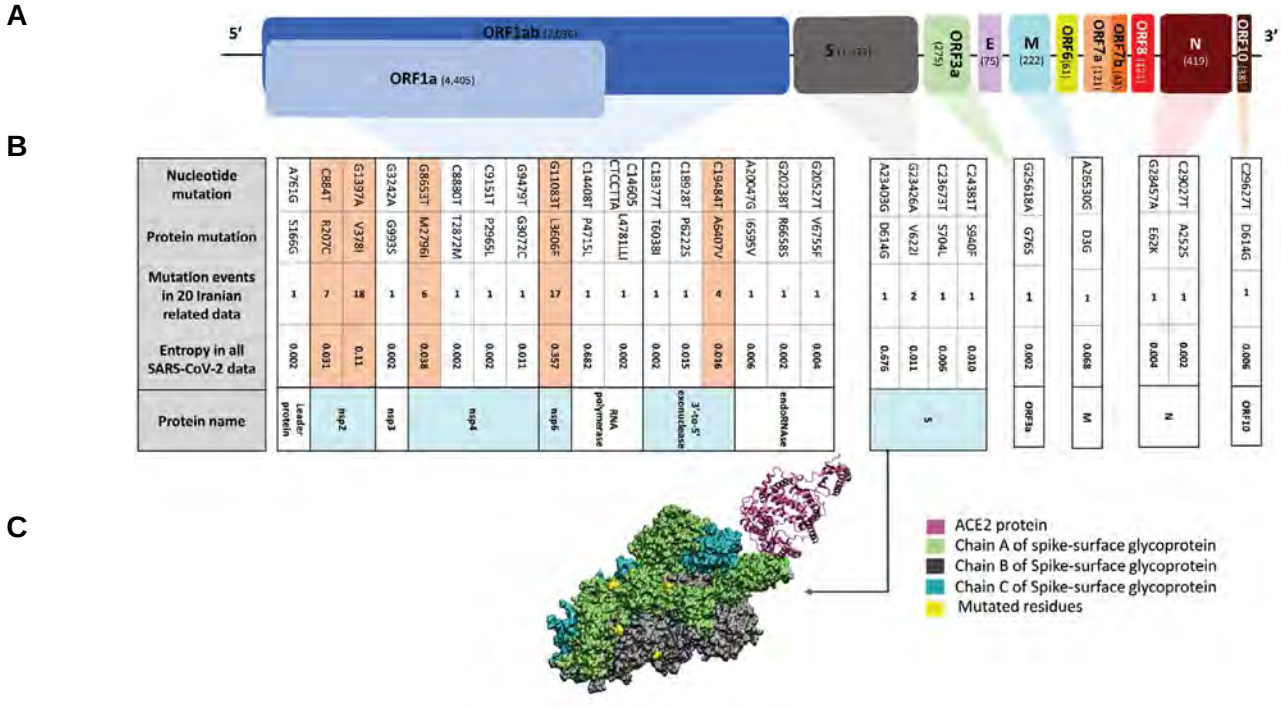

Fig.1: The genomic characterization and the specific mutations in the SARS-CoV-2 sequences of Iranian related COVID-19 patients. **A.** The schematic diagram of the genome organization of SARS-CoV-2 based on the full genome of the SARS-CoV-2 sequence (NC_045512.2). The numbers of the encoded amino acid residues are specified in parenthesis. **B.** The nucleotide and protein mutations, the number of mutation events in data from the 20 Iranian related patients, the entropy values of these mutations in all 3927 SARS-CoV-2 sequences, and the corresponded proteins are depicted. Light orange columns and cyan cells show the common mutations and their corresponded proteins in Iranian related sequences, respectively. **C.** The SARS-CoV-2 and ACE2 complex structure. ACE2, Chain A, B, C of S protein, and mutated residues are depicted in magenta, green, gray, cyan, and yellow, respectively.

Acknowledgements

The authors would like to thank the Genetic Department of Royan Institute for financially support. There is no conflict of interest.

Authors' Contributions

N.S.; Designed the study, analyzed the data and wrote the manuscript. A.A., M.T.; Reviewed the manuscript. M.T.; Proofread the manuscript. All authors read and approved the final manuscript.

References

1. Su S, Wong G, Shi W, Liu J, Lai ACK, Zhou J, et al. Epidemiology, genetic recombination, and pathogenesis of coronaviruses. Trends Microbiol. 2016; 24(6): 490-502.
2. De Wit E, Van Doremalen N, Falzarano D, Munster VJ. SARS and MERS: recent insights into emerging coronaviruses. Nat Rev Microbiol. 2016; 14(8): 523-534.
3. World Health Organization. Summary of probable SARS cases with onset of illness from 1 November 2002 to 31 July 2003. WHO; 2003. Available from: https://www.who.int/csr/sars/country/en/. (26 03 2020).
4. Wang C, Horby PW, Hayden FG, Gao GF. A novel coronavirus outbreak of global health concern. Lancet. 2020; 395(10223): 470-473.
5. Zhu N, Zhang D, Wang W, Li X, Yang B, Song J, et al. A novel coronavirus from patients with pneumonia in China, 2019. N Engl J Med. 2020; 382(8): 727-733.
6. Du L, He Y, Zhou Y, Liu S, Zheng BJ, Jiang S. The spike protein of SARS-CoV--A target for vaccine and therapeutic development. Nat Rev Microbiol. 2009; 7(3): 226-236.
7. Lu L, Liu Q, Zhu Y, Chan KH, Qin L, Li Y, et al. Structure-based discovery of Middle East respiratory syndrome coronavirus fusion inhibitor. Nat Commun. 2014; 5: 3067.
8. Lu R, Zhao X, Li J, Niu P, Yang B, Wu H, et al. Genomic characterisation and epidemiology of 2019 novel coronavirus: implications for virus origins and receptor binding. Lancet. 2020; 395(10224): 565-574.
9. Zhou P, Yang XL, Wang XG, Hu B, Zhang L, Zhang W, et al. A pneumonia outbreak associated with a new coronavirus of probable bat origin. Nature. 2020; 579(7798): 270-273.
10. Zhang T, Wu Q, Zhang Z. Probable pangolin origin of SARS-CoV-2 associated with the COVID-19 outbreak. Curr Biol. 2020; 30(7): 1346-1351.
11. Xiao K, Zhai J, Feng Y, Zhou N, Zhang Xu, Zou JJ, et al. Isolation and characterization of 2019-nCoV-like coronavirus from malayan pangolins. bioRxiv.2020. Available from: https://www.biorxiv.org/content/10.1101/2020.02.17.951335v1. (27 03 2020).
12. Zhang J, Jia W, Zhu J, Li B, Xing J, Liao M, et al. Insights into the cross-species evolution of 2019 novel coronavirus. J Infect. 2020. Available from: https://www.journalofinfection.com/article/S0163-4453(20)30106-7/fulltext. (27 03 2020).
13. Shu Y, McCauley J. GISAID: Global initiative on sharing all influenza data -from vision to reality. Euro Surveill. 2017; 22(13): pii: 30494.
14. Hadfield J, Megill C, Bell SM, Huddleston J, Potter B, Callender C, et al. NextStrain: Real-time tracking of pathogen evolution. Bioinformatics. 2018; 34(23): 4121-4123.
15. Sherwin WB. Entropy and information approaches to genetic diversity and its expression: Genomic geography. Entropy. 2010; 12(7): 1765-1798.
16. Li W, Moore MJ, Vasllieva N, Sui J, Wong SK, Berne MA, et al. Angiotensin-converting enzyme 2 is a functional receptor for the SARS coronavirus. Nature. 2003; 426(6965): 450-454.
17. Hoffmann M, Kleine-Weber H, Schroeder S, Krüger N, Herrler T, Erichsen S, et al. SARS-CoV-2 cell entry depends on ACE2 and TMPRSS2 and is blocked by a clinically proven protease inhibitor. Cell. 2020; 181(2): 271-280.
18. Humphrey W, Dalke A, Schulten K. VMD: Visual molecular dynamics. J Mol Graph. 1996; 14(1): 33-38.
19. Amanat F, Krammer F. SARS-CoV-2 vaccines: status report. Immunity. 2020; 52(4): 583-589.
20. Ahmed SF, Quadeer AA, McKay MR. Preliminary identification of potential vaccine targets for the COVID-19 coronavirus (SARS-CoV-2) based on SARS-CoV immunological studies. Viruses. 2020; 12(3): pii: E254.

IBD Patients Could Be Silent Carriers for Novel Coronavirus and Less Prone to its Severe Adverse Events: True or False?

Shaghayegh Baradaran Ghavami, Ph.D.[1, 2], Shabnam Shahrokh, M.D.[1, 2], Nikoo Hossein-Khannazer, Ph.D.[2, 3], Anastasia Shpichka,Ph.D.[4, 5], Hamid Asadzadeh Aghdaei, M.D.[1, 2], Peter Timashev, Ph.D.[4, 5], Massoud Vosough, Ph.D., M.D.[6*]

1. Basic and Molecular Epidemiology of Gastrointestinal Disorders Research Center, Research Institute for Gastroenterology and Liver Diseases, Shahid Beheshti University of Medical Sciences, Tehran, Iran
2. Gastroenterology and Liver Diseases Research Center, Research Institute for Gastroenterology and Liver Diseases, Shahid Beheshti University of Medical Sciences, Tehran, Iran
3. Department of Immunology, School of Medicine, Shahid Beheshti University of Medical Sciences, Tehran, Iran
4. Institute for Regenerative Medicine, Sechenov University, Moscow, Russia
5. Department of Chemistry, Lomonosov Moscow State University, Moscow, Russia
6. Department of Regenerative Medicine, Cell Science Research Center, Royan Institute for Stem Cell Biology and Technology, ACECR, Tehran, Iran

**Corresponding Address: P.O.Box: 16635-148, Department of Regenerative Medicine, Cell Science Research Center, Royan Institute for Stem Cell Biology and Technology, ACECR, Tehran, Iran.*
Email: masvos@royaninstitute.org

Received: 03/April/2020, Accepted: 20/May/2020

Abstract

Inflammatory bowel diseases (IBDs) are chronic disorders of the gastrointestinal tract. The goal of IBD treatment is to reduce the inflammation period and induce long-term remission. Use of anti-inflammatory drugs including corticosteroids, immunosuppressants and biologicals, is often the first step in the treatment of IBD. Therefore, IBD patients in pandemic of infectious diseases are considered a high-risk group. The public believes that IBD patients are at a higher risk in the current coronavirus 2 pandemic. Nevertheless, these patients may experience mild or moderate complications compared to healthy people. This might be because of particular anti-TNF-α treatment or any immunosuppressant that IBD patients receive. Moreover, these patients might be silent carrier for the virus.

Keywords: Anti-TNF-α, COVID-19, Crohn's Disease, IBD, Ulcerative Colitis

Cell Journal(Yakhteh), Vol 22, Suppl 1, Autumn 2020, Pages: 151-154

Citation: **Baradaran Ghavami Sh, Shahrokh Sh, Hossein-Khannazer N, Shpichka A, Asadzadeh Aghdaei H, Timashev P, Vosough M. IBD patients could be silent carriers for novel coronavirus and less prone to its severe adverse events: true or false? Cell J. 2020; 22 Suppl 1: 151-154. doi: 10.22074/cellj.2020.7603.**

Inflammatory bowel diseases (IBDs) are chronic inflammatory disorders of the gastrointestinal tract; IBDs are categorized as Crohn's disease (CD) and ulcerative colitis (UC) (1). The variation in the gut microbiota and certain genetic backgrounds as well as particular lifestyles are suggested as the main reasons for initiation and progression of these diseases (2). IBDs include two clinical stages, flare-up and remission, and the main therapeutic measures involve establishment and extension of the remission phase and avoiding flare-up occurrence (3). The medications used for management of the condition, are 5-aminosalycilic acid (5-ASA), immunosuppressants and biologicals targeting the immune system (1). Therefore, IBD patients are considered a high-risk group in epidemic and pandemic of infectious diseases.

Interestingly, in the recent pandemic of coronavirus disease (COVID-19), and the SARS-CoV epidemic in 2003, while the fecal samples of these patients were positive for the virus, they did not present any severe respiratory distress syndrome (4). In patients infected with SARS-CoV-2, the gastrointestinal symptoms such as diarrhea and nausea are more common compared to SARS-CoV patients. In addition, it was reported that while the SARS-CoV-2 test is negative for upper respiratory samples, stool samples remain positive for a few weeks after treatment (5). Remarkably, the angiotensin-converting enzyme-2 (ACE2) is the receptor for SARS-CoV-2 and it is expressed in different organs including the lungs, testis and ileum. This protein is also expressed on gut epithelial cells and secreted to the gut lumen (6).

The following two questions should be addressed in this context. First, whether IBD patients show mild or moderate signs and symptoms of COVID-19 compared to the others? Second, in the recent pandemic situation, could IBD patients be considered "silent carriers" and might they increase the disease spread rate?

The innate immune system has a crucial role in protecting body during viral infections. The innate immune system

produces and releases interferon α (IFN-α), an essential cytokine that interferes with the viral replication, virulence and spread in the host during the early phases (7). One of the important activities of coronavirus 2 is suppression of transcription and secretion of IFN-α (8). Moreover, it was shown that, SARS-CoV-2 can block the antiviral effects of IFN-α, *in vitro*. This is an essential mechanism for coronavirus 2 to escape the host innate immune system (9).

Recently, it was considered that there is a regulatory cross-talk between IFN-α and tumor necrosis factor (TNF-α). Of note, this cross-talk was reported between IFN-α and anti-TNF-α biologicals in clinic. Banchereau et al. and Palucka et al. showed that when rheumatoid arthritis patients were treated with anti-TNF-α biologicals (infliximab, adalimumab, and certolizumab pegol), the expression of IFN-α-regulated genes was increased in the peripheral blood mononuclear cell (PBMC) compared to the control group. Moreover, it was shown that when the immune cells produce higher amounts of IFN-α, they are less prone to be infected with SARS-CoV-2 and other viruses (10). Therefore, in patients with IBD who were treated with anti-TNF-α, there might be an increase in the production of IFN-α against viral infections. This could justify why IBD patients who were infected with SARS-CoV-2 , could probably present less severe symptoms compared to others (11). Besides, in IBD patients, particularly those who are under anti-TNF-α treatment, the host innate immune system interferes more efficiently with viral replication cycle and the clinical presentations are more moderate (9, 12).

ACE2 regulates the renin–angiotensin system (RAS) by cleaving several peptides (Ang1-7). This biological activity limits inflammation reflecting a protective role of the ACE2-MasR pathway (13). ACE2 is expressed on the epithelial cells in different organs including lungs, kidneys, liver, brain, blood vessels and particularly, on the cell membrane of the gut and illume epithelial cells (14). ACE2 is known as the main receptor for spike (S) protein of SARS-CoV-2 and is crucial for colonization and entry of the virus into the target cells. The soluble form of ACE2 (sACE2) can act as a decoy molecule and cover the S protein on the virions and block colonization. This can prevent the successful binding of the viral particles to the surface of the cells (15). Remarkably, patients with active UC and CD have higher numbers of ACE2 in their affected tissues (16). Since IBD patients are 3 times more prone to viral infections such as CMV, EBV, varicella zoster virus, and HSV, possible correlations between immunosuppressive therapy/biological treatments and coronavirus infection in IBD patients, should be assessed (17).

It was reported that ACE2 could be a potential target for therapeutic protocols against COVID-19. Therefore, human recombinant soluble ACE2 (hrACE2) could be considered a novel candidate for new treatment strategies (15, 18). Additionally, in two studies, it was shown that soluble ACE2 could block SARS coronavirus 2 replication (4, 19).

RAS and ACE2 are key players in human IBDs (19). It was reported that upregulation of Ang I-VII and ACE2 might be a compensatory response to intestinal inflammation which could result in increased concentrations of circulating ACE2. In fact, in IBD patients, the soluble isoform of ACE2 is found at higher levels in the peripheral blood, compared to normal individuals (11, 20). Interestingly, the expression of ACE2 and Ang (1-7) are increased in terminal ileum and colon in CD and UC patients (21). Though, IBD patients are quarantined and protected well during the pandemic, they could be "silent carrier" of the coronavirus.

TNF-α converting enzyme (TACE) is a protease enzyme that splits ACE2 molecules from the surface of cells (22). Blockage of TNF-α pathway induces TACE activity and increases sACE2 level. Further, it was suggested that TACE might be a potential target for antiviral compounds used for treatment of COVID-19 patients (23). Upregulation of TACE activity increases detachment of the ACE2 form the surface of epithelial cells. Blocking TNF-α by monoclonal antibodies (mAbs) may result in increased TACE activity and higher rate of cleavage of ACE2 from the surface (24). This was observed in IBD patients who are receiving different treatments such as immunosuppressants, corticosteroids and biological medications, for preventing relapse (25).

The main cause of acute respiratory distress syndrome (ARDS) in COVID-19 patients is the cytokine storm. The severity of COVID-19 is associated with increasing serum levels of IL-6, IL-7, IL-8, granulocyte-colony stimulating factor (G-CSF), IFN-γ, macrophage inflammatory protein 1-α (MIP1-α), and TNF-α. This situation increases recruitment of the immune cells into the lungs resulting in hyper inflammation in the patients and increasing adverse events and mortality (26). Accumulating evidence revealed that anti-inflammatory treatments could control ARDS (27). A multicenter, randomized controlled trial, approved the use of tocilizumab (an IL-6 receptor blocker licensed for cytokine release syndrome), in patients with COVID-19 pneumonia. Additionally, Janus kinase (JAK) inhibition could modulate both inflammation and viral entry into the cells in COVID-19 infection (28). Interestingly, IBD patients who regularly take cytokine blockers and immunosuppressant could control cytokine storm and the other related adverse events (11). Based on the specific type of treatment employed for each IBD patient, the severity of inflammation in the lungs and the antiviral immune responses may vary. This might help IBD patients in combating COVID-19 infection though the immune suppression can increase the risk of certain viral infections (29). It should be pointed out that further studies are required in this highly dynamic situation. There is no convincing evidence recommending that patients with IBD should stop their IBD-related medications (30). Nevertheless, elder IBD patients suffering from other comorbidities like obstructive lung diseases, diabetes mellitus, coronary heart diseases and hypertension might have an increased risk of COVID-19 (11). Figure1 schematically depicts this hypothesis.

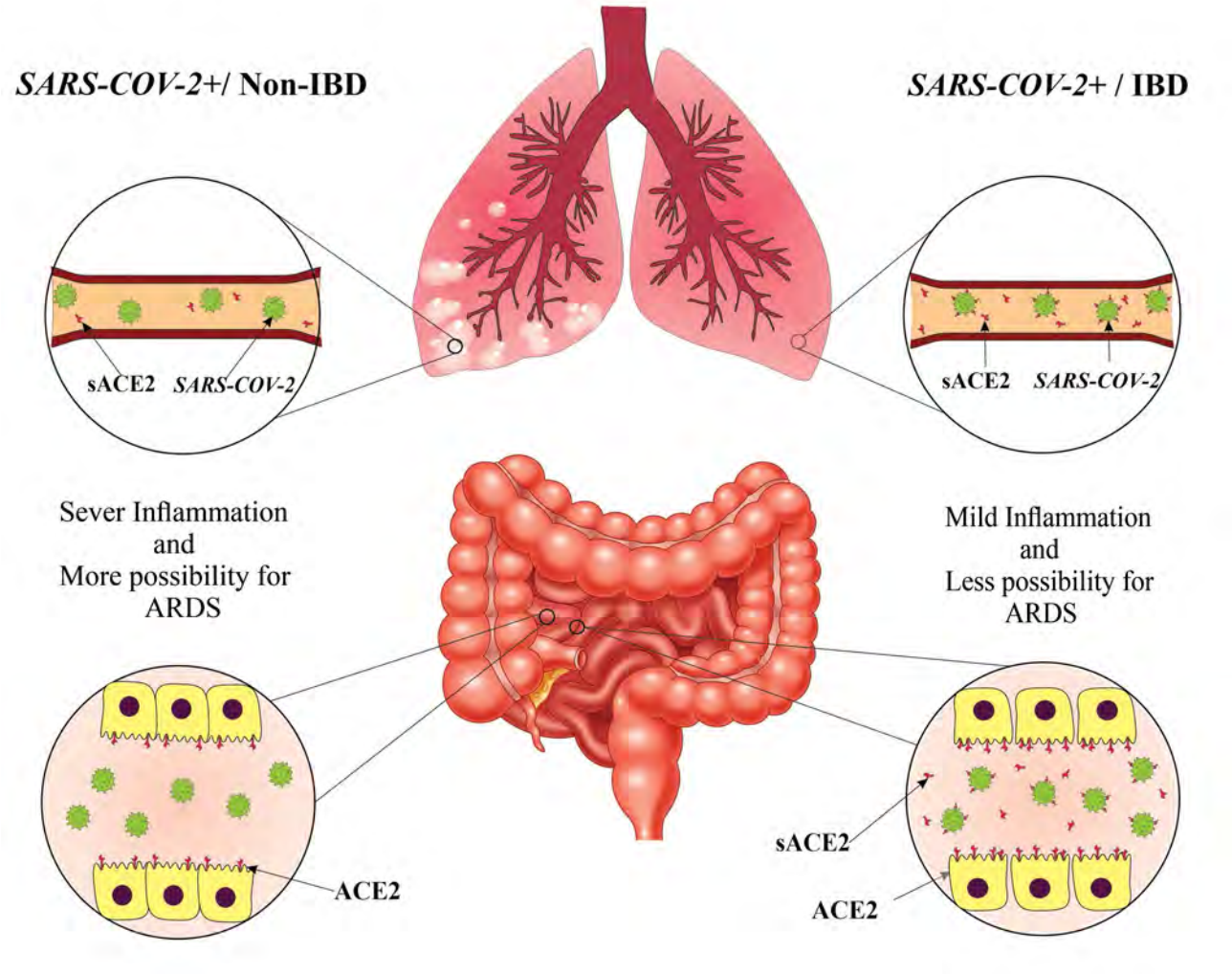

Fig.1: Schematic representation of ACE2 and sACE2 on epithelial cells and in blood circulation respectively in IBD and non-IBD patients. IBD; Inflammatory bowel disease, ARDS; Acute respiratory distress syndrome, and ACE2; Angiotensin-converting enzyme-2.

Though the public believes that IBD patients are at a higher risk for SARS-CoV-2 infection and complications, these patients may experience mild or moderate complications compared to healthy people. However, these patients might be silent carrier for the virus and should maintain their social distancing more strictly. These statements explain our hypothesis that in IBD patients infected with SARS-CoV-2, less severe clinical complications and lower morbidity and mortality rates, might be observed.

Acknowledgments

The authors would like to express their gratitude to Royan institute and Research Institute for Gastroenterology and Liver Diseases, Shahid Beheshti University of Medical Sciences, for their support throughout the course of this work. There is no conflict of interest.

Authors' Contributions

S.B.G., S.S., N.H.K., A.S., H.A.A.; Contributed substantially to the conception and design of the study. P.T., M.V.; Drafted and provided critical revision of the manuscript and provided final approval. substantially to the conception and design of the study. Drafted and provided critical revision of the manuscript and provided final approval. All authors read and approved the final manuscript.

Reference

1. Hanauer SB. Inflammatory bowel disease: epidemiology, pathogenesis, and therapeutic opportunities. Inflamm Bowel Dis. 2006; 12 suppl 1: S3-S9.
2. Younis N, Zarif R, Mahfouz R. Inflammatory bowel disease: between genetics and microbiota. Mol Biol Rep. 2020; 47(4): 3053-3063.
3. Raghu Subramanian C, Triadafilopoulos G. Care of inflammatory bowel disease patients in remission. Gastroenterol Rep (Oxf). 2016 ; 4(4): 261-271.
4. Li W, Moore MJ, Vasilieva N, Sui J, Wong SK, Berne MA, et al. Angiotensin-converting enzyme 2 is a functional receptor for the SARS coronavirus. Nature. 2003; 426(6965): 450-454.
5. Xiao F, Tang M, Zheng X, Li Y, Li X, Shan H. Evidence for gastrointestinal infection of SARS-CoV-2. Gastroenterology. 2020; 158(6): 1831-1833.
6. Gembardt F, Sterner-Kock A, Imboden H, Spalteholz M, Reibitz F, Schultheiss HP, et al. Organ-specific distribution of ACE2 mRNA and correlating peptidase activity in rodents. Peptides. 2005; 26(7): 1270-1277.
7. Katze MG, He Y, Gale M. Viruses and interferon: a fight for supremacy. Nat Rev Immunol. 2002; 2(9): 675-687.
8. Hiscott J, Lacoste J, Lin R. Recruitment of an interferon molecu-

lar signaling complex to the mitochondrial membrane: disruption by hepatitis C virus NS3-4A protease. Biochem Pharmacol. 2006; 72(11): 1477-1484.
9. Frieman M, Heise M, Baric R. SARS coronavirus and innate immunity. Virus Res. 2008 ; 133(1): 101-112.
10. Palucka AK, Blanck J-P, Bennett L, Pascual V, Banchereau J. Cross-regulation of TNF and IFN-α in autoimmune diseases. Proc Natl Acad Sci USA. 2005; 102(9): 3372-3377.
11. Monteleone G, Ardizzone S. Are patients with inflammatory bowel disease at increased risk for Covid-19 infection? J Crohns Colitis. 2020; JJaa061. (In Press).
12. Castilletti C, Bordi L, Lalle E, Rozera G, Poccia F, Agrati C, et al. Coordinate induction of IFN-α and-γ by SARS-CoV also in the absence of virus replication. Virology. 2005; 341(1): 163-169.
13. Salmenkari H, Pasanen L, Linden J, Korpela R, Vapaatalo H. Beneficial anti-inflammatory effect of angiotensin-converting enzyme inhibitor and angiotensin receptor blocker in the treatment of dextran sulfate sodium-induced colitis in mice. J Physiol Pharmacol. 2018; 69(4).
14. Garg M, Angus PW, Burrell LM, Herath C, Gibson PR, Lubel JS. The pathophysiological roles of the renin–angiotensin system in the gastrointestinal tract. Aliment Pharmacol Ther. 2012; 35(4): 414-428.
15. Batlle D, Wysocki J, Satchell K. Soluble angiotensin-converting enzyme 2: a potential approach for coronavirus infection therapy? Clin Sci. 2020; 134(5): 543-545.
16. Garg M, Royce SG, Tikellis C, Shallue C, Batu D, Velkoska E, et al. Imbalance of the renin–angiotensin system may contribute to inflammation and fibrosis in IBD: a novel therapeutic target? Gut. 2020; 69(5): 841-851.
17. D'Amico F, Peyrin-Biroulet L, Danese S. Inflammatory bowel diseases and COVID-19: the invisible enemy. Gastroenterology. 2020; 158(8): 2302-2304.
18. Monteil V, Kwon H, Prado P, Hagelkrüys A, Wimmer RA, Stahl M, et al. Inhibition of SARS-CoV-2 infections in engineered human tissues using clinical-grade soluble human ACE2. Cell. 2020. 181(4): 905-913.
19. Hume GE, Radford-Smith GL. ACE inhibitors and angiotensin II receptor antagonists in Crohn's disease management. Expert Rev Gastroenterol Hepatol. 2008; 2(5): 645-651.
20. Garg M, Burrell LM, Velkoska E, Griggs K, Angus PW, Gibson PR, et al. Upregulation of circulating components of the alternative renin-angiotensin system in inflammatory bowel disease: A pilot study. J Renin Angiotensin Aldosterone Syst. 2015; 16(3): 559-569.
21. Khajah MA, Fateel MM, Ananthalakshmi KV, Luqmani YA. Anti-Inflammatory action of angiotensin 1-7 in experimental colitis. PLoS One. 2016; 11(3): e0150861.
22. Wong E, Cohen T, Romi E, Levin M, Peleg Y, Arad U, et al. Harnessing the natural inhibitory domain to control TNFα converting enzyme (TACE) activity in vivo. Sci Rep. 2016; 6(1): 35598.
23. Haga S, Nagata N, Okamura T, Yamamoto N, Sata T, Yamamoto N, et al. TACE antagonists blocking ACE2 shedding caused by the spike protein of SARS-CoV are candidate antiviral compounds. Antiviral Res. 2010; 85(3): 551-555.
24. Lambert DW, Yarski M, Warner FJ, Thornhill P, Parkin ET, Smith AI, et al. Tumor necrosis factor-α convertase (ADAM17) mediates regulated ectodomain shedding of the severe-acute respiratory syndrome-coronavirus (SARS-CoV) receptor, angiotensin-converting enzyme-2 (ACE2). J Biol Chem. 2005; 280(34): 30113-30119.
25. Actis GC, Pellicano R. Inflammatory bowel disease: Efficient remission maintenance is crucial for cost containment. World J Gastrointest Pharmacol Ther. 2017; 8(2): 114-119.
26. Mehta P, McAuley DF, Brown M, Sanchez E, Tattersall RS, Manson JJ, et al. COVID-19: consider cytokine storm syndromes and immunosuppression. Lancet. 2020; 395(10229): 1033-1034.
27. Chen N, Zhou M, Dong X, Qu J, Gong F, Han Y, et al. Epidemiological and clinical characteristics of 99 cases of 2019 novel coronavirus pneumonia in Wuhan, China: a descriptive study. Lancet. 2020; 395(10223): 507-513.
28. Richardson P, Griffin I, Tucker C, Smith D, Oechsle O, Phelan A, et al. Baricitinib as potential treatment for 2019-nCoV acute respiratory disease. Lancet. 2020; 395(10223): e30-e31.
29. Chen C, Zhang XR, Ju ZY, He WF. Advances in the research of cytokine storm mechanism induced by Corona Virus Disease 2019 and the corresponding immunotherapies. Zhonghua Shao Shang Za Zhi C. 2020; 36(0): E005.
30. Burgueno JF, Reich A, Hazime H, Quintero MA, Irina F, Fritsch J, et al. Expression of SARS-CoV-2 entry molecules ACE2 and TMPRSS2 in the gut of patients with IBD. Inflamm Bowel Dis. 2020. 26(6): 797-808.

Short Communication

Challenges of Iranian Clinicians in Dealing with COVID-19: Taking Advantages of The Experiences in Wenzhou

Yuping Li, M.D.[1#], Yaser Tahamtani, Ph.D.[2, 3#], Mehdi Totonchi, Ph.D.[3, 4#], Chengshui Chen, M.D.[1#], Seyed Mohammad Reza Hashemian, M.D.[5], Fatemeh Amoozegar, B.Sc.[6], Jin-San Zhang, Ph.D.[1, 7*], Yousef Gholampour, M.D.[8*], Xiaokun Li, Ph.D.[1, 9*]

1. Department of Pulmonary and Critical Care Medicine, The First Affiliated Hospital of Wenzhou Medical University, China
2. Department of Diabetes, Obesity and Metabolism, Cell Science Research Center, Royan Institute for Stem Cell Biology and Technology, ACECR, Tehran, Iran
3. Department of Stem Cells and Developmental Biology, Cell Science Research Center, Royan Institute for Stem Cell Biology and Technology, ACECR, Tehran, Iran
4. Department of Genetics, Reproductive Biomedicine Research Center, Royan Institute for Reproductive Biomedicine, ACECR, Tehran, Iran
5. Chronic Respiratory Diseases Research Center, National Research Institute of Tuberculosis and Lung Diseases (NRITLD), Shahid Beheshti University of Medical Sciences, Tehran, Iran
6. Noncommunicable diseases research center, Fasa University of Medical Sciences, Fasa, Iran
7. International Collaborative Center on Growth Factor Research, and School of Pharmaceutical Sciences, Wenzhou Medical University, China
8. Department of Internal Medicine, School of Medicine, Fasa University of Medical Sciences, Fasa, Iran
9. School of Pharmaceutical Sciences, Wenzhou Medical University, and Wenzhou Biomedicine Collaborative Innovation Center, Wenzhou, China

#These authors contributed equally to this work.

**Corresponding Addresses: Department of Pulmonary and Critical Care Medicine, The First Affiliated Hospital of Wenzhou Medical University, Wenzhou 325000, China.*
Department of Internal Medicine, School of Medicine, Fasa University of Medical Sciences, Fasa, Iran.
School of Pharmaceutical Sciences, Wenzhou Medical University, and Wenzhou Biomedicine Collaborative Innovation Center, Wenzhou 325035, China.
Emails: Zhang_JinSan@wmu.edu.cn, Y.gholampoor@fums.ac.ir, Xiaokunli@wmu.edu.cn

Received: 05/May/2020, Accepted: 12/June/2020

Abstract

The novel coronavirus has been spreading since December 2019. It was initially reported in Wuhan, Hubei province of China. Coronavirus disease 2019 (COVID-19) has currently become a pandemic affecting over seven million people worldwide, and the number is still rising. Wenzhou, as the first hit city out of Hubei Province, achieved a remarkable success in effectively containing the disease. A great record was also observed in Wenzhou for the clinical management of COVID-19 patients, leading to one of the lowest death rates in China. Researchers and clinical specialists proposed and formulated combined approaches such as computerized tomography (CT)-scans and molecular assays, as well as using both allopathic and traditional medications to mitigate its effects. Iranian and Chinese specialists and scientists had a communication in clinical, molecular and pharmaceutical aspects of COVID-19. A proper guideline was prepared according to the experiences of Chinese clinicians in managing the full spectrum of COVID-19 patients, from relatively mild to highly complex cases. The purpose of this guideline is to serve a reference in the hospital for specialists so that they may better diagnose cases and provide effective therapies and proposed antiviral and anti-inflammatory drugs for patients.

Keywords: Anti-inflammatory Drug, Antiviral Drug, COVID-19, Diagnosis, SARS-CoV-2

Cell Journal(Yakhteh), Vol 22, Suppl 1, Autumn 2020, Pages: 155-165

Citation: Li Y, Tahamtani Y, Totonchi M, Chen Ch, Hashemian SMR, Amoozegar F, Zhang JS, Gholampour Y, Li X. Challenges of Iranian clinicians in dealing with COVID-19: taking advantages of the experiences in wenzhou. Cell J. 2020; 22 Suppl 1: 155-165. doi: 10.22074/cellj.2020.7604.

Pneumonia with unknown cause has been spreading in Wuhan city (Hubei province, China) since December 2019, while none of the previous vaccines or treatments has been effective. When more than 1,000 patients with coronavirus were identified, the world health organization (WHO) named it coronavirus disease 2019 (COVID-19) on February 2020. WHO also declared a state of emergency before finally recognizing it as a pandemic outbreak on March 11, 2020. Over 7,458,000 infected cases were confirmed in more than 200 countries on June 11, 2020. Major outbreaks of this disease have been reported in China, Italy, South Korea, and Iran, later spreading to many other countries. Mortality of COVID-19 has been approximately 34,114 people in 215 countries, including 4,634 in China, 34,114 in Italy and 8,506 in Iran (1, 2).

Based on the initial reports, the majority of patients were men over 50 years of age. Notably, it was determined that many of them worked in large seafood markets. The reason may be zoonotic transmission between pets and live wild animals traded in the markets; however, scientists observed that the disease is quickly transmitted among the individuals (3, 4).

COVID-19 (also known as SARS-CoV-2) is a RNA virus belonging to the coronaviridae family. It is widely distributed among humans and other mammals. In most cases, the primary symptoms, such as fever, ague, cough and myalgia, fatigue or similar symptoms were observed (5).

Clinical presentations of COVID-19 vary across a broad spectrum of patients with problems ranging from asymptomatic infection and mild upper respiratory tract disease to severe viral pneumonia with respiratory failure and death (6). Morbidity in patients with COVID-19 is secondary to severe alveolar injury and progressive respiratory failure (7). In patients who are mostly between 30 and 79 years old, the symptoms start a few days after virus infection, although can sometimes appear later. In some individuals, there may be no symptom at all (8). WHO has announced that incubation period of the disease lasts up to 14 days, but some researchers believe that it can lasts up to 20 days (9). Based on this, in addition to the highly infectious nature of SAR-CoV-2, the most appropriate approach is quarantine (10).

One of the most successful quarantine applications was in Wenzhou, a city in China that is 900 km away from Wuhan. Wenzhou has a population of 9 million and was one of the first and worst hit cities in of Hubei Province with a more than 504 confirmed cases by the end of February 2020. Wenzhou achieved a remarkable success in controlling the disease outbreak by systemic and rigorous reinforcement of social distancing and home quarantines. The municipal government of the city enforced 25 preventive measures to control the outbreak of coronavirus, such as traffic limitation and reduction of people congregating in both public and private areas, etc. Furthermore, different places were sterilized daily, people used masks and air filtration was implemented when possible. Those who detected positive for COVID-19 (using laboratory tests) and people who returned from the virus epicenter of Wuhan were isolated and carefully monitored either in the hospital or at home. Additionally, only one member of a family could go out to buy home supplies as a method to further contain the spread of the virus. Overall, we know that COVID-19 has caused a great deal of fear and anxiety among people around the world, but this issue have been controlled and Chinese people have managed to control the outbreak correctly (10).

On top of effective control of the disease, Wenzhou also set up a great record for the clinical COVID-19 patients resulting in death rate well below 1%, one of the lowest ratios in China. From January 17, when the first COVID-19 patient was confirmed, researchers and clinical specialists proposed and formulated combined approaches. Several additional diagnostic methods were proposed to screen for SARS-CoV-2, such as computerized tomography Computerized tomography (CT)-scan polymerase chain reaction (PCR), value of C-reactive protein (CRP), immunoglobulin G (IgG) and immunoglobulin M (IgM) levels (11).

There are several additional factors that impact the clinical prognosis of this disease, such as gender, age, regulation of the immune system, physical and nutritional status and expression of human leukocyte antigen (HLA) genes (12). Additionally, some studies showed that HLA expression changes like HLA-A 02:02, HLA-B 15:03, HLA-C 12:03, HLA-B 54:01, HLA-B 07:03, HLA-Cw 08:01, DRB1 03:01, and especially HLA-B 46:01 were significantly associated with high-risk respiratory infectious diseases, like severe acute respiratory syndrome (SARS), middle east respiratory syndrome (MERS) and flu. They can influence the severity of the disease, immune response of the host and susceptibility to these respiratory infectious diseases (13). One study showed that evaluation of HLA classes can be effective in predicting whether a subject will be resistant to infection. It was suggested that HLA-B 46:01 and HLA-B 15:03 are linked to this disease. This study showed that subjects with HLA-B 46:01 are more susceptible to COVID-19. In addition, HLA-B 15:03 potentially plays a role in the release of SARS-CoV-2 peptides in humans. Therefore, this factor could be useful in predicting the most vulnerable individuals to COVID-19 (13). Notably, lymphopenia development, chest CT-scan status, real-time PCR test, rate of oxygen intake, levels of CRP, D-dimer and ferritin levels are all important in determining clinical management (14).

The mortality rate of COVID-19 is about 2% (15), but this is significantly higher in patients with comorbidities and older individuals. In patients over 80 years of age, the mortality rate is 14.8%. Patients with diabetes, cardiovascular disease, chronic respiratory disease, hypertension and cancer are also at increased risk (7.3%, 10.5%, 6.3%, 6% and 5.6%, respectively). Furthermore, the mortality rate is around 3.8% in hospital personnel. These people are already operating in a high risk environment and this higher mortality rates suggest that that disease will be more severe (3).

The outbreak of COVID-19 has lasted several months and there is a lack of definitive information, widely available and accurate diagnostic methods or effective therapy to manage the disease. We also do not have sufficient information about risk factors that may exacerbate the disease and increase mortality in these patients. Interestingly, Wenzhou has enforced multiple precautionary measures to prevent the outbreak of this virus at the right time, so this study suggests that all countries

should adopt the proper approaches and standards to inhibit this disease. While this challenging issue can be controlled, scientists and physicians across the world must communicate with each other in order overcome this outbreak. WHO has recommended knowledge-transfer required to increase awareness of the outbreak, diagnostic, therapeutic and pharmacological methods in COVID-19 field. Therefore, Chinese and Iranian clinical and pulmonary specialists shared several questions regarding clinical and molecular diagnostic methods, different drugs applications and proposed therapeutic methods. Chinese scientists then responded to them based on their own experiences in dealing with COVID-19 patients. This article can be used as a reference tool for practitioners and specialists to improve the common treatment and diagnostic methods for SARS-CoV-2 and the related disease, COVID-19 (15). Iranian clinicians prepared some questions about the diagnosis, therapies, types of drugs, etc. These questions are listed in Table 1. The questions were gathered by pulmonary specialists and scientists and were asked during a webinar. Then Chinese specialists answered these questions based on their own experiences.

In general, WHO guidelines recommend that non-invasive ventilation (NIV) can be used for one hour for patients with severe COVID-19, whereas China's health commission recommends that NIV can be used for maximally two hours in patients with a PaO_2/FiO_2 of 150-200. It is important to use NIV in combination with other therapies. If there is extended use for a longer period of time, such as an entire day, it is important to closely monitor disease progression. We consider it will not be helpful to try NIV for more than one day if there is no improvement in the oxygen saturation levels. In some cases with COVID-19, respiratory rate of patients will not increase even though they have moderate to severe hypoxia (16).

For COVID-19 patients with blood oxygen saturation ≤93% or respiratory rate (RR)≥30 times/min on room air, initial oxygen therapy should be started immediately at 5 l/min and the oxygen should be selected based on the severity of hypoxia as well as the available treatment devices, including nasal catheters, simple masks, oxygen storage masks, etc. If the oxygen storage mask absorbs oxygen at a flow rate of 10-15 l/min and the pulse oxygen saturation is still ≤90% or RR≥30 times/min, then severe acute hypoxic respiratory failure or acute respiratory distress syndrome (ARDS) should be considered and the patient should receive further respiratory support treatment as soon as possible (16).

Table 1: The questions which discussed during the webinar and addressed in the paper

No	Questions
1	According to the guidelines, NIV is not applicable for the severe virus infections. However, do you have any experience, which shows its positive effects on COVID-19 patients? What are the exact indications for using NIV for these patients? Shouldn't we be worried about spreading the virus by using this method?
2	Do you have experience with ECMO for your COVID-19 patients?
3	What are your experiences regarding lung CTs of the COVID-19 patients?
4	Do you have any experience about sampling for PCR diagnosis? Which sampling protocol has more accuracy?
5	How many patients do you have with positive CT which their PCR tests are negative? And, do you categorize these patients (CT+ and PCR-) as the COVID-19 positive/negative patients?
6	Do you have any experience on using BAL for COVID-19? Do you think it works?
7	Do you have any experience about using "Favipiravir" (a new pharmaceutical drug, also named Avigan) for COVID-19 patients? If yes, on how many patients and what was the result?
8	What is the impact of Glucocorticoids for COVID-19 patients? If it is useful, what is the exact steroid type that you use? What is its dose per day and the interval of administration?
9	Do you have any experience about using dexamethasone for patients in ICU?
10	Does plasma exchange work? Do you have any experience on plasma exchange in people who are already cured?

NIV; Non-invasive ventilation, ECMO; Extracorporeal membrane oxygenation, CT; Computerized tomography. PCR; Polymerase chain reaction, ICU; Intensive care unit, BAL; Bronco-alvage, and COVID-19; Coronavirus Disease 2019.

For patients with severe acute hypoxic respiratory failure and mild-to-moderate ARDS (150 mmHg $<PaO_2/FiO_2 \leq 300$ mmHg), high-flow nasal cannula oxygen therapy (HFNO) is preferred, followed by NIV. Changes in the patient's condition should be closely monitored by medical staff who is skilled in performing tracheal intubation during treatment with HFNO or NIV. In patients with mild ARDS who cannot tolerate HFNO, NIV treatment can be attempted. But, it is not recommended to switch therapeutic approach into NIV in patients who have failed HFNO. Regarding the application of NIV, it is important to use the disposable exhalation valve instead of the mask-integrated valve and platform valve. A filter can be added between the mask and the exhalation valve (as shown in Fig.1 and Fig.2). However, this can cause problems, as the filter will increase resistance for water and it can cause water overload. Therefore, filter use should be carefully considered and in case of increasing resistance, it immediately needs to be replaced. The clinically used passive expiratory valve usually includes single orifice valve, mute valve, platform valve and mask-integrated valve. The vent hole of the mask-integrated valve is located on the face of mask, and the exhaled gas is directly discharged. This increases the risk of aerosol transmission of COVID-19 (16, 17).

When patients are under tracheal intubation and on ventilator support, it is recommended to use a heat and humidity exchanger (passive humidification) with bacterial filtration function for the humidification of the invasive ventilator (including transfer ventilator). Alternatively, a dual-heating wire humidifier can also be used for active humidification. It is recommended to use a closed-type automatic water renewal humidification tank or a self-made semi-automatic humidification tank as a water-adding device (Fig.3). It should be noted that active humidification is not recommended to increase the filter at the Y-shaped pipe, since this will increase water content of the filter, consequently increasing the respiratory resistance (16).

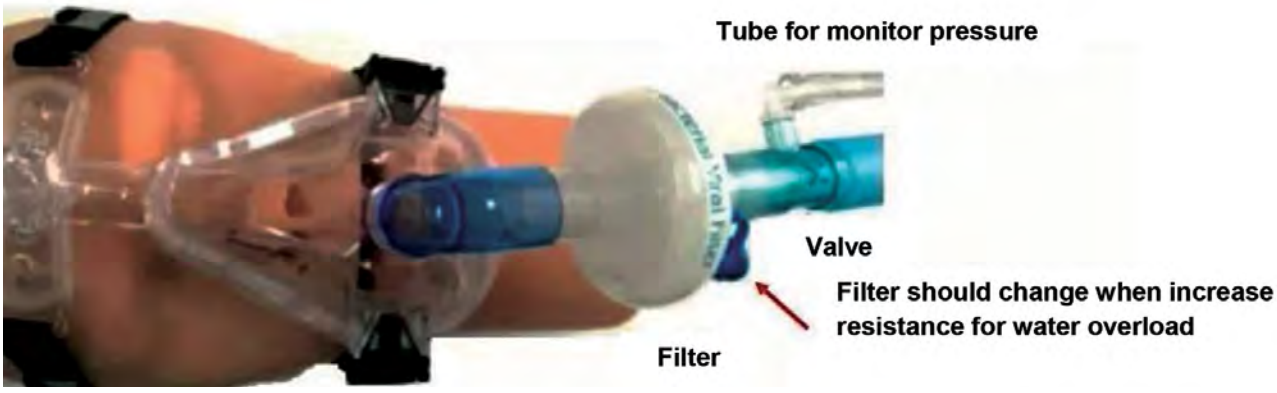

Fig.1: Location of filter near the patient, while non-invasive ventilation (NIV) (between the mask and exhalation valve) is marked by red arrow.

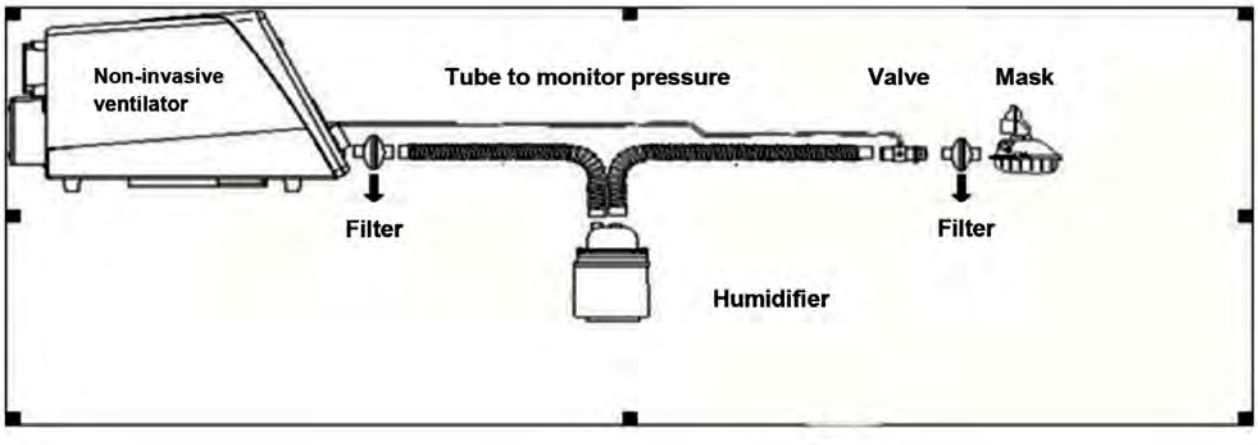

Fig.2: Location of filter, connected in gas outlet of non-invasive ventilation (NIV) and marked by black arrow.

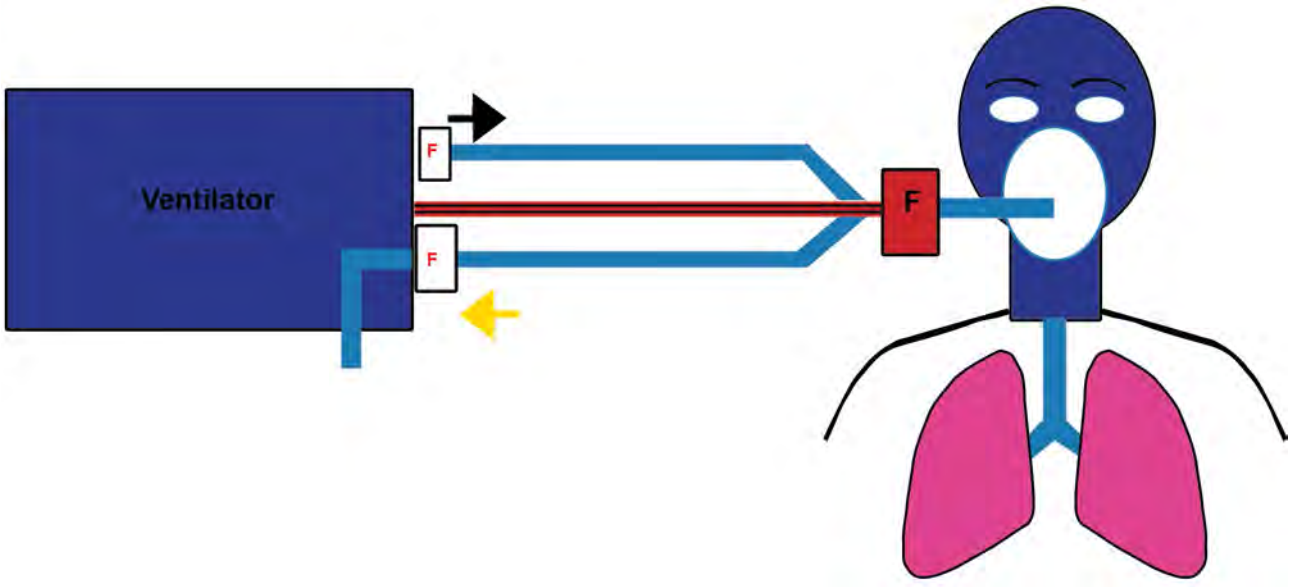

Fig.3: Location of filter (F) in the patient with tracheal intubation filter.

In China, ECMO is often used in the very late stages of disease and the crude mortality rate is not known. Among our six patients, two patients successfully weaned off ECMO and one passed away, while the other three patients are still under treatment. Veno-venous extracorporeal membrane oxygenation (VV-ECMO) was chosen for five patients and veno-arterial extracorporeal membrane oxygenation (VA-ECMO) was selected for one patient (17). Sometimes, patients with severe COVID-19 deteriorate quickly. If the patient's hypoxia does not improve after standard ARDS treatment, ECMO should be started to avoid multiorgan damage caused by either hypoxia or over-ventilation. Based on the previous relevant clinical studies and the recommendations from the International Organization for Extracorporeal Life Support, ECMO should be used in the setting of hypoxic respiratory failure (primary or secondary) caused by any etiology. When the risk of death reaches or exceeds 50%, ECMO should be considered. And by reaching risk of death to 80%, ECMO treatment should be initiated. ECMO can be started under optimal ventilation conditions ($FiO_2 \geq 0.8$, tidal volume 6 ml/kg, Positive end-expiratory pressure (PEEP)$\geq$10 cmH_2O), if there is no contraindication and it meets one of the following conditions: 1. $PaO_2/FiO_2<50$ mmHg More than three hours; 2. $PaO_2/FiO_2<80$ mmHg exceeds six hours; 3. $FiO_2=1.0$, $PaO_2/FiO_2<100$ mmHg; 4. arterial blood pH value <7.25 and $PaCO_2>60$ mmHg more than six hours and respiratory rate >35 times/min; 5. when the respiratory rate is >35 times/min, the blood pH is <7.2 and the plateau pressure is >30 cmH_2O and 6. severe air leak syndrome carrying cardiogenic shock or cardiac arrest (17).

The pathophysiology of critical COVID-19 is heterogeneous in lung injury, but its clinical characteristics are different from those of the other ARDS (18).

Refractory hypoxemia: ARDS, causing by COVID-19, decreases lung volume due to the collapse of a large number of alveoli, decreased lung compliance and hypoventilation, as well as the blood flow ratio disorders. Of these etiologies, decreased pulmonary ventilation and blood flow ratio disorders are the main causes of hypoxemia. Interstitial pulmonary edema in ARDS compresses the small airways and reduction of surfactants causes partial alveolar collapse, resulting in inadequate ventilation of the corresponding lung unit. This, in turn, leads to a decrease in pulmonary ventilation and blood flow ratio, causing functional shunting with extensive atelectasis and alveolar edema. Local lung units have only limited blood flow without ventilation. That is true shunt and the main cause of refractory hypoxemia (19). Hypercapnia that is difficult to correct with conventional ventilation: COVID-19-induced ARDS has different clinical manifestations from the other ARDS and some patients will develop hypercapnia. Mechanism of hypercapnia is due to the non-uniformity of lung damage caused by the new coronavirus. This results in excessive expansion of normal ventilated lung tissue around the collapsed lung tissue. This leads to increased alveolar dead space, CO_2 retention and hypercapnia (19). Low lung expandability: ARDS caused by COVID-19 is a typical endogenous ARDS in the lungs, but response to lung expansion and PEEP is poor. The main mechanism is that local lung injury from virus causes high pressure to open the alveoli. Even if the routine lung expansion is attempted, the collapsed alveoli often cannot be expanded, but the surrounding alveoli are over-expanded. This in turn exacerbates the patient's hypoxemia and hypercapnia. We performed invasive mechanical ventilation on 12 patients with severe COVID-19 and used lung expansion/dilation index to evaluate the results. We found that lung expandability of 11 patients was very low. Therefore, ARDS caused by

COVID-19 should be evaluated for lung expandability during further mechanical ventilation treatment to determine the appropriate ventilation strategy (19).

Acute right heart dysfunction: Hypoxemia, hypercapnia and secondary massive alveolar collapse due to COVID-19 will cause acute pulmonary hypertension, followed by acute right-sided heart failure. The associated hemodynamic changes severely impact the patient's clinical prognosis. The mechanism of pulmonary hypertension, induced by ARDS, starts with alveoli collapse, leading to hypoxia and hypercapnia. This opens calcium ion channels on the cell membrane, depolarizing the cell membrane and increasing the concentration of calcium in the cytoplasm. Ultimately, this leads to vasoconstriction and subsequent pulmonary hypertension. The alveoli collapse might be associated with collapse of alveolar blood vessels, which in turn increases pulmonary arterial pressure. Under inappropriate mechanical ventilation, even if collapsed alveoli are re-expanded, alveolar hyperinflation may still occur in non-gravity-dependent areas of the lung. Alveolar hyperinflation compresses surrounding vascular structures. This increases pulmonary vascular resistance and leads to acute right-sided heart failure (19, 20).

Indications of conventional ARDS prone position ventilation include moderate to severe ARDS [oxygenation index is less than 150 mmHg (1 mmHg=0.133 kPa)]. Additionally, severe hypoxemia and/or hypercapnia should be actively given prone position ventilation. However, severe COVID-19 patients should be treated with prone ventilation as soon as possible. Due to the highly contagious nature of the new coronavirus, medical personnel need to perform tertiary protection. Therefore, the workload of medical personnel is further increased by implementing the prone position. The indication of prone ventilation in COVID-19 patients should be distinguished between severe and critical. For patients with severe disease, active prone ventilation can delay the progression from severe to critical. The prone position should be maintained as long as possible, depending on the tolerance of patient. Prone position ventilation is required for protective lung ventilation in critically ill patients whose hypoxemia and/or hypercapnia have not improved. Prone position ventilation should also be performed in the patients undergoing ECMO therapy. There is medical evidence that ECMO combined with prone position ventilation can improve the clinical prognosis of patients with severe ARDS secondary and COVID-19. It should be noted that COVID-19 patients could have low lung expandability. Therefore, prolonged ventilation should be maintained for at least 12 hours. Additionally, oxygenation changes and respiratory mechanics should be regularly evaluated (21).

One of the most common methods of oxygen therapy is nasal catheter application for infected cases in the mild stage. While this is a non-invasive method, the patient needs to be assisted by others. Therefore, it might not be comfortable for patients. One study confirmed that high-flow nasal cannula (HFNC) is a proper oxygen therapy method for severe and critical stages. HFNC has appropriate outcomes including exposure of warm and humid gas through patients' nasopharynx, which leads to a decrease in metabolic reactions in body, reduction of intubation, improving clinical condition of infected cases with acute respiratory failure; as well, physicians can control and apply this method easily. Despite these positive outcomes, HFNC is not an appropriate option for cases with ARDS in severe stage; the gas flow is high, so the possibility of bio-aerosol dispersion increases (22).

CT-scan and PCR have been used to detect infected cases and viral particles; however, it is important to evaluate sensitivity and specificity of these methods, as well as to assess other practical techniques.

CT scans are very important tools in COVID-19 diagnosis and forming a differential diagnosis, but they are also useful for determining patient prognosis. CT results in COVID-19 cases generally show patchy ground-glass opacities involving multiple lobes. These can be with or without consolidation and are mainly in the peripheral zone. There may also be associated reversed halo signs, vascular thickening, a crazy-paving pattern, or an air bronchogram sign. Patients who have CT scans showing multiple lesions need to be carefully monitored. Despite appearing well on initial presentation, these patients tend to have poorer prognoses and can potentially deteriorate very quickly to severe or critical conditions. Several specialists believe that CT-scan is one of the most useful and widely available medical tools for obtaining a better diagnosis. Clinicians should use the results of the CT scan in combination with reverse transcription polymerase chain reaction (RT-PCR) testing to determine the best course of action. The analysis of advantages of CT-scan images showed that this method is highly sensitive (14).

In China, there is a nationally standardized RT-PCR kit, but its sensitivity can sometimes be as low as 50 percent. The sensitivity mostly depends on the samples (nasal pharyngeal swab shows more positive cases than oral pharyngeal swab; broncho alveolar lavage fluid (BALF) is the most accurate one, sputum is less sensitive than BALF but it may be better than swab). IgM and IgG measurements also are performed which are really helpful. In cases where the results of PCR and CT-scan are different (i.e. CT manifest as typical virus pneumonia and PCR is negative), it must be considered that some errors might have occurred in the PCR results due to the quality of the sample; the process of laboratory testing or the testing kit itself (14). However, these issues tend to be very rare recently because the testing is defined as a combination of tests including the IgG and IgM measurements (11). RT- PCR and the technology of high-throughput sequencing have been used to detect SARS-CoV-2, but high-throughput sequencing is not common because the instrument itself is expensive. Therefore RT-PCR has been used and its sensitivity and specificity have been confirmed (14).

In Wuhan, a physician tried to use bronco-alveolar lavage (BAL) for critical patients who receive ECMO, and it was reported that after 2-3 trials of BAL and removal of some plasma liquid, the lungs became clear, but the final results of the treatment are not clear (When BAL was performed, the patient needed to be completely sedated and was administered a muscle relaxation drug. The physician needed to protect himself with positive pressure head cover) (17, 23).

Furthermore, several additional methods and clinical symptoms have bee also used to detect COVID-19 patients. These methods are explained in following and summarized in Table 2.

Learned from autopsy, there is a lot of viscous mucus in the airway and alveoli with obstruction of the airway in the patients. In these cases, acetyl cysteine and bronchodilator nebulization and tablets of acetyl cysteine are necessary (20).

The other unique feature in critically COVID-19 compared to influenza is that in COVID-19 more patients tend to have a gastric tension (belly tension) (24).

The low oxygen level is the most distinctive feature of COVID-19. In most of other situations, hypoxia is usually associated with tachycardia. However, in part of COVID-19 patients, despite hypoxia, heart rates may appear in normal range (silent hypoxemia) (17, 25).

In some cases, the patient's bilirubin level elevates, particularly when they are given antiviral drugs that have hepatotoxic effects. One study report liver enzymes [Aspartate aminotransferase(AST) and Alanine transaminase (ALT)] were unusually increased in some infected cases with COVID-19 and the rate and extent of ALT and AST elevation in severe COVID-19 patients were higher than those in non-severe patients (11, 23). In normal liver tissues, it is observed that ACE2 was just expressed in epithelial cells of bile duct; however, its level is so low in hepatocytes (7, 11).

Markers consist of CRP, procalcitonin, ferritin, D-dimer, lymphocytes, interleukin 4 (IL-4), interleukin 6 (IL-6), interleukin 10 (IL-10), tumor necrosis factor-alpha (TNF-a), interferon gamma (INF-y) which can help evaluate clinical progress, alert severe and critical tendencies and provide a basis for the formulation of treatment strategies. When patients have high temperature, high CRP and IL-6, high ferritin, increase D-dimer, progress infiltration in CT scan, deteriorate of oxygen index, that means the patient may shift to critically ill disease (11).

Other diagnostic methods have been proposed, including IgM/IgG and enzyme-linked immunosorbent assay (ELISA) kits for coronavirus, this assay could aid to detect virus particles in suspected cases (11, 14). One research study showed that these antibodies are produced against the N protein of SARS-CoV-2. It is also observed that the specificity of IgM and IgG is 100% and 95% respectively and the sensitivity of IgM and IgG is 77.3% and 83.3%, respectively (26). In addition, blood culture and detection of nucleic acids are other ways to diagnose SARS-CoV-2. However, the technique of nucleic acid detection is based on whole genome sequencing and while it is accurate, this method is expensive (14).

Table 2. Further clinical/ laboratorial diagnostics for COVID-19 (more details in B-4)

Indicators	Diagnostic Method	Reference
Clinical		
Obstructive airway	Observational	(20)
Gastric tension	Observational	(24)
Hypoxia	Observational, Oxygen level measurement	(17)
Silent hypoxia	Observational, Oxygen level measurement	(17, 25)
Laboratorial Indicators		
AST, ALT, Bilirubin, ACE2	Radioimmunoassay, Spectophometer	(7, 11)
CRP, Procalcitonin, Ferritin, D -dimer, Lymphocytes, IL-4, IL-6, IL-10, TNF-a, INF-y	ELISA, Radioimmunoassay	(11)
IgM/IgG levels	Serological test, ELISA	(11)
Detection of nucleic acid	Whole genome sequencing	(11)
Virus detection	Blood Culture	(11)

AST; Aspartate aminotransferase, ALT; Alanine transaminase, ACE2; Angiotensin-converting enzyme 2, IL-4; Interleukin 4, IL-6; Interleukin 6, IL-10; Interleukin 10, TNF-a; Tumor necrosis factor-alpha, INF-y; Interferon gamma, and ELISA; Enzyme-linked immunosorbent assay. IgM; Immunoglobulin M, and IgG; Immunoglobulin G.

Here, Chinese and Iranian clinicians discussed about some drugs and therapies in detail and Chinese clinicians expressed their experiences in treating various conditions. To better understand the latest situation on this topic, more recent clinical investigations on new drug or drug combinations has been disscussed separately.

Favipiravir, which is also named Avigen, has been used to treat COVID-19 patients. Chinese specialists do not use Favipiravir at their center, as the primary indication for this drug is influenza. However, a recent clinical trial using Favipiravir to treat COVID-19 in China has shown encouraging results. Below is a brief summary of the study. (This report translated from the Biotechnology Network from Chinese). Results of a "clinical study on the safety and effectiveness of favipiravir in the treatment of patients with new coronavirus pneumonia (COVID-19)" (Registration Number: ChiCTR2000029600). Research suggests that Favipiravir may improve the clinical course of this new coronavirus pneumonia by accelerating viral clearance. This research was completed by the National Engineering Research Center for Emergency Prevention and Control Engineering and the Third People's Hospital of Shenzhen City. Viral clearance is the main internationally accepted gold standard for evaluating clinical efficacy of antiviral drugs. In this clinical study, 35 patients with common new-type coronavirus pneumonia who met the eligibility criteria were treated with Favipiravir (3,200 mg on the first day, 1,200 mg/d on the 2nd to 14th days, divided into two oral doses, the course of treatment until the virus was eliminated, up to 14 days). The study also included 45 patients with COVID-19 who were treated with Lopinavir/Ritonavir tablets (400 mg/100 mg, twice daily, orally) matching for age, gender, and disease severity to the control group. The median time from drug administration to viral clearance, the rate of improvement of chest imaging on day 14 of treatment, and safety were compared between the two groups. The results showed that all baseline characteristics of the two groups of patients were comparable. The median time to viral clearance was shorter in the Favipiravir treatment group, with a median (interquartile range) of 4 days (2.5-9 days) and a control group of 11 days (8-13 days), with significant differences between the two groups (P<0.001). After controlling for potential confounding factors (age, time to onset of symptoms, fever etc.), Favipiravir remains an independent influencing factor for improved chest imaging and early viral clearance. Compared with the control group, the Favipiravir group had fewer adverse reactions and was better tolerated (27).

In general, the consensus reached by experts is that glucocorticoids are not routinely used, and the indications should be strictly controlled. The general agreement is that glucocorticoids are not required in light and common type patients [In China, COVID-19 patients can be divided into four types: mild (only RTPCR positive without pneumonia); moderate, also called as common (RT-PCR positive with pneumonia in CT); severe, and critical pneumonia).] and should only considered in severe and critically ill patients. The indications are established by different criteria including progressive deterioration in oxygenation indicators, quick progression of disease on imaging, and excessive activation of the body's inflammatory response. Additionally, glucocorticoids should be considered if patients have any of following 4 conditions in conjunction with COVID-19: 1. confirmed new COVID-19 pneumonia within the past 10 days that demonstrates rapid progression on imaging; 2. severe hypoxemia (respiratory failure); 3. common type patients with acute exacerbations (high fever, dyspnea) and severe and critically ill patients; or 4. the deterioration of oxygenation index, with or without rapid progress in imaging. To summarize, most experts do not rule out the use of glucocorticoids, but they should be applied early in the critical illness (usually within 10 days of the disease course). Furthermore, mild and moderate patients usually do not need to use glucocorticoids. They should be administered to severe and critically ill patients in the early stages have one of the following three criteria: 1. progressive deterioration of oxygenation index, 2. rapid progression of lesions on imaging and 3. excessive activation of the body's inflammation (28).

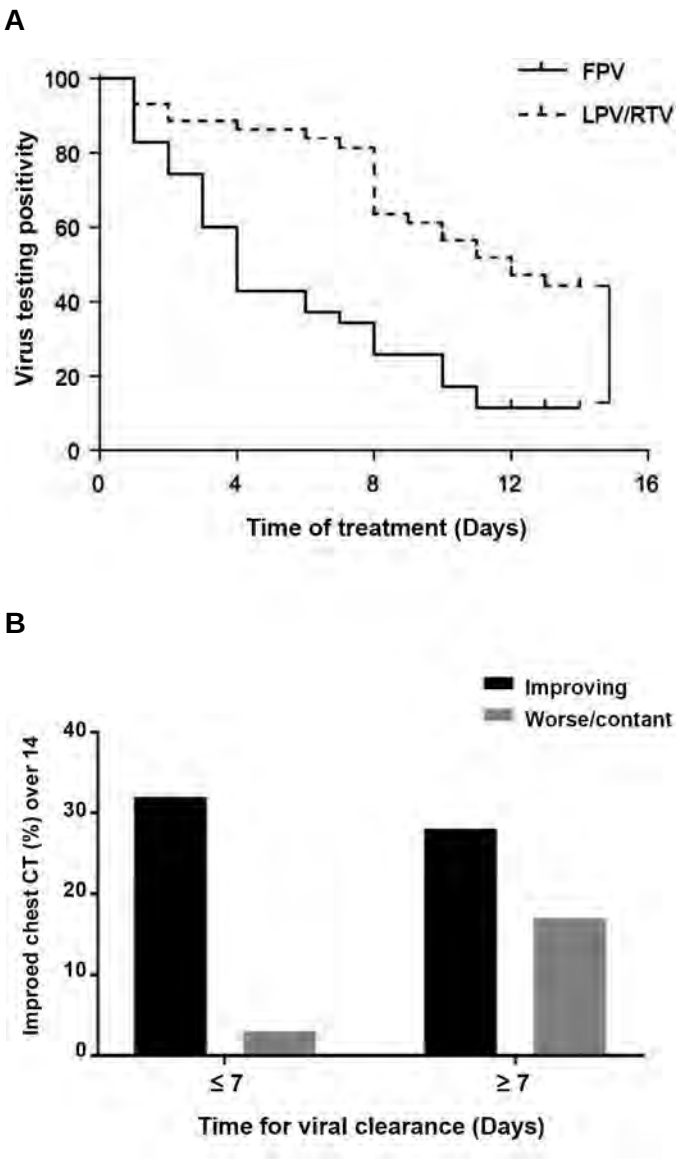

Fig.4: Favipiravir effects on virus testing positivity and chest CT. **A.** Time for virus clearance and survival curve. **B.** Influence of virus clearance rate on the chest CT at day 14 after treatment. CT; Computerized tomography, FPV; Favipiravir, and LPV/RTV; Lopinavir/ritonavir

In theory, glucocorticoids are best used during periods when viral replication is inhibited (whether caused by an antiviral drug or enhanced immune response) and the body's inflammatory response is very intense. It is difficult to grasp the state of excessive activation (inflammatory storm) of the body's inflammatory response (general situation: about 10 days into the course of the disease). Here is a personal opinion for clinical reference; the new coronavirus infection meets the severe clinical manifestations and can be considered as an "inflammatory storm" state when the following conditions are met: persistent high fevers, progressive deterioration of oxygenation, rapid progression of lesions on imaging, continuous decline in the absolute value of lymphocytes, and a significant increase in interleukin 6. The dose and duration of glucocorticoids (Aprenosaurus as a representative; this is the same as methylprednisolone of China): as a representative]: the dose is 40~160 mg/d, for no more than 7~10 days. Glucocorticoids are mainly effective in patients who have developed lung injury. In general, the principle of application is an individualized treatment: it should be administrated at the right time (early, usually within 10 days of the disease), to the appropriate patients (severe and critically ill patients who experience excessive inflammation in the body), with an appropriate dose (usually a medium dose of 40~160 mg/d, and large dose shock is not recommended) and a short course of treatment (not more than 7~10 days). As well, paying attention to the adverse effects of glucocorticoids is crucial. Analysis of contraindications before using glucocorticoids: Glucocorticoids should be used with caution in the following cases: diabetes, known allergies to other steroids, high blood pressure, epilepsy or delirium, glaucoma, active gastrointestinal bleeding in the last three months, problems with hypokalemia correction, secondary microbial infections, immunosuppressed condition (like chemoradiation, major surgery, acquired immune deficiency syndrome) and severe lymphopenia (absolute value <300 / μl).

Nowadays, the use of dexamethasone in ICU patients is a difficult decision to make for clinicians, as the general understanding is that dexamethasone has long lasting effects. Furthermore, in practice, physicians are generally more used shorter half-life methylprednisolone. Investigating the Clinical-Trials. gov website showed that 291 projects have been conducted on COVID-19; Among these projects, 109 studies referred to pharmacological and therapeutic objectives for COVID-19 of which 87 of these trials are in different phases including 4, 36, 36, and 11 studies in phase I, II, III, and IV respectively. On the grounds that COVID-19 is closely related to SARS and MERS, it has been recommended that the drugs which are used to treat SARS and MERS, might be appropriate for COVID-19 treatment too. Therefore, a list of pharmacological agents has been proposed to be investigated. All of the proposed drugs should be precisely evaluated in terms of adult dose, contraindications, toxicities, major drug-drug interactions, etc. Recently, clinicians prescribe Nintendanib and Perfenidone to patients with COVID-19 and idiopathic pulmonary fibrosis. These drugs have anti-oxidant and anti-inflammatory activities. Chloroquine/Hydroxychloroquine which is known as anti-malaria drug, showed anti-inflammatory activities when administered for COVID-19 patients, although its efficacy remains hotly debated. It also is able to inhibit viral entry to host cells by different mechanisms, such as inhibition of proteolytic process. Lopinavir/ Ritonavir is practical for acquired immunodeficiency syndrome (AIDS) treatment and also inhibits 3-chymotrypsin-like protease in SARS. Therefore, the drugs can be proposed for therapeutic purposes in COVID-19; however, some observations showed that these caused side-effects like hepatoxicity and are not appropriate for all conditions of the disease. Ribavirin which inhibits viral RNA-dependent RNA polymerase and has antiviral activity against nCOVs, has been used against SARS and MERS. However, several side-effects such as hematologic and liver toxicity were reported. High dosage of this drug should be used to inhibit viral replication which may cause adverse outcomes in patients. Due to its side effects, its application has been limited in COVID-19 treatment. Umifenovir (Arbidol), which has been confirmed to treat influenza in China and Russia, targets interaction of S protein/ACE2 and inhibits formation of the components of the viral envelop. A randomized control trial has been launched recently in China to investigate its effects on COVID-19. Another drug with destructive effects against RNA viruses is Remdesivir. This drug is an appropriate agent to prevent lung hemorrhage and decreases viral lung titers and used against Ebola virus and now suggested for patients with COVID-19. Several studies showed that Immunoglobins are applicable in several viral diseases such as Ebola, influenza and HIV-1. Therefore, immunoglobins have been considered as a potential therapeutic agents in COVID-19. In addition, it was reported that corticosteroids such as methylprednisolone, hydrocortisone and dexamethasone are effective in SARS-CoV. Nowadays, methylprednisolone is prescribed with oseltamivir, antibiotics and oxygen therapy in the patients infected COVID-19. Other agents which were used in SARS, MERS, or AIDS and are proposed for COVID-19 included Darunavir, recombinant human interferon α2β and thalidomide (28).

There are two criteria for performing plasma exchange: critical severe COVID-19 and COVID-19 that is complicated by liver damage and cytokine storm (high levels of interleukin 6). However, plasma exchange is not a routine procedure and is certainly not a wide-spread practice in the Chinese clinical community. Some treatments are usually applied, including oxygen therapy and application of a wide range of antibiotics, to prevent secondary bacterial infections (28, 29).

Researchers believe that blockers of RNA-polymerase can be effective in reducing RNA-virus proliferation in the body. In addition, some studies recommended inhibitors of Chymotrypsin-like (cinansrin and flavonoids) and papain-like protease (diarylheptanods), also use of blockers to prevent binding S-protein with ACE2, may be effective strategies to decrease this infection.

Other studies demonstrated that types of vaccines, monoclonal antibody, and plasma substitution could be appropriate for the treatment of COVID-19. Hemoperfusion and plasma exchange are applicable for COVID-19 and they cause removal of plasma proteins, cytokines, and toxic factors. However, it is observed that hemoperfusion has adverse outcomes such as reduction of blood glucose, calcium, neutrophils, etc. Furthermore, plasma exchange leads to a decrease in coagulation proteins and antibodies. Therefore, coupled plasma filtration adsorption is proposed. This technique uses a combination of hemoperfusion and plasma exchange and it removes cytokines in infected cases with COVID-19. Another proposed treatment for COVID-19 includes mesenchymal stromal cell (MSC) transplantation. These cells, which include several subtypes, are able to modulate the immune system and inflammatory reactions. Based on pathological characteristics of infected patients, this therapy can be proposed, especially for severe and critical stages. There are several trials which show this therapy is safe rather than others for patients (28).

In the context of the viral pandemic, one of the most important approaches that researchers and physicians should follow is to communicate effectively and quickly with each other and to establish ways to exchange scientific information about different aspects of diagnostics and therapeutics. This communication happened from the earliest moments of the COVID-19 pandemic between a group of Chinese and Iranian clinicians and medical researchers. Present article is the result of this exchange of views which mainly consists of three categories: A. pulmonary techniques for COVID-19 patient, B. clinical and molecular diagnostic methods for COVID-19 and C) Drug combinations and new therapies for COVID-19. A wide range of antiviral and anti-inflammatory drugs, respiratory therapies, plasma exchange, and application of mesenchymal stromal cells as well as the most common/ novel diagnostic methods have been discussed throughout these three sections and the latest investigations in regards to these have been mentioned where relevant.

Acknowledgments

This work has been supported by Wenzhou Medical University, China, Fasa University of Medical Sciences, Iran and Royan Institute, Iran. We express our appreciation to all members of Chronic Respiratory Diseases Research Center at Shahid Beheshti University of Medical Sciences for their helpful deliberations and consultation during this work. The authors declare that there is no financially support and conflict of interest.

Authors' Contributions

Y.L., Y.T., M.T., Ch.Ch.; Have been involved in preparing and categorizing the topics and design of the manuscript. S.M.R.H.; Revising the manuscript for critically important intellectual content. F.A.; Added the new findings and references in different sections of the manuscript. J-S.Z., Y.Gh., and X.L.; Revised the manuscript and developed the final revision. All authors read and approved the final manuscript.

References

1. Phelan AL, Katz R, Gostin LO. The novel coronavirus originating in Wuhan, China: challenges for global health governance. JAMA. 2020; 323(8): 709-710.
2. COVID-19 coronavirus pandemic. 2020. Available from: https://www.worldometers.info/coronavirus/2020. (05 May 2020)
3. Surveillances V. The epidemiological characteristics of an outbreak of 2019 novel coronavirus diseases (COVID-19)—China, 2020. China CDC Weekly. 2020; 2(8): 113-122.
4. Li Q, Guan X, Wu P, Wang X, Zhou L, Tong Y, et al. Early transmission dynamics in Wuhan, China, of novel coronavirus–infected pneumonia. N Engl J Med. 2020; 382(13): 1199-1207.
5. Huang C, Wang Y, Li X, Ren L, Zhao J, Hu Y, et al. Clinical features of patients infected with 2019 novel coronavirus in Wuhan, China. Lancet. 2020; 395(10223): 497-506.
6. Zhou F, Yu T, Du R, Fan G, Liu Y, Liu Z, et al. Clinical course and risk factors for mortality of adult inpatients with COVID-19 in Wuhan, China: a retrospective cohort study. Lancet. 2020; 395(10229): 1054-1062.
7. Li SR, Tang ZJ, Li ZH, Liu X. Searching therapeutic strategy of new coronavirus pneumonia from angiotensin-converting enzyme 2: the target of COVID-19 and SARS-CoV. Eur J Clin Microbio Infect Dis. 2020; 39(6): 1021-1026.
8. Wu Z, McGoogan JM. Characteristics of and important lessons from the coronavirus disease 2019 (COVID-19) outbreak in China: summary of a report of 72 314 cases from the Chinese Center for Disease Control and Prevention. JAMA. 2020 ; 323(13): 1239-1242.
9. Manandhar S, Nakarmi P, Baniya N. A Novel Coronavirus Emerging in World—Key Questions for Developing Countries and Under Developed Countries. North American Academic Research. 2020; 3(02): 473-497.
10. Gong F, Xiong Y, Xiao J, Lin L, Liu X, Wang D, et al. China's local governments are combating COVID-19 with unprecedented responses—from a Wenzhou governance perspective. Front Med. 2020; 14(2): 220-224.
11. Jia X, Zhang P, Tian Y, Wang J, Zeng H, Wang J, et al. Clinical significance of IgM and IgG test for diagnosis of highly suspected COVID-19 infection. medRxiv. 2020. (In Press) (05 May 2020).
12. Veronese N, Demurtas J, Yang L, Tonelli R, Barbagallo M, Lopalco P, et al. Use of corticosteroids in coronavirus disease 2019 pneumonia: a systematic review of the literature. Front Med. 2020; 7: 170.
13. Nguyen A, David JK, Maden SK, Wood MA, Weeder BR, Nellore A, et al. Human leukocyte antigen susceptibility map for SARS-CoV-2. J Virol. 2020; 94(13): e0050-e00520.
14. Li X, Geng M, Peng Y, Meng L, Lu S. Molecular immune pathogenesis and diagnosis of COVID-19. J Pharm Anal . 2020; 10(2): 102-108.
15. Coronavirus disease 2019 (COVID-19) situation report – 57. Available from: https://reliefweb.int/sites/reliefweb.int/files/resources/20200317-sitrep-57-covid-19.pdf (17 Mar 2020)
16. Nasibova EM, Pashayev CN. The use of non-invasive ventilation (NIV) in the treatment of patients with COVID-19. Journal of Anesthesia and Surgery. 2020; 3(2): 1-6.
17. Yuan H, Cao X, Ji X, Du F, Zhou X, He J, et al. A Current emerging respiratory infection: Epidemiological and clinical characteristics, diagnosis and treatments of COVID-19. Diagnosis and Treatments of COVID-19. 2020. Available from SSRN: https://ssrn.com/ab-

stract= 3551344 or http://dx.doi.org/10.2139/ssrn.3551344 (06 Mar 2020).
18. Yuki K, Fujiogi M, Koutsogiannaki S. COVID-19 pathophysiology: A review. Clin Immunol. 2020: 215: 108427.
19. Gattinoni L, Chiumello D, Rossi S. COVID-19 pneumonia: ARDS or not? : Critical Care. 2020; 24: 154.
20. Poe FL, Corn J. N-Acetylcysteine: a potential therapeutic agent for SARS-CoV-2. Medical Hypotheses. 2020: 143: 109862.
21. Sartini C, Tresoldi M, Scarpellini P, Tettamanti A, Carcò F, Landoni G, et al. Respiratory parameters in patients with COVID-19 after using noninvasive ventilation in the prone position outside the intensive care unit. JAMA. 2020; 323(22): 2338-2340.
22. Li J, Fink JB, Ehrmann S. High-flow nasal cannula for COVID-19 patients: low risk of bio-aerosol dispersion. Eur Respir J. 2020; 55(5): 2000892.
23. Hong X, Xiong J, Feng Z, Shi Y. Extracorporeal membrane oxygenation (ECMO): does it have a role in the treatment of severe COVID-19? Int J Infect Dis. 2020. 94: 78-80.
24. Pan L, Mu M, Yang P, Sun Y, Wang R, Yan J, et al. Clinical characteristics of COVID-19 patients with digestive symptoms in Hubei, China: a descriptive, cross-sectional, multicenter study. Am J Gastroenterol. 2020; 115(5): 766-773.
25. Ottestad W, Seim M, Mæhlen JO. COVID-19 with silent hypoxemia. Tidsskrift for Den norske legeforening. 2020.
26. Sean Stowell, Guarner J . Role of serology in the COVID-19 pandemic. Clin Infect Dis. 2020. ciaa510.
27. Cai Q, Yang M, Liu D, Chen J, Shu D, Xia J, et al. Experimental treatment with favipiravir for COVID-19: an open-label control study. Engineering. 2020. [Ahead of print].
28. Hossein-khannazer N, Shokoohian B, Shpichka A, Aghdaei HA, Timashev P, Vosough M. Novel therapeutic approaches for treatment of COVID-19. J Mol Med (Berl). 2020: 98(6): 789-803.
29. Xu W-X, He H-I, Pan S-W, Chen Y-l, Zhang M-l, Zhu S, et al. Combination treatments of plasma exchange and umbilical cord-derived mesenchymal stem cell transplantation for patients with hepatitis b virus-related acute-on-chronic liver failure: a clinical trial in china. Stem Cells Int. 2019; 2019: 4130757.

Is COVID-19 to Blame?

Alireza Asgari, Ph.D.

Aerospace Medicine Research Center, Aja University of Medical Sciences, Tehran, Iran

***Corresponding Address: Aerospace Medicine Research Center, Aja University of Medical Sciences, Tehran, Iran**
Email: ar.asgari@ajaums.ac.ir*

Received: 16/April/2020, Accepted: 21/April/2020

Abstract

Mankind is witnessing economic uncertainty due to a health crisis as never before. In the era of industrialization where the emergence of invisible enemies of humans is causing a great death toll, "nothing seems more universal than health", the old proverb in nearly all human cultures is once again rebirthed by the current COVID-19 pandemic. Nevertheless what is distinctive is that the SARS-CoV-2 seems to be unequally targeting a particular sector of the populations with risk factors for preventable diseases. Comorbidities, mainly non-communicable diseases (NCDs), seem to be the primary contributors of the current pandemic and not the SARS-CoV-2 *per se*. The present letter attempts to underscore the converging pattern of communicable (CDs) and NCDs in *human toll*. For the tens of thousands of lives coming to an end since the turn of the year, we are all truly sad, but thankful to the virus for unearthing the grave need of the mankind to improve his life style and behaviors. It directs us to revisit the values and ultimately save millions of lives in future.

Keywords: Communicable, Convergence, COVID-19, Infectious, Non-Communicable,SARS-CoV-2

Cell Journal(Yakhteh), Vol 22, Suppl 1, Autumn 2020, Pages: 166-168

Citation: **Asgari A. Is COVID-19 to blame?. Cell J. 2020; 22 Suppl 1: 166-168. doi: 10.22074/cellj.2020.7564.**

In the era of industrialization and globalization where the emergence of invisible enemies of humans is growing at a speedy pace with inevitable consequences, nothing seems more universal than health The first 5-page situation report of WHO on 21st of January 2020 announced that it was not until 7th of January 2020 that Chinese scientists identified the new coronavirus as being the cause of their latest 44 cases of pneumonia (1). The SARS-CoV-2 seems to be selecting the older stratum of the world populations where the risk of preventable death is high. Comorbidities, mainly non-communicable diseases (NCDs), seem to be the primary contributors of the current pandemic and not the SARS-CoV-2 *per se*. The present commentary attempts to underscore the converging pattern of communicable (CDs) and NCDs in *human toll*, where only a few frequently asked questions are barely answered, even if asked from the most knowledgeable subject matter experts in the field.

The first United Nation High-Level Meeting (UN HLM) on Health issues was held in 2001 for HIV and yet millions are awaiting a real breakthrough amid tremendous progress in research and management of AIDS. The second HLM was held in 2011 where the impact of NCDs on countries economic growth was brought to surface. Cost of illness, whether direct or indirect, economic loss of productivity and the value of statistical life were the three approaches used to calculate the burden by a collaboration between WHO and the Harvard School of Public Health in 2011 (2). The alarm was substantiated with compelling evidence: more than 60% of all deaths is caused by NCDs which will affect economic growth, more so in low- and middle-income countries. The report anticipated the cumulative cost of NCDs in 2030 to be about 31 trillion USD, by utilizing the burden of NCDs in 2010 and mathematically projecting it into 2030. The EPIC model of WHO, introduced by Abegunde and Stanciole (3), simulated labor and capital features of the economy as two main productive factors that were linked to economic growth. It was concluded by proposing: "a unified front is needed to turn the tide on NCDs". Nearly a decade has passed and yet solid evidence is needed to substantiate whether the world has taken that report seriously in tackling NCDs and if the commitments at national level were scaled to the severity of the threat, despite published doubts (4). The economic catastrophe that inevitably follows the NCDs is felt strongly by the next generation. That is how wide apart the health and economics aspects of NCDs are!

On the same track, the latest UN HLM was convened in September 2019 on Universal Health Coverage issue with the objective of achieving and promoting physical and mental health and well-being of all world inhabitants, leaving no one behind. To cognize the thoughts cloud of the participants, a few keywords were searched for in the published list of pre-registered statements from multi-stakeholder constituency/institutions in that convention (5), including "non-communicable", "communicable"and "infectious". The frequencies of their appearance were 6:1:1, respectively. Presuming that the frequency of words can stand for the level of focus, concern and mindfulness, it seems as if infectious diseases were not at the center of the focus. A few days passed, however, and the whole world was caught by surprise by coronavirus, for the third time in recent decades, but only this time surpassing the thresholds of a pandemic event in less than

a couple of months. Now the COVID-19 has created a real dramatic picture. Since the early days of the current pandemic, human death has tolled to 138,008 by 16th Apr 2020 (JHU corona map) in nearly 4 months, worldwide (6). The worst may yet to come, God forbid, but even then it does not match deaths of NCDs during the same period, more than 200K (7, 8). In a single-centered retrospective study done in Wuhan, China, 50% of non-survivors suffered from chronic diseases (9). Another study by Zhou and colleagues from a pneumonia hospital in Wuhan reported that 67% of non-survivors had comorbidities, hypertension in the first place followed by diabetes (10). The picture is more or less the same in Italy (11) and probably everywhere. The virus has hit and shaken the world badly, but only this time in a unique and unprecedented manner: the *health impact* and the *economic turmoil* are felt simultaneously. *Unhealthiness* and death concurrent with economic distress, leading to immediate unemployment and cash shortages, let aside the health access disparities, travel restrictions, voluntary quarantines, and forced lock-downs, all occurred in about 2 short months!

Following the striking report on the burden of NCDs (2) many countries came to become knowledgeable that economic threats do not necessarily stem from miscalculating megatrends in the emerging markets and/or industries, global recession, disputes and disagreements between oil producing countries, and not even from climate change. However, knowledge *per se* would not bring any change, it needs to be enacted. The number of preventable deaths is still on the rise as if the due interventions are themselves suffering from inefficiency and chronicity. The total number of deaths from NCDs between 2007 and 2017 increased by 27% and that of total YLDs rose more than 50% (4). It seems that humans are not good at responding to events with very slow time course change. Biological principles dictate that if a stimulus intensity rises in several minutes instead of a few seconds, our senses will probably not detect it and the stimulus may easily be ignored, regardless of the absolute magnitude at most times. In fact, we tend to be more vigilant to kinetics of the stimuli rather than their absolute magnitude. As such, we have never advised our family members to eat quality food and engage in physical activity as often as we urge them to wash their hands nowadays, mainly for one reason: we do not see them fall sick and die in a matter of days if they suffer from nutritional inefficacies, hypertension or diabetes. The chronicity of NCDs seems to be the factor that is making all the differences. The chronicity of NCDs renders country health authorities to pass by in silence. The chronicity allows WHO not to declare a state of worldwide emergency.

Convergence of infectious and preventable diseases

It was the general belief of the past century that most infectious diseases are acute illnesses and chronic diseases are mostly non-communicable (12). However, with growing evidence, scientists now believe that a significant portion of chronic diseases are associated with infections. However, the two artificial fields of CDs and NCDs that scientists have long before dichotomized for simplicity are proving insufficient. They are potentiating one another in favor of greater illnesses of humans. Today, pandemic of infectious diseases and epidemics of NCDs are converging on a global scale, a notion that Marias et al. (13). intelligently anticipated to be escalating in the coming decades. COVID-19 is clearly displaying that message, if nothing else. No matter how wild the COVID-19 evolves to become across various world epigenome in the remaining months of 2020, it will not cost humans lives as much as NCDs. To be prepared for future infectious pandemics, the share of NCDs in economic burden of COVID-19 is to be determined and appropriate flags raised. It seems that NCDs, in particular cardiovascular diseases, are the key player in the current crisis. They should once again be stressed to be put at the center of the business sectors' radar in all countries.

Let us focus on the fact that the COVID-19 is not causing all the problems *per se*, it is the comorbidity of the infected that has created all the chaos and confusion. SARS-CoV-2 does not seem to be as cruel as flu virus. As of to date and according to the limited information about its mechanistic path in human body, the comorbidities are killing the host and NOT the COVID-19. If the poor virus had an official speaker and a podium to be questioned by aggressive reporters, it would have pleaded "NOT GUILTY"! Most probably, what the virus is trying to unearth is our vulnerability, predominantly caused by NCDs. It is forcing us to realize that it is our way of living that is backfiring. In other words, SARS-CoV-2 is doing a good job of inversing the chronic character of NCDs into an acute picture, visible and experienced by nearly all individuals across borders.

In the 20th century, influenza and measles, as single-pathogen diseases, were defeated when NCDs were either absent or at their infancy and not hitting all-time records. However, COVID-19 has picked a time to spread where NCDs are at their highest and human microbiome diversity at their lowest (14, 15). Dynamics of COVID-19 behavior in an already health-compromised human body may need a shift in the focus of scientist struggling in the front line of the current viral invasion. In that sense, one potential research priority of delving into the unexpected human toll of the COVID-19 pandemic, is to find a qualitative and quantitative relationship between the clinical outcome of COVID-19 with the type and chronicity of co-existing morbidities and the corresponding microbiome diversity. This approach may partially heal the fragmented studies of epidemiology in different populations. The fact is buried in the tangled web of information in hundreds of hospitals now managing the patients. When the dynamics of the COVID-19 pandemic and its synergies with the epidemics of NCDs, meet the threshold of an official and WHO-tagged *syndemic*, the metaphor of "the blind man and the elephant" may get bridged in order to improve nations' resilience.

As David Jones puts it: "The history of epidemics offers considerable advice, but only if people know the history and respond with wisdom" (16). Can we take a lesson from the present pandemic to prevent, detect, and mitigate chronic diseases and to reduce probability of future viral epidemics, even pandemics? The "viral security" that the world is running after may not be attained without "NCD security" and even other unknown health "securities". Charles Rosenberg states: "epidemics start at a moment in time, proceed on a stage limited in space and duration, follow a plot line of increasing revelatory tension, move to a crisis of individual and collective character, then drift toward closure" (17). As Jones claims in his recent perspective: "societies and their citizens misunderstand the relative importance of the health risks they face. Citizens and their leaders need to think carefully, weigh risks in context, and pursue policies commensurate with the magnitude of the threat" (16). We either need to win or learn the current pandemic, but we cannot afford to lose it.

References

1. World Health Organization. Novel Coronavirus (2019-nCoV): Situation report-5 (25 January 2020). Geneva: WHO; 2020.
2. Bloom DE, Cafiero ET, Jané-Llopis E, Abrahams-Gessel S, Bloom LR, Fathima S, et al. The global economic burden of noncommunicable diseases. Geneva: World Economic Forum; 2011.
3. Abegunde D, Stanciole A. An estimation of the economic impact of chronic noncommunicable diseases in selected countries. Geneva: WHO; 2006.
4. The Lanct. GBD 2017: a fragile world. Lancet . 2018; 392(10159):1683.
5. Moving together to build a healthier world . The UN High-Level Meeting (UN HLM) on Universal Health Coverage; 2019 Sep 23; New York ; 2019. Available from: https://www.uhc2030.org/un-hlm-2019/high-level-meeting-statements-on-uhc/. (15 Apr 2020).
6. Map-COVID-19. John Hopkins Coronavirus Resource Center. Available from: https://coronavirus.jhu.edu/map.html. (15 Apr 2020).
7. Non-Communicable Diseases Progress Monitor 2017. WHO; 2017. Available from: https://apps.who.int/iris/bitstream/handle/10665/258940/9789241513029-eng.pdf;jsessionid=0A327A305EE34E504D105978773BA484?sequence=1.
8. GBD 2016 Causes of Death Collaborators. Global, regional, and national age-sex specific mortality for 264 causes of death, 1980–2016: a systematic analysis for the Global Burden of Disease Study 2016. Lancet. 2017; 390(10100): 1151-1210.
9. Yang X, Yu Y, Xu J, Shu H, Xia J, Liu H, et al. Clinical course and outcomes of critically ill patients with SARS-CoV-2 pneumonia in Wuhan, China: a single-centered, retrospective, observational study. Lancet Respir Med. 2020: pii: S2213-2600(20)30079-5.
10. Zhou F, Yu T, Du R, Fan G, Liu Y, Liu Z, et al. Clinical course and risk factors for mortality of adult inpatients with COVID-19 in Wuhan, China: a retrospective cohort study. Lancet. 2020; 395(10229): 1054-1062.
11. Porcheddu R, Serra C, Kelvin D, Kelvin N, Rubino S. Similarity in case fatality rates (CFR) of COVID-19/SARS-COV-2 in Italy and China. J Infect in Dev Ctries. 2020; 14(2): 125-128.
12. O'Connor SM, Taylor CE, Hughes JM. Emerging infectious determinants of chronic diseases. Emerg Infect Dis. 2006; 12(7): 1051-1057.
13. Marais BJ, Lönnroth K, Lawn SD, Migliori GB, Mwaba P, Glaziou P, et al. Tuberculosis comorbidity with communicable and non-communicable diseases: integrating health services and control efforts. Lancet Infect Dis. 2013; 13(5): 436-448.
14. Pascal V, Pozuelo M, Borruel N, Casellas F, Campos D, Santiago A, et al. A microbial signature for Crohn's disease. Gut. 2017; 66(5): 813-822.
15. Frati F, Salvatori C, Incorvaia C, Bellucci A, Di Cara G, Marcucci F, et al. The role of the microbiome in Asthma: The Gut–Lung axis. Int J Mol Sci. 2018; 20(1): pii: E123.
16. Jones DS. History in a crisis—lessons for Covid-19. N Engl J Med.2020; 382: 1681-1683.
17. Rosenberg CE. What is an epidemic? AIDS in historical perspective. Daedalus. 1989; 118(2): 1-17.